UNIVERSITAS SCIENTIARUM SZEGEDIENSIS · SZEGEDI TUDOMÁNYEGYETEM

SZEGEDI AKADÉMIAI BIZOTTSÁG
SZAB*1961

PROCEEDINGS OF THE

29th International Symposium on Analytical and Environmental Problems

Szeged, Hungary
November 13-14, 2023

University of Szeged

Edited by:
Tünde Alapi
Róbert Berkecz
István Ilisz

Publisher:
University of Szeged, H-6720 Szeged, Dugonics tér 13,
Hungary

ISBN 978-963-306-963-9

2023.
Szeged, Hungary

The 29^th^ International Symposium on Analytical and Environmental Problems

Organized by:
SZAB Kémiai Szakbizottság Analitikai és Környezetvédelmi Munkabizottsága

Supporting Organizations
Institute of Pharmaceutical Analysis, University of Szeged
Department of Molecular and Analytical Chemistry, University of Szeged

Symposium Chairman:
István Ilisz, DSc

Honorary Chairman:
Zoltán Galbács, PhD

Organizing Committee:
István Ilisz, DSc
professor of chemistry
University of Szeged, Institute of Pharmaceutical Analysis
Tünde Alapi, PhD
assistant professor
University of Szeged, Department of Molecular and Analytical Chemistry
Róbert Berkecz, PhD
assistant professor
University of Szeged, Institute of Pharmaceutical Analysis

Scientific Committee:
István Ilisz, DSc
Tünde Alapi, PhD
Róbert Berkecz, PhD
Daniela Sojic Merkulov, PhD
associate professor
University of Novi Sad, Faculty of Sciences, Department of Chemistry, Biochemistry and Environmental Protection

Lecture Proceedings

INFLUENCE OF RAPID HEAT TREATMENT ON THE PHOTOCATALYTIC ACTIVITY AND STABILITY OF STRONTIUM TITANATES AGAINST A BROAD RANGE OF POLLUTANTS

Mahsa Abedi[1], Tamás Gyulavári[1], Zsolt Pap[1,2,3]

[1]Department of Applied and Environmental Chemistry, University of Szeged, Rerrich Béla Sqr. 1, H-6720 Szeged, Hungary
[2]Nanostructured Materials and Bio-Nano-Interfaces Center, Interdisciplinary Research Institute on Bio-Nano-Sciences, Babes-Bolyai University, Treboniu Laurian Str. 42, RO-400271 Cluj-Napoca, Romania
[3]Institute of Research-Development-Innovation in Applied Natural Sciences, Babes-Bolyai University, Fântânele Str. 30, RO-400294 Cluj-Napoca, Romania
e-mail: mahsa.sh.abedi@gmail.com

Abstract

Strontium titanate (STO) photocatalysts were synthesized using a modified Pechini sol–gel method. These photocatalysts were then subjected to rapid calcination at various temperatures with short exposure times. The samples were characterized using a range of techniques, including X-ray diffractometry, scanning electron microscopy, diffuse reflectance spectroscopy, infrared spectroscopy, nitrogen adsorption–desorption measurements, and X-ray photoelectron spectroscopy. The photocatalytic activity of the samples was evaluated by testing their ability to oxidize phenol, oxalic acid, chlorophenol, glucose, and propanol under UV light irradiation. Notably, all the prepared samples exhibited higher photocatalytic activity compared to the commercial STO reference. Increasing the calcination temperature resulted in improved crystallinity and larger primary crystallite sizes, but it also led to reduced band gaps and specific surface areas. The enhanced photocatalytic activity observed in the most efficient samples was attributed to the presence of $SrCO_3$ on the surface of the catalyst. Importantly, the STO photocatalysts exhibited high stability, maintaining their crystalline composition even after exposure to chemicals with different functional groups. Reusability experiments showed that the photocatalytic activity increased over successive reuse cycles, for which further investigations will be carried out to identify the possible causes.

Introduction

Strontium titanate ($SrTiO_3$) is a perovskite-type photocatalyst featuring a 3.2 eV band gap, making it a favorable contender for applications in both water splitting [1, 2], and the photodegradation of organic contaminants [1-4]. The catalyst offers several benefits, including affordability, robust photocatalytic performance, resistance to photo corrosion, and non-toxic nature. However, the primary drawback of $SrTiO_3$ lies in its limited ability to harness solar energy, absorbing only a narrow portion (about 5%) due to its wide band gap. This wide band gap confines its utility for photocatalytic degradation when exposed to UV light [1-5]. Hence, the majority of research endeavors have centered on enhancing $SrTiO_3$ through methods like anion doping [6-8], introducing metal dopants [9, 10], creating oxygen deficiencies [11], depositing noble metals [12], crafting composites [13], or employing dye sensitization [14].

Various methods are employed for $SrTiO_3$ synthesis, including reverse microemulsion, carbon-free combustion, hydrothermal, polymeric precursor, and sol-gel techniques [15, 16]. Among these methods, the sol-gel approach has garnered research interest due to its simplicity and adaptability [16, 17]. The Pechini method, a sol-gel technique, is widely utilized to obtain highly pure oxides [18, 19]. However, perovskite preparation through sol-gel methods necessitates a costly high-temperature calcination step [20]. The calcination temperature significantly impacts the physicochemical properties of photocatalysts, as demonstrated by Jia et al., who observed its strong influence on the stability and photocatalytic activity of doped $SrTiO_3$ photocatalysts [5]. Despite extensive research on sol-gel synthesis of $SrTiO_3$, some aspects, such as the influence of calcination parameters on photoactivity, remain unclear. Calcination, while offering an effective and controllable means to crystallize amorphous materials, is often underexplored [17, 21, 22]. Employing unmodified, optimally calcined $SrTiO_3$ could yield more cost-effective catalysts while maintaining their relatively high photoactivity [17]. While research typically focuses on achieving maximum photocatalytic activity, it is equally important to develop stable photocatalysts for practical applications [23-26]. Notably, the stability of $SrTiO_3$ against pollutants with various functional groups has not been investigated to date.

In this study, unaltered $SrTiO_3$ photocatalysts were synthesized using a distinctive rapid heat treatment process at varying temperatures. The influence of this calcination technique on the characteristics of the specimens was thoroughly examined. We explored their photocatalytic efficiency in degrading phenol, chlorophenol, and oxalic acid under UV exposure and assessed their resilience against a range of compounds with different functional groups.

Experimental

This study employed a modified Pechini sol–gel method, based on the previous research by Chen et al. [27] and Lu et al. [28]. This method involved dissolving $Sr(NO_3)_2$ and citric acid in deionized water, adding titanium(IV) butoxide and ethylene glycol, and subjecting the solution to 4 hours of heating at 100 °C. The resulting amorphous product was collected and dried to obtain the xerogel. Calcination was carried out using a controlled air supply in a tube furnace, with materials labeled as "STO_RHSE_X" (strontium titanate; rapid heating, short exposure; and "X" corresponds to the different calcination temperatures).

Characterization of the catalysts involved various analytical techniques. X-ray diffraction (XRD) was used to measure crystallite sizes. Scanning electron microscopy (SEM) was used to obtain morphological insights, while nitrogen adsorption and the Brunauer–Emmett–Teller model were used to calculate specific surface areas. Optical properties were studied through diffuse reflectance (DR) spectroscopy, determining band gap energies from first-order derivative spectra. Thermal gravimetric (TG) analysis was carried out to determine the minimum calcination temperature. Fourier-transform infrared (IR) spectroscopy and X-ray photoelectron spectroscopy (XPS) were used to study the surface of the samples.

To evaluate photooxidation performance, the study used three pollutants (phenol, chlorophenol, and oxalic acid) under UV light in a temperature-controlled vessel. High-performance liquid chromatography (HPLC) quantified changes in pollutant concentrations. The study also examined the stability of RHSE samples against different functional groups by repeating XRD, IR, and SEM measurements after photocatalytic activity tests, expanding the evaluation to include propanol and glucose.

Following the characterization of material structure and the evaluation of photocatalytic activity and stability, we investigated the reusability of the STO_RHSE samples. Three consecutive phenol degradation measurements were carried out for each sample, and the reusability measurement was repeated two additional times for the best-performing samples to investigate how further the photocatalytic activity can be increased and over how many cycles.

Results and discussion

Following the synthesis, a pale yellow xerogel was obtained, and TG measurements indicated no mass loss beyond 600 °C. Consequently, calcination temperatures ranging from 600–1000 °C were used to prepare the RHSE STO samples. XRD patterns revealed characteristic reflections for $SrTiO_3$ and $SrCO_3$. The primary crystallite sizes exhibited an increase, ranging from 14.7 to 39.2 nm, with the temperature rising from 600 to 1000 °C. Simultaneously, specific surface areas decreased from 54.5 to 2.1 $m^2\ g^{-1}$. As a matter of fact, the calculated primary crystallite sizes increased in line with the calcination temperature, and specific surface areas decreased with higher temperatures. SEM micrographs revealed polycrystalline samples with various shapes and sizes, forming aggregated structures. DRS results showed that the band gap values varied only within a narrow range (3.20–3.25 eV), with slight redshifts resulting from the higher calcination temperatures.

The XPS results could not reveal the reason for the superior activity of the best-performing sample (i.e., STO_RHSE_700). However, IR spectra indicated the presence of $SrCO_3$, which was successfully related to the observed high photoactivity. Stability tests against various functional groups showed that RHSE samples were generally stable, with some changes observed after exposure to oxalic acid.

Photocatalytic activity assessments for phenol, chlorophenol, and oxalic acid indicated that our RHSE samples outperformed the commercial STO reference. RHSE STO samples displayed varying photocatalytic activity related to calcination temperature, with STO_RHSE_700 being the most efficient. The significant photocatalytic performance of STO_RHSE_700 can be rationalized by the existence of $SrCO_3$, which is recognized for its role as a co-catalyst in $SrTiO_3/SrCO_3$ configurations. $SrCO_3$ enhances the separation of charges by capturing photogenerated electrons found in the conduction band of $SrTiO_3$. This capture process diminishes recombination rates, resulting in an overall enhancement of photoactivity [26, 29].

STO_RHSE_700 and STO_RHSE_800 photocatalysts, identified as the most efficient ones, were selected to evaluate the maximum number of cycles for which their activity in phenol degradation tests continues to increase. It was observed that the photoactivity gain of the catalysts decreased after the third cycle, suggesting that the catalysts are approaching their maximum activity levels for phenol degradation under the given experimental conditions. After the third cycle, the active sites on the surface of the catalysts may have become saturated with phenol or other intermediates, which can limit their ability to further degrade phenol. Based on XRD and SEM results, the crystalline composition and morphology of STO_RHSE_700 and STO_RHSE_800 did not change even after five cycles of exposure to phenol solution.

Conclusion

The impact of RHSE treatment on STO photocatalysts was explored. As the temperature increased from 600 to 1000 °C, there was a noticeable growth in the primary crystallite sizes, spanning a range of 14.7 to 39.2 nm. At the same time, the specific surface areas experienced a decline, decreasing from 54.5 to 2.1 m^2 per gram. The morphology and band gap values remained largely unaffected, except for a slight redshift in the band gaps. The photocatalysts demonstrated high stability by retaining their crystalline composition even after exposure to compounds with various functional groups. Notably, the photocatalytic activities predominantly improved with lower calcination temperatures. The most effective sample, displaying enhanced performance against phenol, chlorophenol, and oxalic acid, was the one prepared at 700 °C calcination temperature. The superior photocatalytic activity was primarily attributed to the presence of $SrCO_3$. The photocatalysts remained stable against compounds containing phenolic –OH, alcoholic –OH, –Cl, and –CHO functional groups, although minor changes were observed in their crystalline composition following exposure to relatively concentrated oxalic acid (–COOH). Photoactivity enhancement was observed over the reusability cycles, which is most likely due to a surface-related phenomenon.

Acknowledgments

This study was financed by the NKFI-PD-138248 project. The authors are grateful for the financial support of the 2019-2.1.13-TÉT_IN-2020-00015 project. T. Gyulavári acknowledges the Bolyai János scholarship provided by the Hungarian Academy of Sciences. The research was supported by the ÚNKP-23-4-II New National Excellence Program of the Ministry for Culture and Innovation from the source of the National Research, Development and Innovation Fund. Project no. TKP2021-NVA-19 has been implemented with the support provided by the Ministry of Innovation and Technology of Hungary from the National Research, Development and Innovation Fund, financed under the TKP2021-NVA funding scheme.

References

[1] I. Atkinson, V. Parvulescu, J.P. Cusu, E. Anghel, M. Voicescu, D. Culita, S. Somacescu, C. Munteanu, M. Šćepanović, Z.J.J.o.P. Popovic, P.A. J. Photochem. Photobiol. 368 (2019) 41-51.
[2] M. Ganapathy, Y. Hsu, J. Thomas, C.T. Chang, V.J.J.o.M.S. Alagan, J. Mater. Sci. 56 (2021) 18976-18988.
[3] L.F. da Silva, O.F. Lopes, V.R. de Mendonça, K.T. Carvalho, E. Longo, C. Ribeiro, V.R.J.P. Photochem. Photobiol. Sci. 92 (2016) 371-378.
[4] Y.-X. Song, W.-Q. Ma, J.-J. Chen, J. Xu, Z.-Y. Mao, D.-J.J.R.M. Wang, Rare Met. 40 (2021) 1077-1085.
[5] A. Jia, X. Liang, Z. Su, T. Zhu, S.J.J.o.H.M. Liu, . J. Hazard. Mater. 178 (2010) 233-242.
[6] R. Asahi, T. Morikawa, T. Ohwaki, K. Aoki, Y.J.s. Taga, J. Sci. 293 (2001) 269-271.
[7] H. Irie, Y. Watanabe, K.J.T.J.o.P.C.B. Hashimoto, J. Phys. Chem. 107 (2003) 5483-5486.
[8] T. Umebayashi, T. Yamaki, S. Tanaka, K.J.C.l. Asai, V Chem. Lett. (2003) 330-331.
[9] J. Liu, G. Chen, Z. Li, Z.J.J.o.S.S.C. Zhang, J. Solid State Chem. 179 (2006) 3704-3708.
[10] H. Irie, Y. Maruyama, K.J.T.J.o.P.C.C. Hashimoto, J. Phys. Chem. C. 111 (2007) 1847-1852.
[11] I. Nakamura, N. Negishi, S. Kutsuna, T. Ihara, S. Sugihara, K.J.J.o.M.C.A.C. Takeuchi, J. Mol. Catal. A Chem. 161 (2000) 205-212.
[12] M.V. Dozzi, A. Saccomanni, M. Altomare, E.J.P. Selli, P. Sciences, Photochem. Photobiol. Sci. 12 (2013) 595-601.
[13] B. Tang, H. Chen, H. Peng, Z. Wang, W.J.N. Huang, Nanomaterials. 8 (2018) 105.
[14] G.A. Sewvandi, Z. Tao, T. Kusunose, Y. Tanaka, S. Nakanishi, Q.J.A.a.m. Feng, interfaces, ACS Appl. Mater. Interfaces. 6 (2014) 5818-5826.
[15] S. Gholamrezaei, M. Salavati Niasari, M. Dadkhah, B.J.J.o.M.S.M.i.E. Sarkhosh, J. Mater. Sci. Mater. Electron. 27 (2016) 118-125.
[16] K. Kiran, B. Ashwath Narayana, S.J.S.S.T. Lokesh, Solid State Technol. 63 (2020) 1913-1920.
[17] Z. Pap, É. Karácsonyi, Z. Cegléd, A. Dombi, V. Danciu, I. Popescu, L. Baia, A. Oszkó, K.J.A.C.B.E. Mogyorósi, Appl. Catal. B Environ. 111 (2012) 595-604.
[18] Y. Wu, M. Li, J. Yuan, X.J.J.o.M.S.M.i.E. Wang, J. Mater. Sci. 28 (2017) 10406-10410.
[19] W. Wattanathana, W. Nantharak, S. Wannapaiboon, P. Jantaratana, C. Veranitisagul, N. Koonsaeng, A.J.J.o.M.S.M.i.E. Laobuthee, J. Mater. Sci. Mater. Electron. 29 (2018) 1542-1553.
[20] S. Fuentes, R. Zarate, E. Chavez, P. Munoz, D. Díaz-Droguett, P.J.J.o.m.s. Leyton, J. Mater. Sci. 45 (2010) 1448-1452.
[21] G. Veréb, T. Gyulavári, Z. Pap, L. Baia, K. Mogyorósi, A. Dombi, K.J.R.A. Hernádi, RSC Adv. 5 (2015) 66636-66643.
[22] Z. Pap, V. Danciu, Z. Cegléd, Á. Kukovecz, A. Oszkó, A. Dombi, K.J.A.C.B.E. Mogyorósi, Appl. Catal. B Environ. 101 (2011) 461-470.
[23] K. Mogyorósi, E. Karácsonyi, Z. Cegléd, A. Dombi, V. Danciu, L. Baia, Z.J.J.o.s.-g.s. Pap, J. Sol-Gel Sci. Technol. 65 (2013) 277-282.
[24] T. Gyulavári, G. Veréb, Z. Pap, A. Dombi, K.J.C.T. Hernádi, Catal. Today. 313 (2018) 231-238.

[25] Z.-R. Tóth, S.K. Maity, T. Gyulavári, E. Bárdos, L. Baia, G. Kovács, S. Garg, Z. Pap, K.J.C. Hernadi, Catalysts. 11 (2021) 379.
[26] S. Jin, G. Dong, J. Luo, F. Ma, C.J.A.C.B.E. Wang, Appl. Catal. B Environ. 227 (2018) 24-34.
[27] L. Chen, S. Zhang, L. Wang, D. Xue, S.J.J.o.c.g. Yin, J. Cryst. Growth. 311 (2009) 746-748.
[28] X. Lu, T.S. Pine, D.R. Mumm, J.J.S.S.I. Brouwer, Solid State Ion. 178 (2007) 1195-1199.
[29] B. Boga, N. Steinfeldt, N.G. Moustakas, T. Peppel, H. Lund, J. Rabeah, Z. Pap, V.-M. Cristea, J.J.C. Catalysts. 12 (2022) 978.

LIFE CYCLE ASSESSMENT OF PRODUCTS BASED ON ENVIRONMENTAL PRODUCT DECLARATIONS DATA

Boris Agarski[1], Nikola Maoduš[2], Dejan Ubavin[2], Slađana Jovanović[1], Aleksandar Milošević[1], Milana Ilić Mićunović[1], Đorđe Vukelić[1]

[1]Department of Production Engineering, Faculty of Technical Sciences, University of Novi Sad, 21000 Novi Sad, Trg Dositeja Obradovića 6, Serbia
[2]Department of Environmental Engineering and Occupational Safety and Health, Faculty of Technical Sciences, University of Novi Sad, 21000 Novi Sad, Trg Dositeja Obradovića 6, Serbia
e-mail: agarski@uns.ac.rs

Abstract

Life cycle assessment is a standardised method for assessment of products and processes that consists of the following phases: goal and scope definition, inventory analysis, life cycle impact assessment and interpretation of results. Within the second and third life cycle assessment phases it is necessary to obtain complex data about the material and energy flows and the calculations of various environmental impacts. For this task, the use of life cycle inventory databases is recommended in order to tackle the background processes which are difficult to model manually and time consuming. On the other side, environmental product declarations are standardised type III environmental labels based on life cycle assessment that provide a detailed information on products impact on the environment through its life cycle stages. The information from environmental product declarations can be used as an alternative source of data to build the life cycle inventory and to obtain the corresponding impacts on the environment for several impact categories. In this research, the environmental product declaration data is used to perform the life cycle assessment of building constructions, namely three types of wall constructions. While three types of wall constructions were already analysed with common life cycle assessment approach in previous research [1], this research has alternative approach that uses the environmental product declaration data. The data for the life cycle assessment was built from various environmental product declaration owners in order to cover several construction materials such as: bricks, aerated concrete blocks, expanded polystyrene board, gyps boards, mineral wool, mortar, oriented strand board, wooden frame, polyvinyl chloride foil, and decorative finish render. The results show the differences, advantages and disadvantages between the common and alternative approaches in data gathering for life cycle assessment. Finally, it can be concluded that performing life cycle assessment based on environmental product declaration is a feasible approach that can be used in situations where the life cycle inventory databases are unavailable.

Key words: environmental product declarations, life cycle assessment, construction materials

References

[1] N. Maoduš, B. Agarski, T. Kočetov Mišulić, I. Budak, M. Radeka Life cycle and energy performance assessment of three wall types in south-eastern Europe region, Energy and Buildings, (2016), pp. 605-614.

SURFACTANT-FREE SYNTHESIS OF ZnO/Bi_2WO_6 FLOWERLIKE WITH UV-LIGHT-INDUCED PHOTOCATALYTIC ACTIVITY

Aicha Elaouni,[1,2] **Gergő Ballai,**[2] **Ákos Szamosvölgyi,**[2] **Zoltán Kovács,**[2] **Zsolt Pap,**[2] **Henrik Haspel,**[3,4] **Zoltán Kónya,**[2,3,4] **Hassan Ait Ahsaine,**[1] **Mohamed Saadi**[1]

[1]*Mohammed V University in Rabat - Faculty of Science, Centre des Sciences des Matériaux, Laboratoire de Chimie Appliquée des Matériaux, Rabat, Morocco.*
[2]*University of Szeged - Faculty of Science and Informatics, Department of Applied and Environmental Chemistry, Szeged, Hungary*
[3]*ELKH-SZTE Reaction Kinetics and Surface Chemistry Research Group, University of Szeged, Szeged, Hungary*
[4]*Centre of Excellence for Interdisciplinary Research, University of Szeged, Szeged, Hungary*
e-mail: aicha.elaouni@um5r.ac.ma

Abstract

I hereby present the recent experimental findings and the key concepts of our laboratory's research on photocatalytic degradation. Bi_2WO_6 with a flower-like structure was successfully synthesized by two different surfactants e.i. hexadecyltrimethylammonium bromide (CTAB) and polyvinylpyrrolidone (PVP), via hydrothermal method to control various properties of the resulting material (particle size, morphology, crystallinity, surface area, band gap, etc.). Subsequently, our investigation focused on the creation of a ZnO/Bi_2WO_6 heterojunction photocatalyst designed for efficient photodegradation of pollutants. To analyze the material's characteristics, we employed techniques including X-ray diffraction (XRD), scanning electron microscopy (SEM), transmission electron microscopy (TEM), X-ray photoelectron spectroscopy (XPS), and diffuse reflectance UV-vis spectroscopy (UV-DRS). However, the ZnO/Bi_2WO_6 heterojunction exhibited tunable properties and demonstrated highly efficient phenol degradation with a remarkable degradation rate compared to the as-synthesized Bi_2WO_6.

RANKING OF THE SUSTAINABLE DEVELOPMENT GOALS BY BUSINESS STUDENTS

László Berényi[1]

[1]Institute of Management Science, University of Miskolc, H-3515 Miskolc-Egyetemváros, Hungary
e-mail: laszlo.berenyi@uni-miskolc.hu

Abstract

Research on the social aspects of sustainability problems uses a quite limited toolset. Q-methodology can be suggested as an additional survey method to explore definitive opinions in the field. The paper shows a methodological experiment by ranking the importance of the 17 Sustainable Development Goals. The case study is presented based on 20 responses from business students. The case shows the applicability of the Q-methodology for exploring opinion patterns. The results suggest that the majority of the respondents keep planet-related goals as the most important ones.

Introduction

Sustainability is a complex phenomenon derived from the increasingly urgent need to solve environmental problems [1]. Since social aspects must be considered, and even society can be marked as the source of the problem, the competing interests became challenging to overview. Excellent examples are the endeavors of the United Nations' conferences [2], where numerous principles and action plans were elaborated to cover the different needs of stakeholders and territories. Each case, action, or strategy can be assessed from various viewpoints; I believe there is no ultimate way. At the same time, the expanding knowledge base in the field provides background to make satisfactory decisions. Any contribution to this knowledge base is valuable, including local and general investigations, as well as engineering, social, managerial, and other results. The paper shows a methodological experiment using the Q-methodology [3] to explore sustainability issues. A pilot sample was selected from business and management students at one university to present the opportunities of the method. The results focus on the pattern of the majority opinion.

The objective of the study is the 17 Sustainable Development Goals (SDGs) by the United Nations [4] [5]. The goals and the 5 pillars model (people, planet, prosperity, peace, partnership) suggest building a comprehensive, transparent, and easy-to-use framework for strategy making and evaluation. Still, the number of goals, especially the related 169 targets, is spreading. The research question is how to define the importance of the SDGs.

Several methods can be used for the evaluation, but each has some limitations:

- Scale evaluation methods like the Likert scale or else [6] must consider distortions due to social expectations and usually lead to a left-skewed distribution of the responses, and the results can be meaningless. However, statistical tools are widely available, and great charts can be drawn, but the practical usability of the results is limited. Moreover, the relative importance often remains hidden.
- A direct ranking seems purposeful, but an increasing number of survey items makes the evaluation extremely difficult.
- Pairwise comparison methods can fix some problems mentioned above, but the related survey is long, collecting responses is time-consuming, and the ratio of responses with a clear preference order may be limited. Guilford's method [7] based on pairwise

comparison is not outdated, especially among experts, but the technique does not allow comparison between samples, which limits the generalization of the results.

An old, but nowadays again popular approach is the Q-methodology, which helps to rank a large number of statements and explore typical patterns of opinions. It was developed by a physicist and psychologist, William Stephenson, in the 1930s [3]. Qualitative and quantitative aspects are combined, and the design of the method considers the limitations of human thinking. The respondents express their views by sorting a set of statements from most agree to most disagree, and patterns of beliefs can be drawn. Beyond understanding individual attitudes, it can be used to explore group-level opinion patterns. The Q-methodology is based on the correlation matrix and groups the respondents [8].

The data collection method makes the relative opinion of a respondent about every statement concerning all other statements explicit, presenting a holistic order with integrated trade-offs [9]. Data recording can be managed manually by pre-printed cards of the statements and a blank pattern for organizing them, or software solutions can automate it. The steps of analysis can be summarized as follows based on the literature:

- preparing the initial data matrix of the evaluations,
- calculating correlations,
- selecting the number of factors based on the eigenvalues and the scree plot,
- calculating rotated factors loadings,
- determining factor weights and scores,
- analysis of distinguishing statements,
- presenting patterns of opinions by the final factors.

Experimental

The respondents were asked to organize the SDGs by the question, which is held more or less important compared to the others. The survey for the evaluation used a ready-made Q-sample, including a description of the goals. Normal distribution of the evaluations is assured by the forced sort pattern for the participants [10].

The results in this paper are based on a voluntary online questionnaire following the structure of Easy-htmlq version 2.0.3, and data processing was performed with the free Ken-Q Analysis Desktop Edition (KADE) software. A sample of 20 business and administration students was randomly selected from the database collected in the 2022/2023 academic year.

The factors were defined by principal component analysis with Varimax rotation for maximizing the sum of the variances of the squared correlations between variables and factors.

Results and discussion

The factor analysis shows 7 acceptable factors. The scree plot of the analysis suggests using 2 or 3 of them (Figure 1).

According to the 3-factor solution, the reliability of the questionnaire is good, the percentage of explained variance is 61%, and the correlation between the factors is low, meaning that different opinions are represented in them (Table 1). 18 of 20 respondents have a significant contribution to the patterns.

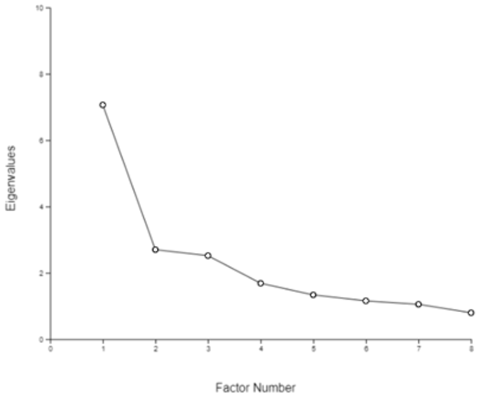

Figure 1. Scree plot of the analysis (KADE output)

Table 1. Factor characteristics (KADE output)

	Factor 1	**Factor 2**	**Factor 3**
No. of Defining Variables	9	4	5
Avg. Rel. Coef.	0.8	0.8	0.8
Composite Reliability	0.973	0.941	0.952
S.E. of Factor Z-scores	0.164	0.243	0.219
		Correlations	
Factor 1	-	0.1717	0.2499
Factor 2	0.1717	-	0.1055
Factor 3	0.2499	0.1055	-

Factor scores and ranking are summarized in Table 2. The dataset presents the weight score and the rank order of the items by factors, ordered by the level of consensus. The first row shows the item with the highest agreement among the respondents, regardless of its position in the ranking. 'Quality education', 'Peace, justice and strong institutions', and 'Clean water and sanitation' were marked as significant consensus statements.

Table 2. Z-scores and ranking orders by factors (based on KADE output)

Statement	**5P**	**Factor 1 Z-score (rank)**	**Factor 2 Z-score (rank)**	**Factor 3 Z-score (rank)**
Quality education	People	0.08 (9)	-0.14 (10)	-0.25 (10)
Peace, justice and strong institutions	Peace	-0.79 (14)	-0.06 (8)	-0.29 (11)
Clean water and sanitation	Planet	1.35 (2)	0.59 (6)	0.93 (4)
Decent work and economic growth	Prosperity	-0.21 (12)	-0.56 (12)	0.26 (8)
Partnership for the global	Partnership	-1.33 (15)	-0.42 (11)	-0.94 (15)
Climate action	Planet	1.97 (1)	1.04 (4)	1.26 (3)
Responsible consumption and production	Planet	0.46 (6)	0.56 (7)	-0.48 (12)
Life on land	Planet	0.8 (4)	-0.09 (9)	-0.67 (13)
Life below water	Planet	0.38 (7)	-1.01 (16)	0.63 (6)
Zero hunger	People	-0.1106 (10)	1.46 (1)	1.37 (2)

Statement	5P	Factor 1 Z-score (rank)	Factor 2 Z-score (rank)	Factor 3 Z-score (rank)
Industry, innovation and infrastructure	Prosperity	-0.2 (11)	-0.96 (14)	-2.07 (17)
No poverty	People	-0.61 (13)	1.4 (2)	0.41 (7)
Affordable and clean energy	Prosperity	0.13 (8)	-1.94 (17)	-0.03 (9)
Good health and well-being	People	0.57 (5)	-0.95 (13)	1.38 (1)
Gender equality	People	-1.84 (17)	-0.98 (15)	0.7 (5)
Reduced inequalities	Prosperity	-1.42 (16)	1.07 (3)	-0.79 (14)
Sustainable cities and communities	Prosperity	0.83 (3)	0.98 (5)	-1.42 (16)

The majority opinion factor includes 9 respondents. In their view (Figure 2), ‘Climate action’, ‘No Poverty’, and ‘Reduced inequalities’ are considered the most important SDGs, while ‘Affordable Energy’, ‘Gender equality’, and ‘Life below water’ are at the bottom of the relative ranking.

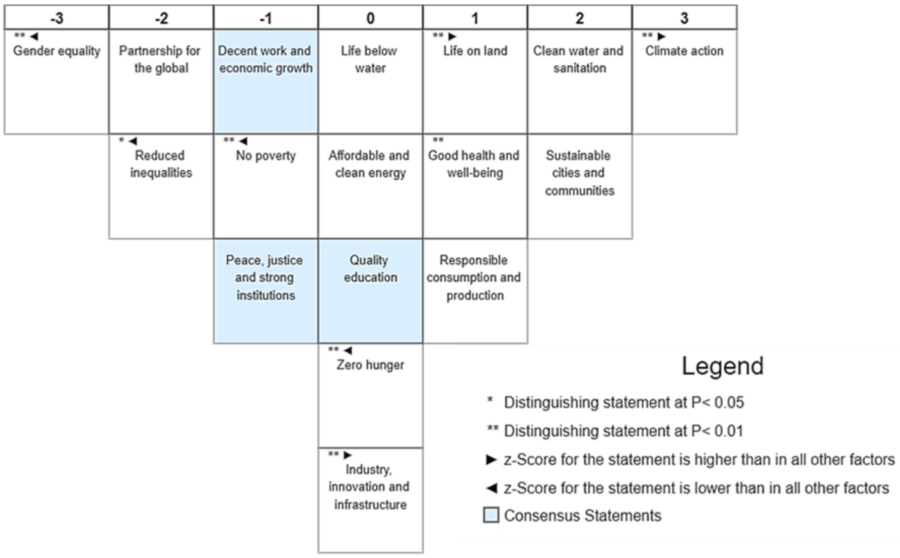

-3	-2	-1	0	1	2	3
** ◄ Gender equality	Partnership for the global	Decent work and economic growth	Life below water	** ► Life on land	Clean water and sanitation	** ► Climate action
	* ◄ Reduced inequalities	** ◄ No poverty	Affordable and clean energy	** Good health and well-being	Sustainable cities and communities	
		Peace, justice and strong institutions	Quality education	Responsible consumption and production		
			** ◄ Zero hunger			
			** ► Industry, innovation and infrastructure			

Figure 2. The q-sort pattern of the majority opinion factor

Translation of the results of the majority opinion pattern to the 5Ps is shown in Figure 3. The results suggest an emphasis on traditional environmental issues while people and prosperity show a scattered picture. Partnership and the need for peace are at the bottom of the list. It is to be noted that the ‘less important’ ranking does not mean the objection of the goal; it is just a relative order. Probably, a Likert-scale evaluation could show slight differences from other items. Factor 2 and Factor 3 give more emphasis to people-related issues than the majority opinion. However, partnership and peace are not among the highest positions in any case.

Learning the opinions of the respondents by Q-sort ranking valuable information can be gained about the shared values. From the viewpoint of management and leadership studies, the under-evaluation of partnership asks for further research since the discipline strongly emphasizes the role of collaboration.

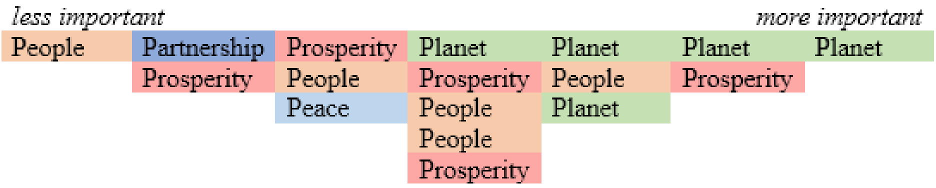

less important						more important
People	Partnership	Prosperity	Planet	Planet	Planet	Planet
	Prosperity	People	Prosperity	People	Prosperity	
		Peace	People	Planet		
			People			
			Prosperity			

Figure 3: Q-sort pattern by the 5Ps

Conclusion

The results show that the majority opinion still keeps environmental (‘Planet’) issues as the most important ingredient of sustainability. At the same time, the limited sample selection does not allow this to be generally stated. The study aimed to show the methodological opportunities of the Q-sort ranking. This method provides an easy way to explore the preferences about an objective, in this case, the SDGs. Although several barriers to statistical analysis can be managed, this method also has serious limitations in presenting the results. I can suggest the application as a preparatory research element that allows further investigations with targeted questions. A practical implication of the study is that knowing the orientation of the respondent’s thinking, especially the majority opinion, the strategic actions can be purposeful, highlighting the preferred values. The interrelations between the SDGs are obvious, and the same target may be available in different ways. A higher level of acceptance can be expected using common values in formulating the actions.

Acknowledgments

The study is related to the OTKA K139225 “Management Readiness Level towards Strategic Technology Management Excellence” project.

References

[1] Hajian, M., Kashani, S.J. Evolution of the Concept of Sustainability. From Brundtland Report to Sustainable Development Goals. Sustainable Resource Management Modern Approaches and Contexts, 2021, 1-24.
[2] Schecter, M.G. United Nations Global Conferences, Routledge, 2005.
[3] Stephenson W. Correlating Persons Instead of Tests. Character and Personality. 4 (1935) 17-24. https://doi.org/10.1111/j.1467-6494.1935.tb02022.x
[4] United Nations. Transforming Our World: The 2030 Agenda for Sustainable Development; United Nations: New York, USA, 2015. A/RES/70/1
[5] Teaching Guide and Resources: Sustainable Development Goals. Available online: https://www.un.org/en/sustainable-development-goals (accessed on 10 11 2022).
[6] Babbie, E. The Practice of Social Research, 15th ed. Cengage, 2020.
[7] Guilford, J.P. The Method of Paired Comparisons as a Psychometric Method. Psychological Review 35 (1928) 494-506.
[8] Watts, S., Stenner, P. Doing Q Methodological Research: Theory, Method & Interpretation; SAGE Publications, 2012.
[9] Zabala, A. Pascual, U. Bootstrapping Q Methodology to Improve the Understanding of Human Perspectives. PloS ONE 11 (2016) e0148087.
[10] Stephenson, W. The Study of Behavior: Q-technique and its Methodology. University of Chicago Press, 1953.

INHIBITION OF MAGNESIUM IONS INDUCED PRECIPITATION FROM SODIUM DODECYL BENZENESULPHONATE−POLYMER MIXTURES BY APPLYING SODIUM CITRATE

Csaba Bús[1], Cora Deák[2], Pál Sipos[1]

[1]Department of Molecular and Analytical Chemistry, University of Szeged, H-6720 Szeged, Dóm tér 7-8, Hungary
[2] Department of Applied and Environmental Chemistry, Rerrich Béla square 1, 6720, Szeged, Hungary
e-mail: bus.csaba@szte.hu

Abstract

Among different type of surfactants, anionic surfactants are generally applied compounds to reduce interfacial tension (IFT) in various fields of industry. Polymeric solutions often possess high viscosity, these materials are commonly used for viscosity control [1]. Presence of divalent metal ions, especially alkaline earth cations in brine water is an important factor during different processes, because these cations considerably affect on both surfactant and polymer solutions. By binding to the surfactant's anionic head group, these cations may cause precipitation from surfactant solutions. Divalent cations are able to interact also with the polymer chains, decreasing the polymer's viscosity, enhancing the negative charge of the polymer chains; these phenomena may cause precipitation also in polymeric solutions [2, 3]. The present study is concerned with the experimental description of the interactions between magnesium ions and sodium dodecyl benzenesulfonate (SDBS)−Flopaam AN125SH mixtures and the complexation of magnesium with sodium citrate. The mixtures contained the polymer in 1.0 g/L concentration and the surfactant in 5.0 g/L concentration. The solvent's magnesium ion content was increased between 0.03−1.5 g/L, and sodium citrate was added to the magnesium ion containing samples in 2.0 and 3.0 molar equivalent relative to the magnesium ion concentration. The samples were characterized by using turbidimetry and rheology measurements (determining consistency index, yield stress, flow number and zero shear viscosity). The infrared spectra of the solid precipitates were also recorded.

The results indicated that sodium citrate is an effective agent to inhibit the magnesium ions caused precipitation up to 1.2 g/L metal ion concentration. Addition of sodium citrate considerably decreased the viscosity of the samples (the consistency index of the SDBS−polymer mixtures decreased from 47.5 mPas to 7.53 mPas), moreover, addition of magnesium ions even in high amounts did not cause the precipitation of the polymer. Nevertheless, the presence of sodium citrate decreased the polymer's viscosity, but according to the rheological parameters all samples were described to possess pseudoplastic flow behavior.

References

[1] Kortemeier, U., Venzmer, J., Howe, A., Grüning, B., Herrwerth, S. Thickening agents for surfactant systems. *SOFW* **2010**, *136*, 30–36.

[2] Ádám, A.A., Ziegenheim, Sz., Janovák, L., Szabados, M., Bús, C., Kukovecz, Á., Kónya, Z., Dékány, I., Sipos, P., Kutus, B. Binding of Ca^{2+} Ions to Alkylbenzene Sulfonates: Micelle Formation, Second Critical Concentration and Precipitation. *Materials* **2023**, *16*, 494.

[3] Sabhapondit, A., Borthakur, A., Haque, I. et al. Characterization of acrylamide polymers for enhanced oil recovery. *J. Appl. Polym. Sci* **2003**, *87*, 1869−1878.

STUDIES ON PHOTOCATALYTIC ACTIVITY OF ONE DIMENSIONAL COORDINATION POLYMERS BASED ON SCHIFF BASE LIGAND

Ildiko Mariana Bută, Maria Andreea Nıstor, Simona Gabriela Muntean

Romanian Academy "Coriolan Dragulescu" Institute of Chemistry, 24 Mihai Viteazu Bvd.,
300223-Timisoara, Romania
e-mail: ildiko_buta@acad-icht.tm.edu.ro

In recent decades, design and synthesis of new materials with photocatalytic properties draw attention in scientific research. Water pollution caused by the presence of non-biodegradable dyes, widely used in the textile and paper industry, has expanded with the increase of industrialization and population [1].

Here, we report the investigation of photocatalytic properties of cadmium(II) and copper(II) coordination polymers: $^{1}_{\infty}[Cd_3L(CH_3COO)_4]\cdot H_2O$ (**CP1**), $^{1}_{\infty}[Cd_2L(NO_3)_2]\cdot CHCl_3$ (**CP2**) $^{1}_{\infty}[Cd_5L_2(CH_3COO)_6]$ (**CP3**), $^{1}_{\infty}[Cu_3L_2(NO_3)](NO_3)\cdot 2MeOH\cdot 2H_2O$ (**CP4**), $^{1}_{\infty}[Cu_3L_2(N_3)](CH_3COO)$ (**CP5**) and $^{1}_{\infty}[Cu_3L_2(H_2O)](ClO_4)_2$ (**6**) based on the Schiff base H_2L (N,N'-bis[(2-hydroxybenzilideneamino)propyl]piperazine) [2] for degradation of industrial dyes. Congo Red (CR), Acid Orange 7 (AO7), Methyl Orange (MO), and Direct Green 6 (DG6) dyes were selected as potential colored pollutants. Photocatalytic experiments were carried out under visible irradiation at 546 nm, and room temperature using 1 g/L compound (**CP1** ÷ **CP6**).

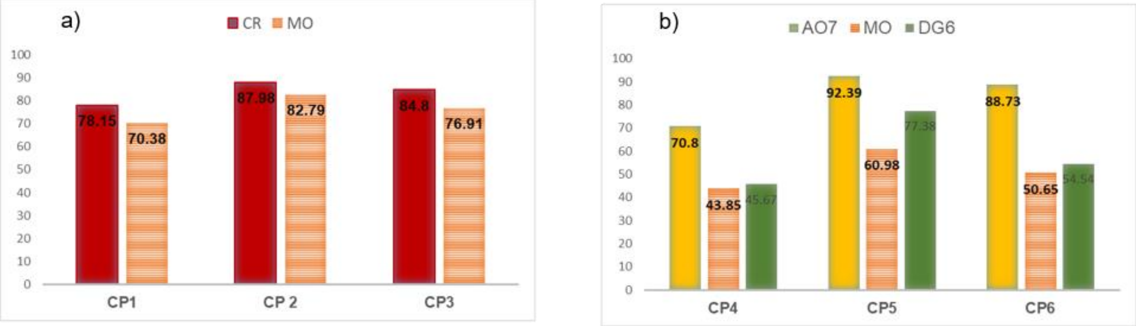

Figure 1. Degradation efficiency of investigated dyes using (a) **Cd^{II}-CP** and (b) **Cu^{II}-CP**

Under irradiation with visible light, catalytic efficiency for the degradation of investigated dyes increased in order: **CP1** < **CP3** < **CP2** using **Cd^{II}-CP** and **CP4** < **CP6** < **CP5** for **Cu^{II}-CP**. The highest photocatalytic activities were obtained using **CP2**: 87.98% for CR, and 82.79% for MO, and **CP5**: 92.39% for AO7, 40.98% for MO, and 77.38% for DG6.

The kinetic of dyes photodegradation was investigated using the Langmuir-Hinshelwood model and the obtained results showed that the degradation process followed a pseudo-first-order kinetic.

Acknowledgements

This work was supported by Project 4.1.3 and Project 2.2 of the "Coriolan Drăgulescu" Institute of Chemistry.

References

[1] M. A Hassaan, A. El Nemr, AJESE 1 (2017) 64-67.

[2]. (a) I. Buta, A. Ardelean, L. Peter, G. Novitchi, E. Hey-Hawkins, M. Andruh, O. Costisor Polyhedron 190 (2020) 114766; (b) I. Buta, M. A. Nistor, P. Lönnecke, E. Hey-Hawkins, S. G. Muntean, O. Costisor J. Photochem. Photobiol. A 404 (2021) 112961.

THE ROLE OF REACTIVE SPECIES IN THE TRANSFORMATION OF TRIMETHOPRIM DURING THE UV-LED/CHLORINE PROCESS

Luca Farkas, **Teodóra Dragic, Tünde Alapi**

Department of Molecular and Analytical Chemistry, University of Szeged, H-6720 Szeged,
Dóm tér 7-8, Hungary
e-mail: fluca@chem.u-szeged.hu

The WHO defined safe drinking water as "water that does not represent any significant risk to health over a lifetime of consumption, including different sensitivities that may occur between life stages”. The production of adequate quality drinking water is a universal problem today, partly due to the biologically active and persistent organic pollutants that cannot be removed by conventional water treatment processes. Among pharmaceuticals, antibiotics have a high ecological, and health risk, because of the development of antibiotic-resistant bacterial strains. Over 30,000 deaths are caused annually by the infections of these strains of bacteria. Consequently, the elimination of antibiotics requires additional or quaternary water treatment processes, such as UV/chlorine method.

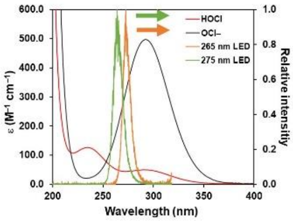

Fig.1: Molar absorbance of HOCl and OCl$^-$ and LEDs emission spectra

For the UV/FAC (FAC: freely available chlorine, i.e. the sum of HOCl and OCl$^-$) process, considering the UV-Vis absorption spectrum of HOCl and OCl$^-$, the LEDs emitting at 265 and 275 nm are a good alternative to traditional low-pressure mercury vapor lamps emitting 254 nm photons. In this study, two types of LEDs (with emission maxima at 265 nm and 275 nm) were used for the photolysis of HOCl/OCl$^-$ solutions. The ratio of protonated and deprotonated forms (pK_a = 7.4) determines the absorption properties of the treated solution and the steady-state concentration of the formed radicals, such as $^\bullet$OH, Cl$^\bullet$, $Cl_2^{\bullet -}$ and ClO$^\bullet$.

The UV photolysis of HOCl and OCl$^-$, the role of the various reactive species in trimethoprim (a widely used antibiotic) transformation were studied under different conditions. The quantum yield of the HOCl photolysis was determined and found to be 0.74 and 0.94 at 265 and 275 nm, respectively. These values for OCl$^-$ photolysis were 0.64 and 0.58. HOCl reacts fast with trimethoprim, while there is no reaction with OCl$^-$. Thus, the pH affects strongly the relative contribution of radical-initiated reactions to the trimethoprim transformation. The trimethoprim reacts fast with $^\bullet$OH and Cl-containing radicals (Cl$^\bullet$, ClO$^\bullet$, $Cl_2^{\bullet -}$) so the transformation rate increased with increasing oxidant concentration, even at high pH. The contribution of $^\bullet$OH-based reaction depends on pH; at acidic and neutral pH the $^\bullet$OH originated from the HOCl photolysis and has a significant role ($[^\bullet OH]_{ss} \approx 4.5\times10^{-13}$ M), while at basic pH the importance of $^\bullet$OH is moderated ($[^\bullet OH]_{ss} \approx 3.2\times10^{-14}$ M), mainly chlorine-containing radicals (Cl$^\bullet$, ClO$^\bullet$, $ClO_2^\bullet$) are formed and responsible for the transformation.

Special attention was paid to the chlorinated products and matrix effect, using biologically treated wastewater as a matrix. The transformation rate of trimethoprim was only slightly affected by this matrix, while the formation of chlorinated compounds was suppressed, due to the reaction of Cl$^\bullet$ and HCO_3^-.

Acknowledgements

This work was sponsored by the National Research, Development and Innovation Office-NKFI Fund OTKA, project number FK132742. Luca Farkas thanks for the financial support (ÚNKP-23-4-SZTE-551) from the New National Excellence Program of the Ministry for Culture and Innovation from the source of the National Research, Development and Innovation Fund.

MULTICOMPONENT SYSTEM BASED ALKANOLAMINE-SUBSTITUTED BENZOIC ACID FOR CORROSION INHIBITION OF IRON IN SALINE MEDIUM

Daniela Haidu, Nicoleta Plesu, Manuela Crisan

"Coriolan Dragulescu" Institute of Chemistry, 300223 Timisoara, Romania
e-mail: danielahaidu1@gmail.com

Abstract

In the past few decades, there has been significant interest from both academia and industry in multicomponent organic crystals constructed from acid-base complexes [1]. Organic salts have been the subject of much research in fields such as corrosion control, medicines, agrochemicals, energetic materials, and protonic conductors. Most well-known organic inhibitors have heteroatoms with polar functional groups, benzene rings, or lone pair electrons (N, O, or S), that act as active sites for adsorption on metal surfaces [2]. According to developments in this field, the inhibitor's structural feature, the corrosive medium's characteristics, and the metal surface's characteristics affect how well corrosion is inhibited.

The present study focuses on the obtaining, structural analysis, and investigation of the anti-corrosive properties of ethylethanolammonium 4-nitrobenzoate (EEA4NB) for iron in 3% NaCl solution, taking into account the trend in the last period towards the development of environmentally friendly corrosion inhibitors [3, 4]. The benzene ring connected to the carboxylate group (COO-) enhances the inhibitor's efficacy and is a crucial functional component that causes adsorption on the metal surface. Additionally, alkanolamines, which combine the chemical and physical properties of amines and alcohols in a single molecule, can form strong and directed hydrogen bonds with benzoic acids [5]. Despite the fact that alkanolamines and substituted benzoic acids are environmentally benign, there aren't many investigations on their application as metallic corrosion inhibitors in $HClO_4$ and chloride solutions in the literature [3, 6]. In this study, a novel environmentally friendly corrosive inhibitor (EEA4NB) was synthesized, purified and structurally characterized by single crystal X-ray diffraction analysis and Fourier transform infrared spectroscopy (FT-IR). All structural data revealed the formation of organic salt with proton transfer from 4-nitrobenzoic acid to nitrogen atom of alkanolamine molecule. Electrochemical assays were used to investigate the inhibitory effect of EEA4NB on iron corrosion in NaCl solution. The values of current density (Jcorr) demonstrate that the EEA4NB layer generated has the ability to inhibit and block the iron surface corrosion sites. The inhibition efficiency (IE), which is calculated from the Jcorr value, exhibits a high percentage of iron surface inhibition above 92% for all concentrations of EEA4NB in solution. At 5 mM, the maximum concentration of EEA4NB, this effect increased to 99.9%. The corrosion resistance (Rcorr) for iron in solution containing 5 mM EEA4NB is 60 times lower than the Rcorr for iron in saline solution alone. The ZEISS STEMI 508 microscope's images show that EEA4NB adsorption has formed a protective coating on the electrode's surface. The image taken on the iron surface at the border between the corroded and exposed areas to saline solution containing 5 mM EEA4NB saline solution is shown in Figure 1.

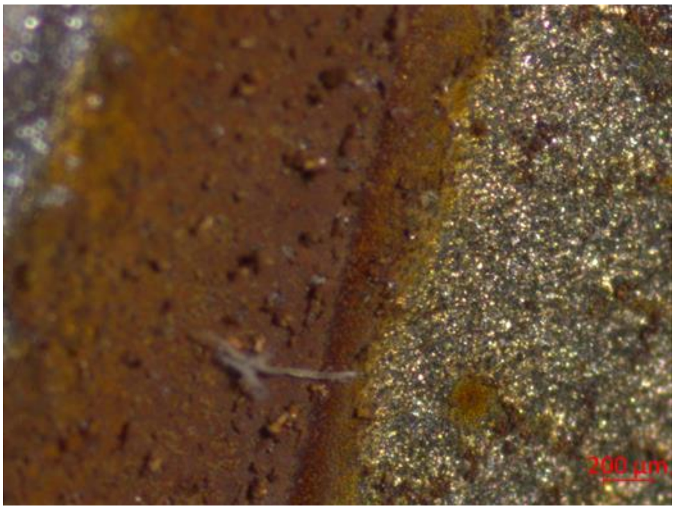

Figure 1. Optical microscope image for surface image with the boundary between exposed area of surface cover with a film formed during exposure to 5 mM EEA4NB and exposed only to saline attack

The results demonstrate the formation of a stable organic layer on the iron surface with anticorrosive properties in the presence of 5 mM EEA4NB [7].

Acknowledgments

The authors are grateful to the “Coriolan Dragulescu” Institute of Chemistry for research support.

References

[1] M. Crisan, P. Bouros, Y. Chumakov, M. Petric and G. Ilia, Cryst. Growth Des. 13 (2013), 143.

[2] K.F. Khaled, Appl. Surf. Sci. 256 (2010) 6753.

[3] C. Li, L. Li, C. Wang. Electrochim. Acta. 115 (2014) 531.

[4] Z. Sibel. Turk. J. Chem. 26 (2002) 403.

[5] A.B.E. Rani, B.B.J. Basu. Int. J. Corros. 2012 (2012) Article ID 380217.

[6] B. Elsener, M. Büchler and H. Böhni, Organic Corrosion Inhibitors for Steel in Concrete, Corrosion of Reinforcement in Concrete: Corrosion Mechanisms and Corrosion Protection, EFC Publication No. 31, The Institute of Materials, London, 2000, pp. 61.

[7] Y. Tong, J. Ye, Q. Wang, H. Zhang, H. Yu & A.-O. Seibou, J. Asian Archit. Build. Eng. 22:2 (2022) 415.

[8] M. Crisan, G. Vlase, N. Plesu, M. Petric, L. Croitor, V. Kravtsov, Y. Chumakov, P. Bourosh and T. Vlase, J. Therm. Anal. Calorim. 134 (2018), 343.

UNLOCKING THE POTENTIAL OF IRON-LOADED ZnO FOR ENHANCED CO_2 CONVERSION A COMPARATIVE INVESTIGATION USING HYDROTHERMAL AND WET IMPREGNATION METHODS

Haythem Basheer, Mohit Yadav, János Kiss, András Sápi*, Zoltán Kónya

Department of Applied and Environmental Chemistry, Interdisciplinary Excellence Centre,
University of Szeged, H-6720, Rerrich Bela ter 1, Szeged, Hungary
e-mail: haythemsuliman@gmail.com

Abstract

In the present work, iron-doped zinc oxide nanocomposites (ZnO-FeOx) were synthesized by two different routes i.e. hydrothermal and wet impregnation for the photocatalytic CO_2 reduction under both visible-light irradiation (VLI) and UV-light irradiation (UVI). The results indicated that the ZnO-FeOx samples exhibited defects as a result of doping in the hydrothermal method, while heterosystem was observed in the case of wet impregnation route. The wet impregnation nanocomposites showed remarkable results and produced CO with a yield of **2.418** µmol/gcat (VLI) and **1.725** µmol/gcat under (UVI). In contrast, the hydrothermal method yielded **0.477** µmol/gcat and **0.36** µmol/gcat of CO under (UVI) and (VLI). These outcomes represent approximately tenfold (wet impregnation) and sevenfold (hydrothermal) improvements compared to bare ZnO. Various factors were thoroughly examined which contributed to the enhanced performances of (ZnO-FeOx) as compared to pristine ZnO. Theoretical investigations using density functional theory (DFT) unveiled the presence of novel impurity energy states in ZnO caued by iron. Furthermore, diffuse reflectance infrared fourier transform spectroscopy (DRIFTS) identified the critical intermediates. Additionally, the study elucidated a charge transfer mechanism involved in photocatalytic CO_2 reduction.

Keywords: *Photocatalysis, CO_2 reduction, RWGS, UV/Visible light irradiation*

Pt NANOPARTICLES ON INERT H-BN SUPPORT: INVESTIGATION OF THE CO_2 HYDROGENATION REACTION

Tímea Hegedűs[1], **Imre Szenti**[1], **Anastasiia Efremova**[1], **Ákos Szamosvölgyi**[1], **Kornélia Baán**[1], **János Kiss**[1,2], **Kónya Zoltán**[1,2]

[1] *Interdisciplinary Excellence Centre, Department of Applied and Environmental Chemistry, University of Szeged, Rerrich Béla tér 1, H-6720 Szeged, Hungary*
[2] *HUN-REN-SZTE Reaction Kinetics and Surface Chemistry Research Group, Rerrich Béla tér 1, H-6720 Szeged, Hungary*
e-mail: hegedustimea@chem.u-szeged.hu

Abstract

Metal nanoparticles, such as Pt were applied in catalysis on various support materials, and have been employed widely in the CO_2 activation reaction. The utilization of this greenhouse gas is a burning question. During catalyst design, it is important to know the behavior of metal nanoparticles and the support alone. The distinct catalytic activity of Pt without any interaction with the support material is unknown experimentally as the support always plays a role in the catalytic reaction [1]. As a chemically inert material, hexagonal boron nitride (h-BN) can be a candidate for this purpose [2]. Therefore, h-BN fibers were synthesized and characterized. The as-prepared fibers show no catalytic activity towards CO_2 hydrogenation. After, controlled-size (4.7 ± 0.6 nm) Pt nanoparticles were impregnated onto the fibers the catalytic activity was 377 nmol/gs at 400°C with almost 100% CO selectivity. DRIFTS measurements supported that the reaction mechanism observed fits the RWGS reaction mechanism. Various surface science techniques proved that the measured activity is attributed to the Pt nanoparticles alone. For the noticed low catalytic activity of Pt nanoparticles the development of new sites is responsible proved by CO vibration spectroscopy studies [3]. Thus, the synthesized h-BN fibers can be employed in catalytic investigations as reference material with the proposed metal and reaction or possibly under different conditions.

Acknowledgments

Supported by the "ÚNKP-23-4-SZTE-554" New National Excellence Program of the Ministry for Culture and Innovation from the source of the National Research, Development and Innovation Fund.

References

[1] S. Kattel, P. Liu, J.G. Chen, J. Am. Chem. Soc. 139 (2017) 9739–9754.
[2] W. Auwärter, Surf. Sci. Rep. 74 (2019) 1–95.
[3] C. Lentz, S.P. Jand, J. Melke, C. Roth, P. Kaghazchi, J. Mol. Catal. A Chem. 426 (2017) 1–9.

MODIFICATION OF GLASSY CARBON NANOPARTICLES USING TITANIUM NANOPARTICLES AS A PLATFORM FOR DETERMINING DICLOFENAC SODIUM

Hidalgo, Juan[1], Turdean, Graziella[2], Galambos, Ildiko[1]

[1]University of Pannonia, Soós Ernő Research and Development Center, Zrínyi Miklós St. 18. H-8800, Nagykanizsa, HUNGARY
2 "Babes-Bolyai" University, Faculty of Chemistry and Chemical Engineering, Department of Chemical Engineering, Research Center of Electrochemistry and Non-Conventional Materials, Arany Janos St.11, RO-400028, Cluj-Napoca, Romania

e-mail: juansannin2595@gmail.com, graziella.turdean@ubbcluj.ro

Abstract

This article presents an investigation on the behavior of a chemically modified glassy carbon electrode as a sensing platform for the detection of Diclofenac Sodium. The study also explores the potential application of this electrode in analyzing real samples, including blood, urine, and wastewater. In addition, the synthesis of Titanium Nanoparticles and filaments used in the electrode modification was carried out using a novel method developed by our research group. This unique combination of materials has significantly enhanced the novelty of the technology, as no previous studies have reported such a combination.

Introduction

Considering the significance of dissolved solids (DS) in groundwater and its relevance to European Union legislation, various methodologies have been utilized to ascertain DS levels. These techniques encompass chromatography, specifically gas chromatography-mass spectrometry [1], as well as liquid chromatography [2]. The current study elucidates the alteration of a glassy carbon electrode (GCE) through the integration of micro flagellar nanotubes and titanium dioxide nanoparticles (TiO_2np) to serve as a substrate for the detection of diclofenac sodium (DS) in wastewater samples.

Experimental

The GC electrodes were modified using the drop-casting method. Initially, two solutions were prepared. In the initial experiment, a solution was prepared by combining chitosan (1 mg) with 5 mL of Acetic Acid (1%) and TiO_2 nanoparticles. In the second experiment, chitosan (1 mg) was utilized in a 5 mL solution of Acetic Acid (1%), along with TiO_2 nanoparticles and nanotubes of filaments. These components were prepared for the purpose of detecting diclofenac sodium (DS). Next, a volume of 3 μM of each solution was applied onto the GC electrode and subsequently dried to facilitate solvent evaporation at ambient temperature. The procedure was replicated on three separate occasions. Furthermore, the determination of the DS was conducted through the utilization of cyclovoltammetry (CV) technique, employing a computer-controlled AutoLab potentiostat (PGSTAT302N, and PGSTAT 12, EcoChemie, Utrecht, Netherlands) operated by GPES 4.7 software.

Results and discussion

The cyclovoltagrams (see Figure 1) show the behavior of the prepared modified sensors in the presence of DS. It can be observed at -0.6 V an oxidation peak appears because of the oxidation of the diclofenac. Also, there is no reverse peak appearing, which shows the irresistibility of the process in which the DS is oxidized, and the reduction reaction does not occur. Furthermore, the anodic intensity peak was greatest when the TiO_2-4HIS-Chit/GCE was evaluated. The I_p was equal to 9.14µA which was 10 times greater than the peak reported by the TiO_2-Chit/GC electrode. Which probes the efficiency of the prepared filaments in the recognition of the DS.

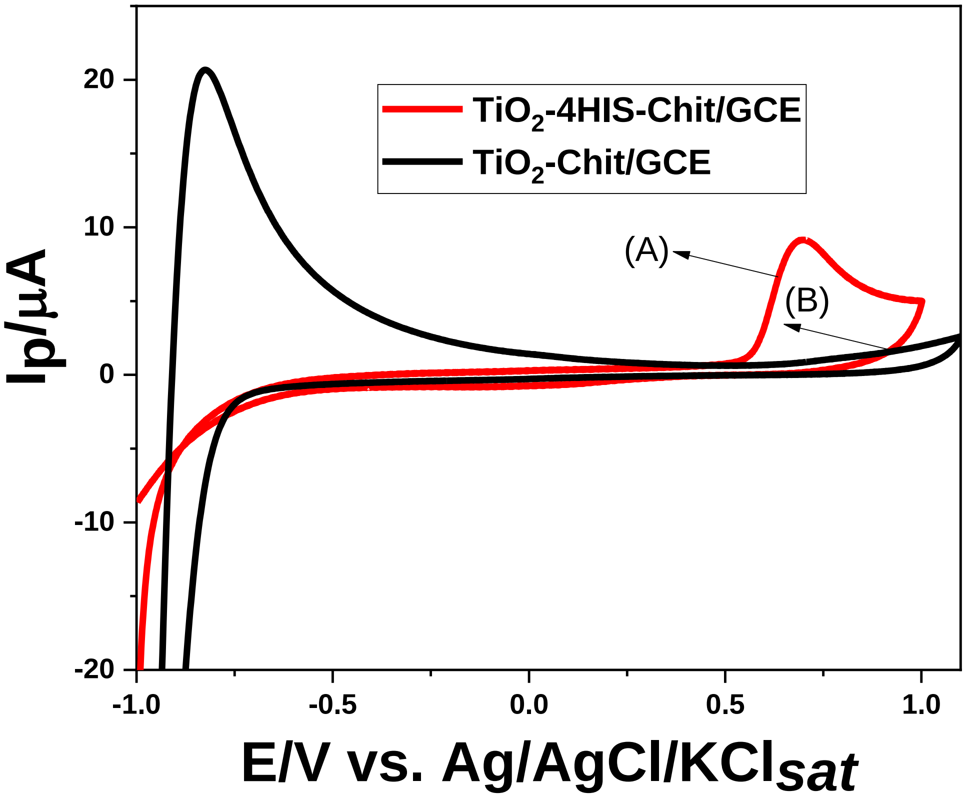

Figure 1. CV of GCE-4HIS-TiO_2Np (a) Chit-TiO_2Np/GCE, (b) in 10^{-3} M diclofenac. Experimental conditions: 0.1 M PBS (pH 4); scan rate, 50 $mV \cdot s^{-1}$, starting potential, -1 V vs. Ag/AgCl, KClsat.

Conclusion

The findings presented in this study demonstrate the efficacy of filament sensing and the enhancement of electrical properties in TiO_2 nanoparticles. In conclusion, it can be stated that the sensors developed in this study have demonstrated efficacy in detecting DS in wastewater samples. Furthermore, the robustness of this technology suggests its potential for application in online monitoring systems.

Acknowledgments

Juan Hidalgo Viteri thanks for the Ph.D. fellowship offered by the Tempus Foundation in accordance with Government Decision 477/21.04.2021. The
authors thank Dr. Jankovics Hajnalka, and Eva Toth (Bio-Nanosystems Research Laboratory) for the filament preparation and characterization.

References

[1] B. Yilmaz, GC–MS determination of diclofenac in human plasma, J. Chromatogr. 71 (2010) 549

[2] E.F. Elkady, Simultaneous determination of diclofenac potassium and methocarbamol in ternary mixture with guaifenesin by reversed-phase liquid chromatography, Talanta 82 (2010) 1604

PARALLEL MEASUREMENT OF SIZE DISTRIBUTION AND SPECTRAL RESPONSES OF PARTICULATE MATTER OF DIESEL ENGINES USING 4-PAS AND SMPS

Szabolcs Hodovány, Tibor Ajtai, Gábor Szabó, Zoltán Bozóki

Department of Optics and Quantum Electronics, University of Szeged, H-6720 Szeged,
Dóm tér 9, Hungary
e-mail: hszabolcs@titan.physx.u-szeged.hu

Abstract

Diesel engine emissions are under scrutiny in various fields. Due to its complex air quality and climate relevancies, the parallel measurement of size distribution and the spectral responses of thermally pretreated diesel particulate matter (DPM) provides a powerful opportunity to better understand its environmental impact and serve as a novel method for emission-based fuel development. In this study, we demonstrate the experimental results of number concentration, size distribution, and absorption spectra measurements of DPM as function of the operational conditions of diesel engines using different fuel types by 4-PAS and SMPS. The number-concentration and the population statistics including TNC, TVC and GMD values as well as the absorption responses including OAC and AAE data at different operational wavelengths were measured at each operational mode of the engine using pure petroleum based B0 and FAME mixed diesel fuels at three different TD temperatures. The thermal evolution of the investigated emission was also investigated at all measurement conditions. The results demonstrate the applicability of multi-wavelength PA spectroscopy for the qualitative investigation of diesel emissions and thermal evolution using a multi wavelength PA instrument - thermodenuder unit combination.

Introduction

In present days due to their climate and adverse health impact the investigation of diesel particulate matter (DPM) has been in gradually increased scientific interest. The diesel emitted particle is one of the dominant sources of light absorbing carbonaceous particulate matter (LAC), which is the second most important climate relevant atmospheric constituent too [1,2]. Diesel engines equipped with a modern, sophisticated after-treatment system also meet the new emission standards. However, further restriction of emissions in this way is limited by durability and maintenance. Emission-based fuel development is one of the most promising alternatives not only for reducing emissions but also for more environmentally friendly fuel development. The controlled parameter for soot emitted by a diesel engine is the number and mass concentration that has a limited ability to describe the air quality and climate implications of the DPM assembly. The size distribution, volatile classification and spectral responses of diesel carbon are critical parameters both in climatic and in health relevancies. A recently introduced in-situ measurement method for volatile classification of DPM is based on measuring the size distribution of a temperature-treated and denuded aerosol assembly [3]. The use of a thermodenuder (TD) for the pretreatment of depleted DPM not only allows the classification of volatiles, but also provides an indirect opportunity to study the state of the particles in relation to a given exhaust gas temperature under steady-state measurement conditions. Measuring aerosol light absorption is also a key, climate-relevant quantity. Moreover, the absorption spectrum of the LAC, which is quantified by its wavelength dependence (AAE) is the only physical quantity that can be measured in real-time, and which serves composition and air quality relevant information’s [4,5].

Experimental

For the measurement, a four-cylinder EURO 4 PC diesel engine with a 2-liter turbocharged common rail injection system was used to generate diesel exhaust emissions. The rear exhaust gas concentration was further reduced 10-fold with ejector diluter (Palas GmbH VKL 10). In any given operating condition of the engine, the exhaust particles were treated thermally before measurement. In our experiments the measurements were performed with two different fuel compositions (B0 and B7) under three different engine loads (defined on fig. 1 as wp#1, wp#2, and wp#3) at three different denuding temperatures (40°C, 150°C, 300°C). B7 For reference petroleum based B0 (bio free) fuel was used. For the investigation of biofuel effect B0 was blended with 7% FAME (Fatty Acid Methyl Ester) (B7). For reference measurements the heating unit of TD was set to 40°C. While, for volatility measurement the TD was heated to 150°C and 300°C respectively.

Results and discussion

The results of number concentration and size distribution measurements using B0 and B7 fuels at three distinct operational conditions of engine and temperatures are shown in Fig. 2. From the fitted data, we derived the characteristic parameters of the identified modes, including the median count (CMD), the geometric standard deviation (GSD), and the total number concentration (TNC). Total volume concentration (TVC) was also inferred using a simple spherical approach in the calculations. Independently of the fuel used, a bimodal size distribution was identified at a reference temperature (40°C) of 820 rpm at 0 Nm. In general, regardless of fuel type, engine operating condition, and sample temperature, B7 fuel provides similar emission characteristics (i.e., GMD and GSD values) as B0, but with a total number concentration (TNC) approximately 10-20% lower for all case.

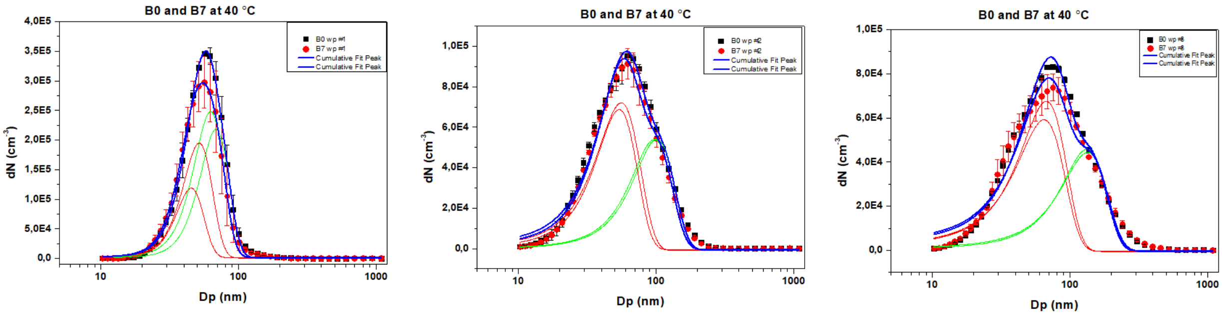

Figure 2. Size distribution and its characteristic parameters using B0 and B7 fuels at three different operatory parameters of the test engine.

The AAE value deduced from the measured absorption at the operational wavelengths of the multi-wavelength photoacoustic instrument using B0 and B7 fuels at different working points of the engine are drawn in Fig. 3. Based on that the AAE value around 1 means the elemental or black carbon fraction dominancy, while the higher value of that indicates presence of organic or in spectral terminology brown carbon fractions. The AAE value of B7 is higher than that of B0. This indicates the presence of organic carbon soot with high absorption ability towards the shorter wavelengths. This tendency means that the volatile organic compounds evaporate from the surface of the particles at higher temperatures.

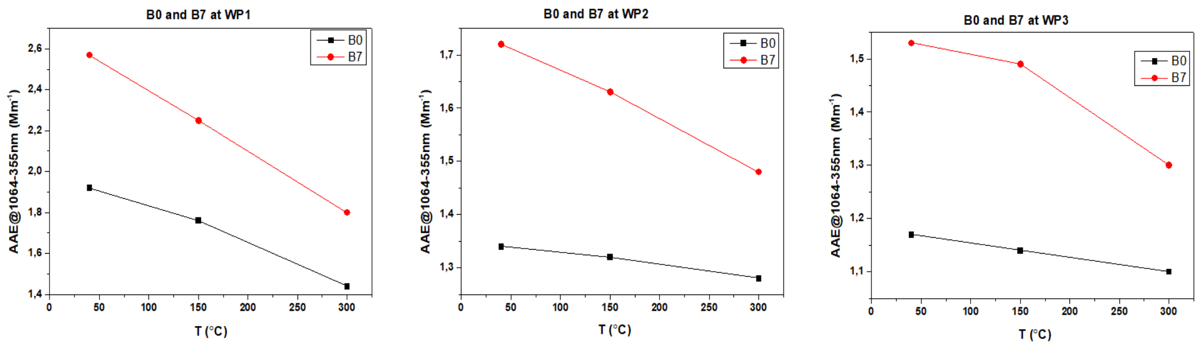

Figure 3. AAE of diesel emission in the function of working points of engine using different type of fuels and sampling temperature.

Summary and conclusion

The number-concentration and the population statistics including TNC, TVC and GMD values as well as the absorption responses including OAC and AAE values were measured at three different engine operating points using pure petroleum based B0 and B0 blended with 7% FAME content (B7) fuels. The absorption spectra quantified by its wavelength dependency (AAE) were deduced from the measured data at any operating condition of engine and fuel types. We have demonstrated experimentally that the size distribution of the wp#1 has bimodal distribution. We also demonstrated in this work that biofuel content cause higher absorption responses towards the shorter wavelengths and that the TNC values shows increased dynamics than that of AAE values with the increased number of wp's. We also experimentally demonstrated the applicability of the multi-wavelength PA spectroscopy for the emission-based fuel development purposes. Finally, we also demonstrated a novel methodology for particle evolution measurement using the combination of PA instrument and a thermodenuder unit.

Acknowledgements

This work was supported by *Production and validation of synthetic fuels in industry-university collaboration* (ÉZFF/956/2022-ITM_SZERZ).

References

[1] Lloyd, A. C., & Cackette, T. A. (2001). Diesel engines: environmental impact and control. Journal of the Air & Waste Management Association, 51(6), 809-847

[2] Bond T. C., Doherty S. J., Fahey D. W., Forster P. M., Berntsen T., DeAngelo B. J.,Flanner M. G., Ghan S., Kärcher B., Koch D., Kinne S., Kondo Y., Quinn P. K., Sarofim M. C., Schultz M. G., Schulz M., Venkataraman C., Zhang H., Zhang S., Bellouin N., Guttikunda S. K., Hopke P. K., Jacobson M. Z., Kaiser J. W., Klimont Z., Lohmann U., Schwarz J. P., Shindell D., Storelvmo T., Warren S. G., Zender C. S. 2013. Bounding the role of black carbon in the climate system: A scientific assessment, Journal of Geophysical Research: Atmospheres. 118, 1–173.

[3] Burtscher, H., Baltensperger, U., Bukowiecki, N., Cohn, P., Hüglin, C., Mohr, M., Matter, U., Nyeki, S., Schmatloch, V., Streit, N. and Weingartner, E., 2001. Separation of volatile and non-volatile aerosol fractions by thermodesorption: instrumental development and applications. Journal of Aerosol Science, 32(4), pp.427-442.

[4] Utry, N., Ajtai, T., Filep, Á., Pintér, M., Török, Z., Bozóki, Z., & Szabó, G. (2014). Correlations between absorption Angström exponent (AAE) of wintertime ambient urban aerosol and its physical and chemical properties. Atmospheric environment, 91, 52-59.

[5] Ajtai, T., Utry, N., Pintér, M., Major, B., Bozóki, Z., & Szabó, G. (2015). A method for segregating the optical absorption properties and the mass concentration of winter time urban aerosol. Atmospheric Environment, 122, 313-320.

DIELECTRIC MONITORING IN CERTAIN LIGNOCELLULOSIC BIOMASS UTILIZATION PROCESSES

Zoltán Péter Jákói[1], Balázs Lemmer[2], Réka Dobozi[2], Cecilia Hodúr[1], Sándor Beszédes[1]

[1]*Department of Biosystems Engineering, University of Szeged, H-6725 Szeged, Moszkvai krt. 9, Hungary*
[2]*Department of Food Engineering, University of Szeged, H-6724 Szeged, Mars tér 7, Hungary*
e-mail: jakoiz@mk.u-szeged.hu

Abstract

In our present study, we wanted to investigate the applicability of dielectric properties measurement to monitor the progress of three distinct but connected subprocesses of lignocellulosic biomass utilization. These involved the enzymatic saccharification of corn-cob residues, followed by the bioethanol fermentation of the hydrolysates, and lastly, the anaerobic biogas co-digestion of industrial wastewater sludge and solid residues from the alcohol fermentation part. Our results revealed that a strong and established correlation can be found between the process indicators and the dielectric constant of the different fermentation media - namely, the absolute sugar concentration during the enzymatic hydrolysis, the ethanol concentration during the alcohol fermentation, and the biogas yield during the anaerobic co-digestion. The relationship between these parameters can be described via linear functions, and the coefficient of correlation *r* varied between 0.97-0.99, while the R^2-value between 0.96-0.99.

Introduction

The growing importance of sustainable growth and the need to lessen reliance on finite resources have increased attention on the use of biomass and the integration of eco-friendly technologies. Serving as a fundamental component in the circular economy framework, biomass utilization strives to eradicate waste and perpetually recycle resources within a self-sustaining system. Lignocellulosic biomass (LCB) stands as the planet's most plentiful biological raw material, accounting for an estimated 80% (or 450 gigatons of carbon) of all different kinds of biomass. Over the past several years, extensive research has been conducted on harnessing LCB for bioenergy generation, positioning it as a viable and eco-friendly substitute for finite energy resources [1]. There are numerous procedures that can be utilized for biomass processing, among which bioethanol production and biogas fermentation are the most commonly used ones. From an environmental and energetic perspective, combining these utilization methods is the most favorable solution, since it can “close” the whole lifecycle of a phytomass of any kind, and can be perfectly integrated into the circular economy concept [2]. The separated hydrolysis and fermentation process (SHF) is one of most frequently employed technologies for biomass saccharification and ethanol fermentation – the first two of the cycle -, since it grants usually great yields and efficiency, and can be precisely controlled. Although the feedstock loses a significant part of its organic matter during these processes, it still contains a significant number of utilizable compounds, making it a great secondary raw material for anaerobic biogas co-digestion [3]. However, the biochemical pathways and reactions that occur during these subprocesses are especially complicated, and the standard analytic methods for controlling are either time consuming, and/or expensive. Therefore, an alternative method for monitoring these utilization methods should be sought out. The applicability of dielectric behavior assessment has been widely investigated, and its reliable use in several fields of science and engineering - for example foresting, soil engineering or food science – has been proved [4]. The underlying principles governing dielectric behavior are established in electrodynamic characteristics. Specifically, the presence of an electromagnetic field of any strength, denoted as *E*, induces what is known as a dielectric displacement, or *D*, in real materials. This can be interpreted as a form of phase shift, represented by δ. Consequently, the dielectric permittivity (ε), which describes how different materials react to the electromagnetic field, is considered a complex function dependent on the angular frequency ω of the field being applied:

$$D_0 e^{-i\omega t} = \varepsilon^*(f) E_0^{-i\omega t} \tag{1}$$

In the equation above, ε^* denotes the complex relative permittivity, ω is the (angular) frequency and $i = \sqrt{-1}$. In case *E* is not excessively high, the proportionality between *E* and *D* remains, and as the frequency increases the emerging δ phase difference becomes more prominent. The frequency at which the phase shift becomes prominent depends on the temperature, and the biological, chemical, and physical characteristics of the material, and can be defined as:

$$\varepsilon^* = \frac{D_0}{E_0} = |\varepsilon| e^{-i\delta} \tag{2}$$

$$\varepsilon^*(\omega) = \left|\frac{D_0}{E_0}\right| (cos\delta - isin\delta) = \varepsilon'(\omega) - i\varepsilon''(\omega) \tag{3}$$

Equation 3 is the separated form of the complex relative permittivity, where ε' – the dielectric constant – denotes the real part, and ε'' – the loss factor – the imaginary part. The dielectric constant quantifies the electric (or electromagnetic) absorbing and storing capabilities of a given material, while the loss factor shows how much of the absorbed energy is converted into other types of energy. As can be seen from the equation, both the dielectric constant and loss factor are frequency dependent, and the distinct frequency where the dielectric constant reaches its maximum (*i.e.* the inflexion point of the dielectric spectra) is called the relaxation frequency. For systems containing high amounts of water, this relaxation frequency occurs around 700-1000 MHz. These dielectric properties highly depend on the chemical – physical structure of a system as well – meaning, that a change in either the chemical or physical structure is reflected in the change of dielectric behavior as well. This makes the measurement of dielectric behavior a promising alternative in the controlling and monitoring of biotechnological processes, such as biomass utilization [5].

Experimental

Corn-cob residues served as raw material for the enzymatic saccharification; of which 10 m/m% aqueous suspensions were made by the addition of purified water. A mixture of different β-1,4-glucanase enzymes was added to the suspensions, and during the 6-days-long hydrolysis, the temperature was kept at 45±1°C, whilst the pH at 5.5±0.4. The sugar end-product of the hydrolysis was measured with dinitrosalicylic-acid based spectrophotometric method every 24 hours. Along with the sugar concentrations, the dielectric properties of the hydrolysates were also measured with a DAK-3.5 open-ended dielectric probe connected to a ZVL-3 vector network analyzer (bandwidth: 30 kHz – 3 GHz). The subsequent ethanol fermentation took place in automatic anaerobic fermenters, and standard *Saccharomyces cerevisiae* strains were used for the bioconversion of glucose to ethanol. The temperature was kept at 30°C, and the pH at 5.5. The ethanol concentration was measured with distillation, and the dielectric properties of the fermentation media were also measured with the aforementioned dielectric system. The solid residues after the fermentation were transferred to laboratory-grade glass fermenters, where they were mixed with 100 cm^3 of industrial wastewater sludge for mesophilic co-digestion. The optimal temperature condition (T=38°C) was achieved in a thermostatic cabinet.

The biogas yield was calculated based upon the absolute pressure inside the reactors, and along with it, the dielectric behavior of the fermentation media was also measured with the dielectric assessment kit.

Results and discussion

In order to evaluate the correlation between the nascent sugar concentration during the enzymatic hydrolysis and the dielectric properties of the medium, we plotted the values of the 900 MHz dielectric constant (i.e., the variable which is affected by the biochemical changes in the material) as a function of the corresponding sugar concentration (i.e., the variable which ultimately leads to the change in dielectric behavior). This can be observed in Figure 1.

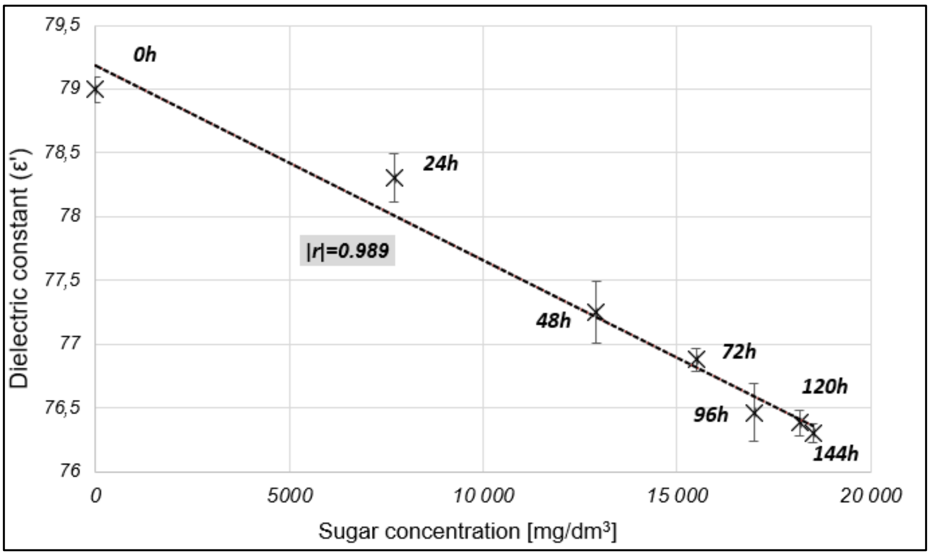

Figure 1. *The relationship between the sugar concentration and the 900MHz dielectric constant during the enzymatic saccharification*

The results obtained suggest that as the hydrolysis converges, the concentration of sugar shows saturation characteristics (i.e. the product concentration eventually reaches its maximum and does not go any further), which is a typical tendency of enzymatic reactions. The maximum value of sugar turned out to be around 18 g/dm^3, which means an approximately 76% bioconversion efficiency. In terms of the dielectric constant, it can be clearly stated that there is a strong and linear correlation between it and the sugar concentration (r = 0.989). It can also be seen that as the sugar concentration increases, the dielectric constant gradually decreases. This might be explained by the fact that the degradation of lignocellulose evidently produces smaller mono-, di- and oligosaccharides, the vast majority of which are soluble. This eventually leads to the reduction of free water molecules, which also implies a decrease in the dielectric constant. This strong relationship suggests that evaluating certain dielectric characteristics (in this case, the dielectric constant) can be a promising, fast, and accurate method for monitoring enzymatic processes.

During the second part of the SHF process, the hydrolysates underwent anaerobic alcohol fermentation, where the ethanol concentration was regularly measured every 24 hours, along with the dielectric characteristics. Figure 2 shows the results obtained for the fermentation process.

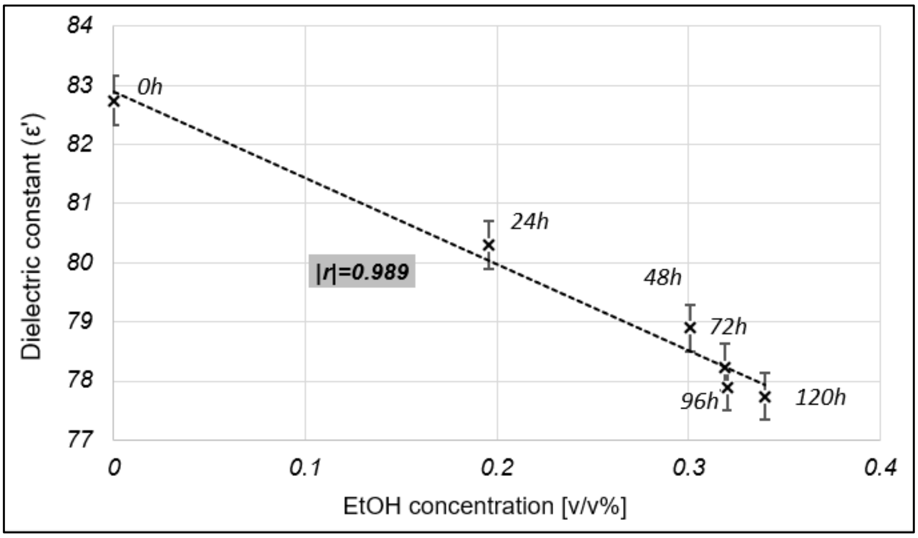

Figure 2. *The dielectric constant as the function of ethanol concentration during the fermentation process*

Like in the case of enzymatic hydrolysis, the ethanol concentration also showed a saturation tendency during the fermentation, which is related to both the concentration of free sugars available and the alcohol tolerance of the microbes. Since the maximum v/v% achieved was around 0.35%, the conversion efficiency did not exceed 40%. A possible explanation for this is that during the degradation of lignocellulose, a huge variety of compounds can be generated (especially from the lignin) that can limit the microbial metabolism. Although the ethanol conversion efficiency was relatively low, the change in dielectric behavior showed strong linear correlation (r = 0.989) with the ethanol concentration as well. Since ethanol has a lower dielectric constant than water, even a small amount of it can influence the dielectric behavior of the medium, which can be observed in Figure 2.

During the anaerobic co-digestion, the solid residues from the alcohol fermentation (after drying) were mixed with 100 cm^3 of industrial sludge. The produced gas volume was measured on every seventh day of the process, along with the dielectric constant of the fermentation media. Figure 3 shows the results obtained.

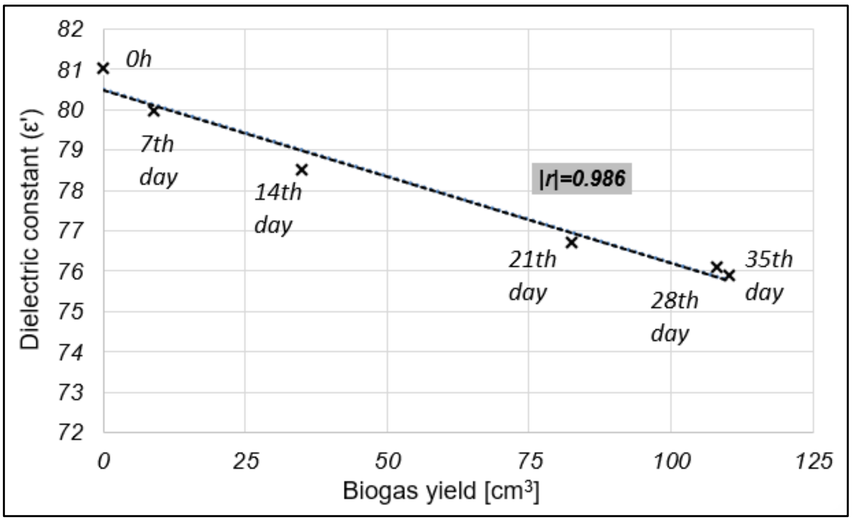

Figure 3. *The connection between the dielectric constant and bigos yield during the anaerobic co-digestion process*

It can be seen from the results that the digestion process reached the steady-state (or "stagnating") phase around the 28th day, after which no detectable difference was experienced in the biogas volume. During this stage the biochemical reactions slow down and eventually no recognizable chemical / physical structural change occurs. This is in great alignment with the dielectric characteristics, namely that the decreasing tendency stops after the 28th day. Like the previous processes, the dielectric constant shows a strong linear correlation with the actual phase of the fermentation media ($r = 0.986$), meaning that it might be used as a fast and accurate monitoring tool for anaerobic biogas fermentation processes tool.

Conclusion

In the present study, we investigated whether certain biomass utilization processes, namely enzymatic hydrolysis of lignocellulose, alcoholic fermentation of the hydrolysates and the biogas co-digestion of fermentation residues, can be monitored by measuring dielectric parameters. Our results revealed that a strong a linear correlation could be established between the dielectric constant, and the indicator parameters of these biomass utilization processes, namely the sugar, ethanol and biogas yield or concentration ($r = 0.989$, 0.989 and 0.986, respectively). This suggests that – after proper optimization – dielectric measurement can be utilized as a fast, reliable, and relatively cheap technique in monitoring and controlling of these, or similar biomass processing technologies.

Acknowledgements

The authors are grateful for the financial support provided by the New National Excellence Program of the Ministry for Culture and Innovation from the source of the National Research, Development, and Innovation Fund, under funding numbers ÚNKP-23-3-SZTE-246, ÚNKP-23-5-SZTE-668, and ÚNKP-23-2-SZTE-249. This project was supported by Bolyai János Research Scholarship of the Hungarian Academy of Sciences (BO/00161/21/4).

MINISTRY OF CULTURE
AND INNOVATION

References

[1] Mao, G., Huang, N., Chen, L., & Wang, H. (2018). Research on biomass energy and environment from the past to the future: A bibliometric analysis. *Science of the Total Environment*, *635*, 1081-1090.

[2] Velvizhi, G., Balakumar, K., Shetti, N. P., Ahmad, E., Pant, K. K., & Aminabhavi, T. M. (2022). Integrated biorefinery processes for conversion of lignocellulosic biomass to value added materials: Paving a path towards circular economy. *Bioresource technology*, *343*, 126151.

[3] Cesaro, A., & Belgiorno, V. (2015). Combined biogas and bioethanol production: opportunities and challenges for industrial application. *Energies*, *8*(8), 8121-8144.

[4] Routray, W., & Orsat, V. (2018). Recent advances in dielectric properties–measurements and importance. *Current Opinion in Food Science*, *23*, 120-126.

[5] Yardley, J. E., Kell, D. B., Barrett, J., & Davey, C. L. (2000). On-line, real-time measurements of cellular biomass using dielectric spectroscopy. *Biotechnology and Genetic Engineering Reviews*, *17*(1), 3-36.

INVESTIGATION OF THE STRONTIUM TITANATE ($SrTiO_3$) AND SOIL EXTRACT INTERACTION

Chagu John[1,*], Ariya Badam[1], Solymos Karolina[1], Gyulavári Tamás[1], Pap Zsolt[1,2,3]

[1]*Department of Applied and Environmental Chemistry, University of Szeged, H-6720 Szeged, Rerrich Béla tér 1, Hungary*
[2]*Nanostructured Materials and Bio-Nano-Interfaces Center, Institute for Interdisciplinary Research on Bio-Nano-Sciences, Babeş–Bolyai University, RO-400271 Cluj-Napoca, Treboniu Laurian 42, Romania*
[3] *Institute of Research-Development-Innovation in Applied Natural Sciences, Babeş–Bolyai University, RO-400294 Cluj-Napoca, Fântânele 30, Romania*
[4]*Department of Geoinformatics, Physical and Environmental Geography, University of Szeged, HU-6722 Szeged, Egyetem u. 2-6, Hungary*
**e-mail: johnchagu7@gmail.com*

Abstract

The study was aimed on the investigation of strontium titanate photocatalysts ($SrTiO_3$) and soil extract interaction. Both commercial and synthesized $SrTiO_3$ photocatalysts were studied in the present work. The latter was obtained via a solvothermal crystallization method (applying different synthesis parameters: treatment time, NaOH source and precursor ratio). The result of the soil solution (extracted from solonetz/basic soils) - catalyst interaction was studied via the photocatalytic activity towards phenol degradation under UV-light. The $SrTiO_3$ nanoparticles were characterized by X-ray diffractometry (XRD), infrared spectroscopy (IR), diffuse reflectance spectroscopy (DRS) and scanning electron microscopy (SEM). The phenol degradation experiments revealed that synthesized $SrTiO_3$ showed higher photocatalytic activity than commercial $SrTiO_3$. The XRD patterns revealed that crystalline structure of each sample was preserved, while the primary crystallite size values obtained decreased following immersion in the basic soil extracts. The IR results showed that the surface properties of both commercial and synthesized $SrTiO_3$ photocatalysts were modified. Based on DRS investigations, all samples immersed in basic soil solutions changed their color. However, no changes were observed in the band gap for commercial $SrTiO_3$ while for the synthesized $SrTiO_3$ smaller changes were observed. The SEM micrographs showed only signs of particle aggregation.

Acknowledgements

Indo-Hungarian TÉT project (2019-2.1.13-TÉT_IN-2020-00015 is thanked for the financial support. . T. Gyulavári is grateful for the financial support of the NKFI-PD-138248 project, the Bolyai János scholarship provided by the Hungarian Academy of Sciences, and that the research was supported by the ÚNKP-23-4 New National Excellence Program of the Ministry for Culture and Innovation from the source of the National Research, Development and Innovation Fund.

GREEN AGENTS FOR SYNTHESIS OF SILVER NANOPARTICLES THROUGH MULTI- ROUND RECYCLING OF WASTE AS AN ALTERNATIVE TO CHEMICAL METHODS: SYNTHESIS AND CHARACTERIZATIONS

Edi Kachal[1], **Andrea Rónavári**[1], **Imre Szenti**[1], **Zoltán Kónya**[1]

[1]*Department of Applied and Environmental Chemistry, IC, University of Szeged, Szeged,*
HU-6720 Rerrich Béla tér 1, Hungary
e-mail: edisk@chem.u-szeged.hu, ronavari@chem.u-szeged.hu

Abstract

Green nanoparticle (NP) synthesis is a novel area of nanotechnology that succeeds in terms of biocompatibility, scalability, cost-effectiveness, and environmental friendliness. Due to the widespread of metal nanoparticles in industrial scale applications, green and efficient process that are required free toxic solvent is being emphasized. Plants have lately been used to produce metal nanoparticles as an alternative approach that apply extracts made from as reducing and capping agent. Due to their excellent properties, silver nanoparticles have been widely used for several applications, including as antibacterial agents, in industrial, household, and healthcare-related products, in consumer products, medical device coatings, optical sensors, and cosmetics. Regarding this, the purpose of our research firstly was to find out whether the green martials Turkish coffee (TC) and Virginia Creeper (VC) extracted and used for synthesis of silver nanoparticles (Ag NPs) could be recycled for further NP synthesis. Another objective was to compare Ag NPs morphology synthesized by biological reagent to chemical reagents as sodium borohydride ($NaBH_4$) as reductant, and sodium citrate and Polyvinyl-Pyrrolidone (PVP) 55k as the stabilizing agents by conventional method. The characteristics of the Ag NPs was confirmed by transmission electron microscopy (TEM), U.V spectroscopy and dynamic light scattering (DLS) measurements.

Introduction

Nowadays, nanotechnology plays a crucial role in various industries, including electronics, chemicals, biotechnology, bioanalytics, and others. (1). Scientists formed a novel area known as "green nanotechnology" via linking the concept of sustainability with nanotechnology. Green improvement took birth out of the repeated thought method and act plans of researchers. Plants and its counterparts are comprehensively used in synthesis of nanoparticles (2). Additional when technology advanced the green route of synthesis was selected for replacing non-ecofriendly by yields with eco-friendly ones. This greener route employs biotic entities of the environment as its incredible ingredient by altering the traditional ingredients in physical and chemical methods of synthesis (3). Metal nanoparticles have been used extensively in current research, between the diverse metal nanoparticles, Ag NPs further have been paid attention throughout the past few years because of their prospective. The modern studies for the preparation of silver nanoparticles with a controlled size will be valuable in numerous approaches such as: chemical reduction of silver ions commonly in the presence of stabilizing agents (4). It is noteworthy that this method and the most of the chemical methods have possible hazards to health and environment. Nonetheless by reduction potential of plant extract, we could be able to reduce the metal ions. Therefore, the potential of plants as biological materials for the synthesis of nanoparticles still should be explored like the mechanism of reduction which is not well described in the articles, their process conditions and concentration of both reducing agent and main precursors. Green synthesis of NPs by means of plants extract has numerous rewards above chemical synthesis, such as easiness, cost effectiveness as well as compatibility for biomedical and pharmaceutical applications (5). Thus, the present study focused on the green materials (TC and VC) extracted and used for the synthesis of nanoparticles, the major key was through the multi-round recycling for further NP synthesis. This study aims to compare the chemical properties of green Ag NPs with those synthesized using chemical reagents, providing a explore a clean, sustainable, direct alternative to chemical approach for Ag NPs synthesis.

Experimental

Preparation of plant extracts in multiple rounds. The selected plant extracts were prepared according to earlier described procedures (6,7) with some modifications. Virginia Creeper (VC) leaves were collected locally (Szeged, Hungary) in September 2023. The leaves washed by deionized water to remove any surface dust and dried at room temperature until achieving constant weight. Afterward, the VC leaves were cut to small pieces. For the duration of first-round extraction, the extracts were prepared by using 5 g of VC small pieces leaves in 100 mL of deionized water set up temperature to 70 °C for 30 min, and then the extracts were paper- and vacuum-filtered to remove residual plant particles. The extracts were stored at fridge for somedays before used for NPs synthesis. A similar procedure was working for coffee (TC) extracts, except that purchased powder coffee (Hazer Babe, Turkish coffee) were boiled directly without any pretreatment. After the first-round extractions remaining plant materials (used upon the first extraction, left behind as “waste”) were air-dried and recycled two further times to gain individual extracts each time (second- and third-round extractions). In these multiple rounds, the extraction technique was undistinguishable as described above for first-round extractions. The extracts formed were labeled according to the name of the plant extract and the order number of the extraction round, namely TC1, TC2, and TC3 for coffee and VC1, VC2, and VC3 of Virginia Creeper extractions, respectively. These extracts were all stored in fridge, then applied separately for Silver nanoparticle (Ag NPs) synthesis as reducing and capping agents. Synthesis of AgNPs, TC-Ag- and VC-Ag – labeled green Ag nanoparticles were synthesized by adding the corresponding extracts (of the first-, second-, and third-round extractions: TC1, TC2, TC3 and VC1, VC2, VC3, respectively) added to 0.002 mole/L aqueous of $AgNO_3$ solution 1:1 volume ratio at 75 °C , PH 7 by continuous stirring for 1h . Then the prepared Ag nanoparticles cooled down and kept in fridge for later use. Whereas chemical reagents citrate and PVP Ag NPs where synthesized by the seed-mediated growth conventional approach (8,9). The method is based on chemical reduction using silver nitrate ($AgNO_3$) as a silver source, sodium borohydride ($NaBH_4$) as reductant, and sodium citrate and polyvinyl-pyrrolidone (PVP) 55k as the stabilizing agents.

Results and discussion

Consideration of the suitability of the plant extracts obtained in several recycling rounds to form Silver nanoparticles (Ag NPs). Following the procedure described earlier (6,7) we achieved Ag NPs synthesis with the benefit of each extract obtained in the multiple round of extraction. Our primary objective was to assess the appropriateness and recyclability of green household waste materials for the generation of Ag NPs and to determine which green material provides sufficient quantities and quality of key components after successive extraction steps to produce AgNPs. During the reaction when certain aqueous green extracts were added to the reaction mixture, while the continuous of reduction of silver ion and constant of growth of Ag nanoparticles, we observed a color change. UV–Vis Spectroscopy was used to measure the localized surface plasmon resonance, The UV spectrum is shown specific peaks in (400 to 450 nm) region for synthesized Ag NPs by various reagents that confirmed the present of silver nanoparticles (Figure 1). Dynamic light scattering (DLS) was used to determine the size distribution (d.nm) (Figure 2). The hydrodynamic size was around 6nm for PVP and 18 nm for citrate whereas for green reagents 19nm for TC and 30 nm for VC.

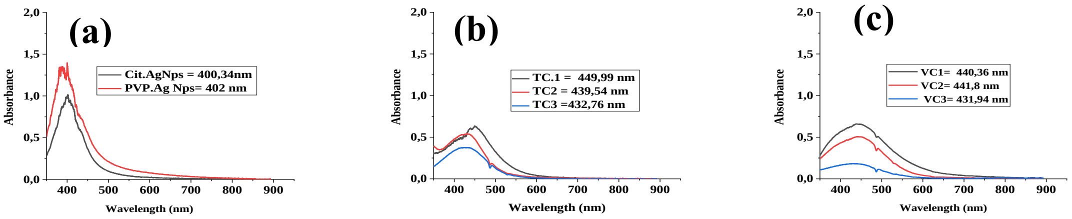

Figure 1. UV-vis absorption spectra of chemical approaches PVP and Citrate AgNPs (a), and green synthesized AgNPs prepared by coffee (TC1,2 and 3) (b) and (c) for VC (1,2 and 3).

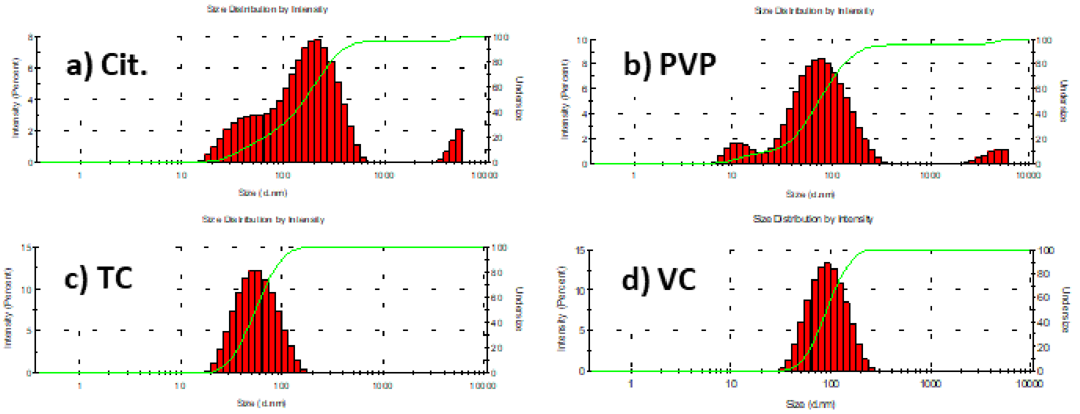

Figure 2. Size distribution (d.nm) Citrate-SB Ag Nps (a) PVP -SB Ag Nps (b) and (c) is TC- Ag Nps and (d) is VC-Ag Nps .

TEM measurements were employed to ascertain the size and morphological characteristics of the obtained Ag NP samples. According to these images (Figure 3) Ag NPs synthesis was successful with chemical reagent as well as green reagents applied. The shape (spherical) of Ag NPs produced by green synthesis was similar to chemical ones. The size of AgNPs by green synthesis appeared larger compared to (SB) Ag NPs as around 5 nm.

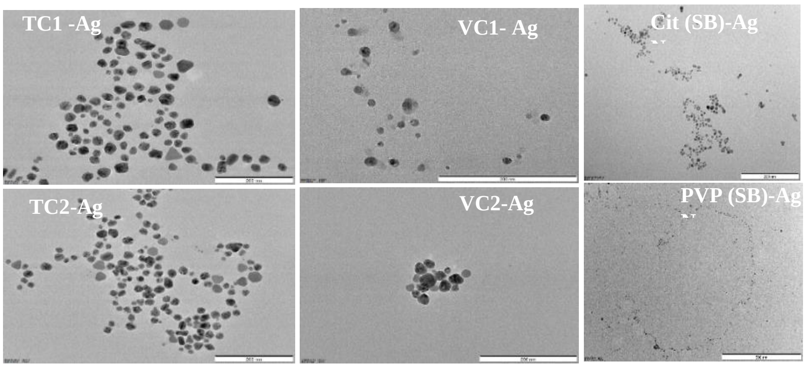

Figure 3. TEM images of silver nanoparticles produced by using various green waste extracts obtained in round extraction of Turkish Coffee (TC1-Ag, TC2-Ag), Virginia Creeper (VC1-Ag, VC2-Ag) compared to chemical reagent sodium borohydride (SB-Ag).

Conclusion

In the last decade, the green production of nanoparticles had been a major ground of research. Nowadays, one of the most basic needs to the field of nano is its compatibility with environment. In this regard, this work focused on investigation of the multiple applicability such as recyclability of (coffee and Virginia Creeper) waste extraction for green Ag NP synthesis and compare the synthesized particles to the conventional produced Ag NPs (SB-Citrate and PVP). All green extracts obtained from first to third round extraction samples of TC, VC were found to be adequate for Ag NPs synthesis, although TC extracts appeared to be better compare to VC extracts. These outcomes show that the well-selected green waste materials can be reprocessed in multiple rounds for nanoparticles synthesis.

Acknowledgements

This work was supported by GINOP_Plusz-2.1.1-21-2022-00080 project and by the János Bolyai Research Scholarship of the Hungarian Academy of Sciences (Grant no. BO/00384/21/7) and by the New National Excellence Program of the Ministry of Human Capacities of Hungary (UNKP-23-5-SZTE-687).

References

[1] Michelle Duval Malinsky, K. Lance Kelly, et al. Chain Length Dependence and Sensing Capabilities of the Localized Surface Plasmon Resonance of Silver Nanoparticles Chemically Alkanethiol Self-Assembled Monolayers.J. Am. Chem. Soc. 2001, 123, 7, 1471–1482

[2] Mahendra Rai, Alka Yadav. Plants as potential synthesiser of precious metal nanoparticles: progress and prospects. IET Nanobiotechnol . 2013 Sep;7(3):117-24.

[3] Shakeel Ahmed, Mudasir Ahmad, et al. A review on plants extract mediated synthesis of silver nanoparticles for antimicrobial applications: A green expertise.Journal of Advanced Research. January 2016 Volume 7, Issue 1, Pages 17-28.

[4] Robert W. J. Scott,Orla M. Wilson, et al. Bimetallic Palladium-Gold Dendrimer-Encapsulated Catalysts.J. Am. Chem. Soc. 2004, 126, 47.

[5] Mahmoud Nasrollahzadeh , S. Mohammad Sajadi et al. Green synthesis of Pd/Fe3O4 nanoparticles using Euphorbia condylocarpa M. bieb root extract. Journal of Molecular Catalysis A: Chemical. January 2015, Volume 396, Pages 31-39.

[6] Andrea Rónavári , Margit Balázs, et al. Multi-round recycling of green waste for the production of iron nanoparticles: synthesis, characterization, and prospects in remediation. Int J Nanomedicine .2023 Feb 9;18(1):8.

[7] Kozma G, Rónavári A, Kónya Z, Kukovecz Á. Environmentally benign synthesis methods of zero-valent iron nanoparticles. ACS Sustain Chem Eng. 2016;4(1):291–297.

[8] Péter Bélteky , Andrea Rónavári, et al. Are Smaller Nanoparticles Always Better? Understanding the Biological Effect of Size-Dependent Silver Nanoparticle Aggregation Under Biorelevant Conditions. Int J Nanomedicine. 2021 Apr 23:16:3021-3040.

[9] Andrea Rónavári , Péter Bélteky, et al. Polyvinyl-Pyrrolidone-Coated Silver Nanoparticles—The Colloidal, Chemical, and Biological Consequences of Steric Stabilization under Biorelevant Conditions. Int. J. Mol. Sci. 2021, 22(16), 8673.

COMPLEXES OF THE NATURAL ANTIBIOTIC MONENSIN A WITH ENVIRONMENTAL DIVALENT METAL IONS

Máté Levente Kis[1], Bálint Hajdu[1], Béla Gyurcsik[1], Ivayla Pantcheva[2], Petar Dorkov[3]

[1]Department of Molecular and Analytical Chemistry, University of Szeged, H-6720 Szeged, Dóm tér 7-8, Hungary
[2]Department of Analytical Chemistry, Faculty of Chemistry and Pharmacy, "St. Kl. Ohridski" University of Sofia, 1164 Sofia, Bulgaria
[3]Research & Development Department, Biovet Ltd., 4550 Peshtera, Bulgaria
e-mail: kis.mate.levente@chem.u-szeged.hu

Abstract

Monensin A is polyether type natural antibiotic with a quasi-ring structure. The structure is the consequence of hydrogen-bond formation between the two terminal functional groups. The outer side of the molecule is lipophilic due to the alkyl function groups. The cavity has a hydrophilic character. Based on the above properties, this molecule is able to coordinate monovalent metal ions and transfer them across cell membrances. This way of transportation may cause bacterial cell death by disruption of the metal ion balance. The environmental divalent metal ions may influence this process. The results of the experiments serve the better understanding of the behavior of monensinate toward these metal ions.

The coordination ability of the monensin molecule can be studied through its chirality in solution by circular dichroism (CD) spectroscopy. The measured CD data showed that the deprotonated ligand forms two different types of divalent metal complexes depending on the metal to ligand molar ratio. In the presence of ligand excess a biscomplex exists, however if the amount of metal ions is incrased, a monocomplex is formed. The $[M(Mon)_2(H_2O)_2]$ biscomplex is neutral and the metal ion's coordination sphere is octahedral. The formation processes followed by UV-CD were presented earlier [1]. CD spectroscopy in the visible and near-infrared range was used to investigate the monensin A complexes with colored metal ions. The colored metal ions can be chirally perturbed by the ligand, thereby they show optical activity in the visible wavelength region [2]. Furthermore, the implementation and evaluation of measurements in this range is simplified by the fact that the free components do not exert CD spectra. The complexation with Co(II) and Ni(II) cations was investigated in methanolic solution, where the ligand was deprotonated by tetramethyl-ammonium-hydroxide. Competition experiments between selected colored and colorless divalent metal ions (Mg(II), Ca(II) and Zn(II)) were also performed. The observed characteristics of the mono- and bis-complexes of Co(II) and Ni(II) were used to investigate the competition with divalent colorless metal cations. The conditional stability constants of these complexes were calculated by PSEQUAD program.

As a conclusion, monitoring the complex formation in the VIS-NIR range with CD spectroscopy reduces the data for evaluation. The evaluation of the measurements with visible chiral complexes can be easily carried out, as the ligand and the metal ion have no CD signal. Moreover the measurment conditions are simplified in these cases. Our data show that, to decide whether the monensin molecule is suitable for chelating agent, it is necessary to consider its interactions with non-native metal ions in the living system and in the environment.

References

[1] I. Pantcheva, A. Nedzhib, L. Antonov, B. Gyurcsik, P. Dorkov, Inorg. Chem. Act. 505, 2020
[2] M.L. Kis, B. Hajdu, P. Dorkov, I. Pantcheva, B. Gyurcsik, Inorganics 2023, 11, 334.

ENANTIOSELECTIVE SEPARATION OF SUBSTITUTED AMINO ACIDS UTILIZING CINCHONA ALKALOID-BASED CHIRAL STATIONARY PHASES

Gábor Németi*[1], Dániel Ozsvár[1], Róbert Berkecz[1], Antal Péter[1], Wolfgang Lindner[2], István Ilisz[1]

[1]*Institute of Pharmaceutical Analysis, University of Szeged, H-6720 Szeged, Somogyi u. 4, Hungary*
[2]*Department of Analytical Chemistry, University of Vienna, Währingerstrasse 38, 1090 Vienna, Austria*
e-mail: nemeti.gabor@szte.hu

Applying chiral stationary phases is a highly favored choice for enantioseparation purposes due to its versatility both in analytical and preparative scales. Among others, *Cinchona* alkaloid-based ion-exchanger type chiral stationary phases are particularly noteworthy in the case of enantioseparation of amino acids and their derivatives.

The changes in the chromatographic parameters were investigated by varying of the methanol and acetonitrile content of the bulk solvent, the nature of the acid and base additives, and the temperature of the stationary phase. The stoichiometric displacement model was used to study ionic interactions by varying the concentration of the additives. Evaluation of structure-retention relationships was done on the basis of the effects of the various structures of the applied analytes and the elution order of their stereoisomers utilizing different selectors as stationary phases.

Acknowledgments

The study was supported by the ÚNKP-23-3-SZTE-191 New National Excellence Program of the Ministry for Culture and Innovation from the source of the National Research, Development and Innovation Fund. This work was also supported by the National Research, Development and Innovation Office-NKFIA through project K137607. Project no. TKP2021-EGA-32 has been implemented with the support provided by the Ministry of Innovation and Technology of Hungary from the National Research, Development and Innovation Fund, financed under the TKP2021-EGA funding scheme.

Zr-BASED METAL-ORGANIC FRAMEWORKS: FROM SYNTHESIS TO APPLICATION

Roxana Nicola[1*], **Carmen Cretu**[1], **Adel Len**[2,3] , **Levente Illés**[4], **Zsolt Endre Horváth**[4], **Ana-Maria Putz**[1]

[1] "Coriolan Drăgulescu" Institute of Chemistry, Bv. Mihai Viteazu, No. 24, 300223 Timisoara, Romania
[2]Institute for Energy Security and Environmental Safety, Centre for Energy Research, Konkoly-Thege Miklós út 29-33, 1121 Budapest, Hungary
[3]Faculty of Engineering and Information Technology, University of Pécs, Boszorkány street 2, 7624 Pécs, Hungary
[4]Institute for Technical Physics and Material Science, Centre for Energy Research, Konkoly-Thege út 29-33, 1121 Budapest, Hungary
email: cc.roxana@yahoo.com

Abstract

Metal-organic frameworks (MOFs) are a new class of crystalline micro/mesoporous hybrid materials, constructed by organic linkers and metal nodes, with significant application potential. Due to their chemical and physical properties, such as high surface area, large porosity, tunable pore size, and flexible functionality, MOFs have gained extensive explorations as a highly versatile platform for functional applications in many research fields [1,2]. Zr based metal-organic framework materials (Zr-MOFs) with increased specific surface area and pore volume have been obtained using the chemical and the solvothermal synthesis methods. The obtained materials were investigated by FT-IR spectroscopy, TGA, SANS, PXRD and SEM methods. The nitrogen porosimetry data evidenced the presence of pores with average dimension of ~4 nm and by SANS the average sizes of the Zr-MOF nanocrystals are suggested to be around 30 nm. The PXRD obtained patterns were characterized by similar features that point to well-crystallized phases specific for the UIO-66 type materials revealing by SEM also that the materials are composed of small and agglomerate crystals. The thermogravimetric analysis reveals that both materials have approximatively two linkers deficiencies per Zr_6 formula unit [3].

[1]. S. Soni, P.K. Bajpai, C. Arora, A review on Metal-Organic Framework: synthesis, properties and application, Charact. Appl. Nanomater. (**2019**) 2.
[2]. B. Maranescu, A. Visa, Applications of Metal-Organic Frameworks as Drug delivery Systems, Int. J. Molec. Sci. 23 (**2022**) 4458.
[3]. C. Cretu, R. Nicola, S.-A. Marinescu, E.-M. Piciorus, M. Suba, C. Duda-Seiman, A. Len, L. Illés, Z.E. Horváth, A.-M. Putz, Performance of Zr-based Metal-Organic Framework Materials as in Vitro Systems for the Oral Delivery of Captopril and Ibuprofen, Int. J. Mol. Sci. 24 (**2023**) 13887.

This work was supported by Program 4 of the "Coriolan Dragulescu" Institute of Chemistry, Research Project 4.2 and the authors thanks to Romanian Academy.

EFFICIENT REMOVAL OF METHYLENE BLUE FROM COLORED WASTEWATER USING MAGNETITE/CARBON NANOCOMPOSITE

Maria Andreea Nistor[1], Robert Ianos[2], Simona Gabriela Muntean[1]

[1] "Coriolan Drăgulescu" Institute of Chemistry, 24 Mihai Viteazul Bvd., 300223, Timisoara, Romania,
[2]Faculty of Industrial Chemistry and Environmental Engineering/ Politehnica University, 6 Pîrvan Blv, RO-300223, Timişoara, Romania
e-mail: sgmuntean@acad-icht.tm.edu.ro

Abstract

In this work, a new nanocomposite based on activated carbon and magnetite (PM) was synthesized and characterized by the most indicated and modern methods. The obtained magnetite/carbon nanocomposite was tested as adsorbent for the removal of *Methylene Blue* (MB) from colored wastewater. In ortder to elucidate the adsorption mechanism, kinetic and thermodynamic studies were carried out. The high adsorption capacity of the synthesized nanocomposite was highlighted by regeneration and reuse studies in consecutive adsorption/desorption cycles.

Introduction

The efficient removal of dyes from wastewater is becoming a worldwide priority for increasing the quality of life [1].Various physical, chemical and biological methods have been tested to remove dyes from wastewater [2]. Among all the decontamination methods, adsorption is considered to be one of the most promising alternative techniques for removing non-biodegradable dyes from wastewater, due to: its simple application, superior efficiency, relatively low costs, as well as the possibility of reusing adsorbents [3]. The application of magnetic nanocomposites as adsorbents for wastewater treatment has proven effective, due to their unique physical and chemical properties and easy separation from the solution [4].

Experimental

The magnetite/carbon nanocomposite was obtained by combustion method [5] using iron oxide as an oxidizing agent and L-arginine as a reducing agent. The synthesized magnetic nanocomposite was investigated as adsorbent material for the removal of cationic dye: *Methylene Blue* (MB) from colored wastewater. The effect of the working conditions: solution pH (2÷12), the amount of adsorbent (0.25÷3 g/L), initial dye concentration (10÷250 mg/L), and temperature (25°C, 40°C, 55°C), on the removal efficiency was investigated. The experimental data obtained at certain time intervals and at equilibrium were correlated with pseudo first-order and pseudo second-order kinetic models, respectively Freundlich, Langmuir, Sips and Redlich-Peterson adsorption isotherms. In order to evaluate the regeneration and reuse performance of the synthesized magnetic nanocomposite, the study was extended to six consecutive cycles of adsorption-desorption.

Results and discussion

The crystalline structure of the synthesized nanocomposite was determined by X-ray diffraction analysis and infrared spectroscopy. The synthesized material has a specific surface of 930 m^2/g and a saturation magnetization value of 4.02 emu/g.

Working under normal conditions: natural solution pH and room temperature very good removal yields greater than 92% were obtained, for MB dyes. Kinetic studies showed that the adsorption process was best described by the pseudo second order model. The data obtained at equilibrium were best correlated by the Sips isotherm model, and the maximum adsorption capacitie was determined as: 132.52 mg/g for MB. The determination of thermodynamic parameters (Gibbs free energy, enthalpy and entropy) indicated that the adsorption process is spontaneous and endothermic in nature.

The regeneration capacity of the synthesized nanocomposite was studied in consecutive adsorption-desorption cycles, yields of over 75% being recorded even after the 6^{th} cycle for the MB dye.

Conclusion

The experimental results indicate that the synthesized magnetite/carbon nanocomposite exhibits a very good adsorption capacity, which recommends it as a versatile and promising material for industrial wastewater treatment.

Acknowledgements

This work was supported by Program no. 2 of the “Coriolan Drăgulescu” Institute of Chemistry of Romanian, Research Project no. 2.4

References

[1] T. Adane, A.T. Adugna, E. Alemayehu, J. Chem. (2021) 1-14.
[2] A. Al Prol, Asian J. Fish. Aquat. Res. (2019) 1-18.
[3] S. Moosavi, C. Lai, S. Gan, G. Zamiri, O. Akbarzadeh Pivehzhani, and M. Johan, *ACS Omega*, 5 (2020) 20684-20697.
[4] M.A. Nistor, S.G. Muntean, R. Ianoş, R. Racoviceanu, C. Ianaşi, and L. Cseh, Appl. Sci., 11 (2021) 9236.
[5] R. Ianoş, C. Păcurariu, and G.Mihoc, Ceram. Int. 40 (2014) 13649-13657.

AMMONIUM REMOVAL FROM AQUEOUS SOLUTION IN PRESENCE OF ORGANIC COMPOUNDS, USING BIOCHAR FROM BANANA LEAVES. COMPETITIVE ISOTHERMS MODELS

Fernanda Pantoja[1], Sándor Beszédes [2], Tamás Gyulavári [3], Erzsébet Illés[4], Gábor Kozma[3], András Sápi[3] and Zsuzsanna László [2],

[1] *Doctoral School of Environmental Sciences, University of Szeged, H-6720 Szeged, Hungary*
[2] *Department of Process Engineering, University of Szeged, H-6725 Szeged, Hungary*
[3] *Department of Applied and Environmental Chemistry, Institute of Chemistry, University of Szeged, Rerrich Béla Sqr. 1, H-6720 Szeged, Hungary.*
[4] *Department of Food Engineering, University of Szeged, H-6725 Szeged, Hungary*
e-mail: fliceth@hotmail.com

Abstract

With the imminent threat of water contamination and its increasingly expensive treatment, the challenge of finding solutions with environmentally friendly and low-cost systems, operations and materials to address the imperative of conserving essential resources. Biochar can remove a wide range of pollutants from water such as ammonium, however, the effectivity of adsorption may be affected by other pollutants of wastewater. Thus, this study aims to determine the efficiency of biochar as an adsorbent of ammonium in aqueous solutions in the presence of some selected organic compounds as bovine serum albumin (BSA), lactose and acetic acid. The biochar was produced from banana leaves at 300°C, then modified with NaOH. Biochar was characterised by SEM and FTIR, specific surface area was determined by BET measurements. Batch experiments were carried out to investigate the ammonium adsorption capacity and the competitive adsorption mechanism. Results show that the highest ammonium removal rate occurs at pH 9 with a dose of 500mg of biochar in 2 hours. The maximum NH_4^+ adsorption capacity was 0.97 mg/g without organic compounds according to Langmuir model in a monolayer condition. The isotherm model that best fits the data obtained is Harkins-Jura model. The presence of organic compounds in the aqueous solution significantly impacts the adsorption of ammonium by biochar. The data obtained during competitive adsorption experiments are fitted to the Aranovich-Donohue isotherm model.

Keywords: biochar, water treatment, adsorption, ammonium removal, competitive adsorption.

Acknowledgements

Project no. 2019-2.1.11-TÉT-2020-00152 has been implemented with the support provided by the Ministry of Innovation and Technology of Hungary.

DRUG DELIVERY SYSTEMS USING Zr-BASED METAL ORGANIC FRAMEWORK MATERIALS

Ana-Maria Putz[1], Roxana Nicola[1], Carmen Cretu[1], Elena-Mirela Picioruş [1] and Corina Duda-Seiman [2]

[1] "Coriolan Drăgulescu" Institute of Chemistry, Bv. Mihai Viteazul, No.24, RO-300223, Timisoara, Romania
[2] West University of Timisoara, Biology-Chemistry Department, Johann Heinrich Pestalozzi No. 16, RO-300115, Timisoara, Romania
e-mail: putzanamaria@yahoo.com

Abstract

Tests of drug loading and release in different buffered solutions were performed. Captopril and ibuprofen were chosen as model drugs. Zr-based metal–organic frameworks were used as drug carriers envisaged for controlled drug release. The carriers demonstrated enhanced drug-loading capacity and showed relatively good results in drug delivery. The cumulative percentage of drug release in phosphate-buffered solution at pH 7.4 was higher than that in buffered solution at pH 1.2. The release rate could be controlled by changing the pH of the releasing solution. Different captopril release behaviors were observed when the experiments were performed using a permeable dialysis membrane. By applying different kinetic models resulted that the mechanism of drug release in various pH media, obeyed Fickian diffusion.

References

[1] C. Cretu, R. Nicola, S.-A. Marinescu, E.-M. Picioruş, M. Suba, C. Duda-Seiman, A. Len, L. Illés, Z.E. Horváth, A.-M. Putz, Performance of Zr-Based Metal–Organic Framework Materials as In Vitro Systems for the Oral Delivery of Captopril and Ibuprofen. *Int. J. Mol. Sci. 24* (2023) 13887.

MERCAPTOPROPYL FUNCTIONALIZED MESOPOROUS SILICA AS CARRIERS FOR CLOTRIMAZOLE

Diana-Oana Rusu, Ana-Maria Putz

"Coriolan Drăgulescu" Institute of Chemistry, Bv. Mihai Viteazul, No. 24, 300223
Timisoara, Romania;
e-mail: dianaoanarusu@yahoo.com

Abstract

Mesoporous silica particles were synthesized by sol-gel method in order to be tested for their drug loading and release properties, starting from mixed silica precursors, tetraethoxysilane and mercaptopropyltriethoxysilane using the co-condensation method. The carriers demonstrated enhanced drug loading capacity of 99.87% and also showed good results in drug delivery. The cumulative percent of drug release in acidic buffered solution was 45.07% after 3 hours of release. The in vitro release data were applied to various kinetics models to predict the drug release mechanism and kinetics. A good coefficient of determination was obtained for Higuchi model. The drug release mechanism in acidic obeyed the Fickian diffusion mechanism. Considering the material characterisation N_2 adsorption-desorption isotherms were determined by N_2-physisorption measurements at 77 K for simple material as well for the material after functionalization with mercaptopropyl. After functionalization, the specific surface area decreases from 1213 m^2/g to 69.34 m^2/g and the pore diameter, from 3.54 to 2.4 nm but the total pore volume increases slightly from 0.8 to 1.05 cm^3.

References

Len, A.; Paladini, G.; Románszki, L.; Putz, A.-M.; Almásy, L.; László, K.; Bálint, S.; Krajnc, A.; Kriechbaum, M.; Kuncser, A.; et al. Physicochemical Characterization and Drug Release Properties of Methyl-Substituted Silica Xerogels Made Using Sol–Gel Process. *Int. J. Mol. Sci.* 2021, *22*.

INVESTIGATION OF FOULING PARAMETERS IN ULTRAFILTRATION WITH 3D PRINTED TURBULENCE PROMOTER

Nikolett Sz.Gulyás[1], Cecilia Hodúr[2], Szabolcs Kertész[2],

[1]Institute of Environmental Science and Technology, University of Szeged, H-6725 Szeged, Tisza Lajos krt. 103., Hungary
[2]Department of Biosystems Engineering, Faculty of Engineering University of Szeged, H-6725 Szeged, Moszkvai krt. 9., Hungary
e-mail: gulyasn@mk.u-szeged.hu

Abstract

Dairy factories annually generate an increasing amount of wastewater, which can cause eutrophication due to high concentrations of amino acids and lipids. To address this issue, membrane technology has emerged as a promising solution, but membrane fouling remains a significant challenge, since it can cause decreased flux, decrease membrane rejection performance, and increased energy demand. There may be a solution to the problem the use of three-dimensional printed (3DP) turbulence promoters integrated into membrane modules. These 3DP elements offer innovative opportunities to mitigate fouling by optimizing membrane modules with turbulence promoters.

In this study we designed and fabricated a 3DP turbulence promoter to mitigate membrane fouling in a classic dead-end membrane separation cell. This turbulence promoter was inserted into the ultrafiltration device, which was tested with commercially available polymer membrane to increase local shear stress on the membrane surface. Their ultrafiltration efficiencies were compared to permeate fluxes, different resistances, and fouling index.

Ultrafiltrations were compared with and without turbulence promoters at different pressures (0.1 and 0.2 MPa) and stirring velocities (100, 200, 300 and 400 rpm).

Acknowledgements

This study was financed by the Hungarian National Research, Development and Innovation Office, project NKFI-FK-142414.

NOVEL PLATINUM COMPLEXES WITH SCHIFF BASES AND α-DIOXIMES, THEIR PHYSICO-CHEMICAL AND BIOLOGICAL STUDY

Csaba Várhelyi jr.[1], Roland Szalay[2], György Pokol[3], János Madarász[3], Péter Huszthy[3], Melinda Simon-Várhelyi[1], Róbert Tőtős[1], Raluca-Anca Mereu[1], Judit Papp[4], Judith Mihály[5]

[1] *Faculty of Chemistry and Chemical Engineering, "Babeş-Bolyai" University, RO-400 028 Cluj-Napoca, Arany János str. 11, Romania*
[2] *Institute of Chemistry, "Eötvös Loránd" University, H-1117 Budapest, Pázmány Péter str. 1/a, Hungary*
[3] *Faculty of Chemical Technology and Biotechnology, Budapest University of Technology and Economics, H-1111 Budapest, Műegyetem rkp. 3, Hungary*
[4] *Faculty of Biology and Geology, "Babeş-Bolyai" University, RO-400 084 Cluj-Napoca, Mihail Kogălniceanu str. 1, Romania*
[5] *Institute of Materials and Environmental Chemistry, Research Centre for Natural Sciences, H-1117 Budapest, Magyar tudósok körútja 2, Hungary*
e-mail: csaba.varhelyi@ubbcluj.ro

Abstract

In our research project we prepared the following platinum(II) complexes with Schiff bases and α-dioximes, such as [Pt(ketone)$_2$A(L$_2$)], (ketone: 2-heptanone, 2-octanone, 3-octanone; A: hydrazine, phenylhydrazine, *o*-phenylene-diamine; L: 1-naphthylamine, 2-aminopyrimidine, 2-methylimidazole, 2-amino-4-methylpyridine) and [Pt(DioxH)$_2$L$_2$], (DioxH$_2$: methyl-phenyl-dioxime, butyl-methyl-dioxime; L: 1-naphthylamine, 2-methyl-imidazole, 2-amino-4-methylpyridine, lepidine, 2-methylpyridine, *m*-toluidine, dicyclohexyl-amine, 4-isopropylamine, cyclohexylamine), by the reaction of PtCl$_2$ in suitable solvent. After a short bibliographical survey, involving the classification and evolution of platinum complexes with possible applications, we analyzed their physico-chemical properties using FTIR, Raman, NMR, UV-VIS spectroscopy, powder X-ray diffraction (XRD), mass spectrometry, thermal analysis (TG, DTG, DTA) and SEM. We also studied the antibacterial effect of complexes on different strains of bacteria. This class of compounds has relevance in biochemistry, some of them are antibacterial agents and potential anti-tumor drugs.

Introduction

Following the discovery of the anticancer properties of cisplatin, there has been a vast interest in the scientific community to develop metal-based drugs. Cisplatin inhibits the replication of cancer cells by forming covalent cross-links with DNA, which distorts its helical structure and prevents repair and replication, resulting in apoptosis [1].

Besides the biological applications of metal complexes with Schiff base type ligands, they can be used in various dye, drugs, polymer industries and exhibit luminescence properties. In biological applications, they have been studied mainly for their insecticidal, fungicidal, antibacterial, anticancer, and inflammatory activities [2].

Over the past decades, the Pt(II) complexes have been extensively investigated as optoelectronic materials owing to their outstanding photoelectronic properties enabling them for potential applications such as light-emitting devices, chemosensors, and luminescent imaging agents [3].

In this paper we report the synthesis and characterization of novel platinum complexes with Schiff bases and α-dioximes.

Experimental

Used materials: $PtCl_4$, Bu-Me-DioxH_2, Me-Ph-DioxH_2, 2-heptanone, 2-octanone, 3-octanone, hydrazine, phenylhydrazine, *o*-phenylene-diamine, 1-naphthylamine, 2-aminopyrimidine, 2-methylimidazole, 2-amino-4-methylpyridine, 2-methylimidazole, lepidine, 2-methylpyridine, *m*-toluidine, dicyclohexylamine, 4-isopropylamine, cyclohexylamine, MeOH, EtOH.

Methods:

- Synthesis of [Pt(ketone)$_2$A(L$_2$)] type complexes

1.5 mmol $PtCl_4$ (0.5 g) was reduced with 1 ml formic acid and dissolved in 5 ml distilled water before its use in the complex synthesis:

$$PtCl_4 + HCOOH \rightarrow PtCl_2 + CO_2 + 2\ HCl$$

3 mmol ketone (2-heptanone, 2-octanone or 3-octanone) and 1.5 mmol diamine (hydrazine, phenylhydrazine or *o*-phenylene-diamine) were dissolved in 5 ml MeOH, and then refluxed for 1–2 hours. The resulting colored solution was added to the aqueous solution of the reduced platinum salt ($PtCl_2$). At last 3 mmol amine (1-naphthylamine, 2-aminopyrimidine, 2-methylimidazole or 2-amino-4-methylpyridine) dissolved in 10 ml MeOH was added. The obtained mixture was refluxed in a water bath for 2–3 hours. After cooling the crystalline complexes were filtered off, washed with MeOH–water mixture (1:1), and finally dried on air. A typical reaction is the following:

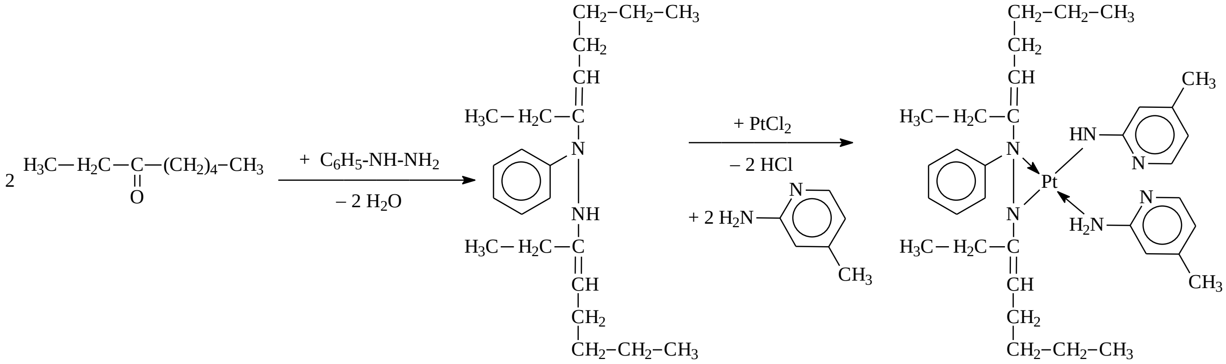

- Synthesis of [Pt(DioxH)$_2$L$_2$] type complexes

2 mmol α-dioxime (Bu-Me-DioxH_2 or Me-Ph-DioxH_2) was dissolved in 20 ml EtOH or MeOH, and then added to the aqueous solution of 1 mmol reduced platinum salt ($PtCl_2$). Afterwards 2 mmol amine (1-naphthylamine, 2-methylimidazole, 2-amino-4-methylpyridine, lepidine, 2-methylpyridine, *m*-toluidine, dicyclohexylamine, 4-isopropylamine or cyclohexylamine) dissolved in 5 ml EtOH or MeOH was added. The obtained solution was heated for 2–3 hours on a water bath. After cooling the crystalline complexes were filtered, washed with MeOH–water mixture (1:1). A typical reaction as an example is shown below:

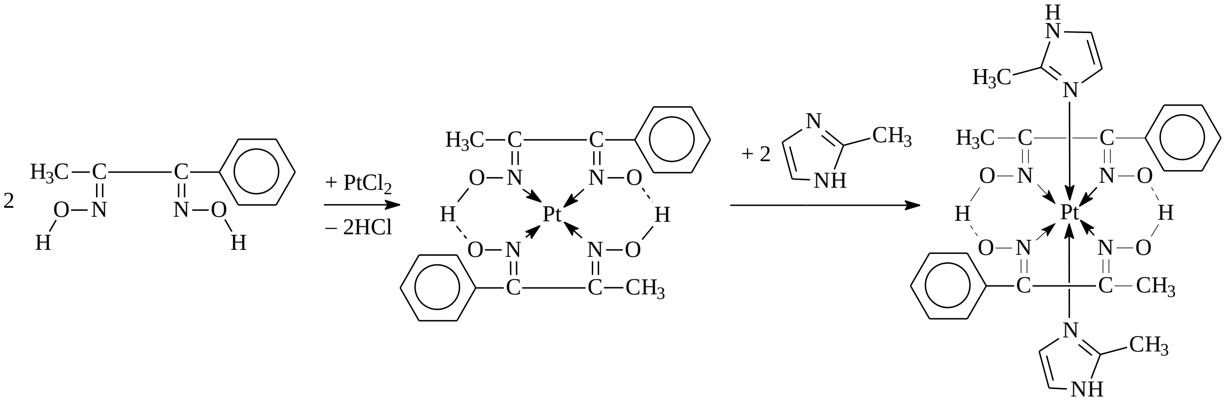

Results and discussion

Microscopic characterization and yields of the prepared complexes are presented in Table 1.

Table 1. Microscopic characterization, calculated molar masses and yields of the prepared complexes.

Nr.	Compound	Calc. mol. mass	Yield (%)	Microscopic characterization
1.	[Pt(2-heptanone)$_2$(hydrazone)(1-naphthylamine)$_2$]	703.83	12	Dark violet irregular microcrystals
2.	[Pt(2-octanone)$_2$(hydrazone)(2-amino-pyrimidine)$_2$]	635.71	12	Brown, small triangle-based prisms
3.	[Pt(2-octanone)$_2$(Ph-hydrazone)(2-am.-pyrimidine)$_2$]	712.82	50	Dark brown, small triangle-based prisms
4.	[Pt(2-octanone)$_2$(o-phenylenediamine)(2-Me-imidazole)$_2$]	685.81	25	Reddish-brown triangle-based prisms (microcrystals)
5.	[Pt(3-octanone)$_2$(hydrazone)]	445.50	34	Dark brown triangle-based prisms
6.	[Pt(3-octanone)$_2$(Ph-hydrazone)]	522.61	16	Brown irregular microcrystals
7.	[Pt(3-octanone)$_2$(hydrazone)(1-naphthylamine)$_2$]	731.88	40	Black triangle-based prisms
8.	[Pt(3-octanone)$_2$(Ph-hydrazone)(1-naphthylamine)$_2$]	808.98	14	Black irregular microcrystals
9.	[Pt(3-octanone)$_2$(Ph-hydrazone)(2-am.-4-Me-Py)$_2$]	738.89	10	Dark brown triangle-based prisms (microcrystals)
10.	[Pt(Ph-Me-DioxH)$_2$(1-naphthylamine)$_2$]	835.82	68	Dark blue triangle-based prisms
11.	[Pt(Ph-Me-DioxH)$_2$(2-Me-imidazol)$_2$]	713.65	41	Blue triangle-based prisms (microcrystals)
12.	[Pt(Ph-Me-DioxH)$_2$(2-amino-4-Me-pyridine)$_2$]	765.73	50	Dark blue triangle-based prisms (microcrystals)
13.	[Pt(Ph-Me-DioxH)$_2$(lepidine)$_2$]	835.82	15	Dark blue triangle-based prisms
14.	[Pt(Ph-Me-DioxH)$_2$(2-Me-pyridine)$_2$]	735.70	15	Dark blue triangle-based prisms (microcrystals)
15.	[Pt(Ph-Me-DioxH)$_2$(m-toluidine)$_2$]	763.75	41	Dark blue triangle-based prisms
16.	[Pt(Ph-Me-DioxH)$_2$(dicyclohexil-amine)$_2$]	912.08	95	Dark blue triangle-based prisms
17.	[Pt(Bu-Me-DioxH)$_2$(m-toluidine)$_2$]	723.77	24	Brown, small triangle-based prisms
18.	[Pt(Bu-Me-DioxH)$_2$(dicyclohexyl-amine)$_2$]	872.10	31	Blue triangle-based prisms (microcrystals)
19.	[Pt(Bu-Me-DioxH)$_2$(4-i-Pr-aniline)$_2$]	779.88	22	Dark violet triangle-based prisms
20.	[Pt(Bu-Me-DioxH)$_2$(cyclohexyl-amine)$_2$]	707.81	24	Dark violet triangle-based prisms (longer needle crystals)

Infrared spectroscopic study

The mid-IR spectra were recorded with a Bruker Alpha FTIR spectrometer (Platinum single reflection diamond ATR), at room temperature, in the wavenumber range of 4000–400 cm^{-1}, and the far-IR range of 500–50 cm^{-1}, respectively, on a Bio Rad – FTS 60A, PIKE Gladi ATR spectrometer, with a resolution of 4 cm^{-1}. The samples were measured in solid state (in powder form). The data of the most characteristic IR bands for some selected complexes are presented in Table 2.

Table 2. IR data of selected complexes.

Comp. cm^{-1}	2	3	5	6	7	8	10	16	17	19
ν_{O-H}	-	-	-	-	-	-	3647 w	3653 w	3224 m	3647 w
ν_{N-H}	3284 m	3281 w	3401 w	3223 w	3229 w	3112 m	3216 m	3163 w	3198 s	3200 m
ν_{C-H}	2925 s	2923 s	2918 w	2930 m	2945 w	2797 s	3056 m	3060 m	2956 m	2955 vs
$\nu_{C=C}$	1618 vs	1615 vs	1690 w	1665 s	1606 m	1606 w	1594 m	1577 w	1614 w	1646 w
$\nu_{C=N}$	1566 vs	1559 vs	1561 s	1598 s	1527 s	1528 s	1577 m	1532 s	1586 vs	1585 vs
δ_{CH2}	1490 m	1457 s	1450 w	1493 m	1459 w	1449 m	1423 m	1443 s	1465 s	1434 s
δ_{CH3}	1362 s	1357 m	1342 w	1377 w	1387 s	1398 vs	1339 m	1375 s	1377 m	1376 s
ν_{N-N}	1206 s	1203 s	1201 m	1244 m	1270 m	1288 m	-	-	-	-
ν_{N-O}	-	-	-	-	-	-	1279 m	1281 vs	1204 s	1264 s
ν_{N-OH}	-	-	-	-	-	-	1159 m	1145 s	1133 m	1192 vs
τ_{O-H}	-	-	-	-	-	-	1016 vs	967 vs	919 vs	1038 s
γ_{C-H}	785 s	757 vs	721 w	752 vs	764 vs	764 vs	697 vs	739 vs	684 vs	741 vs
ν_{Pt-N}	493 vs	436 m	482 w	503 s	455 s	455 s	485 s	510 m	481 s	509 vs
δ_{N-Pt-N}	336 s	328 m	378 m	324 vs	268 s	264 s	326 s	363 s	332 vs	336 vs

(Abbreviations: vs = very strong, s = strong, m = medium, w = weak)

The most important bands for the characterization of complexes are $\nu_{C=N}$ (1527–1598 cm^{-1}) and ν_{Pt-N} (436–510 cm^{-1}). In the far IR region δ_{N-Pt-N} deformation vibrations appear (264–378 cm^{-1}) [4]. In case of Schiff bases, if we compare the amine containing complexes, like **7** and **8**, with the amine missing compounds, like **5** and **6**, the $\nu_{C=N}$ and ν_{Pt-N} valence bands are shifted to lower wave-number values in case of the amine containing complexes, which can be explained with the –*I* effect of the amine nitrogen.

Mass spectrometry

Mass spectra of the samples were recorded on an Agilent 1200/6410B Triple Quad LC-MS/MS system using electrospray ionization (ESI). In the spectra we could detect the molecular ions and some fragments from decomposition.

NMR spectroscopic study

The ^{1}H NMR spectra were recorded in DMSO-d$_6$ in 5 mm tubes at RT on a Bruker DRX 500 spectrometer at 500 MHz, using TMS as internal reference. In the spectra of Schiff bases the aliphatic protons appear at 0.8–2.5 ppm, the aromatic protons appear between 6.7–7.8 ppm and in nitrogen containing aromatic rings at 8–8.6 ppm. In the spectra of dioxime complexes the aliphatic protons appear at 0.9–2.8 ppm, the aromatic protons appear between 6.5–7.7 ppm, in nitrogen containing aromatic rings at 7.8–8.8 ppm and the OH protons appear between 11.3–11.5 ppm.

Thermoanalytical measurements (TG-DTG-DTA)

Thermal measurements were performed with a 951 TG and 910 DSC calorimeter (TA Instruments), in Ar or N$_2$ at a heating rate of 10 K·min^{-1} (sample mass of 4–10 mg).

The thermal stability of complexes is limited within the temperature range of 100–140 °C. In the case of *[Pt(ketone)₂A(L₂)]* type complexes the first step of the decomposition mechanism is the loss of the amino (L) groups between 100–300 °C, then the *ketone* units leave between 300–415 °C. Finally the diamine (A) unit is lost between 415–530 °C. In the case of *[Pt(DioxH)₂L₂]* type complexes the first decomposition step belongs to leaving amino (L) groups, until 270 °C, then the glyoxime units leave. The end of the process is between 420–580 °C. Subsequently, the decomposition of the glyoxime unit is accompanied by big exothermic peaks. This behavior can be explained with the presence of oxygen in the molecule. The general mechanism for decomposition is as follows:

$$[Pt(DioxH)_2L_2] \rightarrow [Pt(DioxH)_2L] \rightarrow [Pt(DioxH)_2] \rightarrow [Pt(DioxH)] \rightarrow PtO$$

$$[Pt(ketone)_2AL_2] \rightarrow [Pt(ketone)_2AL] \rightarrow [Pt(ketone)_2A \rightarrow$$

$$\rightarrow [\ Pt(ketone)A] \rightarrow [PtA] \rightarrow PtO$$

UV–VIS spectroscopy

The electronic spectra were recorded with a Jasco V-670 Spectrophotometer in 10% EtOH/water solutions containing the substance in 10^{-4} mol/dm^3 concentration. Using Sörensen buffer solutions the electronic spectra were also recorded as a function of pH, and then the acidity constants were calculated, too. The obtained values were between $2.2 \cdot 10^{-12} - 3.8 \cdot 10^{-10}$.

Powder X-ray diffraction measurements

The crystal structure of the complexes was studied with powder XRD measurements, carried out on a PANalytical X'pert Pro MPD X-ray diffractometer. As being novel compounds their diffractograms can not be found in the Cambridge database. The dioxime type complexes exhibit crystalline form, the Schiff bases are amorphous, except for $[Pt(3\text{-octanone})_2(hydrazone)(1\text{-naphthylamine})_2]$ which is crystalline.

SEM (scanning electron microscopy) and EDX (energy dispersive X-ray spectroscopy analysis)

The images were taken with a JEOL JSM-5500LV scanning electron microscope. For the study the beam energy was 20 kV in order to obtain the excitation of all the elements and secondary electron detector (SED) were employed for measurement. The morphological study of the sample surface at five significant magnifications 10000x, 5000x, 1000x, 500x and 100x were recorded. In case of compound **3** the amorphous form can be observed.

Biological study

The antimicrobial effects of complexes were studied on *Staphylococcus aureus* Gram-positive bacterium. The investigations were carried out by Kirby-Bauer disk diffusion method. The complexes were dissolved in DMSO in 10 mmol/l concentration, and 30 µl was applied on sterile paper discs. The diameter of inhibition zones were: **3** – 16.33 mm, **10** – 13.66 mm, **16** – 14.83 mm.

Conclusion

In this work new platinum(II) complexes were synthesized and characterized with physico-chemical and biological methods. Thermal decomposition mechanism was monitored with thermoanalytical measurements.

Acknowledgement

The authors wish to express their thankfulness to the "Domus Hungarica Foundation" of Hungary for the several fellowships provided to Csaba Várhelyi jr.

References

[1] A. Jain, Coordination Chemistry Reviews 401 (2019) 213067.

[2] F.N. Sayed, G.G. Mohamed, R.G. Deghadi, Journal of Molecular Structure 1278 (2023) 134904

[3] T. Liu, Y.N. Chen, D.X. Tan, F.S. Han, Journal of Organometallic Chemistry 977 (2022) 122453.

[4] K. Nakamoto, Infrared and Raman Spectra of Inorganic and Coordination Compounds. Part B: Applications in Coordination, Organometallic and Bioinorganic Chemistry, Wiley J., 38, NY 1997.

BOX-BEHNKEN EXPERIMENTAL DESIGN FOR OPTIMIZATION OF VOLTAMMETRIC NANOMATERIAL-MODIFIED ELECTRODES

Javier E. Vilasó-Cadre[1,*], Juan Hidalgo-Viteri[2], Iván A. Reyes-Domínguez[1,3,], Graziella Liana Turdean[2]**

[1]Institute of Metallurgy, Autonomous University of San Luis Potosí, Mexico.
[2]"Babes-Bolyai" University, Faculty of Chemistry and Chemical Engineering, Department of Chemical Engineering, Research Centre of Electrochemistry and Non-Conventional Materials, Romania.
[3]National Council of Humanities, Science and Technologies of Mexico, Mexico City, Mexico.
*e-mail: *a321418@alumnos.uaslp.mx, ** alejandro.reyes@uaslp.mx*

Abstract

In the field of analytical chemistry, experimental designs have been used in some of the most important areas such as separations, spectroscopic analytical methods, chromatography, and electroanalytical methods. In the latter, they have been used to optimize the electroanalytical response, taking into account factors such as sweep and pulse parameters in voltammetric methods, as well as physicochemical conditions. However, the amount of catalyst is the only electrode preparation variable generally considered as part of the experimental factors. This work presents the optimization of two voltammetric sensors using a surface response experimental design considering only factors related to the preparation of the electrode. The two types of sensors most commonly used in voltammetry were considered: a carbon paste electrode (CPE) and a glassy carbon electrode (GCE), both modified with electrocatalytic nanomaterial.

The Box-Behnken experimental design was used to optimize the sensors. In the case of the CPE, the experimental factors were: the amount of nanomaterial in the paste, the amount of mineral oil, and the resting time of the electrode before being used as a voltammetric sensor for an industrial analyte. The response variable for the CPE was the peak current intensity in cyclic voltammograms. In the case of the GCE, the experimental factors were: chitosan concentration, the amount of nanomaterial in the modifier suspension, and the amount of suspension drops deposited on the electrode. The response variable for the GCE was the peak current intensity of the voltammograms for the oxidation of an environmental analyte.

The analysis of variance in the optimization of both electrodes showed the factors with statistically significant influence on the peak current (p-value < 0.05). In addition, second-order effects of both individual factors and interactions were detected for both electrodes. From the mathematical model, the main effects plot was generated for each electrode, which allowed to study the effect of the factors, and it was verified in both cases that an excess of nanomaterial decreases the sensor response due to electron transfer resistance effects at the electrochemical interface. The response surfaces allowed the determination of the optimal response conditions of the sensors, which could be experimentally verified by observing a higher peak current with respect to the non-optimized electrode. This work demonstrated that Box-Behnken experimental designs are a powerful analytical tool to improve the electrochemical response of voltammetric sensors, taking into account factors related only to the electrode preparation, which shows the importance of these in the analytical response.

SIMULTANEOUS ANALYSIS OF STILBENES, CHROMATOGRAPHIC DESIGN AND APPLICATION

Zahraa Ali [1] , Csilla Zsuzsanna Dávid[2] , Andrea Vasas[2] , István Ilisz[1], Róbert Berkecz[1]

[1]Intitute of Pharmaceutical Analysis, University of Szeged, Somogyi utca 4. H-6720 Szeged, Hungary
[2]Department of Pharmacognosy, University of Szeged, Szeged Eotvos u. 6, H-6720 Szeged, Hungary
e-mail: ali.zahraa@o365.u-szeged.hu

Introduction

Stilbenes are non-flavonoid phenolic secondary metabolites found in various medicinal plants and foods. They possess antioxidant, anti-inflammatory, antitumor, cardioprotective, and antiaging effects. Only a few data are available for analysis of stilbenes such as cis-miyabenol C, kobophenol A, carexinol A, and hopeaphenol in the literature [**1**]. Furthermore, no analytical method has been reported for the simultaneous analysis of these stilbenes using ultra-high performance liquid chromatography coupled with tandem mass spectrometry (UHPLC-MS/MS).

Experimental

An efficient targeted UHPLC-MS/MS method was developed for the simultaneous determination of stilbene derivatives in the plant extract. For the development of UHPLC separation of stilbenes, a three-dimensional model of the *in-silico* simulation software DryLab®4 was used based on our preliminary UHPLC-MS/MS measurements. The MS/MS detection was performed using optimized electrospray ionization (ESI) multiple reaction monitoring (MRM) mode.

Results and discussion

For ESI of stilbenes, higher ionization efficiency was observed in the negative electrospray mode than in the positive mode. The fragmentation behaviors of stilbenes were studied based on MS/MS measurements, and the proper fragment ions with related optimized collision energies were selected for UHPLC-MS/MS analysis. The software-based chromatographic modeling succeeded in predicting the retention times and the most appropriate conditions of the separation and was confirmed by HPLC-MS/MS measurements

Conclusion

The developed reversed-phase UHPLC-MS/MS method was successfully applied to analyze stilbenes in plant extract.

Acknowledgements

This work was supported by National Research, Development, and Innovation Office-NKFIA through projects: National Laboratory of Translational Neuroscience (NLTN) "Neurodevelopmental disorders" "Adult nervous system disorders" (RRF-2.3.1-21-2022-00011). Project no. TKP2021-EGA-32 has been implemented with the support provided by the Ministry of Innovation and Technology of Hungary from the National Research, Development and Innovation Fund, financed under the TKP2021-EGA funding scheme. The authors are grateful to Dr. Imre Molnár, the founder of "Molnár-Institute for Applied Chromatography" for providing us a license to DryLab®4.

References

[1] L. Hoferer, V.L.R. Guimarã Abreu, F. Graßl, O. Fischer, M. R. Heinrich, and S. Gensberger-Reigl. ACS Food Sci. Technol. 3, (2023), 1057−1065.

NUCLEASE DOMAINE OF COLICIN E7 UNDER HEAVY METAL

Zeyad H. Nafaee[1,2], **Balint Hajdu**[1], **Éva Hunyadi-Gulyás**[3] **and Béla Gyurcsik** [1]

[1]Department of Molecular and Analytical Chemistry, University of Szeged, H-6720 Szeged, Dóm tér 7, Hungary
[2]University of Babylon, College of Pharmacy, Hillah 51001 Babel, Iraq.
[3]Laboratory of Proteomics Research, Biological Research Centre, Temesvári krt. 62, H-6726 Szeged, Hungary
e-mail: n.zeyad@chem.u-szeged.hu

Introduction

Colicins are a group of protein antibiotics as toxins produced by strains of Escherichia coli in the extracellular medium during environmental stress as part of their defense system. [1] Colicin-producing bacteria are resistant to the action of their own colicin by a small immunity protein that binds and inactivates the cytotoxic domain of colicin. Colicins are classified into two groups according to the cell surface receptor. [1] Type E colicins bind to the protein product of the chromosomal gene btuB.[2] The ~15 kDa C-terminal DNase domain of colicin E7 is translocated into the cytoplasm, followed by hydrolysis of the chromosomal DNA of target cells.[4] NColE7 is a metal-dependent enzyme that binds a single divalent metal ion and it has three domains.[3] The core of NColE7 active site is the 32 amino acids HNH motif located at the C-terminus of the enzyme, which envelops the bound metal ion by three His residues. H544, H569, and H573 constitute the amino acids of the HNH motif and exhibit a characteristic secondary structure (Fig.1). The H545 histidine side-chain is suggested to participate in the generation of the OH^- ion nucleophile by promoting the deprotonation of the catalytic water molecule [5, 6]. Several crystal structures demonstrated that the metal ion can also bind a water molecule [7, 8], or a phosphate [5, 7, 9] or a sulphate [7,10] anion or the scissile phosphodiester bond of the substrate DNA [17,18] via the fourth binding site in the tetrahedral geometry. Previous and recent structural studies showed that the active site of colicin DNases is the HNH motif present also in homing endonucleases. This motif binds a single transition metal ion such as Zn^{2+} ion. Some environmental heavy transition metal ions may replace Zn^{2+} leading to change of the structure and catalytic properties of this enzyme. Ni^{2+} ion can remain from the purification procedure by immobilized metal ion chromatography through oligohistidine tags, Cu^{2+} is a strong Lewis acid and has high affinity to the His residues, and Cd^{2+} was selected as analogue of Zn^{2+}.

Experimental

The pGEX-6P-1 vector with an inserted mutant of NColE7-R447G- was constructed, NColE7-KGNK protein expressed and purified with N-terminal Glutathione-S-Transferase (GST) fusion according to previous described work [11]. After the protein purification, the GST tag was removed according to the described method in [11]. The buffer of the purified protein was exchanged to 20 mM N-2-hydrox-yethylpiperazine-N-2-ethane sulfonic acid (HEPES) pH 7.7 by an Amicon ultra 15 mL centrifugal filter. The purification steps were monitored via 15% (w/v) sodium dodecyl sulphate polyacrylamide gel electrophoresis (SDS PAGE) using a mixture of 116, 66.2, 45, 35, 25, 18.4 and 14.4 kDa unstained proteins as a marker. Intact MS protein analysis was performed by an LTQ-Orbitrap Elite mass spectrometer coupled with a TriVersa NanoMate (Advion) chip-based electrospray ion source. MS measurements were performed in positive mode at 120,000 resolution, The protein concentration was 3.0 µM in 2.5 mM ammonium bicarbonate buffer (pH ~7.8) with various metal ions (added as $ZnCl_2$, $CuCl_2$,

$NiCl_2$ or $CdCl_2$) at different molar ratios. Circular dichroism (CD) spectra were recorded at room temperature utilizing a Jasso J-1500 CD spectrometer using the following parameters. Wavelength range: 280-180 nm; path length: 0.2 mm (Jasco cuvette); D.I.T.: 2 sec; bandwidth: 1.0 nm; scanning speed: 50 nm/min (continuous scanning mode); each spectrum was the average of three accumulated measurements. The concentration of the enzyme was 18.0 μM in 3-10 mM HEPES, pH 7.7. The measurements were carried out with Apo-enzyme and holo-enzyme with various metals salts ($ZnCl_2$, $CuCl_2$, $NiCl_2$ and $CdCl_2$) with various molar ratio. The catalytic activity of the NColE7-KGNK mutant protein was monitored against plasmid DNA (pUC119) as a substrate. The final concentration of the enzyme was 1.0 μM, while the DNA was 74 μM for base pairs in 20 mM HEPES, pH 7.7. The DNA cleavage was performed in apo and holo forms of different metal ions of Zn^{2+}, Cu^{2+}, Cd^{2+} and Ni^{2+} at various molar ratios. The reaction mixtures were incubated at 37 °C for various periods. Aliquots of 5 μL of the reaction mixture were taken four times and the reaction was stopped by adding 5 μL of 2% (w/v) SDS solution (1% (w/v) at final concentration). The products of the DNA cleavage assays were checked via agarose gel electrophoresis (AGE). The products were run in 1% (w/v) agarose gel containing 0.5 μg/mL ethidium bromide for the visualization of the DNA.

Results and Discussion

The interaction of the NColE7-KGNK mutant protein with various transition metal ions was monitored via circular dichroism (CD) spectroscopy and MS spectrometry. As well the effect of transition metal ions on the catalytic activity of the enzyme was investigated in aqueous solutions. The Zn^{2+} ion is the native metal ion for the enzyme, but we used other transition metal ions in this work, like Ni^{2+} ion because it is the most common component of the immobilized metal ion affinity chromatography (IMAC) technique for protein purification, Cu^{2+} ion is a strong Lewis acid which could strongly compete for histidine side-chains, and Cd^{2+} ion has a d^{10} electron system in analogy to Zn^{2+} ion. The binding of Zn^{2+} ion to the apo-enzyme causes a slight but significant change in the CD spectrum, reflected in a red shift of about 2 nm and, this agreed with previous measurements. [11,12] However, addition of one equivalent of non-endogenous metal ions like Ni^{2+}, Cu^{2+}, or Cd^{2+} ions to the apo-protein caused very similar changes in the CD spectra to that related to the effect of Zn^{2+} ion. In the mass spectra two main peaks were detected upon measuring the Apo-NColE7-KGNK protein without the addition of metal ions: one with ~20% relative intensity related to that of the mono-metallated KGNK with Zn(II) and one with ~80% relative intensity. This means that the apo-enzyme easily acquires metal ions from buffers/reagents/containers/sample holders applied during the experiments. The apo-enzyme coordinated the added Zn^{2+} ions, as well as the non-endogenous metal ions (Ni^{2+} and Cd^{2+}) in the active center in mono-metallized enzyme. However, one equivalent of Cd^{2+} ions could not saturate the available Apo-protein fully; a small peak appeared related to the Apo-enzyme. In addition, Ni^{2+} ions could bind to the apo-enzyme, but they could not replace the Zn^{2+} ions, and there was ternary complexes including two different metal ions bound to the protein. Cd^{2+} ions proved to be weaker interacting agents than Ni^{2+} ions. It was difficult to prove whether the Cu^{2+} ion could replace the Zn^{2+} ion in the apo-enzyme via MS because of the small difference in the atomic weight.

The DNase activity of NColE7-KGNK was studied using pUC119 plasmid DNA as a substrate via agarose gel electrophoresis. DNA substrate mainly contains the super-helical form of the plasmid; during the cleavage first, the open circular form appears as a consequence of single-strand nicks. Then, linear DNA is formed upon double-strand cleavage. The DNA solution may contain a residual concentration of Zn^{2+} ions. The addition of one equivalent of Zn^{2+} ions, surprisingly resulting in a less active enzyme compared to the “apo” form. Supplementing one equivalent of Cu^{2+} ions to the protein provided similar behavior to that of Zn^{2+} ions. More efficient DNA cleavage is observed in the presence of Cd^{2+} ions than with Zn^{2+} or Cu^{2+} ions and less than that of the apo-protein in the absence of added metal ions. The enzyme in the presence of Ni^{2+} ions showed much higher activity than the apo-protein and in presence of Zn^{2+} used as a control. Nevertheless, it could not replace the Zn^{2+} ion for the active center.

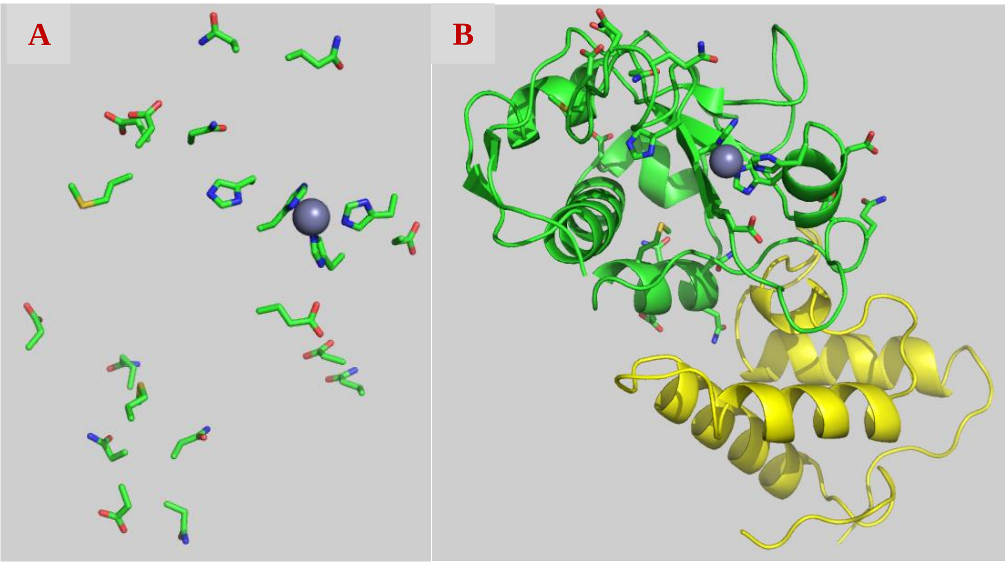

Fig. 1: Sequence and structure of the *E. coli* NColE9 (PDB code: 7CEI). A: The relative positions of the side-chains of the HNH motif and putative metal ion binding residues. B: The cartoon representation of the crystal structure of NColE9-Im9 complex with the putative metal ion binding sites were detected by the X-ray diffraction method.

Conclusion

The colicin E7 was studied in this project in the presence of non-endogenous metal ions such as Ni(II), Cu(II) and Cd(II), which may originate from environmental pollution. The purpose of use of the mutated NColE7 is the decreased activity to monitor the catalytic process. CD and mass spectrometric results revealed that all of the metal ions used in this study bound to the active center of the enzyme in the absence of Zn(II). In another word, they could not compete with Zn(II) in binding to the active site. It was detected that the enzyme is very active in the presence of tiny amount of metal ion. On the other hand, there is very high activity of the enzyme in the presence of Ni(II) and Cd(II) ions which could not be inhibited by the excess of the metal ion, but it was inhibited by Zn(II). These results suggest that the presence of these non-endogenous metal ions like Ni(II) and Cd(II) ions in the environment may lead to highly efficient toxic bacteria that can digest the other bacterial cells faster from the native one leading to biological contamination.

Acknowledgements

This research was supported by the Hungarian National Research, Development and Innovation Office (GINOP-2.3.2-15-2016-00038, GINOP-2.3.2-15-2016-00001, and GINOP-2.3.2-15-2016-00020, as well as 2019-2.1111-TÉT-2019-00089).

References

[1] R. James, C. Kleanthous, G.R. Moore. Microbiology 142 (1996) 1569–1580.
[2] R.D. Di Masi, J.E. White, C.A. Schaintman, C. Bradbeer. J. Bacteriol. 115 (1973) 506-513.
[3] Papadakos, G.;Wojdyla, J.A.; Kleanthous, C. Q. Rev. Biophys. 2012, 45, 57-103.
[4] C. Garinot-Schneider, C.N. Penfold, G.R. Moore, C. Kleanthous, R. James. Microbiology 143 (1997) 2931-2938.
[5] Huang, H.; Yuan, H.S. J Mol Biol 2007, 368, 812-821.
[6] Levin, K.B.; Dym, O.; Albeck, S.; Magdassi, S.; Keeble, A.H.; Kleanthous, C.; Tawfik, D.S. Nat Struct Mol Biol 2009, 16, 1049-1055.
[7] Ko, T.; Liao, C.; Ku, W.; Chak, K.; Yuan, H.S. Structure 1999, 7, 91-102.
8 Sui, M.; Tsai, L.; Hsia, K.; Doudeva, L.; Ku, W.; Han, G.; Yuan, H. Protein Sci 2002, 11, 2947-2957.
[8] Czene, A.; Tóth, E.; Németh, E.; Otten, H.; Poulsen, J.N.; Christensen, H.E.M.; Rulíšek, L.; Nagata, K.; Larsen, S.; Gyurcsik, B. Metallomics 2014, 6, 2090-2099.
[9] Doudeva, L.; Huang, D.; Hsia, K.; Shi, Z.; Li, C.; Shen, Y.; Cheng, Y.; Yuan, H. Protein Sci 2006, 15, 269-280.
[10] Wang, Y.; Yang, W.; Li, C.; Doudeva, L.G.; Yuan. H.S. Nucleic Acids Res 2007, 35, 584-594.
[11] Czene, A.; Németh, E.; Zóka, I.G.; Jakab-Simon, N.I.; Körtvélyesi, T.; Nagata, K.; Christensen, H.E.M.; Gyurcsik, B. J Biol Inorg Chem 2013, 18, 309-321.
[12] Németh, E.; Körtvélyesi, T.; Thulstrup, P.W.; Christensen, H.E.M.; Kožíšek, M.; Nagata, K.; Czene, A.; Gyurcsik, B. Protein Sci 2014, 23, 1113-1122.
[13] Németh, E.; Balogh, R.K.; Borsos, K.; Czene, A., Thulstrup, P.W.; Gyurcsik, B. Protein Sci 2016, 25, 1977-1988.

Poster Proceedings

THE HEAVY METALS IN THE PROCESSING SCREEN PRINTING INKS

Savka Adamović[1], Ivana Tomić[1], Bojan Banjanin[1], Rastko Milošević[1], Dragan Adamović[1], Aleksandra Mihailović[1], Miroslav Dramićanin[1]

[1]Faculty of Technical Sciences, University of Novi Sad, 21000 Novi Sad,
Trg Dositeja Obradovića 6, Serbia
e-mail: adamovicsavka@uns.ac.rs

Abstract

The contents of heavy metals were analyzed in the two types (solvent-based and water-based) of processing screen printing inks. Mass concentrations of heavy metals (copper, iron, zinc, manganese, chromium, nickel, cadmium, and lead) were determined in the tested screen inks by combining the gravimetric method and atomic absorption spectroscopy. The results indicated that the measured mass concentration of copper (2049.9 mg kg^{-1}) in solvent-based cyan ink is 2.4 times higher than in water-based cyan. Other detected metals show higher concentration values with water-based processing inks.

Introduction

The printing industry uses different types of ink, which may be more or less harmful to the environment. It is impossible to determine the ecologically optimal composition of inks because each printing technique dictates the content of specific components due to the quality and speed of printing [1]. The composition of printing inks includes natural and synthetic organic or inorganic pigments whose main disadvantage is their environmental unacceptability [2].

Experimental

The processing screen printing inks (cyan - C, magenta - M, yellow - Y, and black - K) based on solvent (S) and water (W) were digested by using the dryash method (500°C, 6 h). After digestion, 5 g of each sample was weighed (with an accuracy of ±0.01 g) in a ceramic crucible and diluted with 50 mL of 0.5 mol L^{-1} nitric acids (p.a., Merck, Germany). The sample blanks have also been performed with an empty ceramic crucible. After samples were cooled to room temperature in a desiccator, the solutions were filtered through a quantitative cellulose filter paper (Macherey-Nagel, Germany). Heavy metals analyses were carried out by atomic absorption spectroscopy (PerkinElmer Aanalyst 700) according to the standard EPA 7000B method. Heavy metal contents were assessed on a triplicate sample ($n = 3$), and mean values were used [3].

Results and discussion

The mass concentration (γ, mg kg^{-1}) levels of copper, iron, zinc, manganese, chromium, nickel, cadmium, and lead in the CMYK processing solvent and water-based screen printing inks are presented in Figure 1. Based on the obtained results of the analysis of the content of heavy metals in the screen printing inks, it is observed that the highest concentration of copper is in solvent-based cyan (2049.9 mg kg^{-1}), iron in water-based yellow (30.9 mg kg^{-1}), zinc in water-based magenta (160.1 mg kg^{-1}), manganese in water-based cyan (5.4 mg kg^{-1}), chromium in water-based cyan (0.6 mg kg^{-1}), cadmium in water-based black (0.4 mg kg^{-1}), and lead in water-based magenta (2.7 mg/kg). Only in the case of copper, the measured concentration value is 57.7% higher in solvent-based than water-based cyan ink. But, iron, zinc, manganese, chromium, cadmium, and lead concentrations are higher by 82, 96, 95, 98, 79, and 78%, respectively, in water-based CMYK inks.

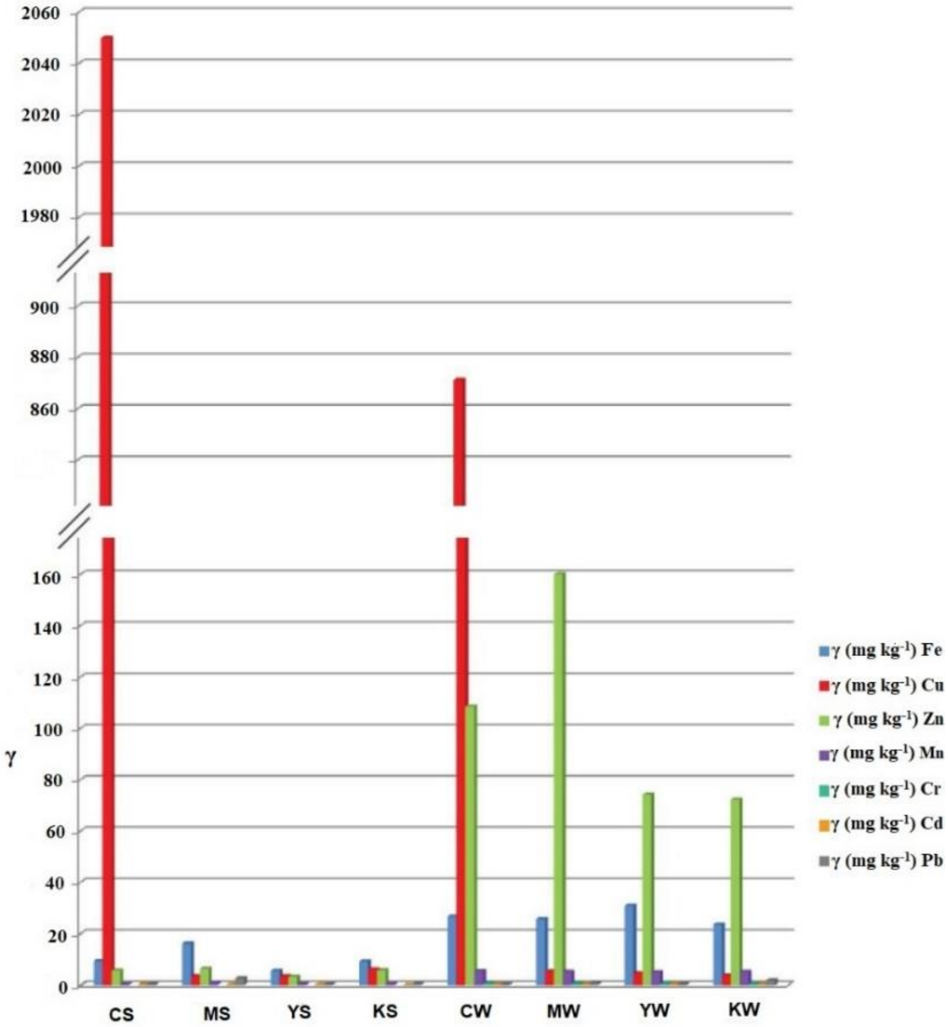

Figure 1. Mass concentration levels of detected heavy metals in the CMYK solvent and water-based screen printing inks

Conclusion

Screen printing inks contain heavy metal compounds (in pigments) and intensive drying agents - siccatives (organic salts of manganese, cobalt, or lead). The proportion of heavy metals in processing screen printing inks must be reduced, neutralized, or replaced with environmentally acceptable substances.

Acknowledgements

This paper has been supported by the Ministry of Science, Technological Development and Innovation through project no. 451-03-47/2023-01/200156 “Innovative scientific and artistic research from the FTS (activity) domain”.

References

[1] H. Kipphan, Handbook of Print Media, Technologies and Production Methods, Springer, Berlin, 2001.
[2] M. Prica, S. Adamović, Printing Materials, Faculty of Technical Sciences, Nvi Sad, 2017 (In Serian).
[3] M. Prica, S. Adamovic, B. Dalmacija, Lj. Rajic, J. Trickovic, S. Rapajic, M. Becelic-Tomin, Process Saf. Environ. Prot. 94 (2015) 262.

AB INITIO STUDY OF STRUCTURAL, ELECTRONIC AND OPTICAL PROPERTIES OF EDGE-FUNCTIONALIZED GRAPHENE QUANTUM DOTS

Tatjana Agatonović Jovin[1], Biljana Todorović Marković[1], Zoran Marković[1]

[1]Vinča Institute of Nuclear Sciences - National Institute of the Republic of Serbia, University of Belgrade, P.O. Box 522, 11001 Belgrade, Serbia
e-mail: tatjana.jovin@vin.bg.ac.rs

Abstract

Graphene quantum dots (GQD) are nano-particles small enough to exhibit unique electronic and optical properties that results from quantum confinement and edge effects. Unlike graphene they exhibit opening of the HOMO-LUMO band gap responsible for their unique optoelectronic properties high photoluminescence (PL) quantum yield, excellent photobleaching resistance and photostability, low citotoxicity, good biocompatibility, high solubility in various solvents, exceptional electrochemical activity and physicochemical stability. These characterisics of the GQDs make them suitable for a wide range of applications from biomedical applications such as diagnostics and therapy, to susteanable agricultural and environmental appications. In this respect carbon-based quantum dots such as GQDs, present promising candidates for usage in biosensing and fluorescence bioimaging applications, allowing a fast, more sensitive and more selectable detection and diagnosis. As biocompatible nanoparticles, they also have the potential to revolutionize the prospects of photodynamic therapy (PDT) in clinical treatments of cancer [1] and other diseases, antibacterial [2] and preventive antivirus PDT [3], being applied as photosensitizer agents. In a meanwhile comprehensive biomedical studies should pave the way for safe and efficient use of carbon-based quantum dots in clinical applications. In the present work, we investigate the effects of size and shape variation, as well as edge-functionalization on the structural and optical properties of GQDs, using the first-principles study based on the density functional theory (DFT) and time-dependent density functional theory (TD-DFT). We investigate edge-functionalized GQDs, with oxygen-containing –OH and –COOH groups, different shapes, such as hexagonal, triangular and rectangular and zigzag/armchair edge configuration, as well as variation of size, in tailoring the optoelectronic properties and photoluminescence behaviour of GQDs leading to a wide variety of applications.

Acknowledgements

This research was supported by the Science Fund of the Republic of Serbia, grant #7741955, Are photoactive nanoparticles salvation the global infection threat? - PHOTOGUN4MICROBES. This research was also supported by the Ministry of Science, Technological Development and Innovation of the Republic of Serbia (grant numbers 451-03-47/2023-01/ 200017.

References

[1] Hua-yang Fan et al. European Journal of Medicinal Chemistry 182 (2019) 111620
[2] Biljana Z. Ristic *et al.* Biomaterials 35 (2014) 4428-4435
[3] Tanja Bulat *et al.* Materials Chemistry and Physics, 311 (2024) 128495

XYLANASE – THE ENZYME WHICH MAKES THE DIFFERENCE IN NUTRITION

Mirela Ahmadi, Lavinia Stef, Gabi Dumitrescu, Dorel Dronca, Petculescu-Ciochina Liliana, Igori Balta, Ioan Pet

Faculty of Bioengineering of Animal Resources, University of Life Sciences „King Mihai I“
from Timisoara, 300645- Timisoara, Calea Aradului 119, Romania
e-mail: ioanpet@usvt.ro, doreldronca@usvt.ro

Abstract

Nutrition plays a critical role in health status both for humans and animals, comprising very complex processes starting with the ingestion of food or feed and ending with the excretion. But in this whole chain of processes, one of the main elements is the enzyme system without which digestion could not be possible. Xylanase is one of the enzymes that can make the difference in the digestion and absorption of some carbohydrates, like the digestion and absorption of fibers, used in various fields - food processing, feed additives, biofuel production, paper and pulp industry, textile industry, as well as waste management. Biochemically, xylanase is an enzyme that breaks down xylan, a complex polysaccharide found in plant cell walls. This paper presents some characteristics of xylanase, the important role in biotechnology, and also some applications of this enzyme.

Keywords: xylanase, enzyme, biotechnology

Introduction

Enzymes play a crucial role in the digestion and nutrition of humans and other animals. They are responsible for breaking down complex food/feed molecules into simpler, more readily absorbable forms, which can be used by the body for energy, growth, and maintenance.

Xylanases are endohydrolytic enzymes that randomly cleave the main chain of β-1,4 of xylan – the polysaccharide specific to the plant cell wall. There are many types of xylanase which are different by hydrolytic activity, substrate specificity, tridimensional folding, and mechanism of action [1] More specifically, xylanases are O-glycoside hydrolases (EC 3.2.1.x) which break down the xylan, producing xylose - which is considered the first source of carbon in plants. Also, xylan is very important in cell metabolism and plant infection, due to the fact that it is produced in plant infection by different pathogens (bacteria, fungus, algae, protozoa, anthropods, and gastropods) [2].

Industries, including those in biotechnology, biofuel production, food processing, and more, often require enzymes to catalyze specific reactions under various process conditions. Enzymes can be valuable tools for enhancing the efficiency and sustainability of industrial processes.

Extremophiles are microorganisms that thrive in extreme environments, such as high temperatures (thermophiles), high pH (alkaliphiles), or low pH (acidophiles). These extreme conditions can be found in certain industrial processes. Enzymes, including xylanases, derived from extremophiles are of interest to researchers and industries because they can function under these challenging conditions.

While there has been a focus on extremophilic xylanases, the statement suggests that cold-adapted xylanases have received relatively less attention. Cold-adapted enzymes, often derived from psychrophiles (organisms that thrive in cold environments), have unique properties that make them valuable in specific industrial applications, particularly those that require enzymatic activity at lower temperatures. These enzymes are of interest because they can function efficiently in refrigerated or cold processing conditions.

The statement reflects a research and industrial bias toward extremophilic enzymes (particularly from thermophiles, alkaliphiles, and acidophiles) due to their potential utility in harsh industrial processes. However, it also points out the relative neglect of cold-adapted xylanases, which may have untapped potential for applications in industries that require enzymatic activity under cold or refrigerated conditions. As scientific understanding of these enzymes continues to evolve, there may be increasing interest in exploring their practical applications in various industrial processes.

Xylanase chemistry

Xylan as a monoglyceride is the major component of hemicellulose. Hemicellulose is formed from a complex of polymeric carbohydrates, containing carbohydrates such as xylan, xyloglucan (heteropolymer of D-xylose and D-glucose), glucomannan (heteropolymer of D-glucose and heteropolymer D-mannose), galactoglucomanan (heteropolymer of D-galactose , D-glucose heteropolymer and D-mannose heteropolymer) and arabinogalactan (D-galactose heteropolymer and arabinose heteropolymer) [3].

Hemicellulose, together with other carbohydrates such as cellulose (1,4-β-glucan) and lignin (complex polyphenolic compound), form the major polymeric constituents found in the cell wall of plants.

Xylan is an important component in wood, being found in larger quantities in the hardwood of angiosperms, where it is found in an amount of 15–30% of the cell wall content, but also in the softwood of gymnosperms, where it is found in the amount of 7–10% and in some annual plants, in the amount of up to 30% [4].

Due to the fact that xylan has a very heterogeneous and complex chemical structure, complete hydrolysis requires the participation of a wide variety of enzymes that must act in symbiosis [5]. Thus, enzymes of the endo-1,4-β-D-xylanases type (EC 3.2.1.8) randomly cleave the base chain of xylan, and enzymes of the β-D-xylosidases type (EC 3.2.1.37) only cleave the monomers of xylose at the non-reducing end of xylooligosaccharides and xylobiosis. The side groups are hydrolyzed by a complex of enzymes such as α-L-arabinofuranosidases (EC 3.2.1.55), acetylxylan esterases (EC 3.1.1.72), α-D-glucuronidases (EC 3.2.1.139), ferulic acid esterases (EC 3.1.1.1.1.), but also p-coumaric acid esterase enzymes (EC 3.1.1.-).

Xylanase – enzyme importance

Xylanases, like natural enzymes, are produced through their own metabolic pathways by different microorganisms (bacteria, fungi and actinomycetes), protozoa and molluscs, but they are also found in the rumen of higher animals [6].

Figure 1 shows the schematic chemical structure of xylan, highlighting the bonds subject to the action of specific xylanase enzymes that completely hydrolyze xylan until the formation of constituent monomeric units [7].

In recent years, xylanase has been needed in large quantities for various industries [8]. Thus, there is a need to find and select various microorganisms that produce larger amounts of xylanase. The production of xylanase must be followed by the optimization of the substrate components in order to obtain quality production, which is also significant from a quantitative point of view.

Studying and unraveling the genetic constituents of xylanase-producing microbes will bring information of great interest that helps to elucidate the enzyme's mode of action. These aspects will be useful in the kinetics of the action of xylanases for their use in industry. Microorganisms, however, also produce other proteins and secondary metabolites, and thus the crude enzyme must be purified in order to obtain purified enzymes.

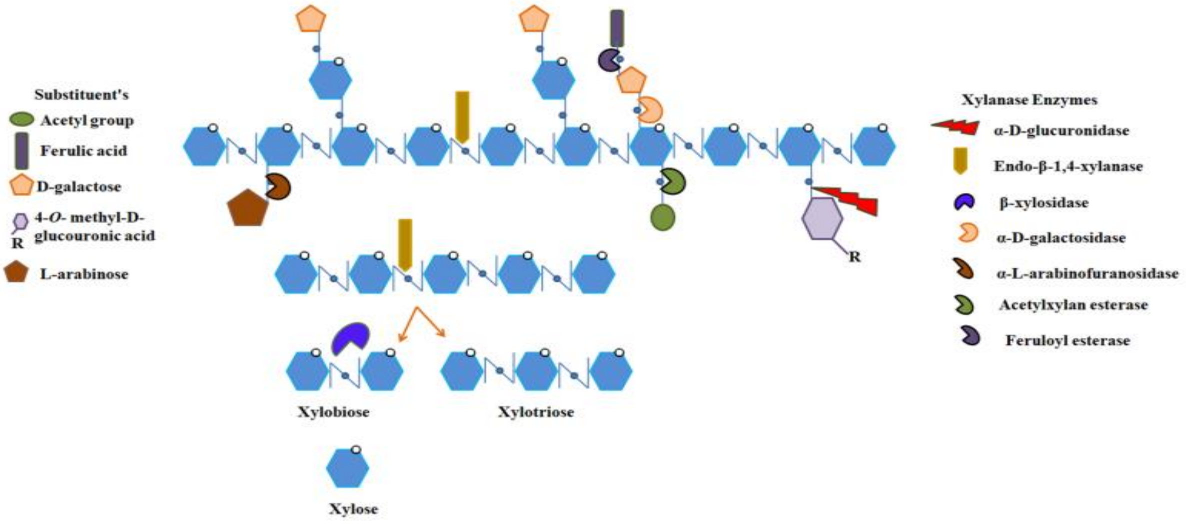

Figure 1. Xylan's chemical bonds attacked by xylanolytic enzyme specific for the complete hydrolysis of xylan [7]

The characterization of the purified xylanase will help in a better stability and specificity of the enzyme towards different substrates, and therefore a more efficient use of xylanases.

Xylanase production

For the production of specific enzymes by microorganisms, it is important that the culture medium provides a substrate with specific essential nutrients. This feature will allow you to check the strains in order to monitor the quality and quantity of enzymes or metabolites produced [9].

Thus, the process of obtaining enzymes is continuously optimized to ensure a higher production of enzymes from a specific strain of microorganisms [10] In this sense, different strategies are applied to improve performance, such as optimizing environments components - which ensure the enzyme-substrate, the regulation of the physico-chemical parameters of growth, but also the improvement of the strain's efficiency through the use of different biotechnological tools [11]. Figure 2 shows the schematic representation of the production method, purification and xylanase characterization [7].

For the production of specific enzymes, different components are selected, which must be optimized, for a better selection of the substrate and enzyme-producing microorganisms, also taking into account the regulation of nutrient concentration from the substrate (carbon, nitrogen, minerals, vitamins, amino acids), but also the optimization of the physico-chemical parameters (temperature, pH, homogenization, gas aeration, humidity, inoculum size, incubation period [12-15].

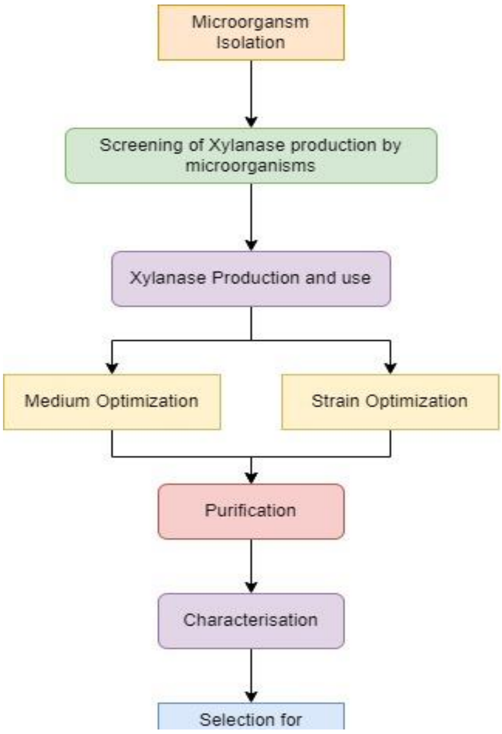

Fig. 2. Xylanase production, purification, and characterisation

Challenges and Future Trends in Xylanase Production

Efforts to discover super xylanases continue, with researchers worldwide searching for microbial sources capable of producing highly active and stable xylanase enzymes. Microbes from extreme habitats are of particular interest due to their ability to withstand harsh conditions, such as high temperatures and pH variations. Advances in biotechnological tools and techniques, including recombinant DNA technology and genetic engineering, enable the selection and transfer of xylanase-producing genes for enhanced production with specific industrial properties. Genomics, proteomics, and metabolomics data, along with bioinformatics tools, can be harnessed to develop strategies for improved xylanase production. Synthetic biology, combined with traditional recombinant DNA technology, offers opportunities to achieve high xylanase production with desired properties, although challenges related to mimicking natural systems in synthetic settings and ethical, socio-economic, and health considerations must be addressed before widespread commercial implementation.

Biofuel Production: Xylanase is used in the production of biofuels, such as ethanol, from lignocellulosic biomass. It helps to break down the xylan present in the cell walls of plant materials, making it easier to extract sugars that can be fermented into biofuels.

Paper and Pulp Industry: In the paper and pulp industry, xylanase is used to reduce the environmental impact of the paper-making process. It helps in the efficient removal of xylan, removing the need for the chemicals otherwise required for bleaching. Studies also show it could be promising in deinking waste paper, which would have a big impact on paper sustainability [16].

Animal Feed: Xylanase is used in animal feed to enhance the digestibility of feed ingredients, particularly in monogastric animals like poultry and swine. Xylanase is widely used to significantly reduce gut viscosity in wheat-based feed by breaking down soluble arabinoxylans, reducing the chance of enteric disease and increasing overall performance. Besides also increasing the nutritional value of cereal feed, studies also show it could have a positive effect on the gut microbiota[17]. The application of a mixture of xylanase and cellulase) in the breeding technology of cattle fed alfalfa, hay or timothy with 30 led to a better digestibility, but which was inferior to the application of the same percentage of xylanase to barley silage. These positive responses demonstrate the importance of interactions between dose, enzyme, and substrate. Also, the improvement of digestion coefficients and the increase in body weight in farm animals were observed [18].

Food Industry: Xylanase is used in the food industry to improve the texture and quality of baked goods, such as bread and pastries. It breaks down xylan in flour, which can improve dough handling and the final product's characteristics [19, 20].

Textile Industry: In the textile industry, xylanase can be used to remove hemicellulose impurities from cotton and other fibers, enhancing the quality of textiles, and possibly reducing the environmental footprint of textile bleaching and dyeing.

Waste Management: Xylanase can also be used in the treatment of agricultural and forestry waste, breaking down xylan-containing materials, which can help reduce environmental pollution.

Xylanase is just one example of the many enzymes and techniques used in biotechnology to manipulate and process biological materials for various industrial and research purposes, which brings new perspective to the future industry.

Conclusion

A wide variety of xylanase enzymes have been isolated, purified, and characterized to be applied in various industries. New biotechnological approaches, such as PCR screening, genome sequencing programs, as well as the study of extremophilic enzymes will bring new insights that support the understanding and much wider applications of xylanases. Xylanases act as a "green" alternative to today's industrial applications (in the production of paper, textiles, food, feed, pharmaceuticals, and biofuels). Adding xylanase to the animal diet had positive effects on growth and development, by improving digestion coefficients and increasing body weight in birds and farm animals. This demonstrates that the use of xylanases in the production technologies of various products can mediate the global economy. The methods already applied for the extraction and production of xylanases can be improved or new development strategies can be developed for an improved and more efficient production both qualitatively, quantitatively, and economically.

References

[1] T. Collins, C. Gerday, G. Feller, FEMS Microbiology Reviews 29 (2005) 3–23.
[2] R.A. Prade, Biotech. Genet. Eng. Rev., 1995, 13, 100-131.
[3] H. Shahrestani, A. Taheri-Kafrani, A. Soozanipour, O. Tavakoli. Biochem Eng J. 109 (2016) 51–58
[4] S. Singh, A.M. Madlala, B.A. Prior, FEMS Microbiol. Rev, 27 (2003) 3-16.
[5] P. Biely, M. Vršanská, M. Tenkanen, D. Kluepfel. J Biotechnol 57 (1997) 151–166.
[6] Q. Beg, M. Kapoor, L. Mahajan, G.S. Hoondal, Appl Microbiol Biotechnol 56 (2001) 326–338
[7] N. Bhardwaj, B. Kumar, P. Verma. Bioresources and Bioprocessing, 6 (2019) 40.
[8] Z. Qiu, P. Shi, H. Luo, Enzyme Microb Technol. 46 (2010) 506–512.
[9] D. Kouzounis, Journal of Animal Science and Biotechnology 13 (2022) 51.
[10] L. Zhang, J. Xu, L. Lei, Y. Jiang, F. Gao, G.H. Zhou, Asian-Australasian journal of animal sciences. 27 (2014) 855–861.
[11] D. Shallom, Y. Shoham, Curr. Opin. Microbiol. 6 (2013) 219-228.
[12] . Van Hoeck, Agriculture 11 (2021) 142-148.
[13] S.S. Dhiman, J. Sharma, B. Battan. BioResources 3 (2008) 377–1402.
[14] V. Juturu, J.C. Wu. Appl Biochem Biotechnol 174 (2014) 81–92.
[15] I. Maalej, I. Belhaj, N.F. Masmoudi, H. Belghith. Appl Biochem Biotechnol. 158 (2009) 200–212.
[16] P. Bajpai, in: Biobleaching. Bajpai P (Ed.). Biotechnology for pulp and paper processing. Springer, Berlin, 2012, pp 93–138.
[17] M. Paloheimo, J. Piironen, J. Vehmaanperä, Xylanases and cellulases as feed additives. Enzymes in farm animal nutrition. Nutr Finnfeeds Malborough, Wiltshire, 2010, pp 12–53.
[18] B. Gorenz, V. Iseri, J. Rubach, R.N. Dilger, Poultry Science 101 (2022) 102220.
[19] H.J. Bae, H.J. Kim, Y.S. Kim. Bioresour Technol 99 (2008) 3513–3519.
[20] T. Li, S. Li, L. Du, Food Chem 121 (2010) 1010–1013.

OPTIMIZATION AND COMPARISON OF HEAT, MICROWAVES, AND ULTRASOUND-ASSISTED EXTRACTION TECHNIQUES TO OBTAIN POLYPHENOL COMPOUNDS FROM HAWTHORN FRUIT *(CRATAEGUS MONOGYNA JACQ.)*

Areej Alsobh, Gyula Vatai, Szilvia Bánvölgyi

Department of Food Process Engineering, Institute of Food Science and Technology,
Hungarian University of Agriculture and Life Sciences, 1118-Budapest,Villányi út 29-4,
Hungary
e-mail: areejalsobh@gmail.com

Abstract

The objective of this study was to evaluate the effectiveness of several extraction methods such as UAE, MAE, and HAE for maximizing the recovery of phenolics and flavonoid compounds from hawthorn fruit. Chemical methods and UV-VIS spectrophotometers were used to analyze extracts obtained by these extraction methods. Response surface methodology was used to maximize the extract contents of TP and TF and the antioxidant activity in these extracts.

The experimental results showed the highest TPC and TFC (87.1±5.42 mg GAE/g and 29.87±2.09 mg QUE /g of dry weight, respectively) can be obtained from the extract of UAE. In the case of MAE extracts, the highest experimental values of extracted TPC (54.11±5.93 mg GAE/g DW), TFC (12.82±1.55 mg QUE/g DW). With HAE the supreme amounts of TPC (80.65±6.08 mg GAE/g DW), TFC (19.93±1.68 mg QUE/g DW). Similarly, antioxidant activity consistent with TPC and TFC was obtained, where the highest AA could be obtained using UAE all the assays. These response values were improved by RSM models, where the actual values calculated from the regression equations modeled by RSM were slightly higher than experimental values. Accordingly, the efficiency of the extraction method from hawthorn fruit was in order UAE > HAE > MAE. In addition, using UAE reduced used-ethanol concentration by around 50% compared to both other extraction methods, and reduced the extraction time by 90% compared to HAE.

Keywords: Hawthorn, Heat-assisted extraction, microwaves- assisted extraction, ultrasound-assisted extractions, Response surface methodology.

ECOLOGICAL DYNAMICS: THE SPREAD OF INVASIVE PLANT SPECIES IN HUNGARY'S ECOSYSTEM TYPES BETWEEN 2009-2018

Márton Bence Balogh [1], **Miklós Kertész** [2], **Katalin Török** [2,3], **Georgina Veronika Visztra** [1], **and Péter Szilassi** [1],*

[1] *Department of Geoinformatics, Physical and Environmental Geography, University of Szeged, H-6720 Szeged, Hungary; balogh.marton.bence@gmail.com (M.B.B.); myosotis.sylvatica12@gmail.com (G.V.V.)*
[2] *Centre for Ecological Research, Institute of Ecology and Botany, H-2163 Vácrátót, Hungary; kertesz.miklos@ecolres.hu (M.K.); torok.katalin@ecolres.hu (K.T.)*
[3] *National Laboratory for Health Security, Centre for Ecological Research, 29 Karolina Street, H-1113 Budapest, Hungary*
** Correspondence: toto@geo.u-szeged.hu; Tel.: +36-62-544-545*

Abstract

Our research focuses on analyzing the spatiotemporal dynamics of five invasive plant species (Ailanthus altissima, Asclepias syriaca, Elaeagnus angustifolia, Robinia pseudoacacia, and Solidago spp.) in various ecosystem types in Hungary from 2009 to 2018.
Using the National Geospatial Database of Invasive Plants (NGDIP) and the Ecosystem Map of Hungary (EMH), we examine how these species' distribution and occurrence changed over time. Our methodology and findings offer valuable insights for invasive species research.
Our results indicate that Asclepias syriaca and Robinia pseudoacacia increasingly threaten grasslands and complex cultivated areas. Ailanthus altissima and Asclepias syriaca are declining in urban settings due to harsher environmental conditions, while Solidago spp. are expanding in wetlands, impacting riparian biodiversity."

Introduction

The dramatic spread of invasive plant species is a worldwide problem for nature conservation. In addition to causing the decline in the abundance of native species [1], invasive plants often pose a threat to human health due to their allergenic characteristics [2] and, in many cases, are reasons for soil degradation [3,4].

The extension of biological invasion can be extremely rapid, causing changes in ecosystem functions and conditions over a few years; this effect might fade with time in the long-term [1]. The maps of the National Geospatial Database of Invasive Plants (NGDIP) of Hungary, based on the Land Use and Coverage Area Frame Survey (LUCAS) point-cover photo data collections (2009, 2012, 2015, and 2018), showed significant changes in the extent of invasive plant distribution of Hungary [5]. Ecosystem types mean land cover and habitat types with functions related to ecosystem services.

The detailed thematic Ecosystem Map of Hungary (EMH), covering the whole territory of Hungary, has a high spatial resolution (20 × 20 m raster size as the minimal mapping unit). It offers a potential basis to evaluate the spreading trends in relation to ecosystem types when overlaid with the distribution of invasive plants of each type in Hungary [6-8].
In our research, we answered the following questions:

- What has been the trend in the level of invasion of different types of land cover (ecosystems) in Hungary between 2006 and 2018?

- Which types of ecosystems of conservation importance are most threatened by the biological invasion of the studied species?

To answer these questions, we calculated the proportions of invaded LUCAS points relative to the total LUCAS points for each year (2009, 2012, 2015, and 2018) and, then, determined the proportion in the distribution of invasion for each ecosystem type for 2009, 2012, 2015, and 2018, respectively. Based on the frequency of invasion of these four samplings in a ten-year period, we were able to identify those land-cover (ecosystem) types where the e occurrence of the species in question changed significantly between 2009 and 2018.

Materials and Methods

The first used database is the National Geospatial Database of Invasive Plants (NGDIP) of Hungary, which is part of the invasive plant monitoring initiative of the Department of Geoinformatics, Physical, and Environmental Geography at the University of Szeged, based on the LUCAS point dataset (survey of land use, land cover, and agricultural statistics for all EU member states. The investigated invasive plants were identified by the ecologists of the Department of Ecology of the University of Szeged through visual interpretation of more than 100,000 LUCAS photos from all the field observation points of 2009, 2012, 2015, and 2018 of LUCAS surveys in Hungary. The analysts aimed to identify invasive plants based on their phenological (morphological) characteristics.

Table 1. Occurrence of invasive species on the National Invasive Species Database (INOTA) of Hungary.

Invasive Species	**Invaded LUCAS Points in 2009**		**Invaded LUCAS Points in 2012**		**Invaded LUCAS Points in 2015**		**Invaded LUCAS Points in 2018**	
	(N)	**Average Invasion**	**(N)**	**Average Invasion**	**(N)**	**Average Invasion**	**(N)**	**Average Invasion**
Ailanthus altissima	86	1.64%	48	1.05%	71	1.56%	80	1.96%
Asclepias syriaca	250	4.92%	132	2.93%	195	4.40%	175	4.50%
Eleaeagnus angustifolia	251	4.94%	69	1.51%	168	3.77%	71	1.74%
Robinia pseudoacacia	1149	27.47%	714	18.20%	630	15.77%	695	20.08%
Solidago spp.	413	8.40%	299	6.89%	323	7.51%	297	7.70%
All LUCAS points in Hungary	LUCAS points in 2009		LUCAS points in 2012		LUCAS points in 2015		LUCAS points in 2018	
	5332 = 100%		4637 = 100%		4625 = 100%		4156 = 100%	

The other used database was the Ecosystem Map of Hungary (EMH) which was published in 2018 as an open-access land-cover database of Hungary. It shows the ecosystem types of Hungary in detail at a fine scale, providing an excellent tool for conservation biology, landscape ecology, and geographic research [9]. The 20 × 20 m raster resolution base map is a hierarchical system, corresponding to MAES Level 2 types of ecosystems or habitats

GIS and statistical methods. We conducted a spatial intersection between the polygons of EMH and the LUCAS points from the NGDIP dataset, then summed the number of points within each habitat type that were invaded and noninvaded with the given species. To allow time-series analysis, we had to treat the data separately by species and years. We subtracted this ratio from the national averages of invaded points for a given year per species. To determine the temporal changes in invasion of the ecosystem types, we subtracted the percentage of the national average invasion rate of each species from the infection percentage of the given ecosystem types in the examined year.

Using Microsoft Excel, we calculated the relative proportion of invaded versus noninvaded points per ecosystem type using the formula below:

$$PR_{(1-17)} = \left[\left(\frac{INV_{(1-17)}}{LUCAS_{(1-17)}}\right) \times 100\right] - \left[\left(\frac{INVH}{LH}\right) \times 100\right]$$

Number of Level 2 ecosystem types: 17
PR—invasion percentage of the ecosystem types; i.e., the proportion of LUCAS points invaded with the given species in the given year within the EMH ecosystem types (%).
INV—Total number of LUCAS points invaded with a given species within a given EMH ecosystem type in the survey year (2009, 2012, 2015, and 2018).
LUCAS—Total number of LUCAS points within a given EMH ecosystem type each year (2009, 2012, 2015, and 2018).
INVH—Total number of invaded LUCAS points in Hungary each year (2009, 2012, 2015, and 2018).
LH—Total number of LUCAS points in Hungary each year (2009, 2012, 2015, and 2018).

We calculated the percentage of LUCAS points invaded with the species each year within the EMH ecosystem types (Tables A3–A7). Using the PR values of the survey years (2009, 2012, 2015, and 2018), we calculated trends of change for each ecosystem type using linear, logarithmic, exponential, and power regression (R^2), and plotted the most significant changes on graphs. If the R2 value of the trend line for the study years was greater than or equal to 0.7 R^2 , then the change in invasion rate within the ecosystem type was considered a strong determination value. Although there is no definitive limit on what counts as a strong correlation, say |r| > 0.70, it is assumed to indicate a strong determination value. [10], The direction of change within the studied period (2009–2018) could decrease if the proportion of infection of an EMH ecosystem type with a given species decreased significantly. An increasing trend can also be distinguished if the proportion of invasion of an EMH ecosystem type with a given species increased significantly with a coefficient of determination above 0.7 R^2 .

Results and discussion

This study revealed the importance of ecosystem types regarding the level of invasion by the five investigated species based on a thorough, national-level analysis. It was already demonstrated in other studies that the invasibility (susceptibility to invasion), or the degree of invasion of habitat types can be very different [11], and mostly driven by human processes [12]. We have demonstrated these differences in the degree of invasion over a period of ten years.

This general picture shows that the studied species mainly invade intensively humanimpacted ecosystems (disturbed, cultivated, and urban); out of eleven types, only three are seminatural, native ecosystems. This demonstrates that if the structural stability ensured by species interactions (competitions and facilitations) is disturbed, newly arriving invasive species can more easily gain importance [13].

The type and intensity of land use have been recorded to influence the severity of invasion by different organisms [14]. In most studied cases, an increase in the frequency of invaded points was detected. This increase is most pronounced in the case of intensively used ecosystems, like arable land, roads and railways, other herbaceous vegetation, permanent crops, complex cultivation areas, and plantations. The higher invasibility of disturbed (mainly humanaffected) ecosystems was reported elsewhere [15,16].

This study has determined the level of invasion and its trends during ten years for five invasive species at a national level as a first survey. The data and the knowledge gained can improve awareness of the process of invasion, which has huge socioeconomic and health impacts [17]. Knowledge of the levels of invasion can help to explore how the abundance of invasive species affects species and communities and discover eventual saturation processes [1].

Shedding light on the invasibility of different ecosystems is also of great importance because it can help to identify the most vulnerable ecosystems for proactive management [18] and support further studies on which characteristics of communities influence the vulnerability against invaders [13]. As the level and the trend of invasion can vary among regions and might be different at finer scales that also influence the cost of invasion impact [17], the national-level survey must be complemented by further investigations.

Conclusion

We identified the main Ecosystem Map of Hungary (EMH) land-use (ecosystem) types within which the infestation rate of the five invasive species under study varied between 2009 and 2018 above a significant trend ($R2 \geq 0.7$). We plotted significant decreasing or increasing changes on graphs.

After completing the analysis, we can state that Ailanthus altissima is spreading rapidly near roads and railways. Asclepias syriaca occurrence is increasing in diverse, mosaic, so called complex landscapes (where the land-cover heterogeneity is high), and in natural grassland habitats. It can be concluded that grasslands are the most threatened ecosystems by plant invasion in Hungary, as Asclepias syriaca and Robinia pseudoacacia are increasingly covered in these areas. It would be important to find the best conservation management technologies (for instance, an increase in grazing livestock) to reduce the spread of these plants. Wetlands are also prone to invasion by the investigated species, especially Solidago spp. and Robinia pseudoacacia. Solidago spp. species spread in wetlands, posing a growing threat to floodplain habitats around water bodies.

The results presented in our research can contribute to the conservation of biodiversity, to understanding the spread and geographical background of invasive plants, and to the development of appropriate conservation management methods.

Acknowledgements

This poster abstract is based on our article: *Changes in the Occurrence of Five Invasive Plant Species in Different Ecosystem Types between 2009–2018 in Hungary*
(https://www.mdpi.com/2073-445X/12/9/1784)

References

[1] Vilà, M.; Espinar, J.L.; Hejda, M.; Hulme, P.E.; Jarošík, V.; Maron, J.L.; Pergl, J.; Schaffner, U.; Sun, Y.; Pyšek, P. Ecological Impacts of Invasive Alien Plants: A Meta-Analysis of Their Effects on Species, Communities and Ecosystems. Ecol. Lett. 2011, 14, 702–708

[2] . Lake, I.R.; Jones, N.R.; Agnew, M.; Goodess, C.M.; Giorgi, F.; Hamaoui-Laguel, L.; Semenov, M.A.; Solomon, F.; Storkey, J.; Vautard, R.; et al. Climate Change and Future Pollen Allergy in Europe. Environ. Health Perspect. 2017, 125, 385–391.

[3] Ehrenfeld, J.G.; Scott, N. Invasive Species and the Soil: Effects on Organisms and Ecosystem Processes. Ecol. Appl. 2001, 11, 1259–1260.

[4] Bielecka, A.; Borkowska, L.; Królak, E. Environmental Changes Caused by the Clonal Invasive Plant Solidago Canadensis. Ann. Bot. Fenn. 2020, 57, 33

[5] Kitka, D.; Szilassi, P. Geographic Factors Influencing the Spreading of Invasive Species: A Gis-Based Case Study in the Southern Great Plain of Hungary. J. Landsc. Ecol. 2016, 14, 155–169.

[6] Kovács-Hostyánszki, A.; Bereczki, K.; Czúcz, B.; Fabók, V.; Fodor, L.; Kalóczkai, Á.; Kiss, M.; Koncz, P.; Kovács, E.; Rezneki, R.; et al. Nemzeti Ökoszisztéma-Szolgáltatás Térképezés

És Értékelés, Avagy a Természetvédelem Országos Programja. Természetvédelmi Közlemények 2019, 25, 80–90.
[7] Tanács, E.; Belényesi, M.; Lehoczki, R.; Pataki, R.; Petrik, O.; Standovár, T.; Pásztor, L.; Laborczi, A.; Szatmári, G.; Molnár, Z.; et al. Országos, Nagyfelbontású Ökoszisztéma-Alaptérkép: Módszertan, Validáció És Felhasználási Lehet˝oségek. Természetvédelmi Közlemények 2019, 25, 34–58.
[8] Tanács, E.; Bede-Fazekas, Á.; Csecserits, A.; Fodor, L.K.; Pásztor, L.; Somodi, I.; Varga, A.; Vári, Á. Assessing Ecosystem Condition at the National Level in Hungary-Indicators, Approaches, Challenges. One Ecosyst. 2022, 7, e81543.
[9] Tanács, E.; Vári, Á.; Bede-Fazekas, Á.; Báldi, A.; Csákvári, E.; Endrédi, A.; Fabók, V.; Kisné Fodor, L.; Kiss, M.; Koncz, P.; et al. Finding the Green Grass in the Haystack? Integrated National Assessment of Ecosystem Services and Condition in Hungary, in Support of Conservation and Planning. Sustainability 2023, 15, 8489.
[10] Anscombe, F.J. Graphs in Statistical Analysis. Am. Stat. 1973, 27, 17
[11] Guo, Q.; Fei, S.; Dukes, J.S.; Oswalt, C.M.; III, B.V.I.; Potter, K.M. A Unified Approach for Quantifying Invasibility and Degree of Invasion. Ecology 2015, 96, 2613–2621.
[12] Chytrý, M.; Jarošík, V.; Pyšek, P.; Hájek, O.; Knollová, I.; Tichý, L.; Danihelka, J. Separating Habitat Invasibility by Alien Plants from the Actual Level of Invasion. Ecology 2008, 89, 1541–1553.
[13] Godoy, O. Coexistence Theory as a Tool to Understand Biological Invasions in Species Interaction Networks: Implications for the Study of Novel Ecosystems. Funct. Ecol. 2019, 33, 1190–1201.
[14] Liu, D.; Semenchuk, P.; Essl, F.; Lenzner, B.; Moser, D.; Blackburn, T.M.; Cassey, P.; Biancolini, D.; Capinha, C.; Dawson, W.; et al. The Impact of Land Use on Non-Native Species Incidence and Number in Local Assemblages Worldwide. Nat. Commun. 2023, 14, 2090.
[15] Nielson, K.G.; Gill, K.M.; Springer, A.E.; Ledbetter, J.D.; Stevens, L.E.; Rood, S.B. Springs Ecosystems: Vulnerable Ecological Islands Where Environmental Conditions, Life History Traits, and Human Disturbance Facilitate Non-Native Plant Invasions. Biol. Invasions 2019, 21, 2963–2981.
[16] Axmanová, I.; Kalusová, V.; Danihelka, J.; Dengler, J.; Pergl, J.; Pyšek, P.; Veˇceˇra, M.; Attorre, F.; Biurrun, I.; Boch, S.; et al. Neophyte Invasions in European Grasslands. J. Veg. Sci. 2021, 32, e12994.
[17] Turbelin, A.J.; Cuthbert, R.N.; Essl, F.; Haubrock, P.J.; Ricciardi, A.; Courchamp, F. Biological Invasions Are as Costly as Natural Hazards. Perspect. Ecol. Conserv. 2023, 21, 143–150.
[18] Ibáñez, I.; Petri, L.; Barnett, D.T.; Beaury, E.M.; Blumenthal, D.M.; Corbin, J.D.; Diez, J.; Dukes, J.S.; Early, R.; Pearse, I.S.; et al. Combining Local, Landscape, and Regional Geographies to Assess Plant Community Vulnerability to Invasion Impact. Ecol. Appl. 2023, 33, e2821

COMPARATIVE MORPHOSTRUCTURAL AND ELECTROCHEMICAL CHARACTERIZATION OF HYBRID ELECTRODE Ti-TiO$_2$/rGO CORRELATED WITH THE SYNTHESIS METHOD

Cornelia Bandas[1*], **Mircea Nicolaescu**[1], **Mina-Ionela Morariu (Popescu)**[1,2], **Corina Orha**[1], **Carmen Lazau**[1]

[1]*National Institute for Research and Development in Electrochemistry and Condensed Matter Timisoara, Dr. A.P. Podeanu no.144, 300569, Timisoara Romania; orha.corina@gmail.com; carmenlazau@yahoo.com; nicolaescu.mircea13@yahoo.com; mina.popescu37@gmail.com*
[2] *"Politehnica" University of Timisoara, P-ta Victoriei no.2, 300006 Timisoara, Romania;*
**Corresponding author: cornelia.bandas@gmail.com*

Recently, graphene has been widely used with excellent results in electrochemical sensors because of its superior electrical conductivity, high surface: volume ratio, and a rapid electron transfer rate. Because graphene's electrocatalytic activity is restricted, it is often combined with metal oxides to obtain hybrid nanomaterials [1]. To fabricate the hybrid of TiO$_2$ nanoparticles, nanospheres, and nanofibers with graphene nanosheets have been reported through various methods, such as sol–gel, hydrothermal and solvothermal method [2]. For the liquids deposition, there are a variety techniques such as dip-coating [3], spray-coating [4], doctor Blade, spin-coating etc.

This research investigated the comparative study of two different methods, as spin-coating and dip-coating, for obtaining the advanced hybrid electrodes based on reduced graphene oxide deposited onto a titanium plate anode, named Ti-TiO$_2$/rGO. TiO$_2$ nanolayer was grown on titanium foil by thermal oxidation (Ti-TiO$_2$) at 500°C in 0.5 M hydrofluoric acid. Dip-coating technique is a facile and low-cost method for fabrication of hybrid electrode Ti-TiO$_2$/rGO (code Ti-TiO$_2$/rGO1). As comparison, spin-coating methodology was used, at speed of 1500 rot and time 10 sec, being deposited 6 layers of TiO2/GO pasta on both sides of Ti support (code Ti-TiO$_2$/rGO2). Specific investigations, such as X-ray diffraction, UV-VIS analysis, and SEM morphology, were used to analyses the morpho-structural and optical properties of the obtained electrodes. The electrochemical characterization will be performed by cyclic voltammetry, in 1M KOH supporting electrolyte, scan range -0.3 V/SCE and 1.4 V/SCE.

References

1. L. Fu, S. Mao, F. Chen, S. Zhao, W. Su, G.Lai, A. Yu, C.-T. Lin , Chemosphere , 297, 2022, 134127;
2. X. Zhang, P. Suresh Kumar, V. Aravindan, H.H. Liu, J. Sundaramurthy, S.G. Mhaisalkar, H.M. Duong, S. Ramakrishna, S. Madhavi, J. Phys. Chem. C 2012, 116, 14780.
3. C. Lazau; C. Bandas; M. Nicolaescu; C. Orha; A. Pop, Proceedings of the International Semiconductor Conference, CAS, 2022, 2022-October, pp. 277–280 DOI: 10.1109/CAS56377.2022.9934754
4. H.T. Chou; S.T. Chen; C.H. Wang; H.C. Hsu; T.Y. Kao; Z.H. Lin, IEEE Journal of Photovoltaics,11, 5, 2021, 1236 – 1242, 10.1109/JPHOTOV.2021.3090168

Acknowledgements

This work was supported by a grant of the Ministry of Research, Innovation and Digitization, CNCS - UEFISCDI, project number PN-III-P1-1.1-TE-2021-0963, within PNCDI III, with contract number TE13/2022 (DD-CyT), partially project code PN 23 27 01 02 INOMAT, 23-27 29N/2023.

THE CORROSION BEHAVIOR OF Ag NANOWIRES-MODIFIED GRAPHITE ELECTRODE IN ARTIFICIAL SWEAT SOLUTION

Bogdan-Ovidiu Taranu, Madalina-Gabriela Ivanovici, Radu Banica

National Institute of Research and Development for Electrochemistry and Condensed Matter,
Dr. A.P. Podeanu street, No. 144, 300569, Timisoara, Romania
e-mail: b.taranu84@gmail.com

Abstract

An electrochemical study was performed to evaluate the corrosion behavior of a graphite electrode modified with Ag nanowires in artificial sweat solution. The electrochemical setup consisted of a PGZ 402 model Voltalab 80 potentiostat (Radiometer Analytical) connected to three electrodes that were inserted into a glass cell. The auxiliary electrode was a Pt plate with S_{geom} = 1.13 cm^2, the reference electrode was an Ag/AgCl (sat. KCl) electrode, and the working electrode was either an unmodified graphite pallet or the Ag nanowires-modified graphite sample. The modification method utilized to obtain the Ag nanowires-based electrode was the drop-casting method. Basically, a volume of 10 μL suspension was removed from an alcohol suspension containing laboratory-synthesized Ag nanowires and subsequently applied on one of the surfaces of a previously polished graphite pallet. The sample was obtained after a 24-hour drying stage at 23 ± 2 °C. Before the corrosion test, it was inserted into a polyamide support to ensure a constant S_{geom} of 0.28 cm^2. This ensemble was immersed in the electrolyte solution consisting of artificial sweat. The corrosion behavior study was carried out at 23 ± 2 °C by performing experiments with electrochemical methods specific to corrosion studies, such as the open circuit potential method and the potentiodynamic polarization technique with Tafel representation. The polarization curves were recorded at the scan rate of 1 mV/s and the VoltaMaster 4 v. 7.09 software was used to determine the values of the following corrosion parameters: the corrosion potential (E_{corr}), the corrosion current density (i_{corr}), the polarization resistance (R_p), the corrosion rate (ν_{corr}), the anodic Tafel slope (β_a) and the cathodic Tafel slope (β_c). The corrosion inhibition efficiency (IE%) was also calculated, with the equation provided by Birdeanu *et al.* [1].

The main conclusion of the study is that the electrode most susceptible to corrosion in artificial sweat solution is the Ag nanowires-modified one. If the investigation were aimed at identifying the sample with the highest corrosion resistance then the modified electrode should have been discarded. However, this is not the case. The study is part of a larger experimental scheme aimed at outlining the antibacterial effect of the Ag nanowires. The low corrosion resistance of the electrode implies an intense release of Ag ions into the electrolyte. As the concentration quickly increases, the environment becomes toxic for bacteria. Future experiments will involve the presence of such microorganisms.

Acknowledgements

This work was supported by a grant of the Ministry of Research, Innovation and Digitization, CCCDI-UEFISCDI, project number PN-III-P2-2.1-PED-2021-2541, within PNCDI II.

References

[1] A.-V. Birdeanu, M. Birdeanu, E. Fagadar-Cosma, J. Alloys Compd. 706 (2017) 220.

PUBLIC GOVERNANCE STUDENTS' OPINION ABOUT THE ROLE OF THE GOVERNMENT IN ENVIRONMENTAL RESPONSIBILITY

László Berényi[1], Nikolett Deutsch[2]

[1]*Department of Public Management and Information Technology, University of Public Service, H-1083 Budapest, Üllői road 82., Hungary*
e-mail: berenyi.laszlo@uni-nke.hu
[2]*Institute of Entrepreneurship and Innovation, Corvinus University of Budapest, H-1093 Budapest, Fővám square 8., Hungary*
email: nikolett.deutsch@uni-corvinus.hu

Abstract

Solving environmental problems goes beyond the scope of natural and engineering sciences. Social issues must be considered since people are the ultimate beneficiaries or sufferers of the related decisions. Due to the complexity of the problems and the required toolset of the solution, social aspects cover several questions. The role of the government is remarkable in financial, policy-making, and other aspects. The study deals with the individual judgment on the role of the government. The scope is limited to Hungarian higher education students as a pilot study. The results show competing patterns that can contribute to a better understanding of personal opinions.

Introduction

The government has a complex role in managing society and the economy. It is to note that the definition of government is multifaceted indeed [1]. The government can be considered as having to serve the citizens by providing rules and interventions if social interest requires it. According to the economic policy, it covers assuring the legal and institutional background, allocation in producing goods and services, redistribution of the incomes, and stabilization [2]. Of course, it is impossible to serve all concerned equally; weighting is necessary considering the policies, goals, and the availability of resources. There are more or less pro-active national policies [3]. In general, the emphasis on environmental protection and sustainability has been appreciated in recent decades. Kulin and Sevä [4] found that enhancing public support for environmental policies can be improved if people think protecting the environment is the government's responsibility.

The Good State and Government Report [5] in Hungary uses six impact areas that can be considered as the social responsibility of the government, including sustainability and public well-being. The report of 2019 noted growth in the performance of positive expectations regarding climate change, while the need for development is still marked for energy and water management, emissions, and social sustainability. Unfortunately, a more recent assessment is not available to show the impacts of the COVID-19 pandemic and the energy crisis in 2022. The main conclusion of the report and the literature in the field is that the government has a versatile set of tasks.

However, it seems to be an oversimplification to focus only on environmental issues, but holistic explanatory research in the field may contribute to the body of knowledge and can support policymakers in the future. Learning the individual perceptions of the government's role in the field can be considered a pilot study.

The research question can be formulated as what the ranking order of people is about the government's most important environmental responsibilities. A second question is whether the ranking orders differ by gender and CSR knowledge.

Experimental

The study uses a limited scope in data collection. It aims to explore the public governance students' opinions about the role of the government about its contribution to solving environmental problems. These students continue their special 5-year studies at the University of Public Service, Budapest. A voluntary online survey was prepared to investigate student opinions about sustainability and social responsibility. The questionnaire includes seven statements (listed in Table 1) about the government's responsibility for environmental issues. The respondents were asked to prioritize the list items.

This paper is based on the responses of the public governance master students in 2022. 160 responses were available for the analysis. The mean values of the rank numbers describe the priority orders, and the distribution of the rank numbers is presented. Kruskal-Wallis H test was applied to check the impact of grouping factors such as gender, CSR knowledge level, and categorization. The statistical analysis is based on [6]. The study attempts to explore patterns of opinion by cluster analysis.

Results and discussion

The respondents kept the most important item establishing a legal, economic, and technical regulatory framework to achieve environmental objectives, and second, providing economic and financial funding for environmental protection (Figure 1).

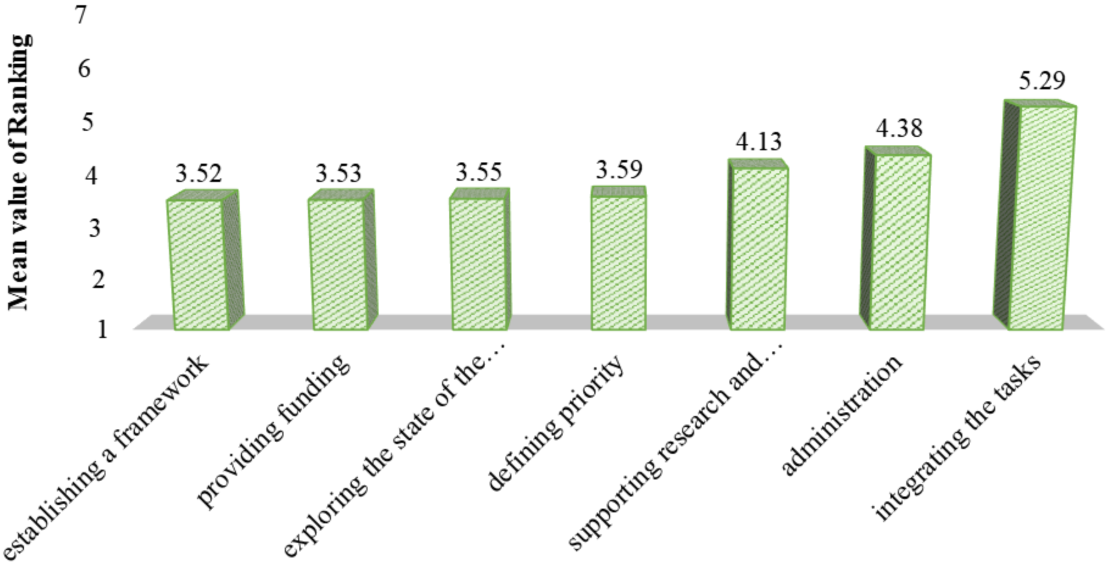

Figure 1. Mean values of the rank orders (lower value means more important issue), total sample

The mean values of the rankings are near each other, and the standard deviation is lower in the second case, suggesting a greater consensus on the importance of providing funds (Table 1).

The analysis of variance shows few significant differences by the grouping factors. Female and male opinions differ significantly from each other about Establishing a legal, economic and technical regulatory framework to achieve environmental objectives (Kruskal-Wallis H=7.533, d_f=1, sig.=0.006). According to the CSR knowledge level, respondents with more CSR knowledge believe less that the government's responsibility is exploring the quantitative and qualitative characteristics of the state of the environment and defining the state to be achieved (Kruskal-Wallis H=6.807, d_f=2, sig.=0.033).

The patterns of opinions were explored by hierarchical clustering. Ward method was applied to find minimum variance within the clusters [6]. A dimension reduction of the 7 survey items was performed by principal component analysis to filter the correlations between the evaluations. The method suggested four independent factors, saving 77.5% of the total variance. The results show a four-cluster solution (Figure 2). The clustering shows significant differences at a 95% confidence level in the evaluations of the items, except for the ranking supporting research and development.

Table 1. Mean values of the evaluations by sub-samples

	Total sample		**Gender**		**CSR knowledge**		
	Mean	*Std. Dev.*	Female	Male	None	Superficial	Detailed
Establishing a legal, economic and technical regulatory framework to achieve environmental objectives (establishing a framework)	*3.52*	*1.893*	**3.86**	**3.02**	3.74	3.14	3.35
Providing the economic and financial funding for environmental protection (providing funding)	*3.53*	*1.773*	3.36	3.78	3.51	3.21	4.17
Exploring the quantitative and qualitative characteristics of the state of the environment and defining the state to be achieved (exploring the state of the environment)	*3.55*	*2.133*	3.6	3.48	**3.8**	**3.55**	**2.52**
Defining the priority tasks for environmental protection (defining priority)	*3.59*	*2.072*	3.58	3.62	3.42	4.07	3.43
Defining and ensuring the performance of research, technical, development, training, and information activities in the field of environmental protection (supporting research and development)	*4.13*	*1.917*	4.03	4.29	4.16	4.05	4.17
Performing public administration tasks in the field of environmental protection (administration)	*4.38*	*1.832*	4.34	4.44	4.19	4.48	5
To enforce and integrate environmental requirements in other tasks of the government (Integrating the tasks)	*5.29*	*1.703*	5.24	5.38	5.19	5.5	5.35
n	*160*		97	63	95	42	23

Table 2 and Figure 2 show that differences in the mean values of the ratings by clusters are the lowest on enforcing and integrating environmental requirements in other tasks of the state and defining and ensuring the performance of research, technical, development, training, and information activities in the field of environmental protection.

A more scattered picture is about the other items, especially administrative tasks and establishing a framework. It is to be noted that lower mean values on the axis of Figure 2 mean the more important role than higher ones.

Table 2. Rank orders by clusters

Rank	**Cluster 1 (n=34)**	**Cluster 2 (n=54)**	**Cluster 3 (n=34)**	**Cluster 4 (n=38)**
1.	establishing a framework	establishing a framework	defining priority	exploring the state of the environment
2.	administration	providing fundings	exploring the state of the environment	providing fundings
3.	integrating the tasks	supporting research and development	establishing a framework	defining priority
4.	defining priority	exploring the state of the environment	supporting research and development	administration
5.	supporting research and development	administration	providing fundings	supporting research and development
6.	providing fundings	defining priority	integrating the tasks	integrating the tasks
7	exploring the state of the environment	integrating the tasks	administration	establishing a framework

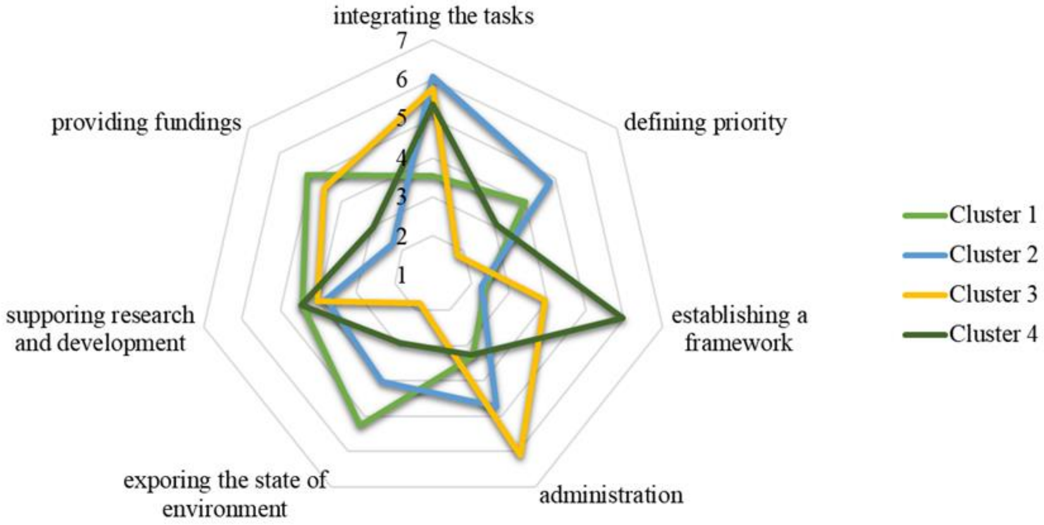

Figure 2. Mean values of the rankings by clusters

Cluster 1 includes the most balanced opinions about the government's role based on the mean values. The members expect to establish a framework, integrate the tasks, and focus on administration while supporting R&D, providing funds, or exploring the state of the environment. Cluster 2 emphasizes providing funds next to establishing a framework, but other factors are equally less important. The members of Cluster 3 agree the most that defining priorities and exploring the state of the environment are the primary governmental tasks. Cluster 4 emphasizes defining priorities and providing funds.

There is a high-level agreement among the factors in the integrative role of the government and supporting R&D.

Conclusion

However, the respondents were master-level students in the field of governmental studies; there is no unambiguous consensus among the students. The results show that there are competing opinions about the role of the government in managing environmental problems. The number of cluster members is higher in the case of Cluster 2. That cluster strongly believes that providing a framework and funding environmental problem solutions are the primary governmental tasks. Another strong opinion is presented in the case of Cluster 3, which emphasizes practical tasks in defining priorities and an active engagement of the government in exploring the state of the environment. The respondents do not highlight the integrative and administrative roles.

The results can be considered partial completion. Involving students from other faculties is planned as future research to find that these opinion patterns are limited to the sample or can be generalized. Although a hypothesis was not formulated since the study is explorative, according to the roles of the government described by the literature, the outcome differs from the author's expectations. The NIMBY phenomenon [7] seems to be reflected in the majority opinion, which needs to be changed for comprehensive results.

References

[1] Takács, P. Az állam fogalma, in: Alkotmányjog I. Alkotmányos fogalmak és eljárások. Universitas-Győr nonprofit Kft., 2014.
[2] Samuelson, P.A., Nordhaus, W.D. Economics. McGraw-Hill Education, 2009.
[3] Steurer, R. The Role of Governments in Corporate Social Responsibility: Characterising Public Policies on CSR in Europe, Policy Science 1 (2010) 49-72.
[4] Kulin, J., Sevä, I.J. Quality of Government and the Relationship between Environmental Concern and Pro-environmental Behavior: A Cross-national Study, Environmental Politics. 35 (2021) 727-752.
[5] Kaiser, T. (Ed.) Good state and Government Report. Dialóg Campus Kiadó, 2019.
[6] Pallant, J. SPSS Survival Manual: A Step by step guide to data analysis using IBM SPSS, 7th ed., Open University Press, 2020.
[7] Dear, M. Understanding and overcoming the NIMBY syndrome, Journal of the American Planning Association, 3, 288-300.

CORROSION BEHAVIOR OF NEW TITANIUM ALLOY FOR BIOMEDICAL APPLICATIONS

Matteo Bertapelle[1], Santiago Brito-Garcia[2], Julia Claudia Mirza-Rosca[2,3], Madalina Simona Baltatu[4], Petrica Vizureanu[4]

[1]Department of Information Engineering, University of Padova, Via VIII Febbraio, 2, 35122 Padova PD, Italia
[2]Dpto. de Ingeniería Mecánica, Universidad de Las Palmas de Gran canaria, Campus Universitario Tafira, 35017, Las Palmas de gran Canaria, Spain
[3]Materials Engineering and Welding Department, Transilvania Univerity of Brasov, 29 Eroilor Blvd., Brasov, Romania
[4]Department of Technologies and Equipments for Materials Processing, Faculty of Materials Science and Engineering, Gheorghe Asachi Technical University of Ia¸si, Blvd. Mangeron, No. 51, 700050 Iasi, Romania;
e-mail: matteo.bertapelle@studenti.unipd.it

Abstract

The biomedical field is in constant evolution and improvement, for such reason we've decided to search for a possible material to overcome the limitations of some of the most common biomaterials utilized, such as Titanium, known for its high biocompatibility and corrosion resistance and used for bone implants and bone fixation parts, or such as Zirconium, a material wuth good chemical stability and mechanical properties, with orthopedical and dental applications, our proposal is a material called R4, an alloy composed of Ti15Mo7Zr15TaSi, which we belive could one day overcome the previous materials in the biomedical field.

Introduction

In this study we chose two commonly used biomaterials Titanium and Zirconium, vastly used in bone implants for their mechanical properties and resistance to biological enviroment, and our alloy called R4, Ti15Mo7Zr15TaSi, which thanks to its composition might be a perfect candidate for orthopedic applications, having mechanical properties similar to the ones of human cortical bone.

For such reason in this study we've decided to analyze a critical aspect for biomaterials, the corrosion behavior, and to compare the new Titanium alloy called R4, with both Titanium, Ti, and Zirconium, Zr.

Experimental

For the experiment we first obtained the samples from the Faculty of Material Science and Engineering at Gheorghe Asachi Technical University in Iasi, Romania, already cut and grinded so that we could have a cylinder of around 2 cm of height, composed of a metallic core and a resin casing, we then proceeded to polish them with alumina suspension in Struers TegraForce-1 polishing machine for 40 seconds. For the electrochemical experiments, a sample was placed in an electrochemical cell with three electrodes: the samples served as the working electrodes, the reference electrode was a saturated calomel electrode and the counter electrode was made of platinum. In order to conduct the experiments, the area of each sample was measured. The mmol/L concentration of the Ringer solution developed by Grifols' Laboratories (Barcelona, Spain) was as follows: Na+ 129.9, Cl− 111.7, K+ 5.4, Ca2+ 1.8, and C3H5O3 27.2. Corrosion potential vs time, linear potential and electrochemical Impedance Spectroscopy were applied using the BioLogic Essential SP-150 potentiostat from Seyssinet-Pariset, France. The tests were

conducted in aerated Ringer solution at 25 °C. and to submerge the sample's part with the exposed material in Ringer solution at 25° C for a time of 24 hours, after this we exported the data from the program EC-lab and used them to obtain various graphs in Excel.
To analyze potential corrosion The "Ecorr vs. Time" method from the Ec-Lab application was used to calculate each sample's corrosion potential during a 24-hour period. Every 300 s or every time there was a 100 mV shift in potential, potential readings were obtained. The information was then gathered and a potential versus time graph was made once the data was examined.
We polished again the samples with alumina suspension in Struers TegraForce-1 polishing machine for 40 seconds and proceeded to do a microhardness test, with microhardness tester machine FM-810, using loads of 1g, 5g, 10g, for 10 measurements each, for a time of 20 seconds each measurement.

Results and discussion

Regarding the Corrosion potential (see Figure 1) we can observe how R4 possesses a tendency to passivate while both Zr and Ti tends to slowly corrode.

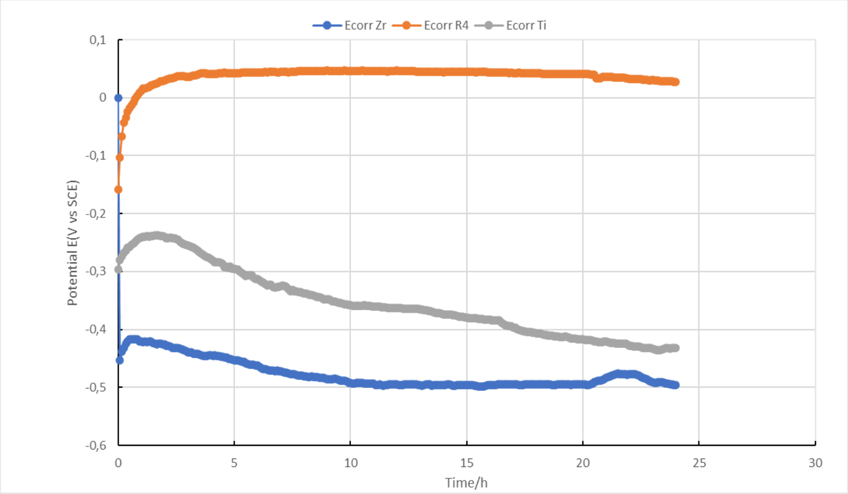

Figure 1. Corrosion Potential of the three analyzed samples in Ringer solution

While evaluationg Bode-phase (see Figure 2) we can see how in both Titanium and R4 alloy we have a large zone with high phase angle, meaning that both have high corrosion resistance poperties, while Zr presents a narrow not point dense pit which can be associated to a passivating effect not very effective that can't protect enough the material,

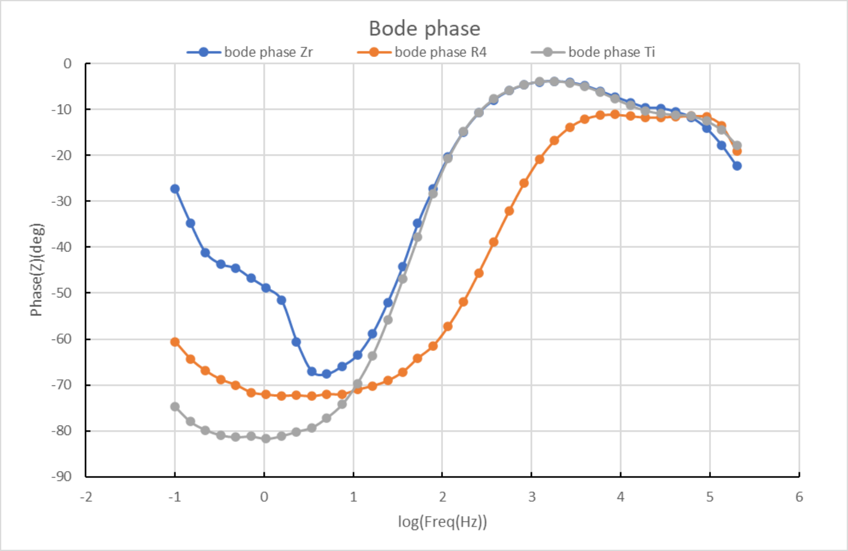

Figure 2. Bode-phase of the analyzed samples in Ringer solution

We can verify what was previously said looking at the Bode-IZI graph (see Figure 3), here we can see that Zr has a high impedence level, corresponding to good corrosion resistance, that is salso true for R4 and Ti, with R4 presenting a longer deminishment with the increase of the frequency.

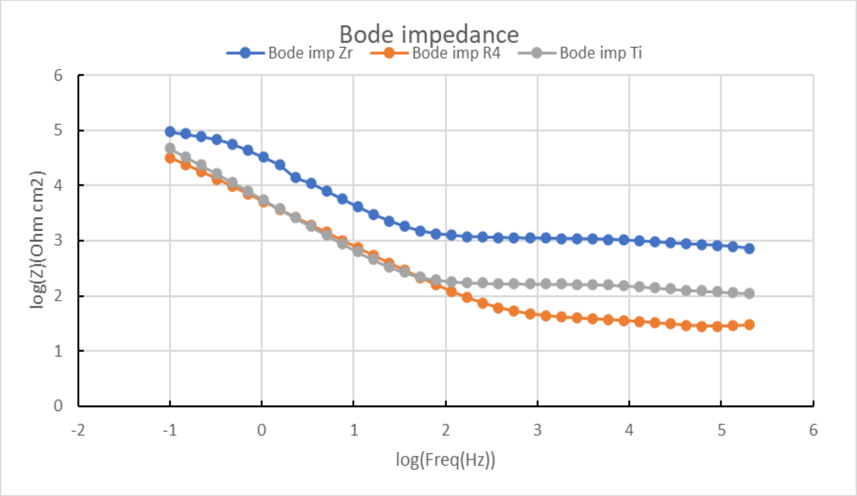

Figure 3. Bode-IZI graph of the analyzed samples in Ringer solution

Again with Nyquist (see Figure 4) we can validate what was said before, with Zr exhibiting highest Corrosion resistance, followed but Titanium and R4

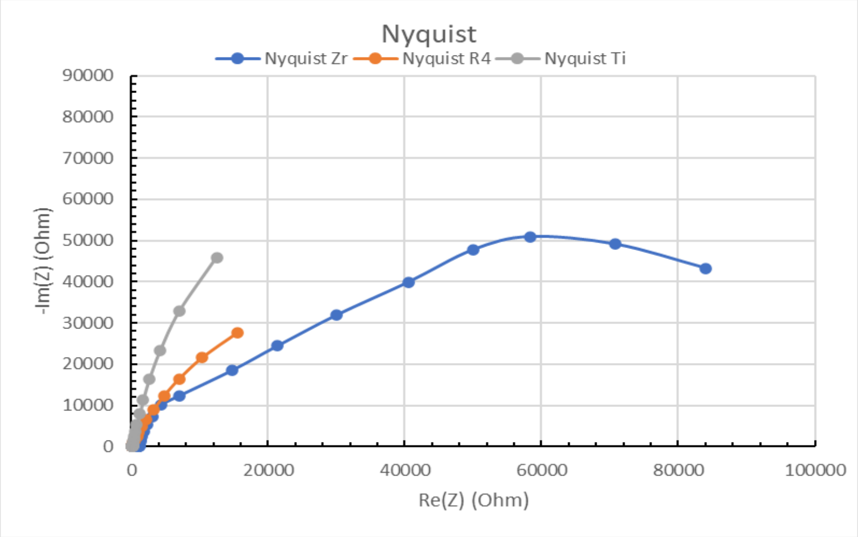

Figure 4. Nyquist of the analyzed samples in Ringer solution

We can finally see that all of the treated materials tend to passivate in some degree, forming an oxide layer that defends them from corrosion, with the most stable material being the R4 alloy. Zirconium instead presents at around 0.2 V pitting corrosion phenomena. (see Figure 5)

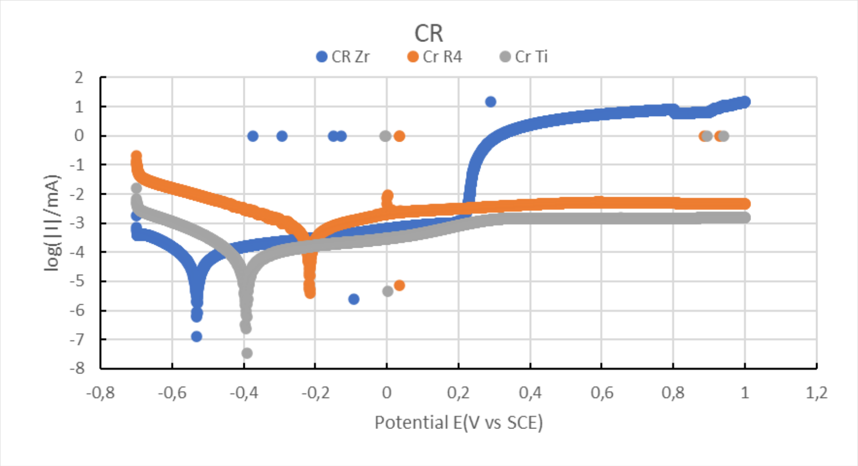

Figure 5. Polarization curves for all the 3 samples in Ringer solution

Conclusion

From our analysis we can state that the R4 alloy presents good corrosion resistance and stability, with passivating capabilityes, which make it a good candidate for biological applications, in fact, its corrosion resistance is slightly superior to the commonly used material, and if we also consider the mechanical properties, that gives us a perfect material for future biomedical applications.

Acknowledgements

I want to thank University of Las Palmas de Gran Canaria, and the University of Padova for the Erasmus+ grant for traineeship and have the opportunity to work on this project.

References

[1] Vizureanu, P. Effect of Si Contents on the Properties of Ti15Mo7ZrxSi Alloys. Materials 2023, 16, 4906.
https://doi.org/10.3390/ma16144906

[2] Baltatu, M.S.; Vizureanu, P.; Sandu, A.V.; Florido-Suarez, N.; Saceleanu, M.V.; Mirza-Rosca, J.C.
New Titanium Alloys, Promising Materials for Medical Devices. Materials 2021, 14, 5934.
https://doi.org/10.3390/ma14205934

APPLICATION OF DIELECTRIC MEASUREMENT FOR MONITORING THE EFFICIENCY OF ENZYMATIC PROCESSES

Sándor Beszédes[1], Réka Dobozi[2], Balázs Lemmer[2], Zoltán Jákói[1]

[1]*Department of Biosystems Engineering, University of Szeged,*
H-6725 Szeged, Moszkvai krt. 9, Hungary
[2]*Department of Food Engineering, University of Szeged, Faculty of Engineering,*
H-6724 Szeged, Mars ter 7, Hungary
e-mail: beszedes@mk.u-szeged.hu

Abstract

The dielectric measurements have proved their applicability in many fields of science and industry practice, as well. However, there is just limited experiences in the case of enzymatic processes. Therefore, the main aim of our research was to investigate the applicability of dielectric measurements for monitoring of enzymatic hydrolysis of lactose and cellulosic biomass. During our measurements, the dielectric constant and dielectric loss factor in the frequency range of 200-2400 MHz was determined using an open-ended coaxial dielectric probe. Based on our results, it can be concluded that the decomposition of lactose can be monitored by measuring both the dielectric constant and the dielectric loss factor at frequencies of 1000 MHz and 1800 MHz, while the enzymatic degradation of cellulose can be detected by the ratio of dielectric constant values measured at 400 and 1800 MHz frequencies. Therefore, it can be concluded that determining dielectric parameters at appropriate measurement frequencies are suitable for non-destructive and rapid monitoring of the efficiency and progress of enzymatic processes.

Key words: dielectric parameters, dielectric monitoring, enzymatic processes

Introduction

The dielectric characteristics of the materials, commonly quantified by its dielectric constant (ε') and dielectric loss factor (ε''), serve as indicators of its interactions with electromagnetic field [1]. The dielectric behaviour has significant effect on the temperature ramp, thermal efficiency, temperature homogeneity of materials subjected to microwave (MW) irradiation, for instance. In multicomponent, and heterogeneous systems, especially in solids, the different dielectric properties of the components alter the propagation of electromagnetic waves in materials under test (MUT) that presents difficulties for achieving uniform alternating electric fields. High power electromagnetic field can generate local overheating ('hot-spots') that makes difficult to maintain uniform temperature. Measurement of dielectric parameters enable to control the power absorption of MW irradiation, estimate the penetration depth of the electromagnetic waves and the conversion efficiency of electric field to heat (heat generation efficiency of MW irradiation). The dielectric constant quantifies the ability of polar components for orientational polarization (rotating) in alternating electromagnetic fields, the loss factor is related to energy absorption of electromagnetic field into the materials, which can generate heat (energy dissipation). The complex permittivity can be calculated by the Cole-Cole relaxation model equation (using static permittivity, frequency, relaxation time, conductance as variables). In some cases, the Cole-Cole dielectric relaxation model can be reduced the Debye model [2].
The dielectric measurement methods include waveguide or resonant cavity methods, open ended probes, impedance measurements and free space methods, as well. Open ended coaxial probes are widely used for the investigation of the dielectric behavior. Beside the numerous

advantages, their high price and the low penetration depth into the MUT can be considered as one of the main disadvantages, which limit the wider-scale applications. In the field of life sciences, the sensors operated at radiofrequency and microwave frequency ranges can be non-invasive alternative methods of conventional analytical techniques for the measurement of glucose concentration in biosystems (in vitro blood glucose measurement with lab-on-chip methodology, for instance) [3]. The change of dielectric loss factor measured at gigahertz frequency range is capable to detect the change of glucose concentration in aqueous solutions, but the presence of salts can reduce the alteration of dielectric behavior, therefore the sensitivity of the dielectric measurement methods decreases [4]. The problems related to electrode polarization effects of salts in aqueous system have also verified for dielectric measurements conducted at megahertz frequency ranges, the change of relative permittivity as a function of glucose concentration decreased if the concentration of ionic compounds (salts) increased [5]. The Maillard-type reactions between reducing sugars (such as glucose) and amino acids can be detected by dielectric measurements as well. In heated media, the intensity of ionic migration is enhanced that affected by the lower viscosity of the solvents, as well. Beside this, the higher temperature led to higher reaction rate between amino acids and sugars. These phenomena resulted in the increment of dielectric loss factor. However, it can be noticed, that during Maillard reaction the number of polarizable molecules decreased, therefore the contribution of dielectric polarization mechanisms to the change of dielectric behavior are decreased [6].

The analysis of the dielectric behaviour of blood plasma shows that in the frequency range of 1-8 GHz dielectric constant decreases, and dielectric loss factor (imaginary part of the complex permittivity) increases as the glucose concentration increases. However, in aqueous glucose solutions opposite trends can be observed for the relationship of glucose concentration with the dielectric parameters. At a given glucose concentration, the dielectric constant decreases while loss factor increases with increasing frequency. The lower temperature results in lower ε' and higher ε" at high concentration ranges, because the lower temperature causes increased viscosity, and in higher viscosity medium the rotation of molecules is impeded, and, furthermore, the higher viscosity is manifested in higher friction of molecules in alternating electromagnetic field [7]. During the enzymatic hydrolysis of lignocellulosic materials, change of the capacitance and the concentration of monomeric carbohydrates release. Therefore, the efficiency of the enzymatic cellulose hydrolysis can be detected by dielectric measurement [8]. In milk, the lactose interacts with water molecules forming water clustered structures. The change of physicochemical structure due the presence and concentration of lactose can have effect on the interaction with electromagnetic field. Alteration of polarisation in the electromagnetic field has effect on the dielectric behaviour of the system. However, the milk cannot be considered as homogenous system, therefore the higher penetration depth of electromagnetic field at microwave frequencies can be applied as a 'volumetric" non-destructive measurement methods compared to methods applying infrared radiation. In lactic-acid bacteria induced coagulation, the hydrogen ions form lactic acid reduces the negative charge of casein. Therefore, the calcium phosphate from casein micelles liberate which led to collapse of micelles resulted in coagulation. During the coagulation the ratio of free to bound water is changed. The relaxation of free and bound water is different in electromagnetic field (in milk: 10-20 GHz vs. 1 GHz, respectively). Because the polarization is depended on the composition and physicochemical structure of milk, analysis of the change in dielectric behaviour can be suitable to monitor the coagulation processes. For example, dielectric measurements in the frequency range of 100 MHz-20 GHz verified, that till 500 MHz the ionic conduction has the main effect on the change of dielectric parameters, and the fat content has not significant effect on the tendency of the change of dielectric loss factor vs frequency at the range of 20-4500 MHz, but there can be found differences in the absolute value of ε". The dielectric loss and dielectric constant are also negatively correlated with the pH during the milk coagulation process [9].

It is verified that dielectric behaviour of the milk and other high water contented biological systems is mainly determined by the polarization effects at frequencies below 3 GHz [10]. Mastitis is one of typical health problems on cows' health status. The change of somatic cell count (SCC) has effect on the physicochemical properties of the milk, and its techno-functional characteristics in dairy industry processing, as well. A recent study concluded that the change somatic cell count in cow milk can be detected by the analysis of the dielectric behaviour. The increment of SCC caused a higher concentration of ionic components that resulted in enhanced ionic polarization in electromagnetic field, therefore the dielectric loss factor is increase, as well. It is also observed, that at higher SCC concentration ranges, the frequency dependence of dielectric spectra reduced [11].

Experimental

The dielectric behaviour of the materials (characterized by the dielectric constant and dielectric loss factor values) in the frequency range of 200-2400 MHz was investigated by a Speag DAK 3.5 dielectric probe connected to a ZVL-3 vector network analyzer with coaxial line. The measurements were based on the determination of reflection coefficient at the interface of sample material and probe. The temperature of MUT/biosystems was controlled with water bath at 20±0.5 °C. For the calibration open, short circuit and deionized water (dielectric load) method was applied. The immersion depth of DAK probe into samples was 10 mm for all measurements.

For the cellulose enzymatic hydrolysis test corn cob residue was used as substrate which has 46±2 w%, 37±1.6 w% and 7±0.5 w% cellulose, hemicellulose and lignin content, respectively. Enzymatic hydrolysis tests were carried out in 3.5 w% suspensions at the temperature of 45°C using 0.1 M sodium acetate buffer for controlled pH of 4.8 using Cellic CTEC2 enzyme blend in a dosage of 60 FPU/g(cellulose). The reducing sugar concentration was measured by DNSA photometric assay. The samples were filtered through a 0.2 μm syringe filter (PES membrane). For the investigation of lactose hydrolysis commercially UHT milk was used with fat content of 1.5%. The incubation temperature was 20±0.5 °C (higher than applied in the dairy technologies to shorten the time demand). The dosage of β-galactosidase enzyme (Maxilact L2000, DSM) was 0.15 v/v%). After the incubation (before the analysis) the enzyme was inactivated using 2 min 90°C heat treatment. The lactose content was measured by refractometer (PAL19S, Atago), the galactose concentration was determined by galactose oxidase colorimetric detection kit (ThermoFischer, absorbance was measured at 560 nm).

Results and discussion

Our results shown, that during the enzymatic decomposition of lactose components in milk the dielectric constant (ε') show increasing tendency. The change of dielectric constant and loss factor due to the decreasing of lactose (and increasing of galactose and glucose monomers) was different in the varying frequency ranges (data not shown). The difference between dielectric properties vs. lactose concentration was the highest at the frequency of 1000 MHz, and has been slightly in the frequency range of 1800-2400 MHz. Therefore, the ratio of dielectric constant and dielectric loss factor (ε") measured at 1000 MHz to that of determined at 1800 MHz was used as dielectric control parameter of the enzymatic process. Our results show, that the dielectric constant is suitable to monitor the lactose hydrolysis process till approximately 45% lactose decomposition degree (Fig. 1.a), while the dielectric loss factor ratio has good linear correlation with the change of lactose concentration in the range of 0-70% (Figure 1.b), respectively. The hydrolysis of lactose to its monomers increase the number of easier polarizable molecules (with lower molecular weight) in the system that can be manifested in the change of dielectric parameters, for example the increasing tendency of dielectric loss factor [6,9].

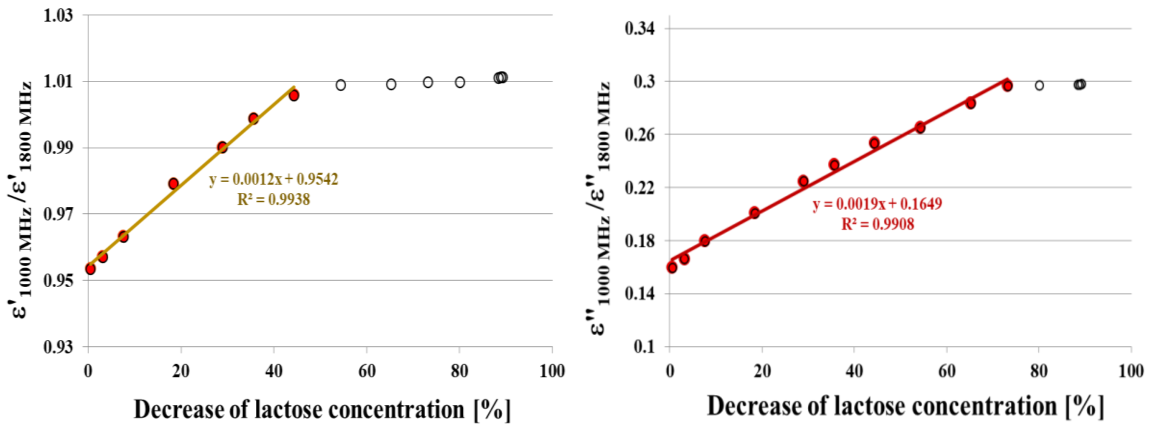

a) *b)*

Figure 1. Relationship between the lactose hydrolysis (decrease of lactose concentration) and dielectric constant (a) and dielectric loss factor (b) ratio (at 1000 MHz and 1800 MHz, t=20°C)

Analysis of the dielectric behaviour during enzymatic hydrolysis of lignocellulosic biomass show, that in the frequency range of 200-2400 MHz the dielectric constant has better correlation with the reducing sugars (RS) concentration compared the sensitivity of dielectric loss factor to the change of RS yield (data not shown). Similar to the experiences related to the dielectric behaviour of milk during lactose hydrolysis, there can be found 'characteristic' measurement frequencies (for minimum and maximum value of loss factor) for the monitoring of cellulose hydrolysis. Ratio of the dielectric constant at the frequency of 400 MHz to 1800 MHz has good linear correlation with reducing sugars yield (mg RS./g dry matters). Progress of cellulose degradation caused decreasing of dielectric constant ratio (Figure 2).

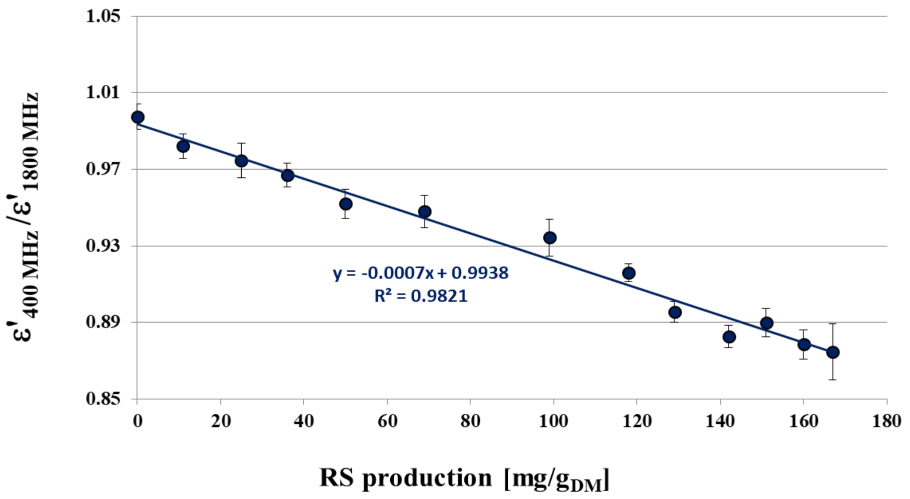

Figure 2. Correlation between RS yield and dielectric constant ratio (measured at 400 MHz and 1800 MHz)

Other studies have also verified, that the presence of sugar monomers (such as glucose) has effect on the relaxation time in electromagnetic field, and increasing of glucose concentration resulted in lower permittivity and dielectric constant in aqueous systems [7, 8].

Conclusion

Our research has verified that both the enzymatic lactose decomposition process used in dairy production technologies and the enzymatic hydrolysis of lignocellulosic biomass can be detected based on the measurement of the dielectric properties. However, to apply a dielectric monitoring method with adequate accuracy for the specific raw material and enzymatic process, the determination of the most sensitive dielectric parameters and appropriate measurement frequencies for the substrate and hydrolysis products can be considered as crucial. However, due to their non-destructive characteristics, the rapid dielectric measurements can be suitable for application in industrial manufacturing technologies, as well.

Acknowledgements

The research was supported by Bolyai János Research Scholarship of the Hungarian Academy of Sciences (BO/00161/21/4).The authors are also grateful for the financial support provided by the New National Excellence Program of the Ministry for Culture and Innovation from the source of the National Research, Development and Innovation Fund, under funding numbers UNKP-23-3-SZTE-246, ÚNKP-23-5-SZTE-668, and UNKP-23-2-SZTE-249.

References

[1.] Okiror, G.P., Jones, C.L. J. Food Eng. 113(1), 151–155. (2012) https://doi.org/10.1016/j.jfoodeng.2012.04.011
[2.] Turgul, V., Kale, I. (2015). E-Health Bioeng. Conf. (EHB) (2015). https://doi.org/10.1109/ehb.2015.7391450
[3.] Dhakal, R., Wang, C., Kim, E.S., Kim, N.Y. Appl. Phys. Lett. 106(7), 073702 (2015) https://doi.org/10.1063/1.4909545.
[4.] Smulders, P., Buysse, M., Huang, M. (2013). Microwav. Optic. Techn. Lett.. 55. 1916-1917. (2013) https://doi.org/10.1002/mop.27672
[5.] Yoon, G. (2010). Biosens. Bioelectr. 26. 2347-2353. https://doi.org/10.1016/j.bios.2010.10.009
[6.] Xu, Y., Xiang, P., Qiu, W., Jin, Y., Deng, S., Tao, N., Jin, Y. LWT. 161. 113355 (2022). https://doi.org/10.1016/j.lwt.2022.113355
[7.] Tao, Y., Yan, B., Zhang, N., Wang, M., Zhao, J., Zhang, H., Chen, W., Fan, D. J. Food Eng.. 316. 110844. (2021) https://doi.org/10.1016/j.jfoodeng.2021.110844
[8.] Bryant, D., Firth, E., Kaderbhai, N., Taylor, S., Morris, S., Logan, D., Garcia, N., Ellis, A., Martin, S., Gallagher, J. Biores. Techn. 128. 765-768. (2012) https://doi.org/10.1016/j.biortech.2012.09.021
[9.] Harindran, A., Vinjanampati, M. J. Microw. Power Electromagn. En. 54.1-21. (2020) https://doi.org/10.1080/08327823.2020.1755484
[10.] Agranovich, D., Renhart, I., Ishai, I., Katz, G., Bezman, D., Feldman, Y. Food Cont. 63. 195-200. (2015) https://doi.org/10.1016/j.foodcont.2015.11.032
[11.] Yang, K., Fang, D., Li, Y., Guo, W., Zhu, X. LWT. 188. 115424. (2023) https://doi.org/10.1016/j.lwt.2023.115424

GLYCOLIPIDOMICS OF HUMAN CEREBELLUM IN DEVELOPMENT AND AGING BY ION MOBILITY TANDEM MASS SPECTROMETRY

Maria-Roxana Biricioiu[1,2], **Mirela Sarbu**[2], **Raluca Ica**[2], **Alina D. Zamfir**[2,3]

[1]Faculty of Physics,West University of Timisoara, 300223 Timisoara, Vasile Parvan 4, Romania
[2]National Institute for Research and Development in Electrochemistry and Condensed Matter, 300224 Timisoara, Plautius Andronescu 1, Romania
[3]Department of Technical and Natural Science, „Aurel Vlaicu" University of Arad, 310032 Arad, Bulevardul Revolutiei 77, Romania
e-mail: maria.biricioiu99@e-uvt.ro

Abstract

In this study ion mobility separation (IMS) mass spectrometry (MS) was for the first time introduced in human cerebellum ganglioside research. The work was focused on a comprehensive mapping and structural characterization of human cerebellar gangliosides and determination of the specific changes induced in their expression by brain development and aging. We have carried out a comparative IMS MS mapping of the native ganglioside mixtures extracted from fetal cerebellum in the second trimester of pregnancy vs. near-term fetus vs. aged cerebellum, followed by IMS CID MS/MS fragmentation analysis.

Introduction

Cerebellum represents a highly specialized region of the brain encompassing approximately 80% of the total brain neurons and regular arrays of neuronal units involved in motor control, learning, cognitive and emotional functions [1, 2]. In recent years, human cerebellum started to be investigated at the molecular level, in order to correlate its functions with the expression of various biomolecules, especially gangliosides, sialylated glycosphingolipids highly expressed in the central nervous system. Among the bioanalytical methods employed so far in the analysis of cerebellar biomolecules, mass spectrometry (MS) provided the most comprehensive information [3].

Experimental

We report here on the first introduction in cerebellum research of ion mobility separation (IMS) mass spectrometry for a systematic mapping of cerebellar gangliosides and determination of the species associated to development and aging. For this purpose, gangliosides extracted from post-mortem tissue biopsies of fetal -in the 15 and 40 gestational weeks (samples 15GW and 40GW)- and 65 years of age (sample 65Y) cerebellum were analyzed by nanoESI IMS MS in the negative ion mode under identical conditions. In the next stage of the research, using CID MS/MS at low and variable collision energy after mobility separation in the transfer cell, were confirmed and characterized the structural conformation of the glycan core and ceramide moiety of three precursor ions that are common in all samples.

Results and discussion

Altogether, no less than 734 molecular ions corresponding to 551 gangliosides were identified by IMS MS separation and screening, which represents almost five times more cerebellar structures than ever reported before. In the absence of specialized software designed for automated interpretation of ganglioside mass spectra, extensive data analysis required manual calculations. As a result, average mass accuracies of 8.358 ppm for C15GW, 7.953 ppm for

C40GW, and 8.456 ppm for C65Y were obtained after assigning all 734 ions. The IMS MS analysis also revealed various intriguing aspects concerning the sialylation and modifications of ganglioside components, encompassing both carbohydrate and non-carbohydrate attachments, across the three extracts. Furthermore, the IMS MS data highlighted substantial deviations in sialylation patterns, as well as a surprisingly diverse array of alterations in the fundamental structure of the glycan core due to fucosylation, *O*-GalNAc attachment, *O*-acetylation, and modifications involving CH_3COO^-. Another significant discovery pertained to the pronounced heterogeneity and substantial differences in the composition and structure of the Cer moieties within the ganglioside species present in C15GW, C40GW, and C65Y. Notably, an unusually high number of compounds exhibiting trihydroxylated sphingoid bases, fatty acid chains with atypical lengths, or a combination of these characteristics were also observed.

The optimized isolation and fragmentation conditions induced efficient ion dissociation with high sequence coverage and a significant number of fragment ions diagnostic for the proposed structures of GD1 (d18:1/18:0), GQ1(t18:18:0) and GQ1(d18:1/18:0). Considering the MS/MS results, which provide evidence on $(Neu5Ac)_2$, the three structural candidates are b-isomers.

Conclusion

The comparative analysis revealed for the first time that: i) 40GW contains the highest number of species (373), followed by 15GW (327) and 65Y (192); ii) fetal cerebellum gangliosidome is characterized by a much higher sialylation degree and species altered by carbohydrate and non-carbohydrate type of modifications than the gangliosidome of aged cerebellum; iii) significant developmentally- and age-regulated changes in the expression and structure of cerebellum gangliosides exist. These variations are to be correlated in the future with the neurological diseases, leading to the discovery of pathways to more effective therapeutic schemes.

Acknowledgements

This work was funded by the Romanian National Authority for Scientific Research, UEFISCDI, project PN-III-P4-ID-PCE-2020-0209.

References

[1] T. Roostaei, A. Nazeri, M.A. Sahraian, A. Minagar, Neurol. Clin. 32 (2014) 859.

[2] K. Parmar, C. Stadelmann, M. A. Rocca, D. Langdon, E. D’Angelo, M. D’Souza, J. Burggraaff, C. Wegner, J. Sastre-Garriga, A. Barrantes-Freer, J. Dorn, B. M. J. Uitdehaag, X. Montalban, J. Wuerfel, C. Enzinger, A. Rovira, M. Tintore, M. Filippi, L. Kappos, T. Sprenger, Neurosci. Biobehav. Rev. 89, (2018), 85.

[3] C. Flangea, A. Serb, E. Sisu, A.D. Zamfir, Biochim. Biophys. Acta. 1811 (2011) 513.

THE INFLUENCE OF PESTICIDE APPLICATION ON THE SOIL SEED BANK IN THE INTENSIVE APPLE ORCHARD

Blagojević Milan[1], Rašković Vera[1], Stošić Nemanja[1], Milan Glišić,[1] Vlajić Slobodan[2], Miloš Rajković[2], Nenad Pavlović[1], Stefan Marković[1]

[1]*Academy of Applied Studies Šabac. Unite for Agricultural Business Studies and Tourism, Republic of Serbia*
[2]*Institute of Field and Vegetable Crops, Novi Sad, Serbia*
email: blagojevicmilan@ymail.com

Abstract

The apple orchard was planted in 1998 on an area of 14.5 ha in the locality of Erdevik, where the soil type is fertile. The type of soil determines the presence of certain plant species, which form the weed flora. The seeds of weeds and cultivated plants, after reaching the ground, remain on the surface, and then gradually penetrate into the deeper layers of the soil and create the so-called soil weed seed bank. The conditions that prevail in the orchard are significantly different from the conditions in the field type of production. Unlike annual field crops, according to Smith and Gross (2006), orchards lack the variability of crop rotation, that is, crop rotation, which affects the composition of the weed seed bank. In the fall of 2022, an analysis of the weed seed bank was carried out at the Erdevik locality, an analysis of the weed seed bank was performed to a depth of 0-30 cm, where the presence of 18 weed species was determined. Weed species are: *Agropyron repens* (L.) Beauv., *Amaranthus retroflexus* L., *Ambrosia artemisiifolia* L., *Polygonum convolvulus* L., *Brassica* sp., *Chenopodium album* L., *Chenopodium hybridum* L., *Datura stramonium* L., *Hibiscus trionum* L., *Lamium purpureum* L., *Polygonum aviculare* L., *Portulaca oleracea* L., *Sorghum halepense* (L.) Pers., *Solanum nigrum* L., *Stellaria media* (L.) Vill., *Setaria glauca* (L.) Beauv., *Urtica dioica* L., *Veronica hederifolia* L. The seeds of determined weeds had a low germination rate of 2.2%. with an abundance of 42341 seeds/m2. The analysis of the weed seed bank was carried out in the row area of the orchard, where pesticides and primarily herbicides are applied, which had an impact on the reduced number of weed seeds in the row, but also on the reduced germination of weed seeds. Intensive methods of cultivation imply a relatively high level of investment, soil cultivation is carried out regularly, usually mechanized, as well as the application of pesticides (herbicides, fungicides, insecticides).

INVESTIGATION OF THE POLYELECTROLYTES' EFFICIENCY IN THE TREATMENT OF LAUNDRY GREYWATER DURING THE COAGULATION-FLOCCULATION PROCESS

Amira Bouzid

Department of environmental engineering, University of Szeged, H-6720 Szeged, Dóm tér 7, Hungary
e-mail: amirabouzid55@gmail.com

Abstract

The global pursuit of a continuous and stable water source is essential in the face of climate change and mismanagement of water resources, which has exacerbated water scarcity. This research aimed to investigate the efficiency of polyelectrolyte as the main coagulant in the coagulation-flocculation treatment process to determine their suitability in producing an alternative water source.

Introduction

In this study, I will be using synthetic laundry greywater (LDGW) as a model water which is considered the most contaminated among other greywater fractions such as bath and even mixed greywater (laundry, bathing and kitchen wastewater all together) and we will be focusing on the coagulation-flocculation process in which we will determine the efficiency of a cationic type polymer agent (ACEFLOC 80902) on LDGW that has been always used as a coagulant aid after metal salts as main coagulants in this process.

The efficiency of the polyelectrolyte will be monitored by measuring the physical and chemical characteristics of greywater before and after treatment and under different flocculation speed and time.

A further investigation of the polyelectrolyte's efficiency response to pH change will be performed. The methods were selected mainly because of their proven efficiency and wide use in the wastewater treatment sector. The parameters investigated were the pH, turbidity, zeta potential, biological oxygen demand (BOD) and the total organic content (TOC).

Experimental

The experimental procedure started by creating synthetic LDGW samples.They were prepared by mixing 0.500 g Detergent/Washing agent (ARIEL gel concentrated, Mountain Spring, Proter and Gamble), 1.00 g Softener (LENOR Sensitive Softener, Proter and Gamble), 0.200 g corn oil (VFI GmbH, Austria), and 0.300 g standard nutrient broth (Scharlau, Spain) for every 1 L of tap water at 40 °C from Debrecen, Hungary.

Initially, 100 mL of synthetic GW was used as sample volume. The measured sample was added to a beaker equipped with a magnetic stirrer and stirred at 800 rpm to ensure sample homogenization is preserved. A selected volume of coagulant was added to the 100 mL GW and the mixture was stirred for 30 seconds after which a sub-sample was extracted using a syringe from the total volume and let to settle for 5 minutes thereafter pH, zeta potential and turbidity were measured. This process was repeated with different volumes of coagulant everytime to create a dose-response curve and from which the optimum volume of coagulant needed for the range of zeta potential between -5mV and +5mV can be determined and used in larger volumes.

At a second stage of the experiment and from the collected data of the adequate volume range of coagulant found with 100 mL samples, we prepared a 4L sample and used the Flocculator

(Jar-test) to perform the coagulation-flocculation process in detailed version. The flocculator has an automatic mixing parameter with different speeds and require a volume of 500 mL in each beaker. After filling each beaker with 500mL of our synthetic GW, we add the coagulant and we activate the automatic stirrer at full speed (300 rpm) for 5 min and then we turn to the slow mixing in different speeds: 10 rpm, 60 rpm, 90rpm and 120 rpm and we repeat the same experiment for two different slow mixing times: 15 min and 30 min in order to find the best condition for which the polyelectrolyte performs the best.

After slow mixing is done, the mixture is left to settle and sediment for 20 minutes. pH, zeta potential, turbidity and TOC were then measured and after which we proceeded with a filtration process and remeasured the mentioned parameters.

Figure 1: Jar Test during coagulation-flocculation process

At a third stage, we have used 2 solutions HCl (0.1 mol/dm3) and NaOH (0.1 mol/dm3) in order to adjust the LDGW to different pH values 5, 7 and 10. Before and after adjusting the pH, different doses of the polymer is added to each 100 ml of solution in order to determine the optimum PE dose each time with each pH alongside with measuring zeta potential, TOC, pH and Turbidity in order to compare between all results obtained.

Results and discussion

This section provides results obtained using the cationic polyelectrolyte (PE) as a main coagulant. To determine the dose at which optimum coagulation occurs a series of zeta potential dose-response curves are created. The results were plotted, and we found that the optimal range is between 2.8 mL and 4.7 mL of polyelectrolyte per 100 mL of LDGW (concentration of 28 mg/L and 47mg/L respectively) and the 0 mV zeta potential value at around 3.8 mL volume of stock coagulant solution which is equal to around 19 mL of polyelectrolyte dose per 500 mL of LDGW.

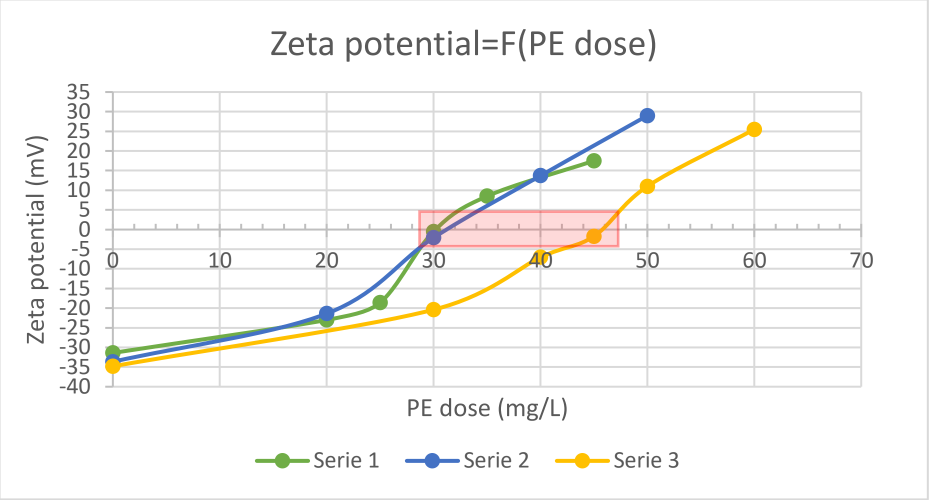

Figure 2: Dose-response curve

At a second stage, using the Flocculator (Jar-Test), with bigger volumes, we have obtained that the best conditions for which the polyelectrolyte performs the best is for 15 mL which is a lower optimum dose than that expected which again shows the impact and the importance of flocculation on the PE performance. Then we proceeded to use different flocculation time and speed to determine its impact on the polyelectrolyte performance and we found that zeta potential in almost all conditions is close to 0 mV which proves in one side the effectiveness of the chosen polyelectrolyte dose and the importance of the flocculation process. For a flocculation speed of 120 rpm and flocculation time of 30 min, the turbidity is very close to that of tap water used in the experiment (4.75 NTU) and this shows the importance of mixing speed that differs from one polyelectrolyte (coagulant) to the other and in this case it is shown that a 120 rpm speed seems to be the right flocculation speed for this cationic polyelectrolyte used. However, for the TOC, the results shows similar results regardless of the time and speed change which shows that PE can be more effective in removing insoluble components.

Table 1: Results of the coagulation-flocculation process under different conditions

	Speed (rpm)	Dose (mL)	Zeta potential (mV)	TOC (mg/L)	pH	Turbidity (NTU)	Slow Mixing (min)
1	60	15	-1.89	55.28	8.30	18.56	15
2	90	15	-1.63	53.33	8.39	11.56	15
3	120	15	-1.35	51.14	8.43	8.51	15
4	60	15	-1.28	51.02	8.28	11.37	30
5	90	15	-1.61	51.97	8.29	6.93	30
6	120	15	-1.13	51.54	8.29	5.05	30

At a last step, the pH test proved that the pH level has indeed a direct effect on the performance of the polymer, for the raw solution with a pH equal to 7.88, the polymer optimum amount (mg/L) that coincides with zeta potential between -5mV and +5mV is shown to be in a range of [37..42], for the higher value of pH =10, there is almost no change in the optimum amount of PE [36,5..42], However in lower values of pH 7 and 5, it is clear that the supposed to be an optimum amount is now more than enough to neutralize the solution as the zeta potential decreased and so did the optimum amount of PE that now became in the range of [35..38] and [24,5..26] respectively.

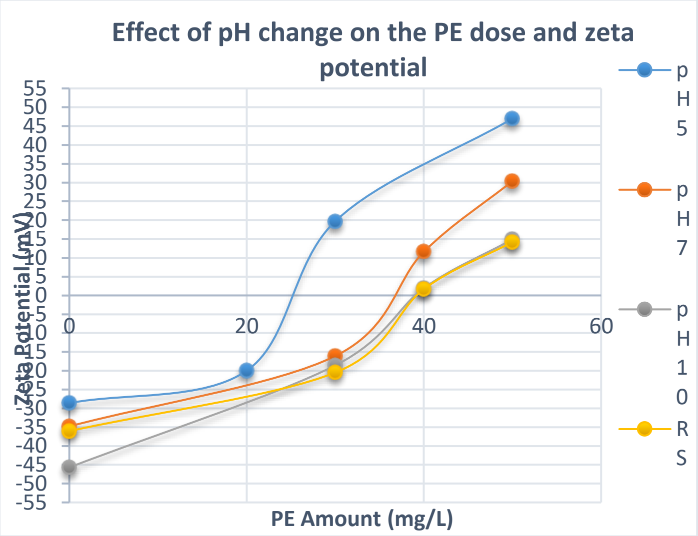

Figure 3: Dose-response curve under different pH values

The TOC values have shown a decrease in all pH levels, For the raw sample and pH 7 the TOC level (around 50 mg/L) is almost the same as that of the raw sample and it can be explained by the fact that they have pretty close pH levels (pH 7.88 and pH 7). however when the pH is either more alkaline (pH 10) or more acidic (pH 5), the TOC level decreased even further and we can notice a more Natural Organic Matter (NOM) removal efficiency when the optimum PE dose is applied (TOC around 40 mg/L) which proves the importance of adjusting the right pH level prior to the use of the proper dose of coagulant.

Based on the measured values, the PE proved its efficiency in LDGW treatment in different pH ranges which is an important advantage in the water treatment sector that the coagulant can work in neutral environment. Moreover, it is also important to note that in real LDGW, pH is usually more alkaline (9-11), which in this case, the PE according to the results found, is expected to work in an effective way as well.

Conclusion

The coagulation-flocculation process using Polyelectrolyte as the main coagulant instead of metal salts followed by a filtration process using a slow sand filter resulted in a successful laundry greywater treatment according to the measured quality parameters of BOD, TOC Turbidity of 6 mg/L, 7.61 mg/L, 1.6 NTU respectively. These results are aligned with the range of limit values set by the international regulations and standards of greywater reuse.

A further investigation of the efficiency of the cationic polyelectrolyte in treating laundry greywater under different pH ranges (5,7 and 10) showed that the optimum dose of PE was reduced from 38 mg/L to ~ 25 mg/L in lower pH (around 5) which can be a cost effective solution to use less chemicals in wastewater treatment as according to previous results obtained in university of Debrecen, an amount of 248.75 mg/L of iron(III) chloride and 18 mg/L for polyelectrolyte was needed to treat mixed greywater and 295 mg/L and 325 mg/L to treat laundry greywater.

It is interesting to test different types of polyelectrolyte especially stronger base cationic ones that can retain a high positive charge at high pH values on real laundry greywater which is usually more alkaline (around 9-11) and determine if it is cost effective comparing it with using metal salts since polyelectrolytes are usually more expensive.

Acknowledgements

I would like to thank my supervisor during my master's studies, Dr. Ildiko Bodnar, for her continuous support, guidance, and mentorship. Dr. Bodnar's insightful feedback and unwavering encouragement significantly contributed to the successful completion of my master's thesis.

References

[1] Wang R, Zimmerman J (2016) Hybrid analysis of blue water consumption and water scarcity implications at the global, national, and basin levels in an increasingly globalized world. DOI: 10.1021/acs.est.6b00571

[2] J. Bratby, Coagulation and Flocculation in Water and Wastewater Treatment. 3rd ed., London, IWA Publishing, 2016, eISBN 9781780407500.

[3] Irshad N.ShaikhM. MansoorAhammed, "Quantity and quality characteristics of greywater", 2020, Civil Engineering Department, SV National Institute of Technology, Surat, 395007, India. Available online at: https://doi.org/10.1016/j.jenvman.2020.110266.

[4] Brian Bolto, John Gregory, Organic polyelectrolytes in water treatment, Water Research, Volume 41, Issue 11, 2007, ISSN 0043-1354, https://doi.org/10.1016/j.watres.2007.03.012.

[5] Modelling Treated Laundry Greywater Reuse for Irrigation Using an Affordable Treatment Method and Seed Germination Test Camila C. A. Cardoso and Ildiko Bodnar

[6] Shoushtarian, F.; Negahban-Azar, M. Worldwide Regulations and Guidelines for Agricultural Water Reuse: A Critical Review. Water 2020, 12, 971. https://doi.org/10.3390/w12040971

VALORIZATION OF SOUR CHERRY KERNELS: EXTRACTION OF POLYPHENOLS USING NATURAL DEEP EUTECTIC SOLVENTS (NADES)

Danica Božović[1], Nemanja Teslić[2], Ivana Dimić[1], Aleksandra Mišan[2], Milica Pojić[2]
Branimir Pavlić[1]

[1]Faculty of Technology, University of Novi Sad, Blvd. cara Lazara 1, 21000 Novi Sad, Serbia,
[2]Institute of Food Technology, University of Novi Sad, Blvd. Cara Lazara 1, 21000 Novi Sad, Serbia
e-mail: danica_bozovic@live.com

Abstract

Cherry (*Prunus cerasus*) is a tree species belonging to the *Rosaceae* family. It is native to Europe and Asia. Cherry is most often consumed fresh, as a dessert fruit. It can also be used to process cherries, such as: juices, marmalades, jams. In order to use by-products, different parts of the cherry, such as seeds, kernels, pomace, are used to isolate bioactive components. The aim of this study was to determine the total phenols yield and the antioxidant activity of the extract from cherry kernels. For extraction, traditional extraction methods (Solid-liquid extraction - SLE) and an innovative extraction method (Natural deep eutectic solvents extraction - NADES) were used. SLE extraction was performed using different concentrations of ethanol (0, 10, 20, 30, 40, 50, 60, 70, 80, 90, 96%). The extraction was performed at room temperature for 24 h, with a shaking speed of 150 rpm. NADES extraction was carried out using 10 NADES solvents, of which 5 were polar and 5 non-polar. All NADES solvents in this work were prepared from organic acids (malonic, citric, lactic, octanic, lauric, decanic) as hydrogen bond donors (HBD) and betaine, choline chloride, glucose as hydrogen bond acceptors (HBA). The NADES extraction was performed with stirring in a heated water bath at 50 °C placed on a magnetic stirrer, for 60 min. Statistical significance ($p < 0.05$) of extraction solvents used such as ethanol in different concentrations, polar and non-polar NADES was determined by analysis of variance (ANOVA). Total phenols in the obtained extracts were determined by the Folin-Ciocalte method, and antioxidant activity determined by the following tests: DPPH, ABTS and FRAP. In the case of SLE extraction, the amount of total phenols ranged from 1.94-3.87 mg GAE/g DW. While in the case of NADES extraction, total phenols ranged from 1.13-2.54 mg GAE/g DW. Regarding DPPH, ABTS and FRAP tests, the extract obtained from SLE using 50% ethanol showed the highest antioxidant activity (5.71 μM TE/g, 9.45 μM TE/g, 25.98 μM Fe^{2+}/g, respectively). Regards to NADES extraction, NADES 1, which based on Choline chloride:Malonic acid in molar ratio 1:1 shown the strongest antioxidant value in case of DPPH test (35.26 μM TE/g) and ABTS test (34.55 μM TE/g). While, extract obtained by NADES 4 (Lactic acid:Glucose=5:1) showed the highest reducing power, and value was 37.05 μM Fe^{2+}/g.

Keywords: hydrophilic NADES; hydrophobic NADES; polyphenols, antioxidant activity

Acknowledgements

This research was supported by the Science Fund of the Republic of Serbia, 7750168, Novel extracts and bioactive compounds from under-utilized resources for high-value applications–BioUtilize.

OCCURRENCE OF POLYCYCLIC MUSKS IN PORE WATER OF THE SEDIMENT-FRESHWATER SYSTEM: PASSIVE SAMPLER APPLICATION

Maja Brborić[1], Sonja Dmitrašinović[1], Sanja Ćojbašić[1], Maja Turk Sekulic[1], Jelena Radonic[1]

[1]University of Novi Sad, Faculty of Technical Sciences, Department of Environmental Engineering and Occupational Safety and Health, Trg Dositeja Obradovica 6, Novi Sad, Serbia;
e-mail: majabrboric @uns.ac.rs.

Abstract

Polycyclic musks are aroma compounds used worldwide as substitutes for natural musks, which have become ubiquitous pollutants in the environment. The land-based input and partition behavior of musks in sediments and fresh water are important for understanding their fate in the aquatic environment. In this study, a 10 sediment samples were collected and used to determine three polycyclic musks: tonalide, galaxolide and cashmeran. All three pollutants were detected in the sediment of the Danube River, but in very low concentrations (< 2 ng/L). In the article, the ex-sity passive methodology of sediment sampling was applied. For this purpose, silicone rubber sheets were used so that, after establishing equilibrium relations between sediment and polymer, the concentration of musk could be determined. Relations of two important parameters for risk assessment- freely dissolved concentration (C_w) in the pore water and the accessible (releasable) concentration in the sediment (C_{AOC}) were deviated the most in the Belegiš locality, with total C_w values of 0.003 ng/L for Galaxolide and Tonalide, and 0.02 ng/L for Cashmeran. The highly significant linear isotherms for musks obtained by the method of equilibrium passive sampling confirmed the partition driven nature of their exchange between water and sediment for the investigated sediments.

Keywords: polycyclic musks, passive sampling, sediment, Danube

Introduction

Synthetic musks (SMs) are aroma compounds that are used worldwide as substitutes for natural musks, and mainly used in the production of household and personal care products (Hua el at., 2023). Due to their low price and widespread availability, the global production and consumption of SMs are increasing rapidly, particularly polycyclic musks (PAMs), galaxolide and tonalide (Hermann et al., 2000). Galaxolide and tonalide have been listed as high volume chemicals by the United States Environmental Protection Agency (Lopez-Gazpio et al., 2012). They can be found in hair care, body washes, toilet soaps, skin lotions as well as makeup products (Lu et al., 2011). Their rapid increase in use worldwide has been primarily due to their economical substitute for natural musk fragrances (Guo et al., 2013). Recently, occurrences of polycyclic musks have been frequently reported in sewage influents, effluents, sludge, surface water and sediments across several major metropolitan regions.

After application, PAMs could be directly discharged into the aquatic environment PAMs in environment are also traced from the effluent of sewage treatment plants, due to the incomplete elimination of SMs in the sewage treatment plants. Despite the application of advanced biological treatment strategies, the removal efficiencies for galaxolide, tonalide, and musk ketone were often lower than 60% (Hong et al., 2021). Also, PAMs have been detected in sediments, surface water, air and biota, suggesting that these contaminants are ubiquitous throughout the environment (Krishnamoorthi et al., 2021). High percentages of PAMs especially galaxolide and tonalide, were found in blood plasma samples of healthy young adults from Vienna, Austria (Hutter et al., 2009).

Passive sampling methods (PSMs) allow the quantification of the freely dissolved concentration (Cw) of an organic contaminant in pore water even in complex matrices such as sediments. Cw is directly related to a contaminant's chemical activity, which drives spontaneous processes including diffusive uptake into benthic organisms and exchange with the overlying water column. Consequently , Cw provides a more relevant dose metric than total sediment concentration. Recent developments in PSMs have significantly improved our ability to reliably measure even very low levels of Cw (Mayer et al., 2013). Application of PSMs in sediments is preferably conducted in the equilibrium regime, where freely dissolved concentrations in the sediment are well linked to the measured concentration in the sampler via analyte specific partition ratios.

Based on previous research on hydrophobic organic contaminants, it is concluded that Cw allows a direct assessment of 1) contaminant exchange and equilibrium status between sediment and overlying water, 2) benthic bioaccumulation, and 3) potential toxicity to benthic organisms (Mayer et al., 2013; Rusinaet al., 2019). Accordingly, the aim of our work was to demonstrate that the use of PSMs to measure Cw of specific emergent contaminants such as polycyclic musks provides an improved basis for mechanistic understanding of fate and transport processes in sediments and has the potential to significantly improve risk assessment and management of contaminated sediments.

Material and Methods

The sampling was performed in Nov 2012. For this investigation, 10 samples of bottom sediment from different sites of Danube River through Serbia (Apatin- D1 (1401 km), Labudnjača- D2 (1367 km), Neštin- D3 (1264 km), Begeč- D4 (1275 km), Ratno Ostrvo- D5 (1257 km), Šangaj- D6 (1250 km), Knićanin- D7 (1214 km), Belegiš- D8 (1199 km), Ritopek- D9 (1141 km), Dubravica- D10 (1103 km)) were collected using a grab sampler (Fig. 1). All sediment samples were analyzed in the laboratory of Research Centre for Toxic Compounds in the Environment - *RECETOX* (Brno, Czech Republic) after two days.

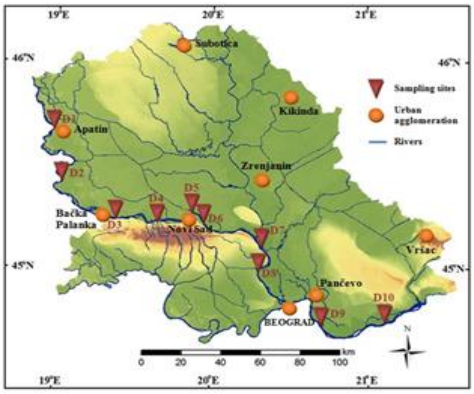

Figure 1. Danube River sampling sites

Passive sampler analysis

As part of the study, transparent strips of silicone rubber, dimensions 300 × 300 mm and thickness 0.5 mm, were used as sorption media of passive samplers. Before use, the silicone strips were extracted with ethyl acetate in a Soxhlet extractor to remove unpolymerized monomers, followed by methanol extraction to remove other impurities. Sorption media of passive samplers were dosed with performance reference compounds (PRC), using a mixture of water and methanol. Polycyclic musks were analyzed using a GC 6890 (Agilent, USA) coupled with an MSD 5975 mass spectrometer (Agilent, USA) operating in EI+ mode. Compounds were separated on an HP-5MS column (film 30 m x 0.25 x 0.25 µm) in selected ion mode (SIM). Helium was used as mobile phase at 1.2 mL/min and constant pressure.

Figure 2. Preparation of passive sediment samplers

Results and discussion

Determination of Cw hydrophobic organic compounds in water samples (by active sampling) is often associated with problems of incomplete phase ("unfinished") separation between bound particles and dissolved analyte and adsorption on sampling instruments such as filters and glass bottles. These effects are even more pronounced for pore water, even if it were possible to obtain large amounts of pore water necessary for satisfactory analyte detection. An alternative is the application of passive samplers, which accumulate compounds mainly through the aqueous phase. When equilibrium is reached, Cw can be estimated through the sampler−water partition coefficient (Kpw) and the measured concentrations in the sampler (Cp).

The usage of passive sampling providing estimates of both bioavailability parameters, i.e. contaminant's accessibility in sediment (C_{AOC}) and Cw in pore water. Equilibrations of passive samplers with sediment at largely different sampler–sediment mass ratios, allow construction of a part of a (de)sorption isotherm, which yields the Cw in the pore water at a low sampler-sediment ratio (minor depletion of the sediment phase) and the accessible or releasable concentration in the sediment at high sampler-sediment ratio (maximum depletion of the sediment phase).

Table 1. Limit of quantification of selected PAM compounds during passive sampler analysis

Compounds	logK_{PW}	LOQ	
		N_P (ng)	Cw (ng/L)
Galaxolide (HHCB)	5,32	2,2	0,003
Tonalide (AHTN)	5,29	1,9	0,003
Cashmeran (DPMI)	4,50	2	0,02

Plots of freely dissolved concentrations (Δ: Cw:0, ng L–1, right y–axis) and accessible concentrations expressed on amorphous organic carbon basis (○ : CAS:0/fAOC, mg kg–1, left y–axis) versus the locations on the x-axis (Fig 3.). The locations are ordered in downstream direction but the distance on the x-axis does not reflect the actual distance, neither do the connecting lines represent the oncentrations in between them. Open, gray and black filled markers indicate f_{AOC} <0.001, f_{AOC} ≥0.001 but <0.002 or f_{AOC} ≥0.002, respectively. Data for a location marked with a "+" passed the quality criterion, QF is "Ok" .

The detected concentration levels of polycyclic musks were very low (< 2 ng/L). At site D8, musk showed some higher $Cw,_0$ levels but these can only be considered indicative as the results did not qualify. For musk cashmeran, logK_{AOC} deviated from the unity line but not significantly, considering its large variability (s = 0.4 log unit).

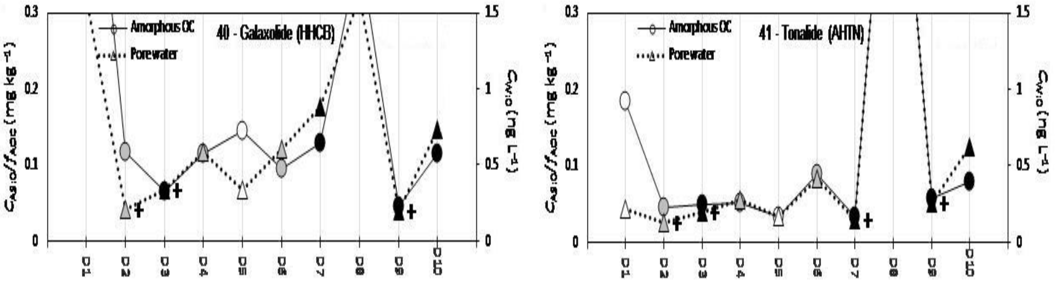

Figure 3. Profiles of freely dissolved concentrations in pore water and available concentrations in the sediment of the Danube River

Conclusion

Based on the overall analysis of the obtained results, it can be established that the Danube riverbank flow at the territory of Serbia have significant potential pollution sources of aquatic systems with polycyclic musks, which is important information to conduct more extensive monitoring and prevent further direct discharge, as well as disposal of ambalage that containing these pollutants by adequate controls, thus diminishing the extremely negative ecotoxicological effects currently present in the aquatic system. Within the framework of such a systematized research process, it would be necessary to include more media (biotic and abiotic) in the analysis as well as more specific points.

Acknowledgements

This research was supported by the Science Fund of the Republic of Serbia, grant number 6707, REmote WAter quality monitoRing anD IntelliGence – REWARDING and the Ministry of Science, Technological Development and Innovation through project no. 451-03-47/2023-01/200156 "Innovative scientific and artistic research from the FTS (activity) domain".

References

[1] Y. Hua, L. Wang, M. Zheng, Y.Xu, J. Liu, L. Fang, X. Pan, A.Liu, Occurrence of synthetic musks in the sediment-seawater system of the Yellow Sea and East China Sea during wet and dry seasons, Science of The Total Environment. 833, 10(2022), 155164.
[2] F. Hermann, O. Thomas, P. Konstanze, Polycyclic musk fragrances in the aquatic environment. Persistent, Bioaccumulative, And Toxic Chemicals II, (2000) 203–222.
[3] J. Lopez-Gazpio, R. Garcia-Arrona, M. Ostra, E. Millan, E. Optimization and validation of a nonaqueous micellar electrokinetic chromatography method for determination of polycyclic musks in perfumes. J. Sep. Sci. 35 (2012) 1344–1350.
[4] N. Liu, Y. Shi, W. Li, L. Xu, Y. Cai, Concentrations and distribution of synthetic musks and siloxanes in sewage sludge of wastewater treatment plants in china. Sci. Total Environ. 476-477 (2014), 65–72.
[5] G. Guo, F. Wu, H. He, R. Zhang, H. Li, Screening level ecological risk assessment for synthetic musks in surface water of Lake Taihu, China. Stoch. Env. Res. Risk A. 27 (2013), 111–119.
[6] V. Krishnamoorthi, N. Patil, E. Nishikant, M. Arun, M. Murugasamy, BR., Ramaswamy, Synthetic musks in surface water and fish from the rivers in India: Seasonal distribution and toxicological risk assessment. J. Hazard. Mater. 414 (2021) 125558.
[7] H.P. Hutter, P. Wallner, H. Moshammer, W. Hartl, R. Sattelberger, G. Lorbeer, et al., Synthetic musks in blood of healthy young adults: relationship to cosmetics use. Sci. Total Environ. 407(2009) 4821–4825.

[8] JH. Hong, JY. Lee, HJ. Ha, JH. Lee, SR. Oh, YM. Lee, et al., Occurrence and sources of synthetic musk fragrances in the sewage treatment plants and the Han River, Korea. Water 13 (2021)392.

[9] P. Mayer, TF. Parkerton,RG. Adams, JG. Cargill, J. Gan, T. Gouin, et al., Passive sampling methods for contaminated sediments: scientific rationale supporting use of freely dissolved concentrations, Integr. Environ. Assess. Manag., 10 (2013) 197-209.

[10] T. Rusina, F. Smedes, M. Brborić, B. Vrana, Investigating levels of organic contaminants in Danube River sediments in Serbia by multi–ratio equilibrium passive sampling. Science of The Total Environment, 696 (2019) 133935.

PRELIMINARY STUDIES OF NEW Ti ALLOYS WITH DIFFERENT Mo CONTENT

Bruma Alessio-Adrian[1], Stanciu Elena-Manuela[1], Pascu Alexandru[1],
Julia Claudia Mirza-Rosca[1,2], Madalina Simona Baltatu[3], Petrica Vizureanu[3]

[1]Materials Engineering and Welding Department, Transilvania Univerity of Brasov, 29 Eroilor Blvd., Brasov, Romania
[2]Mechanical Engineering Deparment, University of Las Palmas de Gran Canaria, Campus Universitario Tafira, Edif. Ingenieria, 35017, Gran Canaria, Spain
[3]Department of Technologies and Equipment for Materials Processing, "Gheorghe Asachi" Technical University of Iasi, Bulevardul Profesor Dimitrie Mangeron 67, Iași 700050, Romania
e-mail: alessio.bruma@student.unitbv.ro

Abstract

This work aims to investigate the mechanical characteristics and biocompatibility of two novel titanium alloys, Ti15Mo7Zr15Ta1Si and Ti20Mo7Zr15Ta0,75Si.These samples have previously undergone cutting, grinding, polishing, and chipping. The studied samples were subjected to electrochemical, metallographic and corrosion behavior. Ti15Mo7Zr15Ta1Si and Ti20Mo7Zr15Ta0.75Si, the study samples, have demonstrated high corrosion potentials, lower corrosion rates, and consequently higher corrosion resistance. In summary, this study's data indicates that both alloys exhibit good corrosion behavior.

Introduction

Biomaterials science has created new materials that can solve many of the medical issues of today and extend and improve human life because of the ongoing relevance of research in biology, chemistry, engineering, and medicine. But as life expectancy has grown in developed nations, so too has the number of elderly and obese people. The latter is a result of leading a more sedentary lifestyle, which increases their risk of developing chronic musculoskeletal conditions like osteoarthritis, which is especially common in the hips and knees, and necessitates more frequent surgical implant repairs.

The new Ti alloys with different Mo content were created by vacuum arc remelting, and this study examined their microstructure, microhardness and corrosion behavior.

Experimental

In order to perform various experiments and ascertain the effect of molybdenum addition in one of the samples, we have analyzed two different compositional alternatives of new alloys containing titanium, molybdenum, zirconium, tantalum and silicon. This has allowed us to obtain the properties of the alloys. Sample 1 composed of Ti15Mo7Zr15Ta1Si (62% Ti, 15% Mo, 7% Zr, 15% Ta, 1%Si) and Sample 2 composed of Ti20Mo7Zr15Ta0.75Si (57,25 % Ti, 20% Mo, 7% Zr, 15%Ta, 0.75% Si) are the chemical compositions of the alloys under study. High-quality elements, such as Zr (99% purity), Mo (99% purity) Ta (99% purity), and Ti (99% purity), were provided by Alfa Aesar through Thermo Fisher Scientific as raw materials. These alloys were produced at the Ghe. Asachi Technical Faculty of Materials Science and Engineering employing a vacuum arc remelting furnace (VAR), which used the heat generated by an electric arc between the electrode and the ingot to fuse a consumable electrode in a vacuum at a measured pace. The alloys were centrifuged, remelted six times (three times for each portion) in an inert argon environment in order to attain a sufficient level of homogeneity, and then solidified as an ingot. The new TiMoZrTaSi alloys were developed using arc melting because it yields the purest ingots possible. Las Palmas de Gran Canaria University received a portion of the ingots for testing and preparation.

Initially, a 4:1 ratio of epoxy resin was added to molds to prepare the surfaces of the two samples for embedding. That is to say, one drop of catalyst was added for every four drops of resin. The samples were then cut with a Buehler IsoMet 4000 precision saw (Buehler, Lake Bluff, IL, USA) longitudinally at a thickness of 1 to 1.5 mm.

Furthermore, the cutting tool was used to make vertical cuts that were roughly 0.5 mm thick. Next, utilizing the Struers TegraPol-11 polishing machine (Struers ApS, Ballerup, Denmark), grinding and polishing were done in two steps: first, with progressive grit silicon carbide papers from 280 to 1200, and then, for the final polish, with 0.1 microns of alpha alumina suspension to polish the surfaces to a mirror finish. The experimental procedures followed ASTM E3-11(2017) for the preparation of samples for metallography.

In order to eradicate any remaining dirt or contaminants, the samples were lastly submerged in a heated "Ultrasons-HD" ultrasonic device from J.P. Selecta (JPS, Barcelona, Spain) for ten minutes. For peer review, see Bioengineering 2022, 9, x. 4 of 23 surfaces with a mirror-like sheen using an alpha alumina suspension. The experimental procedures followed ASTM E3-11(2017) for the preparation of samples for metallography.

In metallography, the phases and compounds that comprise a metallic material are arranged spatially along with any impurities or possible mechanical flaws.

The Axio Vert.A1 MAT ZEISS optical metallographic microscope (Jena, Germany) was used to take surface images of each specimen in order to examine the microstructure.

The attacked surface of each sample was photographed after it was immersed in Kroll's reagent, which is composed of 20 mL glycerin, 30 mL hydrochloric acid, and 10 mL nitric acid, at intervals of roughly 15 s. Three attempts were made to complete the test.

For the electro-chemical tests, the samples were sequentially added to an electrochemical cell that had three electrodes: the samples functioned as the working electrodes, the reference electrode was a saturated calomel electrode, and the counter electrode was a platinum electrode.

To conduct the tests, the area of each sample was established. The Grifols Laboratories' Ringer solution (Barcelona, Spain) had the following mmol/L values: Na+ 129.9, Cl− 111.7, C3H5O3 27.2, K+ 5.4, and Ca2+ 1.8.

The BioLogic Essential SP-150 potentiostat (Seyssinet-Pariset, France) was utilized to perform Corrosion Potential, Corrosion Rate, and Electrochemical Impedance Spectroscopy. The experiments were conducted in an aerated Ringer solution at 25 ◦C.

The corrosion potential was measured using the "Ecorr vs. time" technique over the course of 24 hours, with potential values of ±10 V and potential recordings made every 300 s or 200 mV apart. The acquired data were plotted as a potential vs. time graph, which could exhibit a trend toward passivation or corrosion or stay constant over time.

These experiments were conducted using the "Linear Polarization" approach, and the viability of the approach was confirmed by entering the sample surface area value and the 20-minute test period. The potential scanning, which was conducted with data collected every 0.50 seconds, showed a 0.167 mV/s time-variation relationship between −0.025 and 0.025 V against the open circuit potential (OCP) and an intensity that remained at 100% throughout the process. The corrosion rate estimates for each sample were then determined using EC-Lab's "Tafel Fit" method after these linear polarization curves were presented.

"Potential Electrochemical Impedance Spectroscopy" was chosen for the impedance measurement, and the surface value and the five-minute measurement period were input. For every sample, this measurement was done seven times at ± 300 mV vs. Ecorr in Ringer's solution, with ± 10 V for the maximum and lowest potential values. Equivalent circuits and Bode and Nyquist diagrams were used to illustrate these data.

In compliance with ISO 14577-1:2015, 10 measurements were made for each sample's applied load—in this case, 1, 5, and 10 gf—using the Future Tech FM-810 hardness tester (Kawasaki, Japan). As the stress increases, the mark may include pieces from several phases, giving an approximate measure of the material's overall hardness. It is possible that the mark will only be found in one phase when relatively light weights are positioned, making it possible to evaluate the hardness of that phase. Then, using the observed diagonal lengths, the Vickers microhardness values were automatically calculated by the iVicky software (v2.0, Sinowon, Dongguan, China). Plotting the quantity of indents made against the scan length was done.

Results and discussion

1) Potential (E_{corr})

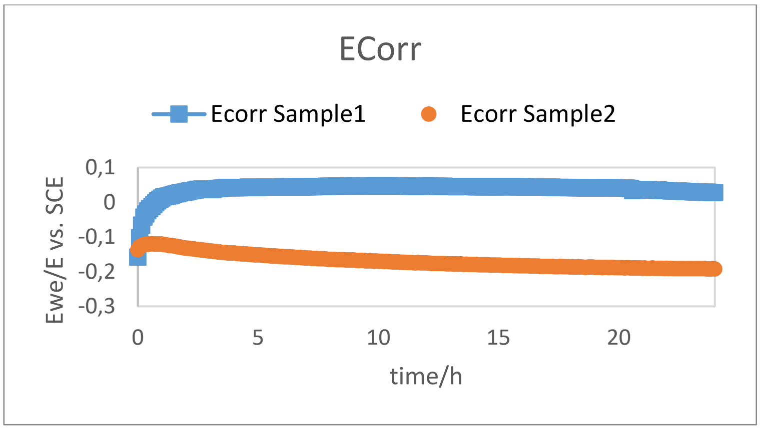

Figure 1. Corrosion potential curves for Ti15Mo7Zr15Ta1Si and Ti20Mo7Zr15Ta0,75Si

As the Molybdenum in the new Ti alloys increase, the corrosion potential becomes more negative. In Figure 1., we have the corrosion potentials for Sample1 Ti15Mo7Zr15Ta1Si and for Sample2 Ti20Mo7Zr15Ta0,75Si. It can be observed that Sample1 is passivating while Sample2 slowly corrodes.

1) Electrochemical impedance spectroscopy (EIS)

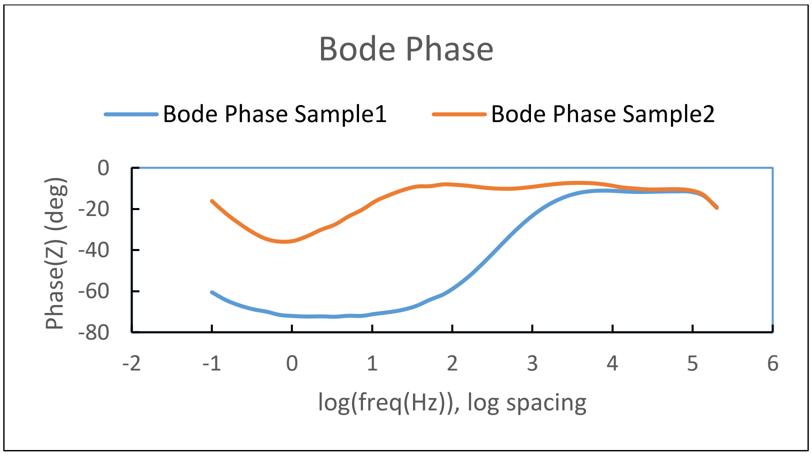

Figure 2. Bode Phase curves for Ti15Mo7Zr15Ta1Si and Ti20Mo7Zr15Ta0,75Si

The Bode Phase of Sample1(Ti15Mo7Zr15Ta1Si) and of Sample2 (Ti20Mo7Zr15Ta1Si) has a difference between the phases (see Figure 2). Sample1 have a low angle beside Sample2 which it´s angle is a little bigger. Because of the increase of the Mo, Sample2 tends to loose corrosion resistance.

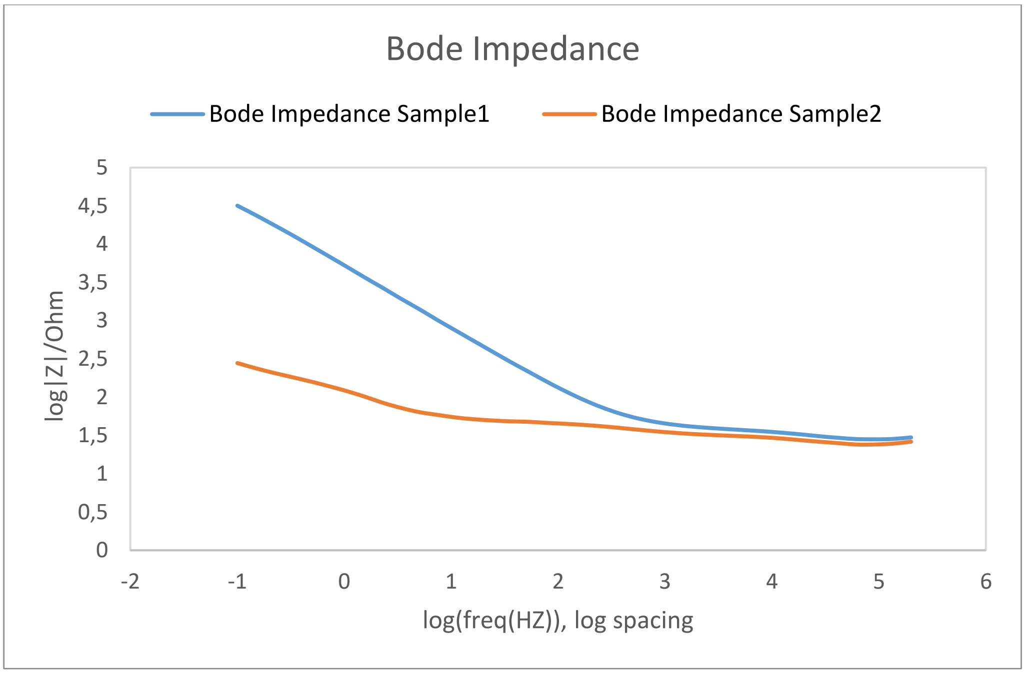

Figure 3. Bode Impedance curves for Ti15Mo7Zr15Ta1Si and Ti20Mo7Zr15Ta0,75Si

Using Figure 3 we can verify what it is said above that sample1 has a higher impedance level that means it is much more resistant to corrosion than Sample2.

Conclusion

From our analysis we can confirm that Sample1 with only 15% Mo is presenting good properties like good corrosion resistance and passivating capability. If we increase the percent to 20% Mo these properties diminish and from that Sample1 can be without fault the future material for biomedical applications.

Acknowledgements

I am very grateful to University of Las Palmas de Gran Canaria and The University Transilvania Brasov Erasmus+ for the occasion to work on this project.

References

[1] Cristina Jimenez-Marcos, Julia Claudia Mirza-Rosca, Madalina Simona Baltatu and Petrica Vizureanu in: „Experimental Research on New Developed Titanium Alloys for Biomedical Applications“ Bioengineering 2022, 9, 686.
https://doi.org/10.3390/bioengineering9110686
[2] Baltatu, M.S.; Vizureanu, P.; Sandu, A.V.; Florido-Suarez, N.; Saceleanu, M.V.; Mirza-Rosca, J.C. in : New Titanium Alloys, Promising Materials for Medical Devices.”
Materials 2021, 14, 5934.
https://doi.org/10.3390/ma14205934

SURFACE MODIFICATION OF GRAPHITIC CARBON NITRIDE WITH COPPER NANOPARTICLES

M. Carević[1], U. Stamenović[1], V.Vodnik[1], M. Čomor[1], T. Vulić[1], M. Otoničar[2], N. Abazović[1]

[1]*Vinča Institute of Nuclear Sciences, National Institute of RS, University of Belgrade,*
P.O. Box 522, 11001 Belgrade, Serbia
[2]*Jožef Štefan Institute, Department of Advanced Materials, 1000 Ljubljana, Slovenia*
**e-mail: milicab@vin.bg.ac.rs*

Abstract

Two different synthetic routes were employed to modify surface of graphitic carbon nitride (g-CN) with copper nanoparticles (CuNPs). Structure, morphology and CuNPs distribution on pre-synthesized g-CN surface are characterized by FT-IR, XRD and TEM. Results suggested that the simpler method based on mixing of precursors in inert atmosphere and room temperature, resulted in better CuNPs distribution compared to method which used refluxing as a step in synthesis.

Introduction

In the pursuit for „green“ semiconductor material with strong spectral response in visible part of the Solar spectrum, g-CN emerged as suitable candidate. This metal-free material can be easily synthesized by simple thermal treatment of nitrogen-rich precursors like urea or melamine. Usually formed as 2D material, it consists of tri -s- triazine units, interconnected by Van der Waals forces, forming layers similar to graphene sheets. With the bulk band gap energy of about 2.7 eV, it is capable for visible light absorption, while high negative potential of conduction band (≃ -1.3 V vs NHE) enables easy formation of reactive oxygen species (ROS). It is used in different photo induced processes like photocatalysts in water splitting [1] or in photoionization in free radical polymerization [1]. Additionally, special interest is given to its antibacterial ability: 2D materials can physically damage cell membrane causing cellular dysfunction and leakage of cytoplasmic components [2] or cell damage can be induced by reaction of photogenerated ROS with phospholipid molecules from cell membrane [2].

However, major drawback for wider usage of g-CN is fast recombination of photogenerated charges. Many different approaches have been probed in order to overcome this issue, including morphology control, surface modification or doping with metal ions and formation of g-CN/metal heterojunctions [2]. In this approach, nitrogen atoms act as anchors and can act as homogeneously distributed sites for adsorption of metal nanoparticles. Different metals (Fe, Zn, Ni, etc.) [2] were used in this approach, but metals like Ag and Cu were of special interest as they alone exhibit also an antimicrobial activity.

Our recent study [3], has shown that copper and its oxide also have significant antimicrobial activity, proven in cases of *Escherichia coli*, *Staphylococcus aureus* and *Candida albicans*. Antimicrobial effect originates from layer of copper oxide formed at the microbial cell wall after CuNPs adsorption, which prevents normal cell function, and subsequently leads to its death [3].

In this study, focus was on finding appropriate route to evenly distribute CuNPs on the surface of the pre-synthesized g-CN. We expect that, comparing to pristine g-CN, Cu-decorated g-CN would exhibit reduced recombination of photogenerated charges, which can be beneficial for its photocatalytic- performance, while, in the same time, antimicrobial efficacy can be improved, comparing to both individual components of heterojunction.

Experimental

Synthesis of g-CN

5g of urea powder (p.a. VWR Chemicals) is placed in ceramic crucible and heated at 550°C for 2h with the ramp rate of 10°C/min. After this time, sample is left to cool naturally, grinded and used without any further treatment.

Synthesis of Cu-gCN nanocomposites

Two synthetic procedures were used for the preparation of Cu-g-CN nanocomposites. Sample labeled as Cu-CN-1 was prepared by "in-beaker" method: under inert atmosphere (Ar$_{(g)}$), 100 ml of Cu^{2+} (0.5 mM; copper(II) chloride dihydrate, Kemika) aqueous acidic solution (pH was adjusted to 3-4 by hydrochloric acid, J.T.Baker) was stirred with g-CN (30 mg). Upon mixing, ascorbic acid (13.2 mM; Sigma-Aldrich) as an antioxidant was added. The color of the reaction mixture changes from milky white to yellowish, indicating some reduction potential of ascorbic acid, as well. Finally, after 30 min, sodium borohydride (13.2 mM; Sigma-Aldrich), as strong reducing agent, was added for complete reduction of Cu^{2+}, which is followed by immediate change in coloration of the reaction mixture to dark green/grey. The reaction under Ar(g) was left for 48 h, during which there was a gradual change in color towards final, dark yellow. The ultimate suspension was left to rest for 24 h, after which it was rinsed with water several times, dried, powdered, and characterized.

Cu-CN-2 was prepared on reflux, in the round bottom flask. Initially, g-CN (0.05 g) was suspended in 20 ml aqueous solution of sodium hydroxide (0.1 M; Aldrich). L-histidine (1 mM; Ferak, Berlin), as a reducing agent, was added, and the reaction was left stirring at 80°C for 5 h. Finally, Cu^{2+} (1 mM) was injected, and the reaction was continued for the next 19 h. There was a change of color from milky white to yellowish. After suspension's cooling to the room temperature, it was left to rest, and, further prepared for the characterization as described above. Structure and morphology of samples are characterized using X-ray diffraction (XRD, PHILIPS 1050 X-ray diffractometer using Ni-filtered Cu Kα radiation and Bragg-Brentano focusing geometry), Fourier transform infrared spectroscopy (FT-IR, ThermoScientific Nicolet 380) and transmission electron microscopy (TEM, JEOL-JEM-2100, 200 kV) techniques.

Results and discussion

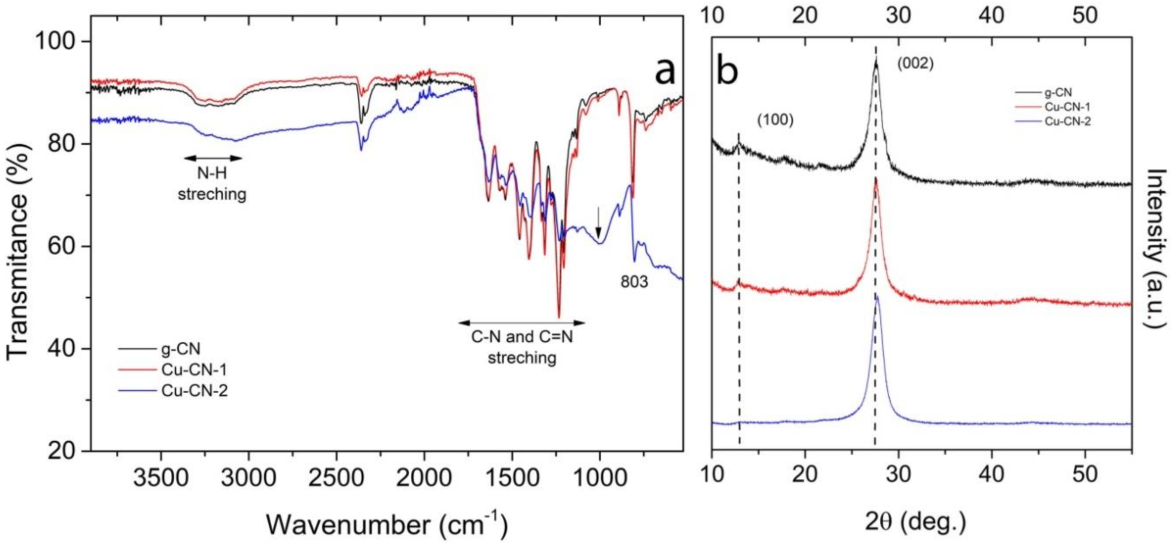

Figure 1. a) FT-IR spectra and b) XRD patterns of synthesized samples

FT-IR spectra of obtained samples are presented in Figure 1a. Three weak bands with maxima at 3277, 3189 and 3080 cm $^{-1}$ originate from N-H stretching vibrations, while bands with maxima placed between 1632 and 1206 cm^{-1} originate from C-N and C=N stretching vibrations of heterocycles. Together with band placed at 803 cm^{-1} that is assigned to breathing mode of triazine rings, all these vibrations are characteristic for g-CN [1]. FT-IR spectrum of Cu-CN-1 sample follows up the same pattern, while in the spectrum of Cu-CN-2 wide band placed at about 1000 cm^{-1} (pointed by arrow) can be assigned to CH_2 vibrations of residual L-histidine [4]. No band that can be assigned to Cu – O bond (at about 530 cm^{-1}) is detected in Cu decorated samples. However, besides difference in peaks intensity, which in the case of Cu-CN-2 can be assigned to presence of residues of L-histidine, there are no distinguished features in the spectra of Cu-decorated samples that can indicate copper presence in the samples.

XRD patterns of synthesized samples are presented in Figure 1b. Diffraction peak at 27.59° (usually indexed as (002)) corresponds to inter-planar stacking of tri-s-triazine layers, while low-intensity peak at 12.87° resembles in-plane structural packing of tri-s-triazine units (indexed as (100)). XRD patterns of both Cu-decorated samples are characterized by both peaks. No additional copper (at about 43.7 or 50.7° [5]) or copper oxide related peaks can be seen in diffractograms, probably due to detection limit of the instrumental method However, comparing to XRD pattern of pristine g-CN, main diffraction peak of Cu-CN-2 is shifted towards 27.76° which indicates additional stucking of layers, as interplanar distance is slightly decreased from 0.323 to 0.321 nm. Such a feature is not desirable as it promotes fast recombination of photogenerated charges. In the same time, significant lowering of relative intensity of low-angle peak indicates on some defragmentation in in-planar packing of triazine units.

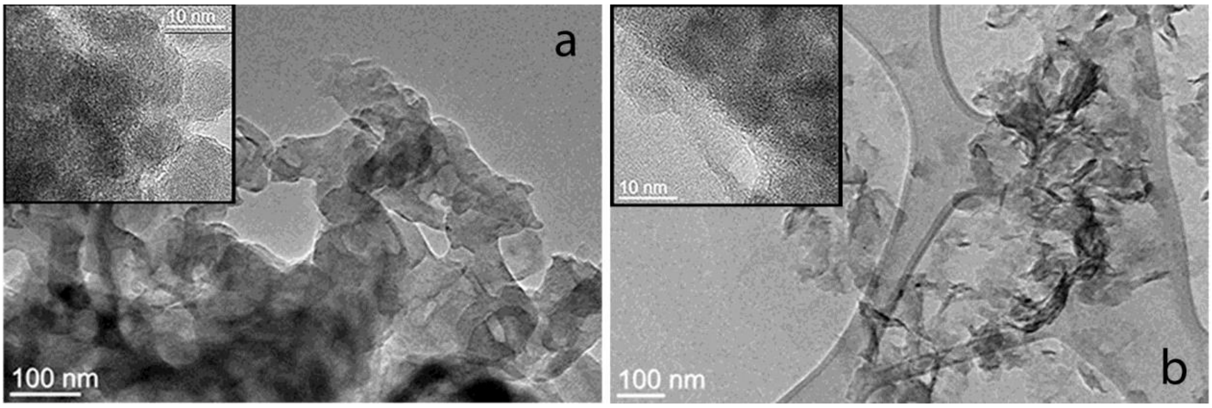

Figure 2. TEM micrographs of a) Cu-CN-1 and b) Cu-CN-2 (insets: higer magnification)

TEM micrographs (Fig. 2) gave final evidence of successful anchoring of copper on g-CN surface. Firstly, synthetic route had obvious influence on g-CN matrix: while Cu-CN-1 consists of inter-connected nanoflakes making one homogeneous structure characteristic for g-CN, g-CN matrix in Cu-CN-2 nanocomposites is partially defragmented in individual sheets. Furthermore, although presences of CuNPs with the sizes in the range from 5 to 10 nm, is obvious in both samples, their distribution is more homogeneous in Cu-CN-1 sample. In Cu-CN-2 sample, CuNPs are partially capped with L-histidine: its terminal carboxyl (hydrophilic) groups can’t anchor to hydrophobic g-CN surface, resulting in less homogeneous Cu nanoparticles distribution in Cu-CN-2 sample.

Conclusion

Two different synthetic routes were employed in decorating pre-synthesized g-CN with CuNPs. FT-IR measurements showed no presence of copper related oxides in obtained samples, while XRD measurements pointed on defragmentation of g-CN matrix in Cu-CN-2 sample. TEM micrographs confirmed presence of CuNPs formation in samples obtained by both synthetic routes: however, simpler "in beaker" method of synthesis provides better distribution of CuNPs on the surface of pre-synthesized g-CN, compared to reflux method.

Acknowledgements

This work was supported by the Ministry of Education, Science and Technological Development of the Republic of Serbia (grant no 451-03-47/2023-01/200017).

References

[1] R. C. Dante, F.M. Sánchez-Arévalo, P. Chamorro-Posada, J. Vázquez-Cabo, L. Huerta, L. Lartundo-Rojas, J. Santoyo-Salazar, O. Solorza-Feria, A. Diaz-Barrios, T. Zoltan, F. Vargas, T, Valenzuela, F. Muñoz-Bisesti, F. J. Quiroz-Chávez, Fuller. Nanotub. Car. N. 24 (2016) 171.
[2] X. Kong, X. Liu, Y. Zheng, P. K. Chu, Y. Zhang, S. Wu, Mat. Sci. Eng. R 145 (2021) 100610.
[3] U. Bogdanović, V. Lazić, V. Vodnik, M. Budimir, Z. Marković, S. Dimitrijević, Mat. Lett. 128 (2014) 75.
[4] A. B. D. Nandiyanto, R. Oktiani, R. Ragadhita, Indones. J. Sci. Technol. 4 (2019) 97.
[5] R. Betancourt-Galindo, P. Y. Reyes-Rodriguez, B. A. Puente-Urbina, C. A. Avila-Orta, O. S. Rodríguez-Fernández, G. Cadenas-Pliego, R. H. Lira-Saldivar, and L. A. García-Cerda, J. Nanomater. 5 (2013) 980545.

ENHANCED ELECTRICAL PROPERTIES OF CERAMICS THROUGH OXYGEN-ENRICHED HYDROTHERMAL SYNTHESIS

Cășuț Cristian[1,2], Marinela Miclău[1], Catalin N. Marin[2], Ursu Daniel[1], Raul Bucur[1]

[1]National Institute for Research and Development in Electrochemistry and Condensed Matter, Plautius Andronescu Str., No. 1, 300224 Timisoara, Romania
[2]West University of Timisoara, Physics Faculty, V. Pârvan Ave., No. 4, 300223 Timisoara, Romania;
e-mail: cristian.casut95@e-uvt.ro

Abstract

Considering the vast range of potential uses and the possibility of intrinsic defect engineering in the perovskite structure, bismuth ferrite ($BiFeO_3$, BFO) is still being extensively researched. $BiFeO_3$ semiconductor defect control may offer an essential approach to overcome unwanted constraints, such as high leakage current, which is linked to the existence of oxygen vacancies (VO) and Bi vacancies (VBi). Our study proposes a hydrothermal method for the reduction of the concentration of V_{Bi} during of $BiFeO_3$ ceramic synthesis [1].

The low conductivity p-type $BiFeO_3$ ceramics have been achieved by utilizing hydrogen peroxide (H_2O_2) as part of the media. Hydrogen peroxide acted as the electron donor in the perovskite structure, controlling V_{Bi} in the $BiFeO_3$ semiconductor, which caused the dielectric constant and loss to decrease along with the electrical resistivity. When comparing the hydrothermally synthesized BFO ceramic, using a hydrogen peroxide-assisted method to two different BFO ceramics used as references, the reduction of Bi vacancies highlighted by FT-IR analysis (fig. 1a) had an expected contribution to the dielectric characteristic, decreasing the dielectric constant (fig. 1b) (with approximately 40%) and loss (fig. 1c) (three times), along with an increase in electrical resistivity (fig. 1d) (three times).

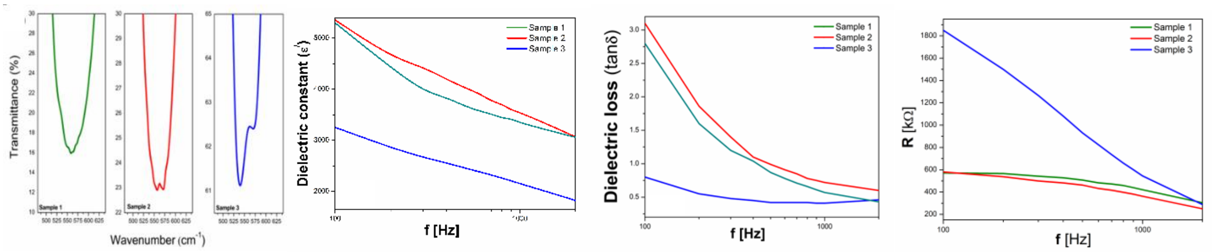

Fig.1 (a) FT-IR spectra of the samples in the range of 480 – 640 cm^{-1}; The frequency dependence of (b) the dielectric constant and (c) dielectric loss b) FT-IR spectra (d) electrical resistance

Acknowledgements Romanian National Authority for Scientific Research and Innovation, the project number *PN 23 27 01 03*, within PNCDI.

References

[1] C. Casut, R. Bucur, D. Ursu, I. Malaescu, M. Miclau; *Materials*, 2023, **16**:3130.
[2] N.M. Shah, N.H. Patel, D.D. Shah, P.K. Mehta; *Mater. Today: Proc.* 2021, **47**:616–620.

OBTAINING AND CHARACTERIZATION OF NOVEL HYBRID COMPOSITE MATERIAL BASED ON $LaMnO_3$:Ag AND POLYVINYLPYRROLIDONE

Adina Căta[1], Antonina Lazăr[1], Ioana M.C. Ienașcu[1,2], Nick Samuel Țolea[1], Daniel Ursu[1], Anamaria Dabici[1], Dan Roșu[1], Paula Sfîrloagă[1,3]

[1]National Institute of Research and Development for Electrochemistry and Condensed Matter, Dr. A. P. Podeanu 144, 300569, Timişoara, Romania
[2]"Vasile Goldiş" Western University of Arad, Faculty of Pharmacy, Liviu Rebreanu 86, 310045, Arad, Romania
[3]Spin-off Nattive-Senz SRL, Dr. A.P. Podeanu 144, 300569, Timisoara, Timis,Romania
e-mail: adina.cata@yahoo.com

Abstract

Polymer-perovskite nanocomposites have attracted the attention of researchers as multifunctional materials for the development of flexible components/devices with many significant technological uses, in which the favorable characteristics of inorganic perovskite nanofiller and organic polymer are effectively integrated [1].

Nanosized filler polymer composites exhibit outstanding properties due to the unique characteristics of nanoparticles, such as the high surface-to-volume ratio and large interfacial area formed between the matrix and nanoparticles, with enhanced mechanical, electrical, and thermal properties. Nanocomposites that combine the advantages of polymer and filler (ceramics) can be processed more easily and are viable alternatives to plain/doped ceramic materials [2].

The procedure for obtaining the hybrid material consists in mixing the precursors in a mass ratio of 20:1 (Polyvinylpyrrolidone/$LaMnO_3$:Ag) and dispersing them in distilled water. The resulting suspension was stirred for 2 hours maintaining the temperature at 80°C, at 400 rpm. The resulting viscous mixture was cast into thin film of 2-5 mm thickness on a flat surface (polypropylene film) and dried at room temperature for 12 hours. The polymer-perovskite film was triturated until a homogeneous mixture with small grain size (up to 1 mm) was obtained and then dried in a forced convection oven, at 60°C for 12 hours.

The major advantage of this method is the obtaining of nanomaterials with small dimensional distribution, of nanometric order, in a relatively short time interval, with controlled morphology and uniform distribution of particles, and with a large specific surface area. Another advantage of this method is the better control over the growth rate of the particles, at a relatively low working temperature (80 °C).

To determine the crystal structure, the obtained hybrid materials were characterized by X-ray diffraction, UV-VIS and RAMAN spectroscopy. Also, to highlight the morphology of the particles, the scanning electron microscopy was used.

References

[1] A.A. Al-Muntaser, R.A. Pashameah, K. Sharma, E. Alzahrani, S.T. Hameed, M.A. Morsi, Opt. Mater. 132(2022), 112799.
[2] S.B. Basturk, C.E.J. Dancer, T.Mc Nally, Mater. Res. Bull., 135(2021), 111126.

Acknowledgements

This work was supported by the Experimental Demonstrative Project 683PED/2022.

THE INFLUENCE OF THE TREND OF URBAN GROWTH OF CITY OF NOVI SAD ON AIR QUALITY IN PARKS

Aleksandra M. Cavic, **Marko S. Carić**

University Business Academy in Novi Sad, Faculty of Economy and Engineering Management
in Novi Sad, 21000 Novi Sad, Cvecarska 2, Serbia
e-mail: aleksandra.cavic22@gmail.com

Abstract

Quality control of air in urban green areas - urban parks are rarely studied spaces, and this paper is based on research on the effects and impacts of microclimatic parameters on the detected suspended particles (PM 2.5 and PM10) with a multidisciplinary influence on public health and the quality of life of Novi Sad citizens. Excessive urbanization of urban environments and global migrations are among the most important causes of increased concentrations of air pollutants, even in urban green areas such as parks. This scientific research is part of a project focused on the effects and discrepancies of microclimatic parameters on detected concentrations of total suspended particles in the city's green parks in Novi Sad. Three urban parks of different sizes and locations with varying microclimatic influences were selected. Measurements of suspended particles (PM) were conducted at Futoški Park (FP), Dunavski Park (DP), and Limanski Park (LP) using a mobile device Aeroqual Series 500. At each location (FP, DP, LP), 10 measurements of suspended particle concentrations were conducted, with the device reporting changes in detected particle concentrations in real time. The results of the measured concentrations of suspended particles indicate variations in detected particle concentrations, with PM2.5 ranging from 4 to 36.1 µg/m3, while PM10 was detected in the range of 7 to 40.1 µg/m3. The measurement period for suspended particle pollution ranged from 12:00 to 17:30, with measured temperature fluctuations from 24.1 to 30.0°C and measured relative humidity oscillating between 39.1% and 54.4%.

Keywords: air quality, suspended particles PM 2.5 µm and PM10 µm, parks, city of Novi Sad, urban growth.

Introduction

According to reports from the World Health Organization (WHO), approximately 90% of the world's population lives in areas that exceed the concentrations deemed safe in prescribed air quality guidelines [1]. Particulate matter (PM 2.5 and PM10) in the air is highly respirable and, as such, very harmful to human health. In recent times, it has garnered significant attention from experts, legislative and regulatory bodies, as well as non-governmental and civil sectors, along with the general public [2].The significant global migrations and the increase in the population are accompanied by urbanization and economic activities. According to United Nations projections, 68% of the world's population will live in cities by 2050. Therefore, it is crucial for cities to implement adequate measures to protect the health of their residents and the environment, as these areas are closely interconnected [3]. This trend of urbanization and population migration is also evident in the city of Novi Sad, which serves as the administrative center and seat of the autonomous province of Vojvodina. Atmospheric particles (PM - particulate matter) represent microscopic suspended particles in Earth's atmosphere, consisting of solid or liquid matter. Anthropogenic particles are formed during combustion processes, such as diesel fuel soot, during photochemical reactions like urban smog, from vehicle exhaust emissions, industrial facilities with high-temperature processes, coal-fired power plants, foundries, steel mills, internal combustion engines, waste incineration, as well as from the resuspension of dust originating from construction sites [2].

Clean air is a fundamental need for every human being, especially in urban ecosystems where lifestyle and high population density lead to a rapid increase in the number of passenger cars and urban public transport on city roads, accompanied by a rise in the construction industry and the number of construction sites. If we consider all the negative impacts on air quality in urban environments, we can identify the benefits of improving public health and reducing pollutants of anthropogenic origin (urban traffic, industry, construction sites, and others). Knowing that the most numerous visitors to city parks are children and elderly individuals, who represent the most vulnerable groups that are most affected by polluted air, measurements of air pollution with suspended particles PM2.5 and PM10 in these locations are crucial. This is particularly important because such measurements are not covered within the framework of the national air quality monitoring in Novi Sad.

Experimental

For indicative air quality measurements, we used the mobile device Aeroqual Series 500 - monitor, which measures and records changes in pollution levels in real-time. This device operates based on the use of semi-permeable sensors that are sensitive to various particles and gases. This technology combines smart measurement techniques and semiconductor sensors based on metal oxides that exhibit changes in electrical resistance in the presence of the measured gas. The sensors are housed in a replaceable sensor head that connects to the base of the monitor. Each sensor head contains only one gas or particle sensor. The sensor head uses a built-in fan for active sampling, directing air towards the sensor, after which the air exits on the opposite end. The device utilizes a long-lasting lithium battery. The device's screen displays the minimum, maximum, and average values of the measured gas in ppm or mg/m3 [8]. The sensor head for measuring PM2.5 and PM10 particles has the following characteristics: the measurement range is from 0.000 to 1.000 mg/m3, with a laser particle counter, a minimum detection limit, and a resolution of 0.001 mg/m3. The accuracy is ± (0.002 mg/m3 + 15% of the reading). The sensor head operates at temperatures between 0 and 40°C and air humidity of 0 - 90% without condensation [9].

For this research, air quality measurements of particulate pollution PM2.5 and PM10 were conducted in three city parks that are considered natural monuments and are under state protection. The selected parks vary in size, occupying different areas, and are located in different parts of the city, each surrounded by varying levels of traffic frequency. These parks were included in the study with the aim of assessing air quality, detecting possible pollution, and comparing the results with measurements from the year 2020 [2]. The research aims to propose measures for further reducing potential environmental pollution and influencing more aggressive greening efforts on other public areas in the city, including the construction and development of new city parks.

Table 2 Average values of measurements

	Temperature (°C)		Relative humidity (%)		PM$_{2.5}$ (μg/m^3)		PM$_{10}$ (μg/m^3)	
Location	2020	2023	2020	2023	2020	2023	2020	2023
FP	18.35	28.35	48	42.65	9	5.2	10.5	9.4
DP	22.1	24.3	41.5	53.6	4.5	16.2	10.5	23.8
LP	22.5	25.16	41	48.77	2.5	12.4	5.5	35.6

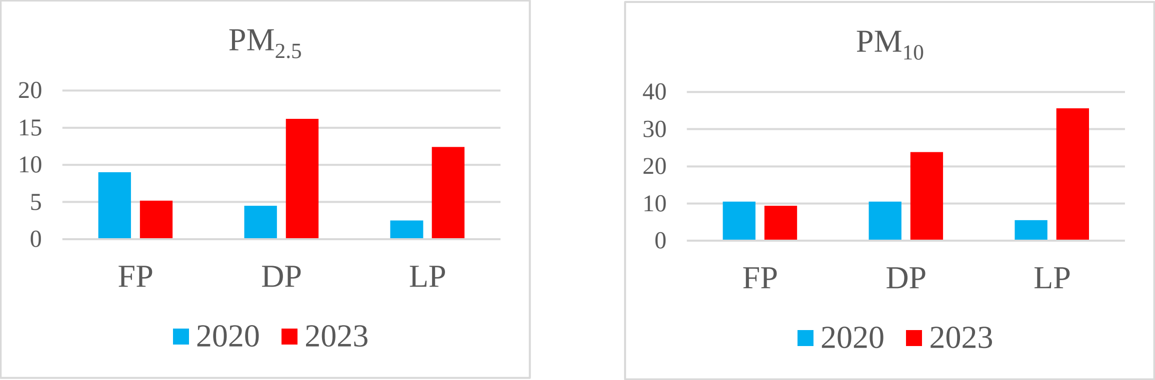

Picture 1 Comparision of particulate matter average values

Results and discussion

The benefits of spending time in urban nature/city parks are significant for both physical and mental health. There are several hypotheses regarding the positive effects of being in nature on the human body, especially for modern individuals who often lack the time to venture into natural settings during their workweek or weekends. Improving air quality can result in sustainable health benefits, including reducing air pollution levels, which can lead to a decrease in premature deaths and diseases such as stroke, heart disease, lung cancer, and chronic and acute respiratory illnesses, including asthma. Implementing sustainable environmental policies to reduce air pollution and mitigate climate change can yield multiple interdisciplinary benefits for urban residents, especially in the transportation, industry, and construction sectors. These benefits include noise reduction and more. Environmental air pollution, both ambient and indoor air, is gaining increasing importance in the healthcare sector every year, particularly when polluted air represents a significant ecological risk to human health, alongside climate change. Each year, it is responsible for nearly 7 million deaths that can be attributed to global causes [1].

By analyzing the measured average values of suspended particles in the city parks, specifically at the locations FP, DP, and LP, in the year 2023 and comparing them with the results from 2020, the following conclusions can be drawn:

1. In FP, the measured values of PM2.5 and PM10 have decreased compared to 2020. PM2.5 values exhibited a more dominant drop, decreasing by 43,3%, while PM10 values decreased by 11,7%.
2. In DP, the values in 2023 have increased compared to 2020. PM2.5 values have risen by a factor of 3.6 and PM10 values have exhibited nearly identical growth, increasing by a factor of 2,26.
3. In LP, there has been an increase in PM2.5 values by a factor of 4.96, and PM10 values have increased by a factor of 6,47.

All the measured values of PM2.5 and PM10 in 2023 were within the time range of 12:00 to 17:30, with measured average temperature fluctuations between 24.30°C and 28.30°C, and relative humidity oscillations ranging from 42.65% to 53.36%. In 2020, the average temperature fluctuations were between 18.35°C and 22.5°C, and the measured average relative humidity oscillated between 41% and 48%. The comparison between data from 2020 (a year marked by COVID-19 with restrictive measures promoting reduced human activities) and 2023 reveals a significant increase in particulate air pollution in 2023, especially when considering the measured values for DP and LP. However, FP experienced a decrease in the concentration of PM2.5 and PM10.

These noticeable differences in suspended particle concentration are the result of multiple factors, including: 1. Park Location: Parks located near major urban thoroughfares with intense motor vehicle traffic and lacking adequate protective green barriers or tree lines on the street side of the park to shield against vehicular exhaust pollution and noise. 2. Population Growth: An increase in the number of residents over the last three years, which has been accompanied by a rise in the number of passenger vehicles on city roads. 3. Construction Sites: The presence of construction sites, which can contribute to air pollution. 4. Climate Change: The presence of climate change effects, such as rising temperatures, increased humidity, and moderately gentle winds. These conditions can also contribute to increased particulate pollution, although not to the same extent.

These factors, combined with the absence of restrictive measures like those implemented during the COVID-19 pandemic, have likely contributed to the observed increase in particulate air pollution, especially in DP and LP. It emphasizes the importance of ongoing efforts to monitor and mitigate air pollution in urban areas. FP, in 2023, shows reduced particle pollution levels compared to measurements taken in 2020, which can be explained by its advantageous location. This park, of medium size relative to other city parks, is enriched with a substantial number of trees and shrubs with extensive canopies that serve as an effective green barrier. These natural features diminish the potential transmission of particle pollution from nearby roadways and adjacent residential areas. The abundant presence of canopy and shrub vegetation within the park creates a robust green barrier, and the park itself acts as an isolated protected ecosystem. These factors, along with favorable climatic conditions, contribute to the reduction of particle pollution. DP, considered the most beautiful urban park located in the city center, exhibits a remarkable surge in the levels of PM particles detected in 2023 compared to measurements taken in 2020. This alarming increase can be attributed to the substantial presence of suspended particles originating from nearby major roadways, as well as the immediate vicinity of two large construction sites (the construction of two extensive underground garages and individual residential unit projects). Additionally, the park's proximity to the Danube River may also play a role in this rise in particle concentration. LP, in terms of its surface area, is the largest compared to the previous two parks. Its location and the proximity to major roadways, extensive vegetation, and the Danube River, along with several nearby construction sites, directly contribute to the detected significant increase in suspended particle levels in 2023 compared to 2020.

Conclusion

Monitoring air quality in urban areas is becoming increasingly important, with a particular focus on urban locations that lack automatic stations for measuring and directly monitoring air quality. The rise in air pollution from particulate matter serves as an alarm for taking necessary measures in terms of early warning and preventive actions. The data presented in this study highlights the significance of this research for the public health of the urban population and the need for installing more monitoring stations in city locations not covered by national, local, regional, and national networks. The focus of this study is on air quality in urban parks to provide better information on air quality and recommendations for spending time in urban green oases. It's essential to enhance and empower the advantages of the flat terrain and expand the existing 100 km of cycling lanes in Novi Sad, suitable for eco-friendly means of transportation. An increasing number of Novi Sad residents opt for bicycles, and the 40,000 residents who currently use them must be a driving force for further investments in new cycling lanes, especially as electric scooters are on the rise. Consistent enforcement of legal and sub-legal acts, sound urban planning, and a multidisciplinary approach to expanding green spaces in cities aim to promote and improve physical activity as a healthy lifestyle and, of course, enhance public health for the urban population of Novi Sad.

Acknowledgements

The authors acknowledge the financial support of the Provincial Secretariat for Higher Education and Scientific Research, Autonomous Province of Vojvodina, Republic of Serbia, within the Project No. 142-451-3066/2023-01.

References

[1] WHO World Health Organization. Ambient Air Pollution: A Global Assessment of Exposure and Burden of Disease. ISBN: 9789241511353 (2016).
[2] Cavic A, Solesa D, Aksentijevic S, Kiurski J., 2020. Air pollution in city parks during the Covid-19 pandemic. International Symposium on Analitical and Environmental Problems (26; Szeged) (104-108). ISBN: 978-963-306-771
[3] https://www.unicef.org/serbia/
[4] Republic of Serbia, Road Traffic Safety Agency, https://www.abs.gov.rs/en/about-rtsa
[5] https://www.gradnja.rs/
[6] Health Effects Institute. State of Global Air 2019. Special Report (Health Effects Institute, Boston, 2019). ISSN 2578-6873.
[7] Statistical Office of the Republic of Serbia, https://www.stat.gov.rs/en-US/publikacije
[8] Kiurski et al., 2019 Kiurski J., Solesa D., Ignjatijevic S, Vapa-Tankosic J. (1029) Characteristic aero polutants of the City Novi Sad (Serbian) Monography, University Business acedemy in Novi Sad, Faculty od Eonomics and Engineering Management in Novi Sad
[9] Aeroqual 2010, Aeroqual Product catalogue
[10] Gržetić I. (2010) Suspended and Respirable Particles in Urban Areas, Faculty of Chemistry, University of Belgrade (In Serbian)
[11] K.L. Medard, H. Hamilton, S.C. van der Moore, J. Chem. Anal. 313 (2007) 163.

ACTIVATION OF PEROXOMONOSULFATE ION BY BIOCHAR FOR THE DEGRADATION OF TRIMETHOPRIM IN AQUEOUS SYSTEMS

[1]Dinesh Chandola, [1]Sinkovics Erik, [2]Zsuzsanna László and [1]Tünde Alapi

[1]Department of Molecular and Analytical Chemistry, University of Szeged, H-6720 Szeged,
Dóm tér 7, Hungary
[2]Department of Biosystem Engineering, Faculty of Engineering, University of Szeged,
Moszkvai Blvd. 9., H-6725 Szeged, Hungary
e-mail: dinesh.chandola@chem.u-szeged.hu

Water treatment processes have recently faced many challenges; one of these is the removal of trace pollutants from biologically treated waters in order to prevent their release into our environment. Advanced Oxidation Processes (AOPs) based on sulfate radical ($SO_4^{\bullet-}$) generation are efficient methods for water treatment that have gained attention in recent years. Highly reactive $SO_4^{\bullet-}$ can be generated in various ways; one of them is the application of biochar, as a sustainable and cost-effective carbon catalyst of persulfate activation.

In this study, the application of various biochars for the activation of peroxomonosulfate ion (PMS) and degradation of trimethoprim antibiotic, as an emerging pollutant of surface waters was examined. Biochars were prepared from different raw materials, such as grass pellets (GP-BC), corncobs (CC-BC), and poplar wood (PW-BC). The effect of pyrolysis temperature (500, 600, and 700 °C) and ball milling on the adsorption properties and activity of biochars was investigated. In catalytic runs, PMS concentration (up to 2.0 mM) and BC dose (up to 3000 mg dm^{-3}) were changed. The contribution of various reactive species was also investigated.

During preliminary experiments, the BCs were used without ball milling, and the dose of BC and PMS was changed. 3000 mg dm^{-3} BC and 2.0 mM PMS were found to be optimal in terms of trimethoprim degradation. The activity depended on the raw material, and 71% (PW-BC), 78% (CC-BC), and 93% (GP-BC) trimethoprim elimination was reached after 120 minutes of treatment. Ball milling highly enhanced the surface area and adsorption capacity, and, consequently, the activity of BCs. In the case of ball-milled GP-BC, a dose of 500 mg dm^{-3} was sufficient to degrade 65% and 88% of the TMP with a 0.1 mM and 0.2 mM PMS dose, respectively, in 60 min. reaction time. However, with a PMS dose of 1.0 mM, trimethoprim completely degraded within 2 minutes. The GP-BC was found to be the most efficient for PMS activation, thus, the effect of pyrolysis temperature was investigated in this case. Even though the increase in pyrolysis temperature (500→700 °C) results in decreased adsorption capacity, the reactivity of BC prepared under 700 °C was the best in terms of PMS activation and trimethoprim degradation. The contribution of various reactive species, such as $^{\bullet}OH$, $SO_4^{\bullet-}$, and singlet oxygen ($^1O_2$), was investigated by the effect of radical scavengers, and singlet oxygen ($^1O_2$) was found to be mainly responsible for trimethoprim degradation. The efficiency of the BC/PMS process was compared to BC/H_2O_2 process, as an alternative method, and BC/PMS was found to be superior. For the BC/H_2O_2 process, less than 20% of trimethoprim could be transformed after 60 min treatment, while using the BC/PMS process, 90% transformation efficiency was reached using the same experimental conditions.

Based on our results, the prepared BCs are suitable for PMS activation and, consequently, for trimethoprim degradation. The activity of BC depends on the quality of the starting row material and the pyrolysis temperature and can be significantly increased by ball-milling due to the increased specific surface area. However, the formed $^1O_2$ is a selective reaction partner, which may limit the applicability of the method in the case of other organic removal.

INVESTIGATION OF THE EFFECTIVENESS OF THE UV/ClO_2 PROCEDURE FOR THE ELIMINATION OF TRACES OF ORGANIC POLLUTANTS FROM AQUEOUS SOLUTIONS

Anett Covic, Tünde Alapi

Department of Molecular and Analytical Chemistry, University of Szeged, H-6720 Szeged,
Dóm tér 7, Hungary
e-mail: covicanett@chem.u-szeged.hu

The removal of persistent organic pollutants with a biological effect requires the development of a water treatment process that can be used as a supplementary or quaternary process. Most often, chlorine-containing substances, such as HOCl, Cl_2, and less often ClO_2, are used for water disinfection in drinking water production. The combination of chlorination with UV photolysis is called the UV/chlorine process, is one of the Advanced Oxidation Processes (AOPs), and can be used to eliminate trace organic pollutants. The application of ClO_2 is getting more and more attention due to its excellent disinfecting effect, and relatively high oxidation potential. Using ClO_2, the disinfection byproducts (including THMs) formation can be reduced; however, toxic chlorite and chlorate formation and chlorination of organic substances pose a potential risk.

The development of UV-LEDs enables their application in water treatments, especially in the UV/ClO_2 process. The absorption spectra of ClO_2 have a maximum of 359 nm (ε =1250 M^{-1} cm^{-1}). Thus high intensity UV-LED emitting at 367 nm is adequate for the efficient photolysis of ClO_2 to generate radicals. The ClO_2/UV process was investigated in the transformation of two pharmaceuticals, namely trimethoprim (TRIM), an antibiotic, and 5-fluorouracil (5-FU), a chemotherapeutic antimetabolite; both are frequently detected in wastewater and surface waters. The effect of pH (3.0 – 9.0), ClO_2 concentration (up to 14 ppm), and photon flux (4.44×10^{-6}–2.45×10^{-5} $mol_{photon}s^{-1}dm^{-3}$) were studied. ClO_2 was added to the treated solution every 5 minutes until the target substance (1.0×10^{-4} M) was degraded.

The UV radiation decomposes the ClO_2 within 3 minutes, even at the highest 14 ppm dosage and lowest photon flux, and results in a complex radical set in an aqueous solution, including reactive oxygen- (ROS) and chlorine-containing species (RCS), such as ${}^{\bullet}OH$, $O^{\bullet}$, $O_2^{\bullet-}$, $Cl^{\bullet}$, $ClO^{\bullet}$, and $Cl_2^{\bullet-}$. The UV/ClO_2 method proved to be more effective for TRIM transformation, mainly due to its high reactivity towards RCS. The pH has no effect on ClO_2 transformation but slightly affects the transformation rate 5-FU (pK_a = 8.0), as a consequence of the different reactivity of its protonated and deprotonated forms. The effect of radical scavengers proved that besides ROS and RCS, singlet oxygen (${}^1O_2$) has an important role in the transformation.

The ecotoxicity of the treated samples slightly increased, most probably because of the formation of chlorinated organic substances and chlorate ions. Results of AOX and ion chromatography measurements proved the formation of these substances.

Biologically treated domestic wastewater having high Cl^- (120 mg L^{-1}) and HCO_3^- (524 mg L^{-1}) concentration reduced the efficiency of the process for both compounds with different extend. The effect of HCO_3^- is complex, as it changes the pH to 9, and behaves as an RCS scavenger changing the radical set in this way.

Acknowledgment

This work was sponsored by the National Research, Development, and Innovation Office-NKFI Fund OTKA, project number FK132742.

PRELIMINARY RESEARCH ON THE USE OF SHEEP'S CHEESE AS A SOURCE OF MINERAL ELEMENTS

Antoanela Cozma[1*], Casiana Mihut[1], Anisoara Duma-Copcea[1], Lia Rotariu[1], Ariana Velciov[2], Sofia Popescu[2], Mihaela Petcu[3], Maria Rada[4]

*1*Department of Soil Sciences, University of Life Sciences "King Michael I" from Timisoara, 300645, Timisoara, Romania e-mail: antoanelacozma@yahoo.com*
2 Department of Food Science, University of Life Sciences "King Michael I" from Timisoara, 300645, Timisoara, Romania ariana.velciov@yahoo.com
3Faculty of Veterinary Medicine, University of Life Sciences "King Michael I" from Timisoara, 300645, Timisoara, Romania e-mail: ptc_mihaela@yahoo.com
4University of Medicine and Pharmacy "Victor Babes" – Faculty of Medicine, 2 Efimie Murgu Sq., 300041, Timisoara, Romania;
e-mail: antoanelacozma@yahoo.com

Abstract

Milk and dairy products represent valuable nutritional foods, which bring many benefits to the health of the human body. The nutritional quality of sheep's cheese is given by nature as well by the content of essential mineral elements that enter into its composition. Therefore, the evaluation of the nutritional quality, of the sheep's cheese mineral intake is conditioned by knowing the concentrations of the mineral elements that are part of this food. The aim of the paper is to determine the concentrations of some essential mineral macro- and microelements: Ca and Mg, respectively: Fe, Zn and Cu from sheep's cheese and to evaluate the mineral intake of this food product in the recommended daily diet. The sheep's cheese taken in the experiment is well represented in terms of the content of: Ca, Mg, Fe, Zn and Cu, essential mineral elements with a beneficial effect on the body. In the analyzed sheep's cheese were identified high amounts of calcium (4892±275 mg/kg) and magnesium (443±38.64 mg/kg), significant amounts of Zn (22.14±1.52 mg/kg) and Fe (9.78±1.29 mg/kg) and appreciable amounts of Cu (1.07±0.17 mg/kg). The mineral profile of this nutritional food shows the following decreasing trend: Ca>> Mg>> Zn >Fe >> Cu.

Introduction

Worldwide, cheese has become a major agricultural product. exceeding the annual production of coffee beans, cocoa, tea or tobacco. Currently, cheese can be obtained from sheep, cow, but also goat or buffalo milk. It serves as one of the good sources of essential nutrients such as proteins, lipids, minerals and vitamins [1,2]. Cheeses can be classified according to several criteria, such as: manufacturing process or country of origin, fat content, type of milk used and the animal from which it is obtained, and the consistency of the varieties . It is a functional food with an important weight in the human diet, being a rich source of essential nutrients such as: proteins, carbohydrates, amino acids, fats, fatty acids, vitamins and essential minerals [3,4]. The type of milk used is very important for the quality of the cheese. The sheep milk is a valuable product with high nutritional value compared to the milk of other domestic species being used mainly for the cheese production [5]. Due to its protein content with high biological value, Telemea cheese is of great nutritional importance. The special characteristics of the cheese are given by the significant amount of minerals, beneficial to human nutrition, such as calcium, magnesium, phosphorus, potassium and sodium. The sheep cheese is part of the category of traditional white brined cheeses from East-Mediterranean countries produced in all countries of the region under various names: Feta,Telemes(Greece); Telemea/Braila cheese

(Romania); Bjalo salamureno sirene/Bjalo sirene (Bulgaria); Bieno sirenje (FYROM); Mohant (Slovenia); Sjenicki, Homoljski, Zlatarski, Svrljiški (Serbia); Pljevaljski, Polimsko-Vasojevaski, Ulcinjski (Montenegro); Travnicki/Vlasicki (Bosnia-Herzegovina); Beyaz peynir, Edirne peyniri (Turkey); Liqvan, Iranian white (Iran); Brinza (Israel); Akawi (Lebanon); Domiati, Mish (Egypt) [8].

Experimental

Sheep's cheese contains important amounts of essential mineral elements, unevenly distributed according to a number of factors including: the origin of the milk used to obtain the cheese, processing and packaging techniques, etc. For this reason, knowing the distribution of these essential mineral elements is very important for assessing the quality of this food product. To achieve the proposed goal, three samples of different salted sheep's cheese (in brine), were purchased, from three agro-food markets in Timişoara, which originated from local producers of the Banat plain area. For each collection point, were taken 500g of local sheep's cheese prepared in the months of May - June of 2023 which (after homogenization) constituted the basis for the preparation of the samples taken for the analysis. The results obtained from the analysis of these average samples were noted in the present paper, according to the place of collection, as: sample A, sample B, sample C. Concentrations of Ca, Mg, Zn, Fe and Cu from sheep cheese samples were determined by atomic absorption spectrometry in the air-acetylene flame. The concentration of the mineral elements in the cheese samples taken in the experiment was achieved by the acetylene flame atomic absorption spectrometry method, following a protocol described by Gogoasa *et al.* [7]. This protocol involves the mineralization of cheese samples through calcination, followed by the solubilisation of ashes in acid HNO_3 0.5 N and measuring the absorbance of mineral elements in the acid solution. The device used was atomic absorption spectrophotometer in air flame - acetylene, brand Varian AA 240 FS, a laboratory water bath and a thermal regulation electric stove. Also, the reagents used are Nitric acid Merck, 65% (ρ = 1.39 g/cm3) to prepare the nitric acid solution 0.5 N; standard solutions for the analyzed elements: Ca, Mg, Fe, Mn, Zn and Cu, obtained from the concentrated standard solution Merck Darmstadt - Germany, 1.000g/ml. The total concentration of analysed microelements was determined by the relationship:

$$C\ [mg/kg] = \frac{a \cdot 50}{m}$$

where: a – element concentration read of the device(mg/l); m –sample mass (g) taken into study

Results and discussion

The experimental results obtained from the analysis of the mineral elements in the sheep cheese samples taken in the experiment are presented in the table 1

Table 1

Total concentration of Ca, Mg, Zn, Fe and Cu in sheep cheese

Specification	Mineral content, mg/kg of raw product				
	Ca	Mg	Zn	Fe	Cu
Sample A	4835	496	20.17	8.46	0.86
Sample B	5254	405	22.36	9.51	1.28
Sample C	4588	428	23.88	11.37	1.10
Average values	***4892±275***	***443±38.64***	***22.14±1.52***	***9.78±1.29***	***1.07±0.17***

As can be seen from Table 1, the distribution of Ca, Mg, Fe, Zn and Cu in sheep cheese analysed samples is non-uniform, being dependent on the origin of the sample and on the nature of the analysed element. The concentration of these elements varies between 0.86 mg/kg Cu - 5254 mg/kg Ca. The best represented among the analyzed elements are the macroelements: Ca (4892±275 mg/kg) and Mg (443±38.64mg/kg). Microelements were identified in much lower concentrations, their average concentrations being: 22.14±1.52 mg/kg Zn, 9.78±1.29 mg/kg Fe and 1.07±0.17 mg/kg Cu. The mineral profile of sheep's cheese shows the following decreasing trend: Ca>> Mg>> Zn >Fe >> Cu. Calcium, essential macroelement, indispensable for the development of the bone system in childhood and adolescence, but also for the maintenance of bone health throughout life.

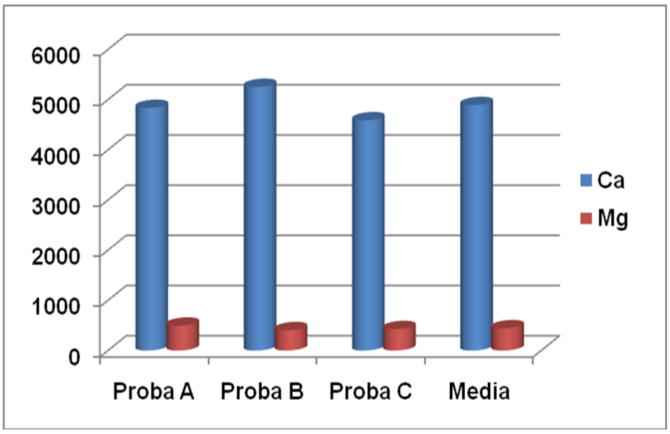

Figure 1. Distribution of Ca and Mg in sheep cheese

Calcium, an essential macroelement, is the best represented among the analyzed elements, the average concentration of this macroelement being 4892±275 mg/kg. Magnesium, an essential macroelement, was identified in much lower concentrations than Ca, but much higher than the microelements: Zn, Fe and Cu. The average concentration of Mg is 443±38.64 mg/kg.

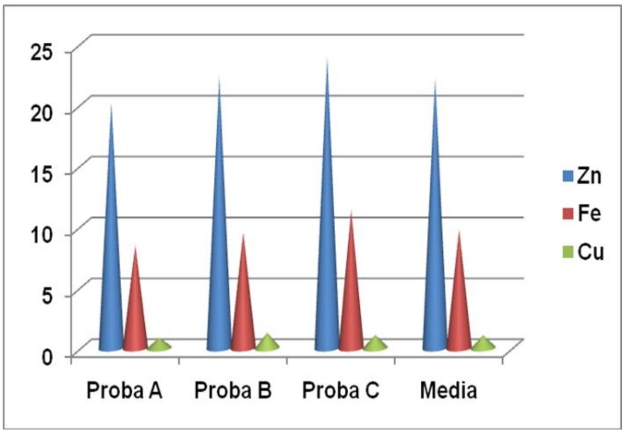

Figure 2. Distribution of Zn, Fe and Cu in sheep cheese

Zinc, an essential microelement, was identified in much lower concentrations than Ca and Mg, but higher than Fe and much higher than Cu. This is the best represented among microelements, its concentration limits being between 20.17 - 23.88 mg/kg. Iron, an essential trace element, was determined in concentrations between 8.46 -11.37 mg/kg. The average Fe concentration

(9.78±1.29 mg/kg) is much lower than Ca and Mg concentrations, lower than Zn concentration and higher than Cu concentration. Copper, an essential microelement, was determined in the lowest concentrations among the elements analyzed (1.07±0.17 mg/kg).

Conclusion

Due to the supply of vitamins (A, D, E, K) and minerals (Ca, P, Mg), fatty acids (FA), cheeses are a basic food that the body needs to function normally. The sheep's cheese taken in the experiment is well represented in terms of the content of: Ca, Mg, Fe, Zn and Cu, essential mineral elements with a beneficial effect on the body. Increased amounts of calcium and magnesium, significant amounts of Zn and appreciable amounts of Cu were identified in the analyzed sheep's cheese. The distribution of mineral elements in the analyzed sheep's cheese shows unevenness, their average concentrations having the following values: 4892±275 mg/kg Ca, 443±38.64mg/kg Mg, 22.14±1.52/kg Zn, 9.78±1.29 mg/kg Fe and 1.07±0.17mg/kg Cu. The mineral profile of this food shows the following decreasing trend: Ca>> Mg>> Zn >Fe >> Cu. In the conditions of the present study, it can be stated that the analyzed sheep's cheese can be considered as a mineralizing food, especially from the point of view of the content of Ca, Zn, and Mg.

References

[1] Cadar O., Tănaselia C., Miclean M., Levei E., Şenilă M., Şenilă L., Analysis of Minor and Trace Elements in Cow, Goat and Sheep Milk in the NW Part of Romania, ProEnvironment 9, pp 87 – 90, 2016

[2] Zamberlin S., Antunac N., Havranek J., Samarzija D., Mineral elements in milk and dairy products, Mljekarstvo 62 (2), Croatia, pp. 111-125, 2012

[3] Walther B., Schmid A., Sieber R., Wehrmuller K**.,** Cheese in nutrition and health, Dairy Science &Technology, EDP Sciences/ Springer, 88 (4-5), pp. 389–405, 2008

[4] V. Levkov, T. Stafilov, N. Pacinovski, K. Bačeva, N. Mateva, N. Gjorgovska, E. Eftimova, T. Kostadinov, The content of mineral elements in curd and traditional white brined cheese, Veterinarija ir Zootechnika (Vet Med Zoot). T. 75 (97). 2017, pp. 36-42

[5] Manuelian C.L., Currò S., Penasa, M., Cassandro, M., De Marchi M**.,** Characterization of major and trace minerals, fatty acid composition, and cholesterol content of Protected Designation of Origin cheeses, J Dairy Sciences.;100(5): 3384-3395, May 2017

[6] Blažić M., Pavić K., Zavadlav S., Marčac N., The impact of traditional cheeses and whey on health, Croatian Journal Food Science Technology, Vol.9(2) pp.198-203, 2017

[7] Gogoasa I., Gergen I., Rada M., Parvu D., Ciobanu C., Bordean D., Marutoiu C., Moigradean D.,AAS detection of heavy metal in sheep cheese (the banat area, Romania), Buletinul USAMV-CN Vol.62., pp 240-245, 2006

[8] Alichanidis E., Polychroniadou A., Characteristics of major traditional regional cheese varieties of East-Mediterranean countries: a review, Dairy Science and Technology, Vol.88, Issue 4-5, pp.495–510, July 2008

DIFFERENT CONCENTRATIONS OF BIOSTIMULATORS IMPACT COLORIMETRIC PARAMETERS OF INTENSIVELY MANAGED TOMATO (*Solanum lycopersicum* L.) FRUITS

Márk Kondacs[1], Anna Divéky-Ertsey[2], László Csambalik[2]

[1]*Moroko Farm Kft., III. Külkerület 223, Szarvas 5540, Hungary, kondacs.mark04@gmail.com*
[2]*Department of Agroecology and Organic Farming, Institute of Rural Development and Sustainable Production, Hungarian University of Agricultural and Life Sciences, Villányi út 29-43., Budapest 1118, Hungary,*
e-mail: csambalik.laszlo.orban@uni-mate.hu

Negative impacts of artificial fertilizers on the agro-environment drive farmers to moderate agrochemicals use. Reduction or abandonment of the easily accessible nutrients would cause decreases in yields; alternative solutions, such as soil and plant biostimulators can contribute to balanced nutrient management. Technologies and nutrient supply solutions of organic farming systems can serve as an example for conventional farmers to substitute agrochemicals and to sustain higher yields, as well as favorable nutritional quality and marketabilty.

In this study, two biostimulants (Kondisol®, Amalgerol®) were applied in three different doses (2, 4, 6 l/ha) in an intensively managed open field tomato (*Solanum lycopersicum* L. cv 'UG 13577') cultivation system, in Szarvas, Hungary (46°53'09"N 20°38'16"E). The applied doses were determined as 50%, 100%, and 150% of the suggested values. Tomato plants were arranged in rows, one plot consisted of 20 plants. Together with control plots, each treatment was done in triplicate; randomized complete block design was applied for the total of 21 plots. Biostimulants were sprayed out in four repetitions, according to the suggested technology of the manufacturers. Intensive tomato cultivation practices were applied according to the cultivation practice of the company owner. After harvesting the fruits in full ripening stage, homogenates were prepared and colorimetric parameters (L*, a*, b*, CIELAB) were measured with a Konica Minolta CR 410 colorimeter in three repetitions. Hue (h^o) and chroma C*), as well as a*/b* values were calculated; data were analyzed using one-way analysis of variance (ANOVA) ($p<0.05$). Chroma values were significantly decreased by using the biostimulators in 2 and 6 l/ha doses. Increases of hue values were experienced after using Kondisol® in 2 and 4 l/ha doses. The most favorable a*/b* values were measured in the case of applying biostimulants in 4 l/ha dose. The results suggest that the applied doses had higher impact on the measured colorimetric parameters, than the biostimulant itself. Deviations from the suggested technology can ruin the color traits of intensively managed tomato fruits.

SYNTEHIS AND CHARACTERIZATION OF Pr^{3+} DOPED YTTRIUM SILICATE VIA SOL-GEL METHOD

George-Daniel Dima[1,2], **Radu Bănică**[1], **Andrei Racu**[1], **Miroslav D. Dramićanin**[1], **Cristina Mosoarca**[1]

[1]*Renewable Energies – Photovoltaics Laboratory – National Institute of Research and Development for Electrochemistry and Condensed Matter, 300569 Timișoara, Dr. A. Păunescu Podeanu, Str., 144, România*
[2]*University Politehnica Timisoara, Faculty of Industrial Chemistry and Environmental Engineering, 6 Pârvan, 300223 Timisoara, Romania*
e-mail: george.dima@student.upt.ro, m.crristina@gmail.com

Abstract

$Y_2SiO_5:Pr^{3+}$ is a widely recognized optical material that is utilized for the conversion of visible blue light into ultraviolet-C radiation (UV-C), thus producing conceivable antibacterial effects [1]. The silicate in question exhibits two distinct allotropic forms. The first form is observed at lower calcination temperatures and exhibits a monoclinic crystal structure with space group P21/c (X_1). The second form, on the other hand, is observed at higher temperatures and possesses the space group I*/a (X_2) [2]. Nevertheless, the literature often fails to adequately address the significance of ensuring the homogeneity of the reaction precursor while synthesizing these silicates. The diffusion coefficient of ions in SiO_2 and Y_2O_3 is influenced by temperature, as indicated by their high melting temperatures. This temperature dependence is observed even at a temperature of 1000°C [3].

The objective of this study is to synthesize Pr^{3+}-doped yttrium silicate using two distinct methodologies. The initial approach involved the utilization of pre-synthesized oxide precursors, while the subsequent method capitalized on co-precipitated oxides. Subsequently, the samples underwent calcination processes at temperatures of 1350 °C and 1050 °C, respectively, as per the aforementioned methods. In the initial scenario, the discrepant velocities observed in the hydrolysis and condensation reactions of tetraethyl orthosilicate, as well as the precipitation of Y^{3+}, no longer exert an impact on the uniformity of the precursor substances. The aforementioned approaches offer a precise means of controlling the composition and uniformity of the synthesized products, rendering them a favorable option for the advancement of superior materials. The produced materials were subjected to analysis using X-ray diffraction (XRD), photoluminescence spectroscopy, and first antimicrobial assays.

Acknowledgements

This study was supported by Romania's National Recovery and Resilience Plan, NRRP, project C9-I8-28/ FC 760107/2023.

References

[1] F. Lai, X. Xu, J. Shen, et al., Silicon, 15 (2023) 1913–1923.
[2] N. Verma, J. Kaur, V. Dubey, N. Dubey, T. Ram, Inorg. Chem. Commun., 147 (2023), 110234.
[3] A. Dwivedi, Anuradha, M. Srivastava, A. Srivastava, R. Kumar, S. Kumar Srivastava, Spectrochim. Acta A Mol. Biomol., 299 (2023) 122782.

INHIBITORY EFFECT OF METOPROLOL IN THE CORROSION OF MILD STEEL IN ACID MEDIA

George Daniel DIMA[1], **Nataliia RUDENKO**[2], **Cristian-George VASZILCSIN**[3], **Mircea Laurențiu DAN**[1],

[1]*University Politehnica Timisoara, Faculty of Industrial Chemistry and Environmental Engineering, 6 V. Pârvan, 300223 Timisoara, Romania*
[2]*University Politehnica Timisoara, Innovation and Technology Transfer Center, 2 V. Pârvan, 300223 Timisoara, Romania*
[3]*National Institute of Research and Development for Electrochemistry and Condensed Matter, Dr. A. P. Podeanu 144, 300569, Timişoara, Romania*
e-mail: mircea.dan@upt.ro

Abstract

The aim of the study is to investigate the inhibitory effect of Metoprolol on the corrosion of OL-45 steel in a neutral 3.5% sodium chloride media. Metoprolol is a part of the beta-adrenergic blocker class that is widely used in the treatment of angina, heart failure, and arterial hypertension. It prevents the heart and the blood vessels from being affected by adrenaline [1]. In this paper, the corrosion inhibition of the drug mentioned was caused by the presence of the aromatic ring and the functional groups that have unpaired electrons, such as the etheric group, amino group, and hydroxilic group [2]. These functional groups provide the capacity for the drug to be adsorbed on the metal surface level, thus preventing the attack of chlorine ions from the corrosive environment [3].

The corrosion behavior has been studied using electrochemical techniques such as cronopotentiometry, chronoamperometry and the Tafel polarization method at a scan rate of 1 mV s^{-1}, in the presence and absence of different amounts of the drug. Quantum chemical calculations have been performed in order to confirm the inhibitory effect of the drug studied. The basis set B3LYP/6-31G* was employed to establish the model of the electronic structure of the molecule that permits the accurate calculation of the molecular descriptors, such as E_{HOMO}, E_{LUMO}, dipole moment, ionization energy, and electron affinity [4]. The theoretical calculus confirms the inhibitory effect of the Metoprolol in neutral media obtained by the electrochemical methods. This study provides important insights for applications in saline industrial settings by highlighting Metoprolol as a viable corrosion inhibitor for OL 45 steel in NaCl conditions.

Acknowledgements

This paper was supported by Politehnica University Timișoara in the frame of PhD studies.

References

[1] D. Felkle, M. Jarczyński, K. Kaleta, K. Zięba, K. Nazimek, Biomedicine & Pharmacotherapy, 153 (2022) 113287.
[2] H. Mobtaker, M. Azadi, N. Hassani, M. Neek-Amal, M. Rassouli, M. Amin Bidi, Journal of Molecular Liquids, 335 (2021) 116183.
[3] Y. Tian, W. Guo, W. Wang, B. Wang, P. Zhang, T.Zhao, Construction and Building Materials, 368 (2023) 130385.4] N. El-Aouni, R. Hsissou, Z. Safi, S. Abbout, F. Benhiba, J. El Azzaoui, R. Haldhar, N. Wazzan, L. Guo, H. Erramli, A. Elharfi, A. El Bachiri, M. Rafik, Colloids and Surfaces A: Physicochemical and Engineering Aspects, 626 (2021) 127066.

MINERAL PROFILE OF FLOURS AND BLENDS CONTAINING GERMINATED ALFALFA SEEDS

Marijana Djordjević[1], Miljana Djordjević[1], Radosław Spychaj[2], Ewa Pejcz[3], Lidija Perović[1], Biljana Cvetković[1], Olivera Šimurina[1]

[1]Institute of Food Technology in Novi Sad, University of Novi Sad, 21000 Novi Sad, Blvd. cara Lazara 1, Serbia
[2]Department of Fermentation and Cereals Technology, Faculty of Biotechnology and Food Science, Wroclaw University of Environmental and Life Sciences, 51-630 Wrocław, J. Chełmońskiego 37, Poland
[c]Department of Biotechnology and Food Analysis, Faculty of Engineering and Economics, Wroclaw University of Economics and Business, 53-345 Wroclaw, Komandorska Street 118/120, Poland
e-mail: marijana.djordjevic@fins.uns.ac.rs

Abstract

Unlike lentil, chickpea, soybean, lupin and bean, alfalfa (*Medicago sativa* L.) represent an underexplored legume regarding the application in food products intended for human consumption. Despite being abundant in nutrients such as proteins, dietary fibers, essential polyunsaturated fatty acids, minerals, vitamins and associated total phenols, its inclusion in staple food formulations such as bakery products is scarce. A possible explanation for this could be the presence of antinutrients and beany flavor in alfalfa-containing products which humper its full usage potential. A simple but effective strategy for overcoming this issue and enhancing the nutritional and sensory profile of alfalfa as well as the bioavailability of corresponding compounds is subjection to bioprocessing treatment such as germination. Germination as a naturally occurring process is also considered convenient regarding enhancement of minerals' bioaccessibility and release from bound complexes with antinutritional factors in legume seeds. Therefore, the main aim of this research was to evaluate the mineral profile of non-germinated (ASC) and germinated alfalfa seed flour (GASC). Additionally, examination was performed on white wheat flour-alfalfa blends containing ASC and GASC in different amounts (5 and 10%) intended for the production of bakery products. Analyzed and quantified were micro- (Fe and Zn) and macro- (Na, Ca, Mg and K) elements by means of atomic absorption spectrometer following the ISO 6869:2000 method.

Significantly higher amounts of all analyzed minerals were detected in non-germinated and germinated alfalfa seed flour compared to white wheat flour. Conducted germination altered mineral profile of the alfalfa flour by inducing an increase in Ca and Zn content (58.06 mg/100 g and 3.60 mg/100 g, respectively) with a simultaneous decrease in Mg, K, and Fe content compared to non-germinated alfalfa seed flour. Consequently, a significant improvement regarding mineral profile was also observed in white wheat flour-alfalfa blends. Distinctive were blends containing 10% alfalfa flour, regardless of type, especially when it comes to Fe content which reached 2.30 mg/100 g.

In conclusion, ASC and GASC can be used for mineral profile enhancement of wheat flour, particularly when included in higher amounts (10%).

Acknowledgments: The work has been conducted in the frame of CEEPUS network HR-0306-15-2223 "For Safe and Healthy Food in Middle-Europe" and it is supported by the Ministry of Science, Technological Development and Innovations of the Republic of Serbia [number 451-03-47/2023-01/200134].

TOWARDS SUSTAINABLE BIOCONVERSION OF LIGNOCELLULOSE: SCREENING OF THE ANTIOXIDANT POTENTIAL OF WASTE STREAMS FROM WHEAT CHAFF PRETREATMENTS

Tatjana Đorđević, Mirjana Antov

Faculty of Technology, University of Novi Sad, Blvd. Cara Laza 1, Novi Sad, Serbia
e-mail: tatjanadjordjevic@uns.ac.rs

Abstract

In recent years, many studies have been conducted on bioconversion technologies and processes to utilize lignocellulosic biomass as feedstock for producing bio-based fuels and fine chemicals. Nevertheless, the life cycle assessment of lignocellulosic-derived products rarely considers waste treatment. To overcome the problems coming from waste accumulation and low recycling efficiency, and to enhance economic feasibility, a novel reuse strategy that enables the utilization of all streams from lignocellulose bioconversion should be investigated.

Wheat chaff, an insufficiently exploited and inexpensive lignocellulosic material, was subjected to ultrasonic (US), alkali (AL) or hydrothermal (HT) pretreatments prior to enzymatic conversion to simple sugars. Applied pretreatments induced various changes in physical and/or chemical characteristics of lignocellulose material resulted in the highest and the lowest production of reducing sugars in liquid waste stream - 5.8 mg/mL and 0.68 mg/mL after HT and US, respectively. The antioxidant potential of waste streams generated after all pretreatment was evaluated using the ABTS and DPPH in vitro assays. The results showed that all waste streams exhibited high antioxidant activity. The waste stream generated after alkali pretreatment had the lowest EC50 values assayed by both applied methods indicating its considerable antioxidant potential. The EC50 values were 0.01 mg/mL and 0.03 mg/L, measured by ABTS and DPPH, respectively. The results suggested that the waste streams from the studied pretreatments could be valuable sources of compounds with excellent antioxidant capabilities that could improve the economic and environmental aspects in wheat chaff bioconversion and valorization route in the future.

Acknowledgements

This study was supported by the Ministry of Science, Technological Development and Innovation of the Republic of Serbia (Grant No. 451-03-47/2023-01/ 200134).

OCCURRENCE OF POLYBROMINATED DIPHENYL ETHERS IN HOUSEHOLD DUST IN BOSNIA AND HERZEGOVINA

Duško Đukić, Nataša Đurišić-Mladenović, Jelena Živančev

University of Novi Sad, Faculty of Technology Novi Sad, Bulevar cara Lazara 1, 21 000 Novi Sad, Serbia
e-mail: duskodjukic93@gmail.com

Abstract

Considering the amount of time people spend in their homes, workplaces, and indoor environments, human exposure to specific indoor pollutants can cause severe health issues. Indoor persistent organic pollutants are causing adverse health effects via dust ingestion and dermal absorption. Worldwide researchers have dedicated their attention to brominated flame retardants (BFRs) due to their ubiquitous occurrences in the environment. The aim of this study was to determine the occurrence and levels of brominated organic pollutants in indoor dust samples (n=40), collected from homes and indoor environments in three settlements from the entity of the Republic of Srpska in Bosnia and Herzegovina. The samples are prepared and analyzed by the method based on gas chromatography with mass spectrometric detection (GC-MS) for the presence of 7 polybrominated diphenyl ethers (PBDE). This research study will report for the first time the levels of 7 PBDE congeners analyzed in dust samples from households in the indoor environments of the Republic of Srpska, Bosnia and Herzegovina. The obtained results will be used for risk assessment which is of great importance in understanding the impact of PBDEs in household dust on human health.

MICROWAVE AND ULTRASOUND-ASSISTED EXTRACTION OF MONOMERIC ANTHOCYANIN PIGMENT CONTENT FROM PLANT RESIDUALS

Réka Dobozi[1], Zoltán Péter Jákói[2], Krisztina Keszthelyi[1], Sándor Beszédes[2]

[1]Department of Food Engineering, University of Szeged, H-6724 Szeged, Mars tér 7, Hungary
[2]Department of Biosystems Engineering, University of Szeged, H-6725 Szeged, Moszkvai krt. 9, Hungary
e-mail: dobozireka@mk.u-szeged.hu

Abstract

Our investigation focused on the intensification of monomeric anthocyanin pigment content (MAC) extraction from raspberry residuals by using microwave (MW) and ultrasound (US) radiation with different solvents, and to monitor the efficacy of these processes by the assessment of the dielectric behavior of the extracts. All the experiments were carried out with using 5 grams of the raspberry raw material mixed with 100 cm^3 of three different solvents – distilled water, hydrochloric acid, and the mixture of HCl and citric acid – separately. For the intensification processes, microwave and ultrasonic radiation were used in three different total irradiated energy input values: 30 kJ, 45 kJ and 60 kJ. The MAC content was analyzed according to the AOAC official method for total monomeric anthocyanin pigment content, while the dielectric behavior of the extracts was analyzed with laboratory dielectric assessment kit. Our results revealed that using MW irradiation as an intensifying process for extraction can be effectively used in the lower irradiated energy range (30 kJ), and the higher level of power (500W) is more efficient, regardless of the applied solvent. If, however, ultrasonic radiation is being used, usually the higher the energy intensity, the higher the yield of MAC can be observed. The assessment of dielectric behavior proved that a strong correlation (r=0.98-0.99) can be found between the dielectric constant (ε') and the MAC concentration of the extracts, regardless of the intensifying method and solvent used.

Introduction

The significance of anthocyanin pigments to food quality lies in their role in enhancing color and visual appeal, and growing attention is being paid to the anthocyanin levels in food products and nutraceuticals due to their potential health advantages. The concentration of these pigments serves as a valuable metric for the quality assurance and procurement guidelines of fruit juices, nutraceuticals, and natural color additives. Anthocyanins account for the red, purple, and blue shades found in most fruits, vegetables, and grains [1]. Six prevalent types of anthocyanidins exist—namely, pelargonidin, cyanidin, peonidin, delphinidin, petunidin, and malvidin. These structures can differ based on glycosidic modifications at the 3 and 5 positions, and further diversity arises from the acylation of sugar groups with organic acids. The extraction process commonly employs solvents like water, methanol, ethanol, often acidified with hydrochloric or citric acid to stabilize the anthocyanins [2]. The extracted solution is then subjected to various purification and concentration methods, such as solid-phase extraction or liquid chromatography. The resulting anthocyanin extracts are widely used in food, pharmaceuticals, and cosmetics for their antioxidant properties and vibrant colors. During the first stage of extraction, using solvents without any intensification method usually grants low or negligible yield [3] and thus, it is usually combined with various thermal and/or mechanical treatments. Among these, the microwave or ultrasound-assisted extraction (MAE or UAE) methods have already shown promising results, compared to conventional hot-water extraction (HWE) [4]. MAE is primarily based on the dielectric heating mechanism caused by the absorption of microwaves, which induce rapid, selective heating inside the bulk material, depending on its dielectric properties. Since plant cells contain high amount of bounded and free water, they can absorb and store electromagnetic energy easily, and due to the polar nature of water molecules, this absorbed electromagnetic energy can be easily dissipated, i.e., can be converted into heat. Therefore, when exposed to microwaves, large amount of heat is generated inside the plant cells, which comes with the increase in pressure as well. When the pressure inside the plant cell exceeds a critical value, the cell wall eventually disrupts [5], and the different substances – anthocyanins, for example - found in the intracellular space or in the cell wall are released. UAE is based on a vastly different principle, namely the ultrasound-induced cavitation. Cavitation is a physical phenomenon that occurs when a substance suddenly changes from a liquid phase to a gas phase due to pressure drop. The explanation is that if the velocity of a liquid in a particular direction increases suddenly, its pressure decreases according to Bernoulli's law. The resulting bubble, if it is placed along the flow line at a point where the pressure exceeds the saturation vapor pressure for the temperature at that point, will suddenly burst, and the liquid surfaces in sudden contact with each other will produce a shock wave. High-intensity ultrasonic irradiation induces high and low frequency cycles in the absorbing liquid. During the high-frequency cycle, small vacuum bubbles or cavities are created, which grow throughout the cycle, and then these bubbles collapse during the low-frequency cycle. When these cavitation bubbles collapse, a momentary (micro- or nanosecond-long), but extremely high increment of temperature and pressure occur. These, and the shockwaves generated by the collapsing of cavities expose the material to mechanical stress and shear, which cause the degradation and disruption of plant cell walls [6].

Applying measurements to identify the dielectric behavior of certain compounds or media have been widely investigated as a promising tool for process monitoring. Dielectric assessment is rapid, sensitive, non-destructive and doesn't necessitate the use of strong chemicals, therefore it can be a great alternative to conventional analytic methods. The fundamental mechanisms behind the dielectric behavior are to be found in electrodynamic properties, namely that an electromagnetic field with any strength E causes a so-called dielectric shift D in real materials, which can be understood as a kind of phase shift δ. In case E is not excessively high, the proportionality between E and D remains, and as the frequency increases the emerging δ phase difference becomes more and more prominent. The frequency at which the phase shift becomes noticeable depends – among others - on the temperature and the chemical, physical properties of the medium, and can be written as:

$$\varepsilon^* = \frac{D}{E} = |\varepsilon| e^{-j\delta} \tag{1}$$

Using the Euler-identity and separating the real and imaginary parts we get:

$$\varepsilon^*(f) = \left|\frac{D}{E}\right| (cos\delta - jsin\delta) = \varepsilon'(f) - j\varepsilon''(f) \tag{2}$$

Based upon the previous equation, the material's response can be characterized by the so-called dielectric properties, e.g. dielectric constant (ε'), dielectric loss factor (ε'') or loss tangent (tanδ). ε', the real part of the complex permittivity shows the electric (or electromagnetic) energy absorbing and storing capability of materials, ε'' – the complex part of the permittivity – shows how much of the absorbed and/or stored energy is converted into heat or other types of energy, while tanδ incorporates the latter two ($tan\delta = \frac{f\varepsilon\prime'' + \sigma}{\varepsilon\prime}$) and denotes quantitatively the dissipation of the electrical energy due to different physical processes such as electrical conduction, dielectric relaxation, dielectric resonance and loss from non-linear processes.

Experimental

The raw material for extraction was raspberry expeller / press cake, a residue originated from the juice-pressing of raspberry fruits. The average water content *W%* was 68.42%, while the dry matter content (*DMC*) 1.579 g. For the extraction process, three different solvents were applied (separately): pure distilled water (pH=6.8), hydrochloric acid (pH=2) and the mixture of HCl and citric acid (pH=2). Using HCl can help disrupt the plant cell wall by depolymerizing it, however the oxidative environment above a certain extent can be harmful for the target components as well. Citric acid can help stabilize the target molecules and making them more resilient to oxidation and/or thermal impacts. For the intensifying operation, microwave (P= 250W and 500W) and ultrasound (200W power) irradiation were being used with different operational times, achieving 30 kJ, 45 kJ and 60 kJ total irradiated energy, respectively. After the extraction step, the total anthocyanin content was analyzed by the standard AOAC differential pH spectrophotometric method. Simultaneously, the dielectric properties of the extracts were determined as well, using a DAK 3.5 (SPEAG GmBh, *Germany*) open-ended dielectric sensor connected to a vector network analyzer (ZVL-3, Rhode&Schwarz GmBh, *Switzerland*) with a 50-ohm coaxial power supply line.

Results and discussion

In the first part of our investigations, we wanted to see how the different solvents and utilized intensifying operations affect the yield of MAC in the extracts. Figure 1 shows the results obtained for the pure water extraction during MAE and UAE with three different total energy outputs, incorporating the dielectric constant of the extracts at f=700 MHz.

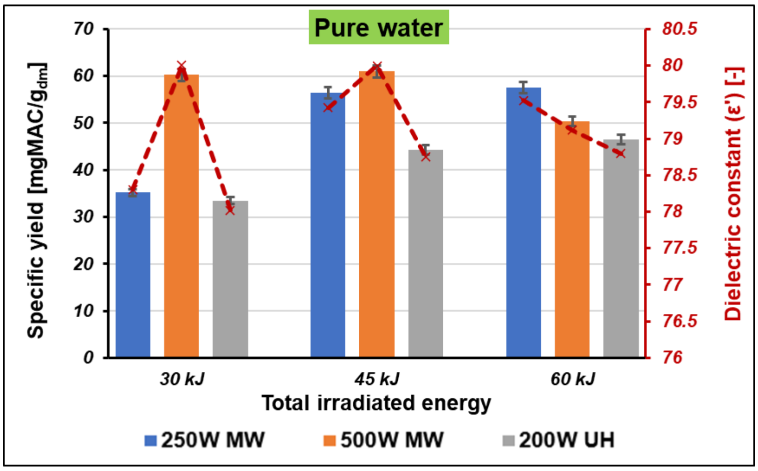

Figure 1. *Specific yield of MAC during the pure water extraction with the different intensifying operations, along with the values of ε'(700 MHz).*

Results indicate that a prominent difference can be found between the different utilized power levels of MAE, especially at low (30 kJ) irradiated energy outputs. Using 500W MW radiation for extraction at 30 kJ energy level resulted in approx. 60 mgMAC/g_{dm} (g_{dm} = grams of dry matter), which is almost two times higher than that of 250W MW or US. The reason behind might be that using higher power means increased electromagnetic (MW) field strength, which ultimately results in higher and faster bulk heating, compared to the 250W power level of MW. Since the ultrasound-assisted extraction is not based on heating mechanisms, the results suggest that a 30 kJ total irradiated energy was not enough in case of ultrasonication to cause enough mechanical stress to disrupt the plant cells. Increasing the total energy from 30 kJ to 60 kJ causes no significant change in terms of 500W MW treatment, whereas the yield obtained with 250W MW is higher. When the total irradiated energy exceeded 60 kJ, the specific yield suddenly decreased in the case of 500W MW, which can be explained by the fact that MACs are usually sensitive to heat, and the extent of heat energy might have induced thermal degradation. This phenomenon can not be observed when the level of MW power was set to 250W, indicating that the profile of temperature increase was steadier, but slower. Using ultrasonication does not increase the temperature of the material considerably, and therefore thermal decay can not be observed there, however the higher the energy output, the higher the disintegration of the cell walls, providing increased yield of MAC. Considering all the different approaches, it can be stated that from an energetic point of view, using 30 kJ total energy with 500W MW irradiation has the greatest efficiency in terms of MAC yield per unit dry matter. Observing the results of the dielectric constant, it can be seen that a similar tendency can be found, i.e., if the yield of MAC was higher, the value of ε' was also higher, indicating a relationship between these two parameters.

Among the acidic solvents, the MAC yield was slightly higher when HCl + citric acid was used regardless of the applied intensifying operation or total irradiated energy. Based on the results, it can be also observed that the addition of citric acid could indeed preserve the target substance to some extent, especially at higher energy outputs (Figure 2). The highest efficiency, like in the case of pure water extraction, was achieved when using 500W MW radiation at 30 kJ total energy.

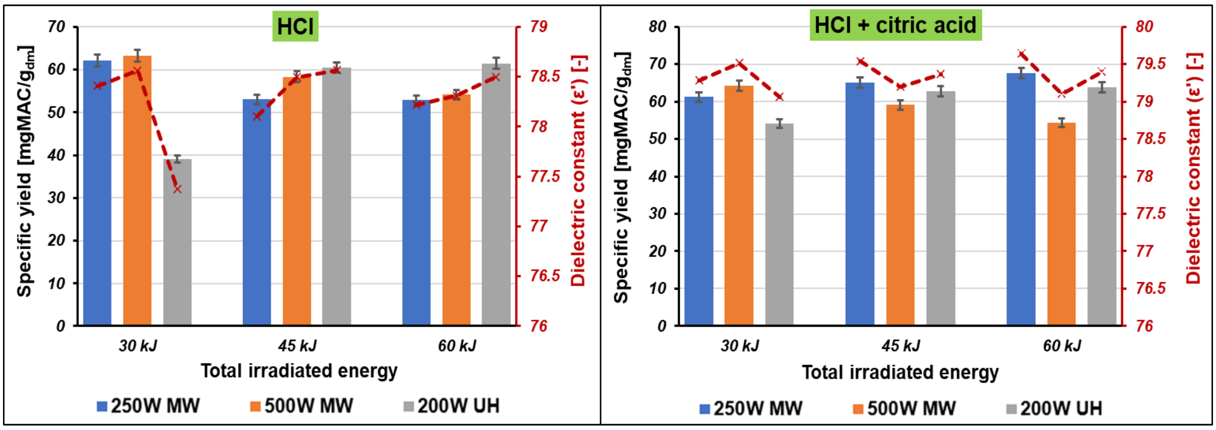

Figure 2. *Specific yield of MAC during the acidic (HCl & HCl + citric acid) with the different intensifying operations, along with the values of ε'(700 MHz).*

Like in the case of water solvent extraction, the trend of the dielectric constant rigorously followed the MAC yield, regardless of the applied treatment, and/or energy output value. The differences in the 'absolute' value of ε' is mostly due to the application of different solvents: the dielectric properties of HCl and citric acid are significantly different than that of pure water. In order to see the strength of this connection, we constructed linear functions between the concentrations of anthocyanin, and the corresponding dielectric constant (Figure 3). These results suggest a strong linear correlation between the specific MAC yield and the dielectric constant of the extracts (with coefficient of correlation r being 0.98-0.99), regardless of the applied solvent, or intensifying method. This ultimately also means that measuring the dielectric behavior of these samples are "non-selective", i.e., it only depends on the exact yield itself, and not on the method or process it was achieved with, making it a potential universal tool for monitoring extraction processes.

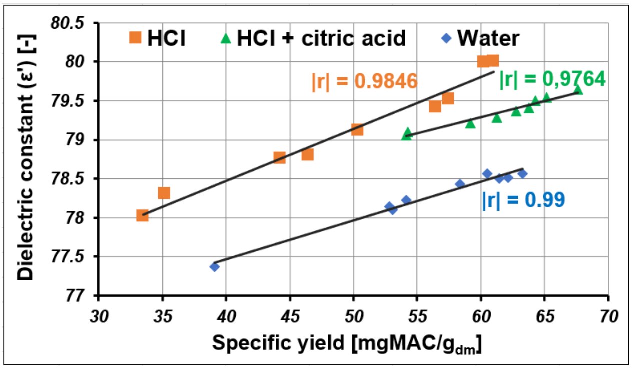

Figure 3. *Correlation between the 700MHz dielectric constant and MAC yield*

Conclusions

Our study focused on the microwave and ultrasound-assisted extraction of anthocyanin from raspberry by using different solvents, and comparing the results for yield with the dielectric behavior of the extracts. The experiments showed that regardless of the applied solvent, using relatively low (30 kJ) total energy output and 500W microwave irradiation resulted in the highest MAC yield, and when the energy level increased, the total yield decreased in case of the MAE – potentially due to thermal degradation. In case of the ultrasound process, the higher the total energy, the higher the MAC yield turned out to be, implying that this method mostly governs mechanical effects in the disruption of plant cell walls. Independent from the solvent or intensifying operation, the 700MHz dielectric constant showed a strong linear correlation with the MAC yield of the extracts, making it a promising, precise monitoring tool.

Acknowledgements

The authors are grateful for the financial support provided by the New National Excellence Program of the Ministry for Culture and Innovation from the source of the National Research, Development and Innovation Fund, under funding numbers UNKP-23-3-SZTE-246, ÚNKP-23-5-SZTE-668, and UNKP-23-2-SZTE-249. This project was supported by Bolyai János Research Scholarship of the Hungarian Academy of Sciences (BO/00161/21/4).

References

[1] Gitelson, A. A., Merzlyak, M. N., & Chivkunova, O. B. (2001). Optical properties and nondestructive estimation of anthocyanin content in plant leaves. Photochemistry and photobiology, 74(1), 38-45

[2] Silva, S., Costa, E. M., Calhau, C., Morais, R. M., & Pintado, M. E. (2017). Anthocyanin extraction from plant tissues: A review. Critical reviews in food science and nutrition, 57(14), 3072-3083.

[3] López, C. J., Caleja, C., Prieto, M. A., Barreiro, M. F., Barros, L., & Ferreira, I. C. (2018). Optimization and comparison of heat and ultrasound assisted extraction techniques to obtain anthocyanin compounds from Arbutus unedo L. Fruits. Food Chemistry, 264, 81-91.

[4] Gamage, G. C. V., & Choo, W. S. (2023). Hot water extraction, ultrasound, microwave and pectinase-assisted extraction of anthocyanins from blue pea flower. Food Chemistry Advances, 2, 100209.

[5] Jákói, Z. P., Lemmer, B., Dobozi, R., Hodúr, C., & Beszédes, S. (2023). Using Dielectric Constant Measurement to Monitor Ethanol Fermentation and Anaerobic Co-Digestion of Lignocellulosic Biomass. Fermentation, 9(10), 902.

[6] Wu, Z., Ferreira, D. F., Crudo, D., Bosco, V., Stevanato, L., Costale, A., & Cravotto, G. (2019). Plant and biomass extraction and valorisation under hydrodynamic cavitation. Processes, 7(12), 965.

EFFECTS OF $SmCoO_3$ ADDITION ON PHASE STRUCTURE, MICROSTRUCTURE AND ELECTRICAL PROPERTIES OF $BaTiO_3$ CERAMICS

Bucur Raul Alin, Farkas Iuliana

National Institute for Research and Development in Electrochemistry and Condensed Matter, Condensed Matter Department, No. 1 Plautius Andronescu, 300224 Timisoara, Romania.
e-mail: raul_alin_bucur@yahoo.com

Abstract

$BaTiO_3$ is the most widely studied ferroelectric material, with applications ranging from tunable dielectrics [1], piezoelectric sensors [2] to elasto-optic elements [3]. Since its discovery [4], interesting characteristics useful for different applications were obtained, by adding different perovskite dopants: $BaSnO_3$ [5], $NaNbO_3$ [6], $(Bi_{0.5}Na_{0.5})TiO_3$ [7] or $Pb(Sn,Ti)O_3$ [8]. Up to date, the influence of rare earth perovskites on the properties of $BaTiO_3$, is not properly discussed. The transitional metal perovskite oxide $SmCoO_3$, is a candidate material for applications in electromechanical devices, such as solid oxide fuel cells [9], gas sensor for O_2 and CO_2 [10] or electrolyte-gated thin-film transistors [11]. Recent reports related to $(Bi_{0.5}Na_{0.5})_{0.94}Ba_{0.06}TiO_3$ lead-free ceramics shows that Sm_2O_3 doped ceramics exhibit a typical relaxor behavior with diffuse phase transition, while enhancing the degree of ferroelectric relaxation behavior as Sm_2O_3 concentration increases [12], with a maximum piezoelectric constant of $d_{33} = 202$ $pC\cdot N^{-1}$ and a quality factor of 101. $SmCoO_3$ doping [13] will contribute to an increase of the quality factor (219) and a good value of the piezoelectric constant $d_{33} = 144$ $pC\cdot N^{-1}$. Both reports observed a promoted grain growth for certain compositions.

The aim of this work is to determine the influence of $SmCoO_3$ on the crystalline structure, unit cell parameters and density, microstructure and electric properties of $BaTiO_3$ ceramics. $SmCoO_3$ doped $BaTiO_3$ ceramics were obtained by solid state method at 1290ºC in air. As the doping percentage increases, the crystalline structure distorts towards the cubic system, but maintaining in the compositional range studied ($0 \le x \le 5$ mol%) a tetragonal symmetry. The refinement of unit cell parameters using Le Bail method show a tetragonality degree (c/a) decreasing from 1.0094 (x=0 mol%) to 1.0040005 (x=5 mol%).

The density of the samples, relative to the computed theoretical density, decrease for higher doping degrees. Anomalous grain growth was observed for x= 0.5 mol%, with grain size around 25 μm, compared to the rest of the compositions, with sizes of around 1 μm. $SmCoO_3$ doping does not significantly influence the Curie temperature, but decrease the value of the dielectric constant at room temperature and at Curie temperature. Also, no specific effect of the grain size was observed related to the temperature dependence of the permittivity. Low dielectric losses were obtained for all samples.

For the frequency dependence of the dielectric constant, a pronounced Maxwell-Wagner effect was noticed at low frequencies for outermost compositions: x= 0, 0.5 and x=3, 5 mol %. In the frequency range 500 Hz to 1 MHz, all ceramics show linear variations of the dielectric constant. The effects of the temperature (room temperature → 250ºC, at 10 kHz) and of the frequency (50 Hz → 3 MHz, at room temperature), on the variation of the real part of the complex permittivity and dielectric loss are investigated.

Our research also show negative temperature coefficient effect over a wide temperature range, as the resistivity decreases exponentially with temperature. As the amount of $SmCoO_3$ in BaTiO3 ceramic increases, the specific electric resistance decreases to a minimum value and then slowly increases again, hence increased dopant concentration does not result in the formation of high volume resistivity layers.

References

[1] K. Uchino, Ferroelectrics 151 (1994), 321–333;
[2] J. Cieminski, H. Beige, J. Phys. D: Appl. Phys. 24 (1991), 1182–1186;
[3] W. Kleemann, J. Mater. Sci. 41 (2006), 129–136;
[4] G.A. Smolensky, J. Phys. Soc. Jpn. 28 (1970), 26;
[5] Y. Liua, R.L. Withersa, X. Weib, J.D.F. Geraldc, J. Solid State Chem. 180 (2007), 858–865;
[6] W. Sakamoto, Y. Hamazaki, H. Maiwa, M. Moriya, T. Yogo, Thin Solid Films 518 (2010), 4256–4260;
[7] H.D. Li, C. Feng, W.L. Yao, Mater. Lett. 58 (2004), 1194– 1198;
[8] S. Gao, S. Wu, Y. Zhang, H. Yang, X. Wang, Mat. Sci. Eng. B 176 (2011), 68–71;
[9] E. Chinarro, J.R. Jurado, Apple Academic Press, Key Engineering Materials 1227 (2001), 206-213;
[10] C.R. Michel, E. Delgado, G. Santillán, A.H. Martínez, A.C. Chávez, Mater. Res. Bull. 42 (2007), 84–93.
[11] P.H. Xiang, S. Asanuma, H. Yamada, H. Sato, I.H. Inoue, H. Akoh, A. Sawa, M. Kawasaki, Y. Iwasa, Adv. Mater. 25 (2013), 2158-61;
[12] P. Fu, Z. Xu, R. Chu, W. Li, G. Zang, J. Hao, Mater. Chem. Phys. 12 (2010), 1065-1070;
[13] L. Shao, R. Chu, Z. Xu, Y. Liu, M. Chen, J. Zhao, G. Li, Physica B. 1 (2013), 164-168;

FABRICATION OF TiO_2 AND TiO_2/CNT MODIFIED PVDF MEMBRANES BY IN SITU POLYMERIZATION AND CHARACTERIZATION OF THEIR PHOTOCATALYTIC ACTIVITY AND FILTERING PROPERTIES

Ákos Ferenc Fazekas[1,2], Tímea Miklós[1], Zsuzsanna László[1], Gábor Veréb[1]

[1]Department of Biosystem Engineering, Faculty of Engineering, University of Szeged,
Moszkvai Blvd. 9., H-6725 Szeged, Hungary
[2]Doctoral School of Environmental Sciences, University of Szeged, Rerrich Béla Sq. 1,
H-6720 Szeged, Hungary
e-mail: fazekas@mk.u-szeged.hu

Abstract

Besides traditional water purification techniques of oily wastewater, such as oil traps, sand filters, flotation, and chemical destabilization, the development of advanced technologies is essential to increase the efficiency of treatments. Membrane filtration is a promising approach as it is a chemical-free and user-friendly treatment, that can be easily combined with other methods, and it effectively removes both micro- and nano-sized oil droplets. In addition to the many advantages of membrane filtration, fouling is the primary obstacle to its widespread use. In this study, we aimed to develop photocatalytically active, TiO_2 and TiO_2/CNT modified PVDF membrane surfaces via a grafting method that can be used to form chemical bonds between the nanoparticles and the membrane matrix. It was also aimed to characterize the photocatalytic efficiency of the modified membranes (TiO_2 and TiO_2/CNT) by the degradation of methyl orange ($c_{initial}=10^{-5}$ mol/dm^3) and to investigate its filtration parameters in the treatment of oil-containing wastewater (c=400 ppm). It was found that the steady-state fluxes of the TiO_2 and TiO_2/CNT modified membranes were six and four times higher, respectively, than those of the unmodified membrane. It was also observed that both reversible and irreversible resistances, and thus, the total resistances, were greatly reduced as a result of the modification. The purification efficiencies were 92% regarding the decrease of the chemical oxygen demand and at least 99% regarding the turbidity measurements for both the modified and unmodified membranes. Furthermore, both types of surface modification were successful in making the membranes photocatalytically active.

Acknowledgements

The authors are thankful for the financial support provided by the Hungarian National Research, Development and Innovation Office—NKFIH (FK_20_135202). This study was also supported by the ÚNKP-23-3-SZTE-245 New National Excellence Program of the Ministry for Culture and Innovation from the source of the National Research, Development and Innovation Fund.

IN SITU ANAEROBIC MICROBIOLOGICAL TREATMENT OF A CHLOROBENZENE CONTAMINATED GROUNDWATER

Balázs Fehér[1], Eszter Csákvári[1], Attila Komóczy[1], József Lendvai[2], Ingrid Zsilinszky[1]

[1]Department of Applied Microbiology, Division for Biotechnology, Bay Zoltán Nonprofit Ltd.
for Applied Research, H-6726 Szeged, Derkovits fasor 2, Hungary
[2]IMSYS Engineering Services Ltd. H-1033 Budapest, Mozaik utca 14/a, Hungary
e-mail: ingrid.zsilinszky@bayzoltan.hu

Abstract

A one-year site investigation was conducted in a contaminated area near a pharmaceutical industry. The main contaminants were chlorobenzene and benzene. Over time, concentration of the contaminants decreased below regulatory level under anaerobic conditions by biostimulation. To confirm the transformation processes and reveal the mechanisms, a corresponding laboratory microcosm study was set up which completed demonstrating the microbial degradation of these two main pollutants. Assumptions about the transformation processes inferred from field data were confirmed by microcosm studies, consequently necessary supplementary information were provided for bioremediation technologies.

Introduction

Accidental activities at a pharmaceutical factory resulted in contamination of groundwater with a mixture of organic pollutants. The primary pollutant of the zone was monochlorobenzene (up to 14 000 μg/l), and benzene (up to 1 300 μg/l) was detected as a secondary contaminant. Although other BTEX compounds, *cis*-1,2-dichloroethylene, vinyl chloride and *tert*-butyl alcohol were also detected, the concentration of these pollutants were in two orders of magnitude lower than chlorobenzene. Possible bioremediation methods were tested with conditions ideal for nitrate reduction. Since the biological degradation, worked excellently due to biostimulation regarding the main pollutants (data not shown), nitrate, phosphate and microelements enriched nutrient solution was applied for the *in situ* treatment of the polluted area on a regular basis. One and a half years after the start of field treatment, then another year later, we investigated groundwater from the contaminated area. The experimental results in summary can provide a guideline for planning biological treatment processes regarding areas with a similar pollution profile.

Experimental

In this work, we compared the results of two consecutive groundwater samplings from the contaminated area, which took place 1 year apart, one in May 2022 and the other in July 2023. We studied the microbiological activity in the affected area primarily by examining the effectiveness of possible bioremediation, which was determined by the biological degradation of pollutants. The *in situ* bioremediation process as well as our tests were carried out under nitrate-reducing conditions, because the most effective way of chlorobenzene degradation, the aerobic way, was not feasible due to the unique characters of the area. Some microcosm studies were set up to acquire knowledge about the microbiological activity of the polluted zone. Microcosm is an artificial and simplified ecosystem which can simulate the behaviour of natural ecosystems under defined and well-regulated conditions. This method is perfect for examining field conditions in laboratory on a small scale. The microcosms were set up using 5 groundwater samples extracted from 5 monitoring wells. The laboratory bottles used for microcosm tests were filled up with the groundwater samples collected from the chlorobenzene-contaminated aquifer, in N_2 (90%), CO_2 (5%), H_2 (5%) containing atmosphere, using an anaerobic workstation. The headspace was 10% of the total volume. Three types of microcosm systems were assembled using every groundwater sample, each in three parallels. Abiotic microcosms were supplemented with mercury(II) sulfate (240 mg/l) to rule out possibility of accidental biological activities, in order to evaluate abiotic degradation and volatilization. Biotic control systems were set up using untreated groundwater. Biostimulated microcosms were amended by adding nitrate, phosphate and microelements to the systems. Microcosms were incubated at 13-15 °C, which corresponds to natural environmental temperature conditions. The concentration of VOC (Volatile Organic Compounds, e.g.: the contaminants), concentration of nitrate, nitrite and phosphate were analyzed weekly by using GC-MS, and HPLC Ion chromatography.

Results and discussion

Analytical results

	2022	**2023**	**2022**	**2023**
	Nitrite (mg/l)		**Nitrate (mg/l)**	
MW-1	<2,50	<2,50	<2,50	<2,50
MW-2	<2,50	5,62	<2,50	76,55
MW-3	<2,50	9,85	115,40	273,34
MW-4	<2,50	6,86	<2,50	145,65
MW-5	<2,50	9,43	<2,50	413,33

As a result of the nutrient injections into the polluted area, the concentration of nitrite and nitrate increased in all areas except for MW-1 labelled groundwater.

Microcosms studies

MW-1

By 2023, the initial concentration of chlorobenzene (6 136 μg/l) and benzene (326 μg/l) in the MW-1 labelled groundwater decreased significantly compared to last year's data. In 2022, an 83.91% decrease in concentration of chlorobenzene was observed only in the biostimulated microcosm after six weeks of incubation, while in case of the biotic control, neither of the contaminants' concentration changed noticeably compared to the abiotic system. In contrast, in 2023, chlorobenzene was already almost completely degraded in both biological systems after two weeks of incubation. The concentration of benzene did not change significantly in 2022 compared to the initial values, but in 2023, the entire amount of benzene was completely degraded in both biotic and biostimulated microcosms.

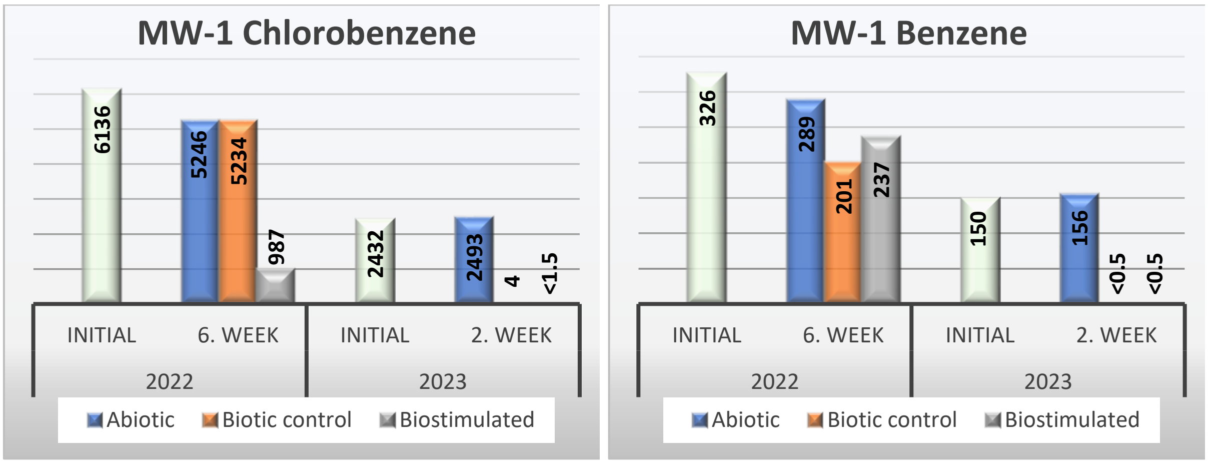

Figure 1. Evolution of concentration (µg/l) of chlorobenzene and benzene in the MW-1 groundwater area

MW-2

In 2023, the initial concentration of chlorobenzene (13 968 µg/l) and benzene (1 183 µg/l) in the groundwater area labelled MW-2 decreased significantly compared to the 2022 data. In 2022, during the 8-week incubation period, concentration of chlorobenzene decreased by only 60.42% in the biostimulated system, while in 2023, almost complete biodegradation occurred in just two weeks, both in case of biotic and biostimulated microcosm. The concentration of benzene did not decrease significantly in 2022 during the 8-week incubation period, however, in 2023, benzene was biodegraded in just two weeks in case of both biological systems.

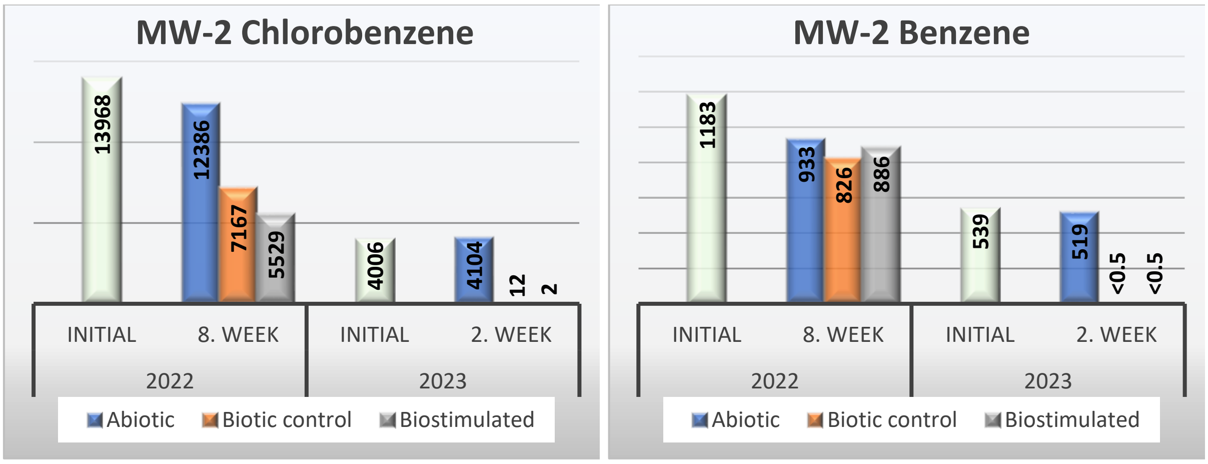

Figure 2. Evolution of concentration (µg/l) of chlorobenzene and benzene in the MW-2 groundwater area

MW-3

By 2023, the concentration of chlorobenzene and benzene in the groundwater area marked MW-3 has reduced by a quarter compared to the data of 2022. In 2022, the initial concentration of chlorobenzene (9 995 µg/l) was reduced by almost half of the value after 8 weeks in both the biotic control and the biostimulated microcosm. On the other hand, in 2023, chlorobenzene was biodegraded in two weeks in both biological microcosms. The concentration of benzene did not change significantly during the 8-week incubation period in none of the biological microcosms compared to the initial value (723 µg/l). However, in 2023, almost 100% of the contamination biodegraded in just two weeks in case of both biotic control and biostimulated systems.

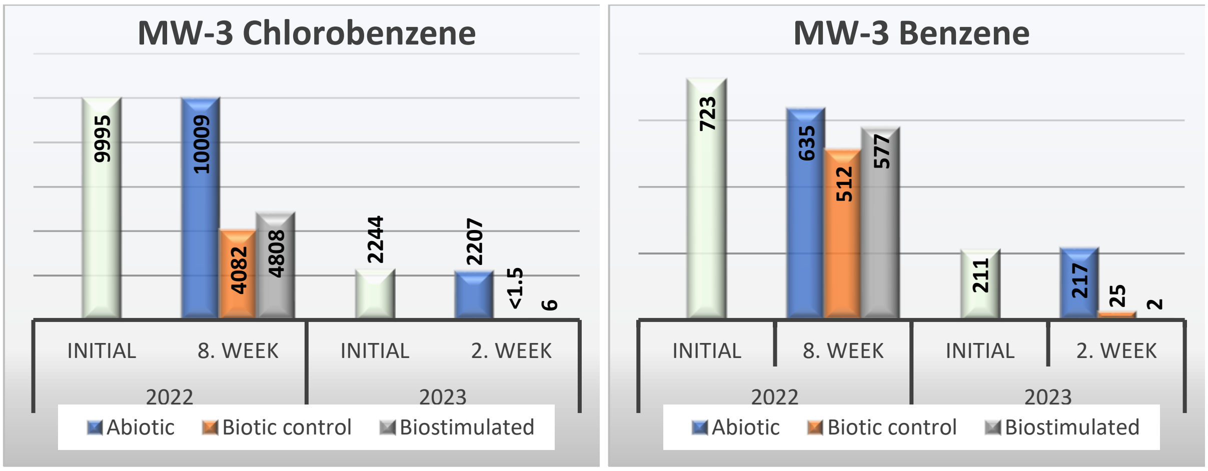

Figure 3. Evolution of concentration (µg/l) of chlorobenzene and benzene in the MW-3 groundwater area

MW-4

The initial concentration of chlorobenzene was ~25% lower in 2023 than in 2022, while the concentration of benzene did not differ significantly during the 1 year of the study. In 2022, after the 8-week incubation period, biodegradation rate of chlorobenzene in biostimulated microcosms was 44.51%, while its concentration in the biotic system did not decrease significantly compared to the initial value (10 562 µg/l). However, in 2023, we noticed an 84.52% decrease in concentration in case of the biotic microcosm within just two weeks. Similarly, also in case of the the biostimulated system, rate of biodegradation was high, almost 100%. In 2022, the initial concentration of benzene (1 278 µg/l) in biological systems decreased by only about 40% in 8 weeks. In contrast, in 2023, 61.56% biodegradation of the contaminant was observed in the biotic control microcosm and almost 100% in the biostimulated system during an incubation period of just 2 weeks.

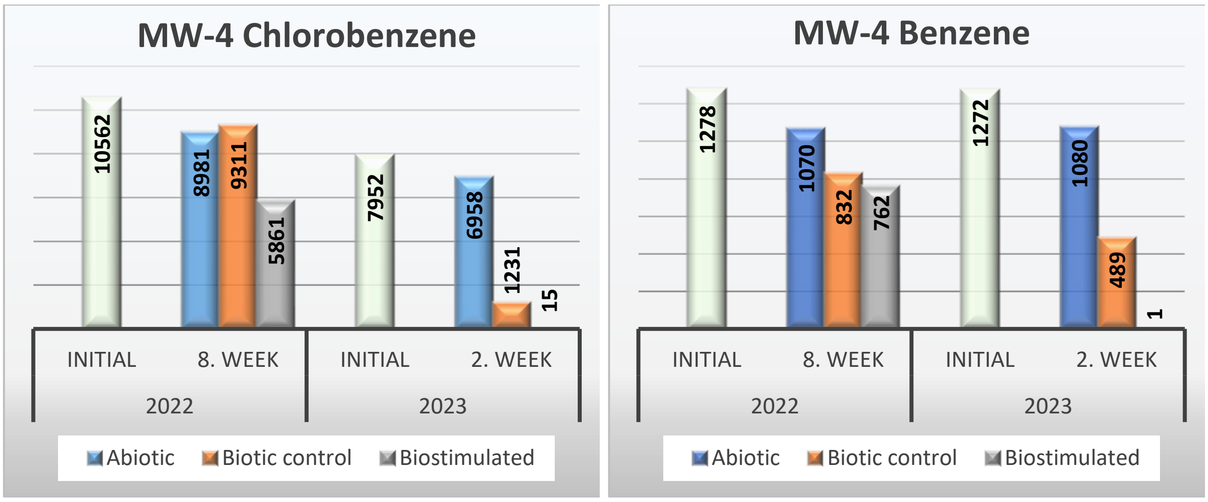

Figure 4. Evolution of concentration (µg/l) of chlorobenzene and benzene in the MW-4 groundwater

MW-5

Based on the microcosm tests compiled from the MW-5 groundwater sample, it was observed that the initial concentration of chlorobenzene in 2023 was significantly lower than in 2022. In 2022, the rate of biodegradation in the biotic microcosm was 65.40%, while in the biostimulated system it was 80.93% during the 8-week incubation period. In contrast, in 2023, chlorobenzene was almost completely biodegraded, both in the biotic and in the biostimulated systems. A significant decrease in the initial concentration of benzene was also observed in 2023. While in 2022, the concentration of benzene decreased by 46.59% in the biostimulated microcosm in 8 weeks, in 2023, the pollutant was completely degraded in both biological systems in just two weeks.

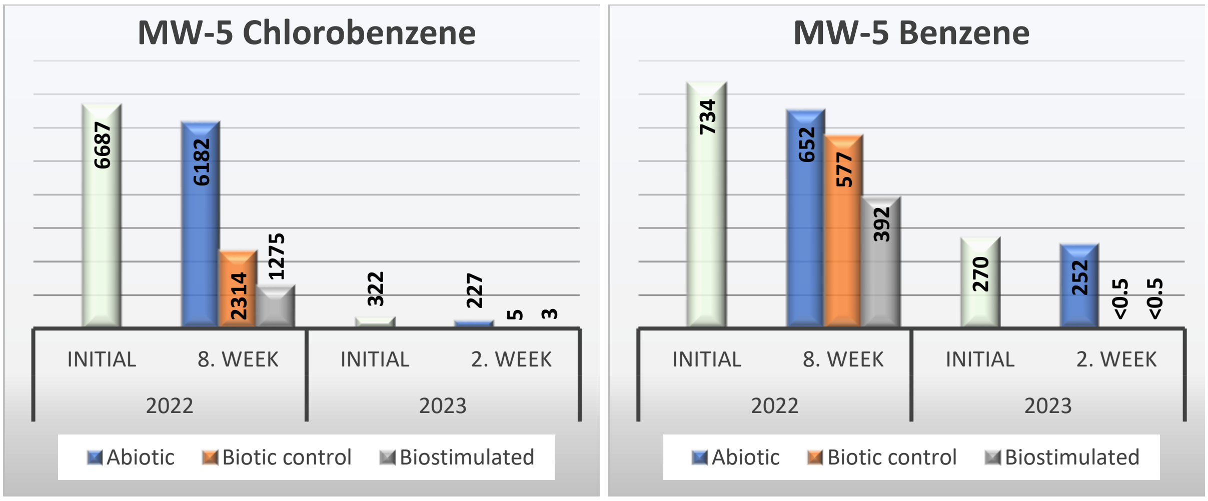

Figure 5. Evolution of concentration (µg/l) of chlorobenzene and benzene in the MW-5 groundwater area

Conclusion

The data gained from field investigations and groundwater analytical results suggest that intrinsic bioremediation process is occurring at the pharmaceutical factory site. The indigenous microbial community at the contaminated site is able to degrade chlorobenzene and benzene if appropriate conditions are provided. We managed to isolate a novel microorganism (*Pseudomonas* sp. EM1) [1] from the groundwater, that is capable of mineralizing chlorobenzene under both aerobic and anaerobic (nitrate reducing) circumstances. The microorganism has been approved as an inoculum. In the future, we intend to use *Pseudomonas* sp. EM1 in chlorobenzene-polluted areas to enhance bioremediation.

Acknowledgements

This work was supported by National Research Development and Innovation Office, Hungary. Project: KFI_16-1-2017-0377 "Intensified Microbiological Degradation and Development of Analytical Methods"

National Research, Development and Innovation Office
Hungary

PROJECT
FINANCED FROM
THE NRDI FUND
MOMENTUM OF INNOVATION

References

[1] I. Zsilinszky, I. Kiss, S. Mészáros, B. Fehér, Proceedings of the 25th International Symposium on Analytical and Environmental Problems 2019 (443-447)

CADMIUM ELECTROANALYTICAL DETECTION AT CARBON PASTE MODIFIED ELECTRODE BASED ON NATURAL CLAY

Ali Sanou[1,2,3], Mariame Coulibaly[3], Carmen Ioana Fort[4], Graziella Liana Turdean[4]

[1]Institut National Polytechnique Félix Houphouet - Boigny, Laboratoire des Procédés Industriels de Synthèses de l'Environnement et des Energies Nouvelles, BP 1313 Yamoussoukro, Ivory Coast
[2]Institut National Polytechnique Félix Houphouet - Boigny, Laboratoire de Thermodynamique; Traitement et Sciences des Surfaces et Interfaces; Ingénierie et Physicochimie des Procédés et de Mécanique des Matériaux (L2-TSIPM), BP 1093 Yamoussoukro, Ivory Coast
[3]Ecole Normale Supérieure, Laboratoire des Sciences Physiques Fondamentales et Appliquées, 08 BP 10 Abidjan, Ivory Coast
[4] "Babes-Bolyai" University, Faculty of Chemistry and Chemical Engineering, Department of Chemical Engineering, Laboratory of Electrochemical Research and Nonconventional Materials, Arany Janos 11, RO-400028 Cluj-Napoca, Romania
email: ioana.fort@ubbcluj.ro

Usually, porous materials [1,2], such as carbon or clays were employed in electrochemistry research for example in electrode acquirements, especially as modifiers. The important properties of clays, such as cation exchange capacity, great surface area, good catalytic support, mechanical stability and low cost, make them suitable as modifiers for electrodes, even if their electrical conductivity is low [3]. Carbon paste electrodes based on clay materials were described to be promising for the electroanalytical detection of heavy metals. While there are many reports on the usage of clay for the construction of clay-based electrodes, the application of natural raw clay has significant importance for the development of eco-friendly electrochemical electrodes. Thus, a carbon paste-modified electrode based on natural clay was prepared. The electrochemical behavior of the obtained modified electrodes and their ability to detect Cd^{+2} has been investigated. The electroanalytical parameters of the investigated modified carbon paste electrode recommend it as a stable, sensitive and reproducible electrode for Cd^{+2} detection. The performances of the new electrode were proved by the results obtained in natural drilling water.

[1] C.I. Fort, L.C. Cotet, A. Vulpoi, G.L. Turdean, V. Danciu, L. Baia, I.C. Popescu, Sensors and Actuators B: Chemical 220 (2015) 712-719.
[2] C.I. Fort, L.C. Cotet, V. Danciu, G.L. Turdean, I.C. Popescu, Materials Chemistry and Physics 138 (2013) 893-898.
[3] Y. Gómez, L. Fernández, C. Borrás, J. Mostany, B. Scharifker,Talanta 85 (2011) 1357

PREPARATION AND STABILITY TESTING OF FLAVOURED WHIPPED CREAM WITH LYOPHILIZED INGREDIENTS

Zsolt Garzó[1], Erzsébet Nyergesné Illés[2]

[1] *Faculty of Food Engineering, University of Szeged, H-6724 Szeged, Mars tér 7, Hungary*
e-mail: garzozsolt@icloud.com
[2]*Institute of Food Engineering, University of Szeged, H-6724 Szeged, Mars tér. 7, Hungary*
e-mail: erzsebet.illes@mk-u.szeged.hu

Abstract

Flavored whipped cream, an innovative culinary creation, has garnered significant attention in recent years for its ability to elevate a wide array of dishes and beverages. Our poster delves into the diverse landscape of flavored whipped cream, shows its origins, production methods, and the multitude of delectable flavor profiles that have captivated the palates of gastronomes worldwide.

Our study begins by tracing the historical roots of whipped cream, from its inception as a simple cream topping to the modern culinary phenomenon it has become. Through a comprehensive review of literature, we explore the evolution of whipping techniques and the pivotal role of emulsifiers in achieving the desired texture and stability.

The production process of flavored whipped cream is then dissected, highlighting the incorporation of various natural and artificial flavoring agents. Techniques such as infusion, extraction, and emulsion are explored in detail, shedding light on the nuanced methods employed by culinary artisans to infuse creams with an array of enticing flavors, from classic vanilla and chocolate to salted caramel and vegan cheese.

Furthermore, our poster delves into the applications of flavored whipped cream in both sweet and savory culinary creations. Through case studies and sensory evaluations, we unveil the transformative impact of flavored whipped cream on diverse dishes, ranging from decadent desserts to innovative savory entrees.

In addition, the study examines the evolving consumer trends and market dynamics surrounding flavored whipped cream, shedding light on its growing popularity in the hospitality industry and its emergence as a staple in home kitchens.

Lyophilized fruits and cheese have emerged as indispensable components in the realm of flavoring, revolutionizing culinary creativity and product development. Their importance lies in their ability to impart concentrated, authentic flavors while offering practical benefits for both chefs and food manufacturers.

Lyophilized fruits, through the meticulous freeze-drying process, retain the essence of fresh fruits in a highly concentrated form. This allows for precise control over flavor profiles, enabling chefs to infuse dishes with vibrant, natural fruitiness regardless of seasonal availability. From adding intensity to desserts and beverages to enhancing the aromatic complexity of savory dishes, lyophilized fruits serve as versatile and reliable flavor enhancers.

Similarly, lyophilized cheese undergoes a transformative preservation process that preserves its distinct taste while eliminating moisture. The resulting cheese products, whether in powdered or crumbled form, serve as potent flavor agents. These versatile cheese powders can be effortlessly integrated into a wide range of dishes, including sauces, dressings, snacks, and baked goods, elevating their taste with a rich, umami depth.

Beyond their flavor-intensifying capabilities, lyophilized fruits and cheese offer logistical advantages in the food industry. They boast extended shelf lives, reducing waste and allowing

for cost-effective inventory management. Their lightweight, compact nature simplifies storage, shipping, and handling.

In conclusion, lyophilized fruits and cheese play a pivotal role in modern culinary innovation and food manufacturing. Their concentrated flavors and practical benefits provide chefs and food professionals with a powerful toolset to craft exceptional and consistent taste experiences, while also addressing logistical concerns in the food supply chain. As essential components in flavoring, lyophilized fruits and cheese are poised to continue influencing the way we approach and savor food.

IMPACT OF GRAPEFRUIT SEED EXTRACT (GSE) ON BIOACTIVE COMPOUNDS OF ARONIA JUICE DURING HEAT TREATMENT

Meriem Serine Hamaidia, Lilla Szalóki-Dorkó, Mónika Máté

Department of Fruits and Vegetables Processing Technology, Institute of Food Science and Technology, Hungarian University of Agriculture and Life Sciences, H-1118, Budapest, Villányi street 29-43, Hungary
e-mail: hamaidiameriemserine@gmail.com, szaloki-dorko.lilla@uni-mate.hu, mate.monika.zsuzsanna@uni-mate.hu.

Abstract

The quest for sources of antioxidant phenolic compounds has encompassed a wide array of plant materials, including vegetables, fruits, leaves, oilseeds, cereal crops, barks, roots, spices, herbs, and crude plant drugs. Among these, berries stand out for their exceptional phenolic content, particularly flavonoids and phenolic acids, known for their potent antioxidant properties [1]. Black chokeberry (*Aronia melanocarpa*), a valuable fruit crop within the Rose family (*Rosaceae*) and the Apple subfamily (*Pomodieae*) [2], is renowned for its rich composition of bioactive compounds, including anthocyanins, procyanidins, phenolic acids, flavonols, and flavanols [3]. Chokeberries, owing to their astringent taste, undergo various processing methods to yield long-lasting products such as juices, nectars, wines, and liqueurs [4]. In response to increased consumer demand and growing recognition of its nutritional benefits, chokeberry juice has gained popularity among juice manufacturers. The stability of polyphenolic compounds during processing is closely tied to the chosen processing technology [5]. Furthermore, for many years, traditional plant extracts, spices, and culinary herbs have been used to improve flavour and extend the shelf life of food products [6]. Grapefruit seed extract (GSE) is a naturally derived functional substance from the grapefruit plant (*Citrus paradise Macf., Rutaceae*). It has gained significant interest in the realm of food packaging applications because of its robust antioxidant properties and wide-ranging antimicrobial capabilities [7]. Grapefruit primarily contains the flavanones narirutin and naringin, along with their aglycone form, naringenin. These constituents have long been acknowledged as distinctive components of grapefruit. The distribution of phenolic acids indicates that the prominent hydroxycinnamic acids are ferulic and p-coumaric acids. As for hydroxybenzoic acids, vanillic and gallic acids are the primary ones identified [8].

This study was conducted to assess the impact of different concentrations of grapefruit seed extract addition (0%, 1%, 2%, 3%) on the levels of anthocyanins and polyphenols in aronia juice subjected to heat treatment (60°C) at different times (5, 10, 30, 60, 120 min). The investigation included total anthocyanins testing, quantification of Total Phenolic Compounds (TPC), and the Ferric Reducing Ability of Plasma (FRAP) assay. Based on the results, FRAP values peak at 60 minutes, with 2% GSE at 1915.53 ± 217.94 mg/L and 1910.46 ± 376.74 mg/L with 3% GSE at 5 min. In addition, the presence of GSE has varying effects on TAC depending on the time point and concentration. For instance, in the 1% GSE condition, the TAC levels remain high at 60 minutes with 85.67 ± 2.62 mg/l, while in 2% TAC remains relatively stable across different time intervals: 69.08 ± 0.10 mg/l, 73.84 ± 4.33 mg/l, 69.86 ± 0.86 mg/l at 5, 30, 120 min, respectively. This demonstrates the potential of GSE to mitigate the heat-induced decline in anthocyanins. Furthermore, the inclusion of GSE appears to result in higher Total Phenolic Compounds (TPC) levels, particularly with 1% GSE, compared to 2% and 3% GSE. Specifically, TPC levels with 1% GSE were measured at 6608.22 ± 227.75 mg/l, 7518.17 ± 374.66 mg/l, and 6639.81 ± 241.85 mg/l at 10, 60, and 120 minutes, respectively. This suggests a potential enhancement of TPC by GSE, especially in the early stages of heat treatment.

In summary, 1% Grapefruit Seed Extract (GSE) concentration shows promise in preserving the compounds in aronia juice during heat treatment, particularly for Total Antioxidant Capacity (FRAP). For Total Anthocyanins content and Total Phenolic Compounds (TPC), both 1% and 2% GSE concentrations are effective, with a slight advantage for 1% GSE, especially in the early stages of heat treatment. These findings have implications for enhancing the compounds' stability in aronia juice during processing. Further research is needed to explore these effects comprehensively and under different conditions.

Keywords: Black Chokeberry, Aronia, Grapefruit Seed Extract (GSE), Anthocyanins, Polyphenols, TPC, FRAP.

References

[1] Oszmiański, J., & Wojdylo, A. European Food Research and Technology. 2005. 221(6). 809-813.
[2] Platonova, E. Y., Shaposhnikov, M. V., Lee, H.-Y., Lee, J.-H., Min, K.-J., & Moskalev, A. Trends in Food Science & Technology. 2021. 114. 570–584.
[3] Oziembłowski, M., Trenka, M., Czaplicka, M., Maksimowski, D., & Nawirska-Olszańska, A. Applied Sciences. 2022. 12(14). 7008.
[4] Wilkes, K., Howard, L. R., Brownmiller, C., & Prior, R. L. Journal of Agricultural and Food Chemistry. 2014. 62(18). 4018-4025.
[5] Bursać Kovačević, D., Gajdoš Kljusurić, J., Putnik, P., Vukušić, T., Herceg, Z., & Dragović Uzelac, V. Food Chemistry. 2016. 212. 323-331.
[6] López-Pedrouso, M., Lorenzo, J. M., & Franco, D. Antioxidants. 2022. 11(9). 1825.
[7] Roy,S., & Rhim, J.-W. Journal of Environmental Chemical Engineering. 2021. 9(1), 104694.
[8] Ballistreri, G., Fabroni, S., Romeo, F. V., Timpanaro, N., Amenta, M., & Rapisarda, P.. Polyphenols in Plants 2019 pp. 191–215.

EFFECT OF SILICON CONTENTS ON THE PROPERTIES OF NEW TITANIUM ALLOY

Christian Hermida-Herrero[1], Santiago Brito-García[1], Julia Claudia Mirza-Rosca[1,2], Madalina Simona Baltau[3], Petrica Vizureanu[3,4]

[1]*Department of Mechanical Engineering, University of Las Palmas de Gran Canaria, 35017 Tafira, Spain.*
[2]*Materials Engineering and Welding Department, Transilvania University of Brasov, 500036 Brasov, Romania.*
[3]*Department of Technologies and Equipments for Materials Processing, Gheorghe Asachi Technical University of Iasi, 700050 Iasi, Romania.*
[4]*Technical Sciences Academy of Romania, Dacia Blvd 26, 030167 Bucharest, Romania.*
e-mail: christian.hermida101@alu.ulpgc.es

Abstract

The use of prostheses promotes the increase of well-being in the population and that is why nowadays we are trying to better understand the results and success in achieving osseointegration of these elements. This gives way to the use of biomaterials. In order to define the characteristics of these materials, analyses and tests are required to determine their behaviour when the material is to be used and applied as an implant. So this research mainly aims to evaluate how silicon influences the mechanical characteristics by comparing two novel titanium alloys.

Introduction

These days, new alloys with a low modulus of elasticity and low cytotoxicity are being researched and developed because of the hip's significant weight bearing capacity and the issues associated with the biomaterials currently in use. Consequently, the decision has been made to look into the potential biomedical uses of the S1 (62% Ti, 15% Mo, 7% Zr, 15% Ta, 1% Si) and S2 (57,25% Ti, 20% Mo, 7% Zr, 15% Ta, 0,75% Si) samples further.

Experimental

The arc remelting process was used in an argon environment to create the alloys. This method was used at the Gheorghe Asachi Technical University in Iasi, Romania, at the Faculty of Materials Science and Engineering. To achieve the required homogeneity, the alloys were melted, then remelted six times (three times in each face), and finally formed into an ingot. Furthermore, part of the ingots were given to Las Palmas de Gran Canaria University (Las Palmas de Gran Canaria, Spain) for their testing and preparation.

To prepare the samples for metallography, they were polished with silicon carbide papers and 0.1 silicon carbide papers and 0.1 micrometre alumina suspensión and after the first examination, the samples were subjected to a Kroll reagent attack.
To perform the microhardness tests, 12 points were taken with forces of 1 gram, 5 gram and 10 gram to calculate and express the Vickers hardness (HV), in accordance with ISO 14577-1:2015. For Electrochemical Tests, each sample was placed in an electrochemical cell with three electrodes for the electrochemical tests: the samples acted as the working electrodes, a saturated calomel electrode served as the reference electrode, and a platinum electrode acted as the counter electrode.

Results and discussion

The compounds and phases that make up a metallic substance are arranged spatially in metallography, together with any impurities or potential mechanical faults.

Vickers hardness versus scan length graphs for both samples exhibit widely spaced maxima and minima, indicating the presence of both soft and hard areas on their surfaces. It is also confirmed that the harder the sample, the higher the percentage of silicon and the applied load. Elechtrochemical tests show that Sample 1 is more stable as Sample 2.

A semi-logarithmic scale of the current results shows the outcomes of the linear polarization technique, which was used to measure the alloys' rate of corrosion. Compared to the other samples under investigation, Sample 2 exhibits higher values of anodic corrosion potential and current (Ecorr and Icorr, respectively), which indicate how much the alloy has been oxidized.

Conclusion

The samples' surfaces displayed biphasic dendritic patterns following their exposure to the Kroll reagent. When silicon was added, the dendrites shrank because silicon is a potent grain refiner in titanium alloys. It encourages the development of fine grains that impede the spread of cracks and strengthen the material's resistance to fatigue.

The potential values of both samples increased during the immersion period without decreasing. By creating a protective oxide layer on the alloy surface, silicon oxide slows down the rate of oxidation and increases the alloys' resistance to deterioration from bodily fluids.

Two distinct phases, *hard and soft*, of the material's microstructure were found by measuring the hardness at various loadings.

Overall, every sample exhibited favorable chemical and biological properties. So we could say that both samples would behave favourably in the human body.

References

[1] Jiménez-Marcos, C., Rosca, J. C. M., Bălţatu, M. S., & Vizureanu, P. (2023). Effect of SI contents on the properties of TI15MO7ZRXSI alloys. *Materials*, *16*(14), 4906. https://doi.org/10.3390/ma16144906

[2] Jiménez-Marcos, C., Rosca, J. C. M., Bălţatu, M. S., & Vizureanu, P. (2022). Experimental research on new developed titanium alloys for biomedical applications. *Bioengineering*, *9*(11), 686. https://doi.org/10.3390/bioengineering9110686

[3] Jiménez-Marcos, C., Rosca, J. C. M., Bălţatu, M. S., & Vizureanu, P. (2023b). Evaluation of new titanium alloys as potential materials for medical devices. *Microscopy and Microanalysis*, *29*(Supplement_1), 196-201. https://doi.org/10.1093/micmic/ozad067.088

NOVEL POLYMER-PEROVSKITE NANOCOMPOSITE BASED ON $LaMnO_3$:Pd AND POLYVINYLPYRROLIDONE

Ioana M.C. Ienaşcu[1,2], **Adina Căta**[1], **Nick Samuel Ţolea**[1], **Antonina Lazăr**[1], **Paula Svera**[1], **Corina Orha**[1], **Cristina Moşoarcă**[1], **Paula Sfîrloagă**[1,3]

[1]National Institute of Research and Development for Electrochemistry and Condensed Matter, Dr. A. P. Podeanu 144, 300569, Timişoara, Romania
[2]"Vasile Goldiş" Western University of Arad, Faculty of Pharmacy, Liviu Rebreanu 86, 310045, Arad, Romania
[3]Spin-off Nattive-Senz SRL, Dr. A.P. Podeanu 144, 300569, Timisoara, Timis, Romania
e-mail: imcienascu@yahoo.com

Abstract

Perovskites represent promising materials due to advantages such as chemical and photo-stability, low production cost, modifiable energy in the band gap, high absorption properties, long carrier lifetime and diffusion length, which can be used in green and sustainable environmental applications [1]. Despite the high dielectric constant and multifunctionality of perovskite materials, they possess high density, brittleness and low dielectric strength, as well as poor processability [2]. PVP is a water-soluble, non-toxic amorphous nonionic polymer, with high solubility in polar solvents, widely used in the synthesis of nanoparticles [3] acting as a nanoparticle dispersant, growth modifier, surface stabilizer, preventing agglomeration of nanoparticles [4]. Due to its amphiphilic nature, PVP can affect the morphology and growth of nanoparticles by providing solubility in various solvents, discriminative surface stabilization, controlled crystal growth, playing the role of a shape control agent and facilitating the growth of specific crystal faces, while preventing the growth others [4].

The aim of this research is to obtain a new hybrid material based on polyvinylpyrrolidone (PVP) polymer functionalized with perovskite structures of the $LaMnO_3$ type doped with Pd, in aqueous medium at 80°C. After mixing the precursors in a mass ratio of 20:1 (PVP:Perovskite) and dispersing them in distilled water, from the viscous mixture, thin films were obtained. These were triturated to obtain particles smaller than 1 mm. The powder was dried and analyzed using SEM/EDAX, X-ray diffraction, UV-VIS, RAMAN spectroscopy in order to completely characterize the nanocomposite. The combination between $LaMnO_3$:Pd perovskite and PVP resulted in a multifunctional material, with favorable characteristics of inorganic perovskite nanofiller and organic polymer effectively integrated.

References

[1] C. Brahmi, M. Benltifa, C. Vaulot, L. Michelin, F. Dumur, A. Airoudj, F. Morlet-Savary, B. Raveau, L. Bousselmi, J. Lalevée, Eur. Polym. J. 157 (2021), 110641.

[2] A.A. Al-Muntaser, R.A. Pashameah, K. Sharma, E. Alzahrani, S.T. Hameed, M.A. Morsi, Opt. Mater. 132(2022), 112799.

[3] K.M. Koczkur, S. Mourdikoudis, L. Polavarapu, S.E. Skrabalak, Dalton Trans. 44 (2015), 17883.

[4] M.I. Voronova, O.V. Surov, N.V. Rubleva, N.E. Kochkina, A.V. Afineevskii, A.G. Zakharov, Compos. Commun. 15 (2019), 108-112.

Acknowledgements

This work was supported by the Experimental Demonstrative Project 683PED/2022.

THE IMPORTANCE OF THE CIRCULAR ECONOMY FOR THE SUSTAINABLE DEVELOPMENT OF THE REPUBLIC OF SERBIA

Jelena Ignjatović, Aleksandra Đorđević

Unit of Agricultural Business Studies and Tourism, Academy of Applied Studies Šabac, Serbia
e-mail: a.djordjevic@akademijasabac.edu.rs

Abstract

It is believed that the first warnings of scientists and various organizations about the development of harmful effects on the environment appeared in the middle of the 20th century, and all of this with the progress and accelerated development of industry. The concept of sustainable development represents a strategy that unites development and environmental problems and points to the simple fact that we are fully connected to what surrounds us. Almost all activities developed by humans depend on the environment. It is important in order to find a way so that what we consume has as little impact on the natural environment as possible. Only what nature itself is capable of regenerating can be taken from nature.

As one of the solutions, the concept of circular economy was born, and represents a regenerative economic system within which production resources, waste, waste emission and energy outflow are reduced by slowing down and extending life cycles in production. This is achieved primarily by designing and creating products, in a way to extend their lifespan, but also by maintenance, servicing and recycling.

However, although there is no clearly defined area of measurement of the circular economy, the term itself creates economic, environmental and social benefits. Recently, the Eurostat methodology has developed a methodology for measuring the development of the circular economy, which is the key importance for monitoring sustainable development. Accordingly, the aim of the paper is to point out the importance of CE development in the Republic of Serbia. According to the available indicators, CE Serbia recorded data in the categories of five indicators. A higher level compared to the EU was recorded in the indicators Waste generation per capita and Generation of waste excluding major mineral wastes per GDP unit, while a lower level was achieved in the categories Resource productivity, Generation of municipal waste per capita and Material import dependency.

Keywords: Circular economy, sustainable development, Republic of Serbia.

EFFECTS OF SUBACUTE DIBUTYL PHTHALATE EXPOSURE ON UDP-GLUCURONOSYLTRANSFERASE 1A9 EXPRESSION IN RAT LIVER

Ivana Ivelja, Jelena Vukčević, Nebojša Andrić, Jelena Marković Filipović

Department of biology and ecology, Faculty of Science, University of Novi Sad, 21000 Novi Sad, Trg Dositeja Obradovića 3, Serbia
e-mail: ivana.ivelja@dbe.uns.ac.rs

Abstract

Di-n-butyl phthalate (DBP) is a plastic additive known for its endocrine-disrupting and reproductive toxicity. DBP is metabolized by UDP-glucuronosyltransferase 1A9 (UGT1A9) in a glucuronidation reaction that takes place in the liver. The aim of our study was to determine whether DBP exposure disturbs UGT1A9 expression in rat hepatic tissue. A total of 24 female *Wistar* rats were divided into four groups and exposed to different DBP doses (100, 500, or 5000 mg/kg diet) over 28 days. Formalin-fixed, paraffin-embedded liver tissue was cut into 5 μm thin sections and immunostained with anti-UGT1A9 antibody. We assessed UGT1A9 levels using ImageJ software, measuring both the optical density (OD) of the immunolabeled UGT1A9, which indicates staining intensity, and the total number of positive cells through the ImageJ plugin IHC profiler. During the sections examination, UGT1A9 was found in abundance in cytoplasm of hepatocytes across all treated groups, as well as, in control group. Interestingly, while the OD remained unaffected by DBP treatment, we found significant changes in the percentage of cells exhibiting high positive and positive UGT1A9 expression. The number of positive cells decreased in the group treated with 500 mg DBP/kg diet while the reduction of high positive cells was observed in all experimental groups. Nevertheless, the total number of positive cells remained consistent. Our results indicate that subacute DBP treatment by changing the percent of high positive and positive immunopositive cells may have the ability to affect UGT1A9 expression.

Acknowledgements

This work was supported by the Provincial Secretariat for Higher Education and Scientific Research of the Autonomous Province of Vojvodina [Grant No. 142-451-3164/2023-01).

EFFECT OF SUBACUTE DIBUTYL PHTHALATE TREATMENT ON THE ACTIVITY AND EXPRESSION OF ANTIOXIDANT ENZYMES IN RAT LIVER

Ivana Ivelja, Jelena Vukčević, Danijela Kojić, Nebojša Andrić, Jelena Marković Filipović

Department of biology and ecology, Faculty of Science, University of Novi Sad, 21000 Novi Sad, Trg Dositeja Obradovića 3, Serbia
e-mail: ivana.ivelja@dbe.uns.ac.rs

Abstract

Di-n-butyl phthalate (DBP), a common plastic additive, is prone to leaching and evaporating from plastic products due to its weak chemical bonds, resulting in its widespread presence in the environment. The aim of our study was to investigate whether DBP applied orally in various doses disturbs the activity and expression of antioxidant enzymes in rat liver . A total of 30 female *Wistar* rats were divided into 4 groups and exposed to DBP in food in doses of 0, 100, 500, and 5000 mg/kg diet, for 28 days. After the study period, tissue samples were collected for evaluating the antioxidant capacity and for RNA extraction. Total superoxide dismutase (SOD) and catalase (CAT) activities were measured spectrophotometrically by monitoring changes in absorbance over the 3min interval, while the expression of the *Sod1*, *Sod2* and *Cat* were obtained by real-time RT-PCR. Our findings revealed that total SOD activity was notably lower in groups treated with 100 and 500 mg DBP/kg diet. Conversely, CAT activity significantly increased in groups exposed to 500 and 5000 mg DBP/kg compared to the control group. However, our RT-qPCR analysis showed no statistically significant changes in the expression of corresponding genes. Our results indicate that subacute dibytil phthalate treatment causes adverse effects on the activity of antioxidant enzymes, potentially leading to oxidative damage.

Acknowledgements

This work was supported by the Provincial Secretariat for Higher Education and Scientific Research of the Autonomous Province of Vojvodina [Grant No. 142-451-3164/2023-01).

UTILIZATION OF BIOPOLYMER PACKAGING MATERIALS IN SUPPORT OF SUSTAINABLE DEVELOPMEN

Ivana Jevtić, Kosana Popović, Ljubica Mijić, Jelena Đuričić Milanković

Academy of Professional Studies Šabac, Department of Medical and Business-Technological Studies, Hajduk Veljkova 10, 15000 Šabac, Serbia
e-mail: ivana.dabic@yahoo.com

Abstract

Packaging is an essential part of everyday life, protecting products, enabling transportation, and contributing to their market success. However, in the context of the growing focus on sustainable development, packaging becomes a key point for innovation and a change in the way we think about products and their protection [1]. Transitioning from a linear to a circular-cyclic industrial system, discarded packaging becomes a raw material in the next production cycle [2]. This system, often referred to as the concept of a circular economy, represents an innovative approach based on sustainability and waste minimization in production and consumption processes. The circular economy connects economic and ecological aspects in an innovative way and sets an ambitious goal to reduce the environmental footprint of the industry [3]. The principle of sustainability applied in the packaging industry is reflected in the approach that considers the life cycle (LCA - life cycle analysis) with an emphasis on material optimization, water and energy savings, waste reduction, and achieving maximum recovery through recycling, incineration, or composting [1]. From an ecological perspective, biopolymer packaging offers a significant advantage, as it is often biodegradable and environmentally friendly [4]. The use of biopolymers helps reduce environmental pollution, lower harmful gas emissions, and supports the principles of a circular economy, making them environmentally friendly alternatives to conventional plastics. The social aspect is also significant, as the use of sustainable packaging and biopolymers can improve consumer health and create jobs in the sustainable industry sector [5]. Sustainable packaging requires collaboration and innovation in all sectors of the economy to achieve sustainable development. When it comes to consumer awareness, ecology, resource conservation, and environmental protection, sustainable packaging becomes a key element in the market. As such, packaging has the potential to play a significant role in achieving sustainable development goals and preserving the planet for future generations.

References

[1] V. Lazić, D. Novaković, Ambalaža i životna sredina, Univerzitet u Novom Sadu, Tehnološki fakultet, Novi Sad, 2010, pp. 12–15.
[2] V. Lazić, J. Gvozdenović, S. Popović, D. Novaković, PTEP, 13 (2009) 226–228.
[3] P. Ghisellini, C. Cialani, S. Ulgiati, S. J. Clean. Prod., 114 (2016) 11–32.
[4] V. Lazić, J. Gvozdenović, Biopolimeri kao ambalažni materijali, Prehrambena industrija, 2007, pp. 19–22.
[5] J. Rydaz, W. Sikorska, M. Kyulavska, D. Christova. Int. J. Mol. Sci. 2015, 16 (2015) 564–596.

MAGNETIC PROPERTIES AND HEMOCOMPATIBILITY OF VARIOUS FERRITE NANOPARTICLES

Anna Katalin Vas[1], **Erzsébet Illés[2]**

[1]University of Szeged, H-6720, Hungary
[2]Department of Food Engineering, University of Szeged, H-6720, Hungary
e-mail: erzsebet.illes@mk.u-szeged.hu

Abstract

Superparamagnetic iron oxide nanoparticles (SPIONSs) are well-known for their great potential in biomedicine, such as active agents for drug-delivery, MRI contrast enhancement and hyperthermia, hence their possible diagnostic and therapeutic application has been the centre of many studies in recent years. Beside magnetite, nickel-ferrite nanoparticles also seem to have promising magnetic properties for utilization in magnetic hyperthermia. These SPIONs, however, require biocompatibilization by surface functionalization as they are unstable in biological fluids. Graphite oxide (GO) is a hydrophilic material, with high surface area and tunable pH-dependent surface charge properties. By synthesizing GO/MNP nanocomposites, it is possible to further enhance the heat production caused by an alternating magnetic field during hyperthermia sessions.[1][2]

To study the effect of the nickel content and the various polymers used as protective layers on the surface of magnetic nanoparticles, nanocomposites were prepared with 1/5 and 1/10 GO/MNP mass ratios. The nickel content was 0%, 10% and 20%, while two different polymers (PAM and PEGMA-AA) were used to fully coat the nanomagnets. The dynamic light scattering (DLS) data on the coagulation kinetics of the various nanocomposite samples showed that there are notable differences in their colloidal stability. The critical coagulation concentrations were higher when PAM polymer was used and the nickel ratio also seemed to have a significant influence when higher NaCl concentrations were applied. The five-minute-long exposure for an alternating magnetic field showed that increasing the frequency (at the same magnetic field strength) resulted in a higher level of heat production.

Hemocompatibility tests of naked SPIONs were also performed in biorelevant media.[3] Peripheral blood smear experiments did not reveal any signs of coagulation or other damage in different blood cells. Development of remarkable protein corona around the nanoparticles was observed for bare ferritenanomagnets by DLS measurements.

References

[1] E. Illés, L. Nánai, Zs. Hegedűs, B. Müller and T. Szabó; Tunable Magnetic Hyperthermia Properties of Pristine and Mildly Reduced Graphene Oxide/Magnetite Nanocomposite Dispersions; Nanomaterials 10(12): 2426. (2020)

[2] Illés E., Szekeres M., Tóth Y. I., Farkas K., Földesi I., Szabó Á., Iván B., Tombácz E.; PEGylation of Superparamagnetic Iron Oxide Nanoparticles with Self-Organizing Polyacrylate-PEG Brushes for Contrast Enhancement in MRI Diagnosis; Nanomaterials 8(10): 776. (2018)

[3] M. Szekeres, I. Y. Tóth, R. Turcu, E. Tombácz; The Effect of Polycarboxylate Shell of Magnetite Nanoparticles on Protein Corona Formation in Blood Plasma; Journal of Magnetism and Magnetic Materials 427: 95–99. (2017)

EVOLUTION OF YTTRIUM SILICATE PHASES IN HYDROTHERMAL SYNTHESIS ROUTE

Madalina-Gabriela Ivanovici, Andrei Racu, Radu Banica, Miroslav D. Dramićanin

National Institute of Research and Development for Electrochemistry and Condensed Matter,
Dr. A.P. Podeanu street, No. 144, 300569, Timisoara, Romania
e-mail: ivanovicigabriela11@yahoo.com

Abstract

The current global pandemic underscores the imperative for the development of more effective strategies in antimicrobial treatments [1]. Optical materials that exhibit ultraviolet-C (UV-C) emission possess the potential as viable choices for these applications. $Y_2SiO_5:Pr^{3+}$ is regarded as one of the extensively investigated silicates exhibiting visible-to-ultraviolet upconversion emission [2]. The enhancement of UV emissions efficiency is a primary objective, and the focus of this study is to acquire and analyze various phases of silicate materials.

Several synthesis methods have been documented in scientific journals for the production of Yttrium silicates, including solid-state reaction, sol-gel method, and hydrothermal route. The primary obstacles encountered in their acquisition pertain to the polymorphism and numerous phases of the oxides [3]. This study aimed to explore a novel hydrothermal method for synthesizing yttrium disilicate. The synthesis process involved two primary starting materials: SiO_2 sol, which consisted of SiO_2 nanoparticles dispersed in ethanol, serving as the silicon source, and an aqueous solution of $Y(NO_3)_3 \times 6H_2O$, providing the yttrium source. These starting materials were combined in a stoichiometric Y/Si molar ratio of 1:1. In order to acquire yttrium disilicate, a series of procedures were undertaken, including the production of a mixture consisting of the initial ingredients, subjecting the mixture to hydrothermal treatment within an autoclave reactor, and subsequently conducting thermal treatment (calcination) of the precursors.

The parameters of hydrothermal treatment and calcination processes exhibit considerable variations in the primary and secondary phases detected through X-ray diffraction, as indicated by the obtained results. Hence, extended durations of synthesis reactions and calcination intervals resulted in the formation of a well-crystallized sample, whereby the predominant phase can be attributed to $Y_2Si_2O_7$.

Acknowledgments

This study was supported by Romania's National Recovery and Resilience Plan, NRRP, project C9-I8-28/ FC 760107/2023.

References

[1] M. Raeiszadeh, B. Adeli, ACS Photonics 7(11) (2020) 2941.
[2] S. L. Cates, E. L. Cates, M. Cho, J.-H. Kim, Environ. Sci. Technol. 48(4) (2014) 2290.
[3] Z. Sun, M. Li, Y. Zhou, Int. Mater. Rev. 59 (7) (2014) 357.

OBTAINING COLORED ANTIOXIDANT COTTON AND COTTON/LINEN FABRICS USING GREEN TEA AQUEOUS EXTRACT

Aleksandra Ivanovska[1], **Jovana Milenković**[2], **Jelena Lađarević**[2], **Leposava Pavun**[3], **Mirjana Kostić**[2]

[1]Innovation Center of the Faculty of Technology and Metallurgy in Belgrade Ltd., 11000 Belgrade, Serbia
[2]Faculty of Technology and Metallurgy, University of Belgrade, 11000 Belgrade, Serbia
[3]Faculty of Pharmacy, University of Belgrade, 11000 Belgrade, Serbia
e-mail: aivanovska@tmf.bg.ac.rs

Abstract

Green tea aqueous extract was prepared and characterized regarding total flavonoids and total phenolic contents as well as antioxidant activity (assessed by ABTS method). The characterized aqueous extract was used for dyeing and functionalization of 100% cotton and cotton/linen (47%/53% and 70%/30%) fabrics. Fabric color strength (K/S) values and their antioxidant activities before and after washing were compared. The obtained results revealed that 100% cotton (GTI), 47%/53% cotton/linen (GTII), and 70%/30% cotton/linen (GTIII) fabrics have *K/S* values ranging between 8.33 and 10.85. After one washing cycle, these values decreased significantly. On the other hand, dyed fabrics showed excellent (100 %) ABTS radical scavenging ability which remained excellent (GTII) or decreased to medium (GTI and GTIII) levels after one washing cycle. Based on the obtained results, it can be concluded that 47%/53% cotton/linen fabric is the most suitable for functional clothing capable of trapping the free radial of oxygen species. The current paper represents a step towards a more sustainable textile industry that could undoubtedly contribute to overcoming the environmental problems caused by the textile industry.

Introduction

Nowadays, water pollution represents one of the main environmental issues worldwide, wherein textile industries are known as the main contributors to water pollution. Namely, to produce one tonne of colored textile materials more than 200 tonnes of water were required. After the conventional textile dyeing and functionalization, high quantities of wastewater consisting of residual dyes, hazardous chemicals, heavy metals, microfibers, and mordants are returned to nature [2]. To overcome this mentioned environmental problem and at the same time minimize the textile workers' exposure to harmful chemicals, non-toxic and biodegradable natural dyes and colorants from sustainable sources were used for simultaneous fiber dyeing and functionalization [2-5].

In light of that, in this paper, cellulose fabrics (100% cotton, 47%/53% cotton/linen, and 70%/30% cotton/linen) were simultaneously dyed and functionalized using green tea (*Camellia sinensis*) aqueous extract. The prepared aqueous extract of green tea is intensely colored, and it was reasonable to assume that it will be capable of dyeing textile materials. On the other hand, herbal teas are rich in polyphenolic compounds, mainly phenolic acids and flavonoids that are known for their antioxidant activities [6]. The stability of fabric color strength values and antioxidant activity was examined both before and after one washing cycle and based on the obtained results, the potential utilization of functionalized cellulose fabrics was proposed.

Experimental

Preparation of tea water extracts

The commercially available dried green tea (*Camellia sinensis*)bought from „Tea House" (Belgrade, Serbia) was ground into a fine powder using a mill. Green tea extract was prepared by immersing 20 g of tea in 1 L of distilled water. The temperature of the mixture was raised to a boiling point and kept at this temperature for 5 min. Thereafter, the mixture was allowed to cool for 2 h, and the solid parts were separated by filtration, while the obtained extract was immediately characterized and used for fabric dyeing and functionalization of cellulose fabrics.

Characterization of the green tea aqueous extract

The total flavonoid and total phenolic contents (*TFC*, and *TPC*) within the tea extract were determined spectrophotometrically according to the methods described by Pavun et al. [7].
The extract antioxidant activity was evaluated using ABTS assay following the procedure given by Lađarević et al. [8].
All spectrophotometric measurements were performed on a Beckman DU-650 spectrophotometer.

Dyeing and functionalization experiments

One hundred grams of 100% cotton (sample I), 47%/53% cotton/linen (sample II) and 70%/30% cotton/linen (sample III) commercially produced fabrics in the plain wave were functionalized with 1 L of prepared extract for one day with constant shaking on a Memmert water bath WNE 14 at 25 °C. After that, the fabrics were rinsed with distilled water, dried at room temperature for 48 h, and characterized. Depending on the chemical composition of undyed fabrics, dyed and functionalized fabrics were denoted as: GTI, GTII, and GTIII.

Characterization of functionalized fabrics

Kubelka-Munk equation[9] was used to calculate the fabrics' color strength (*K/S*) values based on the reflectances recorded on the UV-Vis spectrophotometer (Shimadzu UV-Vis 2600).
The fabrics' antioxidant activity was determined according to the ABTS method described by Glaser et al. [10]. To confirm the differences between the fabrics' *K/S* values before and after washing, the dyed fabrics were washed according to ISO 105-C10 (2010), rinsed, dried at room, and marked as GT0I W, GTII W, and GTIII W.

Results and discussion

Before the utilization for fabric dyeing and functionalization, the prepared green tea aqueous extract was characterized regarding the total flavonoid (*TFC*) and total phenolic (*TPC*) contents, and antioxidant activity (using ABTS assay). *TFC* and *TPC* of the examined extract were found to be 689.7 and 5808 mg L^{-1}, respectively, while it showed 100% antioxidant activity.

Considering the green tea extract's abundance of polyphenolic compounds as well as its excellent antioxidant activity, the prepared extract was used for simultaneous dyeing and functionalization of 100% cotton, 47%/53% cotton/linen, and 70%/30% cotton/linen fabrics. The fabrics' appearances after dyeing and after dyeing and one washing cycle are presented in Figure 1, while the fabrics'*K/S* values are listed in Table I.

GTI GTII GTIII

GTI W GTII W GTIII W

Figure 1. Appearance of the fabrics after dyeing (GTI, GTII, and GTIII) and after dyeing and one washing (GTI W, GTII W, and GTIII W)

Table I *K/S* values of studied fabrics before and after one washing

Before washing	*K/S*	After washing	*K/S*
GTI	9.07	GTI W	1.33
GTII	10.85	GTII	1.15
GTIII	8.33	GTIII W	0.88

From the fabrics'*K/S* values, it is evident that prepared green tea aqueous extract can dye cellulose fabrics, both 100% cotton and cotton/linen blends. Fabrics'*K/S* values decreased in the following order: GTII > GTI > GTIII, Table I. The observed different color strength values are attributed to the fabrics' different chemical compositions and extracts' nature that dictate the possibility of diverse binding interactions between colored bioactive compounds' functional groups and fabric surface groups. After washing with standard detergent, K/S values of all fabrics significantly decreased and accounted for 1.33, 1.55, and 0.88 for 100% cotton, 47%/53% cotton/linen, and 70%/30% cotton/linen fabrics, respectively.

During the utilization of cellulose fabrics as functional clothing, their antioxidant activity plays an important role since high antioxidant activity leads to the reduced production of free radicals that increase oxidative stress, leading to DNA damage. Moreover, they may also contribute to the anti-inflammatory effect.

After dyeing with green tea aqueous extract, all studied fabrics showed maximum (100%) ABTS radical scavenging ability, Figure 2. Similarly, Čuk et al. [11] and Islam et al. [12] concluded that cotton fabric functionalized with green tea aqueous extract having 90% antioxidant activity can be used for free radicals' elimination. It is very important to note that after one washing cycle, functionalized fabrics showed excellent (GTII) to medium (GTI and GTIII)ability for trapping the free radial of oxygen species; i.e., inhibition of ABTS radicals present in testing solutions, Figure 2.

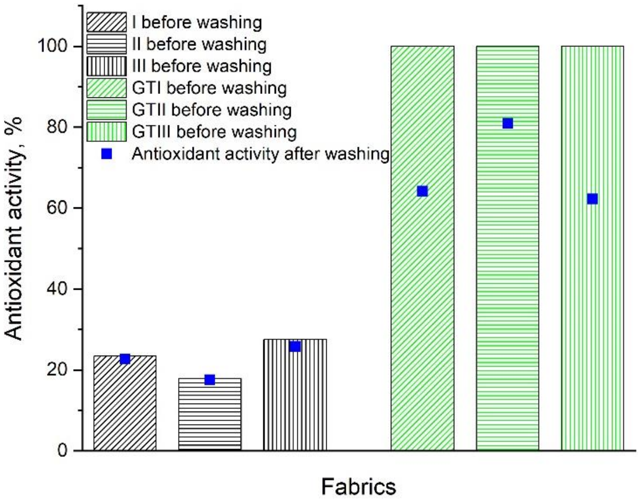

Figure 1. Antioxidant activity of fabrics before and after one washing

Conclusion

Treatment of cotton and cotton/linen fabrics with green tea aqueous extract seems to be very promising for fabric simultaneous dyeing and functionalization or only imparting antioxidant activity, i.e., the ability to trap the free radical of oxygen species, preventing cell deterioration and grow a new cell in the skin. Among all tested fabrics, 47%/53% cotton/linen fabric showed the most stable antioxidant activity after one washing cycle implying that it is the most suitable for functional clothing. The current paper represents a step towards a more sustainable textile industry that could undoubtedly contribute to overcoming the environmental problems caused by the textile industry.

Acknowledgments

This work was supported by the Ministry of Science, Technological Development and Innovation of the Republic of Serbia (Contracts No. 451-03-47/2023-01/200135 and 451-03-47/2023-01/200287).

References

[1] Textile Dyes Pollution: The Truth About Fashion’s Toxic Colours https://goodonyou.eco/textile-dyes-pollution (accessed 2022 - 12 -27)
[2] A. Haji, M. Rahimi, J. Nat. Fibers. 19 (2022) 2785.
[3] S. Joshi, N. Kambo, S. Dubey, P. Shukla, R. Pandey, J. Nat. Fibers. 19 (2022) 8345.
[4] A. Ivanovska, I. Savić Gajić, J. Lađarević, M. Milošević, I. Savić, Antioxidants 11 (2022) 2059.
[5] A. Ivanovska, S. Veljović, M. Reljić, J. Lađarević, L. Pavun, M. Natić, M. Kostić, J. Nat. Fibers. 19 (2022) 11050
[6] A. Kumari, D. Kumar, Chem. Biol. Technol. Ag. 9 (2022) 33.
[7] L. Pavun, P. Đurđević, M. Jelikić-Stankov, D. Đikanović, S. Uskoković-Marković, Czech. J. Food Sci. 36 (2018) 233
[8] J. Lađarević, B. Božić, L. Matović, B. Božić Nedeljković, D. Mijin, Dyes Pigments 162 (2019) 162.
[9] R. Yang, C. He, B. Pan, Z. Wang, Text. Res. J. 92 (2022) 574.
[10] T.K. Glaser, O. Plohl, A. Vesel, U. Ajdnik, N.P. Ulrih, M.K. Hrnčič, U. Bren, Materials 12 (2019) 2118.
[11]N. Čuk, M. Šala, M. Gorjanc, Cellulose 28 (2021) 3215.
[12]S. Islam, B.S. Butola, A. Roy, Int. J. Biol. Macromol. 120 (2018) 1999.

MOLECULAR IDENTIFICATION OF *TRICHOSTRONGYLUS AXEI* ON EUROPEAN BROWN HARE (*LEPUS EUROPAEUS*) IN WESTERN ROMANIA – CASE REPORT

Beatrice Ana-Maria Jitea[1], Sorin Morariu[1], Ion Oprescu[1], Marius Stelian Ilie[1], Mirela Imre[1], Tiana Florea[1], Cătălin Bogdan Sîrbu[2], Gheorghe Dărăbuș[1]

[1]Department of Parasitology and Parasitic Diseases, University of Life Sciences „King Mihai I" from Timișoara, Calea Aradului nr. 119, 300645, Timișoara, Romania
[2]Department of Animal Nutrition and Agriculture, University of Life Sciences „King Mihai I" from Timișoara, Calea Aradului nr. 119, 300645, Timișoara, Romania
e-mail: jiteabeatrice@gmail.com

Abstract

Trichostrongylosis is a cosmopolitan parasitic disease affecting domestic and wild ruminants, equines, and last but not least, leporids. Three species of strongyles commonly parasitize the digestive tracts of leporids, the most prevalent being *Trichostrongylus retortaeformis*. This paper describes the first case of *Trichostrongylus axei* infestation in a wild hare in western Romania. A female wild hare carcass found in Timis County was examined at the Parasiology Department of the Faculty of Veterinary Medicine in Timisoara. A clinical, post-mortem and PCR examination was performed to establish a diagnosis, with molecular analysis confirming the presence of the nematode *Trichostrongylus axei* in European brown hare.

Introduction

The European brown hare (*Lepus europaeus*) is a species native to Europe and parts of Asia [1]. It can be regarded as one of the most important game animals in Europe [2]. In Europe, the brown hare is a major representative of small game and is widespread throughout our country, from the Black Sea basin to mountainous areas. In Europe since the late 1960s, a decline in the European hare population has been observed and has been the subject of numerous studies focusing on the role of habitat [3-5], agriculture [5-8], predation [9] and disease [10-13]. This unfavourable development has been reported in several European countries such as France [14], Denmark [9], Slovakia [15], Poland [16], Serbia [17] and Germany [18].

Apart from common rabbit diseases with a significant impact on rabbit mortality, parasitic diseases are also considered to be a factor in rabbit population reduction [19]. Various parasites, mainly *Eimeria* spp., *Trichostrongylus* spp. and occasionally *Dicrocoelium* spp. and *Linguatula serrata* have been identified in European brown hares [10, 12, 15, 20-23].

The aim of the present study was to identify via molecular analysis the *Trichostrongylus* species present in the European brown hare.

Experimental

Clinical examination

The carcass of a female European brown hare of almost 2 years of age (Figure 1) was found in a forest area in the vicinity of a village in the north of Timis County and was examined in the Parasitic Diseases Clinic of the Faculty of Veterinary Medicine in Timisoara.

Figure 1. European brown hare

After the clinical examination, where no changes were observed, the animal was necropsied. The heart, lungs, liver, spleen and mesenteric lymph nodes were removed and examined separately. Smaller organs were placed in a Petri dish with distilled water and examined under a microscope; the liver and lungs were sectioned into slices of approximately 5 mm to 1 cm and examined; and the intestine was sectioned longitudinally and examined under a stereomicroscope. Parasites found were isolated and preserved in 70% ethanol.

DNA extraction and molecular analysis

The PCR reaction was performed according to the technique described by Yong et al. in 2007 [24]. Amplification was performed by classical PCR and was based on amplification of a ~450 bp sequence for Trichostrongylus spp. modified for the requirements of the mixture.

According to the protocol, the following primers were used: JHTSP (5′-TTATGTGCCACAAATGAAGA-3′ forward primer) and NC2 (5′-TTAGTTTCTTTTCCTCCGCT-3′ reverse primer). A MyTaqTM Red Mix Master Mix (BIOLINE®) was used for the reaction. The final volume of the PCR reaction was 25 µl, of which 12.5 µl MyTaqTM Red Mix (BIOLINE®), 1 µl primer 1 Forward, 1 µl primer 2 Reverse (diluted to a concentration of 10 pmol/µl according to the protocol described by the manufacturer), DNA extracted from the sample to be analysed and ultrapure water. The amplification program was carried out with the My Cycler thermocycler (BioRad®). This program included the steps of DNA denaturation at 95°C for 1 minute; 32 cycles of: denaturation at 95°C for 30 seconds, hybridization at 50°C for 30 seconds and extension at 72°C for 30 seconds; followed by incubation at 4°C. Amplicon analysis and control was performed by horizontal electrophoresis in a 1.5% agarose gel electrophoresis submersion system with the addition of MidoriGreen flourescent dye (Nippon Genetics® Europe) at 120 V and 90 mA for 60 minutes. After migration of the samples into the agarose gel, the image of the gel with migrated DNA fragments was captured using a UV photodocumentation system (UVP®).

PCR results were sequenced at Macrogen Europe® Company (Amsterdam, The Netherlands) and compared with those available in the GenBank database using BLAST alignment.

Results and discussion

Parasites found (n=21) were examined using a stereomicroscope (17 females and 4 males) (Figures 2 and 3). After analysis, two adults were preserved in 90% ethanol for molecular analysis.

Figure 2 Posterior extremity of a *Trichostrongylus axei* female

Figure 3. Posterior extremity of a *Trichostrongylus axei* male illustrating the copulatory bursa and the spicules

Samples examined by the PCR method were successfully processed. The first well contains the molecular marker at 100 bp and well 2 contains the positive DNA sample amplified from *Trichostrongylus* spp. adults (Figure 4).

Samples were checked in GenBank, then compared with available sequences using BLAST. The sequencing results of the samples can be seen in Table 1.

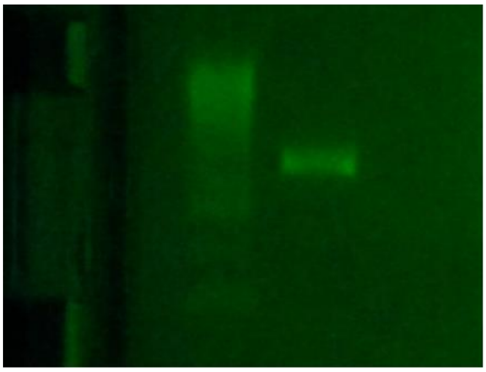

Figure 4. Image of 1.5% agarose gel electrophoresis of amplicons resulting from amplification of extracted DNA with specific primers

Table 1

Results of sequenced samples

Crt. no.	Sample name	Similar sequence	Species
1.	434	ON677948.1	*Trichostrongylus axei*
2.	435	AY439026.1	*Trichostrongylus axei*

Trichostrongylus axei is a ruminant-specific parasite and has never been found in naturally infected hares in western Romania. Experimental infections with *Trichostrongylus axei* and *Trichostrongylus colubriformis* have been performed in hares. Female hares have been shown to be more susceptible to infection with *T. axei* than males, the latter being more susceptible than females to *T. colubriformis* [25].

Natural transmission of some nematode species present in the digestive tracts of ruminants is possible but uncommon in domestic or wild hares. For example, Saulai and Cabaret (1998) reported ruminant-specific parasites, namely *T. colubriformis* and *T. capricola* in *Oryctolagus cuniculus* and *Lepus capensis*, respectively [26]. However, these infections were sporadic despite the large number of ruminant species. In Italy, *T. colubriformis, T. axei, T. vitrinus* and *Ostertagia ostertagi* have been reported in *O. cuniculus* in Sicily [27], while in Sardinia, *T.*

vitrinus and *T. colubriformis* have been reported in wild hares [28]. Regarding *T. circumcincta*, experimental infection of rabbits with larvae has been found to be difficult but reasonable in *L. europaeus*, and not in *O. cuniculus* [29].

Conclusion

This is the first study to confirm the presence of the nematode *Trichostrongylus axei* in the digestive tract of the European brown hare (*Lepus europaeus*) in western Romania.

References

[1] Mori, E., Carbone, R., Viviano, A., Calosi, M., Fattorini, N., Factors affecting spatiotemporal behaviour in the European brown hare *Lepus europaeus*: A meta-analysis. Mamm. Rev. 2022, 52, 454–470.

[2] Tsokana, C.N., Sokos, C., Giannakopoulos, A., Birtsas, P., Valiakos, G., Spyrou, V., Athanasiou, L.V., Burriel, A., Billinis, C., European brown hare (*Lepus europaeus*) as a source of emerging and re-emerging pathogens of public health importance: a review. Veterinary Medicine and Science, 2020, 6(3).

[3] Pavliska, P.L., Riegert, J., Grill, S., Šálek, M., The effect of landscape heterogeneity on population density and habitat preferences of the European hare (*Lepus europaeus*) in contrasting farmlands. Mamm. Biol. 2018, 88, 8–15.

[4] Pépin, D., Angibault, J.M., Selection of resting sites by the European hare as related to habitat characteristics during agricultural changes. Eur. J. Wildl. Res. 2007, 53, 183–189.

[5] Jennings, N., Smith, R.K., Hackländer, K., Harris, S., White, P.C.L., Variation in demography, condition and dietary quality of hares *Lepus europaeus* from high-density and low-density populations. Wildlife Biol. 2006, 12, 179–189.

[6] Panek, M., Habitat factors associated with the decline in brown hare abundance in Poland in the beginning of the 21st century. Ecol. Indic. 2018, 85, 915–920.

[7] Smith, R.K., Vaughan Jennings, N., Harris, S., A quantitative analysis of the abundance and demography of European hares *Lepus europaeus* in relation to habitat type, intensity of agriculture and climate. Mamm. Rev. 2005, 35, 1–24.

[8] Tapper, S.C., Barnes, R.F.W., Influence of Farming Practice on the Ecology of the Brown Hare (*Lepus europaeus*). J. Appl. Ecol. 1986, 23, 39–52.

[9] Schmidt, N.M., Asferg, T., Forchhammer, M.C., Long-term patterns in European brown hare population dynamics in Denmark: effects of agriculture, predation and climate. BMC Ecology. 2004, 4(1).

[10] Brustenga, L., Franciosini, M.P., Diaferia, M., Rigamonti, G., Musa, L., Russomanno, B.L., Veronesi, F., Parasitological Survey in European Brown Hare (*Lepus europaeus* Pallas, 1778) Breeding Facilities in Southern Italy. Pathogens. 2023, 12, 208.

[11] Faehndrich, M., Klink, J.C., Roller, M., Wohlsein, P., Raue, K., Strube, C., Prenger-Berninghoff, E., Ewers, C., Capucci, L., Lavazza, A., Status of Infectious Diseases in Free-Ranging European Brown Hares (*Lepus europaeus*) Found Dead between 2017 and 2020 in Schleswig-Holstein, Germany. Pathogens 2023, 12, 239.

[12] Panayotova-Pencheva, M.S., Endoparasites of the European brown hare (*Lepus europaeus* Pallas, 1778 L.) (Lagomorpha: *Leporidae*) from Bulgaria. Ann Parasitol. 2022; 68(3): 553-562.

[13] Wibbelt, G., Frölich, K., Infectious Diseases in European Brown Hare (*Lepus europaeus*). Wildl. Biol. Pract. 2005, 1, 86–93.

[14] Marboutin, E., Bray, Y., Peroux, R., Mauvy, B., Lartiges A., Population dynamics in European hare: breeding parameters and sustainable harvest rates. Journal of Applied Ecology. 2003, 40(3): 580–591.

[15] Dubinsky, P., Vasilková, Z., Hurníková, Z., Miterpáková, M., Slamečka, J., Jurčík, R., Parasitic infections of the European brown hare (*Lepus europaeus* Pallas, 1778) in south-western Slovakia. Helminthologia. 2010, 47(4): 219–225.

[16] Kornaś, S., Wierzbowska, I.A., Wajdzik, M., Kowal, J., Basiaga, M., Nosal, P., Endoparasites of European brown hare (*Lepus europaeus*) from southern Poland based on necropsy. Annals of Animal Science. 2014, 14(2): 297–305.

[17] Ilić, T., Petrović, T., Dimitrijević, S., Parasitic infections of wild rabbits and hares. Veterinarski Glasnik. 2014, 68(3–4): 241–250.

[18] Sliwinski, K., Ronnenberg, K., Jung, K., Straub, E., Siebert, U., Habitat requirements of the European brown hare (*Lepus europaeus* Pallas 1778) in an intensively used agriculture region (Lower Saxony, Germany). BMC Ecology. 2019, 19(1).

[19] Alzaga, V., Tizzani, P., Acevedo, P., Ruiz-Fons, F., Vicente, J., Gortazar, C., Deviance partitioning of host factors affecting parasitization in the European brown hare (*Lepus europaeus*). Naturwissenschaften. 2009, 96: 1157–1168.

[20] Jitea, B.A.-M., Imre, M., Florea, T., Sîrbu, C.B., Luca, I., Stancu, A., Ciresan, A.C., Darabus, Characterization of the Tongue Worm, *Linguatula serrata* (Pentastomida), Identified from Hares (*Lepus europaeus*) in Romania. Int. J. Mol. Sci. 2023, 24, 12927.

[21] Jitea (Sîrbu), B.A.M., Sîrbu, C.B., Florea, T., Hotea, I., Dărăbuș, Gh., Endoparasites found in *Lepus europaeus* hunted In Western Romania, 22nd International Multidisciplinary Scientific GeoConference SGEM 2022, 691 – 697.

[22] Sergi, V., Romeo, G., Serafini, M., Torretta, E., Macchioni, F., Endoparasites of the European Hare (*Lepus Europaeus*) (Pallas, 1778) in Central Italy. Helminthologia. 2018, 55(2):127-133.

[23] Hora, F., Mederle, N., Badea, C., Tilibaşa, E, Ilie, M., Dărăbus, G., Digestive parasite fauna in hare (*Lepus europaeus*) in Western Romania. Scientific Works. Series C. Veterinary Medicine. 2015, 61, 138 - 141.

[24] Yong, T.S., Lee, J,H., Sim, S., Lee, J., Min, D.Y., Chai, J.Y., Eom, K.S., Sohn, W.M., Lee, S.H., Rim, H.J., Differential diagnosis of *Trichostrongylus* and hookworm eggs via PCR using ITS-1 sequence, Korean Journal of Parasitology. 2007, 45 (1): 69 – 74.

[25] Ciordia, H., Bizzell, W.E., Porter, D.A., Dixon, C.F., The effect of culture temperature and age on the infectivity of the larvae of *Trichostrongylus axei* and *Tricostrongylus colubriformis* in rabbits and guinea pigs. The Journal of Parasitology, 1966, 52, 5, 866 – 870.

[26] Saulai, M., Cabaret, J., Limited role of lagomorphs (*Oryctolagus cuniculus* and *Lepus capensis*) in the dispersion of parasite nematodes of ruminants. Vet. Parasitol. 1998, 77: 301 – 304.

[27] Giannetto, S., Virga, A., Baccarani, E. M., Canestri Trotti, G., Elminti intestinali in conigli selvatici (*Oryctolagus cuniculus*). Atti SISVet., 1998, 52: 165 – 166.

[28] Lai, M., Arru, E., Trichostrongylidae del coniglio selvatico (*Oryctolagus cuniculus*). Parassitologia. 1969, 11: 97 – 99

[29] Stott, P., O'callaghan, M., Phillips, P., Verbyla, A., The experimental establishment of ruminant nematodes in European hares (*Lepus europaeus*). Vet. Parasitol., 2009, 159: 82 – 85.

APPLICATION OF A 3D-PRINTED, HIGH EFFICIENCY SAMPLE INTRODUCTION SYSTEM FOR SINGLE CELL ICP-MS ANALYSIS

Gyula Kajner[1], Ádám Bélteki[1], Martin Cseh[2], Zsolt Geretovszky[2,3], Tibor Ajtai[3], Lilla Barna[4], Mária A. Deli[4], Bernadett Pap[5], Gergely Maróti[5], Gábor Galbács[1,*]

[1]Department of Molecular and Analytical Chemistry, University of Szeged, H-6720 Szeged, Dóm tér 7-8, Hungary
[2]Center of Excellence for Interdisciplinary Research, Development and Innovation, 3D Center University of Szeged, H-6725, Szeged, Tisza Lajos blvd. 107, Hungary
[3]Department of Optics and Quantum Electronics University of Szeged, H-6720 Szeged, Dóm square 9, Hungary
[4]HUN-REN Biological Research Centre, Institute of Biophysics, H-6726 Szeged, Temesvári boulevard 62, Hungary
[5]HUN-REN Biological Research Centre, Institute of Plant Biology, Biological Research Center, H-6726 Szeged, Temesvári boulevard 62, Hungary
e-mail: galbx@chem.u-szeged.hu

Abstract

In this study, the application of an alternative, 3D-printed sample introduction system (SIS) is presented for single cell ICP-MS analysis. The SIS utilized in the experiments was designed by our group with the purpose to enhance single particle detection capabilities. It is able to provide higher transport efficiencies, increased sensitivity, lower background signals and a wider range of detectable particle size in single particle ICP-MS (spICP-MS) analysis compared to the standard SIS. Capitalizing on these features, two single cell ICP-MS (scICP-MS) experiments were done, using single cellular algae (Chlorella) and human endothelial cell suspensions, thereby demonstrating the SIS's ability to facilitate cell biology related studies such as determining the elemental composition/metal uptake of a single cell or monitoring its cell-to-cell variation in cell cultures.

Introduction

Single particle ICP-MS is a relatively novel analytical technique, which was first proposed by Degueldre et al [1], in around 2003. It is able to provide information about the elemental and isotopic composition, size distribution, particle number concentration etc. of nano- and – as later has been also shown – microparticles [2]. Since then, the method has been utilized for various purposes in material science and cell biology [3, 4]. However, the efficiency and applicability of the technique are severely hindered by the inefficient operation of the commonly used ICP-MS sample introduction systems (e.g. a concentric nebulizer coupled with a double-pass or cyclonic spray chamber). These systems are designed to produce as stable and fine aerosol as possible, ensuring plasma stability. However, this comes with undesired features from the perspective of single particle analysis such as low transport efficiency and narrow transmitted droplet size range [5]. To tackle this problem, sample introduction systems (SIS) designed to facilitate efficient particle detection started to appear recently. These systems vary in design, however they usually operate with nebulizers with decreased nozzle dimensions that require lower sample uptake rate, and are often complemented with additional (sheath) gas flows to promote higher droplet transmission [6, 7]. Utilizing these alternative SIS, increased particle detection efficiencies, decreased limit of detections (LODs), and lower sample consumption were reported. However, they are not part of the general ICP-MS laboratory equipment, partly because they pose a significant expense. Last year we presented the design process [8] and later, the application [9] of the first completely 3D-printed version of such a high efficiency sample introduction system for ICP-MS. The system consists of a microconcentric nebulizer coupled with a single-pass spray chamber equipped with an optional sheath gas flow. In this study our goal was to assess the applicability of this system for cell biological purposes, and to compare the capabilities of the 3D-printed SIS to that of the standard one.

Experimental

An Agilent 7700X inductively coupled plasma mass spectrometer was used, coupled with its standard sample introduction system (MicroMist concentric nebulizer coupled with a "Scott-type" double-pass spray chamber) or our custom, 3D-printed sample introduction system (microconcentric pneumatic nebulizer coupled with a single-pass spray chamber equipped with optional sheath gas flow). During spICP-MS measurements, the data acquisition software was set to time resolved analysis (TRA) mode, and the integration time was set to 12 ms. In every experiment the plasma was operated with 15 $L\cdot min^{-1}$ of plasma gas flow rate, 1550 W of R.F. forward power and 10 mm sampling depth. The standard SIS was used with its regular 1.05 $L\cdot min^{-1}$ nebulizer gas flow and 750 $\mu L\cdot min^{-1}$ sample uptake rate with no sheath gas, whereas the 3D-printed SIS was operated with 1.35 $L\cdot min^{-1}$ nebulizer gas flow, 33.3 $\mu L\cdot min^{-1}$ sample uptake, and 0.1 $L\cdot min^{-1}$ sheath gas flow rate.

The high efficiency sample introduction system was printed with a ProJet MJP 3600 MAX type 3D-printer equipped with VisiJet M3 resin (3D Systems, Rock Hill, SC, USA).

In all experiments, trace-quality de-ionized water was used as a diluant. which was obtained from a MilliPore Elix 10 device equipped with a Synergy polishning unit (Merck, Darmstadt, Germany).

For experiments with algae cells, one strain of single cellular algae (d=3.6 µm) was used, which was the Chlorella sp. (MACC-360), obtained from the Monsonmagyaróvár Algae Culture Collection (MACC, Monsonmagyaróvár, Hungary). The cells were cultivated in the form of cell suspensions at 25°C with continous shaking, in an incubator which provided 16:8 h light-dark cycles. Tris acetate phosphate (TAP) medium was used as the growth medium for all culture, which prior to the spICP-MS measurements was replaced with de-ionited water through 5 repeated cycles of cell sedimentation via centrifuge and supernatant replacement. The extra nickel was added to the algae suspension using an analytical grade nickel standard solution (Merck, Darmstadt, Germany)

In experiments involving endothelial cells, human vascular endothelial cells (d=15.4) were used, grown in a dedicated endothelial cell culture medium (ECM) complemented with 5% of fetal bovine serum, 1% of endothelial growth supplement, and 0.5% of gentamincin, all obtained from ScienCell Research Laboratories (ScenCell, Carlsbad, CA, USA). After confluation, the cells were detached from the 60mm Petri dishes they were grown on using a trypsin-EDTA solution. The cells were washed with ECM and after centrifugation, resuspended in PBS (phosphate buffered saline), then fixed with 1% of paraformaldehyde.

Results and discussion

To demonstrate some of the benefits of our 3D-printed sample introduction system can provide, first an experiment was done on a series of cell cultures from the Chlorella algae strain. Four parallel cell cultures, with approximately $5\cdot10^6$ mL^{-1} cell number concentration, were prepared with different Ni^{2+} content in them, ranging from 0 (control) to 150 µM. The cultures' state was examined for 72 hours in every 24 hours via a series of spICP-MS measurements, monitoring the cell population, and cell-to-cell variation of the accumulated Ni^{2+} content. As Figure 1a shows, the added Ni^{2+} ions significantly affected the proliferation rate of the algae in the concentration range used. The cell culture with 50 µM showed significantly higher growth rate as compared to the control sample. Maximum population growth factor could be observed on the culture with 100 µM of Ni^{2+}, although its proliferation was temporarily suppressed initially by the elevated heavy metal content, whereas for the 150 µM culture, population growth was suppressed throughout the whole experiment. Accumulated nickel content in individual cells above detection limit (LOD) was only observable in the case of the culture with the highest concentration. Figure 1b shows the trends related to the heavy metal uptake. Nickel levels appears to be constant for the first two days, then it starts to increase further, whereas LOD values were increasing gradually due to the increasing Ni background in the samples, which probably originate from the cells, that released them after medium changes.

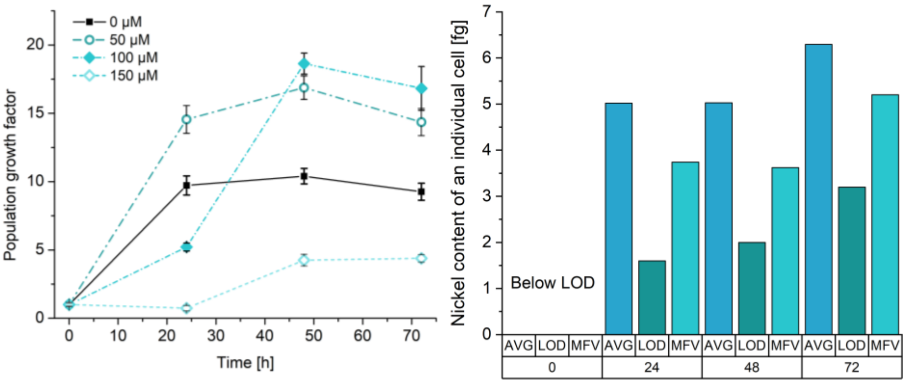

Figure 1. a) Population growth of Chlorella cell cultures in media with different concentrations of Ni^{2+} ions. b) The extent of the accumulation of Ni content in individual Chlorella cells, cultivated in a media with 150 µM Ni^{2+} of ions. The presented statistical indicators were calculated from the Ni content distribution of a few hundred cells (AVG: average, MFV: most frequent value, LOD: limit of detection)

In another experiment, we demonstrated the counting of human endothelial cells. The challenging part of carrying out such measurements comes from the relatively large size (d=15.4 µm) and fragility of these cells.

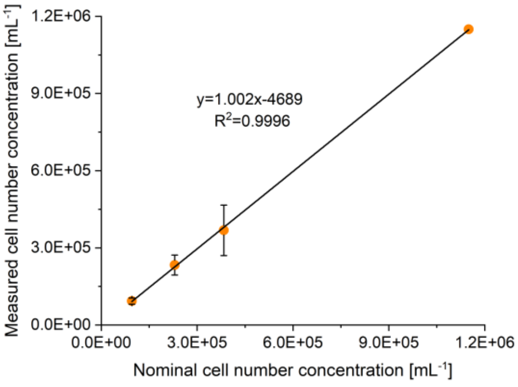

Figure 2. Correlation between the nominal and the determined cell number concentration of endothelial cell suspensions with different dilution rates. Cell detection was done based on the Ni content of the cells, measured at mass 58.

Optical particle counter experiments revealed that this size is above the cut-off size for the standard SIS, whereas the new system has transmission even for droplets with diameters as large as 25 µm, thus making the detection of cells up to this size possible [9]. In the experiment, the endothelial cell dispersion with a cell number concentration of $1.15 \cdot 10^6$ mL^{-1} was diluted in multiple steps until a 12-fold dilution. The cell number concentration of each diluted sample was determined by scICP-MS measurements. The obtained concentation data shows a good linear correlation with the theoretical values (Figure 2), thus demonstrating that the counting of cells of this size is feasible with a decent precision using the new sample introduction system.

Conclusion

Both of the showcased cell biological experiments were made feasible by utilizing of the new, 3D-printed, plastic sample introduction system, as it has provided greatly improved transport efficiencies (the cell fraction that could be detected) compared to what can be achieved with the standard SIS. Furthermore, nickel content of individual cells was only above LOD when the 3D-printed system was used, due to its ability to enhance sensitivity and suppress background signals. As these results indicate, a perfectly functional ICP-MS sample introduction system could be made – for the first time in the literature – using only 3D-printing techniques, that has substantial benefits when applied in scICP-MS measurements.

Acknowledgements

This work was partially funded by the National Research, Development and Innovation Office (NKFIH) of Hungary through projects TKP2021-NVA-19 and K 146733. M.A. Deli acknowledges the support received from the Hungarian Academy of Sciences (NAP2022-I-6/2022). Gy. Kajner is thankful for the financial support received from the ÚNKP-22-2 and ÚNKP-23-3 New National Excellence Programs of NKFIH. The Lendület-Programme of the Hungarian Academy of Sciences (LP2020-5/2020) supported G. Maróti.

References

[1] C. Degueldre, P.Y. Favarger, Colloids Surf. A: Physicochem. Eng. 217 (2003) 137–142.
[2] H. Haraguchi, J. Anal. At. Spectrom. 19 (2004) 5–14.
[3] M. Corte-Rodríguez, R. Álvarez-Fernández, P. García-Cancela, M. Montes-Bayón, J. Bettmer, Trends Anal. Chem. 132 (2020) 116042.
[4] S. Miyashita, A.S. Groombridge, S. Fujii, A. Minoda, A. Takatsu, A. Hioki, K. Chiba, K. Inagaki, J. Anal. At. Spectrom. 29 (2014) 1598-1606.
[5] M. Tharaud, P. Louvat, M.F. Benetti, Anal. Bioanal. Chem. 413 (2021) 923-933.
[6] K. Inagaki, S. Fujii, A. Takatsu, K. Chiba, J. Anal. At. Spectrom. 26 (2011) 623-630
[7] F. Lin, S. Miyashita, K. Inagaki, Y.H. Liu, I.H. Hsu, J. Anal. At. Spectrom. 34 (2019) 401-406.
[8] Gy. Kajner, Á. Bélteki, M. Cseh, B. Vajda, Zs. Geretovszky, G. Galbács, Proceedings of 28th ISAEP, Szeged, Hungary, 2022.11.14.
[9] Gy. Kajner, Á. Bélteki, M. Cseh, B. Vajda, Zs. Geretovszky, E. Papp, M. Braun, G. Galbács, Proceedings of the EWCPS 2023, Ljubljana, Slovenia, 2023.01.29.

C18-UHPLC ANALYSIS OF RETENTION BEHAVIOR OF NEWLY DESIGNED *O*-ALKYLATED ANDROSTANE DERIVATIVES IN TERNARY MIXTURE METHANOL/ACETONITRILE/WATER

Milica Karadžić Banjac[1], **Strahinja Kovačević**[1], **Jasmina Anojčić**[2], **Jovana Ajduković**[2], **Sanja Podunavac-Kuzmanović**[1]

[1]University of Novi Sad, Faculty of Technology Novi Sad, Bulevar cara Lazara 1, 21000 Novi Sad, Serbia
[2]University of Novi Sad, Faculty of Sciences, Trg Dositeja Obradovića 3, 21000 Novi Sad, Serbia
e-mail: mkaradza@uns.ac.rs

Abstract

Different new groups of steroid compounds are the center of attention in a grate number of scientific publications since the majority of compounds are being researched as anticancer drugs. One of the most important feature of potential drug is its lipophilicity. Nowadays, ultra high-performance liquid chromatography (UHPLC) is used as one of the most sophisticated techniques for determination of the retention behavior determination of different biologically active compounds. The series of 18 newly designed *O*-alkylated androstane derivatives was investigated in reversed phase (RP)-UHPLC system using ternary mixture methanol/acetonitrile/water. A good agreement between experimentally observed and *in silico* lipophilicity was noticed given that coefficient of determination of 0.8406 was achieved.

Introduction

Improved anticancer activity of different steroid compounds originates from heterocyclic systems with a nitrogen atom in the steroid nucleus [1,2]. Nowadays, different steroids are taken as a relevant scaffold for new anticancer drugs development since they possess suitable physicochemical properties, high selectivity and reduced side effects when applied as drugs. Different steroid derivatives are proven to achieve results in the treatment of hormone independent tumors, reproductive tissues and a variety of tumor cell lines [3-5]. Scientist are constantly working on design and development of safer, effective and target-specific steroid drugs.

Novel alkylaminoethyl derivatives of androstane 3-oximes were synthesized and their cytotoxic effects were evaluated [6]. *In vitro* cytotoxic activity was investigated against several common human tumor cell lines, as well as on normal fetal lung cells (MRC-5) and human foreskin fibroblasts (BJ). Additionally, *in vitro* screening against cytochrome P450 enzymes were conducted. Also, quantitative structure-activity relationship (QSAR) modeling of cytotoxic activity of these compounds towards malignant melanoma cells was conducted [7]. Univariate linear regression (ULR) and multivariate linear regression (MLR) models were presented as well as several support vector machines regression (SVM)-based quantitative structure-activity relationship (QSAR) models. Previously determined cytotoxic activity of the studied androstane 3-oximes against melanoma G-361 cells was used for molecular docking analysis and molecular dynamics of the most promising compounds.

This study represent the extension of research of this group of 18 newly synthesized *O*-alkylated androstane derivatives in terms of characterization regarding their retention behavior and lipophilicity. Using ternary mixture methanol/acetonitrile/water in RP-UHPLC system the retention behavior of investigated compounds was tested and correlated with their *in silico* lipophilicity.

Experimental

The series of the analyzed compounds was synthesized at the Department of Chemistry, Biochemistry and Environmental Protection, Faculty of Sciences, University of Novi Sad [6]. The IUPAC names of the compounds are presented in Table 1. The studied *O*-alkylated androstane derivatives are generally divided into two series: the series I of 17β-hydroxy-17α-(pyridin-2-yl)methylandrost-4-en-(3*E*,*Z*)-one oximes (the compounds **1-9**) and the series II of (17*E*,*Z*)-(pyridin-2-yl)methylideneandrost-4-en-(3*E*)-one oximes (the compounds **10-18**).

Table 1. The IUPAC names of the analyzed compounds

No.	The IUPAC name
1	17β-Hydroxy-17α-(pyridin-2-yl)methylandrost-4-en-(3*E*)-one oxime
2	17β-Hydroxy-17α-(pyridin-2-yl)methylandrost-4-en-(3*Z*)-one oxime
3	17β-Hydroxy-17α-(pyridin-2-yl)methylandrost-4-en-(3*E*)-one-*O*-[2-(pyrrolidin-1-yl)ethyl] oxime
4	17β-Hydroxy-17α-(pyridin-2-yl)methylandrost-4-en-(3*E*)-one-*O*-[3-(*N*,*N*-dimethylamino)propyl] oxime
5	17β-Hydroxy-17α-(pyridin-2-yl)methylandrost-4-en-(3*E*)-one-*O*-[2-(*N*-methylpyrrolidin-2-yl)ethyl] oxime
6	17β-Hydroxy-17α-(pyridin-2-yl)methylandrost-4-en-(3*E*)-one-*O*-[2-(piperidin-1-yl)ethyl] oxime
7	17β-Hydroxy-17α-(pyridin-2-yl)methylandrost-4-en-(3*E*)-one-*O*-[2-(morpholin-4-yl)ethyl] oxime
8	17β-Hydroxy-17α-(pyridin-2-yl)methylandrost-4-en-(3*E*)-one-*O*-[2-(*N*,*N*-diethylamino)ethyl] oxime
9	17β-Hydroxy-17α-(pyridin-2-yl)methylandrost-4-en-(3*E*)-one-*O*-[2-(*N*,*N*-dimethylamino)ethyl] oxime
10	(17*E*)-(Pyridin-2-yl)methylideneandrost-4-en-(3*E*)-one oxime
11	(17*E*)-(Pyridin-2-yl)methylideneandrost-4-en-(3*Z*)-one oxime
12	(17*E*)-(Pyridin-2-yl)methylideneandrost-4-en-(3*E*)-one-*O*-[2-(pyrrolidin-1-yl)ethyl] oxime
13	(17*E*)-(Pyridin-2-yl)methylideneandrost-4-en-(3*E*)-one-*O*-[3-(*N*,*N*-dimethylamino)propyl] oxime
14	(17*E*)-(Pyridin-2-yl)methylideneandrost-4-en-(3*E*)-one-*O*-[2-(*N*-methylpyrrolidin-2-yl)ethyl] oxime
15	(17*E*)-(Pyridin-2-yl)methylideneandrost-4-en-(3*E*)-one-*O*-[2-(piperidin-1-yl)ethyl] oxime
16	(17*E*)-(Pyridin-2-yl)methylideneandrost-4-en-(3*E*)-one-*O*-[2-(morpholin-4-yl)ethyl] oxime
17	(17*E*)-(Pyridin-2-yl)methylideneandrost-4-en-(3*E*)-one-*O*-[2-(*N*,*N*-diethylamino)ethyl] oxime
18	(17*E*)-(Pyridin-2-yl)methylideneandrost-4-en-(3*E*)-one-*O*-[2-(*N*,*N*-dimethylamino)ethyl] oxime

The chromatographic analysis was carried out by RP-UHPLC system on UHPLC Agilent 1290 Infinity LC System with Diode Array Detector under isocratic conditions with the ZORBAX column Eclipse C18, 95Å, 2.1 × 50 mm, 1.8 µm (1200 bar pressure limit, LC Platform, Low Dispersion UHPLC). Prior to analysis, the compounds were dissolved in methanol (concentration 0.5 mg/mL). Afterwards, the solutions were submerged into ultrasonic bath and filtered by Captiva Econofilter with nylon membrane (25 mm diameter, 0.45 µm pore size, 1000/pk). Temperature in the column was maintained at 25 °C. The injection volume was 10 µL. The flow was set at 0.2 mL/min. The mobile phase used was ternary mixture of methanol, acetonitrile and water (45/45/10 v/v, respectively). The peaks were measured at 210 nm. The chemicals used in analysis are methanol (HPLC gradient grade, Baker), acetonitrile (for HPLC analysis, Acros Organics) and ultrapure water. The retention parameters of the analyzed molecules were expressed as capacity factor (log$k$):

$$\log k = \log((t_r - t_0)/t_0)$$

where t_r is the retention time of a compound and t_0 the dead time (the time of the first disturbance on the chromatogram).

The lipophilicity parameters (log$P$) of the compounds were calculated by ChemBioDraw 13.0 program [8] based on 2D molecular structures.

Results and discussion

One of the representative chromatograms of the analysis of the compound **16** ((17*E*)-(Pyridin-2-yl)methylideneandrost-4-en-(3*E*)-one-*O*-[2-(morpholin-4-yl)ethyl] oxime) is presented in Figure 1, together with its structural formula. The peak detected as the compound of interest is clearly and unambiguously separated from other peaks on the observed chromatogram.

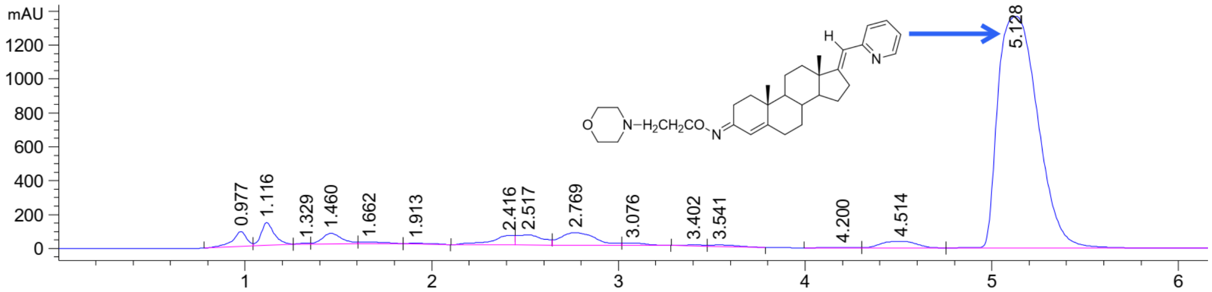

Figure 1. The representative chromatogram of the analysis of the compound **16** ((17*E*)-(Pyridin-2-yl)methylideneandrost-4-en-(3*E*)-one-*O*-[2-(morpholin-4-yl)ethyl] oxime)

Retention and lipophilicity parameters obtained experimentally and *in silico* are presented in Table 2. For all eighteen compounds, dead time, retention time of a compound, capacity factor and lipophilicity parameter are given. It can be noticed that compounds from the series I of 17β-hydroxy-17α-(pyridin-2-yl)methylandrost-4-en-(3*E*,*Z*)-one oximes (the compounds **1-9**) have lower values of log*k* and log*P* parameters, while compounds from series II of (17*E*,*Z*)-(pyridin-2-yl)methylideneandrost-4-en-(3*E*)-one oximes (the compounds **10-18**) have higher values of log*k* and log*P* parameters. According to log*P* parameter values, compound **7** occurs as the one with the lowest lipophilicity (4.07), whilst compound **17** stands out as the one with the highest lipophilicity (5.98).

Table 2. Retention parameters and lipophilicity data of the analyzed androstane compounds

Compounds	t_0	t_r	**log*k***	**log*P***
1	0.974	1.701	-0.127	4.210
2	0.978	1.679	-0.145	4.210
3	1.108	3.257	0.288	4.790
4	0.960	4.296	0.541	4.580
5	1.020	4.746	0.563	4.870
6	1.101	5.328	0.584	5.200
7	1.024	1.717	-0.170	4.070
8	1.099	4.561	0.498	5.150
9	1.054	3.377	0.343	4.470
10	0.965	5.086	0.630	5.040
11	0.963	5.037	0.626	5.040
12	1.001	7.513	0.813	5.620
13	1.000	9.059	0.906	5.410
14	1.100	7.585	0.771	5.710
15	1.100	11.113	0.959	6.040
16	0.977	5.128	0.628	4.910
17	1.009	10.857	0.989	5.980
18	1.034	5.823	0.666	5.310

In Figure 2 the relationship between the lipophilicity (log*P*) and retention parameter (log*k*) of the analyzed series of androstane derivatives is graphically presented. An overview of the distribution of the points around the regression line as well as slope (0.5603) and intercept (-2.3001) are presented.. Very high coefficient of determination (0.8406) indicates the presence of good concurrence between experimentally observed and *in silico* lipophilicity.

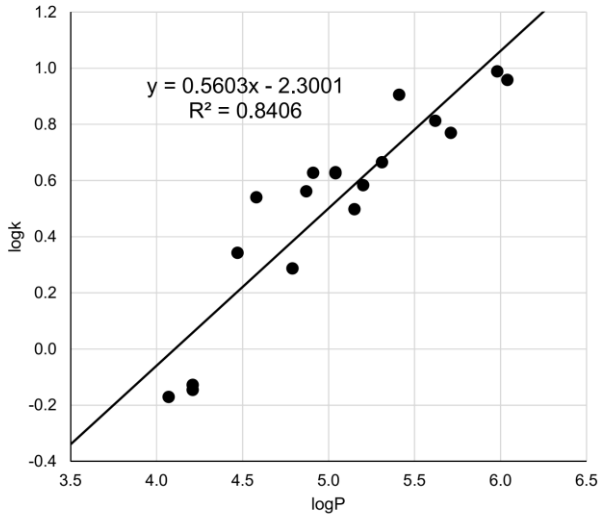

Figure 2. The relationship between the lipophilicity (log*P*) and retention parameter (log*k*) of the analyzed series of androstane derivatives

Conclusion

In the present study, C18-UHPLC analysis of retention behavior of 18 newly designed *O*-alkylated androstane derivatives in ternary mobile phases with methanol and acetonitrile as modifiers was conducted. This study was conducted in order to investigate chromatographic lipophilicity as one of the most important feature of the potential anticancer drug. Results of this study indicate that chromatographic lipophilicity of investigated compounds as future drug candidates of biomedical importance can be successfully correlated with *in silico* lipophilicity descriptor. The lipophilicity parameter can be presented as function of retention value and in that way it reflects the lipophilicity of investigated steroid derivatives.

Acknowledgements

The present research is financed in the framework of the project of the Ministry of Science, Technological Development and Innovation (Project No. 451-03-47/2023-01/200134).

References

[1] N. Zhu, Y. Ling, X. Lei, V. Handratta, A. M. H. Brodie, Steroids. 68 (2003), 603-611.

[2] V.D. Handratta, T.S. Vasaitis, V.C.O. Njar, L.K. Gediya, R. Kataria, P. Chopra, D. Newman, R. Farquhar, Z. Guo, Y. Qiu, A.M.H. Brodie, J. Med. Chem. 48 (2005), 48, 2972-2984.

[3] S.X. Lin, J. Chen, M. Mazumdar, D. Poirier, C. Wang, A. Azzi, M. Zhou, Nat. Rev. Endocrinol. 6 (2010), 485-493.

[4] N. Sharifi, J.L. Gulley, W.L. Dahut, Endocr. Relat. Cancer 17 (2010) R305-R315.

[5] D.S. Jakimov, V.V. Kojić, L.D. Aleksić, G.M. Bogdanović, J.J. Ajduković, E.A. Djurendić, K.M. Penov Gaši, M.N. Sakač, S.S. Jovanović-Šanta. Bioorg. Med. Chem. 23 (2015) 7189-198.

[6] J.J. Ajduković, D.S. Jakimov, L. Rárová, M. Strnad, Y.U. Dzichenka, S. Usanov, D.Đ. Škorić, S.S. Jovanović-Šanta, M.N. Sakač, RSC Adv. 11 (2021) 37449-37461.
[7] S. Kovačević, M. Karadžić Banjac, S. Podunavac-Kuzmanović, J. Ajduković, B. Salaković, L. Rárová, M. Đorđević, M. Ivanov, J. Mol. Struct. 1283 (2023) 135272.
[8] ChemBioDraw 13.0 program, PerkinElmer, https://perkinelmerinformatics.com/

ISOLATION AND PURIFICATION OF LENTIL LECTIN FOR ANALYTICAL APPLICATION IN CARBOHYDRATES RESEARCH

Marija Kostić[1], Branimir Bajac[1], Milica Perović[2], Mirjana Antov[2]

[1]University of Novi Sad, Institute BioSense, Novi Sad, Serbia
[2]University of Novi Sad, Faculty of Technology, Novi Sad, Serbia
e-mail: marija.kostic@biosense.rs

Carbohydrates are highly diverse and ubiquitous natural molecules, with significant roles in many biological processes. Lectins, as carbohydrate-binding proteins that can specifically recognize and reversibly bind different mono- and oligosaccharides, and glycoconjugates, have proven to be an excellent analytical tool in investigating these glycans structures.

The aim of this study was to introduce a relatively low-cost protocol for the isolation and purification of lectin from lentil seeds, whose agglutinating activity could be used in different glycans studies. To characterize samples after each purification step, the Bradford assay for determination of protein concentration, hemagglutinating activity analysis and PAGE electrophoresis were used. After lentil extraction, lectin crude extract was purified by different purification steps including precipitation with ammonium sulfate and ultrafiltration. The highest results in terms of hemagglutinating activity and protein concentration were determined for fraction isolated after precipitation with ammonium sulfate (saturation 40-80%) and whose molecular weight exceeding 50 kDa. In addition, it was shown that isoelectric precipitation of contaminant proteins after precipitation and ultrafiltration enhanced both the agglutinating activity and the purity of the resulting lectin preparation.

ENVIRONMENTALLY BENIGN ASYMMETRIC MICHAEL ADDITION TO MALEIMIDES USING MECHANOCHEMICAL ACTIVATION

Kristóf András Kőszegi,[1,]* **György Szőllősi**[2]

[1]*Department of Molecular and Analytical Chemistry, Institute of Chemistry, Faculty of Science and Informatics, University of Szeged, Dóm tér 8, Szeged, 6720, Hungary.*
[2]*ELKH-SZTE Eötvös Loránd Research Network, Stereochemistry Research Group, Institute of Pharmaceutical Chemistry, Eötvös utca 6, , Szeged, 6720, Hungary.*
**Corresponding author: kristofkoszegi03@gmail.com*

Abstract

The preparation of chiral *N*-substituted succinimides is highly important since they are widely used intermediates in the pharmaceutical industry. Such compounds can be obtained by the Michael addition of nucleofiles to different maleimides. Since the environmental awareness is rising nowadays, there is a huge demand for sustainable synthetic methods that can be applied industrially. Carrying out reactions using efficient alternative activation is key to achieve environmentally friendly procedures. Asymmetric catalytic processes have been developed for Michael additions on maleimides using organocatalysts under batch conditions. Our aim was to carry out the implementation of mechanochemical activation in these reactions because of its huge benefits over the conventional methods, *i.e.* solvent-free conditions and significantly reduced reaction times. In the present study, we examined the impact of milling parameters through the test reaction of isobutyraldehyde and *N*-methylmaleimide. We set the goal to achieve similar conversion and enantioselectivity values as were obtained using thermal activation but without the addition of a solvent and under much less time. As a result of our studies, optimal conditions were determined to carry out the preparation of an *N*-substituted succinimide, which may be a significant step in the development of sustainable industrial synthetic methods of important pharmaceutical fine chemicals.

Introduction

The synthesis of optically pure compounds is crucial for the pharmaceutical industry to produce effective drugs. For that reason, asymmetric catalytic methods have a huge significance and are often used in the production of chiral building blocks [1]. Among these catalytic procedures, because of their environmental benefits, numerous organocatalytic methods have been developed. Asymmetric Michael additions of aldehydes to maleimides catalysed by bifunctional organocatalysts result in products containing quaternary or tertiary stereogenic carbons, which are valuable pharmaceutical intermediates [2]. Outstanding conversion and enantiomeric excess values can be reached using amino acids, their simple derivatives and oligopeptides as organocatalysts in these reactions [3-9]. Out of several examined amino acids, L-phenylalanine (L-Phe) was found to be the most advantageous because of its natural occurrence and provided both great conversion and enantioselectivity. These experiments were carried out in conventional batch reactors, using various solvents and needed long reaction times. However, numerous alternative activation methods can be applied, such as microwave or ultrasound assisted reactions or mechanochemical energy transmission, in order to decrease the necessary time and to increase the sustainability of the processes.

Mechanochemistry bears several advantages over the conventional thermal activation from which the significantly reduced reaction time and the solvent free conditions must be highlighted. It is considered to be a green chemical method; hence it implies great industrial relevance. In the last few decades mechanochemical activation was efficiently applied in performing various organic reactions [10,11]. In these methods the necessary activation energy is provided by the collisions and friction between the grinding media, the components and the wall of the mixing jar.

Although, a variety of asymmetric organic reactions, including stereoselective catalytic transformations, have been performed by milling [12-15], to our knowledge, enantioselective Michael additions to maleimides catalysed by simple bifunctional chiral organocatalysts, such as amino acids, have not yet been reported. Our aim was to examine the feasibility of asymmetric Michael addition reaction of an aldehyde to an *N*-substituted maleimide using mechanochemical activation. By screening the effect of different parameters, such as the number and size of the applied balls and the milling time and frequency, we hoped to reach the same conversion and enantiomeric excess values as under batch conditions but under environmentally friendly circumstances and significantly less time.

Experimental

The isobutyraldehyde (**1**), *N*-methylmaleimide (**2**), L-phenylalanine (L-Phe) and LiOH x H_2O were obtained from commercial sources and were used as received. The conventional magnetically stirred batch reactions were carried out in closed glass vials. After the given time the reactions were quenched by addition of 1 cm^3 aqueous NH_4Cl solution and the products were extracted with 3 x 2 cm^3 ethyl acetate (EtOAc). The combined organic phases were dried over Na_2SO_4 and analysed. Products were identified by mass spectrometry using a GC-MSD system. The conversion and enantiomeric excess (ee) were determined by gas-chromatography (GC-FID) using a chiral capillary column for the separation of the enantiomers.

The mechanochemical reactions were carried in 10 cm^3 ZrO_2 grinding jars with milling balls of 3, 5, 12 and 15 mm diameter made from the same material. In a typical run L-Phe, LiOH x H_2O were measured into to the jars, then the necessary number of balls were added, followed by introducing the given amount of **2** and **1**. The mixture was agitated in a Retsch Mixing Mill MM 400 instrument at the desired frequency for the desired time. When the reaction was completed, the products were dissolved in 3 x 2 cm^3 EtOAc, the combined solutions were washed with 1 cm^3 aqueous NH_4Cl solution, dried over Na_2SO_4 and analysed using the same methods as in case of batch reactions.

Results and discussion

As a test reaction we examined the addition of **1** to **2** resulting in the formation of the succinimide derivative 2-methyl-2-(1-methyl-2,5-dioxopyrrolidin-3-yl)propanal (**3**), using L-Phe as organocatalyst (Scheme 1.). In a similar addition it was found that the amino acid should be *in situ* transformed by reaction with a base in order to obtain high conversion and ee values. A previous study showed that with a β-amino acid the best results are obtained in the presence of LiOH [16].

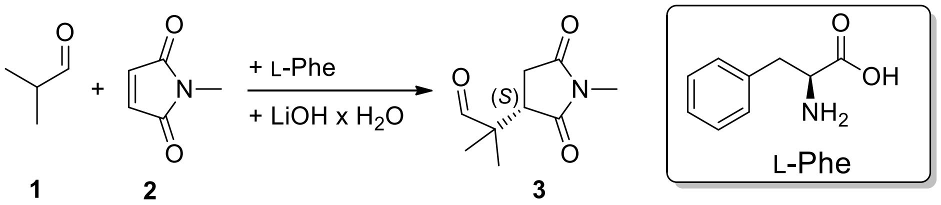

Scheme 1. Michael addition of isobutyraldehyde (**1**) to *N*-methylmaleimide (**2**) catalysed by L-Phe in presence of LiOH.

Our first experiments were carried out in a conventional magnetically stirred system. Two different solvents, CH_2Cl_2 and ethyl acetate (EtOAc) were used to screen the necessary reaction time under the conditions shown in Table 1. Although the ee values do not differ much, high conversions were achieved only in few hours in both solvents, moreover in the latter solvent 24 hours were needed to reach the desired full transformation of **2** (entry 4). Under solvent-free conditions in batch system, the ee was maintained at high level (96%) and in 30 minutes 63% conversion was reached (entry 5). In order to reduce time and have the environmental benefit of a solvent-free method, it was worth trying to examine the test reaction using mechanochemical activation. By milling the reaction mixture for 30 minutes we have obtained over 90% conversion without loss in the enantioselectivity, *i.e.*, 96% (entry 6).

Table 1. Asymmetric Michael addition of isobutyraldehyde (**1**) to *N*-methylmaleimide (**2**) catalysed by L-Phe in batch system.[a]

Entry	Solvent; amount (cm^3)	Time (h)	Conv. (%)[b]	ee (%)[b]
1	CH_2Cl_2; 1	6	77	98
2	CH_2Cl_2; 0.2	0.5	14	97
3	EtOAc; 1	4	40	96
4	EtOAc; 1	24	>99	97
5	–	0.5	63	96
6[c]	–	0.5	92	96

[a] *Reaction conditions*: L-Phe 0.03 mmol; LiOH x H_2O 0.033 mmol, **2** 0.3 mmol, **1** 1.2 mmol.

[b] Conversion (Conv.) and enantiomeric excess (ee) determined by gas-chromatography (GC-FID), *S* enantiomer in excess.

[c] Mechanochemically activated reaction using 25 pieces of Ø 5 mm ZrO_2 grinding balls and 12 Hz milling frequency.

According to the above presented results, the mechanochemical realization of this asymmetric Michael addition is more efficient than the magnetically stirred reaction. Thus, in our further studies we attempted to improve the results of the reaction carried out in the ball-mill by examining the effect of some milling parameters. In the first step, we examined the influence of the applied number of balls on the conversion and ee (Figure 1. **a**). For these measurements we used grinding jars with walls made from ZrO_2 and grinding balls of the same material. We carried out the reactions using balls with the diameter of 5 mm. It was found that the conversion of **2** increased only slightly with the higher amount of grinding media starting from 91% with only 5 pieces (pcs) up to 95% with 35 pcs. However, the enantiomeric excess values reached a maximum of 96% by using 15 pcs. One can see that at high conversions obtained in our experiments the growing grinding surface that ensures the energy transfer has limited effect on the transformation of the maleimide, thus in our further experiments we have applied 15 pcs of balls, which afforded the best ee.

The next step was to examine the effect of the diameter of the applied balls (Figure 1. **b**.). We chose the number of grinding balls as to have similar overall volumes, *i.e.*: 70 pcs of Ø 3 mm, 15 pcs of Ø 5 mm, 1 pc of Ø 12 mm and 1 pc of Ø 15 mm balls. The stereoselectivity was found to be the same (96% ee) regardless of the size of the balls and the milling time. The conversion however differed with the diameter. We set two different milling times for each ball size under otherwise identical conditions and found interesting results (Figure 1. **b**).

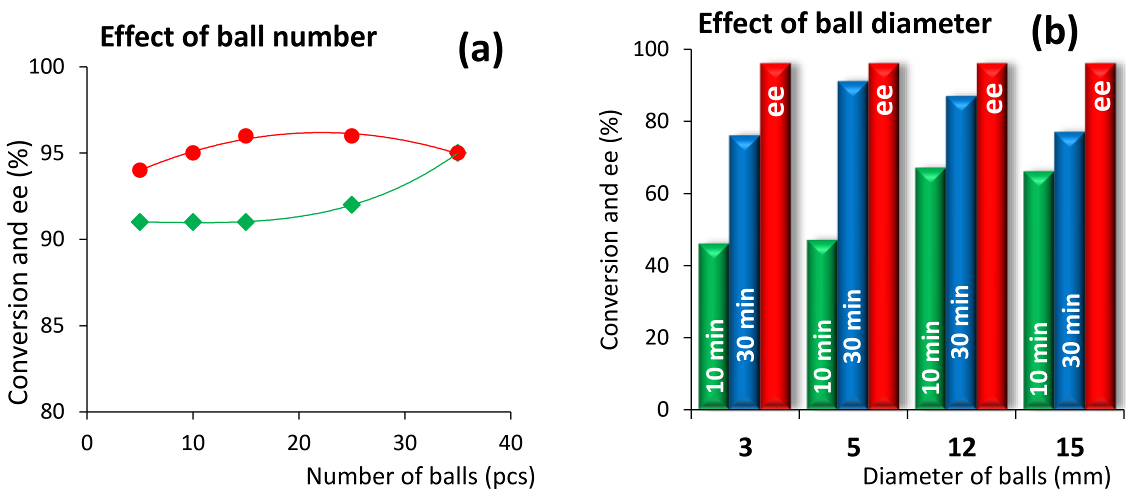

Figure 1. Effect of the number of Ø 5 mm balls on the conversion (◆) and ee (●) (**a**), and effect of the balls diameter on the conversion (green and blue bars) and ee (red bars) (**b**) in the mechanochemical Michael addition of **1** to **2**. *Reaction conditions*: L-Phe 0.03 mmol, LiOH x H_2O 0.033 mmol, **1** 1.2 mmol, **2** 0.3 mmol, 12 Hz, 30 min (10 min green bars).

In the 10 minutes reactions, the conversions were the highest with the Ø 12 mm (67%) and Ø 15 mm balls (66%). However, after 30 minutes milling, the Ø 5 mm balls were found to be the most effective, reaching a conversion of 91%. From these results it may be concluded that by shorter milling the decisive factor was the energy of the collisions, thus, the heavier balls performed better. When longer milling was applied, the effect of the increased number of collisions, *i.e.*, the increased number of the balls became more significant, except in case of Ø 3 mm, which although ensured the highest collision number, due to their low energy were less efficient compared to the Ø 5 mm balls.

After studying the impact of the balls on the conversion and ee, we have also examined the effect of the milling time (Figure 2. **a**).

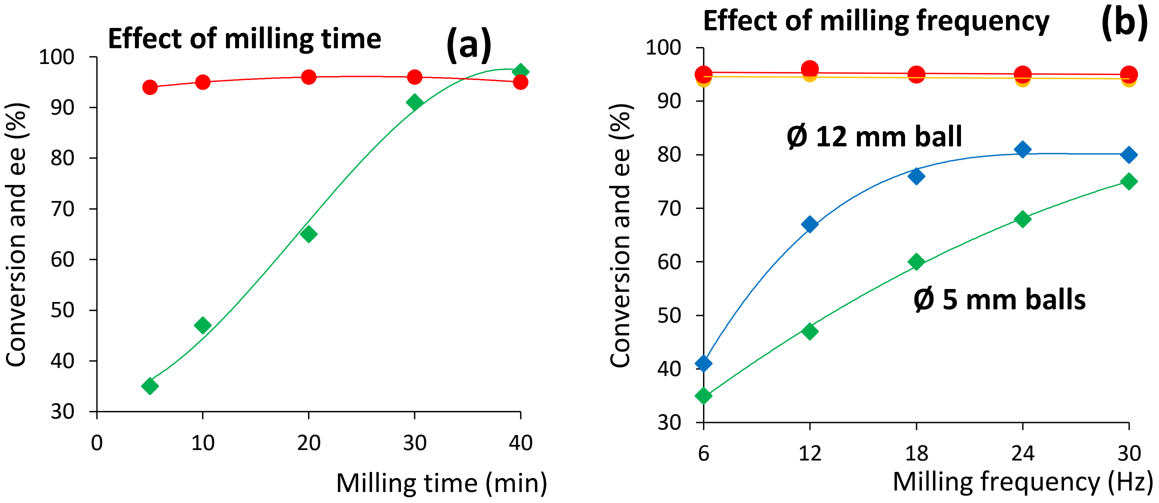

Figure 2. Effect of the milling time (**a**) and milling frequency (**b**) on the conversion (◆, ◆) and ee (●, ●) using 15 pieces of Ø 5 mm balls (◆, ●) or one Ø 12 mm ball (◆, ●). *Reaction conditions*: L-Phe 0.03 mmol, LiOH x H_2O 0.033 mmol, **1** 1.2 mmol, **2** 0.3 mmol, 12 Hz (**a**), 10 min (**b**).

From these measurements, it could be seen that with a reaction time of 40 minutes a conversion of 97% and an ee of 96% could be reached, the latter did not change significantly regardless of the milling time. Furthermore, we examined the influence of the milling frequency (Figure 2. **b**). We used 10 minutes reaction times in order to detect the influence of this parameter. The Ø 12 mm balls provided greater conversions than the Ø 5 mm balls at the same frequency however the shape of the curves was different, and at higher agitation speed the conversion obtained with the latter approaches the value reached with the former. The applied milling frequency did not have an impact on the stereoselectivity, the ee was maintained at 95%.

Conclusion

In summary, we have developed a sustainable method to carry out the asymmetric Michael addition of an aldehyde to an *N*-substituted maleimide by using mechanochemical activation. Compared to the conventional batch systems, we managed to achieve full conversion of the tested maleimide and high enantioselectivity in significantly less time and solvent-free conditions. The use of a natural organocatalyst also adds to the environmentally friendly character of the procedure. In this study the impact of the milling parameters on the reaction results was demonstrated. Based on these, the optimal conditions may be concluded under which the addition of different aldehydes to various *N*-substituted maleimides can be carried out. Our study is a significant step to develop in the future a sustainable method for the environmentally benign preparation of chiral succinimides.

Acknowledgements

This research was supported by the Hungarian National Science Foundation through OTKA Grant K 138871.

References

[1] T. Akiyama, I. Ojima (Eds.), Catalytic Asymmetric Synthesis, John Wiley & Sons, Hoboken, New Jersey, 2022.
[2] P. Chauhan, J. Kaur, S.S. Chimni, Chem. Asian J. 8 (2013) 328.
[3] T. C. Nugent, A. Sadiq, A. Bibi, T. Heine, L. L. Zeonjuk, N. Vankova, B. S. Bassil, Chem. Eur. J. 18 (2012) 4088.
[4] C. G. Kokotos, Org. Lett. 15 (2013) 2406.
[5] A. Schiza, N. Spiliopoulou, A. Shahu, C. G. Kokotos, New J. Chem. 42 (2018) 18844.
[6] A. Sadiq, T. C. Nugent, ChemistrySelect 5 (2020) 11934.
[7] S. Ahmad, M. H. Mahnashi, B. A. Alyami, Y. S. Alqahtani, F. Ullah, M. Ayaz, M. Tariq, A. Sadiq, U. Rashid, Drug Des. Dev. Ther. 15 (2021) 1299.
[8] C. E. Grünenfelder, J. K. Kisunzu, H. Wennemers, Angew. Chem. Int. Ed. 55 (2016) 8571.
[9] C. G. Avila-Ortiz, L. Díaz-Corona, E. Jiménez-González, E. Juaristi, Molecules 22 (2017) 1328.
[10] D. Margetić, V. Štrukil, Mechanochemical Organic Synthesis, Elsevier, Amsterdam, 2016.
[11] V. J. Kolcsár, Gy. Szőllősi, Molecules 27 (2022) 5671.
[12] C. G. Avila-Ortiz, M. Pérez-Venegas, J. Vargas-Caporali, E. Juaristi, Tetrahedron Lett. 60 (2019) 1749.
[13] I. N. Egorov, S. Santra, D. S. Kopchuk, I. S. Kovalev, G. V. Zyryanov, A. Majee, B. C. Ranu, V. L. Rusinov, O. N. Chupakhin, Green Chem. 22 (2020) 302.
[14] V. J. Kolcsár, Gy. Szőllősi, ChemCatChem 14 (2022) e202101501.
[15] V. J. Kolcsár, Gy. Szőllősi, Molecules 27 (2022) 5671.
[16] V. Kozma, Zs. Szakonyi, Gy. Szőllősi, Catalysts 12 (2022) 992.

RETENTION BEHAVIOR OF NOVEL *O*-ALKYLATED ANDROSTANE 3-OXIMES IN RP(C18)-UHPLC SYSTEM WITH METHANOL/WATER MOBILE PHASE

Strahinja Kovačević[1], Milica Karadžić Banjac[1], Jasmina Anojčić[2], Jovana Ajduković[2], Sanja Podunavac-Kuzmanović[1]

[1]University of Novi Sad, Faculty of Technology Novi Sad, Bulevar cara Lazara 1, 21000 Novi Sad, Serbia
[2]University of Novi Sad, Faculty of Sciences, Trg Dositeja Obradovića 3, 21000 Novi Sad, Serbia
e-mail: strahko@uns.ac.rs

Abstract

The retention behavior of newly synthesized *O*-alkylated androstane 3-oximes has been investigated applying reversed-phase ultra-high performance liquid chromatography (RP-UHPLC) with octadecyl stationary phase and methanol/water mobile phase. The set of the analyzed compounds takes into account two groups of steroidal derivatives: 17α-(pyridin-2-yl)methyl and (17*E*)-(pyridin-2-yl)methylidene derivatives. The retention behavior of the compounds in the applied chromatographic system was determined as logarithm of the capacity factor (*logk*). Afterwards, the *logk* values were correlated with *in silico* lipophilicity (logP) in order to establish the quantitative structure-retention relationship (QSRR) model and to confirm that the obtained retention parameters can be considered chromatographic (anisotropic) lipophilicity parameters. The obtained QSRR model successfully correlates the *logk* and logP parameters (the strong correlation has been determined). Considering the lipophilicity parameters, the analyzed compounds can be considered from moderately to highly lipophilic.

Introduction

Generally, steroid compounds are considered to be an excellent basis for development of new anticancer and anti-inflammatory drugs. Androstane derivatives are biologically active compounds whose biological role can be different depending on substituents present in their structure. The novel series of alkylaminoethyl derivatives of androstane 3-oximes possess significant anticancer activity towards various types of cancer (malignant melanoma - G-361, lung adenocarcinoma - A549 and colon adenocarcinoma - HT-29) [1]. Considering their biological potential, the characterization of physicochemical properties of these compounds, particularly the estimation of their lipophilicity, is of a great importance. Also, the set of these compounds was the subject of quantitative structure-activity relationship (QSAR) analysis and molecular docking and molecular dynamics studies that contributed to the better understanding of their anticancer potential [2].

Chromatography is one of the most used analytical techniques in estimation of anisotropic lipophilicity of biologically active molecules. The most applied techniques used for this purpose are high performance liquid chromatography (HPLC) and thin-layer chromatography (TLC). The retention parameters determined by HPLC and TLC are a good basis for the QSRR analysis in which their correlations with different molecular descriptors are investigated. Experimental determination of the chromatographic lipophilicity by RP-HPLC of the series of *O*-alkylated androstane 3-oximes provides the data about their retention behavior and reveals the retention mechanisms in the applied chromatographic system. The chromatographic system with C18 stationary phase and methanol/water mobile phase is the most common system for determination of the chromatographic lipophilicity.

Lipophilicity is one of the most important molecular features of biologically active compounds. It determines the pharmacokinetic/pharmacodynamic properties and absorption, distribution, metabolism and excretion (ADME). Besides, it plays a significant role in toxic behavior of compounds.

Experimental

The general structures of the analyzed compounds are presented in Fig. 1. The series is divided into two groups of compounds: (1) the group I contains nine 17β-hydroxy-17α-(pyridin-2-yl)methylandrost-4-en-(3*E*,*Z*)-one oximes (compounds **1-9**); (2) the group II contains nine (17*E*,*Z*)-(pyridin-2-yl)methylideneandrost-4-en-(3*E*)-one oximes (compounds **10-18**). Prior to the RP-UHPLC analysis, the compounds were dissolved in methanol (0.5 mg/ml).

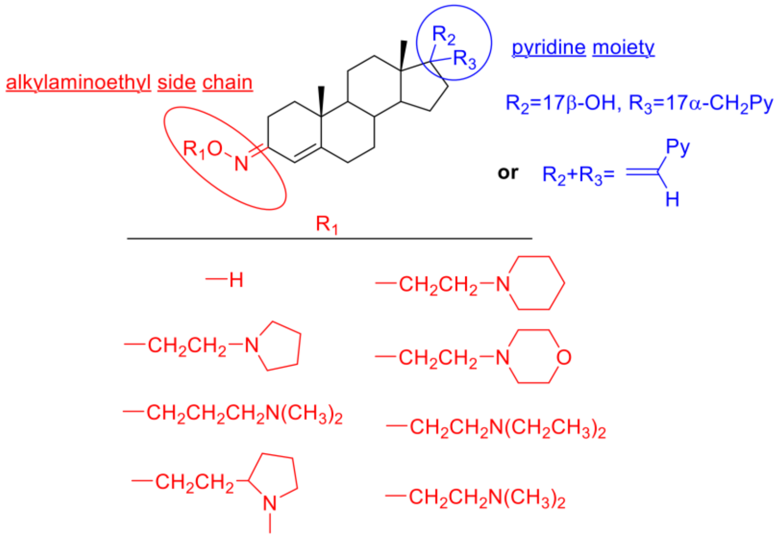

Figure 1. The general molecular structures of the analyzed *O*-alkylated androstane 3-oximes in 17α-(pyridin-2-yl)methyl and (17*E*)-(pyridin-2-yl)methylidene series

The chromatographic analysis was performed on UHPLC Agilent 1290 Infinity LC System with Diode Array Detector under isocratic conditions, by using the column ZORBAX Eclipse C18, 95Å, 2.1 × 50 mm, 1.8 µm (1200 bar pressure limit, LC Platform, Low Dispersion UHPLC) at 25 °C. The flow was set at 0.2 ml/min and the injection volume was 10 µL and. The analysis was carried out by using methanol/water (90/10 v/v) mobile phase. The peaks were recorded at λ_1 = 210 nm. The capacity factor (*logk*) was calculated as follows:

$$logk = \log((t - t_m)/t_m) \qquad (1)$$

where t is the retention time of a compound and t_m is the dead time.

The *in silico* lipophilicity parameter (logP) was calculated by using ChemBioDraw 13.0 program.

Results and discussion

The obtained retention parameters indicate that (17*E*,*Z*)-(pyridin-2-yl)methylideneandrost-4-en-(3*E*)-one oximes (group I) have higher retention in the applied chromatographic system than 17β-hydroxy-17α-(pyridin-2-yl)methylandrost-4-en-(3*E*,*Z*)-one oximes (group II). The reason for that might be the fact that the group II possesses higher lipophilicity. In Fig. 4 there are two chromatograms of representative compounds from group I. The compounds **1** and **2** have the lowest retention since they do not possess highly non-polar substituents. The addition of more non-polar substituents induce the significant increase in the retention time, as it can be seen from Fig. 1. The compound **1** have relatively small retention time comparing to the compound **4** that possesses *N*,*N*-dimethylaminopropyl substituent. The compounds **15** and **17** have the highest retention and the highest lipophilicity.

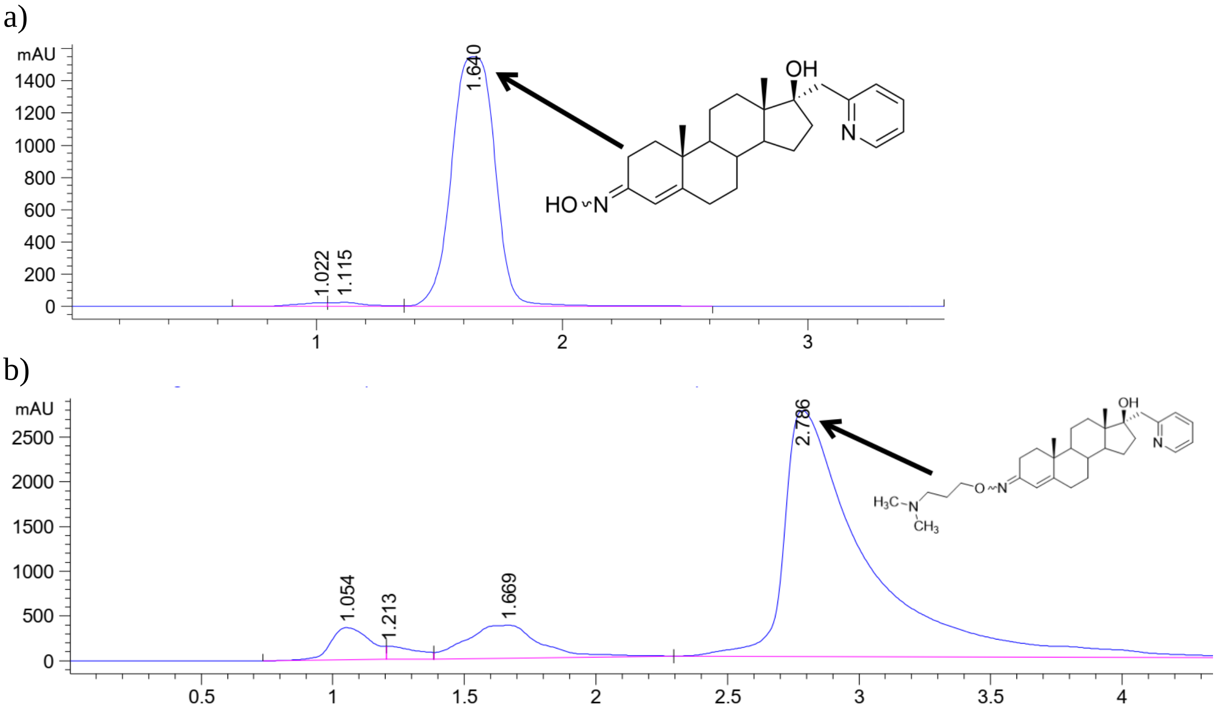

Figure 2. The representative chromatograms of a) the compound **1** (17β-Hydroxy-17α-(pyridin-2-yl)methylandrost-4-en-(3*E*)-one oxime and b) compound **4** (17β-Hydroxy-17α-(pyridin-2-yl)methylandrost-4-en-(3*E*)-one-*O*-[3-(*N*,*N*-dimethylamino)propyl] oxime)

The QSRR model that correlates *in silico* lip ophilicity parameters (logP) with capacity factor of the studied compounds is presented in Fig. 3.

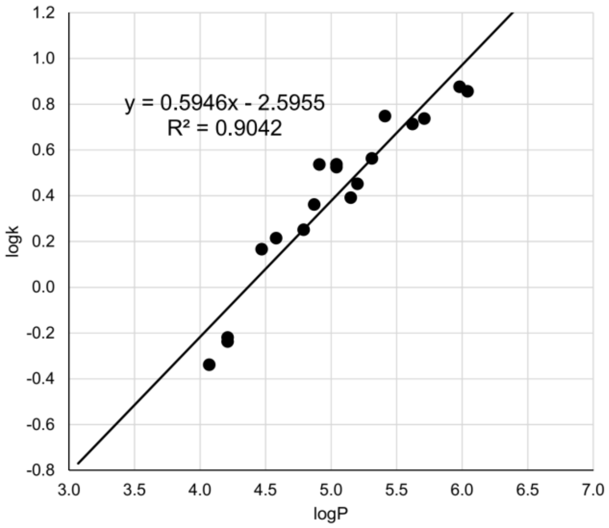

Figure 3. The relationship between the lipophilicity parameter (logP) and retention parameter (*logk*) determined in the applied chromatographic system

The obtained QSRR model indicate the strong linear relationship between logP and *logk* parameters. The determination coefficient is significantly high ($R^2 = 0.9042$) and no outlier has been detected in the set of the compounds. The obtained model implies that *logk* values, determined in the applied chromatographic system, can be considered the lipophilicity measures of the studies series of novel *O*-alkylated androstane 3-oximes.

Conclusion

The retention behavior of the analyzed series of newly synthesized *O*-alkylated androstane 3-oximes, determined in C18-UHPLC system with methanol/water mobile phase, is well correlated with *in silico* lipophilicity parameters. The experimental retention parameters, expressed as *logk* values, can be considered to be anisotropic lipophilicity of the studied androstane derivatives.

Acknowledgements

The present research is financed in the framework of the project of the Ministry of Science, Technological Development and Innovation (Project No. 451-03-47/2023-01/200134).

References

[1] J. J. Ajduković, D. S. Jakimov, L. Rárová, M. Strnad, Y. U. Dzichenka, S. Usanov, D: Đ. Škorić, S. S. Jovanović-Šanta, M. N. Sakač, RSC Adv. 11 (2021) 37449.

[2] S. Kovačević, M. Karadžić Banjac, S. Podunavac-Kuzmanović, J. Ajduković, B. Salaković, L. Rárová, M. Đorđević, M. Ivanov, J. Mol. Struct. 1283 (2023) 135272.

HAPPY MARRIAGE ACROSS THE EVOLUTION: CO-OPERATION OF METHANOGENIC ARCHEA AND ANAEROBIC FUNGI

Etelka Kovács[1], Csilla Szűcs[1], Zoltán Bagi[1, 2], Róbert Veprik[3], Gábor Rákhely[1, 2], Kornél L. Kovács[1]

[1]*Department of Biotechnology, Faculty of Science and Informatics, University of Szeged;*
[2]*Institute of Biophysics, Biological Research Centre, Eötvös Loránd Research Network;*
[3]*Szeged ZOO, Szeged, Hungary*
e-mail: kovacset@bio.u-szeged.hu

Abstract

Four anaerobic fungi (AF) strains, isolated from faeces of anoa, giraffe, bison and moose, were assessed for their ability to degrade lignocellulosic biomass. The effects on biogas production of anaerobic fungi from these animal species were determined in two step batch experiments. The hydrolysis process during the AF incubation led to an initial increase of biogas production, an accelerated degradation of dry matter and an increased concentration of volatile fatty acids. Thus, a separate hydrolytic pre-treatment phase with anaerobic fungi, represents a feasible strategy to improve biogas production from lignocellulosic substrates.

Introduction

Degradation of lignocellulose-rich material into biogas is an attractive strategy to face growing energy demands and moderate greenhouse gas emissions from the exploitation of fossil energy resources. Lignocellulosic residues (e.g. crop residues, green waste, mill waste) are highly frequent (1), they are easily accessible, cheap and do not require additional land to grow on in this way do not trigger "food or fuel" conflicts. This biomass is composed of interwoven cellulose and hemicellulose, coated by recalcitrant lignin (2). This is the explanation why bacteria and archaea in the biogas reactor are not efficient in disintegration of the lignin, leaving a considerable portion of the more easily convertible sugars untouched. Current strategies to release this carbon rely on expensive enzyme cocktails and physicochemical pre-treatment, producing inhibitory compounds that hinder subsequent microbial bioproduction. Microbial pre-treatment utilizing the fibre degrading potentials of aerobic fungi may be a much cheaper alternative but there are some drawbacks e.g. loss of carbohydrates by respiration and biomass build-up and the requirement of long pre-treatment periods (3). Anaerobic fungi (AF) from the phylum *Neocallimastigomycota* are natural inhabitants of the digestive tract of herbivorous animals (4), which decompose a big share of the ingested forage. The AF attach to the plant material and crack the fibres mechanically by growth and expansion of their rhizoids or bulbous holdfasts (5). In addition, AF possess cellulosomes which contain a multitude of lignocellulolytic enzymes. These fungi are an appealing solution as they hydrolyze crude, untreated biomass at ambient conditions into sugars that can be converted into value-added products by partner organisms.

Experimental

The objective of this study was the application of four newly isolated strains to the hydrolysis phase in order to improve hydrolysis of lignocellulosic biomass. The applied isolates were obtained from animals living on a high fibre diet, namely anoa (*Bubalus depressicornis*) (Fig.1.) and giraffe (*Giraffa camelopardalis rothschildi*), bison (*Bos bonasus*) and moose *(Alces alces)*. The effects on biogas production of anaerobic fungi from these animal species were assessed in two step batch experiments, comprised by a hydrolytic/acidogenic stage, followed by a methane production stage. Checking the enzyme activity in hydrolytic stage, beta-glucosidase activity was measured by p-nitrophenyl-β-D-glucopyranoside, for the endoglucanase concentration DNSA-method was used (3,5-dinitrosalicylic acid). The produced organic acids were measured by HPLC. Additionally, gas composition was analysed by GC during the methane production stage.

Figure 1. Anaerobic fungi on soluble carbon substrate from anoa fecal sample.

Results and discussion

In this study, treatment with anaerobic fungi cultures (14-day) increased the total biomethane yield during the experimental period of 20 days.

Methane yield from the same amount of organic total solids (oTS) of black locust and fresh wheatgrass with and without AF+M co-culture pre-treatment was presented in Figure 2. Black locust is a lignin-rich substrate that is difficult for biogas fermenter microbes to degrade. As a result of the AF+M pretreatment, the degradability of black locust increased in the case of the use of both isolates. When 3g of substrate were used, the amount of methane did not increase proportionally, which may indicate inhibition.

In the case of using fresh wheatgrass, the AF+M pretreatment significantly increased the degradability of the substrate both when 0.5g and 1g of substrate were used, no inhibition occured (Fig. 2.).

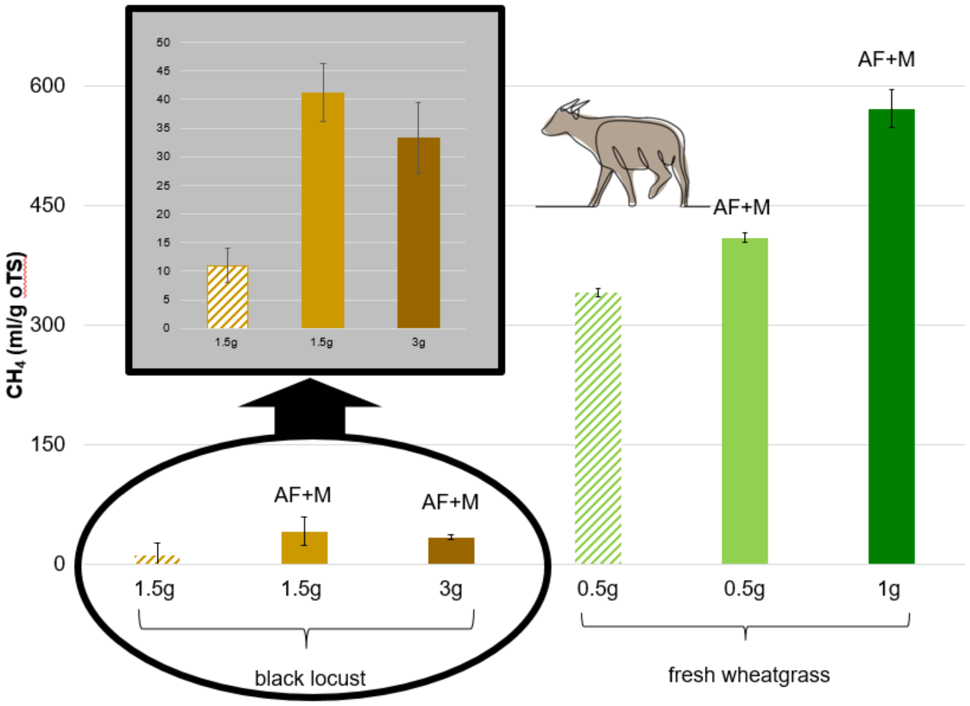

Figure 2. Biomethane yield after the anaerobic fungi pre-treatment using anoa isolate.

Pretreatment with anaerobic fungi significantly improved the degradability of substrates. The results for AF biomethane yields correlated well with the organic acid concentrations measured by HPLC (Fig.3.). From these it can be concluded that the anaerobic fungi degraded the substrate efficiently during the 14-day long treatment. As a result of the pre-treatment, acetic acid, lactic acid, glucose and cellobiose were produced in the highest amounts. These products could be used by methane-producing Archea producing methane during biogas fermentation. The efficiency of biogas fermentation was well characterized by the amount of biomethane produced as well as the concentrations of organic acid measured by HPLC (Fig.3.), which show that methanogens with otherwise slow metabolism were able to use the products of anaerobic fungi from the solution, so inhibition did not occur.

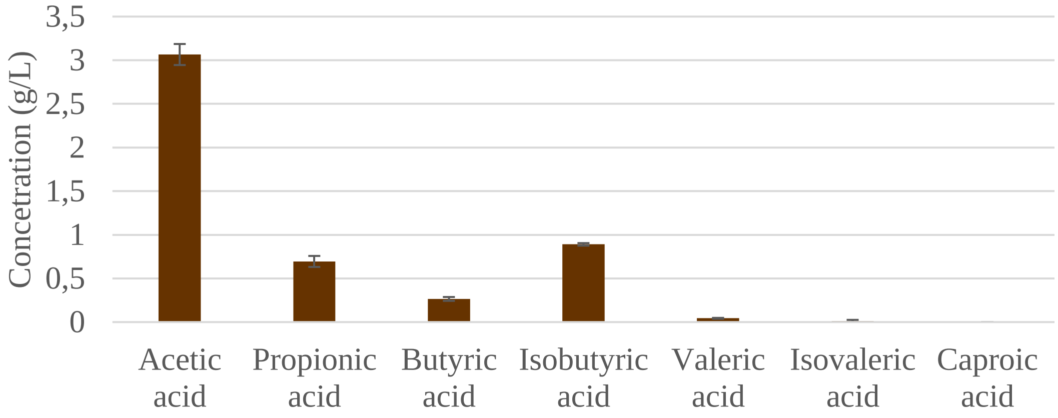

Figure 3. Organic acid concentration at the end of the biogas fermentation using anaerobic fungi from anoa.

Conclusion

Anaerobic fungi isolates from anoa, giraffe, bison and moose are excellent candidates for the conversion of agricultural waste products to biofuels. The four tested isolates efficiently pretreated the hard-to-degrade straw substrate to produce significant amounts of acetic acid, lactic acid, glucose, and cellobiose. The kinetics of the degradation were optimal for the slow metabolism of methanogenic microbes, which were thus able to efficiently utilize the aforementioned by-products and make biomethane from them.

Based on these results AF isolates were effective in enhancing cellulose degradation and successfully increased biogas production.

Acknowledgements

This study has been supported by Hungarian NKFIH fund NKFI-PD 128345. We kindly thank the ZOO in Szeged and Körösvölgyi Állatpark for providing the needed feces for the isolation. We thank Prof. Michael Theodorou for introducing us into the cultivation secrets of anaerobic fungi.

References

1 Williams, L., Gallagher, J., Bryant, D., Ravella, S.R. 2016. Anaerobic digestion and the use of pre-treatments on lignocellulosic feedstocks to improve biogas production and process economics. Advances in biofeedstocks and biofuels, Volume One: Biofeedstocks and their processing, pp. 121.

2 Rodriguez, C., A. Alaswad, K.Y. Benyounis, A.G. Olabi 2017. Pretreatment techniques used in biogas production from grass. Renew. Sust. Energy Rev., 68 (Part 2) (2017), pp. 1193-1204.

3 Isroi, M., Ria, Syamsiah, S., Niklasson, C., Cahyanto, M.N., Ludquist, K., Taherzadeh, M.J., 2011. Biological pretreatment of lignocelluloses with white-rot fungi and its applications: a review. BioResources 6(4), 5224-5259.

4 Liggenstoffer, A.S., Youssef, N.H., Couger, M.B., Elshahed, M.S. 2010.Phylogenetic diversity and community structure of anaerobic gut fungi (phylum Neocallimastigomycota) in ruminant and non-ruminant herbivores. ISME J., 4 (10) (2010), pp. 1225-1235

5 Akin, D.E., Borneman, W.S. 1990. Role of rumen fungi in fiber degradation. J. Dairy Sci., 73 (10) (1990), pp. 3023-3032

A SPECIES DEPENDENT STUDY OF THE EFFECT OF CuO NANOPARTICLE PRODUCED BY CHEMICAL AND GREEN SYNTHESIS ON MICROGREEN PLANTS

Andrea Rónavári[1*], Henrietta Kovács[2], Ágnes Szepesi[2], Péter Pálfi[2], Dalma Ménesi[2], Zoltán Kónya[1]

[1]Department of Applied and Environmental Chemistry, IC, University of Szeged, Szeged, HU-6720 Rerrich Béla tér 1, Hungary
[2]Department of Plant Biology, IB, University of Szeged, Szeged, HU-6726 Közép fasor 52, Hungary
**e-mail: henrietta.kovacs96@gmail.com*

Abstract

Global challenges such as population growth, increasing urbanisation, climate change, and limited access to important plant nutrients have all contributed to the development of nanotechnology as a new innovation and its application in agriculture. Nanoparticles can be synthesized through chemical, physical or biological synthesis methods. However, the applied approach can significantly affect their chemical properties, reactivity and biological activity [1]. In recent years, the use of green synthesis methods has received increasing attention due to their ease of characterization, lower toxicity and favorable production costs. In our work, we examined and compared the species-dependent effects of CuO nanoparticles produced by both chemical and green synthesis on three different microgreen plants. Seed-priming was used for seed treatment and the biomass, pigment, and protein contents of one-week-old plants were investigated.

Introduction

Nanotechnology in agriculture is a potential way to improve sustainable crop production. The use of nanoparticles in crop production is already known to increase germination rates, germination speed and growth. It has positive effects on chlorophyll content, increases cell elongation and enhances nutrient uptake [2]. Furthermore, the use of nanoparticles also plays a role in plant pathogen control, thereby reducing the use of chemical products and contributing to the further development of sustainable crop production [3]. Soilless and nanotechnology-based crop production, including the cultivation of microgreens, could be a revolutionary innovation in traditional farming, which is increasingly important due to the increasing population growth and the reduction of cultivable land with urbanisation [4]. Microgreens are young and immature plants that have been recently introduced as a new category of vegetables, adapting their production at the micro-scale. Microgreens are typically harvested between 10-14 days after their first leaves appeared. Their rapid growth and space-efficient nature make them especially appealing for modern agriculture [5].

The right amount of copper is essential for the proper functioning and development of plants. Copper (Cu) is involved in a number of morphological, physiological and biochemical processes and functions as a cofactor for many enzymes. It plays an essential role in respiration, photosynthesis and the electron transport chain. However, in excessive amounts, it negatively affects plant growth and productivity and has negative effects on mineral nutrition, chlorophyll biosynthesis and antioxidant enzyme activities [6].

Related to this, the subject of these work was to synthesize copper-oxide (CuO) nanoparticles, using chemical and green methods, and then to determine the resulting particles physical and chemical properties. As their effects on microgreen plants have not been well investigated so far, our aim was to characterize the concentration- and species-dependence of chemical and green synthesized NP effects on plants; therefore, experiments were carried out in three agriculturally important plant species, *Brassica rapa cymosa, Lepidium sativum and Eruca sativa*.

Experimental

NP synthesis and characterization

CuO nanoparticles were synthesized through a precipitation method. Initially, copper nitrate ($Cu(NO_3)2\cdot 3H_2O$) was dissolved in 100 mL of deionized water to achieve a 0.2 M concentration. Subsequently, 25% ammonia solution was added drop by drop under vigorous stirring until the pH reached 12. The resulting black precipitate was washed with deionized water until the pH reached 7. Following this, the washed precipitate was dried at 60°C overnight to remove any remaining solvent and then calcined at 450 °C for 2 hours. Finally, the obtained powder was ground and stored at room temperature for further use.

A similar procedure was employed for the green synthesis, with the exception that Virginia creeper (VC) extracts were used instead of ammonia solution. The leaf extracts were prepared by boiling the dry leaves in 100 mL of deionized water at 80 °C for 80 minutes. The extracts were then vacuum-filtered, and the filtrate served as both a reducing agent and a stabilizer for the as-synthesized CuO NPs. "Green" VC-CuO materials were synthesized by adding the plant extracts to the 0.2 M aqueous copper solution in a 1:1 volume ratio at room temperature, with continuous stirring for 24 hours.

Characterization of CuO NPs:

The morphological characteristics of CuO NPs were analyzed using transmission electron microscopy (TEM) with a FEI Tecnai G2 20× microscope at an acceleration voltage of 200 kV. To verify the crystal structure and phase of the nanoparticles, X-ray powder diffraction (XRD) was performed. The XRD scans were conducted with a Rigaku MiniFlex II powder diffractometer, utilizing Cu Kα radiation and a scanning rate of $2°\ min^{-1}$ within the $10°–80°\ 2\theta$ range.

Seed nano-priming

For the treatment of seeds with nanoparticles, seed nano-priming was used. To compare, a CuO NP’s prepared chemically and from wild grapes were used to prepare a stock solution at a concentration of 100 mg/l and then dilutions were performed. A nanoparticle suspension of 100 mg/l was prepared as a treatment solution at dilution levels of 10, 25, 50 and 75 mg/l. Seeds soaked in purified water were used as controls. The nano-priming time was 6 h for broccoli and 1 h for arugula and cress due to the hydrate coating on the seeds. After nano-priming, broccoli seeds were dried at room temperature for 24 hours and stored at 4°C until use.

Microgreen cultivation

Broccoli (*Brassica rapa cymosa*), cress *(Lepidium sativum)* and arugula *(Eruca sativa)* microgreen plants were grown on coconut fibre under hydroponic conditions. The plants were provided with a tomato nutrient solution containing: 1 M $Ca(NO_3)_2$; 1 M $MgSO_4 \times 7\ H_2O$; 0.1 M KH_2PO_4; 0.1 M KCl; 0.1 M $Na_2HPO_4 \times 2\ H2O$; 0.01 M Fe-EDTA and micro-elements. Microgreens were cultivated under a controllable lighting fixture, under LED light containing excess blue light for 7 days. The illumination treatment of all three microgreen species provided the same total photon flux density (TPFD) of 190.3 $\mu mol/m^2/s$.

Biomass measurement

In each tray, 20 seeds were planted on coconut fibre and then grown for 7 days. After harvesting the plants fresh weight of the tray-grown plants was measured.

Figure 1: Preparation and processing of plant samples

Determination of protein content by Bradford Protein Assay

Biochemical parameters and content values are determined as shown in the first figure (Figure 1). The shoot part of the plants is harvested at 7, 10 or 14 days of age, depending on the experiment, the plant sample is homogenized in buffer and absorbance is measured at the appropriate wavelength.

A 200 mg plant sample was homogenized in a pH 7, 50 mM mixed phosphate buffer (KH_2PO_4, Na_2HPO_4). The mixed plant sample was collected in an Eppendorf tube and centrifuged for 10 minutes at 4 °C and 12000 rpm. The supernatant (enzyme extract) of the centrifuged samples was pipetted into another Eppendorf tube. Using Bradford's method, the following reaction mixture was prepared: 900 µl of purified water, 5 µl of enzyme extract and 100 µl of Bradford's reagent. After mixing the samples, the optical density of the samples was determined at 595 nm.

Determination of pigment content

20 mg of plant sample was rubbed in 95% ethanol. The wetted plant samples were centrifuged for 10 min at 4 °C and 12 000 rpm. 200 µl of the supernatant was pipetted three times per sample into 96-well plates and the absorbance was measured at 664, 648, 470, 534, 643 and 661 nm. We measured the amount of chlorophyll a, chlorophyll b and total chlorophyll and determined the ratio of chlorophyll a to chlorophyll b.

Results and discussion

XRD measurements were used to determine the crystal structure and the chemical composition of the synthesized nanoparticles.. The characteristic peaks located at $2\theta = 32.53°$, $35.52°$, $38.87°$, $48.74°$, and $68.24°$ are assigned to (110), (002), (200) , (-202), and (220) plane orientation of monoclinic structure of CuO (JCPDS 892531). According to TEM images, the average size of this VC-CuO sample was around 30 nm, and polydispersity was observed as in case of the chemical sample.

The treatment with nanoparticles can increase the yield/biomass. For this reason, we conducted an investigation to determine whether two types of nanoparticle treatments resulted in differences in biomass mass between species. The results showed a significant difference in arugula after seed nano-priming treatment with CuO nanoparticle concentration of 10 mg/l. (Figure 2, 3).

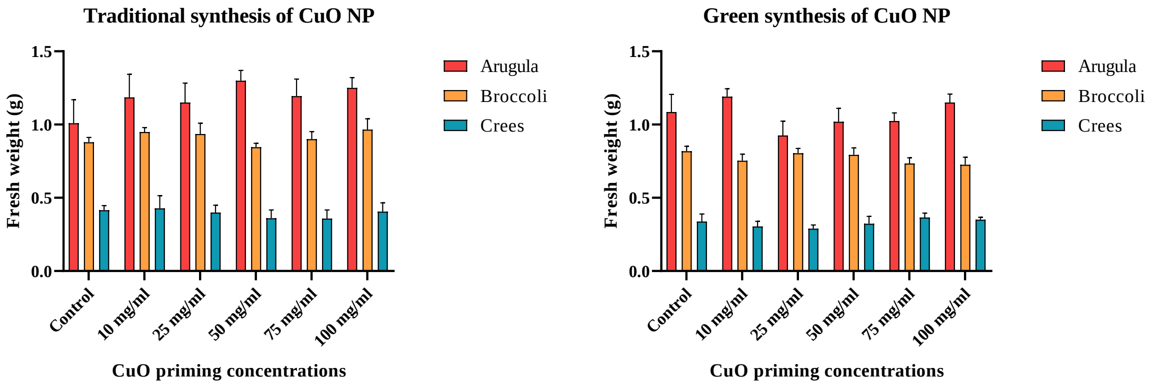

Figure 2: Changes in the biomass of three different plant species after differently synthesized nanoparticle treatments

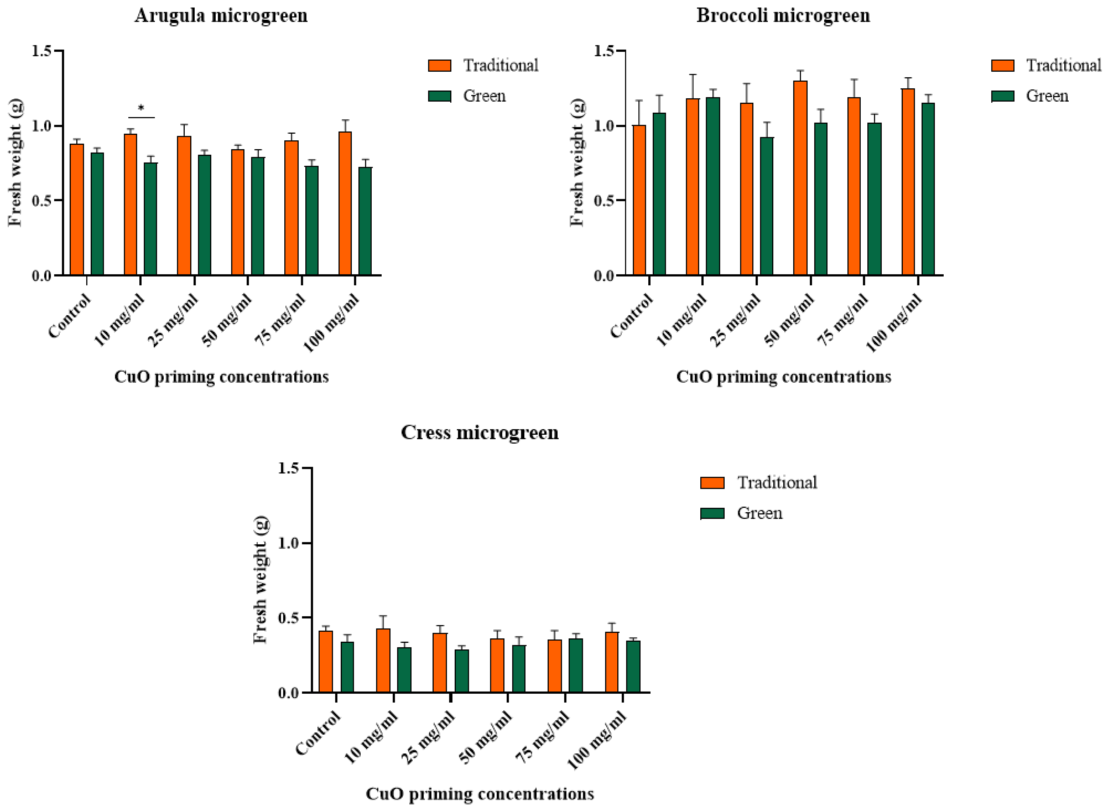

Figure 3: Effect of chemically and green synthesized CuO treatments on biomass by plant species

However, the biomass of the treated plants also showed us that the LED illumination with an excess of blue light had a positive effect on broccoli growth, while the cress did not grow well under the chosen illumination.

Conclusion

Based on the measurements, we successfully synthesized CuO nanoparticles with using plant waste extract of VC. The properties of the obtained nanoparticles were similar to the conventional chemically synthesized nanoparticles. Subsequently, the particles were introduced into microgreens to investigate the concentration- and species-dependent effects of both chemically and green-synthesized nanoparticles on these plants. Our observations revealed differences in the biomass of all three plant species. This finding provides a rationale reason for conducting further experiments to explore the impact of differently synthesized nanoparticles on other parameters, including vitamin C content, antioxidant enzymes activity and the nutritional values of these plants.

Aknowledgements

This work was supported by NRDI OTKA FK No.129061, PD 143320 and GINOP_Plusz-2.1.1-21-2022-00080 projects. This study was supported by the János Bolyai Research Scholarship of the Hungarian Academy of Sciences (Grant no. BO/00384/21/7) and by the New National Excellence Program of the Ministry of Human Capacities of Hungary (UNKP-23-5-SZTE-687).

References

[1] Rónavári, A., Kovács, D., Igaz, N., Vágvölgyi, C., Boros, I. M., Kónya, Z., ... & Kiricsi, M. (2017). Biological activity of green-synthesized silver nanoparticles depends on the applied natural extracts: a comprehensive study. International journal of nanomedicine, 871-883.

[2] Singh, R. P., Handa, R., & Manchanda, G. (2021). Nanoparticles in sustainable agriculture: An emerging opportunity. *Journal of Controlled Release*, *329*, 1234-1248.

[3] Worrall, E. A., Hamid, A., Mody, K. T., Mitter, N., & Pappu, H. R. (2018). Nanotechnology for plant disease management. *Agronomy*, *8*(12), 285.

[4] Maluin, F. N., Hussein, M. Z., Nik Ibrahim, N. N. L., Wayayok, A., & Hashim, N. (2021). Some emerging opportunities of nanotechnology development for soilless and microgreen farming. *Agronomy*, *11*(6), 1213.

[5] Teng J, Liao P, Wang M. The role of emerging micro-scale vegetables in human diet and health benefits—an updated review based on microgreens. *Food & Function*. Published online 2021. doi:10.1039/d0fo03299a

[6] Mir, A. R., Pichtel, J., & Hayat, S. (2021). Copper: uptake, toxicity and tolerance in plants and management of Cu-contaminated soil. *Biometals*, *34*(4), 737-759.

PRELIMINARY STUDIES ON ELECTROCHEMICAL BEHAVIOUR OF SULPHITE ON STAINLESS STEEL IN NEUTRAL MEDIA

Mihaela-Alexandra LĂBOȘEL[1], Nataliia RUDENKO[2], Mircea Laurențiu DAN[1], Nicolae VASZILCSIN[1]

[1]University Politehnica Timisoara, Faculty of Industrial Chemistry and Environmental Engineering, Laboratory of Electrochemistry, Corrosion and Electrochemical Engineering, 6 Pârvan, 300223 Timisoara, Romania
[2]University Politehnica Timisoara, Innovation and Technology Transfer Center
e-mail: mircea.dan@upt.ro

Abstract

SO_2 emissions are widely converted to sulphite through the flue gas desulphurization process, in which SO_2 is scrubbed and then chemically absorbed as sulphite (SO_3^{2-}) in alkaline solutions [1]. Furthermore, the oxidation of SO_3^{2-} ions can produce additional benefits, such as generation of an energy carrier like hydrogen [2]. Sulphite electrooxidation occurs in both acidic and alkaline media, according to the reaction (1) and (2), respectively [3]:

$$SO_3^{2-} + H_2O \rightarrow SO_4^{2-} + 2H^+ + 2e^- \quad (1)$$

$$SO_3^{2-} + 2HO^- \rightarrow SO_4^{2-} + H_2O + 2e^- \quad (2)$$

Several studies regarding the sulphite electrooxidation were performed using noble metals such as platinum [4] and gold [5] due to their good catalytic activity [6], but the high price of these materials is a major drawback for their widespread use, therefore the present paper targets low-cost electrodes such as AISI 420 and Incoloy 800.

In this paper, the anodic oxidation of the sulphite ions on AISI 420 and Incoloy 800 electrodes in neutral solution (1 mol L^{-1} Na_2SO_4) was studied to determine the relationship between the kinetic parameters and the sulphite concentration added in the electrolyte (10^{-3}, 10-2, 10-1, 0.5 and 1 mol L^{-1}). Due to their electrochemical stability in aqueous solutions, in acidic and neutral electrolytes, stainless steal electrodes can be a practical alternative as anode material. Also, their tendency to passivation can be an advantage both due to the high corrosion resistance and the catalytic effict on the anodic oxidation of sulphite [7].

Acknowledgements

This work was supported by University Politehnica Timisoara in the frame of PhD studies.

References

[1] Flagiello D., Erto A., Lancia A. and Di Natale F. (2018), Experimental and modelling analysis of seawater scrubbers for sulphur dioxide removal from flue-gas, Fuel, 214, 254–263.
[2] Han J., Cheng H., Zhang L., Fu H. and Chen J. (2018), Trash to treasure: Use flue gas SO2 to produce H2 via a photoelectrochemical process, Chemical Engineering Journal, 335, 231–235.
[3] Bouroushian M. (2010), Electrochemistry of Metal Chalcogenides, Springer-Verlag Berlin, Heidelberg Berlin.
[4] Skavas E., Hemmingsen T. (2007), Kinetics and mechanism of sulphite oxidation on a rotating platinum disc electrode in an alkaline solution, *Electrochimica Acta*, 52, 3510–3517.
[5] Zelinsky A.G., (2016) Features of Sulfite Oxidation on Gold Anode, *Electrochimica Acta*, 188, 727–733.

[6] Diaz-Abad S., Millan M., Rodrigo M.A. and Lobato J. (2019), Review of Anodic Catalysts for SO2 Depolarized Electrolysis for “Green Hydrogen” Production, *Catalysts*, 9, 63.
[7] MA Lăboșel, GD Dima, DA Duca, N Vaszilcsin, ML Dan, Anodic sulphite oxidation on lead electrode in a neutral environment, Materials Today: Proceedings, Volume 78, Part 2,2023, Pages 302-307.

EVALUATION OF SOLVENT AND SUBSTITUENT EFFECTS ON ABSORPTION SPECTRA OF SPIROHYDANTOINS DERIVED FROM *α*-TETRALONE

Anita Lazić[1], **Jelena Lađarević**[2], **Aleksandra Mašulović**[1], **Kristina Gak Simić**[1], **Luka Matović**[1], **Ivana Đorđević**[3], **Nemanja Trišović**[2]

[1]Innovation Center, Faculty of Technology and Metallurgy, University of Belgrade, Karnegijeva 4, Belgrade, Serbia
[2]Faculty of Technology and Metallurgy, University of Belgrade, Karnegijeva 4, Belgrade, Serbia
[3] Department of Chemistry, Institute of Chemistry, Technology and Metallurgy, National Institute, University of Belgrade, Njegoševa 12, Belgrade, Serbia
e-mail: alazic@tmf.bg.ac.rs

Abstract

A convenient and efficient approach toward the synthesis of six 3-(4-substituted benzyl)-6,7-benzo-1,3-diazaspiro[4.5]decane-2,4-diones (**1**–**6**) by Bucherer-Bergs reaction and further alkylation at position 3 of the hydantoin ring is reported. Further, their chemical structure was confirmed by melting points, elemental analysis, FT-IR, NMR and UV–Vis spectroscopic methods. To gain an insight into interactions which the investigated spirohydantoins establish with their environment, their absorption spectra were recorded in selected solvents of different polarity and the solvent effects on the UV-Vis absorption band positions, intensity and shape, were discussed. Substiuent effects on the solvatochromism of compounds **1**−**6** were analyzed using the Hammett's equation. Considering the broad applications of hydantoin derivatives, as well as the fact that their relative importance may increase in the future, results obtained in this study serve as a basis for further investigations.

Introduction

The hydantoin (imidazolidine-2,4-dione) ring is an important structural fragment of a large number of pharmacologically active compounds [1]. Derivatives of this five-membered cyclic ureide are known anticonvulsants (Dilantin, Cerebyx, Peganon), nonsteroidal antiandrogenic agents (Anandron), antibiotics (Furadantin), muscle relaxants (Dantrium) [2], antiarrhythmics (Azimilide), keratolytics (Alantoin), astringents and antacids [3]. By introducing substituents in N3 and C5 positions of this bioactive nucleus, various analogs with potential pharmacological application are obtained. Structure-activity relationship (SAR) analysis of 3-benzyloxy-5-alkylhydantoins revealed that substitution of benzene ring with chlorine and bromine atoms, as well as the presence of slightly longer lipophilic substituents such as isopropyl and isobutyl groups at C5 position, may be essential for its antiproliferative activity [4]. The antileukemic activity of 1-(3-bromopropyl)-3-methyl-5,5-diphenylimidazolidine-2,4-dione and 1-(3-bromobutyl)-3-methyl-5,5-diphenylimidazolidine-2,4-dione towards human acute histiocytic lymphoma U937 cells and human promyelocytic leukemia HL-60 cells is based on temporary changes in the leukemia cell viability, volume and count [5]. Antiviral activity of 5,5-diphenyl-3-[3-(4-phenyl-1H-1,2,3-triazol-1-yl)propyl]imidazolidin-2,4-dione is based on prevention of adsorption and penetration of human metapneumovirus into host cells [6]. *In vivo* studies have shown that *N*-arylsulfonyl derivatives of imidazolidin-2,4-dione represent new hypoglycemic agents because they effectively reduce blood glucose levels compared to the standard drug glipizide [7]. Potentially pharmacologically active compounds often bear numerous functional groups capable of forming hydrogen bonds, making them soluble and giving them the ability to form specific interactions with their biomolecular targets [8]. Hydrogen bonding influences the interactions of potentially pharmacologically active organic compounds at different levels of complexity, going from those with other small molecules, up to the highest supramolecular assemblies, *e.g.*, proteins and membranes. These interactions considerably affect the pharmacological activity, pharmacokinetics and physicochemical properties of drugs, hence making hydrogen bonding an important subject of study in drug discovery and development [9]. Therefore, solvatochromic study gives an insight into possible different solute–solvent interactions mimicking the interactions of potentially pharmacologically active organic compounds with their environment. In continuation of our long-term research on the influence of chemical structure on the potential pharmacological activity of imidazolidin-2,4-dione derivatives, six 3-(4-substituted benzyl)-6,7-benzo-1,3-diazaspiro[4.5]decane-2,4-diones were synthetized (Scheme 1). To gain insight into the ways in which those compounds interact with their environment, their absorption spectra were recorded in a selected set of solvents. The influence of substituents on the position of the absorption spectra was evaluated in detail using Hammett's equation.

Experimental

General procedure for the synthesis of compounds 1–6

The synthetic route was carried out according to Scheme 1. Starting from commercially available *α*-tetralone, the modified Bucherer-Bergs reaction was carried out by the use of ammonium carbonate and potassium cyanide to afford the 3',4'-dihydro-2H-spiro[imidazolidine-4,1'-naphthalene]-2,4-dione [10]. In the following step, alkylation at position 3 of the hydantoin ring was conducted with various *p*-substituted benzyl-chlorides in the presence of K_2CO_3 in *N*,*N*-dimethylformamide (DMF) [11]. Their chemical structure was confirmed by melting points, elemental analysis, FT-IR, NMR and UV–Vis spectroscopic methods.

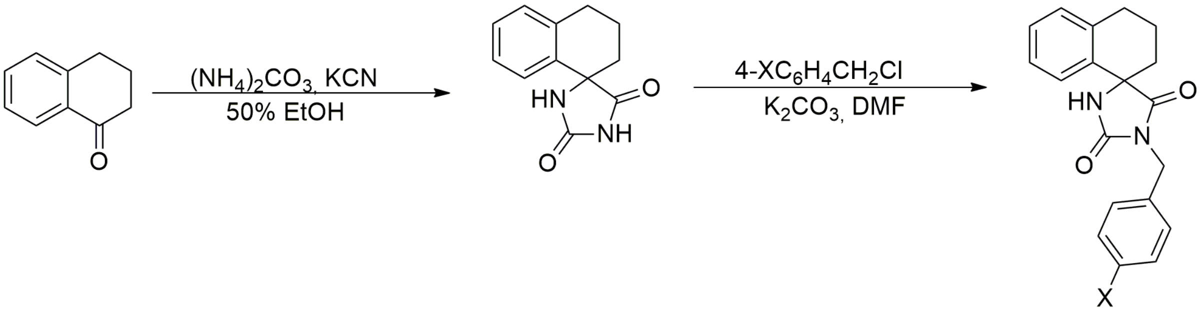

X = H (**1**), CH_3 (**2**), OCH_3 (**3**), Cl (**4**), CN (**5**), NO_2 (**6**)

Scheme 1. Synthetic pathway of the investigated compounds.

The melting points were measured on an Electrothermal melting point apparatus. The FT-IR spectra of the synthesized compounds were recorded in the range of 400 to 4000 cm^{-1} using Bomem MB spectrophotometer. Elemental analysis of the investigated compounds were carried out using microanalyzer Elemental Vario EL III. Absorption spectra were recorded on a Shimadzu 1700 spectrophotometer in solvents of spectroscopic purity (Fluka) at a fixed concentration of 10^{-5} mol dm^{-3}. ^1H NMR spectra were recorded on a Bruker Ascend 400 spectrophotometer at 400 MHz in deuterated dimethyl sulfoxide (DMSO-d_6).

3-(Benzyl)-6,7-benzo-1,3-diazaspiro[4.5]decane-2,4-dione (**1**): White crystalline substance; m.p. 126–129 °C; yield: 75 %; IR (KBr, ν/cm^{-1}): 3246, 2931, 1770, 1701; ^1H NMR (400 MHz, DMSO-d_6): δ = 8.88 (s, 1H, NH), 7.66 (t, 1H, J = 8 Hz, Ar(benzyl)-H), 7.33 (t, 2H, J = 8 Hz, Ar(benzyl)-H), 7.27 (d, 2H, J = 8 Hz, Ar(benzyl)-H), 7.25–7.22 (m, 1H, Ar(tetralin)-H), 7.19–

7.11 (m, 2H, Ar(tetralin)-H), 6.93 (d, 1H, J = 8 Hz, Ar(tetralin)-H), 4.57 (s, 2H; N–CH_2), 2.82−2.79 (m, 2H; CH_2), 2.10−2.04 (m, 2H; CH_2), 1.95−1.81 ppm (m, 2H; CH_2); Anal. Calcd. For $C_{19}H_{18}N_2O_2$: C, 74.49, H, 5.92, N, 9.14. Found: C, 74. 46, H, 5.95, N, 9.14.

3-(4-Methylbenzyl)-6,7-benzo-1,3-diazaspiro[4.5]decane-2,4-dione (**2**): White crystalline substance; m.p.153–156 °C; yield: 71 %; IR (KBr, ν/cm^{-1}): 3269, 2945, 2876, 1756, 1703, 1686; ^{1}H NMR (400 MHz, DMSO-d_6): δ = 8.89 (s, 1H, NH), 7.19 (m, 1H, Ar(tetralin)-H), 7.21–7.15 (m, 6H, Ar(tetralin)-H + Ar(benzyl)-H), 6.90 (d, 1H, J = 8.0 Hz, Ar(tetralin)-H), 4.56 (s, 2H, N–CH_2), 2.83−2.77 (m, 2H, CH_2), 2.45 (s, 3H, CH_3), 2.11−2.04 (m, 2H; CH_2), 1.99−1.85 ppm (m, 2H; CH_2); Anal. Calcd. For $C_{20}H_{20}N_2O_2$: C, 74.98, H, 6.29, N, 8.74. Found: C, 74. 96, H, 6.31, N, 8.74.

3-(4-Methoxybenzyl)-6,7-benzo-1,3-diazaspiro[4.5]decane-2,4-dione (**3**): White crystalline substance; m.p. 136–138 °C; yield: 56 %; IR (KBr, ν/cm^{-1}): 3249, 3025, 2951, 1770, 1698; ^{1}H NMR (400 MHz, DMSO-d_6): δ = 8.90 (s, 1H, NH), 7.24 (d, 2H, J = 8.4 Hz, Ar(benzyl)-H), 7.23 (m, 1H, Ar(tetralin)-H), 7.18–7.13 (m, 2H, Ar(tetralin)-H), 6.93 (d, 2H, J = 8.4 Hz, Ar(benzyl)- H), 6.90 (d, 1H, J = 8.0 Hz, Ar(tetralin)-H), 4.55 (s, 2H, N–CH_2), 3.75 (s, 3H, OCH_3), 2.81−2.78 (m, 2H, CH_2), 2.13−2.05 (m, 2H, CH_2), 1.95−1.81 ppm (m, 2H, CH_2) [12]; Anal. Calcd. For $C_{20}H_{20}N_2O_3$: C, 71.41, H, 5.99, N, 8.33. Found: C, 71. 36, H, 6.04, N, 8.30.

3-(4-Chlorobenzyl)-6,7-benzo-1,3-diazaspiro[4.5]decane-2,4-dione (**4**): White crystalline substance; m.p.130–133 °C; yield: 82 %; IR (KBr, ν/cm^{-1}): 3232, 3105, 2932, 1767, 1703; ^{1}H NMR (400 MHz, DMSO-d_6): δ = 8.91 (s, 1H, NH), 7.36 (d, 2H, J = 8.4 Hz, Ar(benzyl)-H), 7.31 (d, 2H, J = 8.4 Hz, Ar(benzyl)-H), 6.92–6.89 (m, 4H, Ar(tetralin)-H), 4.51 (s, 2H, N–CH_2), 2.89−2.86 (m, 2H, CH_2), 2.19−1.94 (m, 2H, CH_2), 1.92−1.85 ppm (m, 2H, CH_2); Anal. Calcd. For $C_{19}H_{17}ClN_2O_2$: C, 66.96, H, 5.03, N, 8.22. Found: C, 66. 94, H, 5.05, N, 8.22.

3-(4-Cyanobenzyl)-6,7-benzo-1,3-diazaspiro[4.5]decane-2,4-dione (**5**): White crystalline substance; m.p. 182–185 °C; yield: 83 %; IR (KBr, ν/cm^{-1}): 3365, 2935, 2865, 2225, 1774, 1708; ^{1}H NMR (400 MHz, DMSO-d_6): δ = 8.93 (s, 1H, NH), 7.55 (d, 2H, J = 8 Hz, Ar(benzyl)-H), 7.43 (d, 2H, J = 8 Hz, Ar(benzyl)-H), 7.20–7.15 (m, 3H, Ar(tetralin)-H), 6.88–6.84 (m, 1H, Ar(tetralin)-H), 4.52 (s, 2H, N–CH_2), 2.79−2.75 (m, 2H, CH_2), 2.12−2.04 (m, 2H, CH_2), 1.90−1.85 ppm (m, 2H, CH_2); Anal. Calcd. For $C_{20}H_{17}ClN_3O_2$: C, 72.49, H, 5.17, N, 12.68. Found: C, 72. 51, H, 5.14, N, 12.68.

3-(4-Nitrobenzyl)-6,7-benzo-1,3-diazaspiro[4.5]decane-2,4-dione (**6**): Yellow crystalline substance: m.p. 170–173 °C; yield: 88 %; IR (KBr, ν/cm^{-1}): 3204, 3097, 2933, 2840, 1770, 1708; ^{1}H NMR (400 MHz, DMSO-d_6): δ = 8.94 (s, 1H, NH), 8.11 (d, 2H, J = 8 Hz, Ar(benzyl)-H), 7.92 (d, 2H, J = 8.4 Hz, Ar(benzyl)-H), 7.22–7.05 (m, 4H, Ar(tetralin)-H), 4.55 (s, 2H, N–CH_2), 2.79−2.75 (m, 2H, CH_2), 2.12−2.04 (m, 2H, CH_2), 1.95−1.90 ppm (m, 2H, CH_2); Anal. Calcd. For $C_{19}H_{17}ClN_3O_4$: C, 64.95, H, 4.88, N, 11.96. Found: C, 64. 94, H, 4.89, N, 11.96.

Results and discussion

Solvatochromic analysis

Solvatochromic properties of six synthesized compounds were investigated by recording the corresponding UV-Vis absorption spectra in a selected set of solvents of different polarity in the wavelength range 200−400 nm. The values of the wavelengths originating from the higher energy absorption maxima are shown in Table 1, and a representative spectra recorded in ethanol are presented in Figure 1. The observed trends in the change in the intensity of the absorption maximum are in accordance with our previous results [13]. Namely, the absorption spectra of all investigated compounds are characterized by the presence of one dominant band originating from the $\pi\rightarrow\pi^*$ transition and corresponding to the absorption maximum of higher lower energy. Figure 1 shows that the introduction of a substituent in the *p*-position of the phenyl ring results in a bathochromic shift of the absorption maximum in relation to the unsubstituted compound (**1**) in all solvents. In general, with increasing electron-donor as well as electron-acceptor characteristics of the substituent, there is a shift of the absorption maximum towards higher wavelengths. Based on the described trends, it can be concluded that electron-donor groups exert a significant influence on the shift of the electron density from the *p*-substituted benzyl group to the hydantoin ring, contributing to the bathochromic shift [14]. The effect of electron-accepting substituents on the shift of the electron density in the studied molecules is opposite, and also results in positive solvatochromism compared to the unsubstituted compound **1**.

Table 1. The absorption spectra of compounds (**1**–**6**) in a selected set of solvents.

	λ_{max} (nm)					
Solvent/ Compound	**1**	**2**	**3**	**4**	**5**	**6**
Methanol	207	214	222	216	231	269
Ethanol	212	215	225	218	232	270
1-Propanol	216	218	229	221	230	272
1-Butanol	215	216	228	219	234	273
Acetonitrile	210	216	220	215	232	274
Dietyl eter	214	215	228	218	233	273
Cyclohexane	215	216	219	219	235	272

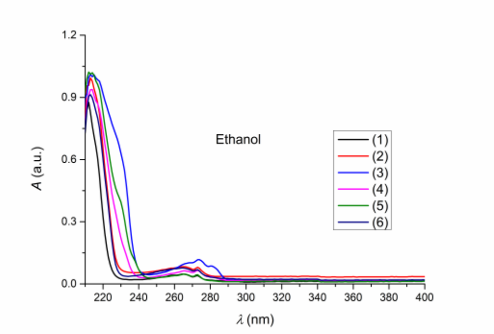

Figure 1. The absorption spectra of compounds (**1**–**6**) in ethanol.

The position of the absorption maxima are more affected by the substitution pattern than the polarity of solvent.The dominant influence of substituents on the shape, intensity and position of the electronic spectra of compounds **1**–**6** was analyzed using linear free energy correlation. The obtained results are represented by the diagram $\nu_{max} = f(\sigma_p)$ (Figure 2), as well as by the corresponding equations, especially for electron-donor (equation 1) and electron-acceptor (equation 2) substituents:

$\nu_{max} = 47.42(\pm0.82) + 9.431(\pm0.48)\sigma_p$ ($R = 0.905$; $s = 0.854$; $F = 4$; $n = 3$) (1)

$\nu_{max} = 47.91(\pm2.03) - 11.048(\pm3.08)\sigma_p$ ($R = 0.895$; $s = 2.45$; $F = 8$; $n = 3$) (2)

The obtained nonlinear dependence is an indicator of the different effect of substituents on the shift of the electron density in the analyzed series of compounds, where the electron-acceptor effect is significantly stronger compared to the electron-donor effect ($\rho_A = -11.048$; $\rho_D = 9.431$).

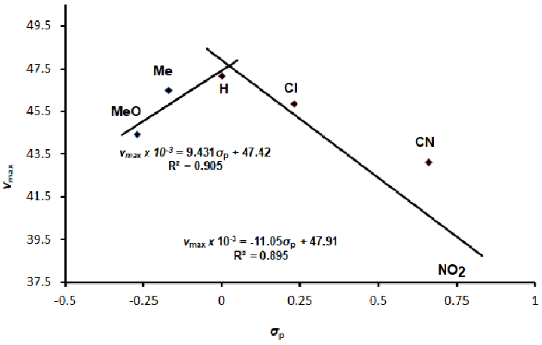

Figure 2. The correlation of ν_{max} and σ_p for compounds **1**–**6** in a selected set of solvents

Conclusion

In this study, we synthetized six 3-(4-substituted benzyl)-6,7-benzo-1,3-diazaspiro[4.5]decane-2,4-diones and confirmed their chemical structure by melting points, elemental analysis, FT-IR, NMR and UV–Vis spectroscopic methods. Substiuent effects on the solvatochromism of compounds **1**−**6** was analyzed using the Hammett's equation. The obtained nonlinear dependence showed that the electron-acceptor effect is significantly stronger compared to the electron-donor effect ($\rho_A = -11.048$; $\rho_D = 9.431$). Considering obtained results, we can conclude that, the investigated spirohydantoins represent interesting starting point for the preparation of new pharmacologically active compounds and better understanding of the structure-activity relationship.

Acknowledgements

This work was supported by the Ministry of Science, Technological Development and Innovation of the Republic of Serbia (Contracts No. 451-03-47/2023-01/200135, 451-03-47/2023-01/200287 and 451-03-47/2023-01/-200026).

References

[1] J.L. Monteiro, B. Pieber, A.G. Corrêa, C.O. Kappe, Synlett. 27 (2016) 83.
[2] L. Konnert, F. Lamaty, J. Martinez, E. Colacino, Chem. Rev. 17 (2017) 13757.
[3] A. Czopek, A. Zagórska, M. Kołaczkowski, A. Bucki, B. Gryzło, J. Rychtyk, M. Pawłowski, A. Siwek, G. Satała, A. Bojarski, M. Kubacka, B. Filipek, Acta Pol. Pharm.-Drug Res. 73 (2016) 1545.
[4] A.A. Mostafa, A.N. Al-Rahmah, R.S. Kumar, A. Manilal, A. Idhayadhulla, Int. J. Pharmacol. 12 (2016) 290.
[5] K. Śladowska, J. Handzlik, K. Kieć-Kononowicz, L. Mazur, Indian J. Exp. Biol. 54 (2016) 553.
[6] G. Mendes, G.H. Aspesi, A.L.A. Arruda, M.T.V. Romanos, C.K.Z. Andrade, J. Braz. Chem. Soc. 27 (2016) 2.
[7] A. Hussain, M.K. Kashif, M.M. Naseer, U.A. Rana, S. Hameed, Res. Chem. Intermed. 41 (2015) 7313.
[8] B. Kuhn, P. Mohr, M. Stahl, J. Med. Chem. 53 (2010) 2601.
[9] G.M. Ghiandoni, E. Caldeweyher, Sci. Rep. 13 (2023) 4143.
[10] E. Naydenova, N. Pencheva, J. Popova, N. Stoyanov, M. Lazarova, B. Aleksiev, Farmaco 57 (2002) 189.
[11] H. Suzuki, M.B.B. Kneller, D.A. Rock, J.P. Jones, W.F. Trager, A.E. Rettie, Arch. Biochem. Biophys. 429 (2004) 1.
[12] A.M. Lazić, I.S. Đorđević, L.D. Radovanović, D.M. Popović, J.R. Rogan, G.V. Janjić, N.P. Trišović, ChemPlusChem 85 (2020) 1220.
[13] N.Trišović, N. Valentić G. Ušćumlić, Chem. Cent. J. 5 (2011) 1.
[14] D.C. Lavanya, K. Yesudas, N.S. Makarov, R.V. Jayathirtha, K. Bhanuprakash, J.W. Perry, J. Mater. Chem. C 3 (2015) 3730.

DETERMINATION OF THE POSITION OF A DOPANT BY DFT ANALYSIS; SOLID-STATE SYNTHESES OF $Zn_3Nb_2O_8$ DOPED WITH Eu^{3+}

Liviu Mocanu, **Mihaela Birdeanu**

National Institute for Research and Development in Electrochemistry and Condensed Matter,
Timisoara, PlautiusAndronescu Str. No. 1, RO-300224, Timisoara, Romania
e-mail: mocanuliv@gmail.com

Abstract

The present paper aims to provide an objective criterion for establishing the position of a dopant (Eu^{3+}) in a given crystalline matrix ($Zn_3Nb_2O_8$). Following the analysis of the general conditions, regarding the size of the doping ion correlated with the reticular distances and / or the size of the coordination polyhedra, it remains to be established the concrete place that it will occupy, substitutional or interstitial. The criterion is based on the principle of minimum energy of the system, as a condition of existence of doped structure, which is why the method is applicable for a large variety of crystalline materials.

Introduction

The design of the properties of a material is increasingly used, as a step prior to its synthesis. The most effective and direct method of modulating the properties of a material with a crystalline structure is to use a certain dopant. All its physicochemical properties are strongly influenced both by the nature and concentration of the dopant and by its position in the host crystal lattice. The development of computing power in the last 3 decades has made possible the emergence of a wide range of software used in materials design, as direct applications of *ab-initio* computational methods of quantum chemistry. DFT is one of these methods, which has gradually become a practical tool in engineering and modeling the properties of crystalline materials. As will be seen in this paper, the efficiency of the method is inextricably linked to the computing power available and inherently correlated with the complexity of the crystal structure analyzed. The convergence of the energy of a crystalline system towards a minimum value in order to achieve a state of stability is the fundamental criterion by which its existence is found. For calculating the energy of crystalline materials, DFT is an increasingly widely used method, providing a good correlation with experimentally determined values. At the outset, it should be emphasized the seemingly paradoxical fact that the calculation difficulties are greater the lower the level of doping. Also, the application of the method is simpler in the substitutional case than in the interstitial case. [3]

Figure 1 shows the elementary cell of $Zn_3Nb_2O_8$ in which 26 ions are identified: 4 Nb, 6 Zn and 16 O with their 300 electrons. In order to refer to low-concentration doping, the elementary cell would have to be multiplied a certain number of times, thus obtaining a supercell. Only in the supercell can we speak of introducing an impurity element at a low concentration in relation to the host ions. The smallest supercell that complies with the spatial symmetry conditions corresponding to the space group C2/c (No. 15) to which $Zn_3Nb_2O_8$ belongs contains 208 ions and a proportionally higher number of electrons, which makes the calculation unfeasible, assuming logistics that far exceed any justification for the case under consideration.However, *ante-factum*, it is possible to determine the place that the doping ion can occupy within the elementary cell, even in this case.

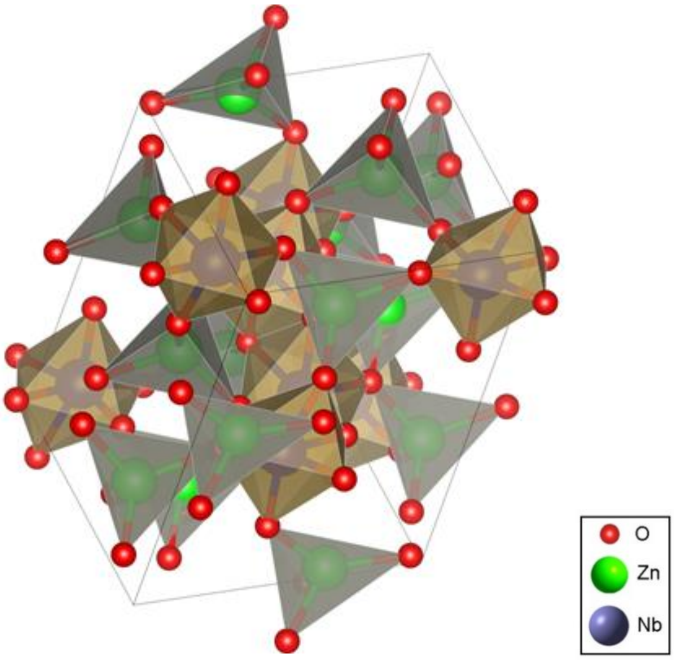

Figure 1. Elementary cell of $Zn_3Nb_2O_8$ obtained by CRYSTAL 14 package

Results and Discussions

Note the coordination polyhedra of Nb and Zn. In the case of Zn we notice two distinct positions, irreducible from a symmetrical point of view, denoted by Zn1 and Zn2 respectively. We will be interested in what substitute positions are eligible for the Eu ion and whether interstitial positions are possible. The fact that the Eu ion originating from Eu_2O_3 is octahedraly coordinated allows us to assume that it can substitute Nb ions within the host network, also octahedrally coordinated. Here, however, begins another type of problem regarding the use of the software. The information it needs to build the elementary cell in the lattice refers to the symmetrically irreducible positions – the asymmetric unit after which it is necessary to communicate to it the group of spatial symmetry with which it must operate. Since in the asymmetric unit there is only one Nb ion, after the reconstitution of the entire elementary cell, all Nb atoms will be replaced by Eu! Basically, we are no longer talking about $Zn_3Nb_2O_8$ but about the structurally equivalent network $Zn_3Eu_2O_8$. The calculation of DFT converges towards a minimum energy, so this material possesses a thermodynamically stable structure. In conclusion, it is permissible for Eu to substitute for Nb. Because, for example, its forbidden band calculated for $Zn_3Eu_2O_8$ is 2.5 eV, much smaller than the original compound's forbidden band of 3.7 eV [1], it is obvious that it will narrow after doping. Testing other substitution positions for both Zn1 and Zn2, similar substitution calculations reveal convergence towards energy minimums in both cases. The synthesis process allows the reaction to take place competitively between Eu and Zn ions, not successively; does not occur the initial formation of the $Zn_3Nb_2O_8$ crystal matrix, after which the Eu^{3+} dislodge the Zn ions in the two positions. On the contrary, Eu with more available electrons in valence layers than Zn, is more reactive, will occupy the places in the network before Zn. In these cases, in which it is practically not a doping but a massive impurification, resulting in a compound of the type $Zn_{3-x}Eu_xNb_2O_8$, the calculation of the band structure reveals the cancellation of the band gap, the material becoming conductor, fact due to a much more number large of weaker electrons tied in the Eu, which easily become mobile in the network.At the same time, Eu ionic radius R = 0,947Å can find a place and interstitial, conserving the spatial symmetry.

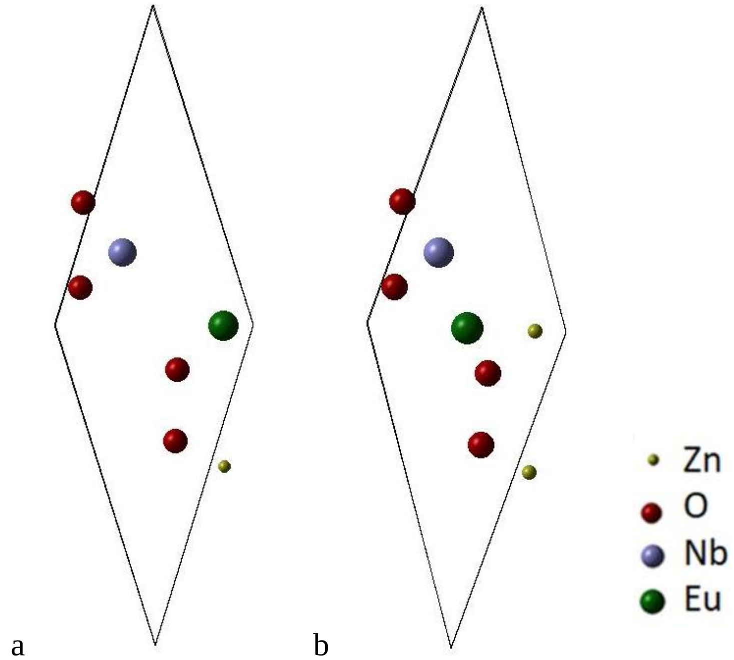

Figure 2 a**.** Eu^{3+} substitutes Zn b. Eu^{3+} - interstitial position

The calculation of DFT in the case of the figure above, with Eu ions placed median in the elementary cell, was not completed by convergence due to mutual influence in between . This inconvenience is canceled in the case of low concentrations, specific to doping. As a experimental study, a series of samples of $Zn_3Nb_2O_8$ doped with Eu^{3+} at various concentrations were obtained by solid-state thermal synthesis. The precursors used were niobium pentoxide Nb_2O_5 (99.9%), zinc oxide ZnO (99.9%) in molar ratio 3:1 to which europium (III) oxide Eu_2O_3 (99.9%) was added in concentrations 0.01%, 0.02%, 0.05%, 0.1%, 0.2% and 0.5% respectively. [1]

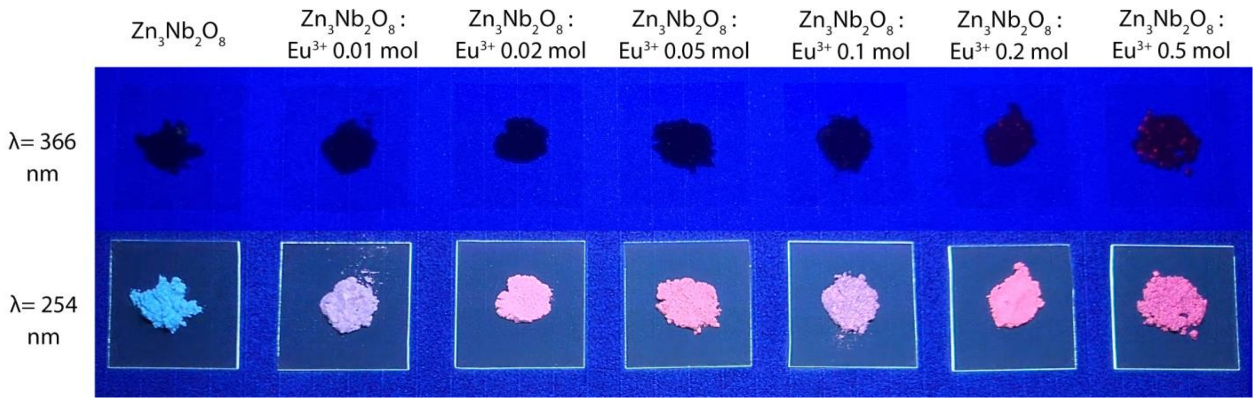

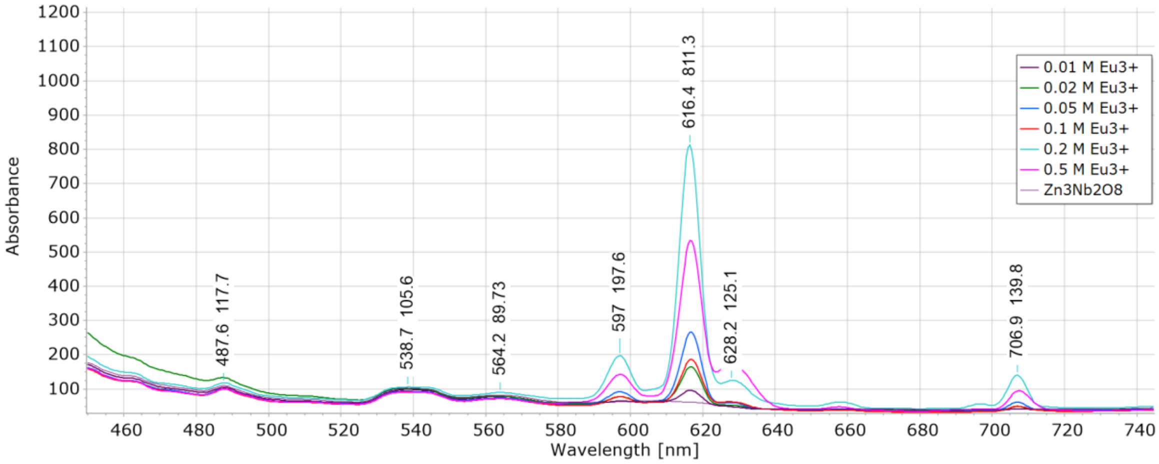

Figure 3**.** Samples and UV-VIS spectra for Eu^3-doped $Zn_3Nb_2O_8$. at these concentrations.

Conclusion

The DFT method used in CRYSTAL 14 software offers the possibility to determine the position of a dopant in a given crystal matrix. Its advantage lies in its general and objective character, overcoming the difficulties that arise in the case of dopants that do not bring significant changes in the crystal lattice, preserving its symmetry. Experimental arguments, of which the diffraction spectrum XRD being the most important, encounter some inherent difficulties for the following reasons. In the case of interstitial doping, in principle, some additional picks occur due to the appearance of new crystalline diffraction planes in the host matrix and some displacement of some of them due to cross-linking changes. In the case of substitutional doping, where no additional plans appear in the network, no additional picks occur, because only the distance between plans can be modified; some picks move one way or the other, as distances between planes decrease or increase. But these effects depend decisively on the concentration of the dopant and its ionic size.

Acknowledgements

The study was carried out within the project PN 23 27 01 02 INOMAT, 23-27 29N/2023

References

1. M. Birdeanu, I. Fratilescu, C. Epuran, L. Mocanu, C. Ianasi, A. Lascu,E. Fagadar-Cosma, International Journal of Molecular Sciences, 2023,24,8920. https://doi.org/10.3390/ijms24108920.
2. R.A. Evarestov ; Springer (Eds.), Quantum Chemistry of Solids The LCAO First Principles Treatment of Crystals, Berlin, Germany, 2007, pp. 105−140.
3. R. Dovesi, R. Orlando, A. Erba, C.M. Zicovich-Wilson, B. Civalleri, S. Casassa, L. Maschio, M. Ferrabone, M. De La Pierre, P. D'Arco, Y. Noël, M. Causà, M .Rérat, B. Kirtman, Int. J. Quantum Chem. **2014**, 114, 1287–1317.

THE DEVELOPMENT OF AN INNOVATIVE TECHNOLOGY FOR BIOMASS UTILIZATION USING ARTIFICIAL INTELLIGENCE

Corina Macarie, Paula Sfirloaga, Bogdan Taranu, Ionel Balcu, Doru Buzatu

National Institute for Research and Development in Electrochemistry and Condensed Matter,
144 Dr. A. PaunescuPodeanu, 300569, Timisoara, Romania, Tel.: +40 256 222119
e-mail address:mac_cora@yahoo.com

Abstract

The paper aims at the development of an innovative technology for biomass utilization using artificial intelligence.For the elaboration of the technical solution a very important role is played by the efficient pre-treatment of the reed which is characterised by several criteria. Biomass preparation involved the following methods: physical and chemical methods of biomass pretreatment.The samples were mechanically prepared, followed by preliminary characterization analyses: moisture, total solids content, determination of total organic carbon content, qualitative analysis by FT-IR spectroscopy, SEM - EDAX scanning electron microscopy and metal concentration.

The studies were performed using a PGZ 402 Radiometer Analytical potentiostat using a classical 3-electrode electrochemical study setup. To begin with we investigated the behaviour of both solutions obtained on the bright nickel electrode, platinum counter electrode and ESC reference electrode.

Obtaining hydrogen in an electrolyzer without separation of the electrode spaces is possible. Depending on the working conditions and the electrolyte solution obtained from the enzymatic fermentation of reed - or cellulose extract - it is possible to obtain hydrogen without oxygen being released from the anode. This can only happen if there is ethyl alcohol in the electrolyte. The higher the amount of ethyl alcohol in the electrolyte, the more hydrogen can be obtained. As the electrode reactions proceed the ethyl alcohol is consumed. When its concentration becomes very low, the anode potential increases and the release of oxygen begins.

Acknowledgements

This work was supported by “Plan Sectorial” Project 1PS / 09.11.2021"Development of innovative technologies using artificial intelligence for the exploitation of biomass in lake areas inorder to sustain green energy sustainability".

References

[1] Calcerrada AB, de la Osa AR, Llanos J, Dorado F, de Lucas-Consuegra A. Hydrogen from electrochemical reforming of ethanol assisted by sulfuric acid addition. Appl Catal B-Environ 2018;231:310–6.

[2] Da Silva Veras T, Mozer TS, da Costa Rubim Messeder dos Santos D, da Silva César A. Hydrogen: trends, production and characterization of the main process worldwide. Int J Hydrogen Energy 2017;42(4):2018–33.

[3] Holladay JD, Hu J, King DL, Wang Y. An overview of hydrogen production technologies. Catal Today 2009;139(4):244–60.

MULLITE TEMPLATING EFFECT AND PARTICLE SIZE INFLUENCE ON THERMO-MECHANICAL PROPERTIES OF CORDIERITE-MULLITE CERAMIC STRUCTURES

John. W. Makokha[1], Imre Szenti[1,2], Tamás Boldizsár[2], András Sápi[1,2], Nagy László[3], Zita Sándor[3]

Department of Applied and Environmental Chemistry, University of Szeged, H-6720 Szeged, Rerrich Bela ter 1, Hungary.
email: sapia@chem.u-szeged.hu

Abstract

In this study, we present findings on mullite templating effect on microstructure and how the particle sizes of SiC and Al_2O_3 influence the thermomechanical properties of cordierite-mullite ceramic structure. Initial SiC and Al_2O_3 were milled at 600rpm for 2 hours to synthesize submicron particles. Three sample sets consisting of CHS96, initial particle size and 600rpm 2hr-milled particles were synthesized. Kaolin, clay, Al_2O_3, talc, mullite, chamotte and SiC were mixed in appropriate ratios for two hours and aged for 24 hours. Liquidity levels were adjusted within the range of 180-250, and the thixotropy set between 30-70. The green samples were moulded for one hour, dried between 30-50^{O}C for 48 hours, and then fired at 1350^{O}C for 3½ hours. The Field Emission Scanning Electron Microscope (FESEM) results showed the formation of acicular mullite with interspersed cordierite in the mullite phase. X-ray Diffraction (XRD) analysis of the fired samples confirmed the presence of distinct peaks corresponding to cordierite, mullite, SiC and Al_2O_3 phases at 2θ angles of 29.7^{O}, 31.2^{O}, 35.7^{O} and 43.8^{O}, respectively. The coefficient of thermal expansion (CTE) in SiC samples reduced from 3.75×10^{-6}/ k to 3.50×10^{-6}/ k. This was attributed to enhanced thermal conductivity, which rose from 1.322 to 1.792 W/ mk in the SiC specimens. The thermal conductivity in Al_2O_3 samples was found to be lower compared to SiC samples. The CTE and Thermal conductivity were found to be independent of SiC particle size. Al_2O_3 particles enhanced flexural strength of the samples while SiC particles lowered the bending strength. Al_2O_3 particles that were milled at 600rpm for 2 hours resulted in a bending strength of approximately ≈40 MPa, while SiC particles, under similar conditions, yielded a bending strength of ≈34.8 MPa.

Keywords: Templating Effect, Particle Size, Bending Strength, Thermal Conductivity, X-Ray Diffraction, FESEM

CHEMICAL ANALYSIS OF BLUEBERRY FRUITS (*VACCINIUM CORYMBOSUM* L.) FOR PESTICIDE RESIDUES IN THE MAČVA DISTRICT

Marković Stefan*, Robinić Jelena, Pavlović Nenad, Stošić Nemanja, Blagojević Milan

Academy of Applied Studies Šabac. Unite for Agricultural Business Studies and Tourism,
Republic of Serbia
**e-mail: markovicstefaan@gmail.com*

Abstract

Quality and healthy nutrition is the goal of every consumer on the market. Blueberry (*Vaccinium corymbosum* L.) is a very healthy and attractive fruit, with high nutritional value and a rich content of antioxidants. Nowadays, producers are faced with the problem of the appearance of diseases and pests in their plantations, caused by a change in the climate, which favors the better development of fruit rot in the first place. The quality control of fruits that reach the market and in supermarkets is at a very demanding level, and there are only a few registered pesticides on the market that are used in blueberry protection treatments. Chemical analysis of fruits for pesticide residues is crucial when exporting blueberries to the European and world markets. In order for blueberry fruits to reach the market, chemical analyzes for pesticide residues must be carried out. As part of the analysis, blueberry fruits are tested for over 600 active substances, primarily active substances cyprodinil, azoxystrobin and fludixonil. Export is enabled only to those distributors whose fruits have passed a chemical analysis in which it has been confirmed that the pesticide residues are in the optimal amount. *Botrytis cinerea* has a major impact on fruit quality, where fruit infection during the growing season affects fruit quality after harvest. Correct and timely application of fungicides in disease control ensures the quality of the fruits, as well as the minimal risk of excessive amounts of fungicide residues on blueberry fruits. The aim of this research is to examine the content of pesticide residues on blueberry fruits, which were applied at different moments during the growing season. The results of the research will help agricultural producers in more efficient application of pesticides in their blueberry plantations, as well as the implementation of all measures to protect human health and the environment.

Keywords: pesticides, blueberry, quality, health

GLOBAL G.A.P. IN ORDER TO OBTAIN THE HIGHEST QUALITY AGRICULTURAL PRODUCT

Marković Stefan*, Rasković Vera, Stošić Nemanja, Blagojević Milan, Glišić Milan, Pavlović Nenad

Academy of Applied Studies Šabac. Unite for Agricultural Business Studies and Tourism, Republic of Serbia
**e-mail: markovicstefaan@gmail.com*

Abstract

The food industry faces the challenge of food safety, as well as food quality and standards. The change in consumer attitudes was largely influenced by incidents related to food quality and safety, where the conclusion was drawn that it is necessary to pay more attention to this issue globally. Consumers demand healthy, high-quality and biologically valuable food, they demand from producers responsibility in environmental protection, respect for workers on farms, as well as care for animals. However, in addition to consumers, the attitude towards food production also began to change in the food industry. The reasons for such relationships can be sought in changes in the food markets, which are increasingly oriented towards safe and healthy food. Food safety, food security and environmental sustainability are essential prerequisites for the well-being of societies around the world. Failure in food quality and safety cannot be the fault of only one member of the chain (producer - processor - consumer), where it is necessary for all these actors to work together and successfully eliminate the possibility of errors. The purpose of this paper is an analysis of the current representation of the use of Global G.A.P. in agricultural production, the conditions that need to be met in order for a product to be certified, what the certification process looks like and what the obtained certificate enables the producers.

Keywords: global G.A.P., food safety, food quality, human health

APPLICATION OF 1-MCP IN ORDER TO MAINTAIN THE QUALITY OF BLUEBERRY FRUITS (*VACCINIUM CORYMBOSUM L.)*

Marković Stefan*, Robinić Jelena, Pavlović Nenad, Stošić Nemanja, Blagojević Milan, Glišić Milan

Academy of Applied Studies Šabac. Unite for Agricultural Business Studies and Tourism,
Republic of Serbia
**e-mail: markovicstefaan@gmail.com*

Abstract

Blueberry (*Vaccinium corymbosum L.*) belongs to the berry group, and due to the very thin skin, its fresh storage is very limited and the fruits deteriorate relatively quickly. Due to the deterioration of the fruits, blueberries lose their quality and nutritional value, and therefore their market value decreases, as well as the possibility of placing them on the market in general. By inhibiting the synthesis of the hormone ethylene in the fruit, the possibility of storing the fruits, in this case blueberries, is extended, as well as the preservation of quality, nutritional value and the possibility of better transporting the fruit to the market. 1-methylcyclopropene is an inhibitor of the hormone ethylene, and it has no negative effects on fruits and vegetables. 1-Methylcyclopropene is a gas released in cold storages with normal or controlled conditions with the help of an activator. As part of this experiment, tests were carried out on blueberry fruits that were treated with 1-MCP and fruits that were not treated. The parameters that were monitored were the weight of the fruit, the content of soluble dry matter (ºBRIX), the composition of total acids, the firmness of the fruit and the amount of released ethylene. The content of soluble dry matter was measured using a refractometer, and total acids were determined by titration. Differences were observed when measuring the released ethylene with the SCS56 device, expressed in ppm, and with the firmness of the fruit, which was measured using a hand-held penetrometer FT327. Differences in the obtained results were observed in the loss of fruit weight, where the dehydration of the fruits that were not treated was greater compared to the treated fruits, average by 9.6%. Significant differences were observed in fruit firmness, where treated fruits maintained a 14,3% higher average fruit firmness compared to untreated fruits.

Key word: blueberry, ethylene, 1-MCP, sugar, acids

ADDRESSING THE ENVIRONMENTAL PROBLEMS OF WASTEWATER: REDUCING THE POLLUTION WHILE PROVIDING MULTIFUNCTIONAL WOOL FABRICS

Aleksandra Mašulović[1], Aleksandra Ivanovska[1], Mirjana Kostić[2], Anita Lazić[1], Luka Matović[1], Dušan Mijin[2], Jelena Lađarević[2]

[1]*Innovation Center of the Faculty of Technology and Metallurgy, University of Belgrade, Karnegijeva 4, 11000 Belgrade, Serbia*
[2] *Faculty of Technology and Metallurgy, University of Belgrade, Karnegijeva 4, 11000 Belgrade, Serbia*
e-mail: amasulovic@tmf.bg.ac.rs

Abstract

The reduction of water pollution represents one of the priority topics of the EU's goal to achieve climate neutrality by 2050. Considering this, the concept of reusing the same dyebath for multiple dyeing cycles is proposed. For this purpose, two pyridinium-based azo pyridone dyes with improved solubility and affinity towards different fibers, are used for dyeing wool fabric. It is demonstrated that the dye concentration in wastewater could be reduced up to four times by recirculation of the same dyebath 5 times. The dyed fabrics obtained in each cycle are further characterized regarding color strength (*K*/*S*) and ultraviolet protection factor (UPF), while their antioxidant potential is evaluated by ABTS (2,2'-azino-bis(3-ethylbenzothiazoline-6-sulphonic acid)) test. The results revealed that the proposed concept could be used for obtaining multifunctional wool fabrics by following the principles of sustainable development of reducing the effluent load in wastewater.

Introduction

The practices within the textile industry have given rise to numerous environmental and social issues, including high emissions, high water and/or energy consumption and heavy pollution [1]. Among them, the disposal of colored effluents from the textile industry into the natural ecosystem constitutes a major concern. It is estimated that textile production is responsible for about 20% of global clean water pollution from dyeing and finishing products. To tackle the adverse impact on the environment, the European Union aims to reduce textile waste and increase the life cycle and recycling of textiles as part of the plan to achieve a circular economy by 2050 [2]. The proposals encompass boosting sustainable products and empowering consumers to participate in the green transition.

Moreover, much effort has been made to develop eco-friendly dyes from natural sources, but synthetic dyes are still superior due to their excellent dyeing capabilities and color fastness properties. Among them, azo pyridone dyes have gained wide commercial application due to the simplicity of their preparation, good color fastness, high tinctorial strength, thermal and optical stability [3]. Generally, they are applied to textile as disperse dyes, colorants characterized by low water solubility which are, in their colloidal form, suitable for dyeing and printing of hydrophobic fibers. Recently, it has been shown that the introduction of the pyridinium ring into pyridone molecule resulted in enhanced water solubility of the dyes and improved affinity towards various natural and synthetic fibers, especially wool and cellulose diacetate fibers [4].

In order to address environmental issues caused by the textile industry, this work aims to reduce wastewater by using the same dyebath for multiple dyeing cycles while providing multifunctional wool fabrics at the same time. Two pyridinium-based pyridone dyes bearing different substituents in *para*-position of the phenyl ring (Figure 1) were used for dyeing wool fabrics. The results show that the same dyebath can be efficiently used up to 5 times. In addition, the obtained fabrics from different cycles are further characterized by *K*/*S* values and UPF factor, while antioxidant activity is evaluated by ABTS test.

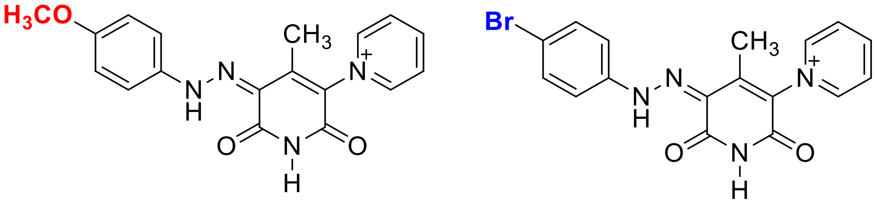

1 **2**

Figure 1. Structure of the pyridinium-based azo dyes used for dyeing wool fabrics.

Experimental

Dyeing experiments

Wool fabric (7 cm × 7 cm) was used for dyeing experiments. The dyeing of the wool was performed at pH 8.5 and 80 °C for 60 min under constant shaking. The dyebath was prepared by dissolving the corresponding amount of dye (1% o.w.f., i.e. on the weight of fiber) in distilled water (C_0 = 0.2 mg/mL). After dyeing, the fabric was washed with warm distilled water and dried in the air at room temperature. The procedure was repeated four times for each dye using the previous dyebath. The dye exhaustion after each dyeing cycle was determined by UV-Vis absorption spectra on a Shimadzu 1700 spectrophotometer.

Characterization of the fabrics

Reflectance fabric spectra were recorded on the Shimadzu UV-Vis-Nir 3600 plus spectrophotometer using Datacolor ColorTools QC version 1.2.1 software. Thereafter, the color strength of dyed fabrics was calculated from the reflectance values (*R*) by using the Kubelka-Munk equation [5]. The fabric UPF was determined according to the standard test method EN 13758–1:2001 + A1:2006 using the Shimadzu UV-Vis 2600 spectrophotometer.

Determination of antioxidant activity

The antioxidant potential of the wool fabrics was determined using ABTS test according to the procedure described in the literature [6].

Results and discussion

The dyes used in this study were characterized previously, and it has been shown that they exist in the hydrazone form in an acidic medium, while in an alkaline medium dyes exist in the equilibrium between hydrazone form (cationic form) and deprotonated (zwitterionic) form [4]. The screening of the dyeing process (by using multifiber fabric) showed that the best dyeing performance was achieved for wool and cellulose diacetate fabrics at pH of 8.5. Thus, in this study, two dyes bearing different substituents (methoxy group (**1**) or bromine atom (**2**), Figure 1) are selected for the dyeing wool fabrics with the aim to reduce waterwaste by using the same dyebath multiple times.

The dye exhaustion after each dyeing cycle was determined by UV-Vis absorption spectra (Figure 2). The results show that the dye exhaustion after the first cycle was relatively low (17 and 20% for dyes **1** and **2**, respectively). Thus, the remaining solution was further used for the next dyeing cycles. The dyeing experiments showed that the same dyebath could be efficiently used for dyeing wool up to 5 times for each dye. After the fifth cycle, the total exhaustion of the dyes was 79 and 82%, for **1** and **2** respectively, indicating that the dye load in the wastewater could be reduced up to four times by recirculation of the same dyebath.

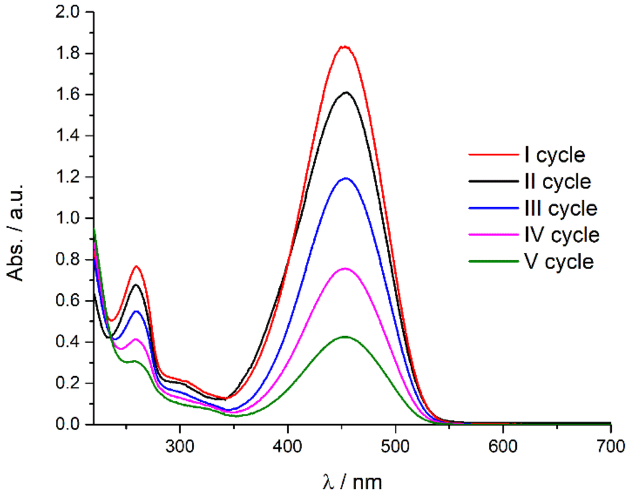

Figure 2. UV-Vis spectra of the dye solutions after each dyeing cycle with dye **1**.

Dyed fabrics were further characterized by reflectance spectra that were further used for the calculation of the color strength (*K*/*S*), Table 1. The results listed in Table 1 show, as expected, that *K*/*S* values decrease with a higher number of dyeing cycles being the highest for the first cycle and the lowest for the fifth cycle. It should be emphasized that even though the decline is substantial, wool fabric *K*/*S* value after the fifth dyeing cycle is still satisfactory (> 1). Considering dyes, it should be pointed out that higher color strength is obtained for bromine-substituted dye **2** for each cycle indicating better adhesion of this dye to wool fabric.

Table 1. *K*/*S* values and the visual appearance of the dyed fabrics for different dyeing cycles

	Dye **1**		Dye **2**	
I cycle	12.74	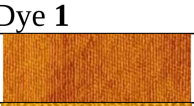	23.65	
II cycle	5.43		12.44	
III cycle	4.32		6.46	
IV cycle	2.95		3.91	
V cycle	1.62		1.99	

Further, the fabrics are characterized by UPF factor. Obtained results revealed that wool fabrics dyed with dye **2** irrespectively on the dyeing cycle and fabrics dyed with dye **1** for the first three cycles have excellent UV protection (UPF values are 50+). Fabrics obtained after the fourth and fifth dyeing cycles with dye **1** show unsatisfactory UV protection.

Figure 3 depicts the antioxidant activity of the dyed wool fabrics over the different dyeing cycles. The results show moderate radical scavenging ability of the fabrics dyed with **1** for the first three cycles, while fabrics dyed with **2** have low antioxidant potential. It can be also observed that increasing the number of dyeing cycles significantly reduces the antioxidant capability of the wool fabrics dyed with **1**, while for fabrics dyed with **2**, no significant changes in their activity could be observed.

It can be summarized that most of the investigated dyed fabrics, besides good color strength have remarkable UV protection properties and moderate antioxidant activity (in the case of samples dyed with **1** for the first three cycles) and therefore provide additional value to the textile, making them suitable for application as protective fabrics.

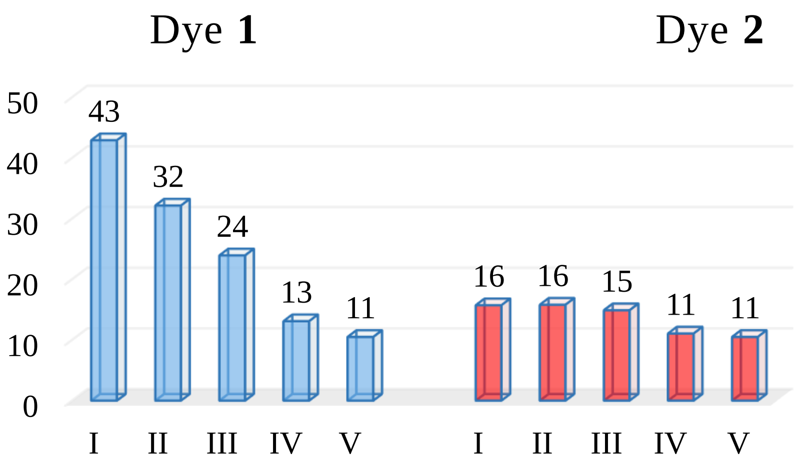

Figure 3. Antioxidant potential of the dyed fabrics for different dyeing cycles.

Conclusion

In this study, two pyridinium-based pyridone azo dyes are used for dyeing wool fabrics. The same dyebath was used 5 times in order to reduce the concentration of the dye in the wastewater (up to 4 times) while providing multifunctional fabrics having different color shades. The obtained wool fabrics are characterized by excellent color strength and remarkable UPF factors (except fabrics dyed with **1**, fourth and fifth cycles). Wool dyed with **1** for the first three cycles shows moderate antioxidant activity. All these properties provide additional value to the textile, making them suitable for protective fabrics. Reusability of the same dyebath for five dyeing cycles will ensure better source usage and recycling that will provide environmental benefits and cost effectiveness of the dyeing process and wastewater treatment.

Acknowledgments

This work was supported by the Ministry of Science, Technological Development and Innovation of the Republic of Serbia (Contracts No. 451-03-47/2023-01/200135 and 451-03-47/2023-01/200287).

References

[1] K. Shirvanimoghaddam, B. Motamed, S. Ramakrishna, M. Naebe, Sci. Total Environ. 718 (2020) 137317.
[2]https://eur-lex.europa.eu/legal-content/EN/TXT/?qid=1583933814386&uri=COM:2020:98:FIN
[3] J. Lađarević, B. Božić, L. Matović, B. Božić Nedeljković, D. Mijin, Dyes Pigments 162 (2019) 562.
[4] A.D. Mašulović, J.M. Lađarević, A.M. Ivanovska, S.Lj. Stupar, M.M. Vukčević, M.M. Kostić, D.Ž. Mijin, Dyes Pigments 195 (2021) 109741.
[5] G. Zhang, J. Zhou, R. Pan, Fibers Polym. 22 (2021) 412.
[6] T.K. Glaser, O. Plohl, A. Vesel, U. Ajdnik, N.P. Ulrih, M.K. Hrnčič, U. Bren, L.F. Zemljič, Materials 12 (2019) 2118.

GRAPHENE OXIDE-SILVER NANOWIRES COMPOSITES FOR PROTECTION AGAINST MODERN POLLUTION – ELECTROMAGNETIC WAVES

Mila Milenković[1], Miroslav Huskić[2], Andjela Stefanović[1] , Mohamed Sebbache[3], Kamel Haddadi[3] and Svetlana Jovanovic[1]

[1]Vinca Institute of Nuclear Sciences-National Institute of the Republic of Serbia, University of Belgrade, P.O. Box 522, 11000 Belgrade, Serbia
[2]Fakulteta za tehnologijo polimerov, Ozare 19, 2380 Slovenj Gradec, Slovenija
[3]Univ. Lille, CNRS, Centrale Lille, Univ. Polytechnique Hauts-de-France, UMR 8520 - IEMN - Institut d'Electronique de Microélectronique et de Nanotechnologie - Lille, France
e-mail: svetlanajovanovic@vin.bg.ac.rs

Abstract

With the development of the electronic industry, telecommunication, transportation, energy storage devices, and wireless technologies, the need for materials that are able to block electromagnetic waves (EMWs) in low-frequency regions of the spectrum is increasing. A new type of pollution named pollution by EMWs is an inevitable component of modern life. Although materials efficient in blocking the propagation of EMWs are developed, these materials show drawbacks regarding durability and mechanical properties, as well as a high production price and processability. Thus, new eco-friendly and durable materials are needed. Herein, we produced composites based on graphene oxide and silver nanowires to create an efficient shielding barrier for low frequencies (0-15 GHz) EMWs.

Introduction

The industrial progress and development of new electronic devices made everyday life more simple and conformable. At the same time, all devices that generate, transfer, and use electrical energy, emit in the area around them Electromagnetic Waves (EMWs). In this way, a new type of environmental pollution, so-called EMW pollution becomes an inevitable component of everyday life [1].

Current research laboratories and researchers across the world are facing issues with EMW inferences which lead to prolonged measurements, shortening of the equipment lifetime, and unwanted signal and noise [2].

Thus, there is currently a large demand for efficient EMW shielding materials. The efficiency of the materials to block EMW propagation is related to reflected (SE_R), absorpted (SE_A), and multiple reflected EMWs (SE_{MR}) [3]. The total shielding efficiency of material (SE_T) is the sum of these three components and it is expressed in dB. Commercial applications demand a SE_T of 20 dB is considered an acceptably efficient material since it blocks 99% of the total incident energy [4].

Common shielding materials are metals such as Cu, Al, and Ag [5], but they are hard to process, chemically unstable, and rigid which makes them unfavorable for current technological requirements. Another group of shielding materials is conducive polymers (CPs) with high SE_T, lightweight, good mechanical properties such as flexibility and resistance to humidity [6]. But, CPs showed the issues regarding processability [7]. Particularly interesting and highly efficient shielding materials are MXene due to its high electrical conductivity which is a key parameter for EMI shielding materials and it is between 5 S cm^{-1} to above 20,000 S cm^{-1} [8, 9].

Considering mechanical, chemical, and electrical properties, but also ecological and economic aspects of production, graphene and its derivates, are one of the promising materials for EMI shielding [10]. Thanks to its mechanical strength, elasticity, lightweight, chemical stability, and tunable electrical properties, graphene derivates become a spotlight of shielding material [11]. Graphene was isolated from graphite using a simple experiment, an adhesive tape and graphite in 2004 [12], and later in 2010, Geim and Novoselov won a Nobel prize. Graphene is a single atomic layer of graphite and contains only sp^2 hybridized C atoms [12].

Since then, various methods for the production and modification of graphene have been reported, such as chemical vapor deposition (CVD), electrochemically exfoliated graphite, and Hummers oxidation of graphite followed by chemical reduction [11].

Herein, we prepared graphene oxide by oxidizing graphite with an improved Hummers method [12] and produced silver nanowires (AgNWs) by chemical reduction of Ag ions with ethylene glycol in the so-called polyol method [13]. After, two separately produced nanomaterials were mixed in different mass ratios and deposited using vacuum filtration producing homologous and uniform free-standing films. The efficiency of these films in blocking EMWs was studied.

Experimental

For GO synthesis, graphite powder (KS6, TIMREX®, Bodio, Switzerland) was used as a starting material [12]. First, graphite powder was sonicated in ccH_2SO_4 in a concentration of 43 mg mL^{-1}, and then three times the larger amount of $KMnO_4$ was carefully added while the temperature was kept at 4 °C, for 30 min, followed by heating at 40 °C for 30 min. In the next stage, a double volume of water was gradually added, and for another 15 min, the temperature was kept at 90 °C. The reaction was stopped by pouring the mixture into water. GO was cleaned from residual acid and ions using centrifugation (3500 for 30 min) till a pH of 7. The precipitate was then dried under reduced pressure and GO in the form of powder was collected.

Separately, AgNWs were produced using a previously described method [13].

To produce GO-AgNWs composites, GO powder was dispersed in water at a concentration of 1 mg mL^{-1}, while AgNWs were sonicated shortly in ethanol at the same concentration. Then, different volumes of both dispersions were mixed at room temperature for 30 min. The mass ratio of GO and AgNWs varied from 20:80 to 50:50. Samples were named GO-AgNWs 20:80 and 50:50. After mixtures were stabilized, they were transferred in a system for vacuum filtration to produce free-standing films. For each dispersion, the same volume (15 mL) was poured. After drying, samples were detached from the membrane surface.

For reduction, films were heated at 90 °C for 8 hours in a water solution of L-(+)-ascorbic acid (AA, 15 mM) [11]. After reduction, films were washed in 400 mL of water and dried.

To analyze the morphology of the surface of free-standing films, a scanning electron microscope (SEM) was used. All measurements were performed in a high vacuum. A high-resolution scanning electron/focused ion beam (dual-beam) microscope Tescan® LYRA 3 FEG / XMH SEM was used. Images were captured using a secondary electron detector. The acceleration voltage was 10kV.

Tetmogravimetic analysis of composites was conducted using the Mettler Toledo TGA/DSC 3+ instrument. The samples were heated from ambient to 700 °C at a scan rate of 5 K min^{-1}, under nitrogen purge (20 mL min^{-1}).

Shielding properties of free-standing films were characterized in the microwave regime using a homemade dedicated coaxial test cell operating in reflection and transmission mode. In its essence, the test cell consists of two semi-rigid coaxial cables that sandwich the free-standing film. Special attention is paid to minimizing RF crosstalk and parasitic RF radiations using grounded metallic structures. The test cell is connected to a Keysight Technologies Streamline P5008A Vector Network Analyzer (VNA), with operating frequency set to 150 KHz-18 GHz, input RF power of -15 dBm, at 25 °C. The test cell is connected to the VNA using highly stable coaxial cables.

Results and discussion

Morphology of samples was investigated using SEM and images are presented in Figure 1. In Figure 1a), a cross-sectional view of GO film is presented, showing lamellar morphology and a thickness of around 12.58 µm. In the case of composites GO-AgNWs, the bright, rodlike structures packed between graphene sheets could be observed. These images indicated that GO sheets are closely wrapped around AgNWs and located in the middle of the composite (Figure 1c and d). TGA measurements (Figures 1e and f) showed better thermal stability of composites after reduction (red curves). The weight loss between 100 and 231 °C could be attributed to the removal of the labile oxygen groups (such as carboxylic and aldehydes groups) and residual water [15] and it is 13.67% for GO-AgNWs 50:50 and 4.73 % for GO-AgNWs 20:80. After reduction, these values were 2.52% and 1.05%, respectively. These changes indicated successful chemical reduction with AA. The second weight loss between 260 and 460 °C is a result of the decomposition of stable oxygen groups as epoxides [15]. At 460 °C weight loss for GO-AgNWs 50:50 was 71.87% and 90.50% after reduction, while for GO-AgNWs 20:80 was 87.29%, and after reduction 95.46%. The results indicated the removal of epoxy groups.

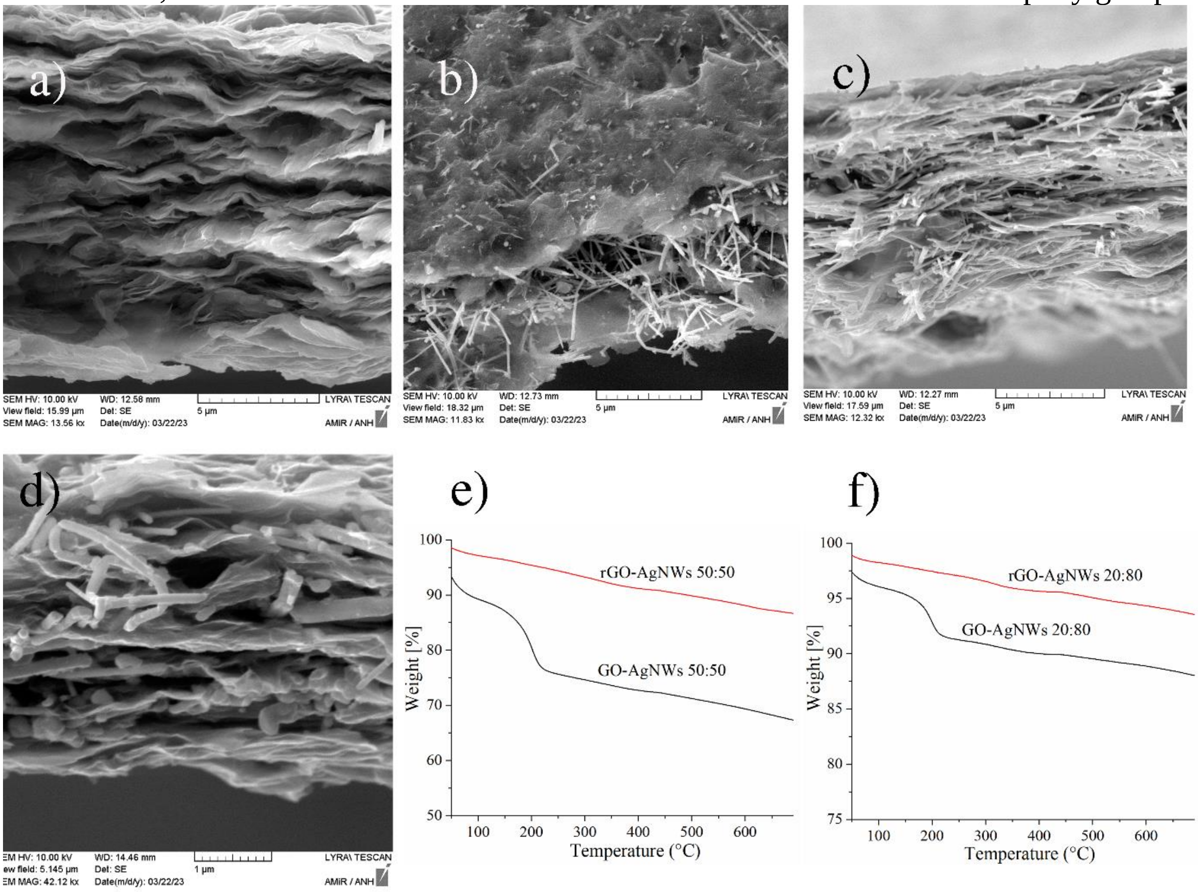

Figure 1. SEM images of GO (a), top (b) and cross-sectional view (c) of GO-AgNWs 50:50, and rGO-AgNWs 50:50 (d), TGA of (r) rGO-AgNWs 50:50 (e) and (r)GO-AgNWs 20:80 (f).

Results obtained by investigating the shielding properties of rGO-AgNWs 20:80 are presented in Figure 2.

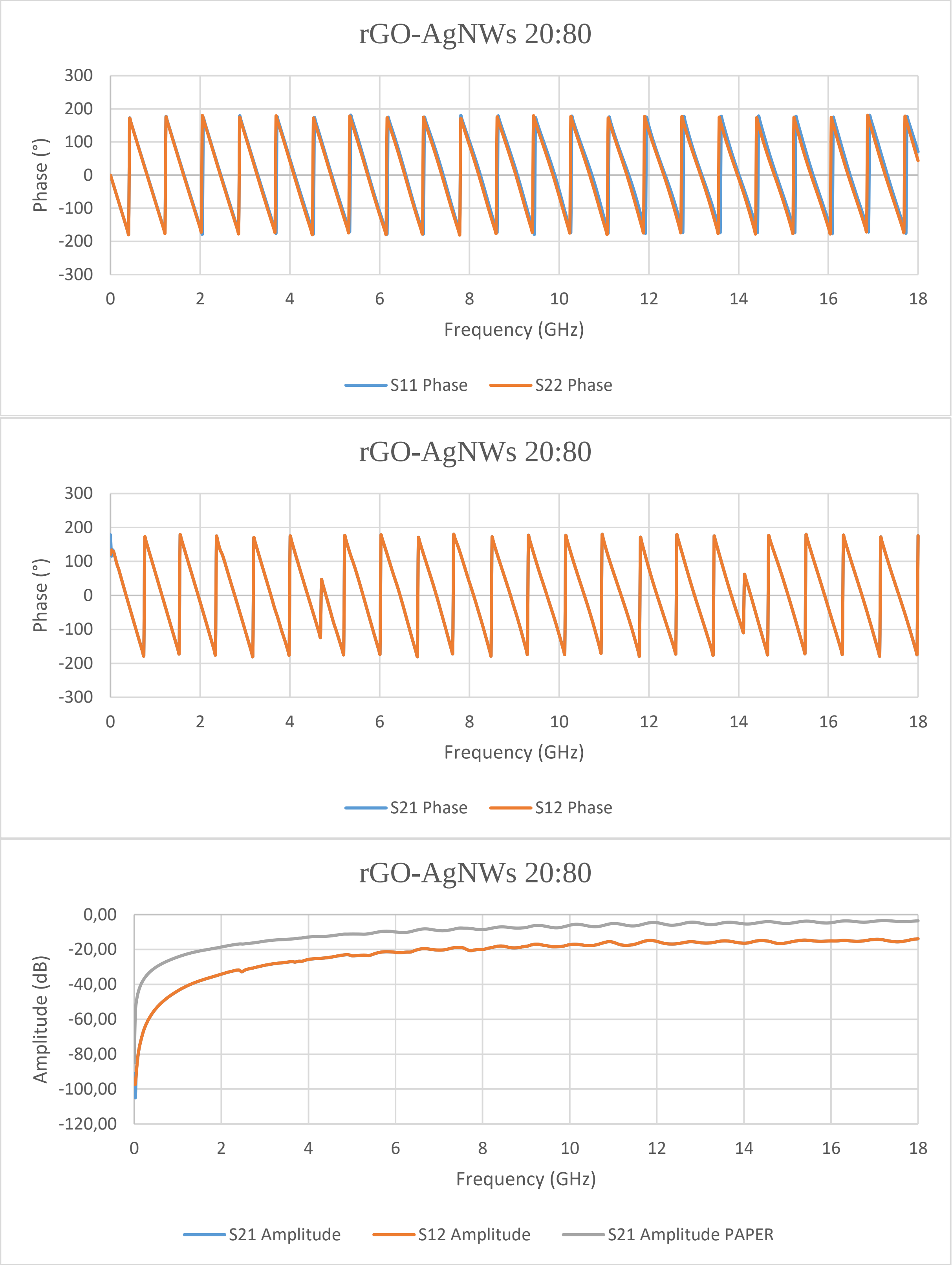

Figure 2. Measured amplitudes of the transmission coefficient of the coaxial test cell loaded with rGO-AgNWs 20:80 as shielding materials.

The measured complex reflection coefficients vary from 0 to 3.5 dB. As the set-up is calibrated at the output of the coaxial cables, the microwave paths in the test cell (from coaxial input up to the coaxial aperture are not taken into account by the calibration procedure). In addition, each sample is inserted between two cellulose papers (named PAPER) that need to be taken into account to isolate the signature of the sample only. In particular, the PAPER only shows a variation of the amplitude of the complex reflection between 0 to 5.5 dB. Therefore, better reflection is observed between PAPER only and PAPER loaded with the material. In addition, the amplitude of the transmission coefficient falls when the PAPER is loaded with the material under test. For instance, the amplitude is shifted from around 20 dB at 2 GHz. These results indicated that the obtained composite is an efficient shielding material, considering that the shielding efficiency of 20 dB is acceptable for commercial applications [4].

Conclusion

A new type of environmental pollution caused by low-frequency range electromagnetic waves needs to be addressed urgently. In this paper, composites based on graphene oxide and silver nanowires were studied as a potential solution for the growing problem regarding EMW shielding. Composite rGO-AgNWs 20:80 showed a satisfying shielding efficiency to block the propagation of EMWs.

Acknowledgements

This project has received funding from the European Union's Horizon Europe Coordination and Support Actions programme under grant agreement No 101079151 - GrInShield. M. M., A. S. and S. J. thank the Ministry of Education, Science, and Technological Development of the Republic of Serbia (grant number 451-03-68/2023-14/200017).

References

[1] G. Redlarski, B. Lewczuk, A. Żak, A. Koncicki, M. Krawczuk, J. Piechocki, K. Jakubiuk, P. Tojza, J. Jaworski, D. Ambroziak, Ł. Skarbek, D. Gradolewski, Biomed. Res. 2015 (2015).
[2] P. Mathur, S. Raman, J. Electron. Mater. 49 (2020) 2975–2998.
[3] M. Jaroszewski, S. Thomas, and A.V. Rane, Advanced materials for electromagnetic shielding: fundamentals, properties, and applications, Wiley, 2018, pp. 464.
[4] D. Kong, J. Li, A. Guo, X. Xiao, Chem. Eng. J. 408 (2021) 127365.
[5] C. Liang, Z. Gu, Y. Zhang, et al. Nano-Micro Lett. 181 (2021) 13.
[6] J. Kruželák, A. Kvasničáková, K. Hložekováa, I. Hudeca, Nanoscale Adv., 2021,3, 123-172
[7] Z. Zeng, M. Chen, H. Jin, W. Li, X. Xue, L. Zhou, Y. Pei, H. Zhang, Z. Zhang, Carbon, 96 (2016) 768-777.
[8] M. Han, C.E. Shuck, R. Rakhmanov, D. Parchment, B. Anasori, C.M. Koo, G. Friedman, Y. Gogotsi, ACS Nano, 14, 4 (2020) 5008-5016.
[9] T.S. Mathis, K. Maleski, A. Goad, A. Sarycheva, M. Anayee, A.C. Foucher, K. Hantanasirisakul, C.E. Shuck, E.A. Stach, Y. Gogotsi, ACS nano, 15, 4 (2021) 6420-6429.
[10] S. Jovanović, M. Huskić, D. Kepić, M. Yasir, K. Haddadi, Graphene and 2D mater. (2023).
[11] J. Prekodravac, D. Kepić, J.C. Colmenares, D. Giannakoudakis, S. Jovanović, J. Mater. Chem. C, 9 (2021) 6722-6748.
[12] K.S. Novoselov, A.K. Geim, S.V. Morozov, D. Jiang, Y. Zhang, S.V. Dubonos, I.V. Grigorieva, A.A. Firsov, Science, 306 (2004) 666-669.
[13] J. Chen, B. Yao, C. Li, G. Shi, Carbon, 64 (2013) 225-229.
[14] J. Maa, M. Zhan, RSC Adv. 4 (2014) 21060-21071.
[15] C. S. Rattana; N.N. Witit-anun, P. Chindaudom, S. Oaew, C. Kedkeaw, P. Limsuwan, Procedia Eng. 32 (2012) 759- 764.

SHAPE-DEPENDENT CARBONIZED PANI-COATED TiO_2 NANOCRYSTALS AND ITS USE IN THE DECOMPOSITION OF ORGANIC POLLUTANTS

Milica Milošević[1], Marija Radoičić[1], Gordana Ćirić-Marjanović[2], Jelena Spasojević[1], Ivana Vukoje[1], Aleksandra Radosavljević[1], Zoran Šaponjić[3]

[1]Department of Radiation Chemistry and Physics, "Vinča" Institute of Nuclear Sciences -
- National Institute of the Republic of Serbia, University of Belgrade,
Mike Petrovića Alasa 12 - 14, Vinča, Belgrade, Serbia
[2]Faculty of Physical Chemistry, University of Belgrade,
Studentski Trg 12 - 16, Belgrade, Serbia
[3]Institute of General and Physical Chemistry, Studentski trg 12/V, Belgrade, Serbia
e-mail: milicam@vin.bg.ac.rs

Abstract

Differently-shaped TiO_2 photo-nanocatalysts play a principal role in the remediation of environmental and pollution challenges considering their proven potential for treating organic contaminants in wastewaters [1]. However, increasing the photoactivity of TiO_2 *i.e.* its optical response from UV into visible region is a constant challenge of many ongoing researchers [2]. An proceed towards this demand may be the creation of hybrid functional nanocomposites by coating the TiO_2 nanocrystals (NCs) with electronically coupled conductive polymers (*e.g.*, polyaniline (PANI), polypyrrole, etc.) [3]. By the carbonization process of mentioned conductive polymers at high temperatures, obtained final material possess carbon-like structure which impart additional properties [4]. Thus, the evolution of carbonized PANI (CPANI)-coated TiO_2 NCs opens up the possibility for tailoring the photocatalyst with distinctive properties. This study implies development of new nanocomposites based on CPANI and colloidal TiO_2 nanoparticles (NPs) (TPC) and CPANI and TiO_2 nanotubes (NTs) (TTPC). Sol-gel and hydrothermal synthesis paths were used to obtain TiO_2 NCs. The influence of their size and shape on the photocatalytic activity of formed carbonized nanocomposites was estimated. TPC and TTPC nanocomposites were synthesized according to the steps: 1) the non-carbonized PANI/TiO_2 class was firstly prepared by the chemical oxidative polymerization of aniline with ammonium peroxydisulfate in the presence of TiO_2 NPs or NTs and 2) the subsequent carbonization process was applied (650 °C). Developed hybrid nanocomposites were morphologically and structurally characterized by TEM measurements and Raman spectroscopy, while their functionality was estimated through the photocatalytic degradation processes of Methylene blue and Rhodamine B. All TPC and TTPC nanocomposites showed excellent photocatalytic properties, however, shape-depending of used TiO_2 NCs.

Acknowledgements

This work was supported by the Ministry of Education, Science and Technological Development of the Republic of Serbia (Grant no. 451-03-47/2023-01/200017).

References

[1] M.M. Mahlambi, C.J. Ngila, B.B. Mamba, J. Nanomater., 2015 (2015) Article ID 790173.
[2] A. Truppi, F. Petronella, T. Placido, M. Striccoli, A. Agostiano, M.L. Curri, R. Comparelli, Catal., 7 (2017) Article number 100.
[3] K.R. Reddy, M. Hassan, V.G. Gomes, Appl. Catal. A-Gen., 489 (2015) 1.
[4] M. Radoičić, Z. Šaponjić, I.A. Janković, G. Ćirić-Marjanović, S.P. Ahrenkiel, M.I. Čomor, Appl. Catal. B: Environ., 136-137 (2013) 133.

SCREENING OF NATURAL DEEP EUTECTIC SOLVENT (NADES) TOWARDS IMPROVED ISOLATION OF POLYPHENOLIC ANTIOXIDANTS FROM STRAWBERRY TREE FRUIT (*Arbutus unedo* L.)

Sanja Milošević[1], Anica Bebek Markovinović[2], Nemanja Teslić[3], Aleksandra Mišan[3], Milica Pojić[3], Irena Brčić Karačonji[4,5], Karlo Jurica[6], Dario Lasić[7], Predrag Putnik[8], Danijela Bursać Kovačević[2,*], Branimir Pavlić[1,*]

[1]Faculty of Technology, University of Novi Sad Blvd. cara Lazara 1, 21000 Novi Sad, Serbia;
[2]Faculty of Food Technology and of Biotechnology, University Zagreb, Pierottijeva 6, 10000 Zagreb, Croatia;
[3]Institute of Food Technology, University of Novi Sad, Blvd. cara Lazara 1, 21000 Novi Sad, Serbia;
[4]Institute for Medical Research and Occupational Health, Ksaverska cesta 2, 10000 Zagreb, Croatia;
[5]Faculty of Health Studies, University of Rijeka, Viktora Cara Emina 5, 51000 Rijeka, Croatia;
[6]Special Security Operations Directorate, Ministry of the Interior, Ulica grada Vukovara 33, 10000 Zagreb, Croatia;
[7]Andrija Štampar Teaching Institute for Public Health, Mirogojska 16, 10000 Zagreb, Croatia;
[8]Department of Food Technology, University North, Trg dr. Žarka Dolinara 1, 48000 Koprivnica, Croatia.
e-mail: sanjamilosevic9898@gmail.com

Abstract

Strawberry tree fruits (*Arbutus unedo* L.) from *Ericaceae* family is plant originating from Mediterranean with promising bioactive content. Traditional use of A. unedo refers to jams, preserves, wines, and liqueurs. Due to confirmed biological activity (gastrointestinal, dermatological, and cardiovascular) natural deep eutectic solvent (NADES) extraction was used for obtaining high-quality extracts. This rapid and simple extraction is eco-friendly, due to use of non-toxic solvents with creating minimal waste streams. The main goal in this study was to investigate the most appropriate NADES solvents in regard to the highest content of phenolic compounds (TP) and antioxidative capacity. Twenty different NADES mixtures according to [1] were prepared and used on strawberry tree fruits. The extraction parameters were: temperature at 50 °C, solid/liquid ratio of 1:10 m/m, extraction time of 60 min, and stirring speed 600 rpm. The only independent variable was the solvent while the other four were held constant, which is known as the OFAT approach (one factor at a time). Analysis of variance (ANOVA) and post-hoc Tukey-test were used to determine the significant differences among NADES mixtures ($p \leq 0.05$). After NADES extraction, followed selection of the most suitable NADES solvents, where obtaining was based according to TP content and antioxidant activity. Results showed that NADES mixtures highly effected TP content and DPPH assay ranging from 2.23-19.99 mg GAE/g and 7.38-25.82 mg TE/g, respectively. Solvent mixture of choline chloride and glycerin, with a molar ratio 1:2 (N9) provided the highest content of TP. Moreover, N6 solvent (betaine-glycerin-water, with a molar ratio 1:2:1) stood out as the most convenient for neutralization of DPPH radicals. Therefore, NADES mixtures made of glycerin, choline chloride and betaine, such as N6 and N9, enabled the high isolation of polyphenols and antioxidants from *A. unedo*. In this way, it was confirmed that strawberry tree fruit represented a highly valuable raw material for isolation of phenolic compounds with antioxidant capacity.

But further optimization of NADES extraction will be necessary in order to obtain as high as possible contents of bioactives from this plant.

Acknowledgements

This research was supported by the Science Fund of the Republic of Serbia, 7750168, Novel extracts and bioactive compounds from under-utilized resources for high-value applications–BioUtilize and by Croatian Science Foundation through the funding of the Hurdle Technology and 3D Printing for Sustainable Fruit Juice Processing and Preservation project, IP 2019–04-2105.

References

[1] B. Pavlić, Ž. Mrkonjić, N. Teslić, A. C. Kljakić, M. Pojić, A. Mandić, A. Stupar, F. Santos, A. R. C. Duarte, A. Mišan, Molecules, 2022, 27(5), 1508.

THE INFLUENCE OF CARBONIZED POLYMER DOTS ON MECHANICAL PROPERTIES OF POLYURETHANE FOIL

Aleksandra Mišović[1], Zoran Marković[1], Miroslav Huskić[2], Rebeka Lorber[2], Biljana Todorović Marković[1]

[1]Vinča Institute of Nuclear Sciences – National Institute of the Republic of Serbia, University of Belgrade, P.O. Box 522, 11000 Belgrade, Serbia
[2]Faculty of Polymer Technology, Ozare 19, 2380, Slovenj Gradec, Slovenia
e-mail: aleksandra.misovic@vin.bg.ac.rs

Nanocomposites of carbonized polymer dots (CPD) and polyurethane (PU) are promising materials. In order to use a material in a wide range of applications, it is necessary to know its mechanical properties. In this study, two CPD/PU nanocomposites, with different CPD, from citric acid/urea (CAUR) and from phloroglucinol (PHL), as well as the reference PU foil, were mechanically characterized.

CAUR-CPD was synthesized by 2.1 g of citric acid and 1.8 g of urea, dissolved in 50 mL of acetone. PHL-CPD was synthesized by 500 mg of PHL mixed in 50 mL of acetone. Both solutions were transferred to a Teflon-lined autoclave for heating. After the condensation reactions, the products of CAUR-CPD and PHL-CPD were filtered and centrifuged to remove the unreacted precursors. The CAUR-CPD/PU and PHL-CPD/PU nanocomposites were prepared by dipping PU foil (0.2 mm thick) in CAUR-CPD or PHL-CPD solution in acetone. The swelling-shrink-encapsulation method was used to encapsulate the CAUR-CPD and PHL-CPD in PU. The samples were dried in a vacuum furnace to eliminate acetone from the composites.

The mechanical properties were determined on universal testing machine Shimadzu, AG-X plus 10 kN. The samples were prepared in the form of plates with a width of 8 mm. The distance between the grips was 50 mm. The strain rate was set to 1 mm/min for determination of E modulus and to 50 mm/min until the end. Each sample was measured 5 times and the average values were taken.

The reference PU sample showed the highest elastic modulus (33.3 MPa) and tensile strength (25.8 MPa). The nanocomposites, CAUR-CPD/PU and PHL-CPD/PU, showed similar mechanical properties: a lower elastic modulus (18.8 and 18.6 MPa, respectively) and tensile strength (14.6 and 16.9 MPa) but much higher strain at break (650 and 608 %) than the reference PU foil (434 %).

Acknowledgements: The research was supported by the Science Fund of the Republic of Serbia (Grant No. 7741955), Are photoactive nanoparticles salvation the global infection threat? PHOTOGUN4MICROBES, the Ministry of Science, Technological Development and Innovation of the Republic of Serbia (Grant No. 451-03-68/2023-14/200017), and the HE TWINNING project GrInShield (Grant No. 101079151).

MAGNESIUM-DEPENDENT ATPASE AS A POSSIBILITY FOR THE INVESTIGATION OF DEPONATING ENVIRONMENTAL LOADS IN A HEPATOCYTE MODEL

Zsolt Molnár[1], Miklós Mózes[1], Marianna Radács[1], Péter Hausinger[2], Márta Gálfi[1], Krisztián Sepp[3]

[1]*Institute of Applied Health Sciences and Environmental Education, Juhász Gyula Faculty of Education, University of Szeged, Hungary*
[2]*Invasive Cardiology Unit, Department of Internal Medicine, Albert Szent-Györgyi Medical School, University of Szeged, Szeged, Hungary*
[3]*Department of Internal Medicine, Albert Szent-Györgyi Medical School, University of Szeged, Szeged, Hungary*
e-mail: molnar.zsolt.02@szte.hu

Abstract

Chemicals that load the environment can be chlorobenzenes with massive chemical stability. They induce a dose-dependent toxic effect in the cells of affected tissues, and because of their high frequency of occurrence in the food chain, they can be used as expositors in environmental exposure models. In this work, we wanted to investigate the magnesium-dependent ATPase activity of chlorobenzenes in hepatocytes.

Introduction

Changes in material and energy transfer can be detected in cells exposed to chlorobenzenes (ClB) [1]. ClB affect homeostasis and/or its regulation, including psycho-immuno-endocrine regulation [2]. The known effects of ClB in toxic doses have been confirmed in embryogenesis, increased risk of spontaneous abortion, intrauterine growth retardation, premature birth, and lower birth weight [3]. Furthermore, their carcinogenic, and immunotoxic effects are known [4]. However, it is very important to emphasize that these agents can also generate changes in psychological processes, such as mental and psychomotor functions [5].

Hepatocytes (HC) are significant cells in systemic relationships and xenobiotic transformations [6]. In the mentioned endodermal cells, the key of discrete energy transfer is Mg^{2+}-dependent ATPase [7]. Mg^{2+}-dependent ATPase is an integrated ectomembrane ATPase, its operation involves the hydrolysis of 3'-5'-adenosine triphosphate (ATP). These membrane units provide energy for many cellular biological processes by converting ATP molecules into 3'-5'-adenosine diphosphate (ADP) and then to 3'-5'-adenosine monophosphate (AMP) molecules, $\{P_3O_{10}^{5-}\}$ groups by generating $\{P_2O_7^{4-}\}$ and $\{PO_4^{3-}\}$ groups [8]. Hydrolysis-controlled energy changes depend significantly on the pH, temperature, and metal ion concentration of the system. In this sense, Mg^{2+} plays a key role, as they are important substrates for the formation of [Mg^{2+}-ATP] complexes, which can be further cleaved by the Mg^{2+}-dependent ATPase, and the mentioned transport process can take place [9]. The purpose of this study was to monitor the effects of different doses of ClB treatments on changes in energy transfer (Mg^{2+}-ATPase) of HC.

Experimental

In vivo protocol

Male Wistar rats (Charles River, Isaszeg, Hungary, medically certified) from different litters (weighing 120-250 g, aged 4-6 weeks at the beginning of the research) were used for cell culture model systems. Animal care and research protocols were in full accordance with the guidelines of the University of Szeged, Hungary. During the research period, rats were kept under controlled relative air humidity of 55-65% and 22±2°C ambient temperature. The experimental animals lived under automated diurnal conditions (12 h dark and 12 h light system). Standard pellet food (CRLT/N, Charles River, Magyarország) and tap water were available *ad libitum*. Male Wistar rats were treated with combined ClB (1:1 mixture of 1,2,4- trichlorobenzene /CAS number: 2199-72-6, Sigma Aldrich, USA, St. Louis) and hexachlorobenzene / CAS number: 93952-14-8, Sigma Aldrich, USA, St. Louis), in 1 mL of 0.015% ethanol in distilled water was administered daily) in a dose of 0.1, 1.0 and 10.0 μg/b.w. kg via a gastric tube. Rats were exposed to ClB for 30 (n=5), 60 (n=5) and 90 (n=5) days. Control groups were established: stress control (n=5, gastrostomy tube insertion group), absolute control (n=5, untreated group), positive control group (n=5, receives ClB solvent, 0.015% ethanol solution via gastric tube) and negative control group (n=5, receives water via gastric tube). At the endpoints of the experiment (30, 60 and 90 days), after pentobarbital anaesthesia (4.5 mg/b.w. kg, Nembutal, Abbott, USA) the animals were killed and decapitated.

In vitro protocol

Rat HC were separated under a dissecting microscope. From liver tissue by enzymatical (trypsin: 0.2 % /Sigma Aldrich, USA, St. Louis/ for 30 minutes; collagenase / Sigma Aldrich, USA, St. Louis /: 30 μg/mL for 40 minutes; dispase / Sigma Aldrich, USA, St. Louis/: 50 μg/mL for 40 minutes, phosphate buffer was used /PBS-A/; temperature: 37°C) and mechanical dissociation (using a nylon-blutex filter with pore diameter of 48 μm), primary monolayer cell cultures were prepared. Monolayer HC cultures were maintained in Williams' Medium E medium (Sigma, Germany) [10]. Cell proliferation induction was performed on separate reference systems treated with 1 mg/mL benz[c]-acridine (BcA) for 168 h. *In vivo* HC pretreated with ClBs were treated with exposure of ClBs (0.1; 1.0; 10.0 μg/mL) for 168 h.

Mg^{2+}-ATPase activity determination

The Mg^{2+-}dependent ATPase activity after ClB treatment was measured using the modified method of Martin and Dotty to follow discrete energy changes in cell energy transfer. ATPase activity is expressed as control %.

Statistical analysis

To compare the means of different treatment doses (0.1, 1.0, 10.0 μg/b.w. kg) to the controls during 30-, 60-, and 90-days long treatments (n=5 in each group of time and dose) two-way ANOVA was performed. Dose and time were used as the two factors for analysis.

The two-way ANOVA showed a significant difference between the group averages overall ($p<0.001$). Statistical analyses were carried out using IBM SPSS Statistics, version 21 software (IBM Corporation, Armonk, NY, USA).

Results and discussion

According to environmental aspects, if a process originating from an impact factor causes a change in the studied environmental factor or its state, in this case alterations in enzyme activity may be as direct effects. The results are presented to the absolute control group.

Number of tumour clones as a result of ClB treatments

	Hepatocyte
AC	0
BcA	65.7±5.1*

Table 1. The number of tumour clones in response to the absolute reference control (AC) and benz[c]-acridine (BcA) treatment (number of cells±sem, *:p<0.001)

From the data in Table 1, BcA significantly induced tumour clones in the model system, confirming that the experimental setup is suitable for the numerical detection of tumour cells.

	Hepatocyte		
ClB treatment	**30 days**	**60 days**	**90 days**
ClB 10.0 µg/bw.kg	0	1.6± 0.05*	1.9±0.008*
ClB 1.0 µg/bw. kg	0	0.71±0.05*	0.03±1.39*
ClB 0.1 µg/bw.kg	0	0	0.54±0.01*

Table 2. The number of tumour clones in the different cell populations as a result of each ClB treatment (number of cells±sem, *:p<0.001)

The data in Table 2 clearly show that the number of tumour clones in the HC cell cultures increased depending on the dose and time.

Changes in Mg^{2+}-dependent ATPase due to exposure to ClB

The activity of Mg^{2+}-dependent ATPase capable of AC group activity (100%) was significantly increased by benz-(c)-acridine treatment in HC (178.7±8.19%).

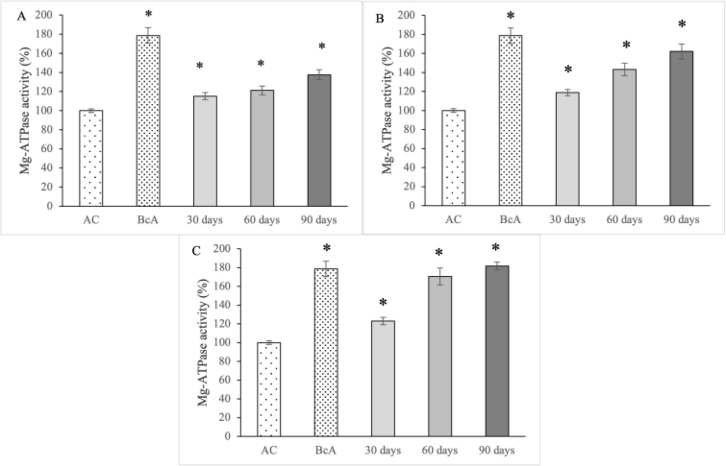

Figure 1. Effects of different exposures to the ClB mix on the activity of Mg^{2+}-dependent ATPase in HC cell cultures (A: 0.1 µg/bw. kg, B: 1.0 µg/bw. kg, C: 10.0 µg/bw. kg doses, *:p< 0.001, n=5/group)

The data in Figure 1 clearly show that the enzyme activity increased significantly (p<0.001) as a function of time and dose. After 90th day of the experiment, 1.0 µg/bw. kg dose exposures (162.1±7.8%) gave a value that approximates the effect of benz-(c)-acridine.
Enzyme activity exceeded (181.7±4.2%) the value of the reference system after 90 day by the effects of a dose of 10.0 µg/bw. kg of ClB.

ClB can also be classified as artificial compounds created during chemical reactions, which can generate changes in many physiological processes. Living systems are affected by complex environmental exposures *in vivo*; however, if these exposures are very low (subtoxic concentrations), they can exert their effects in a latent manner for a long time. If the artificial ClB can generate changes in the central axis and in the peripheral elements, then in a more appropriate approach, we should call these agents homeostatic disruptor compounds. ClB-mix exposures caused a dose-dependent increase in cell proliferation, accompanied by an increase in Mg^{2+}-dependent ATPase activity. However, extremely low doses of ClB treatments did not result in significant changes in transformation activity. According to our morphological observations, ClB treatments induced tumour clone formation in the first generations of primary cell cultures in a time- and dose-dependent manner. As a result of treatment with a higher dose of ClB, tumour clone formation was generated in all primary cell cultures we examined after only 60 days. The initiation effect of ClB was expressed less in the central regulatory elements but more intensively in the peripheral cells. HC cell cultures responded with a sensitive reaction to the chemical agents included in the experiment. If we examine Mg^{2+}-dependent ATPase activity, which indicates the discrete energy transfer of cells, after 30 days all cell types showed an increase in the typical activity because of ClB treatment. The Mg^{2+}-ATPase, located in cell membrane, provides energy through increased hydrolysis of ATP. The release of the energy inherent in the macroergic bond also led to protein production at the cellular level.

Conclusion

The Mg^{2+}-dependent ATPase enzyme shows that the energy from ATP splitting is connected to the cell's own energy supply, and this also manifests itself in increased cell activity. Tumor cells can be characterized by increased cell proliferation activity and increased protein production [10]. This means that ClB included in the model study have an effect on both initiation and promotion. Thus, it can be established that ClBs exert a general effect on cells.

Acknowledgements

This study was supported by EFOP-3.6.1-16-2016-00008, EFOP-3.4.3-16-2016-00014, TÁMOP-4.2.4.A/2-11/1-2012-0001 and Juhász Gyula Faculty of Education’s "Scientific and Artistic Activity Support Grant".

References

[1] A.C. de Tomaso Portaz, G.R. Caimi, M. Sánchez, F. Chiappini, A.S Randi, D.L. Kleiman de Pisarev, L. Alvarez, Hexachlorobenzene induces cell proliferation, and aryl hydrocarbon receptor expression (AhR) in rat liver preneoplastic foci, and in the human hepatoma cell line HepG2. AhR is a mediator of ERK1/2 signaling, and cell cycle regulation in HCB-treated HepG2 cells. Toxicology. (2015) 336:36-47.

[2] J.L. Barber, A.J. Sweetman, D. Wijk, K.C. Jones, Hexachlorobenzene in the global environment: emissions, levels, distribution, trends and processes. Sci Total Environ. (2005) 349, 1-44.

[3] K. Sepp, Zs. Molnár, A.M. László, T. Alapi, A. Serester, Zs. Valkusz, M. Gálfi, M. Radács, Study of the potential endocrine-disrupting effects of phenylurea compounds on neurohypophysis cells in vitro. Int J Endocrinol. (2019) 1546131.

[4] S.N. Young, R.O. Pihl, C. Benkelfat, R. Palmour, M. Ellenbogen, D. Lemarquand, The effect of low brain serotonin on mood and aggression in humans. Influence of baseline mood and genetic factors. Adv Exp Med Biol. (1996) 398, 45-50.

[5] A. Ichihara, T. Nakamura, K. Tanaka, Use of hepatocytes in primary culture for biochemical studies on liver functions. Mol Cell Biochem. (1982) 43(3): 145-60.

[6] V.M. Vasic, M.B. Čolovic, D.Z. Krstic, Mechnaisms of Na^+/K^+–ATPase and Mg^{2+}-ATPase inhibition by metal ions and complexes. Hem. ind. (2009) 63: 499–509.
[7] A. Horvat, T. Orlic, A. Banjac, T. Momic, S. Petrovic, M. Demajo, Inhibition of rat brain ecto-ATPase activity by various drugs. General Physiology and Biophysics. (2006) 25: 91-105.
[8] R. Betto, L. Senter, S. Ceoldo, E. Tarricone, D. Biral, G. Salviati, Ecto-ATPase activity of a-sarcoglycan (adhalin). The Journal of Biological Chemistry. (1999) 274: 7909-7312.
[9] A. Chihara, T. Nakamura, K. Tanaka, Use of hepatocytes in primary culture for biochemical studies on liver functions. Mol Cell Biochem. (1982) 43(3): 145-60.
[10] Z. Zhang, Y. Zhang, S. Xia, Q. Kong, S. Li, X. Liu, C. Junqueira, K.F. Meza-Sosa, T.M.Y. Mok, J. Ansara, S. Sengupta,Y. Yao, H. Wu, J. Lieberman, Gasdermin E suppresses tumour growth by activating anti-tumour immunity. Nature. (2020) 579(7799): 415-420.

STUDY OF MOLYBDENUM STABLE OXIDE FILM IN SIMULATED BODY FLUID

Andreea-Cristina Musat[1], Elena-Manuela Stanciu[1], Alexandru Pascu[1], Julia Claudia Mirza Rosca[1,2], Madalina Simona Baltatu[3], Petrica Vizureanu[3]

[1]Materials Engineering and Welding Depart., Transilvania University of Brasov, 29 Eroilor Blvd., 500036, Brasov, Romania
[2]Mechanical Engineering Department, University of Las Palmas de Gran Canaria, Campus Universitario Tafira, Edif. Ingenieria, 35017, Gran Canaria, Spain
[3]Department of Technologies and Equipment for Materials Processing, "Gheorghe Asachi" Technical University of Iasi, Bulevardul Profesor Dimitrie Mangeron 67, Iași 700050, Romania
Email: andreeamusat46@gmail.com

Abstract

This study's main goal is to thoroughly compare the mechanical attributes and biocompatibility of the recently created titanium alloy Ti15Mo7Zr15Ta1Si (62% Ti, 15% Mo, 7% Zr, 15% Ta, 1% Si) to that of the pure metal Mo. The samples underwent a series of meticulous preparation procedures, including chip preparation, polishing, grinding, and cutting, to enable a thorough evaluation. These preparation steps were essential for ensuring the samples' consistency and uniformity, which allowed for accurate and reliable analyses of their mechanical and corrosion-related properties. The samples' microstructure and surface morphology were also investigated using metallographic techniques, allowing a thorough examination of any potential flaws, grain boundaries, or phase compositions.

Additionally, electrochemical tests were used to investigate the materials' corrosion resistance and electrochemical characteristics in environments that mimicked physiological conditions. The samples were subjected to a variety of electrochemical analyses, such as polarization curves and impedance spectroscopy, in order for the researchers to fully comprehend the corrosion behavior of the materials and their suitability for biomedical applications.

Introduction

Titanium is a non-toxic element, even in large doses. Several studies have examined what would happen if humans consumed up to 0.8 mg of titanium daily, showing that Ti was eliminated without being absorbed or assimilated. A number of studies have demonstrated that titanium implants do not experience rejection because of its biocompatibility, favorable interactions with the host bone, and excellent corrosion resistance.

Molybdenum is a substance that is frequently used to alloy titanium Since Mo is a stabilizing element, some research in the field has shown that a percentage of about 20% Mo can reduce the modulus of elasticity and result in proper mechanical properties, similar to those of human bone. With regard to Cr, Ni, and Co, it is also a biocompatible element with a low level of toxicity.

The purpose of this experiment is to compare the degree of corrosion of molybdenum with that of the alloy and to observe if it is quite favorable for the medical environment, so the experiment is carried out in a liquid environment, namely in Ringer's solution.[1]

Experimental

Epoxy resin was first added to molds in a 4:1 ratio to prepare the surfaces of the two samples for embedding. In other words, four drops of resin were added for every one drop of catalyst.

The samples were then longitudinally cut at a thickness of 1 to 1.5 mm using a Buehler IsoMet 4000 precision saw (Buehler, Lake Bluff, IL, USA).

The cutting tool was also used to make roughly 0.5 mm thick vertical cuts. Next, grinding and polishing were carried out in two steps using the Struers TegraPol-11 polishing machine (Struers ApS, Ballerup, Denmark): first, using silicon carbide papers with increasing grit sizes between 280 and 1200,

The samples, which contain Molybdenum metal and Ti15Mo7Zr15Ta1Si alloy, were cleaned and leveled to create a suitable surface for the experiment by using a "Struers" polishing machine at a speed of 150 rpm, for 3-6 minutes, with a force of 20N-40N. After using an 800P grit abrasive paper to remove impurities, they were cleaned with water and alcohol.

The samples were then heated "Ultrasons-HD" ultrasonic equipment from J.P. Selecta (JPS, Barcelona, Spain) for ten minutes to remove any last traces of dirt or contaminants. 4 of 23 surfaces were coated with an alpha alumina suspension to give them a mirror-like sheen. For peer review, see Bioengineering 2022, 9, x. The experimental techniques used to prepare samples for metallography were in accordance with ASTM E3-11(2017). The phases and compounds that make up a metallic material, as well as any impurities or potential mechanical flaws, are arranged spatially in metallography.

In an electrochemical cell with three electrodes—the samples served as the working electrodes, the reference electrode was a saturated calomel electrode, and the counter electrode was a platinum electrode—the samples were sequentially added for the electrochemical tests.

The region of each sample was determined before the tests were carried out. The mmol/L values for the Grifols Laboratories' Ringer solution (Barcelona, Spain) were Na+ 129.9, Cl 111.7, C3H5O3 27.2, K+ 5.4, and Ca2+ 1.8. [1]

The Corrosion Potential, Corrosion Rate, and Electrochemical Impedance Spectroscopy procedures were carried out using the BioLogic Essential SP-150 potentiostat from Seyssinet-Pariset in France. The tests were carried out at 25°C in an aerated Ringer solution.

By entering the sample surface area value and the 20-minute test period, the "Linear Polarization" approach used in these experiments was found to be viable. Data were collected every 0.50 seconds during the potential scanning, which revealed a 0.167 mV/s time-variation relationship between 0.025 and 0.025 V against the open circuit potential (OCP) and an intensity that remained at 100% throughout the procedure. These linear polarization curves were presented and the corrosion rate estimates for each sample were obtained using EC-Lab's "Tafel Fit" technique. The surface value and the five-minute measurement period were entered, and the impedance measurement method was selected as "Potential Electrochemical Impedance Spectroscopy". This measurement was carried out seven times for each sample at 300 mV vs. Ecorr in Ringer's solution, with 10 V being the highest and lowest potential values. To illustrate these data, equivalent circuits and Bode and Nyquist diagrams were used.[3]

The Future Tech FM-810 hardness tester (Kawasaki, Japan) was used to take 10 measurements for each sample's applied load, in this case 1, 5, and 10 gf, in accordance with ISO 14577-1:2015 [32]. The mark may contain fragments from various phases as the stress increases, providing an approximation of the material's overall hardness. When relatively light weights are positioned, it is possible that the mark will only be discovered in one phase, allowing one to gauge the difficulty of that phase. The Vickers microhardness values were then computed automatically by the iVicky software (v2.0, Sinowon, Dongguan, China) using the observed diagonal lengths. The number of indents made were plotted against the scan length.[2]

Results and discussion

With reference to the corrosion potential depicted in Figure 1, it is clear that molybdenum and Ti15Mo7Zr15Ta1Si behave differently. A stable corrosion potential over time indicates that Ti15Mo7Zr15Ta1Si has a significant tendency to passivate, according to the data. By strengthening the material's resistance to corrosion, this passivation phenomenon which is typified by the creation of a protective oxide layer improves its longevity and performance in harsh environments.

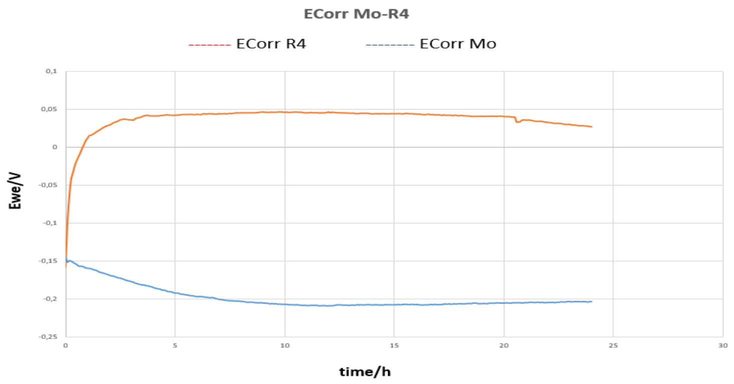

Figure 1. Corrosion Potential

On the other hand, the graph shows that molybdenum corrodes gradually, indicating that it is susceptible to the corrosive effects of the surrounding medium. When using molybdenum in applications where exposure to corrosive agents is anticipated, this gradual corrosion tendency highlights the need for careful consideration. It also highlights the significance of implementing appropriate protective measures or investigating alternative materials with higher corrosion resistance for such environments.

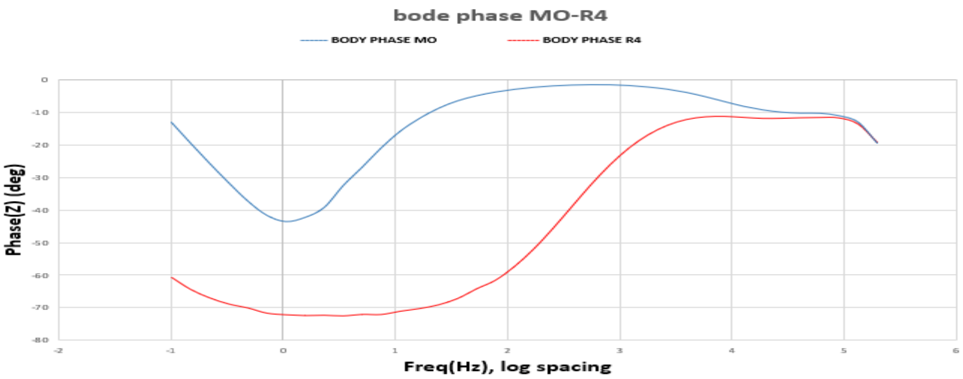

Figure 2. Bode-Phase in Ringer solution

When analyzing the Bode spectra (Figure 2), we can see that Ti15Mo7Zr15Ta1Si has a large zone with a high phase angle (almost -80 deg.), indicating that it has high corrosion resistance properties, while Mo exhibits a narrow, non-point dense pit that may be related to a weak passivating effect that cannot adequately protect the material.

According to the Bode-IZI spectra, which confirmed what had been stated previously in relation to the Bode-phase graph (Figure 2), Ti15Mo7Zr15Ta1Si exhibits high impedance levels, which are indicative of strong corrosion resistance. On the other hand, Molybdenum, characterized by its remarkably lower impedance level, significantly enhances its resistance to corrosion. This property positions it as an invaluable asset in environments where the prevalence of corrosive agents poses a persistent threat to the structural integrity of materials.

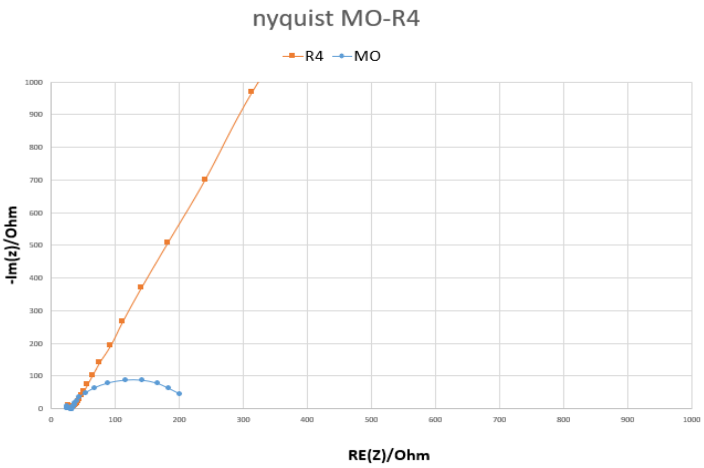

Figure 3. Nyquist spectra in Ringer solution

Finally, it is evident from the data that the Ti15Mo7Zr15Ta1Si alloy, characterized by its remarkable stability, displays a propensity for passivation, a process in which it forms a protective oxide shield. This oxide shield acts as a formidable barrier against corrosion, further enhancing its resistance to the degrading effects of corrosive agents. In contrast, Molybdenum exhibits a different behavior, notably manifesting pitting corrosion phenomena when subjected to potential values of approximately 0.1 V versus the standard saturated calomel electrode (SCE). This observation underscores the vulnerability of Molybdenum to localized corrosion, emphasizing the importance of considering these materials' distinct corrosion characteristics when selecting them for specific applications.

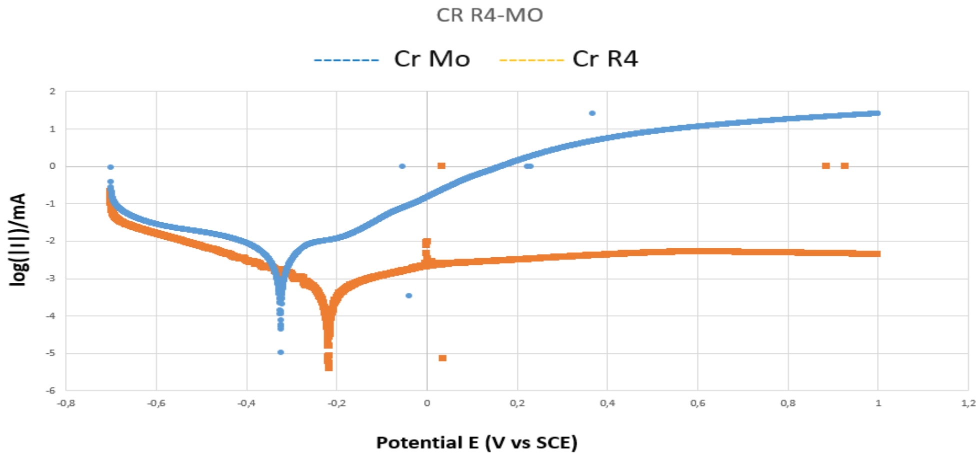

Figure 4. Corrosion Rate

Linear polarization curves in Ringer solution

Conclusion

While molybdenum is typically known for its resistance to corrosion in specific environments, its behavior can change when complex solutions like Ringer's solution are present. This environment in particular, which is frequently used to simulate physiological conditions in biological experiments, contains a variety of ions and substances that may cause specific reactions with molybdenum, resulting in gradual corrosion over time. Due to its exceptional qualities of strong corrosion resistance, remarkable stability, and innate passivating abilities, the Ti15Mo7Zr15Ta1Si alloy stands out significantly. These characteristics make it a very strong candidate for a wide range of biological applications. Its superior corrosion resistance highlights its potential for use in challenging biological and biomedical environments where corrosion can degrade the performance and longevity of materials. This corrosion resistance surpasses that of the commonly used materials. It is ideally suited for implantable medical devices, prosthetics, and other biomedical tools due to its resistance to the physiological conditions found inside the human body and impressive mechanical strength.

Acknowledgements

I am grateful for the invaluable opportunity presented to me by the University of Las Palmas de Gran Canaria, along with the University Transilvania of Brasov Erasmus+, for the enriching traineeship experience that allowed me to contribute to this project. The collaborative environment and the guidance provided by the esteemed faculties and mentors have been instrumental in shaping my understanding and skills in this field.

References

[1] Jiménez-Marcos, C., Rosca, J. C. M., Bălţatu, M. S., & Vizureanu, P. (2022). Experimental research on new developed titanium alloys for biomedical applications. Bioengineering, 9(11), 686. https://doi.org/10.3390/bioengineering9110686

[2] Jiménez-Marcos, C., Rosca, J. C. M., Bălţatu, M. S., & Vizureanu, P. (2023). Effect of SI contents on the properties of TI15MO7ZRXSI alloys. Materials, 16(14), 4906. https://doi.org/10.3390/ma16144906

[3] Jiménez-Marcos, C., Rosca, J. C. M., Bălţatu, M. S., & Vizureanu, P. (2023b). Evaluation of new titanium alloys as potential materials for medical devices. Microscopy and Microanalysis, 29(Supplement_1), 196-201. https://doi.org/10.1093/micmic/ozad067.088

PHYSICO-CHEMICAL AND BIOLOGICAL CHARACTERIZATION OF POMEGRANATE (*PUNICA GRANATUM* L.) PEEL EXTRACT MICROENCAPSULATES

Milica Radan[1], Nada Ćujić Nikolić[1], Snežana Kuzmanović Nedeljković[1], Zorana Mutavski[1], Nemanja Krgović[1], Smilja Marković[2], Tatjana Stević[1], Jelena Živković[1], Katarina Šavikin[1]

[1] *Institute for Medicinal Plants Research Dr Josif Pančić, Tadeuša Košćuška 1, 11000 Belgrade, Serbia*
[2] *Institute of Technical Sciences of SASA, Knez Mihailova 35/IV, 11000 Belgrade*
e-mail: zmutavski@mocbilja.rs

Abstract

Peel of the pomegranate (*Punica granatum* L.) fruit takes up for approximately 50% of the total weight, is a byproduct which is usually discarded as waste. However, pomegranate peel (PP) is considered as a rich source of potent phenolic compounds, including ellagic acid and its derivatives which possess several functional and nutraceutical qualities, including lowering blood pressure, reducing oxidative stress, decreasing blood sugar and cholesterol levels, and restoring heart health [1, 2]. The main aims of this study were to develop preserved microencapsulated systems of the pomegranate peel (PP) extract by spray-drying using two biocompatible carriers (pectin and its mixture with HP-β-CD) and to evaluate their physico-chemical properties as well as *in vitro* antimicrobial, antioxidant, and antidiabetic activities. Obtained micro-sized powders were characterized with high values of powder yield (> 78%) and satisfied moisture content, flowability and cohesive properties. According to the DSC analysis, carrier addition showed favorable impact on the thermal stability (up to 200°C) of examined microencapsulated samples. Chemical analysis showed that total phenolic content in spray-dried powders of PP varied between 373.15 to 427.88 mg GAE/g DW, with the punicalagin, punicalin, gallic acid, and ellagic acid as the most abundant individual bioactive compounds. Despite dilution effect, comparable free radical scavenging ability in DPPH assay was observed for microencapsulated and carrier-free powders (IC_{50}: 6.51-7.60 μg/mL). Furthermore, examined samples showed great potential to control elevated glycemic levels demonstrating potent inhibition effects against α-amylase and α-glucosidase enzymes. Molecular docking analysis provided more deeper insight into molecular mechanisms of action, revealing high affinity of ellagic acid to inhibit α-amylase enzyme, while punicalagin and punicalin more selectively inhibited α-glucosidase. Antimicrobial activity assay revealed that the Gram-positive bacteria, including *S. aureus* and *S. epidermidis* as representative skin pathogens, were the most susceptible with the minimum inhibitory concentration of 1.75 mg/mL. On the whole, valorization of PP through microencapsulation process with pectin and pectin/HP-β-CD as coating materials represents a sustainable approach for the development of ellagitannin-rich products that have the potential to be developed into phytopharmaceutical and functional foods for the prevention and management of metabolic diseases.

References

[1] Y. Mo, J. Ma, W. Gao, L. Zhang, J. Li, J. Li, J. Zang. Front Nutr. 9;9:887113 (2022)
[2] H. B. U. Ain, T. Tufail, S. Bashir, N. Ijaz, M. Hussain, A. Ikram, M. A. Farooq, S. A. Saewan. Food Sci Nutr. 23;11(6):2589-2598 (2023)

THE IMPORTANCE OF BEETROOT CONSUMPTION IN EVERYDAY LIFE

Vivien Csoszor[1], Anna Maria Nagy[2,3], Éva Stefanovits-Bányai[2], Mónika Máté[4], Zsuzsanna Mednyánszky[1]

[1]MATE Institute of Food Science and Technology, Department of Nutrition, H-1118 Budapest, Somlói út 14-16, Hungary
[2]MATE Institute of Food Science and Technology, Department of Food Chemistry and Analytics, H-1118 Budapest, Villány Street 29-43, Hungary,
[3]Holi-Medic Ltd., H-1117 Budapest, Fehérvári Street 44, Hungary,
[4]MATE Institute of Food Science and Technology, Department of Fruit and Vegetables Processing Technology, H-1118 Budapest, Villány Street 29-43, Hungary,
Email: holimedic@gmail.com

Abstract

There is a growing worldwide demand for healthy foods, such as fruit and vegetables, including beetroot (*Beta vulgaris* L. ssp. *esculenta* convar. *crassa* provar. *rubra),* with its extremely valuable content. During the measurements (amino acids, betanin and vulgaxanthin, polyphenol content, antioxidant capacity), the peel and flesh of commercially available spherical and oblong morphology beets as well as 4 organic beetroot juices of different origins (some with additional components) were examined. Based on the results, it was established that carrot root and biojuices have different amino acid compositions. It has been proven that the peel of beets is extremely rich in valuable components, which is also worth considering when consuming. When examining beetroot juices, added supplements, e.g. lemon juice, have an influencing effect on the measured parameters.

Introduction

Beetroot (*Beta vulgaris* L. ssp. *esculenta* convar. *crassa* provar. *rubra)* belongs to the *Chenopodiaceae* family, which includes about 1400 species [1,2,3]. It is rich in nutritional components, e.g. vitamins C, B1, and B2, due to its minerals (Fe, Mg, Ca, K), valuable amino acids (e.g. cysteine, methionine, glutamic acid), significant folic acid content, polyphenolic compounds [4,5,6,7,8,9.] and other bioactive components (betanin, vulgaxanthin) [10], it has a very beneficial physiological effect, e.g. on cardiovascular diseases, colon cancer, Alzheimer's disease and the list could go on [11,12,13,14,15.]

Materials and methods

For measurements, spherical and elongated morphological beets (*Beta vulgaris* L. ssp. *esculenta* convar. *Crassa* Provar. *rubra)* and organic beetroot juices were used, obtained commercially, and the following markings were used during measurements (Table 1). The chemicals used were purchased from Sigma-Aldrich.

Analytical methods

Sample preparation

The beets were peeled, then the peel and carrot root were homogenised separately (amino acid determination) and lyophilised (analytical measurements). From the lyophilised samples, a 20 mg/ml solution was prepared with distilled water. The solutions were placed in a cooled ultrasonic water bath for 1 hour, then after centrifugation (6000 rpm, 20 min10°C), the clean supernatants were stored in a refrigerator at -32°C until measurements. There was no sample preparation for beetroot juices.

Table 1: Markings used in measurements

Marking	Meaning
CHK	Elongated beetroot peel
CHB	Elongated beetroot carcass
CGK	Spherical beetroot peel
CGB	Spherical beetroot carcass
C1	dm bio rote bete saft (100% beetroot juice)
C2	Nature's Blessing with Organic Beetroot Juice (99% beetroot juice, 1% lemon juice)
C3	Spar Natur Pur Bio Rote Rübe (100% beetroot juice)
C4	Biopont Organic beetroot juice (99% beetroot juice, 1% cherry puree)

Determination of amino acids: AAA 400 Automatic Amino Acid Analyzer operating on the principle of ion exchange column chromatography. Results are given in mg/kg.

The extraction of samples was done with 10% trichloroacetic acid during 1 h agitation on a shaker at room temperature. After filtration through a 0.2 µm pore membrane filter, the detection of samples was done by an automatic amino acid analyser (Ingos Ltd., Czech Republic) equipped with an Ionex Ostion LCP5020 cation exchange column. The Li^+-citric buffer system (Ingos Ltd., Czech Republic) was used for the stepwise separation of free amino acids.

Determination of total phenolic contents (TPC) by Folin-Ciocalteu method: The Folin-Ciocalteu spectrophotometric method by Singleton and Rossi [16], at 760 nm is an electron transfer based on assay and shows the reducing capacity, which is expressed as phenolic content. Gallic acid (GA) was used to prepare the standard curve. The results were expressed as µM GA/g of dry matter (DM).

Determination of antioxidant capacities by FRAP (Ferric Reducing Antioxidant Power) method: Measurement of ferric reducing antioxidant power of the peel extracts was carried out based on Benzie and Strain's procedure [17], at 593 nm. Ascorbic acid (AA) was used as a standard to prepare the calibration solutions. Results were expressed as µMAA/g DM.

Determination of betanin- and vulgaxanthin: by spectrophotometric method ($\lambda = 476$, 538, 600 nm) by Joachim [18]. Results were expressed as mg/g dry matter and mg/L.

Results and discussion

There is no significant difference between in the % distribution of the flesh and peel of different form beetroots (Table 2).

2. Table: Flesh-peel ratio of different varieties of beets

	Flesh %	**Peel %**
Long	84,80±1,89	14,88±1,85
Spherical	81,54±4,22	18,11±4,23

In total free amino acid content, the spherical and the C2 beetroot juice showed the best results (Figure 1). Based on the distribution of individual amino acids, cysteine and its precursor, cystathionine, are examined together, and based on the results, it can be stated that an average of 10.3 mg is contained in 1 kg of beetroot and 7.36 mg in 1 litre of beetroot juice.

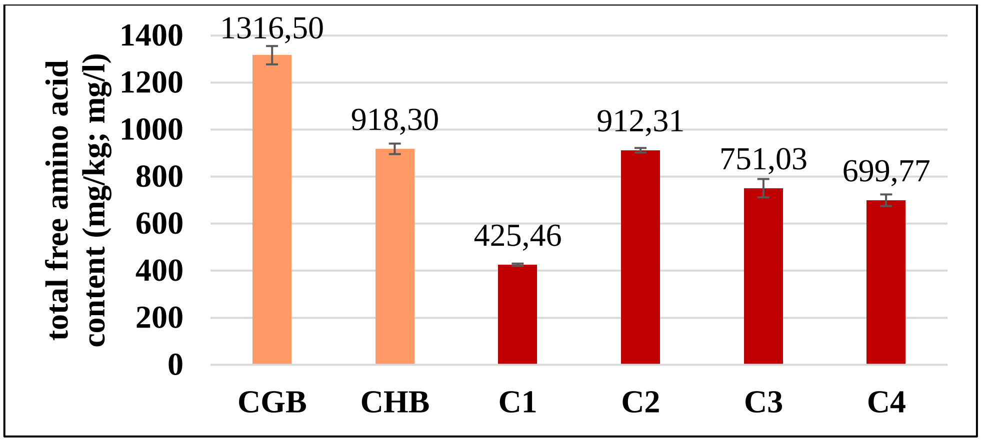

Fig. 1. Total amino acid content of beetroot beets and organic beetroot juices

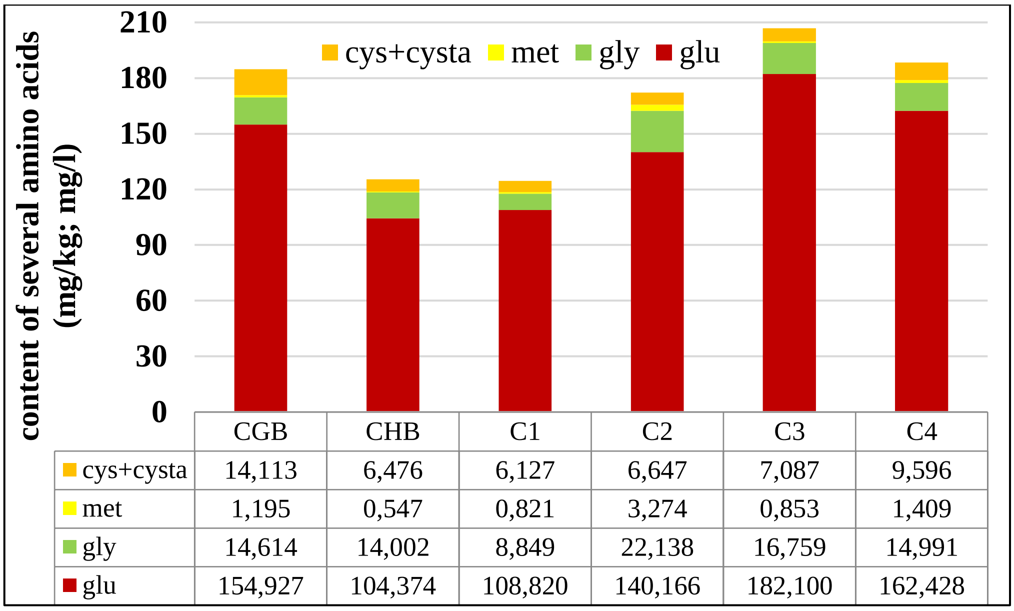

	CGB	CHB	C1	C2	C3	C4
🟧 cys+cysta	14,113	6,476	6,127	6,647	7,087	9,596
🟨 met	1,195	0,547	0,821	3,274	0,853	1,409
🟩 gly	14,614	14,002	8,849	22,138	16,759	14,991
🟥 glu	154,927	104,374	108,820	140,166	182,100	162,428

Fig. 2. Distribution of some amino acids in beetroot beets and organic beetroot juices

Examining the data of individual amino acids statistically, it can be seen that during the examination of beets, only the glycine content of the samples does not show significant differences (p=0.298). In the case of beetroot juices, samples C3 and C4 differ the least in glutamic acid, glycine and methionine content (p=0.239; p=0.185; p=0.183), while in cysteine content, they show even less significant difference, as we did not notice any significant difference at 95% significance level in samples C1-C2 (p=0.723), C1-C3 (p=0.281) and C2-C3 (p=0.809).

When examining the total polyphenol content (Figure 3), it can be stated that there is no significant difference between the corresponding parts of the two samples in the polyphenol content measured in the beet root and measured in the peel. Still, there is also a significant amount in the peel, which must be taken into account during kitchen processing.

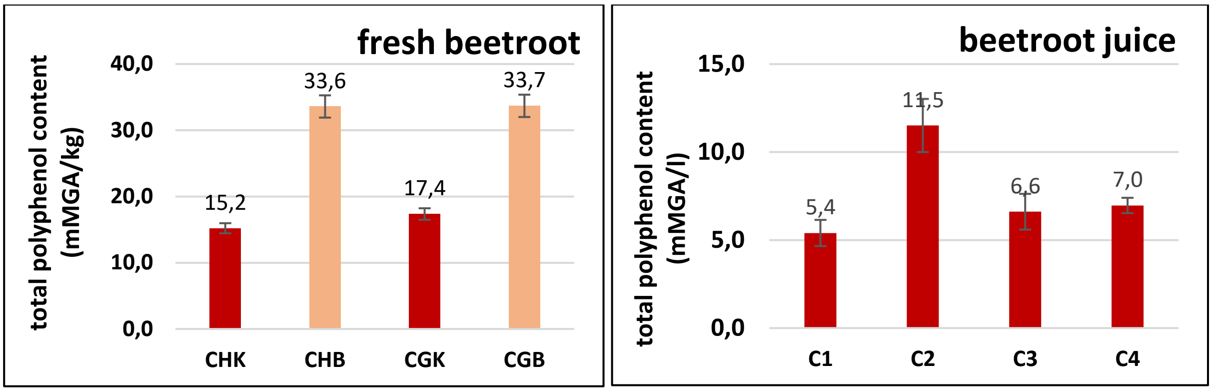

Fig. 3. Total polyphenol content of the various parts of beetroot and beetroot juices

In the case of organic beetroot juices, it can be stated that sample C2 has a significant polyphenol content compared to samples C1 (p=0.005), C3 (p=0.022) and C4 (p=0.028). This outstandingly high value can be attributed to the 1% lemon juice content.

Regarding the antioxidant capacity examined with FRAP (Figure 4), the carrot roots show a completely identical course as we saw for the polyphenol content.

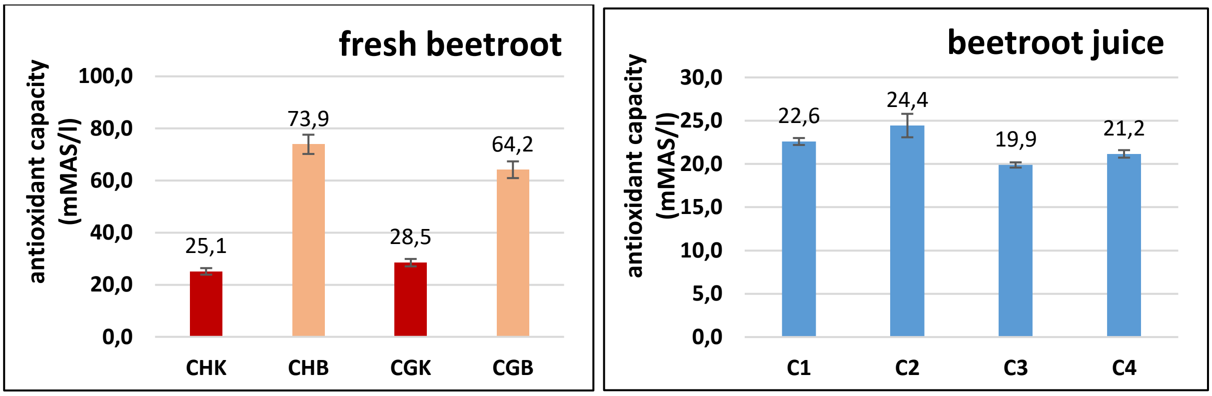

Fig. 4. Antioxidant capacity of beet carcasses and beetroot juices

In the case of beetroot juice (Figure 4), beetroot juices show balanced antioxidant capacity. Among the colouring substances, betanin is present in higher amounts in all samples (carrot root and organic beetroot juice), which in some cases can mean a 4-fold difference. The betanin content in peels is much higher, about twice as high as in carrot roots (Figure 5).

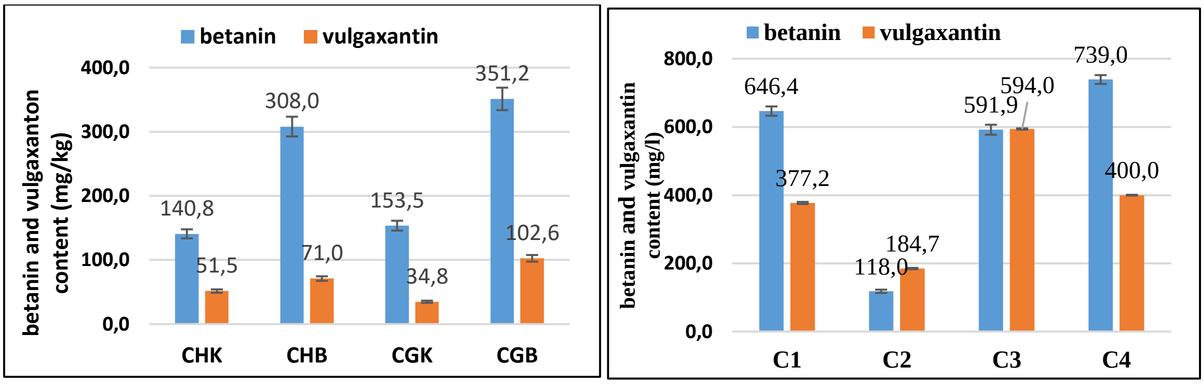

Fig. 5. The formation of betanin and vulgaxanthin in beet carcasses and beetroot juices.

Such a difference in vulgaxanthin content can not be observed; only in the case of the peel of the oblong beetroot sample an outstanding result can be observed. While in the case of peel, there was a significant difference between the measured values in the case of betanin (p=0.017) and vulgaxanthin (p<0.001) content, on the contrary, no significant difference was observed in the case of carrot roots (p=0.079; p=0.228). However, if we take into account the peel-to-flesh ratio as before, it can be seen that the carrot body of the round sample has the highest value, both in the case of betanin and vulgaxanthin content. This is followed by the beet fleshpeel of the long beetroot and then the peels, with values about half as large.

When examining organic beetroot juice samples (Fig. 4), interestingly, the C2 sample has the lowest value for the two colours, which is due to the dosed lemon juice.

Conclusion

During the examination of beetroot varieties and organic beetroot juices, it was proven that the peel of beets is extremely rich in valuable components, which should also be taken into account when consuming them and possibly incorporating them into our diet with proper processing. The study of organic beetroot juices showed that it is worth knowing the exact composition of the product at the time of purchase or before consumption since the added additives can significantly influence the individual favourable development of nutritional values.

References

[1] N. Chhikara, K. Kushwaha, P. Sharma, Y. Gat, A. Food Chem. 272 (2019) 192–200.
[2] A. Kovács (ed.): Growing root vegetables. Agricultural Publishing House, Budapest (2011)
[3] M.T. Hájos, T. Rubóczki, V. Raczkó, Int. J. of Hort. Sci., 21(3-4) (2015) 31-35.
[4] Gy. Judge, K. Lindner: Nutrient table. Medicina Publishing House, Budapest (1999)
[5] B. Nemzer, Z. Pietrzkowski, A. Spórna, P. Stalica, W. Thresher, T. Michałowski, S. Wybraniec, Food Chem. 127(1) (2011) 42–53.
[6] S.C. Chew, S. Loh, G.L. Khor, Int. Food Res. J. 19 (2012) 189–197.
[7] T. Vargas-Rubóczki, M. Takács-Hajos, Acta Agr. Debr.sci. (2019) 115-119.
[8] K. Tamilselvan, S. Nadanasabapathi, R. Kumar, Int. Food Res. J. 21 (2014) 1305-1312.
[9] D. Babarykin, G. Smirnova, I. Pundinsh, S. Vasilyeva, G. Krumina, V. Ageychenko, 7(3) (2019) 61–79.
[10] T. Clifford, G. Howatson, D.J. West, E.J. Stevenson, Nutr. 7(4) (2015) 2801-2822.
[11] U. Gröber, J. Schmidt, K. Kisters, Nutr. 7(9) (2015) 8199-8226.
[12] R. Swaminathan, The Clin. Biochem. Rev. 24(2) (2003) 47–66.
[13] S.J. Moat, D. Lang, I.F. McDowell, Z.L. Clarke, A.K. Madhavan, M.J. Lewis, J. Goodfellow, The J. of Nutr. Biochem. 15(2) (2004) 6479.
[14] B.A. Jennings, G. Willis, Cancer let. 356(2, Part A) (2015) 224–230.
[15] J.H. Yoo, G.D. Choi, S.S. Kang, Arterios., Throm., and Vasc. Biology 20(8) (2000) 1921–1925.
[16] V.L. Singleton, J.A. Rossi, Am. J. of Enol. and Viticult. 16 (1965) 144-158.
[17] I.F.F. Benzie, J.J. Strain, Biochem. 239(1) (1996) 70–76.
[18] H. von E. Joachim, Food. Chem. (1) (2011) F3.1.1 to F3.1.*7*

FRACTIONATED HIGH-PRESSURE EXTRACTION OF POLYPHENOLS FROM ELDERBERRY BY-PRODUCT

Nataša Nastić[1], Naiara Fernández[2], Jelena Živković[3], Zorana Mutavski[1,3] Anita Milić[1], Katarina Šavikin[3], Senka Vidović[1]

[1]Faculty of Technology, University of Novi Sad, Bulevar cara Lazara 1, 21000 Novi Sad, Serbia
[2]iBET, Instituto de Biologia Experimental e Tecnológica, Apartado 12, 2781-901 Oeiras, Portugal.
[3]Institute for Medicinal Plants Research "Dr Josif Pančić", Tadeuša Košćuška 1, Belgrade, Serbia.
e-mail: natasa.nastic@uns.ac.rs

Abstract

The main focus of this study was to propose new streams to use plant waste, specifically to put on the demonstration of the possibility to implement emerging, green and safe technology into food and pharmaceutical industries in order to enable more economical waste management. For the isolation of valuable compounds from elderberry press cake (by-product left after pressing of juice), solvents and techniques considered as "acceptable" and "generally regarded as safe" in the food and pharmaceutical industries have been applied. Polyphenols rich elderberry press cake extracts were obtained employing a fractioned high-pressure methodology, supercritical fluid (SFE) and enhanced solvent extractions (ESE). SFE-CO_2+ESE comprising a first SFE-CO_2 step in order to remove the low polarity CO_2-soluble compounds, and a second ESE step in order to extract polar compounds like anthocyanins have been carried out, as well as ESE without any pretreatment. The process kinetics of the extraction and increase of extraction yields (EY) were monitored at time intervals from 10 to 90 min, while EYs of ESE were measured after 30-220 min of extraction. Higher extract yield occurred in extract obtained by SFE-CO_2+ESE (28.70%) showing its advantage over ESE. According to the kinetics results for the two-step extraction approach, extraction time of 100 min might be sufficient to achieve the similar final EY obtained after 220 min. HPLC of obtained extracts was utilized for quantification of polyphenolic compounds, showing cyanidin-3-O-sambubioside as a main compound, followed by rutin and cyanidin-3-O-glucoside. This work is the first to produce anthocyanin-rich fractions from black elderberry press cake using such high-performance technique.

Introduction

The importance of green chemistry application and its technologies in improving sustainability is growing, which is reflected in the reduction of water and energy consumption, and the use of hazardous materials, as well as in achieving sustainability in social, economic and environmental performance. Starting from the last decade of the 20th century until today, the efforts have been directed to development of new technologies that comply with strict environmental requirements, so most of the recent research focuses on the development of green technologies and their potential application in industry [1]. Since these are new technologies, it is necessary to constantly and rapidly work on the acquiring new knowledge and comprehensively expand it in all directions and in terms of all green technologies.

Therefore, this study was focused on agro-food waste which is attractive in its composition and in that sense, its processing using green techniques can give a new product with added value and functionality. Black elderberry press cake (*Sambucus nigra* L.) is a byproduct from the production of black elderberry juice. It is mostly composed of hemicellulose and cellulose, but it also represents an important source of polyphenolic compounds [2]. Namely, the recent studies reported that the main part of the black elderberry polyphenolics - anthocyanins remain in the press cake after juice pressing [3]. Plant-based products rich in anthocyanins have a pharmacological relevance and therapeutic application due to their antioxidant properties. Anthocyanins can reduce neurological diseases and heart diseases risk, and exert an anti-inflammatory role related to obesity and diabetes [4,5]. However, despite the high nutrition and pharmacological value and economical interest in bioactive substances this by-product is underutilized.

In the recent years, thanks to new scientific cognitions related to the mechanisms of separation of compounds from complex matrices, significant progress was made in the technology of pharmacologically active compounds of natural origin and their isolation. Special attention was paid to the development of chemical processes which make use of solvents that do not pollute the environment. Beside of these solvent characteristics, focus of the scientific community was directed to the solvents which are at the same time non-toxic and safer, but efficient enough for bioactive compounds extraction from various natural resources. Therefore, for the isolation of valuable compounds from elderberry press cake, with consideration to safety, low price, selectivity and solvating properties of solvents, this study investigated the possibilities of supercritical fluid extraction (SFE) and enhanced solvent extraction (ESE). These techniques will be used in order to improve polyphenols', specifically anthocyanin's thermal stability without the need of employing high temperatures during isolation, limiting inactivation of the anthocyanins and generally achieving high extraction efficiency. The obtained extracts were analyzed by high performance liquid chromatography with diode array detection (HPLC-DAD) to identify and quantify the main phenolic compounds.

Experimental

Fresh black elderberry press cake (*Sambucus nigra* L.) was provided by a factory focusing on harvesting and processing forest fruits (NISHA d.o.o., Belgrade, Serbia). The raw material was dried using a vacuum dryer and ground in a blender. The average particle size (1.05 ± 0.16 mm) and moisture content (6.69 ± 0.13%) were determined.

The fractionated high pressure extraction assays were performed using the extraction unit described by Seabra et al. [6]. Experiments were carried out with and without a previous defatting step with SFE-CO_2 followed by ESE with CO_2/EtOH-H_2O mixture, to obtain polyphenols rich fractions in the second step. The influence of SFE-CO_2 pretreatment was studied concerning the total extraction mass yield (EY). The EY was expressed as the mass of obtained dry extract (g) per g of dry plant material, i.e., percentage (%). The process kinetics of the extraction and increase of EYs were monitored at time intervals of 10, 20, 30, 45, 60, and 90 min, while EYs of ESE were measured after 30, 40, 70, 100, 130, 160, 190, and 220 min of extraction. The ESE process conditions, pressure (20 MPa), temperature (40°C), and CO_2/EtOH/H_2O mixture proportion (80:1:19, %, v/v/v) were held constant. The same pressure and temperature were applied for SFE-CO_2 pretreatment. Extraction conditions were selected taking into consideration the results obtained by Seabra [7] and the literature information concerning the anthocyanin stability Jackman et al. [8].

Analyses of individual polyphenolic compounds were carried out on an Agilent 1200 RR system (Agilent, Waldbronn, Germany) with a diode array detector. A reverse-phase Lichrospher RP-18 (Agilent) column (250 mm × 4 mm, 5 µm) was used, and the column temperature was maintained at 25°C. The mobile phase consisted of solvent A (10%, v/v solution of formic acid in water) and solvent B (acetonitrile), using gradient elution as follows: 1% B, 0–0.5 min; 1–7% B, 0.5–1 min; 7% B, 1–4 min; 7–10% B, 4–7.5 min; 10–14% B, 7.5–

11.5 min; 14–25% B, 11.5–15.5 min; 25–40% B, 15.5–18.5 min; 40–75% B, 18.5–22 min; 75% B, 22–25 min. The injection volume was 10 µL, the flow rate was 1 mL/min and the detection wavelengths were set at 290, 350 and 520 nm. The contents of the compounds were calculated using calibration curves. The results are presented as micrograms per gram of dried extract (µg/g DE).

Results and discussion

Two different extraction approaches, namely fractionated high-pressure extraction (SFE-CO_2+ESE comprising a first SFE-CO_2 step in order to remove the low polarity CO_2-soluble compounds, and a second ESE step in order to extract polar compounds like anthocyanins) and only ESE, were exploited to isolate polyphenols from elderberry press cake. The elderberry press cake SFE (first step) and ESE (second step) in both extraction approaches exhibited a typical overall extraction curve profiles. For all SFE and ESE experiments, total extraction time was set to 90 and 220 min, respectively, to guarantee the diffusional period. Both experimental extraction kinetics curves regarding ESE and polar fraction isolation are clearly divided in two distinct zones (Figure 1). In the first zone, the yield increases with increasing extraction time, indicating a faster solubility of active compounds into the extraction media. In the second zone, the yield was maximized into the steady-state yield, indicating that mobility of active compounds from elderberry press cake into the extraction media approaches zero in the remaining time. In conclusion, extraction time of 100 minutes might be sufficient to achieve the similar final extraction yield obtained after 220 minutes.

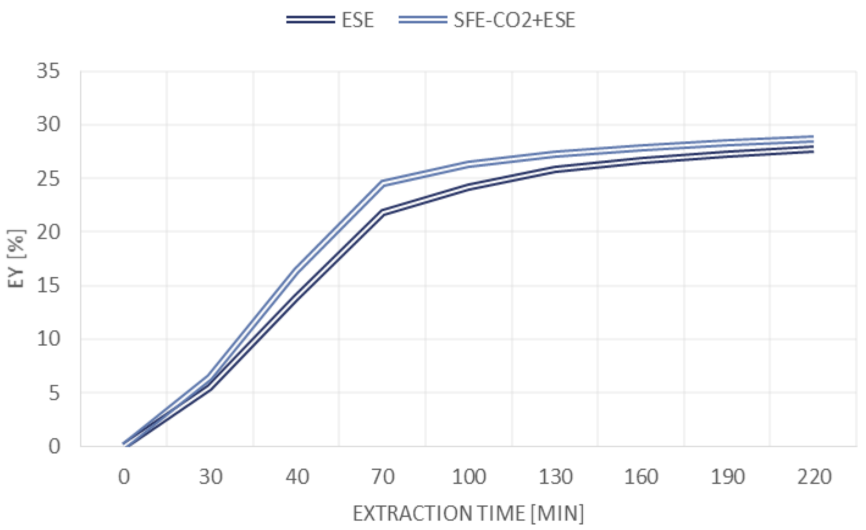

Figure 1. Kinetic curves regarding ESE and polar fractions in both extraction approaches.

During the first SFE-CO_2 step, essentially lipophilic compounds were extracted (Table 1). An extract fraction presenting a yellow color, without anthocyanins, was obtained during the first few minutes of the ESE continuous process (second step), for both extraction approaches. These fractions should contain the low polarity compounds. Higher yields of polar fractions were obtained for fractioned high-pressure extractions with ethanolic mixture in the second step (ESE) when compared to those obtained only by ESE. The main contribution to this difference was essentially due to the first step, wherein the less polar substances were extracted. Since anthocyanins are mainly located in outermost layer of elderberry skin cell walls wherein the fatty acids and waxes exist, an effective lipophilic substances removal, in a first SFE-CO_2 step, can make polar material more available for extraction. Higher yields of polar and non-polar compounds obtained by $SFE-CO_2$+ESE show its advantage over ESE.

Table 1. EYs of elderberry press cake extracts obtained by ESE and $SFE-CO_2$+ESE.

			ESE	**SFE-CO_2+ESE**
		Extraction time [min]	EY [%]	
SFE-CO_2	non-polar fraction	10	-	1.02
		20	-	2.71
		30	-	3.80
		45	-	6.78
		60	-	8.59
		90	-	9.08
ESE	non-polar fraction	30	6.09	0.38
	polar fraction	30	5.53	6.38
		40	13.91	16.32
		70	21.80	24.48
		100	24.22	26.27
		130	25.79	27.23
		160	26.70	27.88
		190	27.25	28.31
		220	27.72	28.70

[1] The phenolic compounds in black elderberry press cake extracts were identified and quantified by HPLC-DAD analysis. The polyphenolic profile of elderberry press-cake extracts is presented in Table 2. A significant difference was observed in the concentrations of quantified compounds in ESE with and without pre-treatment, being the $SFE-CO_2$+ESE more effienct in terms of phenolic compounds contet. The highest concentration had cyanidin-3-O-sambubioside (2559.37 µg/g DE), followed by rutin and cyanidin-3-O-glucoside.

[2]

[3] Table 2. Characterized compounds in elderberry press cake extracts using HPLC-DAD.

[4]

Sample	C3Gal [µg/g DE]*	C3Sam [µg/g DE]*	C3Glu [µg/g DE]*	RUT [µg/g DE]*	IQ [µg/g DE]*	p-KUM [µg/g DE]*	PC [µg/g DE]*
SFE-CO_2 + ESE	60.66 ± 3.50^{a}	2559.37 ± 270.48^{a}	1187.17 ± 81.38^{a}	1794.70 ± 264.33^{a}	683.08 ± 43.90^{a}	21.85 ± 2.80^{b}	501.59 ± 50.53^{a}
ESE	tr	tr	tr	tr	tr	97.68 ± 5.02^{a}	tr

*Different letters within a column indicate a significant difference between samples at $p < 0.05$; SFE - supercritical fluid extraction; ESE - enhanced solvent extraction; DE - dried extract; C3Gal - cyanidin-3-O-galactoside; C3Sam - cyanidin-3-O-sambubioside; C3Glu - cyanidin-3-O-glucoside; RUT - rutin; IQ - isoquercitrin; p-KUM - p-kumaric acid; PC - protocatechuic acid. Tr – trace.

Conclusion

In this work, green-based extraction approaches were applied to extract mainly phenolic compounds from black elderberry press cake being a part of the zero-waste valorization concept. SFE-CO_2+ESE has proven to be highly efficient for the extraction of polyphenolic compounds from black elderberry press cake. The highest concentration was reported for cyanidin-3-O-sambubioside, followed by rutin and cyanidin-3-O-glucoside. These results showed that two step extraction approach enabled the production of natural fractions from industrial elderberry press cake with acceptable characteristics to be used for the development of nutraceuticals and different food formulations.

Acknowledgements

[5] The authors are grateful to the Serbian Ministry of Education, Science and Technological Development (451-03-68/2022-14/200134). The publication is based upon work form COST Action Green Chemical Engineering Network towards upscaling sustainable processes, CA18224, supported by COST (European Cooperation in Science and Technology).

References

[1] S. Vidović, J. Vladić, N. Nastić, S. Jokić, in: K. Knoerzer, K. Muthukumarappan (Eds.), Innovative Food Processing Technologies, Elsevier, Amsterdam, The Netherlands, 2021, pp. 705–721.
[2] A. Przybylska-Balcerek, T. Szablewski, L. Szwajkowska-Michałek, D. Świerk, R. Cegielska-Radziejewska, Z. Krejpcio, E. Suchowilska, Ł. Tomczyk, K. Stuper-Szablewska, Molecules 26 (2021) 2910.
[3] Z. Mutavski, N. Nastić, J. Živković, K. Šavikin, R. Veberič, A. Medič, K. Pastor, S. Vidović, Biology 11 (2022) 1465.
[4] F. Blando, N. Calabriso, H. Berland, G. Maiorano, C. Gerardi, M.A. Carluccio, M. Andersen, Int. J. Mol. Sci. 19 (2018) 169.
[5] J. Zhang, J. Wu, F. Liu, L. Tong, Z. Chen, J. Chen, H. He, R. Xu, Y. Ma, C. Huang, Eur. J. Pharmacol. 858 (2019) 172500.
[6] I.J. Seabra, M.E. Braga, M.T. Batista, H.C. de Sousa, Food Bioproc. Tech. 3 (2008) 674-683.
[7] I.J. Seabra, Extraction of valuable compounds from agro-residues of elder (*Sambucus nigra*), pine (*Pinus pinaster*) and tara (*Caesalpinia spinosa*). Doctoral dissertation. Coimbra, Portugal, 2010.
[8] R.L. Jackman, R.Y. Yada, M.A. Tung, R.A. Speers, J. Food Biochem. 11 (1987) 201-247.

SUSTAINABLE RECOVERY OF VALUABLE COMPOUNDS FROM WILD MUSHROOMS

Nataša Nastić, Senka Vidović, Aleksandra Gavarić, Slađana Krivošija, Mirjana Sulejmanović, Siniša Simić

Department of Pharmaceutical Engineering, Faculty of Technology, University of Novi Sad,
Bulevar cara Lazara 1, 21000 Novi Sad, Serbia
e-mail: natasa.nastic@uns.ac.rs

Abstract

Serbia, along with the broader Balkan region, is known for its abundance of various mushroom species. Some of these mushrooms are collected and used for food but remain relatively under-researched in terms of their nutritional characteristics and potential pharmacologically valuable compounds. The objective of this work was to develop a sustainable process for the extraction of non-polar valuable compounds from wild edible mushrooms using for the first time supercritical carbon-dioxide extraction. The extractions were performed at the pressure of 30 MPa, temperature of 40 °C and and extraction time of 4 h. Five selected types of wild edible mushrooms *Lycoperdon saccatum, Pleurotus ostreatus, Craterellus cornucopioides, Russula cyanoxantha* and *Cantharellus cibariu* were analysed. The results showed that the highest EY was measured in *C. cornucopioides* (3.32%), followed by *C. cibariu* (2.18%) and *R. cyanoxantha* (2.06%). The chemical characterization of these extracts was performed by GC/MS. The main compounds detected were free carboxylic acids, as well as some aldehydes, alcohols, steroids, and aromatic compounds. After transesterification, methyl esters of carboxylic acids were quantified using GC/FID analysis. Oleic (25.41-67.69%), linoleic (6.64-40.25%) and palmitic acids (9.57-15.22%) were determined as the most abundant in all five species. The studied mushrooms species could potentially be used in well-balanced diets and as a source of valuable helath-promoting compounds.

Acknowledgements

The authors would like to acknowledge the financial support of the Ministry of Science, Technological Development and Innovation of the Republic of Serbia (451-03-47/2023-01/200134).

ROLE OF ASPHALTENES IN THE CRUDE OIL EMULSION STABILITY

Tibor István Ördög[1], Lilla Balassa[2], Sándor Puskás[1], Imre Dékány[2]

[1]Group Oilfield Development and Solutions MOL PLC. H-1117 Budapest, Dombóvári str. 28.
[2] Physical Chemistry and Material Science Department, University of Szeged, H-6720 Szeged, Rerrich Béla sqr.1.
email:tordog5@gmail.com

Abstract

In the terciery crude production technologies the applied surfactant adsorption processes has to be clearly idetified. In this complex environment the asphaltenes has special role in the emulsion stabilisation. Asphaltenes covered solid mineral particles could stabilize the o/w emulsion in the crude oil/ brine environment.

Introduction

In naturally occurring crude oil, there are high molecular weight organic compounds in the crude oil phase, while the other phase of crude oil is an aqueous medium in which electrolytes (calcium, magnesium salts, water-soluble organic substances) are found. Depending on the oil-water ratio, there are o/w (oil in water) and w/o (water in oil) dispersions. In this work, we report on the role of asphaltenes occurring in o/w type emulsions and dissolved in the oil phase, with the aim of obtaining information on the stabilizing effect of asphaltene dissolved in the organic phase. It should be noted that, in addition to electrolytes, the brine phase used as a dispersion medium also contains sand and clay particles from the reservoir rock - washed out by brine migration flows - which also affect the stability of the crude emulsion.

Experimental

The stability test is important because the crude oil emulsion that has come to the surface must be separated into an oil and water phase before being sent to the oil refinery. In this separation technology, the stabilizing layer created at the o/w interface, which consists of asphaltene, mineral particles modified by asphaltene, plays an important role [1]. The schematic diagram 1 presented below shows the assumed so-called the structure of the interfacial layer of a Pickering-type emulsion droplet.

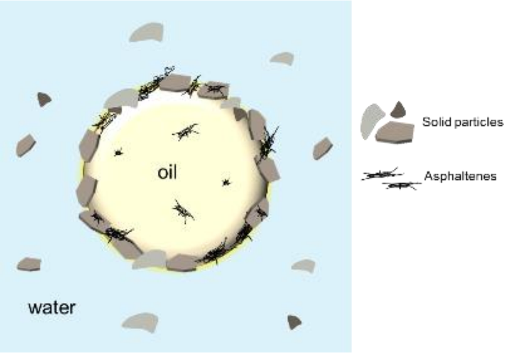

Schematic Diagram 1.

Results and discussion

In this work, we want to provide information on the extent to which the amount of asphaltene adsorbed on the mineral components affects the stability of the emulsion, or concentration of surfactants - which are essential in petroleum production technologies - how does it affect the mineral or the adsorption of surfactants on asphaltene-modified minerals. It is important to know this because in the case of crude oil displacement technologies with surfactants, it is necessary to know the adsorption processes from injected surfactant solutions in the rock pores of the reservoir layer. This means that we are studying surfactant adsorption processes occurring at the solid-liquid interface, and in order to study it quantitatively, surfactant adsorption isotherms were determined using sodium dodecylbenzene sulfonate (NaDBS) anionic surfactant. Figure 1. represents an example of Langmuir adsorption isotherm of untreated and partially treated reservoir layer rock sample. Figure 2. shows the adsorption isotherm and ce/ns representation of the 1.rock sample.

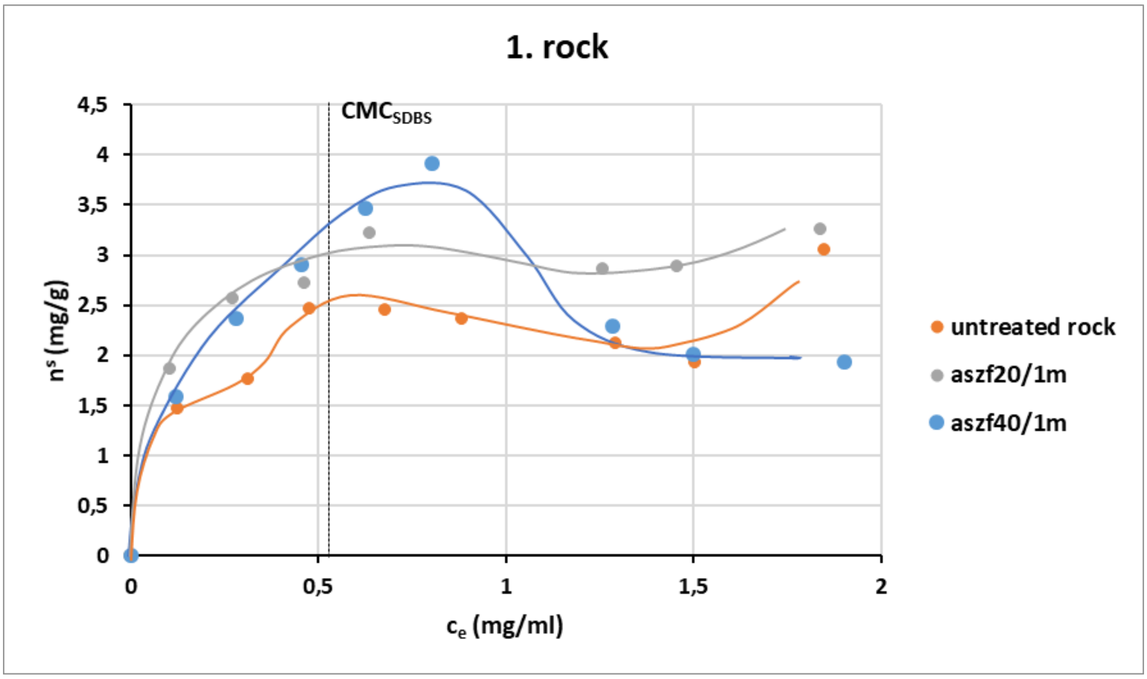

Figure 1. Adsorption isotherm of 1.rock sample

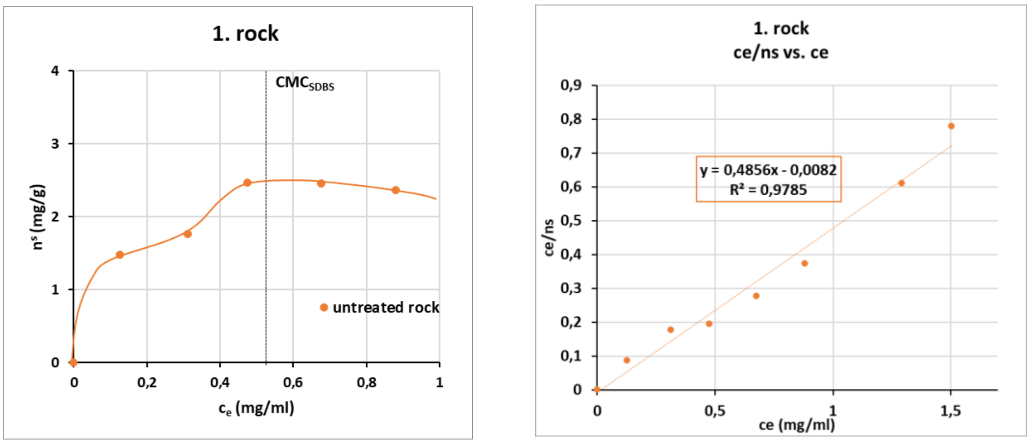

Figure 2. Adsorption isotherm and ce/ns representation of 1.rock sample

We will provide quantitative information about the adsorption capacity and the adsorption mechanism of the reservoir rock or from the surface of the emulsion stabilizing particles. Figure 3. represents the maximum adsorption capacity of NaDBS on the 1.rock sample.

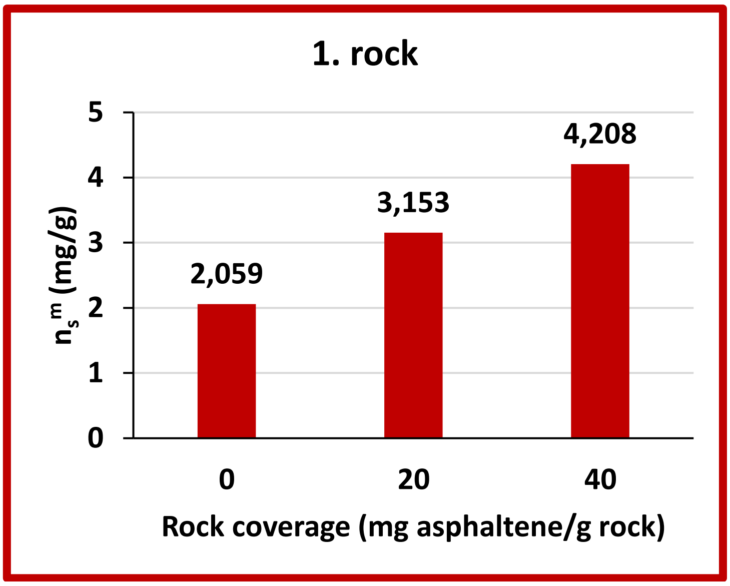

Figure 3. Maximum adsorption capacity of NaDBS on the 1.rock sample

Conclusion

We found that asphaltene adsorbed on the surface of the mineral particles in advance and in increasing amounts increases the amount of surfactant needed to displace crude oil. Knowledge of surfactant adsorption during practical application is important because it affects the costs of crude oil production.

Acknowledgements

Authors thank for the management of the Department of Physical Chemistry and Material Science of Szeged University for the resources applied in this project work and for MOL Group Oilfield Development and Solutions management for the support of this paper preparation.

References

[1] Á. Patzkó, I. Dékány: Colloids and Surfaces, 1993 (71), 299-307

GROUNDWATER QUALITY MONITORING STUDY IN THE WEST REGION OF ROMANIA

Adina Pacala[1], **Mihai Stefanescu**[2], **Gabriela-Geanina Vasile**[2]

[1] *National Research and Development Institute for Industrial Ecology ECOIND, Timisoara Subsidiary, 300431 Timisoara, Bujorilor u. 115, Romania*
[2] *National Research and Development Institute for Industrial Ecology – ECOIND Bucharest, 060652 Bucharest, 57-73 Drumul Podu Dambovitei, district 6, Romania*
e-mail: adina.pacala@ecoind.ro

Abstract

In the present study it was investigated the groundwater quality and its suitability for drinking purposes in several urban and rural areas from Timis, Arad and Bihor counties (West Region of Romania). We have established general and specific techniques for the analytical investigation of the inorganic and organic matrix in the environmental components of water from underground sources, for the identification and quantification of persistent pollutants with toxic potential, especially considering the presence of chlorobenzenes and organo-chlorinated pesticides, organophosphorus pesticides, plant treatment agents (triazine pesticides), benzene and benzene derivatives, polycyclic aromatic hydrocarbons and toxic metals, specifically tracking the presence of arsenic in groundwater resources in the Western Region of Romania.

Introduction

Although groundwater is considered safe, high concentrations of heavy metals such as arsenic (As) can present potential problems and hazards to human health.

With several newly affected regions reported in the last decade, a significant increase has been observed in the global scenario of arsenic contamination [1].

Almost 108 countries are estimated to be affected by arsenic contamination in groundwater (with a concentration exceeding the maximum permissible limit of 10 ppb recommended by the World Health Organization) [2].

The largest of these are from Asia (32) and Europe (31), followed by regions such as Africa (20), North America (11), South America (9) and Australia (4) [3].

Arsenic, even if it is part of the class of metalloids, according to European Union legislation, is included in the category of heavy metals alongside other elements (antimony, cadmium, chromium (VI), copper, lead, mercury, nickel, selenium, tellurium, thallium and tin).

Special attention must be paid to the monitoring and removal of arsenic from water, as it is known that long-term exposure to arsenic can cause health problems.

Underground sources of drinking water are considered to be one of the most important causes responsible for chronic health problems related to arsenic poisoning of the population, at the world level, but also at the national level. Arsenic toxicity is a complex phenomenon and is generally classified into acute and subacute [4].

We pay special attention to the Pannonian Basin. This basin covers a large part of Hungary, the Western Plain of Romania, Northern Serbia, North-Eastern Croatia, a small part of Slovenia, Slovakia and Austria. It is in fact a large area of South-East Central Europe affected by arsenic contamination of natural water resources.

According to a European study in 2011, it is considered that approximately 500.000 people living in Hungary and Romania are exposed to increased levels of arsenic in drinking water [5].

The application of pesticides and other chemical agents for plant protection and to weeds control, as well as the expansion of industrial production have led to land pollution and direct threat to groundwater, rivers and lakes that are sources of drinking water [6].

Due to the critical role of groundwater in numerous fields of life, the dynamic changes in groundwater resources are among the main subjects of sustainable management of groundwater assets.

Groundwater monitoring is nowadays mandatory in all member state level in European Union (i.e., Water Framework Directive (EU) 2020/2184 of the EUROPEAN PARLIAMENT and of the COUNCIL of 16 December 2020 on the quality of water intended for human consumption) [7].

In this study, we mainly focus to act in accordance with the legal provisions of this directive adopted, whereas it is clearly specified on pct. 17: ″When necessary in light of the identification of hazards, Member States should monitor pollutants which they identify as relevant, such as nitrates, pesticides or pharmaceuticals identified under Directive 2000/60/EC, or because of their natural presence in the abstraction area, such as in the case of arsenic, or because of information from water suppliers, for example regarding a sudden increase of the concentration of a specific parameter in raw water″.

For the purpose of appropriate monitoring, as mentioned in the first paragraph letter (c) of Article 8, we have proposed adequate conventional monitoring in groundwater, in the Western Region of Romania, in the catchment areas for abstraction points, or in groundwater sources, of some relevant parameters, substances or pollutants.

Experimental

Groundwater quality monitoring was carried out in 35 sampling points selected from the three different counties: Timis, Arad and Bihor, located in Western part of Romania.

The sampling campaign took place during May 2023, the groundwater sources analyzed had varying depths, between 10 and 300 m, most of them being located in the rural area.

To determine the degree of pollution of groundwater resources intended for human consumption in the Western Region of Romania, 35 representative drills were selected and analyzed: groundwater samples from Timiș County (14 locations: 6 communes, 8 villages), Arad County (8 locations: 7 cities, 1 commune), Bihor County (13 locations: 2 peri-urban areas, 7 communes, 4 villages) (Figure 1).

In addition to many physical-chemical water quality indicators analysed, for the identification and quantification of persistent pollutants with toxic potential, the presence of chlorobenzenes and organochlorinated pesticides, organophosphorus pesticides, plant treatment agents (triazine pesticides), benzene and benzene derivatives, polycyclic aromatic hydrocarbons were analysed by gas chromatographic methods (GC-ECD, GC-FPD, GC-MS) and liquid chromatographic methods (HPLC-FLD, HPLC-UV). The detection technique used for Hg was Atomic Fluorescence Spectrometry (AFS) and for As was Inductively Coupled Plasma Optical Emission Spectrometry (ICP-OES).

Figure 1. The sampling locations investigated in the Western Region of Romania

Results and discussion

The chemical status of groundwater is determinated with respect to the quality of groundwater, and concentrations in monitoring points selected must be compared to the European standards and Threshold Values (TV) which are considered the main objectives for a good status of the groundwater body status. The list of minimum parameters which must be considered for each groundwater body are stiplulated in Groundwater Directive (2006/118/EC) [8].

In order to comprehensively evaluate the degree of pollution of groundwater, a wide range of physical-chemical indicators was analysed and the results of the present study are generally similar to what was reported in other studies, especially regarding the fluctuation of pH and electrical conductivity (Figure 2).

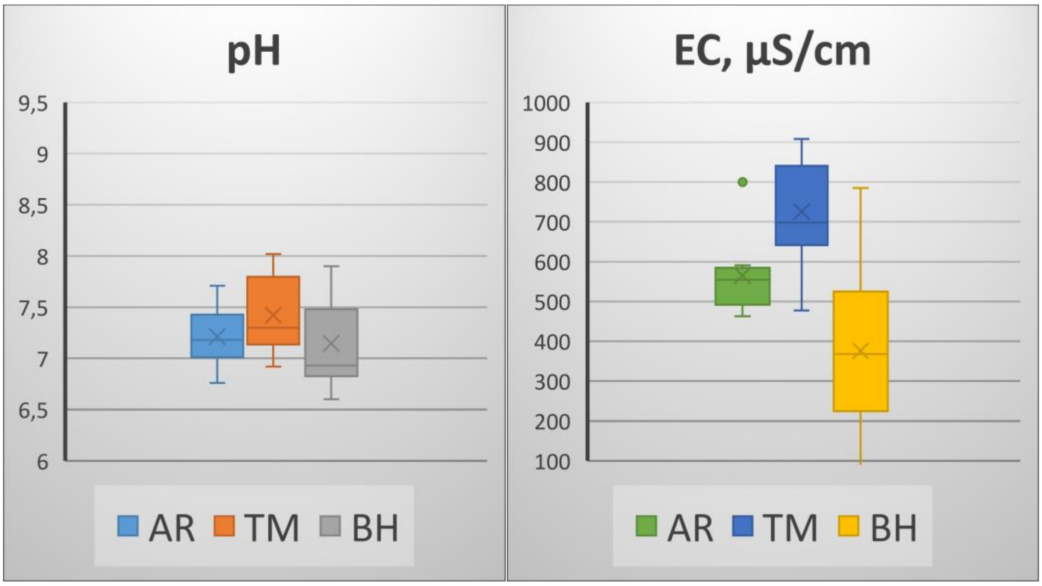

Figure 2. The fluctuation of pH and electrical conductivity (EC) depending on the investigated areas

Nutrients such as nitrogen, that are not taken up by plants, are lost to the environment and become pollutants when present in excessive amounts. This includes high levels of nitrate (NO_3) in groundwater, which pose a threat to the environment and to human health. Reducing high levels of nitrate in groundwater has been a target of European Union (EU) policy since the adoption of the Nitrates Directive. Mineral fertilisers and manure are the main sources of nitrate concentrations in EU groundwaters and an estimated 80% of the nitrogen discharge to the EU aquatic environment stems from agriculture. The Groundwater Directive [8] and the Drinking Water Directive [7] set the maximum allowable concentration for nitrate at 50mg NO_3/L and for pesticides at 0,1 µg/L individual and 0,5 µg/L total, in order to protect human health and water resources.

The presence of chlorobenzenes (1,2,4,5-tetrachlorobenzene; pentachlorobenzene; hexachlorobenzene and organochlorinated pesticides (α-HCH; β-HCH; γ-HCH; δ-HCH; 4,4'-DDD; 4,4'-DDT; 4,4'-DDE; heptachlor; heptachlorepoxide; aldrin; dieldrin; endrin; alachlor; α-endosulfan), organophosphorus pesticides (malathion; parathion; dichlorvos; diazinon; chlorfenvinfos; chlorpyrifos; metamidofos; mevinfos), plant treatment agents (triazine pesticides: simazine, atrazine, propazine), benzene and benzene derivatives (toluene, ethylbenzene, o-xylene, m-xylene, p-xylene, chlorobenzene, 1,2-dichlorobenzene, 1,3-dichlorobenzene, 1,4-dichlorobenzene, 1,2,3-trichlorobenzene, 1,2,4-trichlorobenzene) and polycyclic aromatic hydrocarbons (PAHs) was analysed.

The contents for all types of pesticides, plant treatment agents and PAHs analyzed, nitrate and mercury content were within the maximum permissible limits for all the 35 representative drills analyzed.

The groundwater sources from the West Region of Romania that require water treatment, are generally characterized by high concentrations of iron and manganese, also arsenic being present in fairly high concentrations (even about 400 µg/L in two isolated Timis County locations) and in certain situations exceedances may occur for ammonium (e.g the rural area around Ineu city, Arad County).

This study provides a comprehensive review of these 35 groundwater resources selected according to their current status. More appropriate monitoring programs need to be designed to ensure the quantity and quality of data for the West Region of Romania.

Conclusion

Conventional groundwater quality monitoring methods depend on wells and site analysed, which is expensive, time-consuming, and labor-intensive, but these types of methods applied in this monitoring study provide point-in-time measurement and are accurate.

This study results improve groundwater monitoring for a better quality of life in rural communities using local groundwater sources, contributing to the risk assessment and risk management of the catchment areas in the West Region of Romania, for abstraction points of water intended for human consumption. Concluding, the quality of the groundwater from the West Region of Romania is of good quality and applying specific treatment procedures, these groundwater sources can be used for drinking purpose.

Acknowledgements

This work was carried out through the “Nucleu” Program within the National Research Development and Innovation Plan 2022-2027 with the support of Romanian Ministry of Research, Innovation and Digitalization, contract no. 3N/2022, Project code PN 23 22 03 03.

References

[1] I. Neamtiu, M.S. Bloom, G. Gati, W. Goessler, S. Surdu, C. Pop, S. Braeuer, E.F. Fitzgerald, C. Baciu, I.R. Lupsa, D. Anastasiu, E.Gurzau, Int. J. Hyg. Environ. Health. 218(4) (2015) 371–379.

[2] Guidelines for drinking-water quality: fourth edition Incorporating the first and second addenda. Chemical fact sheets: Arsenic, World Health Organization (2022).

[3] E. Shaji, M. Santosh, K.V. Sarath, P. Prakash, V. Deepchand, B.V. Divya, J. Geoscience Frontiers 12(3), (2021) 101079.

[4] M. Vidović, Z. Nikić, B. Milovanović, Geograph. Pannon. 10 (2006) 43-46.

[5] A.L. Lindberg, W. Goessler, E. Gurzau, K. Koppova, P. Rudnai, R. Kumar, T. Fletcher, G. Leonardi, K. Slotova, E. Gheorghiu, M. Vahter, J. Environ. Monit., 8(1), (2006) 203-210.

[6] M. Tudi, H.D. Ruan, L. Wang, J. Lyu, R. Sadler, D. Connell, C. Chu, D. T. Phung, J. Int. J Environ Res Public Health. 18(3), (2021) 1112.

[7] EU, 2020, Directive (EU) 2020/2184 of the European Parliament and of the Council of 16 December 2020 on the quality of water intended for human consumption.

[8] EC, 2014, Directive 2006/118/EC of the European Parliament and of the Council of 12 December 2006 on the protection of groundwater against pollution and deterioration.

PHOSPHATE REMOVAL EFFICIENCY OF SIMPLE AND THERMALLY ACTIVATED MOLLUSK SHELLS

Alexandra-Ioana Bucur[1], Raul Alin Bucur[1], Mihai-Cosmin Pascariu[1,2], Radu Banica[1]

[1]National Institute of R&D for Electrochemistry and Condensed Matter,
144 Dr. Aurel Păunescu-Podeanu, RO-300569 Timisoara, Romania
[2]„Vasile Goldiș" Western University of Arad, 86 Liviu Rebreanu, RO-310414 Arad, Romania
e-mail: mihai.cosmin.pascariu@gmail.com

Abstract

Chemicals from various industries are dumped in the form of residual water and can be harmful for living organisms if they exceed certain concentrations [1]. Therefore, finding new and improved methods for their extraction from wastewaters and subsequent reuse represents a perpetual scientific and technical objective. For example, less expensive methods are based on adsorption using cheap substrates, where the adsorbent has to fulfill a number of criteria, like selectivity, efficiency and low production cost.

Due to the high environmental risk sometimes posed by the huge amount of mollusk shells, naturally found on seashores or dumped as a result of food processing [2], a lot of interest was shown towards using these residues as useful natural cheap materials for building a circular economy. According to scientific literature, in some cases shells exhibit excellent metal adsorption properties. Their efficiency has been proven in both natural and modified form, *i.e.* by using thermal treatment, chemical treatment or added biomass [3].

This study involved the modification of Black Sea shells, which are commonly found on the Romanian shore, by using thermal treatment. Also, some preliminary results of phosphate removal efficiency from synthetic wastewater by the modified shells are presented. It was hypothesized that the thermal treatment increases the phosphate removal efficiency, so raw shells were tested for comparison.

The protocol involved the washing and drying of seashells, and their fragmentation to specific sizes. Fragments with certain dimensions were then isolated through sieving and used for further modifications and testing. The modification of shells' surface was performed by thermal treatment [3] and the results were evaluated by scanning electron microscopy. The phosphate removal efficiency was tested using synthetic water ran through a custom-made reactor of our own design and the results showed that both natural and modified shells are efficient. The best results were obtained for thermally treated shells when using the proper pH, which makes this material a promising path for wastes reintegration and reuse.

Acknowledgements

This work was supported by the Nucleu Program within the National Research Development and Innovation Plan 2022–2027, carried out with the support of MCID, project no. PN 23 27 02 01, contract no. 29N/2023.

References

[1] N.T.H. Nhung, V.D. Long, T. Fujita, Materials (Basel, Switzerland) 16 (2023) 1095.

[2] A. Bucur, R. Banica, M.C. Pascariu, M. Poienar, C. Mosoarca, R. Bucur, A. Negrea, I. Hulka, Dig. J. Nanomater. Bios. 17 (2022) 153.

[3] A.I. Bucur, M. Poienar, R.A. Bucur, C. Mosoarca, R. Banica, Braz. J. Chem. Eng. (2023).

INFLUENCE OF EXTERNAL NUCLEATION CENTERS IN THE SOLVOTHERMAL SYNTHESIS OF SILVER NANOWIRES

Mihai-Cosmin Pascariu, Daniel Ursu, Cristina Mosoarca, Radu Banica

National Institute of R&D for Electrochemistry and Condensed Matter,
144 Dr. Aurel Păunescu-Podeanu, RO-300569 Timisoara, Romania
e-mail: mihai.cosmin.pascariu@gmail.com

Abstract

The influence of external heterogeneous crystallization active centers, such as nucleation centers on the glass surface, porous SiO_2, and activated carbon, on the growth of silver nanowires [1] is a topic still in its infancy. For this reason, in this study, silver nanowires were synthesized in a microwave field, in the presence of external nucleation seeds other than AgCl, in order to observe the influence of temperature increase on the morphology of crystals obtained on various substrates in a pressurized reactor. The SynthWAVE 3000 microwave reactor was used to obtain metal nanocrystals with varied shape factors. SCS glass spheres, silica gel and activated carbon, were impregnated with the reaction mixture. The samples were placed in the reactor, pressurized to approx. 26 bar at 20 °C, heated to 160 °C, separated by filtration or centrifugation and washed with ethanol, after which the impregnated ones were dried in an oven and the others were kept in suspension.
The samples were morphologically characterized by scanning electron microscopy (Figure 1).

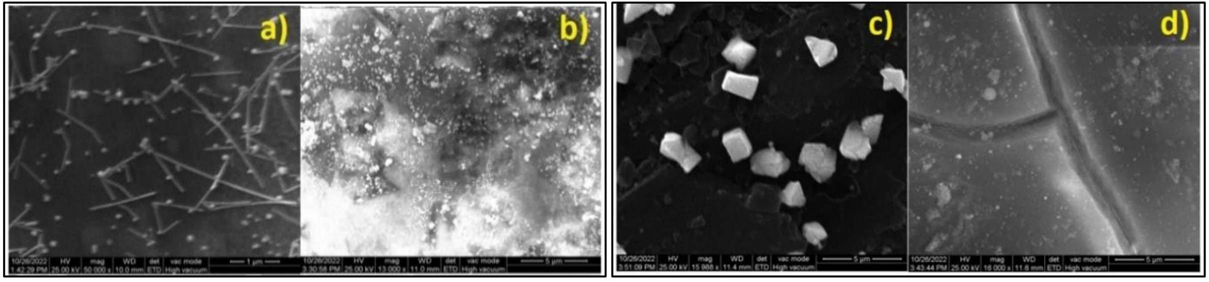

Figure 1. SEM images of microwave-grown silver nanowires (a) without substrate, (b) on the surface of glass spheres, (c) on the surface of activated carbon, and (d) in silica gel matrix

The existence of external nucleation centers, other than AgCl, causes the crystallization of the metal in completely different morphologies. In their absence, a mixture of metal nanoparticles and nanowires, with thicknesses generally less than 100 nm and lengths of several micrometers, is formed. Silver nanoparticles of quasi-spherical shape and very small sizes are also formed in the case of glass spheres and silica gel, while when using activated carbon, silver microparticles are formed very uniformly distributed on the surface of the support. This shows that inorganic substrates represent heterogeneous nucleation centers, strongly competing with AgCl nanocrystals, while activated carbon, although it has a higher specific surface area, does not show a high density of nucleation centers for the metal.

Acknowledgements

This work was supported by a grant of the Ministry of Research, Innovation and Digitization, CCCDI-UEFISCDI, project number PN-III-P2-2.1-PED-2021-2541, within PNCDI III.

References

[1] D. Ursu, R. Banica, M. Vajda, C.B. Baneasa, M. Miclau, J. Alloys Compd. 902 (2022) 163890.

VIRUS CHARACTERIZATION TOMATO CHLOROSIS VIRUS - ToCV

Pavlović Nenad*, Rašković Vera, Marković Stefan, Stošić Nemanja, Blagojević Milan, Glišić Milan

Academy of Applied Studies Šabac. Unite for Agricultural Business Studies and Tourism, Republic of Serbia
**e-mail: pavlovicnenad41@gmail.com*

Abstract

Tomato chlorosis virus (ToCV) causes an important disease that affects tomatoes, beside that it has been found to infect other economically important vegetable crops and a wide range of wild plants. First noticed in Florida (USA) and associated with "yellow leaf disorder" in the mid-1990s, ToCV has been found in 35 countries and theritories to date, representing a paradigmatic example of the emergence of a plant pathogen. ToCVs are semi-persistently transmitted by whiteflies (*Hemiptera: Aleirodidae*) belonging to the genera *Bemisia* and *Trialeurodes.* Transmission of whitefly is very efficient and cases of 100% infection are often observed in the field. To date, no resistant or tolerant tomato plants are commercially available and disease control relies primarily on insect control. In tomato, ToCV causes yellowing that can first be seen on the lower leaves and the later development of leaf thickening, bronzing and necrotic spots on older leaves. Typically, this process takes place slowly, so it is often not physically noticeable, but the crops still get sick and there are minor admixtures, which is the first significant consequence when it comes to this virus.

Key words: *Tomato chlorosis virus*, ToCV, tomato, virus.

INHIBITORS OF ACETOLACTATE SYNTHETASE

Pavlović Nenad*, Rašković Vera, Marković Stefan, Stošić Nemanja, Blagojević Milan, Glišić Milan

Academy of Applied Studies Šabac. Unite for Agricultural Business Studies and Tourism, Republic of Serbia
**e-mail: pavlovicnenad41@gmail.com*

ALS inhibitors belong to a group of herbicides that work by specifically targeting the ALS enzyme in plants, while they have no effect on the same enzyme in humans and animals. This selectivity is a key feature that minimizes the potential environmental and health risks associated with herbicide use. When ALS inhibitors are applied to an area with weeds, they are absorbed through the leaves and roots of the plant. Once in the plant, these herbicides interfere with the ability of ALS to catalyze amino acid biosynthesis, leading to disruption of the plant's integrity. The plant becomes weak, unable to produce protein and eventually dies. ALS inhibitors have a high degree of selectivity for weeds, which makes them a valuable preparation in integrated weed management. They allow farmers to control weeds without harming crops. ALS inhibitors are effective against numerous types of weeds, including broadleaf and grass weeds, making them versatile in different crops. Their selective mode of action reduces the likelihood of off-target effects, thereby reducing the impact of herbicide application on the environment. While ALS inhibitors offer several advantages, there are also challenges and concerns with their use: Overreliance on ALS inhibitors can lead to the development of herbicide-resistant weed populations. Appropriate management strategies, including herbicide rotation and diversification are essential to mitigate this risk. Some ALS inhibitors can persist in the environment, potentially leading to undesirable effects, such as damage to beneficial plants and aquatic ecosystems. Despite their selectivity, ALS inhibitors should be handled carefully to minimize human exposure and potential health risks. Today, ALS inhibitors have become a valuable and modern tool in 21st century agriculture and are used for effective weed management.

Key words: ALS inhibitors, herbicide, weeds

POTENTIAL OF ENZYMATIC EXTRACTION OF SOY PROTEIN AS GREEN ALTERNATIVE TO ALKALINE EXTRACTION

Milica Perović[1], Mirjana Antov[1,2]

[1]Faculty of Technology, University of Novi Sad, Blvd. Cara Laza 1, Novi Sad, Serbia
e-mail: perovicmilica@uns.ac.rs

Abstract

In recent time, growing global population together with changes in socio-demographics has driven the search for new, sustainable protein sources based on plants which will be able to complement/replace animal proteins in various food applications (*Henchion et al*., 2017). Among different plants, soy occupies a prominent place because soy protein is a complete protein that contains all essential amino acids required for normal human growth and development (*Singh et al*., 2008). The aim of this study was to investigate the efficacy of cell wall degrading enzymes in green extraction protocol in recovery of protein from defatted soy grit. Effects of different commercial enzymes (cellulase, pectinase and xylanase used alone or as combinations, as well as comercial enzyme coctail) were determined by measuring protein extraction yield. In addition, aqueous extraction of protein was performed and put as a control. Applied green protocols resulted in increased protein yield up to 118% compared with control. Furthermore, enzymatic extraction with Enzyme complex (as a commercial cocktail) enabled protein extraction with yield in the same amount as conventional 1 h alkaline extraction. In conclusion, enzymatic extraction with commercional enzyme preparations exhibited highly positive effect on recovery of protein from soy grit. Our findings showed that enzymatic extraction enabled production of soy protein isolate in amounts corresponded to alkaline extraction but through *green* and environmental-friendly *protocol.*

Reference

Henchion, M., Hayes, M., Mullen, A., Fenelon, M., & Tiwari, B. (2017). Future Protein Supply and Demand: Strategies and Factors Influencing a Sustainable Equilibrium. Foods, 6(7), 53. https://doi.org/10.3390/foods6070053

Singh, P., Kumar, R., Sabapathy, S.N., Bawa, A.S. (2008). Functional and edible uses of soy protein products. Compr. Rev. Food Sci. Food Saf. 7, 14–28. https://doi.org/ 10.1111/j.1541-4337.2007.00025.x.

Acknowledgement

The financial support by the Ministry of Education, Science and Technological Development, Republic of Serbia (*Project* no: 451-03-47/2023-01/ 200134*)* is greatly acknowledged

STUDY OF THE RHEOLOGICAL AND SENSORY PROPERTIES OF MAYONNAISE WITH DIFFERENT COMPOSITIONS

Cintia Viktória Farkas, Balázs Jójárt, Erzsébet Illés, Gáborné Pintér

Faculty of Engineering, Department of Food Engineering, University of Szeged, H-6724
Szeged, Mars tér 7, Hungary
e-mail:agoston@mk.u-szeged.hu

Abstract

The food industry takes many aspects into account when developing a product, but of course its primary aim is to produce a food that is safe and that will appeal to consumers. Current consumer trends focus on the careful selection of food ingredients, attentive reduction of their quantity, and the use of natural ingredients. In our experimental work, we aimed to develop different mayonnaise recipes and to instrumentally characterize the samples, testing their viscosity, heat stability and sensory properties. The results were evaluated to asceratein the most favourable composition that can be prepared also at home and has similar properties as the industrially produced mayonnaise. Using natural ingredients, we investigated how the variation in the amount of each component (sugar, salt, apple vinegar), at constant amount of sunflower oil, affects the measured parameters (consistency, viscosity, stability, sensory properties). In addition, various compounds were tested as emulsifiers, e.g. lyophilized egg powder, cheese powder or fresh egg yolk. New insights have been gained into the emulsifying capacity of lyophilized egg yolk powder and its effect on the consistency and viscosity in an emulsion-type food product, mayonnaise. We chose Univer mayonnaise as a control sample and compared the measured data of mayonnaise produced with 11 different formulations and evaluated the differences and similarities. The mayonnaise samples made from lyophilized products (egg yolk and cheese) were found to be favourable for the instrumental texture analysis. Among these, the mayonnaise made with 10% lyophilized egg yolk powder showed the highest hardness value. In terms of viscosity, increasing amounts of egg yolk powder and salt increased the dynamic viscosity value, while the presence of sucrose altered the viscosity of the emulsion by inhibiting droplet movement and aggregation. The results of the statistical data evaluation indicated that the only component of the mayonnaise samples that influenced the heat stability was the amount of added sucrose. Based on the sensory evaluation, the most preferred mayonnaise was the commercially available Univer mayonnaise, followed by our sample with the highest content of lyophilised egg yolk powder. The statistical analysis of the sensory evaluation of the grouped samples concluded that the difference in sweetness between the samples was too large. For the salty taste sensation, the difference between the average rankings of all groups was not large enough to be statistically significant. For the other sensory attributes such as colour, odour/smell, fluidity, stickiness, viscosity and bubbliness, the statistics found significant differences between the rankings of the means.

EVALUATION OF THE ORGANIC MATTER AND CLAY CONTENT CONTRIBUTION TO THE CORRECTED REMEDIATION VALUES OF THE TRACE ELEMENTS MAXIMUM ALLOWED CONCENTRATIONS IN THE AGRICULTURAL SOILS OF PROKUPLJE MUNICIPALITY, SERBIA

Radmila Pivić, Aleksandra Stanojković-Sebić, Zoran Dinić, Jelena Maksimović

Institute of Soil Science, Teodora Drajzera 7, Belgrade, Serbia
e-mail: drradmila@pivic.com

Abstract

In the samples of Prokuplje Municipality agricultural soil, it was assessed the contribution of the organic matter and clay content influence on the corrected remediation values of the total forms of Cd, Cr, Pb and Ni maximum allowed concentrations (MAC). A total of 25 samples were analyzed, of which 8 samples were on Fluvisol type of soil, 3 samples were on Vertisol type of soil, 12 samples were on Eutric cambisol type of soil, and 2 samples were on Humofluvisol type of soil. In composite soil samples, taken from a depth of 0-30 cm, certain parameters of soil fertility (content of clay fraction and total forms of Cd, Cr, Pb and Ni), were determined.The interpretation of the obtained results was carried out in relation to the MAC of tested microelements defined in the Regulation on permitted levels of hazardous and harmful substances in the soil, and based on the formula for calculating threshold and remediation values according to Ordinance on the program of soil quality systematic monitoring, indicators for risk assessment from soil degradation, and methodology for developing remediation programs. A high correlative dependence related to the content of organic matter was determined for Vertisols and Humofluvisols, while it was low for Eutric cambisol and Fluvisol. The correlative dependence related to the content of clay fraction showed a strong correlation, for all examined soils.

Introduction

The origin of heavy metals in soil can be geochemical and anthropogenic. The geochemical origin refers to the practical, natural origin of heavy metals in the soil. Certain igneous rocks are characterized by a high content of some heavy metals, especially those that contain ore minerals. Sedimentary rocks comprise about 75% of the rocks that are located near the surface of the earth's crust and therefore have primary importance as the parent substrate of the soil [1]. According to Daskalopoulou et al. [2], high concentrations of trace elements in the soil can affect soil fertility and thus represent an ecological and human health risk if they enter the food chain or are washed into the aquifer.

The mobility of trace elements is influenced by the content of the clay fraction, organic matter and soil pH value [3,4]. In the soil pH interval from 5.50 to 8.00, Cr is almost insoluble, while the solubility of Cd decreases with increasing pH, so that at pH values higher than 7.50, its immobilization occurs. In soils with pH values from 3.80 to 7.10, Cd is less mobile than Ni [5]. The value of organic matter and clay fraction content in the ratio 1:3 influence the mobility of Cd to an insignificant extent. The mobility of Cr and Ni is not affected by the content of organic matter in the soil, while the mobility of Pb is equally affected by the content of clay and organic matter [6]. Based on the data obtained as part of the research [1], the results of organic matter and clay fraction content analysis were processed and their contribution to the assessment of the maximum allowed concentrations (MAC) of investigated trace elements corrected values was determined in accordance with Official Gazzetes of RS [7,8]

Experimental

The municipality of Prokuplje forms the central part of the Toplica sub-region in Serbia, which geographically lies in 43˚10' and 43˚20' of north latitude, and 21˚00' and 21˚50' of east longitude. It covers 75,896 ha, of which agricultural soil occupies 45,083 ha or 60% of the area. The study area has a moderately continental climate with mild transitions between seasons in the basin and long and harsh winters in the mountainous region [1].

The locations of the sampled soil and the type of soil are shown in Table 1.

Table 1. Sampling points and soil type

Sampling point	Coordinate		Soil tipe	Sampling point	Coordinate		Soil tipe
	X	Y			X	Y	
1.	4790957	537876	Fluvisol	14.	4787859	538423	Fluvisol
2.	4784989	530198	Fluvisol	15.	4787338	540137	Humofluvisol
3.	4791875	543018	Vertisol	16.	4787900	537437	Eutric cambisol
4.	4793753	542981	Vertisol	17.	4787938	537389	Eutric cambisol
5.	478768	537310	Eutric cambisol	18.	4791118	549879	Eutric cambisol
6.	4791055	537796	Eutric cambisol	19.	4789092	534040	Fluvisol
7.	4789104	550116	Eutric cambisol	20.	4790716	550010	Eutric cambisol
8.	4790791	532767	Fluvisol	21.	4792163	542846	Vertisol
9.	4784843	529900	Eutric cambisol	22.	4794467	542419	Eutric cambisol
10.	4792496	542907	Eutric cambisol	23.	4796588	547347	Eutric cambisol
11.	4786837	541028	Humofluvisol	24.	4794110	547390	Eutric cambisol
12.	4788473	536928	Fluvisol	25.	4792246	534794	Fluvisol
13.	4788369	536468	Fluvisol				

From the 25 soil samples, sampled and tested, 8 samples are on Fluvisol type soil, 3 on Vertisol type soil, 12 samples on Eutric cambisol type soil, and 2 samples on Humofluvisol type soil [9]. Soil sampling in a disturbed state was done from a depth of 30 cm, according to the instructions, which refer to standard sampling methods [10, 11].

In 25 composite soil samples, prepared in accordance with standard method [12], soil acidity was analyzed potentiometrically, using glass electrode [13], calcium carbonate by volumetric method [14], total C content was analyzed on elemental CNS analyzer Vario EL III [15], SOM (soil organic matter) was calculated using the formula: SOM content (%) = organic C content (%) x factor 1.724 [16]. Granulometric composition was analyzed by determination of particle size distribution in mineral soil material [17]. Determination of the total trace elements forms (Cd, Cr, Pb, Ni) was done by inductively coupled plasma-atomic emission spectrometry - THERMO iCAP 6300 Duo (radial/axial view versions) ICP-OES, after the digestion of the samples with aqua regia [18,19].

The interpretation of the trace elements content in soil samples was carried out based on the guidelines [8], where the following parameters are defined: MAC for Cd = 3 mg kg^{-1}, MAC for Cr = 100 mg kg^{-1}, MAC for Pb = 100 mg kg^{-1}, MAC for Ni = 50 mg kg^{-1}.

For adjusted established MAC [7] it was applied the equation defined by Official Gazzete of RS [8], as follows:

$$\mathbf{(SW, IW)_b = (SW, IW)_{sb} * \frac{A + (B * \%\ clay) + (C * \%\ SOM)}{A + (B * 25) + (C * 10)}}$$

In the equation, A, B and C present the constants dependent on the type of trace element; $(SW, IW)_b$ is corrected threshold or remediation value for a particular soil; $(SW, IW)_{sb}$ is threshold or remediation value from the table of Official Gazzete of RS [7], which determines the corrected MAC value.

Results and discussion

Soil organic matter (SOM) is a complex, naturally occurring material, and plays a critical role in soil fertility, the global carbon cycle, and the portion of pollutants in soil [20]. The level of organic carbon in the soil is closely related to the structure of the soil and is one of the main factors of aggregation [21]. With an increased content of clay particles, the content of organic carbon in the soil tends to increase.

Table 2 shows the values of the examined chemical parameters and the content of clay fraction depending on the soil type and the corresponding statistical parameters. The research results showed that the reaction of the soil solution of the tested samples ranges from acidic to neutral in Eutric cambisol, Fluvisol and Vertisol, while in Humifluvisol it is in the range of slightly acidic to neutral. According to the carbonate content, only certain Vertisol samples are highly carbonated, while samples of other soil types are classified as weakly carbonated and carbonate-free soils. The content of organic matter in the examined samples of all soil's ranges from medium to high, depending on the content of the clay fraction (Table 2).

Table 2. Tested chemical parameters depending on the soil type and clay fraction content

Soil tipe	Parameter	pH 1M KCl	$CaCO_3$	SOM	Clay (<0.002 mm)
			%	%	%
Eutric cambisol	Min	4.80	0.42	2.20	11.40
	Max	6.80	0.42	4.03	53.00
	Average	5.52	0.42	2.76	31.84
	STDEV	0.61	IGDM	0.57	13.02
	CV	0.35	IGDM	1.59	7.52
Fluvisol	Min	5.20	0.04	1.84	18.60
	Max	7.20	2.73	4.31	51.30
	Average	6.19	1.20	3.04	39.03
	STDEV	0.78	1.16	1.03	10.79
	CV	0.45	0.67	1.75	6.23
Vertisol	Min	4.60	10.90	2.98	28.30
	Max	7.20	10.90	5.48	49.10
	Average	5.83	10.90	3.83	36.37
	STDEV	1.31	IGDM	1.43	11.16
	CV	0.75	IGDM	2.21	6.44
Humofluvisol	Min	5.70	0.46	2.11	31.60
	Max	6.80	0.46	3.12	33.60
	Average	6.25	0.46	2.62	32.60
	STDEV	0.78	IGDM	0.71	1.41
	CV	0.45	IGDM	1.51	0.82

The content of Ni in the tested soil types was in the great majority of samples above the MAC (in Eutric cambisol in 6 samples, Fluvisol in all tested samples, in Vertisol in 2 out of 3 tested samples, and in Humofluvisol in 1 of the 2 tested samples. By analyzing the content of trace elements in soil samples, the content of Cd, Cr, Pb in all samples on the tested soil types was below the MAC [8].

By applying the equation for determining the corrected MAC value, taken from Official Gazzete of RS [7], which includes the coefficients of the organic matter content and the clay fraction in the calculation, it was determined that the content of the tested elements in no type of soil exceeds the corrected MAC value. The determination coefficient between the ratio of the corrected MAC value for each element and each type of soil and the MAC value determined by the Regulation [19] and the content of organic matter, i.e. the content of the clay fraction, was determined (Table 3).

Table 3. The average content of the total forms of tested trace elements depending on the soil type and determination coefficient between the ratio of the corrected MAC value for each element and each type of soil and MAC value determined by the Regulation [8] and the content of organic matter and clay fraction, respectively

Soil type	Average content of element mg/kg - R^2			
	Organic matter content			
	Ni	Pb	Cr	Cd
Eutric cambisol	46.96	15.93	50.36	0.29
	$y = 0,0066x + 2,6868$ $R^2 = 0,1396$	$y = 0,0174x + 2,8206$ $R^2 = 0,1727$	$y = 0,0094x + 2,6868$ $R^2 = 0,1396$	$y = 0,026x + 3,152$ $R^2 = 0,242$
Fluvisol	66.81	16.23	68.71	0.32
	$y = 0,0101x + 2,6268$ $R^2 = 0,1432$	$y = 0,0278x + 2,8036$ $R^2 = 0,1945$	$y =0,0145x + 2,6268$ $R^2 = 0,1432$	$y =0,0425x + 3,2977$ $R^2 = 0,3012$
Vertisol	46.43	16.83	49.7	0.29
	$y = 0,0445x + 2,3819$ $R^2 = 0,9808$	$y = 0,096x + 3,2399$ $R^2 = 0,9849$	$y = 0,0636x + 2,3819$ $R^2 = 0,9809$	$y = 0,1036x + 4,4875$ $R^2 = 0,99$
Humoflu -visol	63.35	45.95	65.15	0.35
	$y = 0,1768x - 1,223$ $R^2 = 1$	$y = 0,2852x + 2,5429$ $R^2 = 1$	$y = 0,2525x - 1,223$ $R^2 = 1$	$y = 0,2252x + 5,5376$ $R^2 =1$
Clay fraction content				
Eutric cambisol	46.96	15.93	50.36	0.29
	$y = 0,35x + 25$ $R^2 =1$	$y = 0,8326x + 32,179$ $R^2 = 0,9979$	$y =0,5x + 25$ $R^2 = 1$	$y = 1,0435x + 45,544$ $R^2 = 0,9828$
Fluvisol	66.81	16.23	68.71	0.32
	$y = 0,35x + 25$ $R^2 =1$	$y = 0,8222x + 32,196$ $R^2 = 0,9953$	$y =0,5x + 25$ $R^2 =1$	$y =0,994x + 45,107$ $R^2 = 0,9633$
Vertisol	46.43	16.83	49.7	0.29
	$y = 0,35x + 25$ $R^2 = 1$	$y =0,754x + 31,76$ $R^2 = 0,9998$	$y = 0,5x + 25$ $R^2 =1$	$y =0,8107x + 41,538$ $R^2 = 0,9985$
Humoflu -visol	63.35	45.95	65.15	0.35
	$y = 0,35x + 25$ $R^2 = 1$	$y =0,5648x + 32,457$ $R^2 = 1$	$y =0,5x + 25$ $R^2 = 1$	$y =0,4459x + 38,387$ $R^2 =1$

Conclusion

In the Serbian legislation, screening values in soil are defined as the maximum allowed concentrations, maximum limit values, corrective maximum limit values, remediation values and corrected remediation values. The obtained results indicate that the constant C, related to the product, which is used in the calculation for a specific element (C=0.021 for Cd; C=0 for Cr; C=1 for Pb; C=0 for Ni) has a greater dependence on sandy soils, which is expected considering the source of the formula, which is primarily intended for the studied soils. The highest determination coefficient related to the content of organic matter was determined for Vertisol and Humofluvisol soils, while it is low for Eutric cambisol and Fluvisol soils. The correlative dependence related to the content of the clay fraction shows a strong correlation, for all tested soils, which is in agreement with the assigned constants B for the tested elements (B=0.007 for Cd; B=2 for Cr; B=1 for Pb; B=1 for Ni). Soil is a "complex matrix" that is affected by many factors, but also their mutual influences, which depending on the conditions and factors at a given moment, can be from completely synergistic to completely antagonistic [22]. Monitoring and interpreting the condition of such a matrix requires a more complex interpretation compared to the current interpretation based on simple relationships between the values of soil condition parameters defined by the legislation of the Republic of Serbia.

Acknowledgment
Ministry of Science, Technological Development and Innovation of the Republic of Serbia, Contract No. 451-03-47/2023-01/200011.

References

[1] Institute of Soil Science, Hazardous and harmful substances in agricultural soil, irrigation water and cultivated crops of the Municipality of Prokuplje in order to obtain health-safe products, Study, 2019 (in Serbian).
[2] K. Daskalopoulou, S. Calabrese, S. Milazzo, L. Brusca, S. Bellomo, W.D'Alessandro, K. Kyriakopoulos, F. Tassi, F. Parello, Ann. Geophys. 57 (2014) 1.
[3] A. Kabata-Pendias, Trace Elements in Soils and Plants, 4th ed. CRC Press, Taylor & Francis Group, Boca Raton, Florida, 2011.
[4] R. Pivić, Z. Dinić, J. Maksimović, D. Poštić, R. Štrbanović, A. Stanojković-Sebić, Matica Srpska J. Nat. Sci. Novi Sad 138 (2020) 97.
[5] D.C. Adriano, Trace Elements in Terrestrial Environments: Biogeochemistry, Bioavailability, and Risks of Metals, 2nd ed. Springer Science, 2001.
[6] The Dutch Environment Ministry, Soil Remediation Circular 2009, Ministry of Housing, Spatial Planning and Environment Directorate-General For Environmental Protection, 2009.
[7] Official Gazzete of RS, Regulation on the Program of Systematic Monitoring of Soil Quality, Indicators for Assessing the Risk of Land Degradation and Methodology for Developing Remediation Programs, "Sl. *glasnik* RS", 30/2018 and 64/2019, 2019 (in Serbian).
[8] Official Gazzete of RS 23, Regulation on Permitted Quantities of Dangerous and Harmful Substances in Soil and Water for Irrigation and Methods of Their Testing, "Sl. *glasnik* RS", 23/94, 1994 (in Serbian).
[9] WRB, World Reference Base for Soil Resources, World Soil Resources Reports, 106, FAO, Rome, Italy, 2014.
[10] ISO 18400-102:2017, Selection and application of sampling techniques, Geneva.
[11] ISO 18400-105:2017, Packaging, transport, storage and preservation of samples, Geneva.
[12] SRPS ISO 11464:2004, Soil quality-Pretreatment of samples for physico-chemical analyses, Belgrade.
[13] SRPS ISO 10390:2007, Soil quality - Determination of pH, Belgrade.
[14] SRPS ISO 10693:2005, Soil quality - Determination of carbonate content, Belgrade.
[15] SRPS ISO 13878:2005, Determination of total nitrogen content by dry combustion (“elemental analysis”), Belgrade.
[16] R. Džamić, D. Stevanović, M. Jakovljević, Agrochemistry Manual, Faculty of Agriculture, University of Belgrade, 1996 (in Serbian).
[17] ISO 11277:2009(E), Determination of particle size distribution in mineral soil material-Method by sieving and sedimentation, Geneva.
[18] ISO 11466:1995, Soil quality-Extraction of trace elements soluble in aqua regia, Geneva.
[19] ISO 22036:2008, Soil quality - Determination of trace elements in extracts of soil by inductively coupled plasma-atomic emission spectrometry (ICP-AES), Geneva.
[20] M.J. Simpson, A.J. Simpson, In: In: J.C. Lindon, G.E. Tranter, D.W. Koppenaal, (Eds.), Encyclopedia of Spectroscopy and Spectrometry, 3rd ed. Academic Press, Oxford, 2017, pp. 170.
[21] C.J. Bronick, R. Lal, Geoderma 124 (2005) 3.
[22] M. Manojlović, Diffuse pollution of agricultural soil, prevention and management. Guide Book, Increasing national capacities to assess the risk of diffuse agricultural soil pollution, TCP/SRB/3803/C3, 2022.

COMPARATIVE STUDY OF TI AND TI ALLOY FOR POSSIBLE MEDICAL APPLICATION

Adriana Pop[1], Elena-Manuela Stanciu[1], Alexandru Pascu[1], Julia Claudia Mirza Rosca[1,2], Madalina Simona Baltatu[3], Petrica Vizureanu[3].

[1] *Materials Engineering and Welding Depart., Transilvania University of Brasov, 29 Eroilor Blvd., 500036, Brasov*
[2] *Mechanical Engineering Department, University of Las Palmas de Gran Canaria, Campus Universitario Tafira, Edif. Ingenieria, 35017, Gran Canaria, Spain*
[3] *Department of Technologies and Equipment for Materials Processing, "Gheorghe Asachi" Technical University of Iasi, Bulevardul Profesor Dimitrie Mangeron 67, Iași 700050, Romania*
e-mail: popadrianaa948@gmail.com

Abstract

In the realm of modern medicine, the quest for innovation and improvement is relentless. One significant development that has transformed the landscape of medical devices and implants is the use of titanium and titanium alloys. Just as Titan stands as a resilient moon in the outer reaches of our cosmic neighborhood, titanium and its alloys have emerged as robust and versatile materials for a wide array of medical applications.

From orthopedic implants to dental prosthetics, and even in cutting-edge biomedical engineering, titanium's exceptional combination of strength, biocompatibility, and corrosion resistance has made it an indispensable asset in modern medicine.

Titanium and its alloys are not just elements on the periodic table; they are key elements in the quest for stronger, longer-lasting, and more effective medical treatments and devices.

Introduction

In the biomedical field one of the most widespread materials is Titanium but it's not flawless, the need of improvement is in fact real, it possesses high biocompatibility and high corrosion resistance, but its mechanical properties such as high Young's modulus and density make it troublesome for bone applications due to stress shielding phenomena, we propose a alloy R4 Ti15Mo7Zr15Ta1Si, that might be able to overcome Titanium, thanks to the mixture of different elements in its compositions that give it fantastic mechanical properties, close to the one of human bone, avoiding the all present stress shielding phenomena.

To do so we need first to test the corrosion resistance of the material to be able to demonstrate that it can compare with Titanium, in fact one of the most critical problems in human body is material degradation via corrosion.

Experimental

We were able to learn about the properties of the alloys by doing several experiments to determine the impact of titanium and titanium addition in one of the samples. The chemical make-up of the study samples is titanium and Ti15Mo7Zr15Ta1Si (62% Ti, 15% Mo, 7% Zr, 15% Ta, and 1% Si). These alloys were created using a vacuum arc remelting furnace (VAR), which utilized the heat produced by an electric arc between the electrode and the ingot to gradually fuse a consumable electrode in a vacuum at the "Gheorghe Asachi" Technical Faculty of Materials Science and Engineering. A portion of the ingots were given to Las Palmas de Gran Canaria University for analysis and processing.

Epoxy resin was first put to molds in a 4:1 ratio to prepare the surfaces of the two samples for embedding. The samples were then longitudinally sliced at a thickness of 1 to 1.5 mm using a Buehler IsoMet 4000 precision saw (Buehler, Lake Bluff, IL, USA).

The surfaces were then ground and polished in two steps using the Struers TegraPol-11 polishing machine (Struers ApS, Ballerup, Denmark): initially, with progressive grit silicon carbide papers from 280 to 1200, and then, for the final polish, with 0.1 microns of alpha alumina suspension to polish the surfaces to a mirror finish. The experimental techniques used to prepare samples for metallography were in accordance with ASTM E3-11(2017).

The samples were then heated "Ultrasons-HD" ultrasonic equipment from J.P. Selecta (JPS, Barcelona, Spain) for ten minutes to remove any residual traces of dirt or impurities.The phases and compounds that make up a metallic substance, as well as any impurities or potential mechanical faults, are grouped spatially in metallography.

Each specimen's surface was photographed using the Axio Vert.A1 MAT ZEISS optical metallographic microscope (Jena, Germany) in order to investigate the microstructure.

Each sample was immersed in Kroll's reagent, consisting of 20 mL glycerin, 30 mL hydrochloric acid, and 10 mL nitric acid, at intervals of approximately 15 s, and the attacked surface was photographed following. The test was finished in three tries.In an electrochemical cell with three electrodes—the samples served as the working electrodes, the reference electrode was a saturated calomel electrode, and the counter electrode was a platinum electrode—the samples were consecutively added for the electrochemical tests.

The area of each sample was determined in order to carry out the tests. The mmol/L values for the Grifols Laboratories' Ringer solution (Barcelona, Spain) were Na+ 129.9, Cl 111.7, C3H5O3 27.2, K+ 5.4, and Ca2+ 1.8.

The Corrosion Potential vs time, linear polarization and Electrochemical Impedance Spectroscopy procedures were carried out using the BioLogic Essential SP-150 potentiostat from Seyssinet-Pariset in France. The tests were carried out at 25°C in an aerated Ringer solution.Using the "Ecorr vs. time" method, the corrosion potential was measured over the course of 24 hours with potential readings of 10 V and potential recordings made every 300 s or 200 mV apart. The gathered information was used to create a potential vs. time graph, which may show a tendency toward passivation or corrosion over time or remain constant.

Results and discussion

1. Corrosion Potential

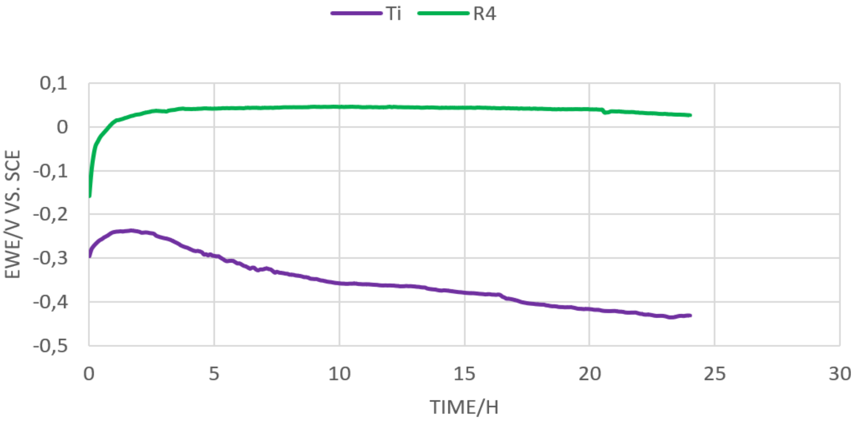

Fig. 1 – Corrosion potential vs time in Ringer solution

This graph about corrosion potential (Fig. 1) shows that the pure Ti element tends to slowly corrode while the R4 tends to be passive.

2. Bode Phase and Bode Impedance

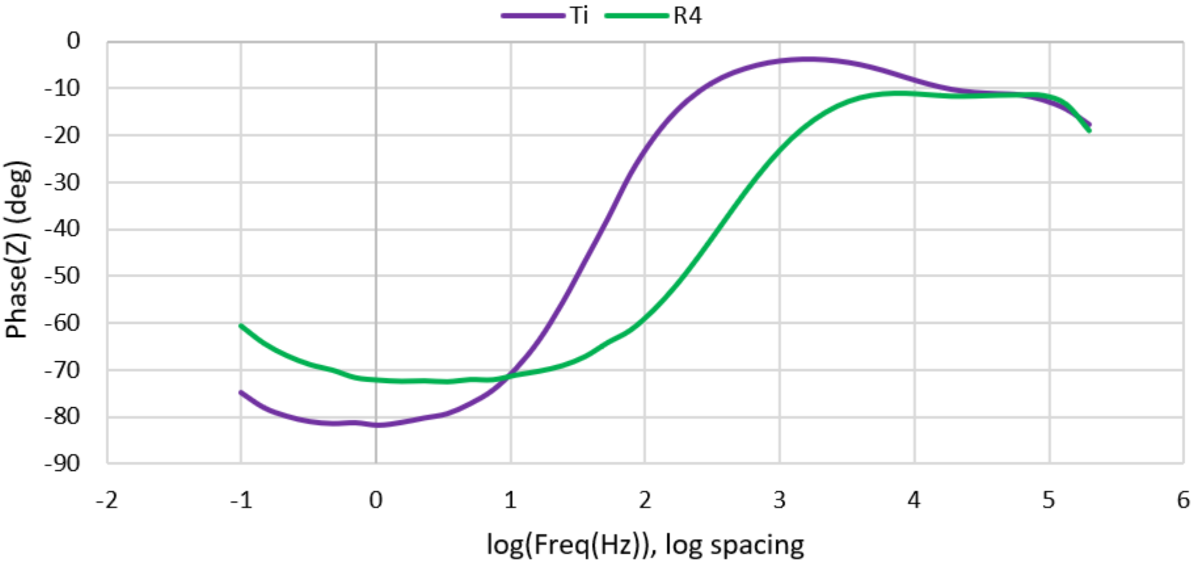

Fig. 2 – Bode-phase spectra in Ringer solution

When evaluating the Bode-Phase, as depicted in (Fig. 2), we can observe a consistent pattern in both Titanium and R4 alloy. This pattern reveals a compact zone with a low phase angle.

The Bode Phase is an important aspect of impedance spectroscopy used to assess the electrochemical behavior of materials. In the context of corrosion resistance, a low phase angle signifies that the impedance of the material is primarily resistive rather than capacitive. In simpler terms, this means that the material has a strong ability to hinder the progression of corrosive processes, the compact, low-phase-angle region in the Bode Phase plot is a promising sign of their performance in the face of corrosive factors, underlining their suitability for a wide range of industries and applications.

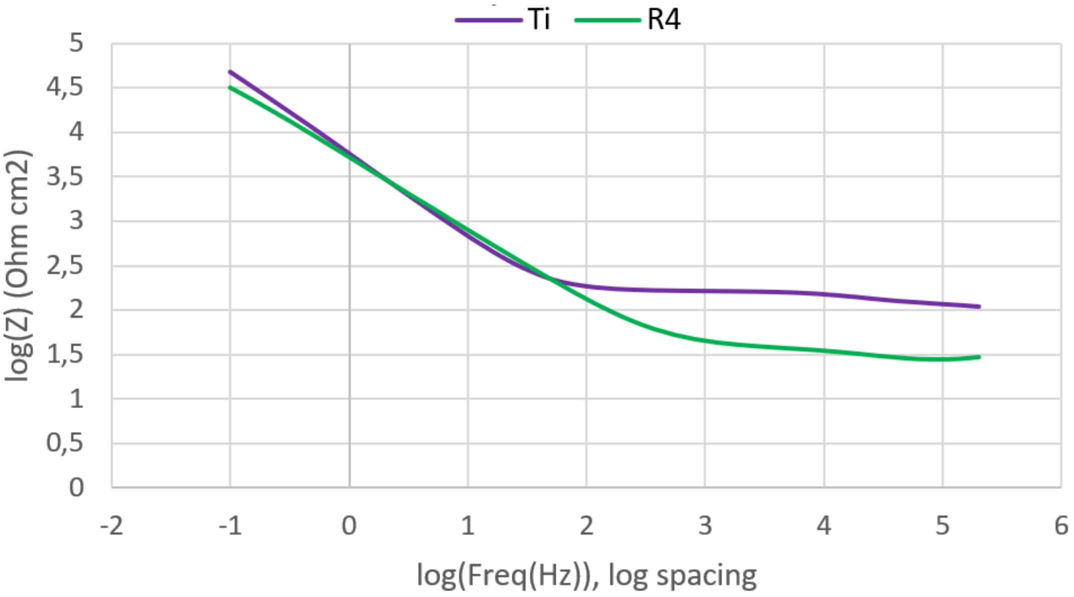

Fig. 3 – Bode_IZI spectra in Ringer solution

The observed behavioral difference between R4 and Titanium in this particular situation takes on significant relevance. The fact that R4 exhibits a more protracted diminishment with increasing frequency points to a few crucial facts: first, the Bode Impedance analysis (Fig. 3) is an effective tool that provides insights into the electrochemical behavior of materials; second, the observed behavior of R4 with its protracted diminishment as frequency increases highlights its exceptional potential for applications requiring robust corrosion resistance and stability across a wide range of conditions.

3. Nyquist

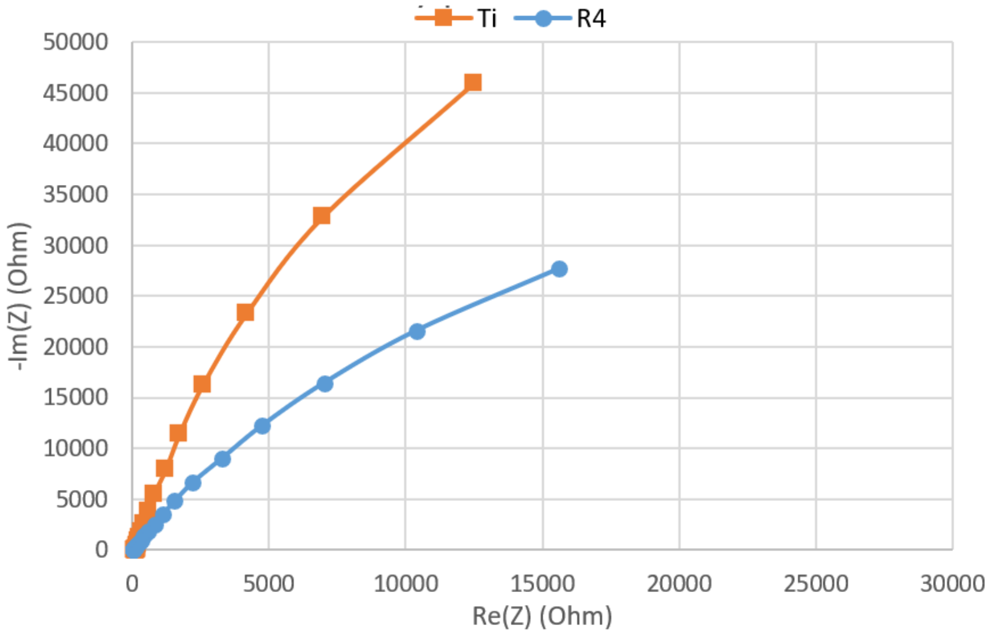

Fig. 4 – Nyquist

Diagrama Nyquist este o altă tehnică importantă în analiza electrochimică utilizată pentru a evalua comportamentul unui material în ceea ce privește impedanța și răspunsul la frecvență. Când comparăm diagrama Nyquist a titanului cu cea a aliajului R4, putem observa diferențe care oferă informații valoroase despre comportamentul lor electrochimic.

According to the Nyquist plots, Titanium has a better impedance response than R4, which indicates that it is more resistant to corrosive conditions.

4. Corrosion rate

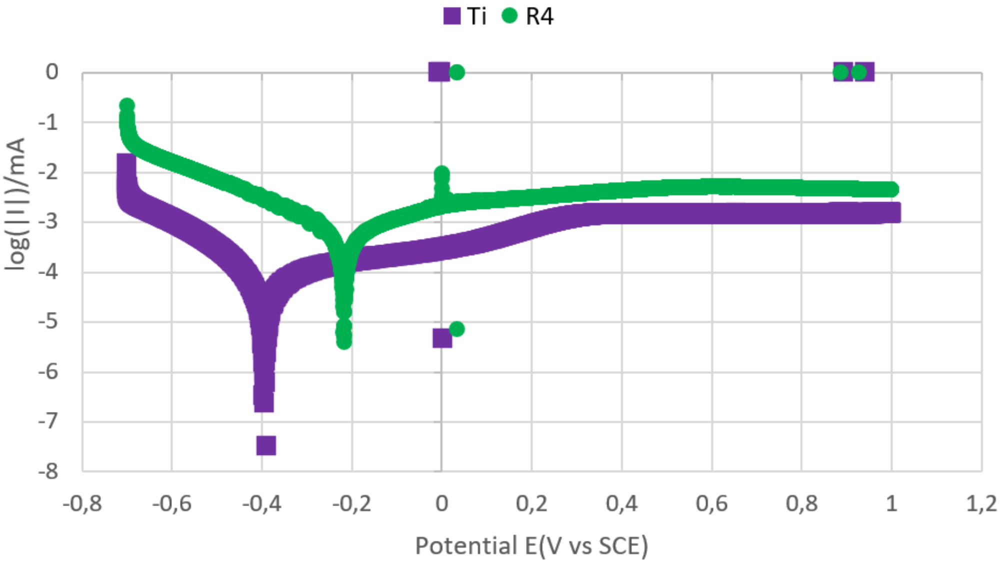

Fig. 5 – Liniar polarization curves for the samples in Ringer solution

In conclusion, the fact that both treated materials have a tendency to passivate and create an oxide shield is encouraging evidence of their capacity to resist corrosion, and this quality has important ramifications for their use in medical field. The R4 alloy stands out due to its more consistent passivation response, which makes it the material of choice in real-world applications where durability and long-term corrosion protection are crucial.

The selection of materials is crucial for medical applications such the production of orthopedic implants, surgical equipment, and other vital medical devices. These items must endure sterilizing processes, bodily fluids, and possibly long-term implantation in the human body because they frequently come into contact with bodily fluids and tissues.

Conclusion

The behavior of pure Ti material and the R4 alloy were compared, and important insights into their potential for use in medicine were gained. Both materials show a propensity to create a passive layer, which points to their potential for corrosion resistance. But the R4 alloy stands out because it exhibits a more reliable and effective passivation reaction.

This discovery is exceptionally significant in the medical industry when it comes to choosing materials. The stability of R4's passivation suggests that it can provide much greater durability and longevity compared to materials with less stable passivation reactions since it can keep its integrity in conditions like biological fluids and even inside the human body.

In order to ensure the security and efficiency of medical equipment, this comparative research helps with material choice and engineering decisions. In conclusion, it can be said that pure Ti material is still a possibility in some situations, while the R4 alloy offers a preferable option for medical applications, offering improved potential for performance and long-term protection.

Acknowledgements

I would like to extend my heartfelt gratitude for the invaluable opportunity provided through the Erasmus+ project in collaboration with Universidad de Las Palmas de Gran Canaria and Universitatea Transilvania din Brașov. This experience has been truly transformative, opening doors to personal growth, academic enrichment, and cross-cultural exchange.

The partnership between our institutions has not only broadened my horizons but also fostered enduring friendships and connections. The warm welcome, guidance, and support that I received during my time at your esteemed institutions have left an indelible mark on my academic and personal journey.

Thank you once again for making this Erasmus+ project a life-changing experience for me.

References

[1] Jiménez-Marcos, C., Rosca, J. C. M., Bălţatu, M. S., & Vizureanu, P. (2023). Effect of SI contents on the properties of TI15MO7ZRXSI alloys. *Materials*, *16*(14), 4906. https://doi.org/10.3390/ma16144906

[2] Jiménez-Marcos, C., Rosca, J. C. M., Bălţatu, M. S., & Vizureanu, P. (2022). Experimental research on new developed titanium alloys for biomedical applications. *Bioengineering*, *9*(11), 686. https://doi.org/10.3390/bioengineering9110686

[3] Jiménez-Marcos, C., Rosca, J. C. M., Bălţatu, M. S., & Vizureanu, P. (2023b). Evaluation of new titanium alloys as potential materials for medical devices. *Microscopy and Microanalysis*, *29*(Supplement_1), 196-201. https://doi.org/10.1093/micmic/ozad067.088

UTILISATION AND EFFECT OF DRIED APPLE PEELS IN PREPARATION OF A NEW DRY SAUSAGE PROTOTYPE

Georgeta-Sofia Popescu[1*], Mihaela-Maria Stanciugelu[2,3], Florina Radu[1], Ariana-Bianca Velciov[1], Antoanela Cozma[4], Luminita Pirvulescu[5], Daniela-Florentina Marcu[6], Lia Sanda Rotariu[5], Elisabeth Spataro[7], Despina Bordean[1]

[1]Department of Food Science, Faculty of Food Engineering, University of Life Sciences "King Michael I" from Timisoara, 300645, Timisoara, Romania
[2] Faculty of Sciences, "Lucian Blaga" University of Sibiu, Sibiu, 550012, Romania
[3] Brukenthal National Museum, Natural History Museum, Sibiu, Romania
[4]Department of Soil Sciences, Faculty of Agriculture, University of Life Sciences "King Michael I" from Timisoara, 300645, Timisoara, Romania
[5]Faculty of Management and Rural Tourism, University of Life Sciences "King Michael I" from Timisoara, 300645, Timisoara, Romania
[6]"1 Decembrie 1918" University of Alba Iulia, 510009 – *Alba Iulia, Romania*
[7]Faculty of Biology, Babes- Bolyai University, Cluj-Napoca,400015 Romania
**e-mail: sofiapopescu@yahoo.com*

Abstract

The purpose of this study was to develop a new recipe to obtain a special innovative pork sausage, to develop the manufacturing process, technological stages, and nutritional analysis of the final product. We obtained this product starting from a classic recipe (of pork sausage), it was added by adding of dry apple peels

The apples are fruits with a rich content of ascorbic acid, and biominerals, and also have a high content of antioxidants.

Our work has focused on evaluation of the sensory characteristics, biochemical, and nutritional characteristics a type of sausage obtained by adding of dry apple peels (sausage DAP). Sensory examination was performed by analyzing the appearance, texture and taste.

The main physico-chemical features observed in the sample of sausage (simple sausage and sausages prepared with added dry apple peels) were: the content of humidity (%), ash (%), soduim chloride (%), protein (%), fat (%), carbohydrates (%) and energetic value (kcal/100g). Following the research that have been undertaken in this work, the obtained product (sausage obtained by adding of dry apple peels – sausages DAP) can be included in the category of secure products of consuming.

This prototype can be considered a food variant due to its high nutritious properties and to its distinguished taste too.

Keywords: sausage, apple peels, antioxidants, pork meat, sensory and nutritional properties

Introduction

Sausages are a meat product usually made from ground meat, often pork, beef or poultry, along with salt, spices and other flavors. Some sausages include other flavoring ingredients. The word "sausages" can refer to meat free of sausages, which can be formed into pies or stuffed into a skin. When called "sausages", the product is usually cylindrical and embedded in a skin. Usually a sausage is formed in a carcass

The paper aims as main objective the study of sensory characteristics and the main physical - chemical properties of the sausage obtained by adding of dry apple peels (sausage DAP). The addition of antioxidants to meat products is done to prevent lipid oxidation, delay the development of off- flavours and improve colour stability.

The study was designed to evaluate the effect of dry fruit on physico-chemical properties and sensory profile of pork sausages. This study aimed to improve the nutritional quality of dry sausages using dry fruit rich in bioactive compounds.

Experimental

The samples that were taken in the analysis were homemade dry sausages prepared by us and other two dry pork sausages samples purchased on the Romanian supermarket.

Notations used: sausages from different industrial manufacturers purchased on the Romanian supermarket (SM1, and SM2) and homemade sausages dried (CA1 - sausages with dry apple peels, CAM2 - control sausage).

The sausages were prepared according to the traditional recipe from Oltenia Region. In the case of sausages with dried fruit, we used the same recipe, but we added blueberries dried fruits. The fruit ratio: (meat + meat and fat) was 1:20.

The spice mixture content we used For preparation of the pork sausages: coriander *(Coriandrum sativum)* -13%, allspice *(Pimenta dioica*, also called *Myrthus pimento)* -15%, black pepper *(Piper nigrum)* -29%, thyme *(Satureja hortensis)* - 43%. Apple peels are leftovers after preparing various cakes. which were then dried and packed.

In the manufacture of sausages, we went through the following stages: choosing the connective tissue (lean meat) and fatty meat, cutting the meat and hard fat into cubes of 5 ÷ 7 cm; obtaining minced meat with the electric mincing machine (with a sieve that has 6 mm holes); measuring ingredients; adding them to the mixture of meat and lard and homogenize the composition.The meat paste was stuffed into pork intestines. The sausages underwent the drying process. The ripening process lasted 30 days until the desired sensory, physical and (bio)chemical and microbial characteristics of the products were reached.

Physicochemical analysis and nutritional characteristics

All chemicals used for analyses were of an analytical grade. All samples were analysed for physicochemical parameters within the next 48 hours upon arrival into the Laboratory.

The moisture content in sausages samples were determined gravimetrically at 103°C in an oven (according to ISO 1442:1997) [3].

The NaCl content was determined through the Mohr method according to STAS 9065-5/73 [4].

The amount of crude protein and ***fat*** in the samples was determined on the dry sample. Fat content was estimated by Soxhlet extraction by using petroleum ether [5]. The Kjeldahl method was used to determine the crude protein content (the FOSS 8400-8420 apparatus) were following the manufacturer's application notes.

Total carbohydrates were calculated by difference. ***The energy value*** was calculated by using the following equation: energy (kcal) = 9 × (g lipid) + 4 × (g protein + g carbohydrate).

All determinations were performed in duplicate, calculating the arithmetic mean of the two separate determinations. The data were statistically analysed using the program Microsoft Excel.

Results and discussion

The results of *water content* of samples are shown in Figure 1. The result was the arithmetic mean of the two parallel determinations (for each sample), which do not differ by more than 0.5 g of water per 100 g of sample to be analysed.

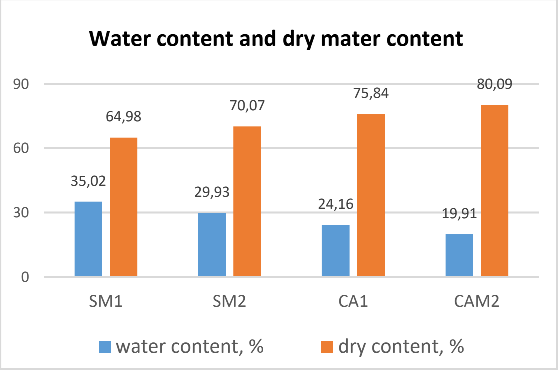

Figure 1. Water and dry mater content of sample

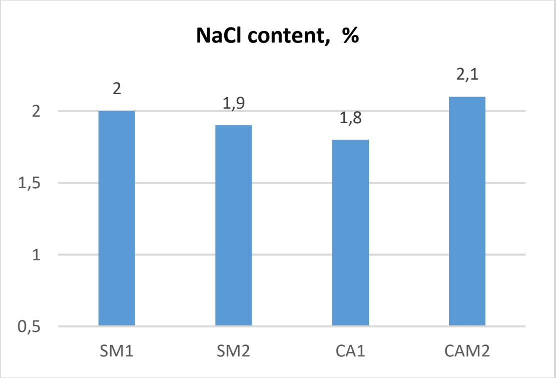

Figure 2. Salt content of analysed samples

The salt content of the sausage samples varied below the maximum limit of 2.3%. The percentage of salt in samples showed values between 1.8% and 2.1% (Figure 2). The lower content in salt (NaCl, %) is for CS1. This sample had the highest water content.

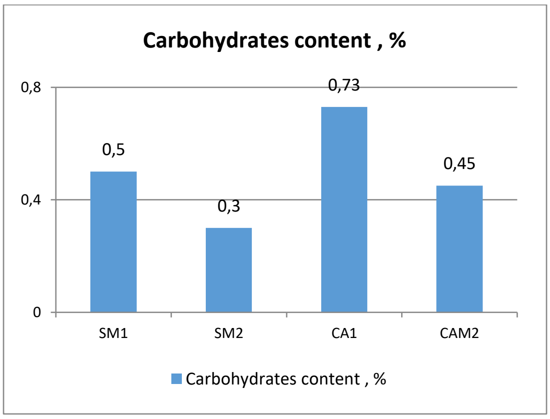

Figure 3. Carbohydrates content in sausage samples

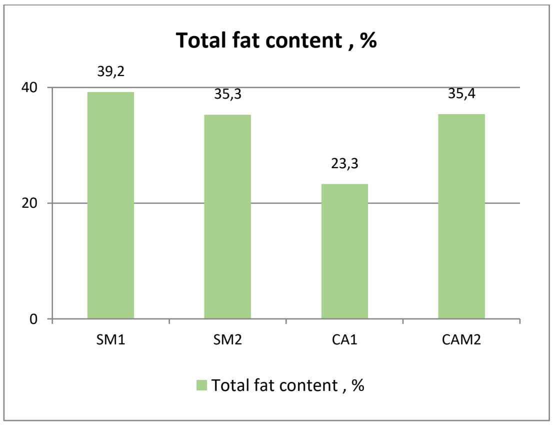

Figure 4. Total fat content in sausage samples

Total carbohydrates content from the sausage samples is showed in figure 3. The highest carbohydrate content was found in the homemade sample (CA1) in which was added dried apple peels.

In figure 4 is showed total fat content from the sausage samples, where is placed the value of arithmetic means of the two parallel determinations for each sample.

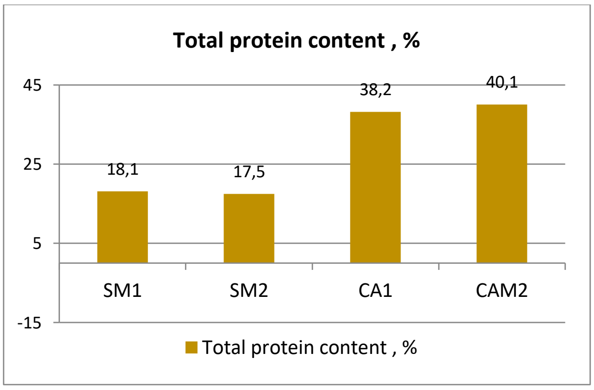

Figure 5. The crude protein content of the sausage samples

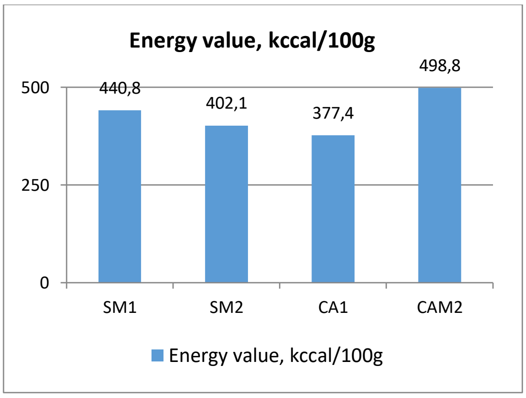

Figure 6. Caloric content of sausage sample

The fat content in our sample was between 23. % and 40 %. The lowest content of fat was found in sample of homemade sausage with dry fruit in composition. This can be explained by replacing a portion of fat with dried fruit.

Total crude protein content from samples are presented in Figure 5.

The data regarding the energy sausages value is shown in Figure 6. The energy sausages value was calculated.

The highest caloric content is for simple homemade sausages (CAM2), control samples, sample without dry fruit in composition. This sample have a highest content of dry mater, and the lowest content of water. The sausages with dry blueberry have a low caloric content. In conclusion, the replacement of pork fat with dry apple peels were reduced the fat content of sausages (see figure 4). The caloric content (the energy value) of sample with dry fruit was decrease.

Conclusion

Our results indicate some different between the sausage with dry fruit peels in the composition and without added dry fruit.

Our research consists in developing an innovative meat product by using dry apple peels rich in bioactive compounds.

The salt and fat content of the analysed sausage samples had values below the maximum permissible limits.

The replacement of pork fat with dry fruit were reduced the fat content of sausages and consequently the caloric content of sample with dry fruit was decrease.

These fruits have high content of antioxidants. The addition of antioxidants to meat products is done to prevent lipid oxidation, delay the flavours development and improve colour stability.

Following the undertaken research in this work, the obtained product (sausages with fruit) can be included in the category of safe products for consumers.

Due to the high content of bioactive substances in dry fruit it was increased the nutritive and phytomedical potentials of homemade sausages with dry fruit.

In conclusion, this sausage prototype can be considered a food variant due to its high nutritious properties and to its distinguished taste.

References

[1] Laranjo, M.; Gomes, A.; Agulheiro-Santos, A.C.; Potes, M.E.; Cabrita, M.J.; Garcia, R.; Rocha, J.M.; Roseiro, L.C.; Fernandes, M.J.; Fernandes, M.H.; et al. Characterisation of Catalao“ and „Salsichao“ Portuguese traditional sausages with salt reduction. Meat Sci., 2016, 116, 34–42.

[2] D. Alpers, W.F Stenson., D Bier. Manual of Nutritional Therapeutics, Fourth Edition, Lippincott Williams and Wilkins, Philadelphia – USA, 2002.

[3] ISO Standard ISO 1442, Meat and meat products - Determination of moisture content. International Organization for Standardization. Genève, Switzerland, 1997.

[4] STAS 9065-5/73 – Carne si preparate din carne. Determinarea conținutului de clorura de sodiu.

[5] AOAC Official Methods of Analysis, AOAC, Washington, DC, USA, 17th edition, 2000.

EXPLORING TRENDS IN ENVIRONMENTAL POLLUTION AND HAZARDOUS CHEMICAL WASTE REPORTING

Nebojša Radović[1], Željka Nikolić[2], Olga Tešović[3]

[1]University of Belgrade - Faculty of Chemistry, Studentski trg 12-16, Belgrade, Serbia
[2]Institute of General and Physical Chemistry, Studentski trg 12-16, Belgrade, Serbia
[3]PhD, Doctor of Law, Research fellow, Kosjerić, Serbia
e-mail: nradovic@chem.bg.ac.rs

Abstract

In contemporary society, environmental pollution and hazardous chemical waste are pressing concerns. This study investigates reporting trends related to environmental pollution and hazardous chemical waste in twelve scientific journals and daily newspapers. Notably, we found that the year 2013 marked a significant peak with the highest number of articles on these topics. Understanding the publishing and reporting trends of these subjects is pivotal for informed public education and underscores the significant influence of scientific research in shaping media reporting. As the global community faces increasing environmental challenges, accurate and scientific-based reporting is essential for fostering public awareness and facilitating effective solutions.

Introduction

Environmental pollution represents one of the greatest challenge of modern human society [1]. Common pollutants in the environment are chemical substances that can exist in various forms, such as chemical elements or compounds, either independently or in mixtures (which can be of homogeneous or heterogeneous composition) [2]. Chemical materials that possess properties classifying them as hazardous waste present a substantial challenge in terms of proper management [3]. Considering that hazardous waste management involves all activities aimed at establishing standardized procedures for categorization, labeling, packaging, transportation, processing, and storage of hazardous waste, it inevitably raises the question: how informed is the general public about the dangers that hazardous chemical waste can present to the human community? Common ways of disseminating information to the general public are achieved through communication channels such as newspapers, radio, television, the internet, and social media [4].

The most of the information on topics related to environmental pollution and hazardous chemical waste that needs to be communicated to the general human society must be based on scientifically confirmed truths to avoid partial or complete misinformation [5]. Since the significance of objective and timely public information is an important precondition for understanding existing threats and problems, it can be concluded that scientific research on environmental pollution and hazardous chemical waste are the foundation for media reporting on these topics [6].

The aim of this paper is to provide data on reporting in scientific journals and daily newspapers on the aforementioned topics of environmental pollution and hazardous chemical waste. Additionally, our goal is to attempt to identify any existing trends in this data.

Methodology

For the analysis of environmental pollution (EP) and hazardous chemical waste (HCW) reporting in scientific journals (SJ) and daily newspapers (DNP), twelve websites representing online platforms of these SJ and DNP were selected. All selected SJ are journals categorized as

Q1 for the year 2022 according to the Scimago Journal & Country Rank (SJR). The chosen DNP comprise well-known daily newspapers with high circulation and readership, published and read in various parts of the world (USA, Great Britain, India, China, Australia).

Data collection for the number of articles on EP topics involved searching websites using the keyword "Environmental pollution". For collecting data on the number of HCW articles, the keyword "Hazardous chemical waste" was employed. The choice of these keywords may not be considered comprehensive and entirely reliable, but they serve as effective tools for searching and identifying of EP and HCW related articles within the selected SJ and DNP. Furthermore, website searches could have varied in terms of the parameters set by the search algorithms. Data retrieval from the SJ Nature and Science websites encompassed all journals of these publishers, while all other websites were surveyed concerning a specific SJ and DNP. The website searches were conducted from the same IP address (Belgrade, Serbia) using the same computer. Prior to each SJ and DNP search, browsing history and cache memory were cleared. Searches were conducted without logging into user accounts, utilizing the same web browser (Mozilla Firefox) with the same website www.google.rs. All searches were carried out during five consecutive days in September 2023.

Table 1. presents essential information on the SJ and DNP employed for the analysis of reporting on EP and HCW topics during 2000-2022 period.

Table 1. Basic information on selected SJ and DNP

Name of SJ/DNP	Type	Web address	Abbreviation
Nature	SJ	www.nature.com	NAT
Science	SJ	www.science.org	SCI
Environmental Pollution	SJ	www.sciencedirect.com/journal/environmental-pollution	ENPOLL
Journal of Hazardous Materials	SJ	www.sciencedirect.com/journal/journal-of-hazardous-materials	JHM
Waste Management	SJ	www.sciencedirect.com/journal/waste-management	WMAN
International Environmental Agreements: Politics, Law and Economics	SJ	www.springer.com/journal/10784/	IEA
Review of European, Comparative & International Environmental Law	SJ	www.onlinelibrary.wiley.com/journal/20500394	RECIEL
Financial Times (International edition)	DNP	www.ft.com	FT
The Australian Financial Review	DNP	www.afr.com	AFR
The Wall Street Journal	DNP	www.wsj.com	WSJ
China Daily (English)	DNP	www.chinadaily.com.cn	CD
The Times of India	DNP	www.timesofindia.indiatimes.com	TOI

Results and discussion

After gathering data related to the number of articles published on the topics of EP and HCW in the chosen SJ and DNP, results have been obtained and are exhibited in Tables 2. and 3.

Table 2. Published articles in the selected SJ&DNP concerning EP during 2000-2022 period

Year	NAT	SCI	ENPOLL	JHM	WMAN	IEA	RECIEL	FT	AFR	WSJ	CD	TOI
2000	67	71	212	58	25	0	0	0	64	1335	0	26
2001	63	63	247	42	24	14	0	0	38	1392	136	131
2002	100	85	312	32	24	17	87	0	46	1101	352	250
2003	66	74	302	43	35	15	76	0	49	988	309	217
2004	122	69	303	67	41	13	21	17	48	1029	268	103
2005	111	70	353	100	47	14	13	47	75	1244	569	79
2006	91	60	458	230	62	15	29	99	70	1636	989	62
2007	126	62	497	324	81	14	17	133	82	2248	1085	100
2008	147	68	556	397	119	15	62	103	99	2119	812	200
2009	172	58	474	765	146	11	29	120	104	2571	820	496
2010	158	81	493	520	107	14	18	121	61	3236	1366	368
2011	194	74	506	497	101	9	24	131	62	3185	3332	645
2012	242	81	449	332	112	11	34	131	25	2970	3464	863
2013	266	94	504	287	121	18	19	198	22	3532	7717	969
2014	348	90	475	229	112	12	36	141	80	3687	5595	910
2015	555	89	500	295	172	13	16	259	111	3522	5421	1206
2016	867	100	960	303	174	21	22	200	57	2938	3550	1164
2017	992	120	1114	307	208	18	28	249	93	2088	3670	1186

2018	978	155	1506	364	259	19	31	279	82	1656	1575	1264
2019	1246	145	1642	506	211	14	27	282	92	1793	1240	1337
2020	1630	195	2133	1089	226	18	40	232	58	1566	457	1087
2021	1836	940	2406	1741	264	21	21	276	95	1924	490	1039
2022	2121	237	2016	1739	209	24	42	234	64	1805	449	1277
Total	12498	3081	18418	10267	2880	340	692	3252	1577	49565	43666	14979

Table 3. Published articles in the selected SJ&DNP concerning HCW during 2000-2022 period

Year	NAT	SCI	ENPOLL	JHM	WMAN	IEA	RECIEL	FT	AFR	WSJ	CD	TOI
2000	4	7	6	77	31	0	0	0	3	2761	0	4
2001	7	3	9	87	22	2	0	0	1	2773	1	10
2002	4	9	8	95	39	4	25	0	1	2531	6	18
2003	5	4	13	92	32	3	42	0	3	2632	2	15
2004	4	1	7	131	32	1	2	5	1	2196	5	9
2005	9	3	15	204	33	1	3	39	3	2233	12	15
2006	12	5	20	398	43	0	9	42	0	2355	24	11
2007	18	5	16	561	62	5	5	44	1	2674	18	7
2008	13	4	17	612	82	1	24	47	0	2947	12	14
2009	21	5	11	1221	101	0	5	48	0	3296	18	36
2010	18	2	15	770	93	5	4	64	1	4838	29	22
2011	10	2	15	655	77	0	2	48	1	5167	104	44
2012	20	12	21	409	90	0	7	54	0	4941	65	62
2013	17	8	16	318	92	1	11	69	1	6037	83	49
2014	27	4	13	255	102	1	12	57	0	5208	38	46
2015	45	7	17	308	141	4	2	84	4	4494	39	62
2016	55	9	51	297	161	4	8	48	0	3835	43	52
2017	87	10	52	330	145	2	7	51	2	3058	22	62
2018	61	8	73	335	166	3	14	61	0	2414	18	68
2019	102	13	91	484	135	2	3	82	0	2136	57	69
2020	141	17	121	820	119	1	5	55	1	1941	14	38
2021	156	64	155	1264	107	3	5	76	1	1723	10	58
2022	207	27	158	1091	115	2	9	79	0	1918	10	65
Total	1043	229	920	10814	2020	45	204	1053	24	74108	630	836

Based on the data presented in Tables 2. and 3, it can be concluded that the highest number of articles on the both topics, EP and HCW, (a total of 20449, expressed as the sum of EP and HCW) were published in the all selected SJ and DNP during the year 2013. Furthermore, Figure 1. illustrates the trend in the total number of published articles on the both topics, EP and HCW, during the period from 2000 to 2022.

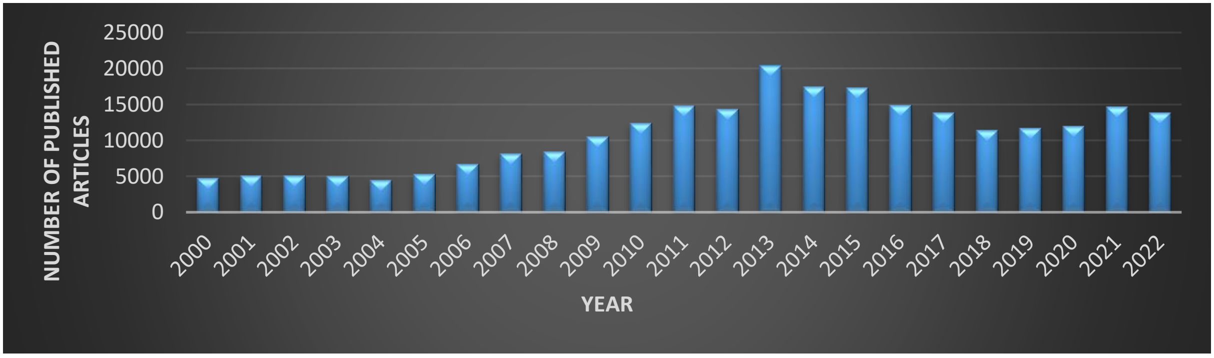

Figure 1. Published articles of EP+HCW topics during 2000-2022 period

In Figure 2, the ratio of the number of published articles on HCW to the number of published articles on EP (expressed as HCW/EP in %) for each individual SJ and DNP is displayed. Specifically, HCW/EP values for WSJ, JHM, and WMAN range from 70.14% to 149.52%, confirming an increased focus on reporting HCW topics in these SJ and DNP. In the case of JHM and WMAN, such a HCW/EP ratio is expected since these are SJ dedicated to HCW topics. Assuming that the editorial board of the WSJ recognized the financial and economic significance of HCW issues, the exceptionally high HCW/EP value (149.52%) can be attributed to this editorial policy.

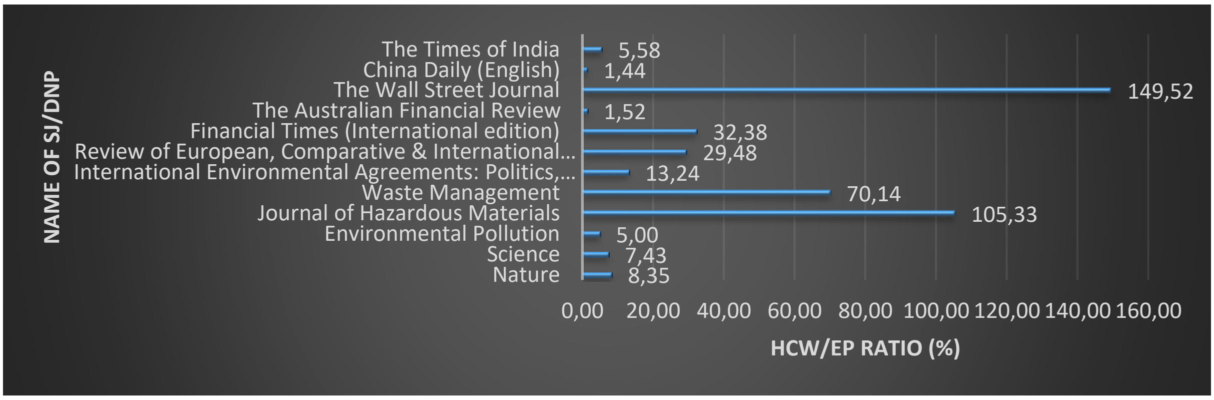

Figure 2. HCW/EP ratio for each individual SJ and DNP during 200-2022 period

To determine the presence of a linear dependency between the number of published articles on individual topics, EP and HCW, for each SJ and DNP, a linear regression analysis method was applied. In Table 4, it can be observed that in all SJ and DNP, except for IEA and AFR (83% of SJ and DNP), the value of R is greater than 0.70, indicating the existence of a linear dependency between the number of published articles on EP and HCW topics [7].

Table 4. Linear regression R-values (x-axis: EP; y-axis: HCW)

	NAT	SCI	ENPOLL	JHM	WMAN	IEA	RECIEL	FT	AFR	WSJ	CD	TOI
R	0.9873	0.9668	0.9785	0.8868	0.8989	0.4239	0.8655	0.8936	0.0950	0.8770	0.7192	0.9624

In addition, this study evaluates the number of EP+HCW articles published in two distinct three-year periods: the COVID-19 period (from 2020 to 2022) and the pre-COVID-19 period (from 2017 to 2019). It measures this against the total number of articles on EP+HCW topics published during the entire study period from 2000 to 2022, expressed as a ratio (in %).

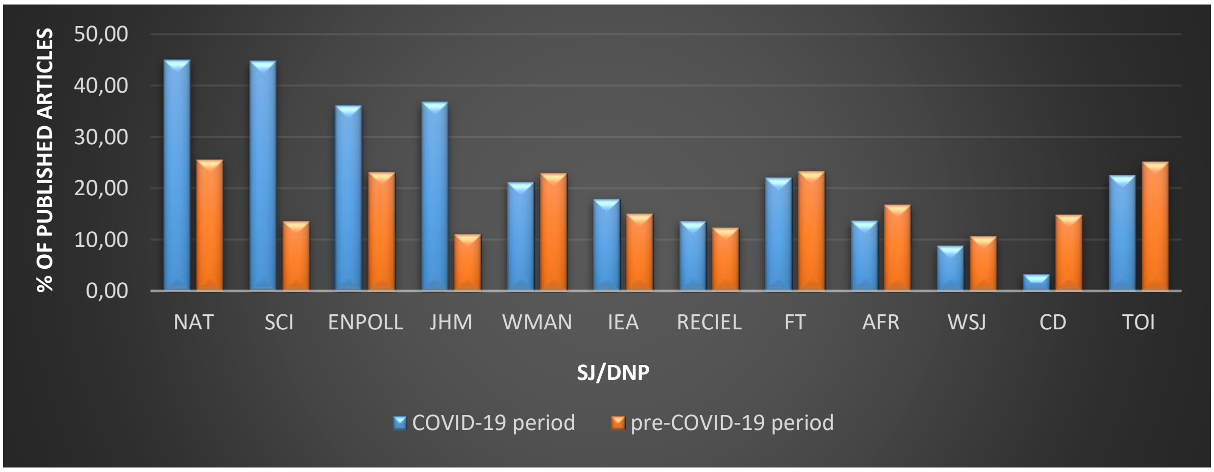

Figure 3. EP+HCW articles production during the COVID-19 and pre-COVID-19 periods

From Figure 3, it is evident that NAT and SCI, as well as ENPOLL and JHM (all SJ), experienced a significant increase in the production of articles on EP+HCW topics during the COVID-19 period compared to the pre-COVID-19 period. This can be attributed to the fact that during the COVID-19 restrictions, researchers had more time available for writing and publishing scientific papers. Conversely, CD experienced a significant decrease in the production of articles on EP+HCW topics during the COVID-19 period compared to the pre-COVID-19 period, which can be linked to the focus of this DNP on reporting events related to COVID-19, given that China was significantly impacted by this public health crisis. All others DNP (FT, AFR, WSJ, and TOI) as well as SJ (WMAN, IEA, and RECIEL) did not exhibit any significant differences in the production of articles on EP+HCW topics between the pre-COVID-19 and COVID-19 periods.

Conclusion

Analyzing 12 selected scientific journals and daily newspapers, this study examined reporting trends during the period from 2000 to 2022 on environmental pollution and hazardous chemical waste. The year 2013 marked a zenith with more than 20000 articles on these subjects. Within 83% of all observed journals/newspapers, a linear correlation between the percent of articles published on environmental pollution and hazardous chemical waste subjects in an individual journal/newspaper is confirmed. During the COVID-19 period, there were varying reporting trends on aforementioned topics, as some scientific publications increased their production.

Acknowledgements

The Ministry of Science, Technological Development and Innovation of Republic of Serbia supported this study (Contract number: 451-03-47/2023-01/200168 and 451-03-47/2023-01/200051).

References

[1] Kampa, M., & Castanas, E. (2008). Human health effects of air pollution. Environmental Pollution, 151(2), 362–367. https://doi.org/10.1016/j.envpol.2007.06.012

[2] Lin, B.-L., Meng, Y., Kamo, M., & Naito, W. (2021). An all-in-one tool for multipurpose ecological risk assessment and management (MeRAM) of chemical substances in aquatic environment. Chemosphere, 268, 128826. https://doi.org/10.1016/j.chemosphere.2020.128826

[3] Núñez-Delgado, A., Dominguez, J. R., Zhou, Y., Race, M., & Domingo, J. L. (2021). New research on reduction and/or elimination of hazardous substances in the design, manufacture and application of chemical products. Environmental Research, 201, 111601. https://doi.org/10.1016/j.envres.2021.111601

[4] Herodotou, C., Ismail, N., Aristeidou, M., Miller, G., Benavides Lahnstein, A. I., Ghadiri Khanaposhtani, M., Robinson, L. D., & Ballard, H. L. (2022). Online Community and Citizen Science supports environmental science learning by young people. Computers & Education, 184, 104515. https://doi.org/10.1016/j.compedu.2022.104515

[5] Scheufele, D. A., Krause, N. M., & Freiling, I. (2021). Misinformed About The "Infodemic?" Science's Ongoing Struggle With Misinformation. Journal of Applied Research in Memory and Cognition, 10(4), 522–526. https://doi.org/10.1016/j.jarmac.2021.10.009

[6] Bai, J., Tang, X., & Zheng, Y. (2023). Serving the truth: Do directors with media background improve financial reporting quality? International Review of Financial Analysis, 85, 102452. https://doi.org/10.1016/j.irfa.2022.102452

[7] Mansournia, M. A., Waters, R., Nazemipour, M., Bland, M., & Altman, D. G. (2021). Bland-Altman methods for comparing methods of measurement and response to criticisms. Global Epidemiology, 3, 100045. https://doi.org/10.1016/j.gloepi.2020.100045

ANTIBACTERIAL ACTIVITY OF KOMBUHA BEVERAGE FROM HYSSOP (*Hyssopus officinalis* L.) WASTE MATERIAL

Aleksandra Ranitović[1], Dragoljub Cvetković[1], Olja Šovljanski[1], AnaTomić[1], Tara Budimac[1], Milica Aćimović[2]

[1]Faculty of Technology Novi Sad, University of Novi Sad, Boulevard cara Lazara1, 21102 Novi Sad, Serbia,
[2]Institute of Field and Vegetable Crops National Institute of the Republic of Serbia, Maksima Gorkog 30, 21101 Novi Sad, Serbia
e-mail: a.ranitovic@uns.ac.rs

Kombucha is a fermented tea beverage which is traditionally obtained during fermentation (with consortium of acetic acid bacteria and yeasts - tea fungus) of sweetened black and green tea leaves (*Camellia sinensis* L.). Apart from the traditional ones, kombucha is also grown on alternative substrates, different medicinal and spicy plants. Different types of such plants are grown in large quantities on the territory of Serbia. After distillation of medicinal plants during the production of essential oils a significant amount of solid (solid plant waste mass) and liquid (liquid plant waste and hydrolates) by-products remains. The potential of these waste can be directed towards obtaining kombucha beverage with functional and health benefits.

This paper introduces obtaining kombuha beverages from waste materials remain after distillation of hyssop (*Hyssopus officinalis* L.) (solid plant waste, in amount 10g/l and liquid plant waste, diluted in a ratio of 1:50) and determination of its antimicrobial activity.

During seven days of fermentation, chemical (pH and titratable acidity) and microbiological (number of yeasts and acetic acid bacteria) parameters were determined. Antibacterial activity of kombucha beverages and control samples (acetic acid solutions, uninoculated plant waste substrates and neutralized Kombucha beverages) was determined by agar-well diffusion method. Tested strains were: Gram-negative (*Escherichia coli* ATCC25922, *Salmonella* Typhimurium ATCC14028, *Pseudomonas aeruginosa* ATCC27853) and Gram-positive bacteria (*Listeria monocytogenes* ATCC35152, *Bacillus cereus* ATCC11778, *Staphylococcus aureus*ATCC 25923).

The results indicate a high potential of hyssop waste material as a substrate for kombucha fermentation. Using both liquid and solid waste, obtained beverages reach optimal acidity after 5 and 7 days, respectively. Also, the number of yeasts and acetic acid bacteria shows a typical growth curve for kombucha fermentation. Both beverages possess expresive antibacterial activity against all tested strains as well as acetic acid solution. Beverage from liquid waste has higher activity due to higher acetic acid concentration. Uninoculated substrate and neutralized Kombucha beverage did not show any activity. Commercialization of beverages obtained from waste material, could contribute to solving the problem of accumulated waste material, which would have a significant environmental contribution.

Acknowledgements: The financial support of the Ministry of Education, Science, and Technological Development of the Republic of Serbia (contract no. 451-03-47/2023-01/200134) is gratefully acknowledged.

YIELD AND AMOUNT OF LAVENDER ESSENTIAL OIL (*LAVANDULA ANGUSTIFOLIA* MILL.) IN THE FLOWER NURSERY "PERIĆ" DURING 2021.

Rašković Vera[1], Blagojević Milan[1], Stošić Nemanja[1], Milan Glišić[1], Nenad Pavlović[1], Stefan Marković[1], Vlajić Slobodan[2], Miloš Rajković[2]

[1]Academy of Applied Studies Šabac. Unite for Agricultural Business Studies and Tourism, Republic of Serbia
[2]Institute of Field and Vegetable Crops, Novi Sad, Serba
email: blagojevicmilan@ymail.com

Abstract

Lavender (*Lavandula angustifolia* Mill.) is a perennial shrub from the Lamiacea family. The yield and quality of lavender flowers, as well as the essential oil content, are affected by many factors such as the age of the plant, environmental factors, and cultivation technology. The aim of the work was to examine the yield of fresh and dried lavender flower mass, as well as the essential oil content per hectare in a 6-year-old plantation. The research was conducted in the flower nursery "Perić" in Orašac. The yield of fresh mass of flowers was measured immediately after harvesting and was 873.6 g per plant (bush), i.e. 6987.2 kg/ha (8000 plants per ha). For the dry flower yield, it was necessary to dry the harvested flowers at room temperature in a dark room for a period of 20 days. After that, weighing was carried out and the dry flower mass was 97.06 g per plant (bush), i.e. 776.48 kg/ha. The amount of essential oil in lavender (*Lavandulae flos*) was measured with a Clevenger-type apparatus (Clevenger 1928). 55-60 kg of fresh flower mass is needed to extract one kilogram of essential oil. The amount of essential oil obtained was 116.45 kg/ha, i.e. 14.56 g of essential oil per plant (bush). This research was supported by the Ministry of Science, Technological Development and Innovation of the Republic of Serbia Grant No: 451-03-47/2023-01/200003.

THE INFLUENCE OF METEOROLOGICAL FACTORS ON SEED GERMINATION AND SPROUT LENGTH OF MELON (*CUCUMIS MELO* L.) WITHOUT THE PRESENCE OF PHYTOPATHOGENIC FUNGI ON THE SEEDS

Rašković Vera[1], Blagojević Milan[1], Nenad Pavlović[1], Stošić Nemanja[1], Vlajić Slobodan[2], Miloš Rajković[2], Milan Glišić[1], Stefan Marković[1]

[1]Academy of Applied Studies Šabac. Unite for Agricultural Business Studies and Tourism, Republic of Serbia
[2]Institute of Field and Vegetable Crops, Novi Sad, Serba
email: blagojevicmilan@ymail.com

Abstract

Quantification of seed germination in relation to changing environmental conditions, which can be used as data for ecological studies on melon seeds. A creeping cultivated melon plant belongs to the gourd family (Cucurbitaceae). The response of seed germination rate to temperature (T) and water potential (Ψ) can be described using heat-time (TT), hydrotime (HT) and hydrothermal time (HTT) models.). The minimum temperature for the germination of melon seeds is 12 to 15 °C. Melon seeds can retain their germination for 7 to 8 years, if properly stored. Practice has verified that three-year-old seeds in some varieties give better production results in terms of yield and fruit quality. The minimum temperature for melon plant growth is 13 to 15°C, and the optimal temperature for growth and development is 25-30°C. According to water requirements, these are plants that tolerate drought because they are xerophytic plants. During the year 2021, the seeds of the SV1232MG melon hybrid and domestic melon seeds were treated at temperatures of -16°C for 15 and 20 days. Seeds analyzed for the presence of phytopathogens. In addition to negative temperatures, hybrids and domestic melon seeds were also treated with temperatures of +60°C for 20 minutes and for 5 hours. After treating the melon seeds, they were placed in petri dishes with a diameter of 8 mm on double filter paper moistened with 5 ml of deionized water. Each treatment was seeded with 50 melon seeds. The parameters of the air conditioning chamber were set at 24°C and 40 hours after installation, the first measurement of the number of germinated seeds was made and the length of the sprout was measured. Statistical data processing was done in the InfoStat 2020 program, using the ANOVA posthoc Dunnet test for the significance level $p \leq 0.01$. The length of the sprout in treatment V (-16 for 15 days) is 23.5 mm in the hybrid and 19.2 mm in the domestic population, with a statistically significant difference compared to the other tested treatments. Observing the reaction of the domestic population for the germ length parameter, with the exception of the V treatment (-16 for 15 days), no statistically significant differences were recorded in the other treatments and also in the control. In hybrids, there are differences between treatments, but they are not statistically significant. Examination of the germination of the domestic population revealed a strong positive correlation of 0.73 between germination after 40 hours and germination after 16 days in the III treatment (seeds exposed to +60°C for 5 hours). Statistically significant differences were recorded between individual treatments after 40 hours of germination readings. After 16 days of germination readings, a statistically significant difference was found between all treatments. An extremely strong positive correlation of 0.91 was found between the germination rate measured after 40 days and after 16 days, in the examined hybrid. No statistically significant difference was found in the observed reading times between control and seed exposure treatment at +60°C for 20 min. While there are statistically significant differences between the other treatments and the control as well as the mentioned treatment. According to the results of this research, it can be seen that exposure to low and high

temperatures primarily has a positive effect on the germination and germination of domestic melon seeds compared to hybrid melon seeds.

WATER QUALITY FOR BLUEBERRY (*VACCINIUM CORYMBOSUM* L.) IRRIGATION

Robinić Jelena, Marković Stefan*, Stošić Nemanja, Blagojević Milan, Pavlović Nenad

Academy of Applied Studies Šabac. Unite for Agricultural Business Studies and Tourism,
Republic of Serbia
**e-mail: markovicstefaan@gmail.com*

Abstract

Water represents a significant factor in primary agricultural production, where until now this percentage has been neglected. The problems of producers who have poor water quality best illustrate the importance of water quality in agricultural production. Irrigation with poor quality water leads to the problem of a significantly lower yield, and not infrequently to crop failure. In addition to the microbiological integrity of water and the control of heavy metal contamination (lead, mercury, cadmium, chromium...), one of the biggest problems of negative consequences of using poor quality water for irrigation is secondary salinization and alkalization. Dissolved salts in water carry with them the danger of their accumulation in the soil during long-term irrigation. When it comes to water quality, it most often refers to two parameters, that is, the electrical conductivity (EC) of the water and the pH value of the water. In intensive production systems, it is necessary to know the content of calcium oxide (CaO), hydrocarbonate (HCO_3) and magnesium oxide (MgO) in water. EC (electrical conductivity of water) represents the ability of water to conduct electricity. The conductivity of water depends on the amount of salt in it, so that a larger amount of dissolved salts in water affects a higher conductivity. The problem of salinization occurs when the concentration of salt in the soil increases to a limit that causes a decrease in water intake by the plant, which further leads to a decrease in yield. Blueberry plants are shallow rooted, salt sensitive and thrive in low soil pH (4.0-5.5). Irrigation of blueberry plants is essential for high-quality fruit, and the quality of the irrigation water will determine the vigor and quality of the harvested fruit. This paper outlines critical nutrients and irrigation water characteristics for blueberry plants that should be determined prior to plant establishment. Since well water is hard and contains lime, actions such as acidifying the water will correct the pH and dissolve the minerals. However, planting blueberries should be avoided when toxic levels of chlorine, boron, and sodium are present in the irrigation water.

Key words: water quality, EC, pH, salt, soil

THE EFFECT OF GRAPHENE AND GRAPHENE-OXIDE NANOPARTICLES ON THE AEROBIC GRANULAR SLUDGE WASTEWATER TREATMENT PROCESS

Andrea Rónavári[1*], Alfonz Kedves[1], Zoltán Kónya[1,2]

[1]*Department of Applied and Environmental Chemistry, University of Szeged, H-6720 Szeged, Rerrich Béla tér 1, Hungary*
[2]*MTA, Reaction Kinetics and Surface Chemistry Research Group, H-6720, Szeged, Rerrich Béla tér 1, Hungary*
e-mail: ronavari@chem.u-szeged.hu

Abstract

The responses of aerobic granular sludge (AGS) to the presence of graphene and graphene-oxide nanoparticles (G and GO NPs) at various concentrations (1, 5 and 10 mg/L) during biological wastewater treatment processes were investigated. Bioreactor performance and extracellular polymeric substance (EPS) secretion were assessed. The results showed that the effects of G and GO NPs on bioreactor performances were dependent on the material and dose applied, especially in terms of chemical oxygen demand (COD) and phosphorus removal. Nitrite and nitrate removal rates were unchanged. The secretion of EPS, which could alleviate the toxicity of GO NPs, also changed. GO NPs were found to be more toxic than G NPs, indicating that structural changes may affect their activity.

Introduction

Carbon-based nanomaterials, such as fullerenes, carbon nanotubes, and graphene derivatives, have gained widespread use, and thus, their global production is continuously increasing [1]. The extremely interesting properties of graphene such as its great mechanical strength, high electrical, thermal and magnetic properties, and unique optical properties have made it a potential candidate to be used in several fields of engineering. They are widely used in industry as sensors and semiconductors as well as in energy storage and water purification [2]. Notably, its favorable biocompatibility, extensive surface area, impressive optical properties, and the ease with which it can be bio-functionalized, along with its derivatives like graphene oxide (GO) have gained attention in areas such as drug/gene delivery and tissue engineering. Due to their versatility, graphene and their derivatives are the most commonly produced carbon-based nanomaterial. However, graphene and graphene oxide NPs exhibit biotoxicity towards various microorganisms and can reduce soil enzyme activity. While the effects weaken with time and can be reversed after a single dosage, their increasing production raises concerns about environmental release and concentrations in wastewater [3]. Moreover, their long-term stability in water leads to their accumulation in wastewater treatment plants, potentially impacting biological wastewater processes. The conventional activated sludge (CAS) process, commonly used for sewage treatment, may be negatively affected by G and GO NPs, prompting the exploration of aerobic granular sludge (AGS) processes. AGS offers advantages, including tolerance to toxins, excellent settling, diverse microbial composition, and concurrent removal of organic matter, nitrogen, and phosphorus. Due to the need to understand the effects of G and GO NPs on AGS, we conducted experiments to assess the response of AGS towards these materials. We monitored reactor performance, including chemical oxygen demand, ammonium nitrogen, nitrite nitrogen, nitrate nitrogen, and phosphorus removal, and EPS production.

Experimental

Synthesis and characterization of G and GO NPs

A modified Hummer's method was used to prepare GO NPs [4]. All chemicals used were of reagent grade (Sigma-Aldrich). Firstly, 9 g of graphite powder and 9 g of sodium nitrate were mixed with 420 mL concentrated sulfuric acid solution at 0 °C in an ice bath for 30 min. This solution was oxidized by slowly adding 54 g of potassium permanganate and stirring at ambient temperature for 1 day. The mixture was then supplemented with 1000 mL deionized water and 20 mL 30 % (w/w) hydrogen peroxide and stirred at 0 °C for 1 h. Thereafter, the product was washed with an excess of distilled water, and the resulting brownish GO NPs were freeze-dried. G NPs were purchased purchased from Sigma Aldrich. To assess particle size and morphology of G and GO NPs, transmission electron microscopy (TEM) at 200 kV were used (FEI Tecnai G2 20 X-Twin microscope and Hitachi S-4700 Type II FE-SEM microscope). The crystalline structure of the particles was characterized via X-ray diffraction (XRD) using a Rigaku MiniFlex II powder X-ray diffractometer with a Cu Kα irradiation source. The scanning rate was $2°\mathrm{min}^{-1}$ over a 2θ range of 5°–40°.

Configuration of AGS reactors

The control AGS sequencing batch reactor (SBR) was fed with synthetic wastewater (SWW), whereas other AGS reactor were fed with G and GO NP-contaminated SWW at different concentrations (1, 5 10 mg/L G and GO NPs, G1, G5, G10, GO1, GO5, GO10). The chemical oxygen demand (COD), NH_4-N, NO_2-N, NO_3-N, and PO_4-P concentrations were continuously measured, while the extracellular polymeric substance (EPS) content, were determined at the end of experiments.

Results and discussion

In case of control bioreactor, the effluent chemical oxygen demand, nitrate, nitrite, ammonia, phosphorus contents were stable during the whole experiment. In all experiments, the concentrations of nitrite and nitrate remained stable throughout the whole operation period, even in the control bioreactor (Figure 1). These observations correspond to the previous AGS studies wherein copper-oxide and silver nanoparticles did not influence the removal efficiency of these components [5,6].

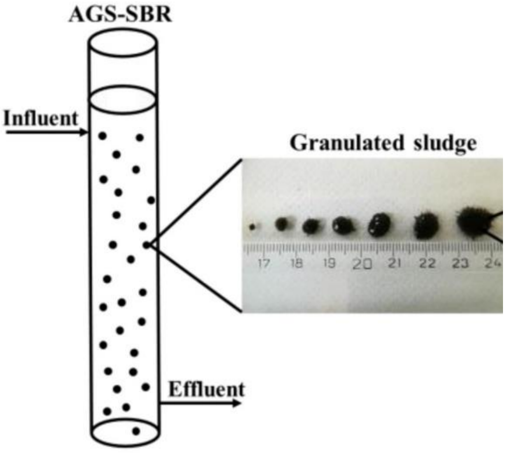

Figure 1. The schematic figure of the reactor [4]

The exposure to both graphene (G) and graphene oxide (GO) particles at various concentrations (1, 5 and 10 mg/L) did not have a detrimental impact on the reactor effluent's nitrate level, nitrate concentrations remained stable throughout the experiment. However, during this exposure, there was a notable and significant increase in ammonia concentration. At a low concentration of 1 mg/L, neither G nor GO nanoparticles affected COD removal even after 10 days. When exposed to 5 mg/L of GO nanoparticles, a slight increase in COD was noted after 6 days, while G nanoparticles exhibited stable COD removal, indicating their tolerance by the aerobic granular sludge. All the two nanomaterials significantly impacted COD removal when exposed to a higher concentration of 10 mg/L. GO NPs were more toxic with effluent COD exceeding limits, while G NPs had a milder effect, indicating granular sludge's ability to tolerate them.
Biological phosphorus removal in AGS changed in the same tendence as in case in COD removal. The phosphorus removal was adversely affected by graphene and graphene-oxide nanoparticles as well. G and GO at 1 mg/L did not significantly alter phosphorus removal. However, GO NPs at 5 mg/L slightly increased phosphate content in the effluent after 10 days. Moreover, GO NPs in higher concentrations strongly hindered phosphate removal by granular sludge. On the other hand, G NPs, even at the highest concentration, had a lesser impact, resulting in effluent phosphate contents. This suggests that microorganisms responsible for phosphorus removal tolerated G NPs better than GO NPs, likely due to the well-known high antimicrobial effects of GO NPs causing bacterial cell disruption. Similar observations were also reported, wherein ZnO and CuO NPs negatively influenced the phosphorus removal in case of AGS [5,6].
Extracellular polymeric substances (EPS), the primary components of granular sludge, are metabolic byproducts of various microorganisms and play a crucial role in protecting against toxic substances. Hence, it is essential to monitor EPS changes in granular sludge. In control AGS, PS levels did not change during nanoparticles exposure. This was in line with earlier studies, where AGS system was treated with different NPs (CeO_2, CuO, and ZnO) [5,6,7]. On the other hand, PN secretion increased significantly with nanomaterial introduction (Figure 2.).

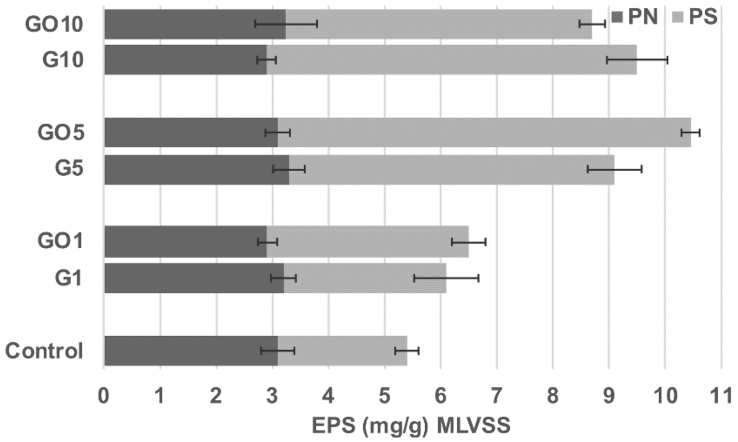

Figure 2. Effects of GO NPs on EPS contents of AGS

With G NPs addition, the PN and EPS levels slowly rose with increasing NP concentrations. This indicates that G NPs had low toxicity initially, allowing microorganisms to adapt and produce more extracellular polymeric substances.

The introduction of GO nanoparticles also enhanced the amount of EPS in sludge, although their utilization in high concentration (10 mg/L) caused high toxicity towards microorganisms which were not able to secrete the appropriate amount of EPS. The higher toxicity of GO NPs compared to G NPs may be due to structural alterations, as GO NPs tends to aggregate less than G nanoparticles.

Conclusion

In this study, the impact of graphene (G) and graphene oxide (GO) at various concentrations (1, 5, and 10 mg/L) on nutrient removal and extracellular polymeric substances secretion in aerobic granular sludge (AGS) SBRs was investigated. Overall, the findings highlight the complex and concentration-dependent effects of graphene and graphene oxide nanoparticles on AGS performance, especially in terms of COD and phosphorus removal. The research highlights AGS's ability to adapt to nanoparticle exposure, with G nanoparticles exhibiting lower toxicity and GO nanoparticles displaying higher toxicity, possibly due to structural variations. These observations emphasize the significance of carefully assessing nanoparticle effects in wastewater treatment and the need for further research to comprehend and mitigate their potential environmental consequences.

Acknowledgements

This work was supported by the National Research, Development and Innovation Office of Hungary under grant No. PD 143320 (A.R.).

References

[1] Chung, C., Kim, Y. K., Shin, D., Ryoo, S. R., Hong, B. H., & Min, D. H. Accounts of chemical research, 46(10), 2211-2224. (2013).
[2] H.N. Nguyen, D.F. Rodrigues. J. Hazard. Mater. 343: 200–207 (2018).
[3] Guo, C., Wang, Y., Luo, Y., Chen, X., Lin, Y., & Liu, X. Ecotoxicology and environmental safety, 156, 287-293. (2018).
[4] A. Kedves, L. Sánta, M. Balázs, P. Kesserű, I. Kiss, A. Rónavári, Z. Kónya. J. Hazard. Mater. 121905 (2019).
[5] X. Quan, Y. Cen, F. Lu, L. Gu, J. Ma, Sci. Total Environ. 506–507: 226–233 (2015).
[6] X. Zheng, D. Lu, W. Chen, Y. Gao, G. Zhou, Y. Zhang, X. Zhou, M.-Q. Jin. Environ. Sci.Technol. 51: 10503–10510 (2017).
[7] Q. He, S. Gao, S. Zhang, W. Zhang, H. Wang. Bioresour. Technol. 238: 95–101 (2017).

RAMAN AND AFM STUDY OF NAFION/AGNWS/PDMS MEMBRANES

Florina Stefania Rus, Radu Banica

National Institute for Research and Development in Electrochemistry and Condensed Matter,
300569 Timisoara, Aurel Paunescu Podeanu Street No. 144, Romania
e-mail: rusflorinastefania@gmail.com

Abstract

The synthesis of composite functional materials with unique optical, mechanical, or electrical properties has garnered increasing attention in recent times. Researchers are especially interested in developing self-cleaning surface materials because of the positive environmental impact on both indoor and outdoor air quality. Integration of inorganic nanoparticles into a polymer matrix results in functional hybrid nanocomposite materials with specialized chemical and physical characteristics. The parts of the composite, the dimension and shape of the nanomaterial particles, and the type of bonding that occurs between the polymer and the nanomaterial phases all influence the hybrid system's characteristics.

The aim of the present study was to obtain a new hybrid composite with self-cleaning property consisting of Nafion/AgNws/PDMS membranes as active compound. The PDMS is a material with a number of advantageous stamping and molding qualities. It offers a surface with good gas permeability, strong thermal stability, low interfacial free energy, chemical inertness, a good host material for this study because of its optical trans-parency in the ultraviolet-visible-near-infrared region [1]. To create interdigitated electrodes, polydimethylsiloxane membranes were profiled and heated above the boiling point of the solvent before being sprayed with an ethanolic suspension of silver nanowires and a 0.1% Nafion 117 solution. Raman, UV-VIS spectroscopy and AFM microscopy were used to characterize the samples in order to evaluate the PDMS/AgNws/Nafion hybrid structure. AFM tests on the depressive disorders of the sample profiles were performed to estimate the surface of the sample observed in the 3D pictures at a greater resolution. The AFM pictures in Figure 1 show a rather smooth and compact surface of the nafion, with no large-sized pores in the material's depth.

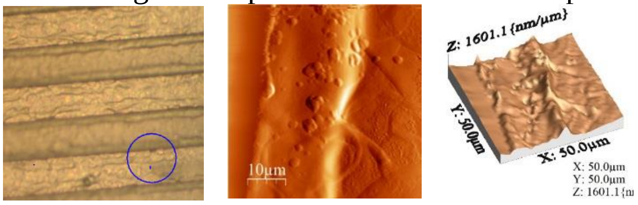

(a) (b) (c)

Figure 1. (a-b) - 2D image and c) 3D image of the PDMS/AgNws/Nafion hybrid structure at 10x magnification

As a measure of the surface texture, the values of the surface roughness at both scales were calculated for analyzed surface. At the micrometric level, the principal roughness is determined by the edges of the droplets sprayed on the heated surface, which have heights in the tens of nanometers.

Acknowledgements

This work was supported by a grant of the Ministry of Research, Innovation and Digitization, CCCDI-UEFISCDI, project number PN-III-P2-2.1-PED-2021-2541, within PNCDI II.

References

[1] Gale, B.K., Eddings, M.A., Sundberg, S.O., Hatch, A.C., Kim, J., & Ho, T.A. (2008). Low-Cost MEMS Technologies.

INVESTIGATION OF ANTIOXIDANT AND ANTIMICROBIAL EXTRACTS OF SANGO RADISH AND KOHLRABI MICROGREENS AND THEIR ENCAPSULATION

Anja Saveljić, Olja Šovljanski, Teodora Cvanić, Vanja Travičić, Aleksandra Ranitović, Jelena Vulić, Gordana Ćetković, Jasna Čanadanović-Brunet

Faculty of Technology, University of Novi Sad, Bulevar Cara Lazara 1, Novi Sad, Serbia
e-mail: anja.saveljic@uns.ac.rs

Abstract

The development of functional foods has been fueled by several factors, including human health promotion, urbanization, its effects, food security, busy lifestyles, and a competitive food market. The term functional food includes food with added value beneficial to consumers' health outside of merely meeting their nutritional needs. Microgreens are regarded as functional foods because of their high mineral nutrient and phytochemical contents. They are vegetable or herb seedlings consumed at an early growth phase, 7–21 days after germination, and are a new specialty crop with great market value. The *Brassicaceae* family's species, which includes radish and kohlrabi crops, are rich in bioactive substances and have a good nutritional profile. These substances include some phytochemicals such as chlorophyll, polyphenols, carotenoids, anthocyanins, ascorbic acid, and total and reducing sugars, and show antioxidant, anti-inflammatory, anti-diabetic, and some even antimicrobial activity. Because of the high water content in microgreens, they are susceptible to spoilage and have short shelf life. Encapsulation is a good option for the preservation of bioactive compounds and their further use. It entails covering the active substance or its mixture with a polymer to shield it from harmful external factors and enable the regulated release of the active substance in a specific environment.

This research aimed to determine the presence of important bioactive compounds (phenolics and chlorophyll) and the potential of various biological activities (antioxidant, antihyperglycemic, antimicrobial, and perform encapsulation of obtained extracts using pea protein. Extracts were obtained using combined ultrasound-assisted extraction with maceration on laboratory shakers, with acetone: ethanol (50:50) solvent on lyophilized plant samples.

Three antioxidant assays (DPPH, ABTS, RP), phenolics and chlorophyll content, as well as antihyperglycemic activity, were performed spectrophotometrically. The antimicrobial potential was determined using the disk-diffusion method against 6 different bacterial species and two yeasts. Encapsulation was performed using pea protein as wall material and the efficiency of encapsulation was measured according to the internal and external content of total phenolics. Results of Sango radish and kale extracts showed a high presence of phenolic compounds (52,12 and 126,97 mg/100 g FS) and chlorophylls (94,85 and 266,34 mg/100 g FS). Furthermore, antioxidant potential proved to be significant with the highest scavenger activity against ABTS radicals (489,61 and 653,49 μM TE/100 g FS). Antimicrobial tests showed a lower bacteriostatic effect of Sango radish against the bacteria *E. coli* (14 mm), *S.* Typhimurium (12 mm), and *S. aureus* (15 mm) and an antifungal effect of not detected. Meanwhile, kohlrabi extract showed no antimicrobial activity. Encapsulation was performed with an efficiency of 63,65% for Sango radish and 68,61% for kohlrabi extract encapsulates.

PURIFICATION OF STERIGMATOCYSTIN WITH LIQUID-LIQUID CHROMATOGRAPHY

Noémi Regina Sebők[1], Kukolya József[2], Mónika Varga[1], Csaba Vágvölgyi[1], András Szekeres[1]

[1]University of Szeged, Faculty of Science and Informatics, Departement of Microbiology,
Közép fasor 52. Szeged H-6726
[2]Research Group for Food Biotechnology, Institute of Food Science and Technology,
Hungarian University of Agriculture and Life Sciences, 1022 Budapest, Hungary
e-mail: sebok.noemi024@gmail.com

Fungi play an important role in causing grain spoilage in stored food, posing a significant challenge to food safety. The Food and Agriculture Organisation (FAO) estimates that approximately 25% of the world's food crops are affected by mycotoxins during both their growth and storage phases. Sterigmatocystin (STC) is a mycotoxin, also known as the precursor of Aflatoxin B1 (AFB1) for biosynthesis, and its chemical structure is similar as well. AFB1 is the most potent carcinogenic mycotoxin known [1]. They are naturally occurring hepatotoxic and carcinogenic mycotoxins. The International Agency for Research on Cancer classifies sterigmatocystin in Group 2B. Although STC is highly toxic, no country has set a maximum limit for it due to the low incidences. STC is produced by several species of *Aspergillus*, including *A. versicolor*, *A. nidulans*, or *A. creber*. STC has been found in stored grains or cheese, but not in the field [2]. The first pure isolation of this mycotoxin was in 1954 [3], but it took another 8 years to clarify its complete chemical structure [4]. The STC consists of a xanthone nucleus attached to a bisfuran structure similar to aflatoxins. STC is soluble in acetone, benzene, ethyl acetate, and chloroform, slightly soluble in ethanol, methanol, and diethyl ether, but insoluble in petroleum ether and water [5].

In our work, the development of a proper preparative method capable of liquid-liquid chromatographic separation of STC was aimed. For this purpose, the 'best solvent' approach was applied using the shake flask method to find the suitable biphasic solvent system. Within this testing period, the biphasic hexane-acetone-water, hexane-methanol-water, hexane-methanol-acetonitrile, hexane-ethanol-water, chloroform-methanol-water and Arizona solvent system were applied to measure the peak areas of the STC and the three major impurities by HPLC-UV separations in the upper and lower phases of the systems. On the basis of the partition coefficients and separation factors of the examined components, the most appropriate system was selected for the liquid-liquid chromatographic separation of STC.

This study funded was by the National Research, Development, and Innovation Office (NKFI grant K128659 and K139312).

References

[1] International Agency for Research on Cancer (IARC) (2006).
[2] J.D. Miller, H.L. Trenholm (Eds.), Mycotoxins in Grain: Compounds Other Than Aflatoxin. Eagan Press, Minnesota, 1994.
[3] Y. Hatsuda, S.J. Kuyama, Agric. Chem. Soc. Jpn. 28, (1954) 989.
[4] E. Bullock, J.C. Roberts, J.G. J. Underwood, Chem. Soc. 10, (1962) 4179.
[5] S. Tabata, in: J.W. Fuquayand (Eds.), Encyclopedia of Dairy Sciences, Academic Press, Cambridge, 2011, pp. 801.

TREATING POLLUTED WATER USING INNOVATIVE MATERIALS OBTAINED FROM THE RECYCLING PROCESS OF SOME WASTE

Adina-Elena Segneanu[1], Melinda Cepan[2] Claudiu Cepan[2], Maria Mihailescu[2], Marin Catalin[1], Ioan Grozescu[2]

[1]*West University of Timisoara, ICAM"*
[2]*Politehnica University of Timisoara*
e-mail: ioangrozescu@gmail.com

Abstract

Water is the source of life and the basic element of activities/processes. That is why it is particularly important to depollute polluted water and return it to the industrial and agricultural circuit and, as far as possible, make it potable.

Introduction

The research team aims to obtain new materials and develop new methods for treating polluted water. In the context of the circular economy concept, we focused on the process of recycling organic and/or inorganic waste as well as obtaining innovative materials used for the adsorption processes of organic pollutants or heavy metals from polluted water. Also, the development of new methods of polluted water treatment using the new obtained materials is another objective of the research. They are used as waste, the power plant ash and the vegetable waste like tree bark, clam shells, eggshell etc. The characterization of the newly obtained materials is done by analytical techniques such as TEM, SEM-EDX, FT-IR, BET, AAS etc.

Experimental

Before use, the waste is thermally treated at temperatures that do not affect the adsorption capacity and is micronized by mechanical grinding. The adsorption materials used are zeolite and iron oxides (eg magnetite). The composite material consisting of one, two or three wastes together with adsorbents (zeolite or iron oxides) is combined in well-defined proportions, compacted in the ball mill and immersed in the synthetic aqueous solution containing the pollutant whose adsorption is being studied. In order to optimize the adsorption process of heavy metals on the new obtained material, the role of the specific parameters of the process was studied: the pH of the solutions, the temperature, the ratio between the constituents, the contact time, the initial concentration of the pollutant. Atomic adsorption spectrometry is used to determine the adsorption capacity of materials.

Results and discussion

As a result of the experiments, new composite materials were obtained, consisting of two and three recyclable materials in different ratios, usually: 1/1; 1/2; 2/1 etc., or 1/1/1/; 1/2/1; 1/1/2; 2/1/2; 2/2/1 etc. Power plant ash and vegetable waste were used: egg shell, clam shell together with zeolite or magnetite. Different concentrations of the pollutant and different values of pH, temperature, and contact time were used. The yield of the adsorption process was between 85% and 98%.

Conclusion

In the context of the circular economy, waste as recyclable materials, is of particular interest polluted water treatment processes because some of them have a good capacity to adsorb nutrients such as nitrogen and phosphorus and/or heavy metals from wastewater, with a yield of up to 98%. Through a simple treatment, the recovered nutrients can be returned to the agricultural circuit.

References

[1] WHO (World Health Organization), Health through safe drinking water and basic sanitation;
http://www.who.int/water_sanitation_health/mdg1/en/index.html (2008).
[2] P. Ghisellini, C. Cialani, S. Ulgiati, A review on circular economy: the expected transition to a balanced interplay of environmental and economic systems. J. Clean Prod. 114, (2016) 11–32;
[3] R.K., Gautam, S.K. Sharma, S. Mahiya, C. Chattopadhyaya Mahesh, Major contaminants in industrial and domestic wastewater a contamination of heavy metals in aquatic media: transport, toxicity and technologies for remediation, Heavy Metals in Water: Presence, Removal and Safety (ed. Sharma S.K.) (The Royal Society of Chemistry, 2015).
[4] Fernández-Reyes B., Ortiz-Martínez K., Lasalde-Ramírez J.A., Hernández-Maldonado A.J., Engineered adsorbents for the removal of contaminants of emerging concern from water. Contaminants of Emerging Concern in Water and Wastewater: (2020) 3–45.
[5] Qasem N.A.A., Mohammed R.H., Lawal D.U., Removal of heavy metal ions from wastewater: a comprehensive and critical review. npj Clean Water 4 (2021) 36.
[6] Segneanu, AE., Marin, C.N., Vlase, G. et al, Highly efficient engineered waste eggshell- fly ash for cadmium removal from aqueous solution, Scientific Reports,, 12 (2022) 9676.
[7] Cepan C, Segneanu A-E, Grad O, Mihailescu M, Cepan M, Grozescu I., Assessment of the different type of materials used for removing phosphorus from wastewater, Materials,14(16) (2021) 4371

MATERIALS WITH IMPROVED ADSORBENT PROPERTIES, FOR RETAINING Cd^{2+} AND Ni^{2+} FROM WASTEWATER

Adina-Elena Segneanu[1], Melinda Cepan[2] Claudiu Cepan[2],
Maria Mihailescu[2], Ioan Grozescu[2]

[1]West University of Timisoara, ICAM"
[2]Politehnica University of Timisoara
e-mail: ioangrozescu@gmail.com

Abstract

In the most cases, wastewater contains both heavy metals in different concentrations and a number of other organic pollutants. Treating wastewater to remove and, if possible, recover heavy metals is vital for the entire food chain. To achieve this goal, we have designed new materials with improved absorption properties. Thus, we used some recyclable wastes such as power plant ash and eggshell together with zeolites and iron oxides, especially magnetite. The characterization of the new material, designed to retain heavy metals from waste water was done by analytical techniques such as SEM/EDAX, FT-IR, BET, AAS etc.

Introduction

Water is vital to the maintenance of life and the development of most industrial processes, processing and production of goods. Worldwide, intensive efforts are being made to treat wastewater and make water drinkable, especially in areas where the availability of drinking water is a major problem. The lack of advanced or strategic depollution materials and their purchase price, lead to costs that make their use in wastewater treatment processes difficult to access. In accordance with the concept of circular economy, the identification of recyclable materials, waste in general, cheap and reusable, is of particular importance for this field.

Experimental

The materials used are morpho-structurally characterized, then they are mechanically micronized and compacted in a ball mill. The combinations are made in different ratios of two or three precursors, of micrometric dimensions; mixed for homogenization and compacted in the ball mill, obtaining a composite material. It is immersed in the synthetic aqueous solution containing the pollutant whose adsorption we wish to study; the mixture is mechanically stirred at 400 rpm. The optimization of the heavy metal adsorption process on the new designed materials was achieved by studying the influence of the following specific parameters: temperature, pH, contact time and the initial concentration of the pollutant. Atomic adsorption spectroscopy is used to perform analytical determinations and subsequently the efficiency of the pollutant adsorption process is calculated.

Results and discussion

Experimentally, for the recovery of Cd2+ and Ni2+ from wastewater, in a ratio of 1:1:1, the following combinations were used: i) central ash with zeolite and magnetite, ii) central ash with eggshell and magnetite, and iii.) eggshell zeolite and magnetite. Conclusive results were obtained under the following conditions: temperature = 297 K; pH = 7.5; contact time = 240 min; mechanical agitation.

Conclusion

The circular economy is based on extending the life cycle of all products on the market and has the impact of reducing the consumption of natural resources; in this context, some wastes are recommended to be used in wastewater treatment processes, because they have a good capacity to adsorb heavy metals. Recovery of Cd2+ and Ni2+ from wastewater using new composite materials can be done with up to 96% efficiency. The composite materials thus obtained can be discharged from the pollutant and reused in a number of 10 to 12 cycles. Thus, it can be stated that the transition from the linear economy model to the circular model is an opportunity for a business to develop sustainable innovations.

References

[1]. Ghisellini P., Cialani C., Ulgiati S. **2016**, A review on circular economy: the expected transition to a balanced interplay of environmental and economic systems. J. Clean Prod. 114: 11–32.

[2]. Gautam R.K., Sharma S.K., Mahiya S., Chattopadhyaya Mahesh C. 2015, Major contaminants in industrial and domestic wastewater a contamination of heavy metals in aquatic media: transport, toxicity and technologies for remediation, Heavy Metals in Water: Presence, Removal and Safety (ed. Sharma S.K.), The Royal Society of Chemistry.

[3]. Zhang L., Dan H., Bukasa O.T., Song L., Liu Y., Wang L., Li J., **2020,** Low-cost efficient magnetic adsorbent for phosphorus removal from water, ACS Omega5, 39: 25326–25333,

[4].Annane K., Lemlikchi W., Tingry S., **2021**, Efficiency of eggshell as a low-cost adsorbent for removal of cadmium: kinetic and isotherm studies. Biomass Conversion and Biorefinery. Springer.

[5]. Lei T., Li SJ., Jiang F. et al., **2019**, Adsorption of cadmium ions from an aqueous solution on a highly stable dopamine-modified magnetic nano-adsorbent. Nanoscale Res Lett. 14,352.

[6]. Segneanu, AE., Marin, C.N., Vlase, G., Cepan C., Mihaiescu M.,Muntean C., Grozescu I., **2022**, Highly efficient engineered waste eggshell-fly ash for cadmium removal from aqueous solution. *Sci Rep* 12, 9676.

[7]. Öden M.K., Karasakal E.N., Çildir S., **2022**, Nickel (II) removal from synthetic wastewater by adsorption using waste pea shell, International Journal of Environmental Trends, 6(1): 10-20.

[8]. Al-Abbad E.A., Al Dwairi R.A., **2021**, Removal of nickel (II) ions from water by Jordan natural zeolite as sorbent material. Journal of Saudi Chemical Society, 25(5):101233.

[9]. Charazińska S., Burszta-Adamiak E. Lochyński P., **2022**, Recent trends in Ni(II) sorption from aqueous solutions using natural materials. Rev Environ Sci Biotechnol 21, 105–138.

DETERMINATION OF AOX CONTENT IN WASTEWATER AND MINERAL WATER SAMPLES

Marjana Simonič

University of Maribor, Faculty of Chemistry and Chemical Engineering, 2000 Maribor, Smetanova 17, Slovenia
e-mail: marjana.simonic@um.si

Abstract

The aim of the work was to validate the analytical method for determination of adsorbable organically bound halogens (AOX) in wastewater samples. We have determined selectivity, working range, accuracy, precision, and matrix effect. The real wastewater samples were analysed on AOX content We have developed a useful method for high AOX polluted wastewaters.

Introduction

Adsorbable organic bound halogens (AOX) is an expression for organic compound which adsorb on activated carbon and contain halogens, mainly chlorine [1]. They are expressed as chlorine in accordance with European standard [2]. One of the main sources of AOX in municipal wastewaters is thought to be hospital wastewater [3]. AOX has toxic effects on aquatic organisms. It can accumulate in the food chain and cause persistent effects in the environment [3]. Around three thirds of the total AOX can be removed by direct filtration process using a microfiltration membrane or an efficient chemical precipitation process [4].

Different separation processes were appropriate for the treatment of wastewater, such as filtration or degradation processes, such as sequencing batch reactor (SBR) [3]. Due to increasing content of persistent compounds such as pharmaceuticals and AOX, advanced oxidation processes are more suitable recently for municipal wastewtaer treatment with effluents from hospital [5].UV/H_2O_2, Fenton, fotofenton processes, etc. have been studied in last decades.

The increased concentrations of AOX were reported in swimming pool wastewater [6]. The urea removal process using anti-chlorourea oligomer promoted the conversion of organic matters to chlorinated disinfection byproducts, and then to brominated disinfection byproducts. Consequently the AOX expressed as total adsorbable halogens (TOX) significantly increased. Highly toxic bromated disinfection byproducts resulted in up to 7-fold increase in the cytotoxicity.

The main objective of the work reported here was to determine the AOX concentrations in the selected polluted wastewater samples. A coulometric method was chosen. Validation of the method was demonstrated, determining accuracy, precision, measuring range, and matrix effect.

Experimental

Samples

Industrial wastewater sample was taken from the company effluent (Maribor, Slovenia) and analysed as a real water sample. Next sample was swimming pool wastewater. Samples were taken in dark glass ware, 0.5 L, cleaned with surfactant (Ecolab). Samples were quantified in triplicates, and standard deviations were calculated.

Matrix effects in wastewater samples were determined.

Calibration curve and sample preparation

AOX standard (100680, Supelco), 20 mg/L 4-chlorophenol solution was used. Working standard solutions were prepared daily by diluting the stock solution with Milli-Q water in the range from 0.1 mg/L to 2 mg/L. The AOX cell test 100675 was applied connected with photometer. Firstly, adsorption column in prepared and sample enriched. AOX adsorb on activated carbon followed by digestion. AOX were finally determined using photometer Spectroquant NOVA 60. The column was placed into empty cell and reagent AOX-1 was added. Then the column was washed by AOX-2 and AOX-3 reagent three times with each. Into the cell the 100 mL wastewater sample was poured, and 6 drops of AOX-4 reagent was added for pH adjustment (from 1.5 and 2). The column was detached from reservoir. 10 mL of AOX-5 was filled using syringe and coupled with the column with activated carbon (Figure 1) and 2 micro-spoons of AOX-6 reagent. Cell was closed, shaken, and put into thermos-reactor at 120 °C for 30 mins. When the cell was cooled to room temperature 5 drops of AOX-4 reagent was added, 0.2 mL of AOX-1K and 7 mL of sample. After 15 min the concentration of AOX in photometer was read. The same procedure was applied for determination of AOX in samples.

Figure 1. AOX syringe attached with sample in a cell

Results and discussion

Calibration curve

Calibration curve is presented in Figure 2.

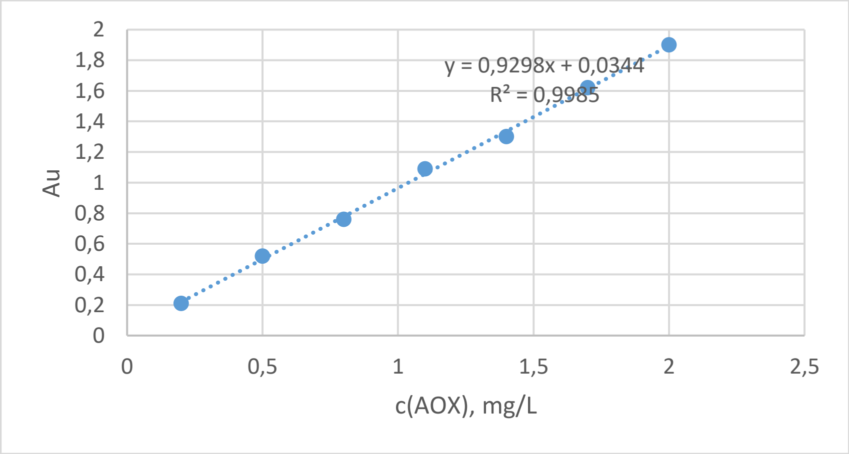

Figure 2. The calibration curve for AOX in the concentration range from 0.2 mg/L to 2 mg/L

The correlation coefficient R^2 values were greater than 0.998, and the quality coefficient was 1.8 %. The linearity was confirmed. Reproducibility was confirmed with *RSD* lower than 5 %.

Homoscedasticity test

The ten replicates were measured for the lowest (0.1 mg/L) and highest concentration level (2.0 mg/L). Standard deviation and variance were calculated, and *F*-test was performed. The results are presented in Table 1.

Table 1: Homoscedasticity test

	Average value (mg/L)	*Variance (mg/L)*	
AOX(0.1 mg/L)	0.104	1.927	
AOX(2 mg/L)	2.108	34.082	
F_c			10.9
F_{tab}			4.0

Calculated *F*-value was higher compared with tabular *F*-value, $F_c > F_{tab}$ therefore the data were heteroscedastic.

Accuracy

Accuracy was confirmed by interlaboratory test. Three replicates of samples were analysed. The results are gathered in Table 2. The differences were small.

Table 2. Accuracy test

	Result (mg/L)	*Overall results (mg/L)*	*Difference*
Sample 1	0.350	0.340	3.0 %
Sample 2	0.220	0.230	4.5 %

Repeatability

Repeatability was confirmed by two-day analyses of two samples in 10 replicates. Table 3 presents the results. *RSD*-s were below 5 %.

Table 3. Repeatability test

	Result average (mg/L)	*Stdev (mg/L)*	*RSD*
Sample 1	0,50	0,020	4.0 %
Sample 2	0,52	0,022	4.2 %

Water sample analysis

The AOX was determined in an industrial wastewater. The average value of 10 replicate was determined at 0.27 mg with standard deviation 0.003 mg/L and RSD 1.4 %. Without matrix, the *RSD* was determined at 1.1 %. There was no difference and RSD below 10 %.

The second sample was swimming pool wastewater and AOX were measured at 0,22 mg. The average value of 10 replicate was determined at 0,23 mg with standard deviation 0,006 mg/L and *RSD* 2.1 %. Without matrix, the *RSD* was determined at 1.1 %. The difference was low and *RSD* below 10 %.

Matrix effect

Standard addition method was applied for study of matrix effect. Four standard solutions were added to the wastewater sample and the curve was determined. The *t*-test was performed:

$$t_c = b_1 * b_2 / (s_{b1}^2 + s_{b2}^2)$$

where t_c = calculated t-value

b_1 and b_2 are slopes of calibrate curve and curve gained after standard addition, s_{b1} and s_{b2} are their standard deviations.

The calculated t_c was 1.20 and 1,2 for wastewater and pool water. Tabular t_{tab} was 2.57 (at 95 % confidence level), thus $t_c < t_{tab}$ and the matrix does not affect the measurement for both types of wastewater samples..

Conclusions

The aim of this study was to determine the concentration of AOX in wastewater samples using coulometry. The method conditions were verified by determination of matrix effect, linearity, precision, accuracy, and LOD. The standard addition method was used and based on the slopes with the t-test it was determined that the matrix affects the measurements. The linearity of the method was confirmed with the correlation coefficients greater than 0.999 from 0.2 to 2.0 mg/L. The low *RSD* (≤ 4.0 %) clearly indicates the reproducibility and the successful application of the developed method for the quantitative measurement of AOX in highly polluted wastewater samples.

Acknowledgements

The author would like to thank Aleksandra Savič for laboratory work performance and funder the Slovenian Research and Innovation Agency Programme P2-0032.

References

[1] T. Benabdallah El-Hadj, J.Dosta, R. Torres, J. Mata-Alvarez, Biochem Eng J., 36 (2007) 281-287.
[2] SIST EN ISO 9652: 2005 Water Quality – Determination of adsorbabble organicaaly bound halogens, Geneva 2005.
[3] I.H. Farooqi, F. Basheer, J. Water Process Eng., 19 (2017), 60-66.
[4] S. M. Hocaoglu, M. D. Celebi, I. Basturk, R. Partal, J. Water Process Eng, 43 (2021) 102205.
[5] G. Moussavi, E. Fathi, M. Moradi, Process. Saf. Environ. Prot., 126 (2019) 259-268.
[6] D. Zhang, L. Chen, S. Dong, J. Luo, Z. Xu, W. Chu, Water Res. 223 (2022) 118987.

KINETIC ASPECTS OF SILVER IONS RELEASE FROM Ag-POLY(*N*-ISOPROPYLACRYLAMIDE/ITACONIC ACID) HYDROGEL NANOCOMPOSITES

Jelena Spasojević[1], Ivana Vukoje[1], Nikolina Nikolić[1], Milica Milošević[1], Dragan Ranković[2], Aleksandra Radosavljević[1]

[1]Vinča Institute of Nuclear Sciences, National Institute of the Republic of Serbia, University of Belgrade, Mike Petrovića Alasa 12-14, 11351 Vinča, Belgrade, Serbia
[2]Faculty of Physical Chemistry, University of Belgrade, Studentski trg 12-16, 11000 Belgrade, Serbia
e-mail: jelenas@vin.bg.ac.rs

Abstract

In recent years, drug delivery systems have been one of the most investigated solutions for safer and more efficient therapy. Among many investigated materials, hydrogels with incorporated drugs and/or active substances can be produced in different ways to meet the criteria of biocompatibility, non-toxicity, continuous drug delivery, etc. In our previous work, the Ag-P(NiPAAm/IA) hydrogel nanocomposites were produced by radiolytic method, which enabled the synthesis and sterilization of materials in one technological step. Because of silver ions release, these hydrogel nanocomposites showed good antibacterial potential against both gram-positive and gram-negative bacteria. In this study, we go a step forward and investigate the silver release mechanism by fitting experimentally obtained data with several commonly used kinetics models of drug release.

Introduction

During the past decades, hydrogels have gained considerable interest because of their unique properties and versatile applications. Their 3D network can absorb and retain large amounts of water and/or other physiological fluids, giving them a soft structure similar to living tissue. Such types of materials are recognized as promising systems for drug and/or active compound delivery. Nanocomposite materials based on polymer hydrogels with embedded metal nanoparticles have attracted tremendous attention due to an extremely wide range of applications, especially in biomedicine [1, 2]. In a previous study, novel multifunctional silver-poli(*N*-isopropylacrylamide/itaconic acid) (Ag-P(NiPAAm/IA)) hydrogel nanocomposites were prepared by gamma irradiation induced synthesis. This “green” technique uses biologically harmless and biocompatible radiolytic products of water, enabling the production of crosslinked nanocomposites without the use of any additional substances, which can be harmful, toxic, or difficult to remove from the system. Moreover, this method also enables simultaneous synthesis and sterilization of materials, which is a very important prerequisite for their use in the field of biomedicine [3, 4]. Among the numerous nanoparticles, probably the most investigated and the most promising have become the silver nanoparticles (AgNPs) due to their ability to prevent the growth and development of single-celled organisms and therefore can be used as a therapeutic agent against Gram-positive and Gram-negative bacteria, fungus or viruses. Furthermore, AgNPs also possess strong anti-septic and anti-inflammatory properties, with low systemic cytotoxicity effects [5]. Nowdays, great emphasis has been placed on the development of suitable wound dressing, with appropriate antibacterial effects, which could be able to protect the injury site from further insult, contamination, and infection [6].

In this study, the Ag^+ ions release from Ag-P(NiPAAm/IA) hydrogel nanocomposites was investigated in a physiological simulated condition. To evaluate the mechanism of silver release, the experimentally obtained data were fitted using zero-order, first-order, Ritger-

Peppas, Higuchi, Kopcha, and Makoid-Banakar models. Moreover, the diffusion coefficients of silver release from hydrogel nanocomposites were determined.

Experimental

Series of P(NiPAAm/IA) hydrogels were prepared by adding the IA into NiPAAm solutions (10 wt%) to obtain comonomer mixtures with the weight ratios 100/0, 98.5/1.5, 97/3 and 95.5/4.5. Those mixtures were saturated with argon for 30 min, poured into specially designed glass molds, and exposed to γ-irradiation (absorbed dose of 50 kGy; dose rate 0.5 kGy/h). The obtained hydrogels were cut into discs (diameter ≈ 10 mm, thickness ≈ 4 mm) and immersed in distilled water (changed daily for one week) to remove unreacted residues. Furthermore, the P(NiPAAm/IA) hydrogel discs were swelled in the solution of $AgNO_3$ (1.0×10^{-2} mol/dm^3) and 2-propanol (0.2 mol/dm^3), and then exposed to γ-irradiation to perform reduction of Ag^+ ions (absorbed dose of 18 kGy; dose rate 17 kGy/h). As a result, the formation of AgNPs was confirmed by obtaining yellow-colored Ag-P(NiPAAm/IA) hydrogel nanocomposites.

The release of Ag^+ ions from the Ag-P(NiPAAm/IA) hydrogel nanocomposites was monitored in phosphate buffer solution (PBS, pH 7) at 37ºC. Nanocomposite samples were immersed in 10 ml of PBS, which was changed at predetermined time intervals with new 10 ml, to maintain the perfect sink condition. The total content of silver within the Ag-P(NiPAAm/IA) hydrogel nanocomposites was determined upon treatment in HNO_3 (1:1 v/v) to induce the oxidation of all AgNPs into Ag^+ ions. The Ag^+ ions concentration was determined by atomic absorption spectrometry, and the results represent the mean of three measurements.

Results and discussion

The release of Ag^+ ions from Ag-P(NiPAAm/IA) hydrogel nanocomposites was monitored in PBS at 37ºC in order to simulate the physiological condition. The obtained results for cumulative silver release indicate that after 4 days of monitoring, the Ag-P(NiPAAm/IA) (100/0) hydrogel nanocomposite released the smallest amount of initial concentration of silver (59.9 %), whereas samples with 1.5 wt%, 3 wt% and 4.5 wt% of IA in copolymer network released 73.8 %, 71.1 % and 78.2 % of initial concentration of silver, respectively. Moreover, it is obvious that the initial burst release of Ag^+ ions is followed by the slower release in the middle and later phases.

To evaluate the kinetics and to determine the mechanism of release, the experimental data were fitted and compared with several commonly used kinetics models of the drug release process. The cumulative Ag^+ ions release profiles were analyzed by zero-order (Eq. (1)), first-order (Eq. (2)), Ritger-Peppas (Eq. (3)), Higuchi (Eq. (4)), Kopcha (Eq. (5)) and Makoid-Banakar (Eq. (6)) models [2, 7, 8]:

$$M_t = M_0 + k_0\,t, \tag{1}$$

$$ln(M_\infty - M_t) = lnM_0 - k_1\,t, \tag{2}$$

$$\frac{M_t}{M_\infty} = k_{\mathrm{RP}}\,t^n, \tag{3}$$

$$\frac{M_t}{M_\infty} = k_H\,t^{1/2}, \tag{4}$$

$$\frac{M_t}{M_\infty} = A\,t^{1/2} + B\,t, \tag{5}$$

$$\frac{M_t}{M_\infty} = k_{MB}\,t^n\,\exp(-Ct), \tag{6}$$

where M_t is the amount of silver released in time t, M_0 is the amount of silver released in time t=0 (M_0=0), M_∞ is the initial amount of silver in hydrogel nanocomposites, while M_t/M_∞ is the fraction of silver released at each time point; k_0 is a zero-order rate constant, k_1 is the first-order rate constant, k_{RP} is constant dependent on the polymer network properties, n is the diffusional exponent which indicates the transport mechanism during the release, k_H is the Higuchi dissolution rate constant, A and B are the Kopcha constants indicating the dominant process during the release, k_{MB} is the Makoid-Banakar constant and C is an empirical parameter. The mathematical modeling of Ag^+ ions released from hydrogel nanocomposites is presented in Fig. 1, while the obtained fitting parameters are summarized in Table 1.

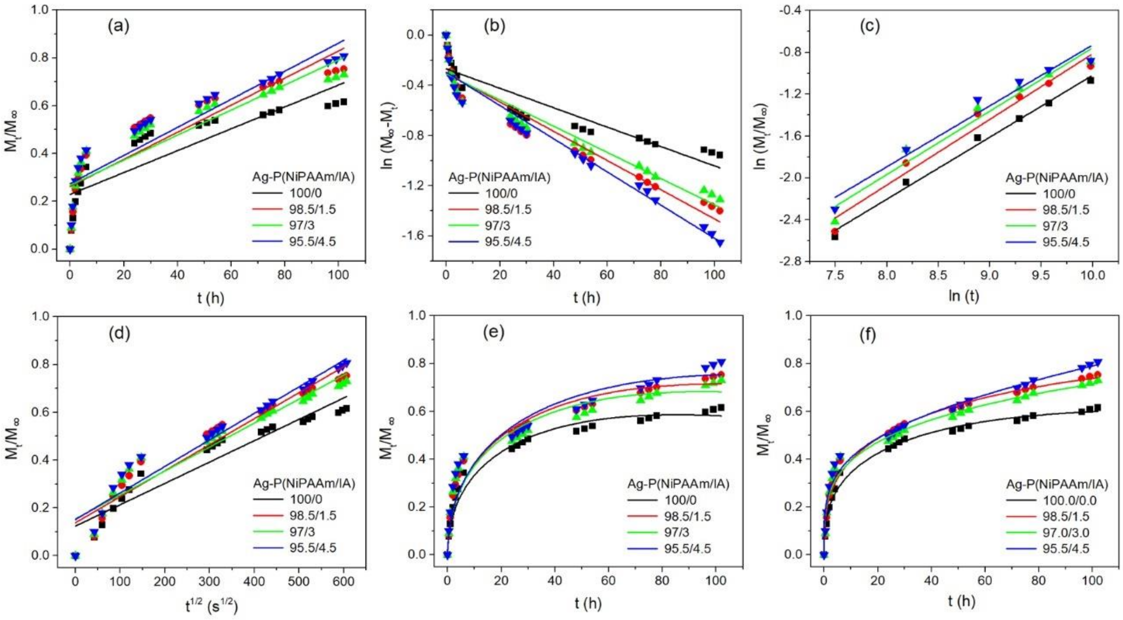

Figure 1. Mathematical modeling of cumulative Ag^+ ions release from Ag-P(NiPAAm/IA) hydrogel nanocomposites: (a) zero-order model, (b) first-order model, (c) Ritger-Peppas model, (d) Higuchi model, (e) Kopcha model and (f) Makoid-Banakar model.

The curvilinear nature of cumulative release profiles suggests that silver release from the hydrogel nanocomposites follows neither the zero-order nor first-order kinetics. This observation is supported by the lowest values of correlation coefficients (R^2). The Ritger-Peppas model showed that silver release from investigated samples follows anomalous or non-Fickian diffusion ($n \approx 0.58$-0.61) when both mechanisms (diffusion and relaxation of polymer chains) influence the release process. The high values of R^2 (0.95-0.99) indicate the good fitting between the model and experimentally obtained data, but only at an early stage of releasing ($M_t/M_\infty < 0.6$). In this case, that is the stage of the initial burst release of Ag^+ ions. As expected, the values of Higuchi dissolution rate constants are higher for systems with improved swellability (higher IA content). The formation of a concentration gradient is the main trigger for the diffusion of Ag^+ ions from the polymer matrix into the surrounding medium. The Higuchi model shows a good fit with silver release data ($R^2 \approx 0.97$-0.98), as well as the Kopcha model, but with slightly lower R^2 (0.95-0.98). The Kopcha model can be used to quantify the relative contributions of diffusion and polymer relaxation to drug release. The data in Table 1. clearly show that the values of the diffusional constant (A) are far greater than that for the relaxation constant (B), suggesting that Ag^+ ions release from the Ag-P(NiPAAm/IA) hydrogel nanocomposites is primarily controlled by a Fickian diffusion process. However, the mathematical model that best describes Ag^+ ions release is the Makoid-Banakar model in which the R^2 values are the highest (0.98-0.99). Makoid-Banakar model provided a slightly better fit for the experimental data, compared to the Ritger-Peppas model. When the value of parameter $C \rightarrow 0$, the Makoid-Banakar model becomes equal to Ritger-Peppas. The values of C are low but not equal to zero, so the introduction of an exponential parameter in the model, related to the dissolution of AgNPs, evidently provides a better correlation with the experimental data.

Table 1. Kinetic parameters of Ag^+ ions released from hydrogel nanocomposites obtained by different models, and diffusion coefficients determined by Etters approximation.

Model	Parameters	Sample Ag-P(NiPAAm/IA)			
		100/0	98.5/1.5	97/3	95.5/4.5
Zero-order	$k_0 \times 10^6$ (1/s)	1.27	1.57	1.46	1.63
	R^2	0.74	0.78	0.77	0.81
First-order	$k_1 \times 10^6$ (1/s)	2.15	3.24	2.90	3.68
	R^2	0.83	0.85	0.85	0.84
Ritger-Peppas	$k_{RP} \times 10^4$ ($1/s^n$)	9.64	8.34	10.95	14.24
	n	0.59	0.60	0.61	0.58
	R^2	0.99	0.96	0.95	0.95
Higuchi	$k_H \times 10^3$ ($1/s^{1/2}$)	0.89	1.09	1.00	1.11
	R^2	0.97	0.98	0.98	0.97
Kopcha	$A \times 10^3$ ($1/s^{1/2}$)	2.11	2.37	2.34	2.37
	$B \times 10^6$ (1/s)	-1.90	-1.97	-2.00	-1.85
	R^2	0.98	0.97	0.95	0.95
Makoid-Banakar	$k_{MB} \times 10^3$ ($1/s^n$)	9.35	14.40	24.16	28.40
	n	0.35	0.32	0.27	0.25
	$C \times 10^4$	7.38	3.18	0.37	-2.62
	R^2	0.99	0.99	0.98	0.98
Diffusion coefficient	$D_E \times 10^3$ (cm^2/s)	3.34	6.44	6.66	11.60
	R^2	0.90	0.97	0.97	0.99

Finally, the diffusion coefficients of Ag^+ ions from the polymer matrix were determined by the Etters approximation, using the following equation:

$$\frac{M_t}{M_\infty} = \left[1 - exp\left(-K\left(\frac{D_E\, t}{\delta^2}\right)^a\right)\right]^{1/b}, \qquad (7)$$

where D_E is the diffusion coefficient of silver for the entire range of releasing ($0 < M_t/M_\infty < 1$), t is the time and δ is the thickness of the xerogel, while a = 1.3390, b = 2.6001 and K = 10.5449 are the constants [9]. As can be seen from Table 1, the diffusion coefficients of Ag^+ ions release increase with increasing IA content in a polymer matrix, which is expected. Namely, with increasing IA content, the swelling capacity of hydrogel nanocomposites increases because of increased porosity, leading to the faster diffusion of the medium into the hydrogel nanocomposites. Therefore, the higher content of the swelling medium enables easier and faster dissolution of silver and its diffusion from the hydrogel nanocomposites. According to the values of R^2, the least fit is observed for the homopolymer network (100/0) probably due to the initial burst release of Ag^+ ions.

Conclusion

In order to evaluate the kinetics and to determine the mechanism of Ag^+ ions release from the Ag-P(NiPAAm/IA) hydrogel nanocomposites the several drug delivery models were employed. It was demonstrated that the Makoid-Banakar showed the best fitting to the silver release profiles, indicating that diffusion is the dominant mechanism. This was supported by the Kopcha model, while the Higuchi model confirms that the dissolution of AgNPs and the formation of a concentration gradient play a key role in the release process. In addition, diffusion coefficients of silver release increase when the hydrogel nanocomposites are in more hydrated form (more porous network).

Acknowledgements

This work was supported by the Ministry of Science, Technological Development and Innovations of the Republic of Serbia (Contract No. 451-03-47/2023-01/200017).

References

[1] J. Spasojević, A. Radosavljević, J. Krstić, D. Jovanović, V. Spasojević, M. Kalagasidis Krušić, Z. Kačarević-Popović, Dual responsive antibacterial Ag-poly(N-isopropylacrylamide/itaconic acid) hydrogel nanocomposites synthesized by gamma irradiation, Europen Polymer Journal 215 (69) 168-185.

[2] J. Krstić, J. Spasojević, A. Radosavljević, A. Perić-Grujić, M. Đurić, Z. Kačarević-Popović, S. Popović, *In Vitro* Silver Ion Release Kinetics from Nanosilver/Poly(vinyl alcohol) Hydrogels Synthesized by Gamma Irradiation, Journal of Applied Polymer Science 131 (2014) 40321.

[3] M.T.S. Alcantara, N. Lincopan, P.M. Santos, P.A. Ramirez, A.J.C. Brant, H.G. Riella, A.B. Lugao, Simultaneous hydrogel crosslinking and silver nanoparticle formation by using ionizing radiation to obtain antimicrobial hydrogels, Radiation Physics and Chemistry 165 (2019) 108369.

[4] N. Nikolić, J. Spasojević, A. Radosavljević, M. Milošević, T. Barudžija, L. Rakočević, Z. Kačarević-Popović, Influence of poly(vinyl alcohol)/poly(N-vinyl-2-pyrrolidone) polymer matrix composition on the bonding environment and characteristics of Ag nanoparticles produced by gamma irradiation. Radiation Physics and Chemistry 202 (2023) 110564.

[5] S. Bhowmick, V. Koul, Assessment of PVA/silver nanocomposite hydrogel patch as antimicrobial dressing scaffold: Synthesis, characterization and biological evaluation, Materials Science and Engineering: C 59 (2016) 109-119.

[6] Y. Xie, X. Liao, J. Zhang, F. Yang, Z. Fan, Novel chitosan hydrogels reinforced by silver nanoparticles with ultrahigh mechanical and high antibacterial properties for accelerating wound healing, International Journal of Biological Macromolecules 119 (2018) 402-412.

[7] M. Askarizadeh, N. Esfandiari, B. Honarvar, S. Ali Sajadian, A. Azdarpour, Kinetic Modeling to Explain the Release of Medicine from Drug Delivery Systems, ChemBioEng Reviews, https://doi.org/10.1002/cben.202300027.

[8] K. Nešović, A. Janković, V. Kojić, M. Vukašinović-Sekulić, A. Perić-Grujić, K. Yop Rhee, V. Mišković-Stanković, Silver/poly(vinyl alcohol)/chitosan/graphene hydrogels – Synthesis, biological and physicochemical properties and silver release kinetics, Composites Part B: Engineering 154 (2018) 175-185.

[9] M.P. Mullarney, T.A.P. Seery, R.A. Weiss, Drug diffusion in hydrophobically modified N,N-dimethylacrylamide hydrogels. Polymer 47 (2006) 3845-3855.

BIOLOGICAL AND CATALYTIC ACTIVE NANOCOMPOSITES OF METAL NANOPARTICLES (Ag, Au, AND Cu) AND CONDUCTIVE POLYMERS (POLYANILINE AND POLYPYRROLE) FOR VARIOUS APPLICATIONS

Una Stamenović, Vesna Vodnik, Dijana Mašojević

Vinča Institute of Nuclear Sciences - National Institute of the Republic of Serbia, University of Belgrade, Belgrade, Serbia
e-mail: una.bogdanovic@gmail.com

Abstract

A special group of functional materials with advanced features and accordingly promising applications are the nanocomposites of the metal nanoparticles (MNPs) - gold (Au), silver (Ag), and copper (Cu) and intrinsically conductive polymers - polyaniline and polypyrrole [1-7]. Thanks to the characteristics of these MNPs such as tunability of the plasmon resonance through variation of their size, shape, and composition, in combination with polymers, it is possible to create nanocomposites for specific biomedical and catalytic use as a variety of biological/catalytic processes occurring at nanometer scale. These processes are also related to the surface effects of the MNPs, i.e. the reactive (111) crystallographic planes present on their surface, together with the electrical characteristics and morphology of the polymer, as well as the synergistic activity of both components. Biocompatible polymers with good conductivity and electrochemical activity, such as polyaniline or polypyrrole, are good choices for the formation of functional composites with these MNPs, by *in-situ* polymerization processes. In addition, they protect the MNPs from agglomeration or oxidation and improve their physicochemical characteristics, functions, and variety of applications. The electrocatalytic response of the different prepared nanocomposites for oxygen reduction reaction, and direct borohydride fuel cells, together with their antimicrobial activity, currently investigated in this field in our group, are the subject of the presented work.

Acknowledgements

The research were funded by the Ministry of Science, Technological Development and Innovation of the Republic of Serbia, via direct financing of Vinča Institute of Nuclear Sciences - National Institute of Republic of Serbia (contract number: 451-03-47/2023-01/200017).

References

[1] U. Bogdanović, V. V. Vodnik, M. Mitrić, S. Dimitrijević, S. D. Škapin, V. Žunič, M. Budimir, M. Stoiljković, ACS App. Mater. Interfaces 7 (2015) 1955.
[2] U. Bogdanović, I. A. Pašti, G. Ćirić-Marjanović, M. Mitrić, S. P. Ahrenkiel, V. V. Vodnik, ACS App. Mater. Interfaces 7 (2015) 28393.
[3] U. Stamenović, N. Gavrilov, I. A. Pašti, M. Otoničar, G. Ćirić-Marjanović, S. D. Škapin, M. Mitrić, V. Vodnik, Electrochim. Acta 281 (2018) 549.
[4] J. Milikić, U. Stamenović, V. Vodnik, S.P Ahrenkiel, B. Šljukić, Electrochim. Acta 328 (2019) 135115.
[5] J. Milikić, A. Tapia, U. Stamenović, V. Vodnik, M. Otoničar, S. Škapin, D. M.F. Santos, B. Šljukić, Int. J. Hydrog. Energy 47(2022) 36990.
[6] D. Mašojević, U. Stamenović, M. Otoničar, S. Davidović, S. Škapin, T. Barudžija, V. Vodnik, Mater. Lett. 338 (2023) 134051
[7] J. Milikić, U. Stamenović, V. Vodnik, M. Otoničar, S. Škapin, B. Šljukić, Mol. Catal. 547 (2023) 113310

RESPONSE OF ARUGULA (*ERUCA SATIVA* MILL.) TO INORGANIC, ORGANIC AND METALLURGICAL SLAG AMENDMENTS TO ACID SOIL

Aleksandra Stanojković-Sebić[1], Radmila Pivić[1], Aleksandar Stanojković[2]

[1]Institute of Soil Science, Teodora Drajzera 7, 11000 Belgrade, Republic of Serbia
[2]Institute for Animal Husbandry, Autoput 16, 11080 Belgrade- Zemun, Serbia
e-mail: astanojkovic@yahoo.com

Abstract

The aim of this study was to determine an influence of Ca - containing metallurgical slag application, sampled from steel factory area, as well as the influence of commercial lime material and fertilizers, on macro and trace elements content in aerial biomass of arugula, grown on Eutric Cambisol (a soil with high acidity), through greenhouse semi-controlled pot experiments, in 2019. The influence of metallurgical slag was compared to those of commercial lime material ($CaCO_3$) solely and in combination with inorganic and organic fertilizers. Content of N was determined using elemental CNS analyzer, P - by spectrophotometer, and K - by flame emission photometry. In the determination of Fe, Zn, Cu and Cd, ICP-AES was used. Used metallurgical slag, in combination with mineral and organic fertilizer, showed positive effects on the main chemical composition of arugula and its yield. The high and toxic concentrations of trace elements in plant comparing to plants from untreated soil were not significantly increased and were within the permissible levels in plants in all the treatments in spite of their high content in metallurgical slag. The evaluated results obtained in present study showed high potential in usage of the studied alkaline metallurgical slag when it is combined with inorganic and organic fertilizers, to acid soils toward amelioration their fertility without adverse effects.

Introduction

Arugula (*Eruca sativa* Mill.) is an annual herbaceous plant from the Brassiccaeae family. It belongs to the group of leafy vegetables, since the leaf is mainly used for nutrition, has modest heat requirements and is resistant to frost, so it can be produced practically all year round. It is best suited to soils with a neutral reaction, although it can also be grown on soils with an alkaline reaction. However, it is considered that acidic soil condition can significantly affect the reduction of its growth and development [1].

Acidic soils are widespread and limit plant production all over the world [2], with a similar situation in the Republic of Serbia. The productivity of those soils increasingly becoming a limiting factor in plant production. The constant increase in their surface area is the result of intensive production technology, uncontrolled use of inorganic fertilizers, the impact of acid rain, as well as the lack of organic fertilizers usage [3].

In Serbia, Eutric Cambisols [4], used in this reserch, are considered to be mostly medium-heavy soils, with a marked texture difference through the profile. The degree of base saturation is above 50%, where pH in water is around 5.5 [5]. Intensification in use of cambisols, in the manner of inorganic fertilizers overuse, causes their transformation into marginal, often acid soils, with reduced organic matter. Amelioration of these soils (optimum dose of nutrients and their source) play an important role in enhancing the productivity of crops [6]. It is considered that the first step in creating favorable conditions in these soils for productive plant growth is their acidity reduction. The use of traditional commercial alkaline liming materials to acid soils for the amelioration of acidity consequently improving crop production is a common practice [7]. Along with these materials present in Serbia and regarding its alkaline nature, metallurgical slag, sampled from steel factory area, can be of great importance. Although the significant quantities of metallurgical slag are generated as waste material every day from steel industries, its physicochemical property offers a high potential for its utilization in agriculture. As metallurgical slag contains fertilizer components such as CaO, SiO_2 and MgO, its alkaline property remedies soil acidity. In addition to these three components, it also contains components such as FeO, MnO and P_2O_5, and some slags may contain elevated levels of trace metals such as Fe, Cd, Cr, Cu, Pb, Mo, Ni and Zn, that occur naturally in soil, and many of them are essential plant nutritive. Although there are varying concentrations of trace elements in metallurgical slags, their bioavailability is very low [8]. Metallurgical slag has been used for a broad range of agricultural purposes. On field trials in Pennsylvania the yields of corn, wheat, oats, buckwheat and soybeans with metallurgical slag application were as good or better than an equivalent amount of limestone [9].

The aim of this research was to investigate the effect of Ca-containing metallurgical slag, a by-product from steel factory, on yield and chemical composition (N, P, K, Fe, Zn, Cu, Cd) of the aerial biomass of arugula, grown on Eutric Cambisol (a soil with high acidity) performed in semi-controlled greenhouse conditions. The effect of metallurgical slag were compared to those of commercial lime material ($CaCO_3$) in combination without and with standard inorganic NPK and organic (NPK nutrients of animal origin) fertilizers.

Experimental

The study was performed in Institute of Soil Science in greenhouse semi-controlled vegetative experiments using plastic pots, from the first decade of March to the first decade of May, in 2019. Each pot was filled with 3 kg pot^{-1} of homogenized Eutric Cambisol, brought from an experimental field in Mladenovac town, located about 55 km from Belgrade, Serbia (grid reference: 44°24' N, 20°40' E). In every plastic pot ten arugula seeds were sown. Arugula plants were grown according to the standard growing methods (watering and regular weed control), and without using any plant protection products.

Chemical characteristics of Eutric Cambisol plowed layer, used in present research, were determined in our previous study [10]. Accordingly, the soil is characterized by acid reaction (pH in 1M KCl 4.98), low content of available P (7.98 mg 100 g^{-1}), medium to well supplied with available K (21.8 mg 100 g^{-1}), medium provided with total N (0.28%) and organic matter (3.05%), and very highly provided with available elements: Ca (440 mg 100 g^{-1}), Mg (58 mg 100 g^{-1}), Fe (63 mg kg^{-1}), Mn (43 mg kg^{-1}) and Co (0.26 mg kg^{-1}). According to textural composition, Eutric Cambisol is a clay loam and has a relatively favorable particle size distribution for the plant cultivation.

The following seven designed treatments were carried out in three replications: control - untreated soil (T1); $CaCO_3$ (T2); NPK inorganic fertilizer (NPK) + $CaCO_3$ (T3); NPK organic fertilizer (NC) + $CaCO_3$ (T4); metallurgical slag, MS (T5); NPK + MS (T6); NC + MS (T7). Before sewing the arugula, the amount of fertilizers, $CaCO_3$ and slag was measured according to the experimental design and mixed with soil (calculated as for 1 ha): NPK inorganic fertilizer (15:15:15) = 500 kg ha^{-1}; NC organic fertilizer = 170 kg ha^{-1}; $CaCO_3$ = 4 t ha^{-1}; MS = 4 t ha^{-1} (same as the amount of $CaCO_3$). Both MS and $CaCO_3$ with granulation of 0.2 mm were used in the experiment.

The samples of metallurgical slag used in present study were taken during spring 2009 from different deposition sites of Steel factory – Smederevo, Serbia (previously US Steel, now Hesteel Smederevo Steel Plant) located approximately 60 km South-East from Belgrade.

Chemical composition of used MS was determined in our previous study [3]. Accordingly, this material has very alkaline reaction (pH in H_2O 12.48), with the content of calcium in oxide forms (CaO) from 33-45%, of which about 50% is easily soluble in 1 M ammonium acetate; content of the total Mg was mainly in forms of MgO, while nearly all the amount of P is in available forms for plants; contents of the total Fe (15.34 %) and Mn (1.80 %) are high, but with lower amounts of their soluble forms; content of the total Zn is in lower amounts (14.60 %), while the total content of Cu is a little higher (228.80 %).

Organic fertilizer applied in present research is a solid NPK 4:3:4 nutrient of animal origin, commercially called Nervosol Complex (NC). According to its main chemical composition, it consists of 4% of total N, 4% of organic N, 3% of P (P_2O_5 form), 4% of K (K_2O form), and 30% of organic C [11].

The aerial biomass (stems with developed leaves) of arugula plants was taken at the beginning of rosette formation from each experimental variant and replicate in experimental pots. Biomass was then air-dried and the yield of plants was measured and expressed in g pot^{-1}, after which it was dried for 2 hours at 105°C and weighed again for chemical analyses, using gravimetric method for determination of dry matter content of plant tissue [12]. The content of total N was determined on elemental CNS analyzer Vario EL III [13]. The content of P was determined by spectrophotometer with molybdate, and the content of K - by flame emission photometry [14]. The content of trace elements - Fe, Zn and Cu, as well as the toxic heavy metal Cd, was determined using inductively coupled plasma-atomic emission spectrometry (ICP-AES), after microwave oven extraction and moisture content [15].

The effects of experimental treatments on the studied chemical parameters and yield of the plants were evaluated using the SPSS ANOVA, followed by Duncan's Multiple Range Test (DMRT). Significant differences between means were tested by the LSD test at P = 0.05.

Results and discussion

Plant analysis can play a major role when diagnosing mineral nutrition and trace elements problems, whether for research purposes, or for solving practical field problems for farmers and growers. The concentrations of all analyzed macroelements (Table 1) and trace elements (Table 2) in arugula aerial biomass were *significantly affected* by all treatments applied (T1-T7).

Table 1. Macroelements content in arugula and its yield depending on the treatment used

Treatments	Macroelements (% in dry biomass)*			Yield* (g pot^{-1})
	N	P	K	
T1 - control (untreated soil)	3.10 ± 0.01^{d}	0.64 ± 0.02^{b}	2.89 ± 0.03^{e}	6.31 ± 0.51^{b}
T2 - $CaCO_3$	3.31 ± 0.31^{a}	0.81 ± 0.03^{b}	3.83 ± 0.11^{bc}	6.44 ± 0.12^{b}
T3 - NPK + $CaCO_3$	4.28 ± 0.19^{b}	0.84 ± 0.02^{b}	3.86 ± 0.27^{b}	6.69 ± 1.62^{b}
T4 - NC + $CaCO_3$	4.52 ± 0.13^{b}	0.69 ± 0.01^{b}	3.35 ± 0.26^{d}	6.52 ± 0.70^{b}
T5 - MS	3.81 ± 0.15^{c}	0.70 ± 0.02^{b}	3.41 ± 0.17^{d}	6.52 ± 1.32^{b}
T6 - NPK + MS	5.13 ± 0.17^{a}	2.76 ± 0.22^{a}	5.85 ± 0.13^{a}	7.89 ± 1.79^{a}
T7 - NC + MS	4.86 ± 0.09^{a}	0.92 ± 0.07^{b}	3.93 ± 0.19^{c}	7.93 ± 5.33^{a}
P value	***	***	***	***
LSD (0.05)	0.239	0.377	0.329	0.272

*means ± standard deviation; LSD - least significant difference; *, **, *** - statistical significant differences at $P<0.05$, $P<0.01$ and $P<0.001$, respectively; values followed by the same letter in a column are not significantly different at $P<0.05$.

Results of the main macroelements content (N, P, K) in arugula aerial parts show high statistically significant differences (*P****) between the treatments at $P<0.05$ for all studied elements, particularly for P and K (Table 1). Regarding to that, there is a noticeably tendency of an increase in the content of N, P and K in tested plant material in the treatments that included NPK inorganic and NC organic fertilizer, respectively, in combination with MS (T6 and T7), in relation to other treatments including control. The results of arugula yield were in accordance with chemical ones, meaning that the yield was highly significantly higher (*P****) at $P<0.05$ in treatments T6 and T7 (Table 1). The promotion of arugula biomass growth which led to the promotion of its yield could be explained by improved organic and inorganic nutrition mixing with metallurgical slag. According to Prasad and Power [16], the optimum pH range in soil for growth of most crops is between 5.5 and 7.0, within which most plant nutritives are available. Most plant nutrients will not dissolve when the soil is either too acidic or too alkaline. Depending upon individual needs of vegetables, such as availability to plant roots, the pH level determines what nutrient elements, such as N, P, and K, become available to plants and how efficiently they are absorbed when they dissolve in water or soil moisture. Crops, including arugula, grown on acid soil low in organic matter are likely to be injured more by acidity than on soil having the same acidity but higher in organic matter content [17, 18]. However, application of organic and inorganic fertilizers in combination with lime, such as metallurgical slag, proves to be an excellent package for improving productivity and health of acid soils.

The concentration of trace elements in arugula aerial parts shows that there are statistically highly significant differences (*P****) between different treatments at $P<0.05$ for all studied trace elements (Table 2). The content of Fe, Zn and Cu in plants from all treatments were in the range of normal and critical concentrations, but far below the toxic values [19, 20, 21]. Zn can become toxic since its activity increases rapidly with decreasing pH, and at pH above 7.0 its bioavailability to crops is substantially reduced [22]. There were not found toxic levels of Cu and Fe in aerial plant parts in the treatments where solely metallurgical slag was applied in spite of their significant content in this liming material. According to the reference values [19, 20, 21], the content of Cd was within the safety limits and permissible levels in all the treatments, which is a highly desirable outcome since Cd is a highly mobile element and can be easily translocated to the aerial plant parts, causing a toxicity [23].

Table 2. Effect of applied treatments on the content of trace elements in arugula biomass

Treatments	Trace elements (% of dry biomass)[*]			
	Fe	Zn	Cu	Cd
T1 - control (untreated soil)	100.35 ± 1.07^{c}	48.58 ± 2.02^{de}	6.88 ± 0.13^{d}	0.64 ± 0.05^{b}
T2 - $CaCO_3$	263.34 ± 7.82	60.22 ± 8.63^{c}	7.67 ± 0.45^{c}	0.42 ± 0.02^{e}
T3 - NPK + $CaCO_3$	57.34 ± 4.11^{d}	63.56 ± 3.70^{abc}	8.30 ± 0.26^{abc}	0.53 ± 0.03^{c}
T4 - NC + $CaCO_3$	49.33 ± 2.55^{d}	46.68 ± 1.81^{e}	8.25 ± 0.15^{abc}	0.45 ± 0.01^{d}
T5 - MS	123.66 ± 3.49^{b}	69.77 ± 3.03^{a}	8.45 ± 0.08^{a}	0.63 ± 0.09^{b}
T6 - NPK + MS	26.67 ± 6.43^{e}	60.93 ± 4.64^{bc}	8.24 ± 0.12^{abc}	0.76 ± 0.02^{a}
T7 - NC + MS	28.32 ± 6.51^{e}	56.43 ± 4.91^{cd}	8.33 ± 0.23^{ab}	0.52 ± 0.01^{c}
P value	***	***	***	***
LSD (0.05)	14.862	6.909	0.577	0.059
Reference value (MPL)				
Normal	50[1]	15[3]	3[3]	<0.1-1[3]
Critical	250[1]	150[2]	15[2]	5[2]
Toxic	600[2]	200[2]	20[2]	10[2]

[*] means ± standard deviation; LSD - least significant difference; *, **, *** - statistical significant differences at $P<0.05$, $P<0.01$ and $P<0.001$, respectively; values followed by the same letter in a column are not significantly different at $P<0.05$; MPL - maximum permissible levels; literature source: [1][19], [2][20], [3][21].

Conclusion

The results of the paper indicate that the treatments with combination of metallurgical slag and organic and mineral fertilizer, respectively, showed positive effects on the content of main and beneficial biogenic macroelements in aerial parts of arugula, particularly in relation to control. Such improved nutrition would explain the promotion of arugula biomass growth which led to the promotion of its yield (the results on arugula yield were in accordance with chemical ones). The contents of trace elements in plant, including toxic Cd, comparing to untreated soil, were not significantly increased and were within the permissible levels in plants in all the treatments. Consequently, high potential has been estimated in the application of the studied alkaline metallurgical slag, particularly, when combined with mineral and organic fertilizers, to acid soils toward amelioration their fertility without adverse effects.

Acknowledgment

Ministry of Science, Technological Development and Innovation of the Republic of Serbia, Contract No. 451-03-47/2023-01/200011.

References

[1] R. Lešić, J. Borošić, I. Buturac, M. Ćustić Herak, M. Poljak, D. Romić, Vegetables, 3rd updated edition, Zrinski, Čakovec, 2016.
[2] H.R. Von Uexkuell, E. Mutert, Plant Soil 171 (1995) 1.
[3] R.Pivić, A.Stanojković, S.Maksimović, D.Stevanović, Fresenius Env. Bull. 20 (2011) 875.
[4] WRB, World Soil Resources Reports, 106, FAO, Rome, Italy, 2014.
[5] G.M. Antonović, Pedological Lexicon, Acta Biol. Jugosl., special series, Union of Biological Scientific Societies of Yugoslavia, Belgrade, 1999.
[6] S.K. Yadav, U.V. Khokar, R.P. Yadav, Integrated nutrient management for strawberry cultivation. Indian J. Hortic. 67 (2010) 445.
[7] Y. Huang, X. Guoping, C. Huigao, W. Junshi, W. Yinfeng, C. Hui, **Procedia Environ. Sci.** 16 (2012) 791.
[8] National Slag Association, http://www.nationalslag.org/tech/ag_guide909.pdf
[9] J.W. White, F.J. Holben, C.D. Jeffries, Mustards - A Brassica Cover Crop for Michigan, Penn State Bulletin *AES* 341 (1937).
[10] J. Maksimović, Ž. Dželetović, Z. Dinić, A. Stanojković-Sebić, O. Cvetković, R. Pivić, *Agric. conspec. sci*. 83 (2018) 113.
[11] N. Đurić, B. Kresović, Đ. Glamočlija, Systems of Conventional and Organic Production of Field Crops, Grafos Internacional, Pančevo, Serbia, 2015.
[12] R.O. Miller, in: Y. Kalra (Ed.), Handbook of Reference Methods for Plant Analysis, CRC Press, Taylor & Francis Group, Boca Raton, Florida, 1998, pp. 51.
[13] SRPS ISO 13878:2005 (2005), Institute for Standardization, Belgrade, Serbia (in Serbian).
[14] B. Đurđević, in: D. Miklavčić (Ed.), Manual in Plant Nutrition, Faculty of Agriculture, Osijek, Croatia, 2014, pp. 60, 62.
[15] Y.P. Kalra, Handbook of Reference Methods for Plant Analysis. CRC Press, Taylor & Francis Group, Boca Raton, Florida, 1998.
[16] R. Prasad, J.F. Power, Soil Fertility Management for Sustainable Agriculture. CRC Press, Lewis Publishers, Florida, 1997.
[17] https://harvesttotable.com/vegetable-crop-soil-ph-tolerances
[18] https://homeguides.sfgate.com/vegetables-prefer-acidic-soil-51176.html
[19] E-D. Schulze, E. Beck, K. Müller-Hohenstein, D. Lawlor, K. Lawlor, G. Lawlor, Plant Ecology, Springer-Verlag, Berlin, Heidelberg, Germany, 2005.
[20] R. Kastori, N. Petrović, I. Arsenijević-Maksimović, in: R. Kastori (Ed.), Heavy Metals in the Environment, Institute of Field and Vegetable Crops, Novi Sad, Serbia, 1997, pp. 196.
[21] A. Kloke, D.R. Sauerbeck, H. Vetter, In: J.O. Nriagu (Ed.), Changing Metal Cycles and Human Health, Springer-Verlag, Berlin, Heidelberg, New York, Tokyo, 1984, pp.113.
[22] N. Bolan, V.P. Duraisamy, Soil Res. 41 (2003) 533.
[23] E. Sipter, E. Rozsa, K. Gruiz, E. Tatrai, V. Morvai, Chemosphere 71 (2008), 1301.

MEASUREMENT OF EMI SHIELDING PERFORMANCE OF GRAPHENE OXIDE AND ELECTROCHEMICALLY EXFOLIATED GRAPHENE THIN FILMS

Andjela Stefanović[1,2], Dejan Kepic[1], Miroslav Huskić[3], Kamel Haddadi[4], Mohamed Sebbache[4], Svetlana Jovanović Vučetić[1], Biljana Todorović Marković[1]

[1]Vinča Institute of Nuclear Sciences - National Institute of the Republic of Serbia, University of Belgrade, P.O.B. 522, 11001 Belgrade, Serbia
[2]Faculty of Chemistry, University of Belgrade, Studentski trg 12-16, 11158 Belgrade
[3]Faculty of Polymer Technology, Ozare 19, 2380 Slovenj Gradec, Slovenia
[4]University of Lille, CNRS, Centrale Lille, University Polytechnique Hauts-de-France, UMR 8520-IEMN, F-59000 Lille, France
e-mail: andjela.stefanovic@vin.bg.ac.rs

Abstract

Graphene and its derivatives have become the scientific community's focus due to their remarkable electronic, mechanical, and optical properties. In this work, we prepared two graphene-based materials, graphene oxide (GO) and electrochemically exfoliated graphene (EEG), and performed morphological and structural analysis. Both materials showed good dispersibility in water. GO is composed of mainly single- and few-layer graphene sheets, while EEG is predominately multi-layer graphene. EEG showed better thermal stability under nitrogen flow compared to GO. We also performed ElectroMagnetic Interference (EMI) shielding performance measurements of these materials.

Introduction

Electromagnetic pollution is becoming a major worry for us due to the exponential growth of wireless electronics and communication tools [1].

Electronic devices such as laptops and mobile phones emit electromagnetic radiation (EMR), which is a natural byproduct of contemporary technology [2]. The specific absorption rate, or quantity of incoming electromagnetic radiation absorbed over a broad frequency band, determines how these various radiation types influence living things. Beginning with larger wavelengths of non-ionized low-energy radiation like radio waves and microwaves, this spectrum moves through infrared and visible light before ending with shorter wavelengths of higher-energy radiation like ultraviolet, X-rays, and gamma rays [3].

Numerous studies have connected EMR to a number of health hazards, even though the effects of EMR on human health are not yet completely understood, such as DNA damage, cellular stress, lower sperm count and even cancer.

The risks connected with exposure to EMR from electronic devices are particularly of concern, as these devices are typically localized near the body, such as laptops put in laps and mobile phones kept in trouser pockets. Laptops are built up with Radio Frequency electronic devices operating in the frequency range 0.3 - 2.4 GHz whereas mobile phones use RF frequency signals between 0.01 and 4 GHz [2]. Conductive polymer composites (CPCs)-based EMI shielding materials have several advantages over traditional metal-based EMI materials, including being lightweight, low density, inexpensive, easily fabricated, and having good corrosion resistance [1].

Reducing phone usage and utilizing airplane mode when feasible are some ways to safeguard against EMR from computers and mobile phones. Other methods include employing shielding covers or pouches for laptops and phones. It is crucial to remember that even while these methods might lessen exposure to EMR, the danger may still exist. Existing EMR-blocking textiles have the drawback of potentially blocking helpful signals like cellular and Wi-Fi. In addition, the efficiency of these fabrics can depend on the frequency and intensity of the radiation, as well as the specific fabric and its construction [2].

To produce CPCs-based EMI materials, numerous conductive fillers, including carbon black (CB), carbon nanotubes (CNTs), graphene, carbon nitrides, and metal nanoparticles/nanowires, were used to mixture with insulated polymer matrix [1].

Experimental

GO and electrochemically exfoliated graphene (EEG) were prepared as described previously [4] [5]. Briefly, GO was obtained by modified Hummers' method by oxidation of graphite powder (Sigma-Aldrich) with concentrated sulfuric acid, sodium nitrate and potassium permanganate under elevated temperature (98 °C). After the completion of the reaction, the mixture was diluted, added 2 ml of 30% hydrogen peroxide and the powder was purified by several cycles of centrifugation and washing until reaching neutral pH. EEG was prepared in a two-electrode system using highly oriented pyrolytic graphite rods as both the counter and the working electrode and 0.1 M ammonium persulfate as electrolyte. A direct current (DC) voltage of +12 V was applied, and the voltage was kept constant until the exfoliation process was finished which was indicated by the total consumption of the working electrode. The obtained material was purified by several cycles of centrifugation after which the material was dispersed in water using an ultrasonic bath.

Transmission electron microscopy (TEM) analyses were performed on the TEM-JEOL JEM-1400 microscope operated at an accelerating voltage of 120 kV. The samples were dispersed in ethanol using an ultrasound bath and a drop of dispersion was deposited on lacey carbon copper grids (200 mesh) and dried in air. Raman spectra were recorded on a DXR Raman microscope (Thermo Scientific). Each spectrum was obtained at room temperature using a 532 nm excitation line with a power of 2 mW. The spectral resolution was 1 cm-1 and the acquisition time was 10 × 10 s. The confocal pinhole diameter was 50 µm. Each sample was recorded at four different places and an average spectra was used. Thermogravimetric analysis (TGA) tests were performed on a TGA/DSC 3+ (Mettler Toledo instruments, Greifensee, Schweiz) under nitrogen (20 ml/min) at a heating rate of 5 °C/min, from 25 to 1000 °C. Samples were prepared by passing 15 ml of 1 mg/ml water dispersions through 0.2 µm PC Membrane using a vacuum.EMI shielding efficiency measurements were conducted using a Vector Network Analyzer (VNA) from Keysight Technologies (Streamline P5008A) operating in the frequency range 150 kHz-53 GHz. The VNA is connected through high stable coaxial cables to a dedicated coaxial set-up to measure the complex reflection (S11) and transmission (S21) up to 18 GHz. Preliminary to the microwave characterization of the samples, a vector calibration is performed at the output of the coaxial cables to remove systematic errors. Input RF power was set to -15 dBm, intermediate frequency (IF) bandwidth was set to 100 Hz resulting in a time per frequency of 10 ms. All measurements were conducted at room temperature. Each sample is sandwiched between two thin films of cellulose (named PAPER in the following) to avoid any contamination of the coaxial apertures.

Results and discussion

In this work, we used two types of graphene material: one obtained from graphitic powder by following the modified Hummers' method and one obtained from highly oriented pyrolytic graphite rod by electrochemical exfoliation. Both materials, namely graphene oxide (GO) and electrochemically exfoliated graphene (EEG) are well dispersible in water and form stable dispersions. While the water dispersion of EEG is black in color, the dispersion of GO is brownish which might be an indication of a higher oxidation degree of GO compared to EEG.

To investigate the structural properties of both materials we performed TEM analysis (figure 1). GO sample has a higher degree of single-layer and few-layer graphene than EEG which indicates better exfoliation of GO. Graphene sheets have lateral sizes of up to several hundreds of nanometers and graphene sheets are planar with some wrinkles and folds at the sheet ends. Contrary to GO, the TEM images of EEG reveal the presence of predominately few- and multi-layer graphene with larger sheet dimensions, usually up to several micrometers. Based on the Z-contrast of TEM images a stacking of graphene sheets is notable.

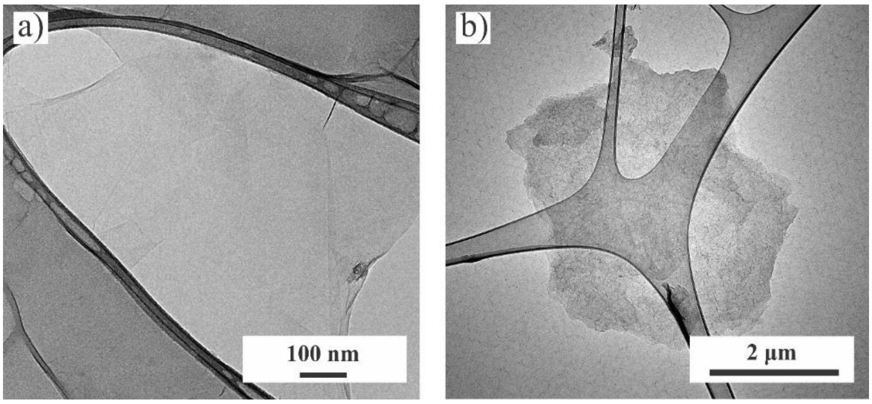

Figure 1. TEM images of a) GO and b) EEG.

Raman spectra of GO and EEG (figure 2) reveal typical graphitic features at 1350 cm^{-1} and 1593 cm^{-1} [6]. The first peak at 1593 cm^{-1} is also known as the G band and originates from the double-degenerate vibrational mode (E_{2g}). It is a first-order scattering process at the crossing of the longitudinal optical (LO) and transverse optical (TO) phonon branches at the Γ point in the first Brillouin zone of graphene. The other peak at 1350 cm^{-1}, denoted as the D peak, is a defect-induced band. It is activated by symmetry breaking induced by the presence of defects or the edges of graphene. Besides, the spectra also show bands that appear at 2700 cm^{-1} and 2930 cm^{-1} that correspond to 2D and D+G bands. The intensity ratio between D and G peaks, also known as I_D/I_G ratio, is an important characteristic of the graphene structures which is related to the defect density and the crystallite size. The I_D/I_G ratio for GO is 0.9, while the I_D/I_G ratio for EEG is 1.2.

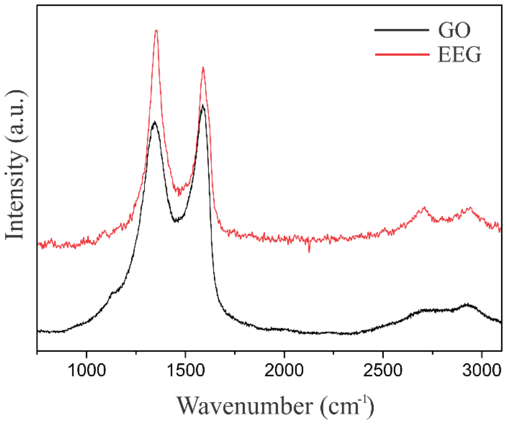

Figure 2. Raman spectra of GO and EEG.

The difference in GO and EEG structure is well reflected in their thermal stability. We performed TGA analysis of both materials under nitrogen and TGA curves are presented in figure 3. The first mass loss region is associated with the loss of adsorbed moisture, the second mass loss around 200 °C is attributed to the breakdown of thermally labile oxygen-containing functional groups, and the third region to the decomposition of the carbon lattice. TGA curves reveal a significant portion of oxygen functional groups in GO compared to EEG. Additionally, EEG shows better carbon lattice stability - at 1000 °C the residual mass of EEG is 55.14% while GO is 2.8%.

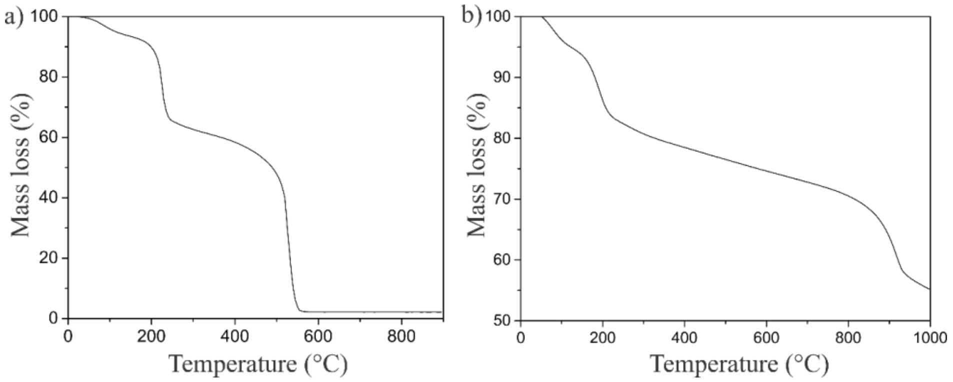

Figure 3. TGA curves of a) GO and b) EEG.

The EMI shielding performance of GO and EEG was estimated by measuring the amplitude of the S-parameters. The data are reported in figure 4. From Fig. b), transmission coefficient of the GO sample does not show any difference with the reference signal (PAPER only), indicating a poor EMI efficiency. Fig. 4 (c) and (d) EEG sample show clear difference between reference and loaded measurements. At 2 GHz, the difference of amplitude of the transmission coefficient S21 is around 10 dB corresponding to 10% of the RF power reflected transmitted through the sample.

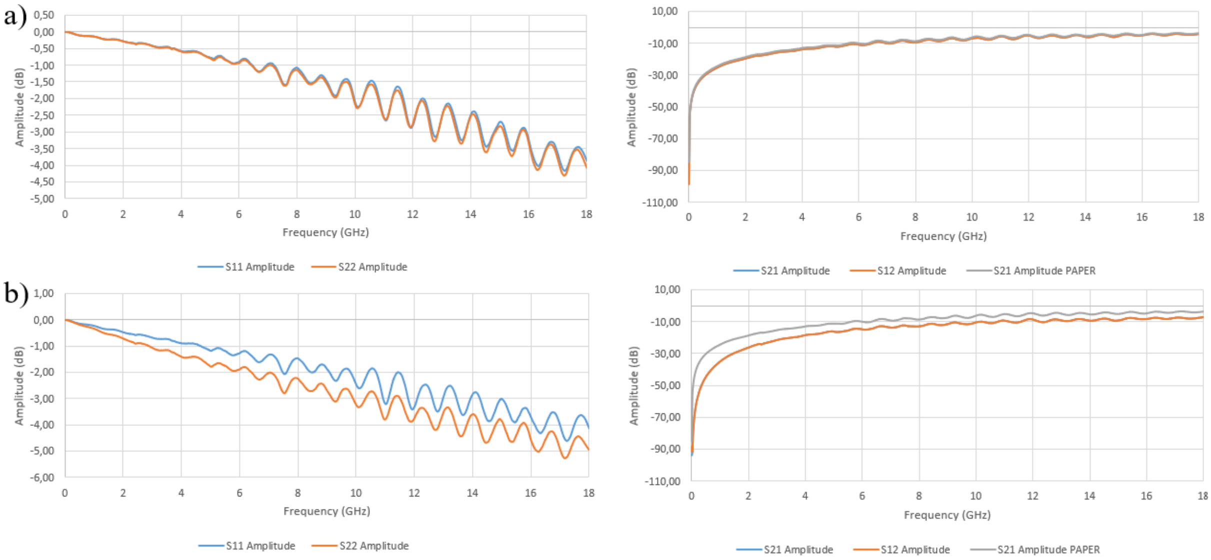

Figure 4. Electromagnetic shielding effectiveness of a) GO and b) EEG in vertical plane.

Conclusion

In this work, we used two types of graphene-based materials – graphene oxide obtained by modified Hummers' method and exfoliated graphene obtained by electrochemical exfoliation. Both materials are well dispersible in water and form a stable dispersions. GO is mainly composed of single- and few-layer graphene sheets, while EEG is predominately multi-layer graphene. Both GO and EEG showed typical features of graphene in the Raman spectra, while I_D/I_G ratio is higher for EEG compared to GO. EEG also showed better thermal stability. EMI shielding performance measurement revealed relatively good performance of the EEG material whereas GO material does not show EM shielding.

Acknowledgements

This project has received funding from the European Union's Horizon Europe Coordination and Support Actions programme under grant agreement No 101079151 - GrInShield. The research was also supported by the Science Fund of the Republic of Serbia, #7741955, Are photoactive nanoparticles salvation for global inflectional treath? - PHOTOGUN4MICROBES and by the Ministry of Education, Science and Technological Development of the Republic of Serbia, grant number 451-03-47/2023-01/200017.

References

[1] Y. Luo, Y. Guo, C. Wei, J. Chen, G. Zhao, Q. Yuan, Y. Zhu, Carbon. 215 (2023) 118480.

[2] U. Ahmed, T. Hussain, H.S. Ahmad, Intern. Jour. of Therm. Sci. 194 (2023) 108594.

[3] S. Ayesha, Z. Abideen, G. Haider, F. Zulfiqar, A. El-Keblawy, A. Rasheed, K.H.M. Siddique, M. B. Khan, E. Radicetti, Plant Stress, 9 (2023) 100198.

[4] Z. Marković, M. Budimir, D. Kepić, I. Holclajtner-Antunović, M. Marinović-Cincović, M. Dramićanin, V. Spasojević, D. Peruško, Z. Špitalský, M. Mičušik, V. Pavlović, B. T. Marković, RSC advances, 6 (2016) 39275-39283.

[5] D. Kepić, S. Sandoval, Á. P. Del Pino, E. György, L. Cabana, B. Ballesteros, G. Tobias Kepić, Chem. Phys. Chem, 18 (2017) 935-941.

[6] L.M. Malard, M.A. Pimenta, G. Dresselhaus, M.S. Dresselhaus, Physics reports, 473 (2009). 473 51-87.

Carpocapsa pomonella - OCCURRENCE IN APPLE ORCHARDS DURING 2022-2023 IN MACHVA

Stošić Nemanja[1], Blagojević Milan[1], Rašković Vera[1], Bajagić Marija[2], Ljiljana Tanasić[1], Marković Stefan,[1] Nenad Pavlović[1]

[1]*Academy of Applied Studies Šabac. Unite for Agricultural Business Studies and Tourism, Republic of Serbia*
[2]*University of Bijeljina, Faculty of Agriculture, Bijeljina, Republika Srpska*
email: nemanjastosic.vpssa@gmail.com

Abstract

In the location of Mrđenovac (Repubilka Srbija, Mačva), during 2021-2023, the presence and representation of Carpocapsa pomonella in apple orchards was monitored. It is specific that the apple orchard is surrounded on two sides by large forests, which would favor the development of all insects. Apple planting with the varieties Granny Smith, Red-Cif, Pink lady was planted on M-9 rootstocks during the fall of 2015. On pheromone traps in 2021, the first appearance of imago was recorded on April 16, while the largest number was determined on May 12. presence was also recorded until the last decade of September. In 2021, the first appearance of imago was recorded a little later on April 29, while the largest number was recorded on June 11. During 2022, the presence of the first imagos was recorded on April 26, and the largest number on August 30. During 2023, the presence of the first imagos was recorded on 07.05., and the largest number on 03.09. The number of imagos on traps varies at peaks of occurrence from 6 to 12 imagos on a pheromone trap. The intensity of development and the number depended from the very beginning where we had a higher number than the appearance itself, as in 2021, the intensity of the attack and the number was as high as the late peak of 11.6. in number it is the result of a strong and long attack of insects for that year. Percentage-wise, due to the level of Carpocapsa pomonella attacks, the greatest damage was recorded in 2021. According to the percentage representation, depending on the variety, the yield was reduced in 2021 by between 1 and 6.5 percent. The greatest damage was done by the Granny Smith variety in 2021 with 6.5 percent, and the least Pink Lady with a 1 percent reduced yield.

CHANGES IN THE STRUCTURAL STABILITY OF CHESTNUT PUREE DUE TO THE ADDITION OF DIETARY FIBRE

Beatrix Szabó-Nótin, **Mónika Máté**

Department of Fruit and Vegetable Processing Technology,
Institute of Food Science and Technology, Hungarian University of Agriculture and Life Sciences
H-1118, Budapest, Villányi street 29-43. Hungary
e-mail: szabo-notin.beatrix@uni-mate.hu

Abstract

Our work involved the production of spoonable chestnut puree products with different inulin types (FTX, HP, GR, HSI) in order to obtain a spoonable stock. The evaluation of the samples were based on the water activity, dry material content, colour, and rheological properties.

Introduction

Chestnut consumption is particularly widespread and popular in Hungary. Chestnuts can be eaten whole, e.g. as roasted chestnuts, as a popular delicacy at Christmas fairs, but the most common commercial form is quick-frozen puree or quick-frozen paste. Chestnut paste is the mashed chestnut version, which according to the Hungarian Food Guide should not contain added sugar or sweeteners, and is usually used in cakes and various meat dishes. Chestnut purée with added sugar and/or sweeteners is a dessert in its own right [1].

Recently, the largest producer of chestnut products in Hungary has started to produce and market a product which, according to the Hungarian Food Guide, is a chestnut puree, but not quick-frozen, but stored in vacuum packaging in the refrigerator (5-10°C). This product inspired the product development described in this thesis. Inulin, which functions as dietary fibre and prebiotic in the human body, is low in calories and suitable for diabetics. In the food industry, it is mainly used as a thickener in dairy products and as a fat replacer and fat substitute [2, 3]. The chestnut product we have developed has a good digestive effect due to its inulin content, which makes it suitable for a healthy diet and a product that can be eaten as a dessert on its own.

Materials

Basic ingredients needed for the preparation of chestnut puree product were the follows: chestnut paste (Prima Maroni Ltd.), maltitol powder (Paleocentrum Ltd), and FTX, HP? GR? HSI inulin (Orafti Ltd.)

Preparation of chestnut puree products

The ingredients were mixed, and after that stored at 5°C for 48 hours. The ingredients are shown in Table 1.

Table 1. Ingredients of the chestnut puree product

Name of the product	Chestnut paste (%)	Inulin (%)	Maltitol (%)
MControl (MC)	80	0	20
M10GR 10%	80	10	10
M15HSI 5%	80	5	15
M10HSI 5%	85	5	10

Determination of dry material content and water activity

Determination of dry material content of the biscuits was performed by using a MAC-50 rapid moisture analyzer (Radwag Waagen GMBH, Hilden, Germany). To determine the water activity, Novasina, LabMaster-aw equipment was used.

Colour measurements

Colour is a determining factor in the definition of the quality of any food. The colour of the surface of three biscuit samples were also measured with 3 parallels using a Konica Minolta CR400 chromameter. Results were expressed as L*, a*, and b* values. L* is a measure of the brightness from black (0) to white (100), while a* describes the redgreen color (a*> 0 indicates redness, a* < 0 indicates greenness), and b* describes yellow-blue color (b*> 0 indicates yellowness, b* < 0 indicates blueness). To determine the total color difference between two samples using all the three coordinates, the following formula was used [4]:

$$\Delta E^{*} = \sqrt{(\Delta \mathrm{L}^{*})^2 + (\Delta \mathrm{a}^{*})^2 + (\Delta \mathrm{b}^{*})^2}$$

Rheology measurements

The rheology properties were investigated with the Physica MCR 51 (Anton-Paar) rheometer in oscillation mode using the amplitude sweep method. The oscillation measurements were performed with a plate-plate measuring system, P-PTD 200 type measuring plate, and a PP50/s 50 mm diameter rough surface measuring head. Two parallel measurements were performed for each sample and the data were recorded using Rheoplus v.3.2 software.

Amplitude sweep method was performed with a deflection of 0.01 to 400% (0.0-6mm), a constant 10 rad/s frequency and a constant temperature of +10 °C. During the measurement, 40 measurement points were taken with a time interval of 5 seconds between each point. The storage modulus (G') and loss modulus (G") were determined as a function of increasing shear stress.G''_0 was determined, the initial loss modulus, and G'_0, the initial elastic modulus, and calculated the end of the linear viscoelastic range, the LVE. The LVE value is the point at which the elastic modulus decreases by 5% from the initial value, i.e. G'_0*0.95. This point includes the value τ_{LVE}, which is the value of shear stress below which the applied force causes the sample to undergo a reversible change in shape, i.e. if the applied force is removed, our test material will return to a state similar to the initial position. In practice, this indicates the stability of the sample at rest. The higher the value of the end of the LVE range, the stronger the structure formed. After the LVE endpoint, the measured storage modulus decreases due to the increasing deformation force and at a certain shear stress, the intersection of the two measured modulus curves (CO) is observed in singles, which marks a kind of yield point, from which point the material behaves as a viscoelastic fluid (G">G') rather than a viscoelastic solid (G'>G") [5].

Sensory evaluation

During the sensory evaluation, the judges had to score the biscuits on a 100-point scale. The sensory attributes were given different scores. Texture was 30 points, colour and smell and overall impression 10 points and taste 40 points.

Statistical analysis

For the statistical analysis the mean values were compared by 2-way analysis of variance (ANOVA) when evaluating the sensory attributes of the products ($\alpha = 0.05$). The statistical analysis was carried out using SPSS ver.No.23.

Results and discussion

Table 1 contains the dry material content and water activity. In case of the dry material content and water activity, there are significant differences between the samples (Sig=0.015 and Sig.=0.01). While the water activity of the M15HSI5 sample was almost identical (Sig.=0.83) to the control sample.

Sample	Dry material content (%)	Water activity
MC	44.37	0.764
MGR10	45.1	0.804
M10HSI5	38.17	0.802
M15HSI5	47.53	0.793

Table 1. Dry material content and water activity of the samples

In the rheograms shown in Figure 1, it can be seen, that there is a crossover point for all samples, all samples liquefy during the measurement, which suggests that the addition of maltitol to the chestnut paste weakens its stability and softens its structure.

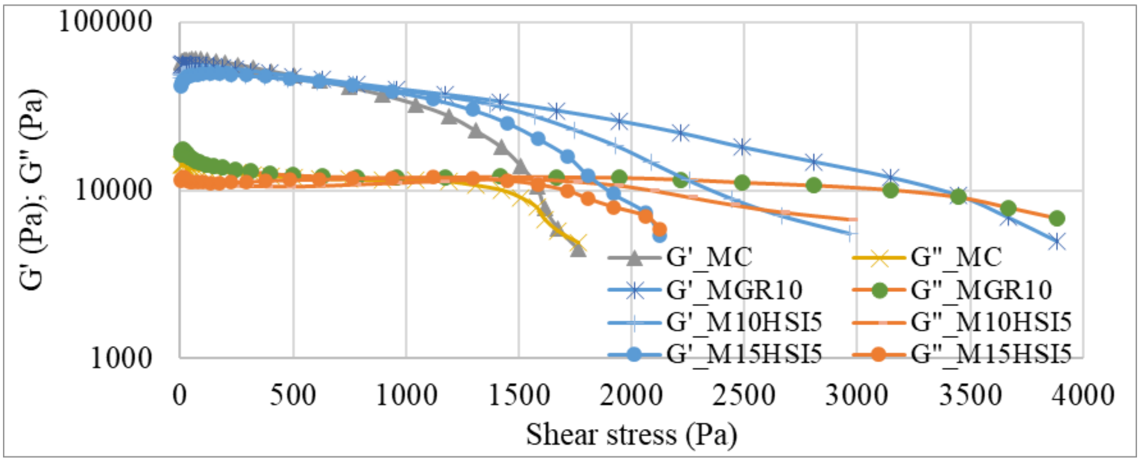

Figure 1. Apmlitude rheograms of the samples

The τ_{CO} values read from the amplitude sweep rheograms are shown in Figure 2. At the lowest shear stress, 1850 Pa was sufficient to force the control sample to flow, followed by the M15HSI5 sample, which flowed near 1940, then the M10HSI5 sample, and finally the MGR10 sample, which was the most stable, requiring a shear stress of 3820 Pa. Based on these results, the control sample and the M15HSI5 sample were the softest and easiest to lubricate.

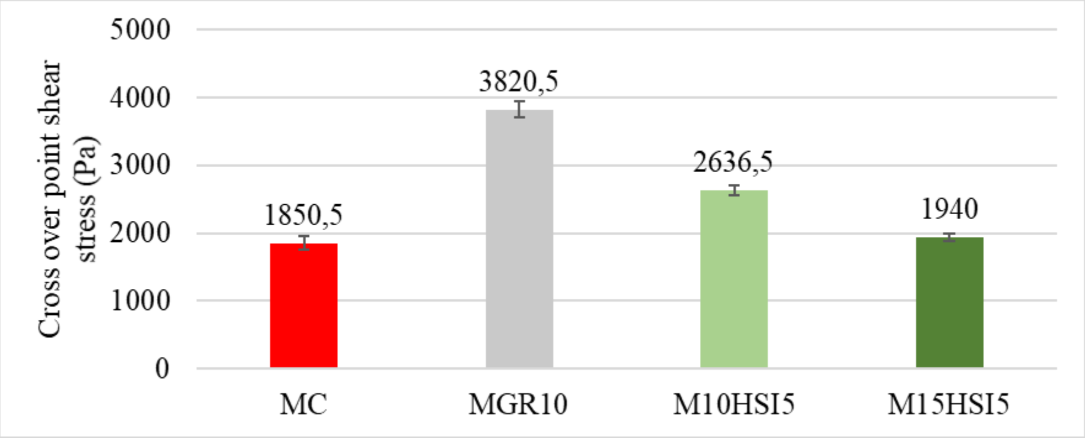

Figure 2. CO point values of the samples

Colour factors were examined. It can be seen that the addition of maltitol makes the samples uniformly darker (Figure 3.)

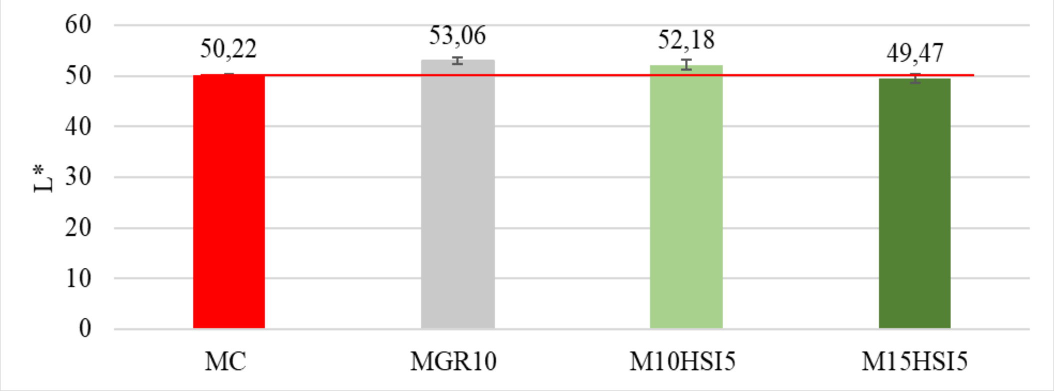

Figure 3. L* value of the samples

The most similar sample to the control sample is M15HSI5, the only one that does not show a significant difference (Sig.=0.22) compared to the control sample. MGR10 and M10HSI5 were significantly lighter than the control.

In case of the sensorial evaluation, it can be say, that the MC sample and the samples containing HSI inulin were considered by the judges to be of adequate consistency or too soft for a spoonable dessert (Figure 4). The consensus was that Prima Maroni's product and the MGR10 sample were too hard for a spoonable dessert.

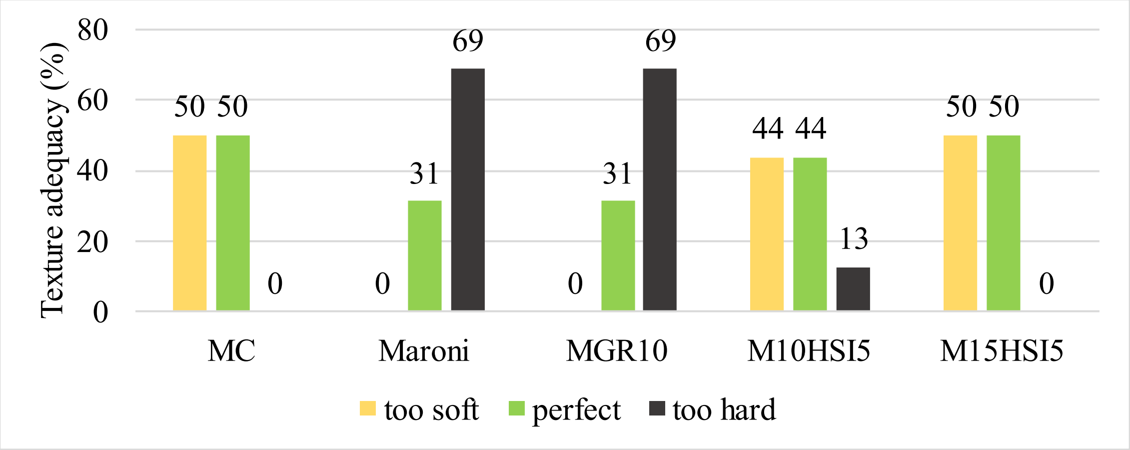

Figure 4. Texture adequacy (%) of the sample

Conclusions

The results of the organoleptic evaluation confirmed my instrumental measurements, thus the sample containing 15% maltitol and 5% HSI inulin was the best overall, with the right sweetness, no unpleasant side flavours and the consistency for a spoonable chestnut dessert.

References

[1] MAGYAR ÉLELMISZERKÖNYV 2-604 számú irányelv. (2013. 05). Forrás: https://elelmiszerlanc.kormany.hu/download/9/4b/a2000/2-604.pdf

[2] Tiwari, A., Sharma, H., & Kaur, M. (2015). The effect of inulin as a fat replacer on the quality of low-fat ice cream. *International Journal of Dairy Technology*, 68 (3) p. 374-380. doi:10.1111/1471-0307.12176

[3] Karimi, R., Azizi, M., Ghasemlou, M., & Vaziria, M. (2015). Application of inulin in cheese as prebiotic, fat replacer and texturizer: A review. Carbohydrate Polymers, 119, (30) p. 85-100. doi:10.1016/j.carbpol.2014.11.029

[4] Mokrzycki, W.S., & Tatol, M. (2011): Color difference Delta E - A survey. Machine

[5] Mezger, T. (2011). *The Rheology Handbook, 3rd revised edition.* Hanover: Vincentz Network GmbH & Co. KG. Forrás: ISBN 978-3-86630-890-9

Graphics and Vision, 20 (4), pp. 383-411.

COMPARISON OF COLOUR PROPERTIES OF CROSSBRED ELDERBERRY GENOTYPES

Lilla Szalóki-Dorkó, Nikoletta Molnár, Mónika Máté

Department of Fruit and Vegetable Processing Technology, Institute of Food Science and Technology, Hungarian University of Agriculture and Life Sciences, H-1118 Budapest, Villányi út 29-43., Hungary
e-mail: Szaloki-Dorko.Lilla@uni-mate.hu

Abstract

Elderberry (*Sambucus nigra L.*) is a good source of anthocyanins, therefore, a preferred source of natural food colourant in the food industry to adjust food colour. Today, the growers have a strong intention to cultivate elderberries with high pigment and water-soluble solid content which are the value-determining properties. In this study four different crossbred genotypes (Haschberg×Samocco, Haschberg×Wild, Haschberg×Sampo, Sampo×Wild) were examined in two ripening stages from the aspects of colour properties. HSc genotypes had the highest total anthocyanin concentration above 800 mg CGE/100 g in both ripening stages. The lowest pigment values were measured in SW elderberry samples furthermore the ripening had significant ($p<0.05$) effect on this hybrid because ca 33% more total anthocyanin was found in the ripening stage 2. Finally, crossbred elderberry genotypes can have better colour properties than the elderberry varieties alone, but the ripening process can influence the measured parameters. Furthermore, it is necessary to examine the samples of the following vintages also to establish more comprehensive conclusions.

Introduction

Today, utilization of natural plant pigments is becoming more preferred as an alternative of synthetic food colourants in the food industry. Among them anthocyanins are suitable for food colouration with a low pH level such as soft drinks, water ice cream, sauce, confectionery, table jellies, conserves because anthocyanin molecules are more stable in acidic medium [1–3]. The source of anthocyanins can be including black currant, sour cherry, elderberry, purple wheat, and blood orange etc. Elderberry can be a potential natural colouring food because of high amount of anthocyanins [4–5] and it is easy to grow in plantation in Hungary. Many cultivars of elderberries are planted in Europe, the most common is the 'Haschberg' cultivar with several selections, which are mainly grown for fruit [4]. Globalization of the market for juice or concentrate resulted that new genotypes with different quality characteristics have appeared, but their colouring properties are less known.

Therefore, the aim of this study is to evaluate the new crossbred elderberry genotypes grown in Hungary as a potential source of natural food colourant considering the different ripening stages.

Experimental

Elderberry fruit (*Sambucus nigra* L.) samples were harvested in 2022 from mid-August (ripening stage 1) and at the end of August (ripening stage 2). Four different crossbred elderberry genotypes, namely Haschberg×Samocco (HSc), Haschberg×Wild (HW), Haschberg×Sampo (HS), Sampo×Wild (SW) were sampled growing location of Nagyvenyim (46°570 N, 18°510 E), Hungary.

After crushing the berries total water-soluble solid content (Brix%) using digital refractometer (ATAGO PAL-3) was measured in triplicates while prior the other measurements extraction step was done. Extraction solvent was 60% (v/v) aqueous methanol containing 1% (v/ v) formic acid. Samples were extracted for 30 min at the room temperature and 15 min in an ultrasonic bath. After extraction, samples were centrifuged at 4180 *g* for 5 min at room temperature. The supernatant was used for the measurements.

Colour parameters (L*, a*, b*) were determined with digital colorimeter (CR-400 Chroma Meter, Konica Minolta) and the colour difference values (ΔE*) were calculated from them based on this equations: $\Delta E^*_{ab}=((\Delta a^*)^2+(\Delta b^*)^2+(\Delta L^*)^2)^{½}$. Total anthocyanin concentration (TAC) was assessed using the pH differential method at 520 and 700 nm [6] The values were expressed in mg cyanidin-3-glucoside (CGE)/100g.

T-test was used for analysis of difference between the elderberry samples and the ripening stages in case of Brix values and TAC. Significant difference was considered when *p* value was <0.05.

Results and discussion

The Brix values of the samples can be seen in the Table 1. Using elderberry concentrate as a colouring food is evaluation of the total soluble solid content is very important from the economical aspect because during the evaporation technology the higher Brix value of the fresh fruit, the less water should be evaporated to reach the targeted concentrate.

The Brix values of the samples were between 12.03 and 16.23 Brix% in the case of the first ripening stage while data of the later-harvested samples varied between 10.9 and 14.17 Brix%. According to the statistical analysis there is significant difference between the ripening stage of 1 and 2 in case of HW and SW (*p*=0.002 and *p*=0.007).

Table 1. Total water soluble solid content of crossbred elderberry genotypes during ripening

Brix%	Ripening stage	
Elderberry sample	1	2
HSc	12.33 ± 0.29	10.90 ± 0.87
HS	12.03 ± 0.91	13.13 ± 0.35
HW	16.23 ± 0.51	11.07 ± 0.46
SW	12.13 ± 0.23	14.17 ± 0.67

Total anthocyanin concentration of crossbred elderberry genotypes in the Figure 1. HSc had the highest values (816.61 and 864.25 mg CGE/100g) in both ripening stages which was expected due to the high pigment content of Samocco Danish variety alone based on our earlier study [7], furthermore the maximum maturity stage of this hybrid was not found. SW1 had the lowest TAC, however in the next ripening stage ca. 33% more anthocyanin content was measured. The effect of ripening was not detected clearly in elderberry samples of HW1 because almost the same TAC was observed (500.22 and 491.97 mg CGE/100g). Sampo Danish variety crossbred with Haschberg had 542.86 and 422.97 mg CGE/100g. According to our results Samocco and Wild elderberries can enhance the pigment content of hybrid with Haschberg variety. Significant differences were found in case of HS and SW elderberries (*p*=0.007 and *p*<0.000) considering the ripening stages.

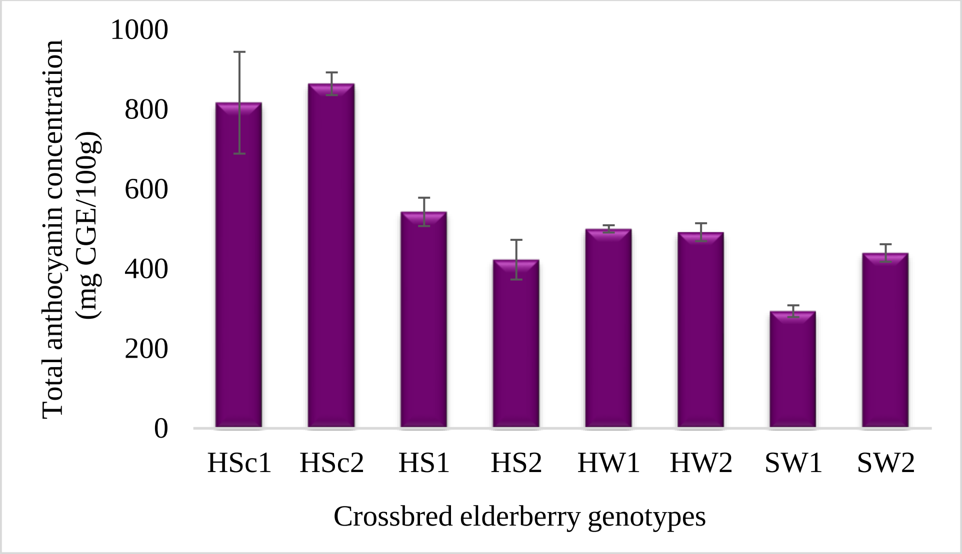

Figure 1. Total anthocyanin concentration of crossbred elderberry genotypes

As regard the colour parameters, the calculated colour difference values (ΔE*) were varied between 0.20 to 3.60 (Table 2.). It can be seen, there was no visible difference between the HSc1 and HSc2 samples. In the case of the HS1 and HS2, as well as the SW1 and SW2 samples, there was barely noticeable difference between the two ripening stages. The well visible difference was detected between HW2 and HSc samples. There is only a noticeable or barely visible difference between the other samples based on maturity and genotypes.

Table 2. The colour difference values (ΔE*) between the crossbred elderberry genotypes

ΔE*	**HSc1**	**HSc2**	**HS1**	**HS2**	**HW1**	**HW2**	**SW1**	**SW2**
HSc1		0.23	1.69	2.11	1.23	3.60	1.95	2.14
HSc2	not visible		1.57	2.04	1.16	3.49	1.92	2.08
HS1	visible	visible		0.62	0.57	1.96	0.87	0.74
HS2	visible	visible	barely visible		0.88	1.56	0.69	0.20
HW1	barely visible	barely visble	barely visible	barely visible		2.39	0.89	0.93
HW2	well visible	well visible	visible	visible	visible		2.10	1.64
SW1	visible	visible	barely visible	barely visible	barely visible	visible		0.54
SW2	visible	visible	barely visible	not visible	barely visible	visible	barely visible	

Conclusion

Elderberry fruit is used for natural food colourant in the food industry because of high anthocyanin content. The growers have an increasingly demand for new crossbred genotypes with higher value-determining values. Among the examined hybrid elderberries Haschberg×Samocco had the highest anthocyanin concentration however the water-soluble solid content was lower. Sampo and Wild can be also promising with Haschberg variety due to the high Brix value and pigment concentration, mostly in case of ripening stage 2. Our results revealed that crossbred elderberry genotypes can have better colour properties than the elderberry varieties alone, however the ripening can influence the measured parameters which have effect on the quality of elderberry. Furthermore, it is necessary to examine the samples of the following vintages also to establish more comprehensive conclusions.

Acknowledgements

The authors wish to thank Elderberry Grower Cooperative (Vál, Fejér megye, Hungary) for providing elderberry genotypes.

References

[1] P. Bridle, C.F. Timberlake, Food Chem. 58 (1997) 103–109.
[2] X. Luo, R. Wang, J. Wang, Y. Li, H. Luo, S. Chen, X. Zeng, Z. Han, *Foods 11* (2022) 2166.
[3] B. Alappat, J. Alappat, *Molecules* 25 (2020) 5500.
[4] R. Veberic, J. Jakopic, F. Stampar, V. Schmitzer, Food Chem. 114 (2009) 511– 515.
[5] L.S.M. Jakobek, M. Medvidovic-Kosanovic, I. Novak, Dtsch. Lebensmitt. Rundsch. 103 (2007) 58–64.
[6] J. Lee, R.W. Durst, R.E. Wrolstad, *J. AOAC Int.* 88 (2005) 1269–1278.
[7] L. Szalóki-Dorkó, M. Stéger-Máté, L. Abrankó, Int. J. Food Sci. Technol. 50 (2015) 1317–1326.

DOUBLE-LAYER CAPACITANCE STUDY OF A NICKEL PHOSPHITE/PROPHRYIN-MODIFIED GRAPHITE ELECTRODE WITH WATER-SPLITTING CATALYTIC PROPERTIES

Bogdan-Ovidiu Taranu

National Institute of Research and Development for Electrochemistry and Condensed Matter,
Dr. A.P. Podeanu street, No. 144, 300569, Timisoara, Romania
e-mail: b.taranu84@gmail.com

Abstract

An electrode exhibiting water-splitting catalytic properties was manufactured by applying a combination between $Ni_{11}(HPO_3)_8(OH)_6$ and 5,10,15,20-tetrakis(4-methoxyphenyl)porphyrin on graphite substrate. The specimen was coded $G_{NiPh\text{-}TMeOPP}$ and its double-layer capacitance was investigated. The obtained value of 7.475 mF/cm^2 is higher than the ones determined for the unmodified graphite support and for the nickel phosphite-based graphite electrode. This result indicates that $G_{NiPh\text{-}TMeOPP}$ is the most likely to find application in the field of supercapacitors.

Introduction

The constant search for new catalysts possessing water splitting properties takes part within the broader context represented by the global energy crisis and climate change [1]. Nickel phosphite and porphyrins are among the materials identified so far as exhibiting electrocatalytic activity for the two half-cell reactions involved in the electrochemical decomposition of H_2O, namely the oxygen and the hydrogen evolution reactions [2-5]. Regarding $Ni_{11}(HPO_3)_8(OH)_6$, it is a member of the metal phosphites class and it has been reported as a highly active, very stable, robust and structurally versatile electrocatalyst for overall water splitting [3]. It was also investigated by Taranu *et al.* in water electrolysis studies [6-8]. As for porphyrins, there are many published articles in which these compounds have been revealed as catalytically active for the decomposition of water [9-12]. What makes them suitable for such an application are their specific structure and properties. Porphyrins are a class of aromatic organic pigments sharing the tetrapyrrole porphine macrocycle that can be substituted with a wide variety of functional groups and can bound in its centre almost any metal ion [13,14]. Whether free-base or metalated, porphyrin molecules can spontaneously associate to form stable and well-defined aggregates that have properties of their own, including water splitting electrocatalytic ones [4,15].

In a study published by Taranu *et al.* [8], the catalytic activity for the hydrogen evolution reaction (HER) of free-base porphyrin aggregates combined with nickel phosphite was investigated in alkaline medium. The experimental results have shown that the combination between the metal salt and the metal-free 5,10,15,20-tetrakis(4-methoxyphenyl)porphyrin was the most catalytically active for the specified reaction. The purpose of the current investigation is to further characterise the electrode manufactured using the specified mixture, but in terms of its electric double-layer capacitance (C_{dl}). This parameter, representing the capacitance from stored charge in the double-layer region at the electrode/electrolyte solution interface [16], is relevant when trying to determine whether an electrode material can be utilized in the field of supercapacitors. It should also be pointed out that $Ni_{11}(HPO_3)_8(OH)_6$ and members of the porphyrin class have been reported as suitable for the mentioned application [17-19].

Experimental

The nickel phosphite was obtained hydrothermally at high temperature and high pressure, in accordance with the literature [6,20]. 5,10,15,20-Tetrakis(4-methoxyphenyl)porphyrin (TMeOPP) was also synthesized following a previously published procedure [21], and its chemical structure can be seen in Scheme 1. Tetrahydrofuran (THF), purchased from Sigma-Aldrich, was employed to obtain the porphyrin solution that was used in the electrode manufacturing process. Other reagents involved in the study were potassium chloride (Merck), ethanol (Honeywell) and acetone (Chimreactiv). All aqueous solutions were prepared with laboratory produced double distilled water. A spectroscopic graphite rod (ø = 6 mm), type SW.114 ("Kablo Bratislava", National Corporation "Electrocarbon Topolcany" Factory, Bratislava, Slovakia), served as the substrate of the nickel phosphite/porphyrin modified electrode.

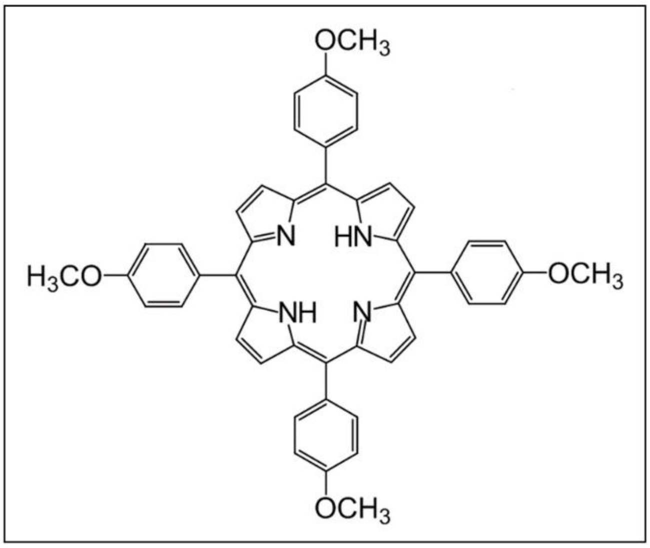

Scheme 1. The chemical structure of 5,10,15,20-tetrakis(4-methoxyphenyl)porphyrin

The manufacturing process involved several steps: (1) The graphite rod was introduced inside a polyethylene tube; (2) A thermal treatment at 180 °C ensured the sealing between the rod and the tube; (3) The surface of one of the rod ends was polished with silicon carbide paper (grit sizes of 800 and 1200) and felt; (4) The polished surface was washed with double distilled water and dried at 23 ± 2 ºC; (5) The nickel phosphite/TMeOPP composition was applied from a suspension on the dried graphite surface; (6) The modified surface was exposed to 40 ºC for 4 h and 23 ± 2 ºC for 20 h to ensure solvent evaporation.

As for the suspension containing the metal salt and TMeOPP, it was realized by first dissolving the porphyrin in 500 µL THF so as to obtain a 0.15 mM solution and by subsequently adding to it 1.5 mg nickel phosphite. After 40 minutes of ultrasonication, a volume of 10 µL was removed from the suspension and was drop-casted on the graphite substrate – see step (5) from the manufacturing process. The resulted modified electrode was coded $G_{NiPh-TMeOPP}$. Other specimens used in the study were the unmodified graphite support (G_0) and an electrode modified only with nickel phosphite (G_{NiPh}).

A Voltalab PGZ 402 potentiostat (Radiometer Analytical) connected to three electrodes inserted into a glass cell was employed throughout the electrochemical investigations. Each sample was utilized as working electrode (S_{geom} = 0.28 cm^2), the auxiliary electrode was a Pt plate (S_{geom} = 0.8 cm^2) and Ag/AgCl (sat. KCl) was the reference electrode. All the potentials are quoted versus the specified reference and all experiments were performed at 23 ± 2 °C in unstirred electrolyte solution.

In order to determine the C_{dl} value for every specimen a previously reported protocol was followed [22]. Basically, cyclic voltammograms were recorded in neutral medium (0.1 M KCl solution) at different scan rate (v) values and in a potential range where no faradic currents were present. The voltammetric data were subsequently used in Equation (1) to calculate the capacitive current density (i_{dl}). Lastly, the C_{dl} value was determined as the absolute value of the slope from the linear dependence between i_{dl} and the scan rate [23].

$$i_{dl} = (i_a + i_c)/2 \tag{1}$$

Where: i_{dl} [A/cm^2] is the capacitive current density; i_a and i_c [A/cm^2] are the absolute values of the anodic and cathodic current densities at a potential value where only double-layer adsorption and desorption features are present [24].

Results and discussion

The i_{dl}-v graphical representation for the studied specimens is shown in Figure 1, and Table 1 presents the obtained C_{dl} and R^2 values. The C_{dl} values are expressed both is mF/cm^2 (areal C_{dl}), as well as in mF (by considering the 0.28 cm^2 geometric surface of the electrodes). It can be seen that the highest value was found for $G_{NiPh-TMeOPP}$ and this result indicates that out of the investigated samples the electrode modified with the combination between nickel phosphite and TMeOPP is the most likely to find application as electrode material in supercapacitors.

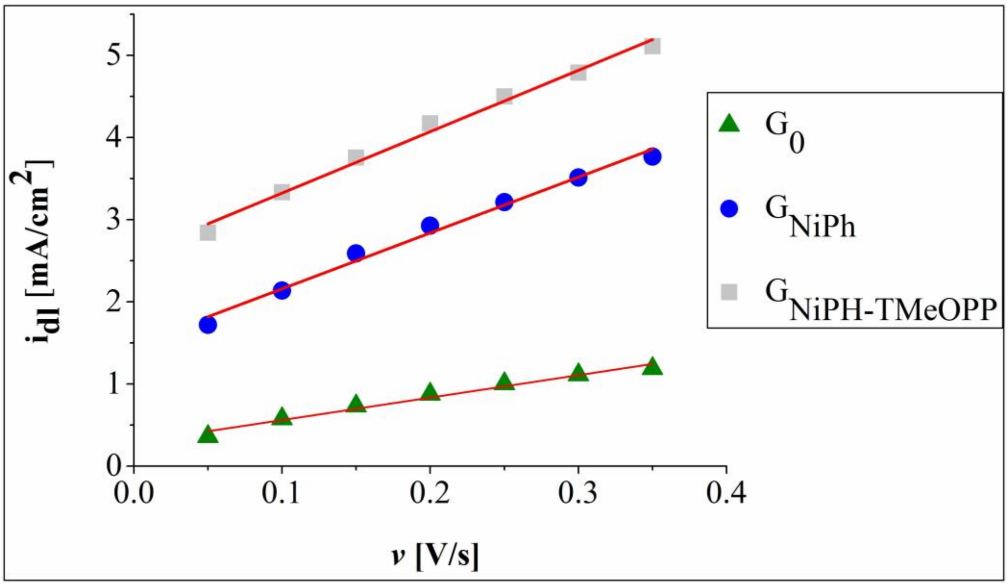

Figure 1. The i_{dl}-v plot for the G_0, G_{NiPh} and $G_{NiPh-TMeOPP}$ electrodes, obtained using the results from the cyclic voltammetry study of these specimens in 0.1 M KCl electrolyte solution, at v = 0.05, 0.1, 0.15, 0.2, 0.25, 0.3 and 0.35 V/s

The higher C_{dl} for $G_{NiPh-TMeOPP}$ can be explained in terms of the porphyrin species. As previously reported [8], compared with G_{NiPh}, $G_{NiPh-TMeOPP}$ benefits from the properties of both materials and it exhibits a larger electroactive surface area due to the intercalation between elongated nickel phosphite structures and self-assembled bundle-like TMeOPP aggregates.

Table 1. The C_{dl} and R^2 values obtained for the investigated electrodes

Electrode code	C_{dl}		R^2
	[mF/cm^2]	[mF]	
G_0	2.732	0.765	0.9734
G_{NiPh}	6.798	1.903	0.9869
$G_{NiPh\text{-}TMeOPP}$	7.475	2.093	0.9891

Conclusion

The double-layer capacitance of an electrode manufactured by drop-casting a combination between a transition metal phosphite – $Ni_{11}(HPO_3)_8(OH)_6$ – and a metal-free symmetrically substituted porphyrin on graphite support was successfully determined. The obtained value was higher than the ones found for the unmodified electrode and for the specimen manufactured by applying only the nickel phosphite on the graphite substrate, making the combination of the two materials more suitable to be used in the supercapacitors field.

References

[1] X. Xiao, L. Yang, W. Sun, Y. Chen, H. Yu, K. Li, B. Jia, L. Zhang, T. Ma, Small 18 (2022) 2105830.

[2] P. W. Menezes, A. Indra, C. Das, C. Walter, C. Gobel, V. Gutkin, D. Schmeiber, M. Driess, ACS Catal. 7 (2017) 103.

[3] P. W. Menezes, C. Panda, S. Loos, F. Bunschei-Bruns, C. Walter, M. Schwarze, X. Deng, H. Dau, M. Driess, Energy Environ. Sci. 11 (2018) 1287.

[4] B.-O. Taranu, E. Fagadar-Cosma, Processes 10 (2022) 611.

[5] I. Fratilescu, A. Lascu, B.O. Taranu, C. Epuran, M. Birdeanu, A.-M. Macsim, E. Tanasa, E. Vasile, E. Fagadar-Cosma, Nanomater. 12 (2022) 1930.

[6] B.-O. Taranu, M. G. Ivanovici, P. Svera, P. Vlazan, P. Sfirloaga, M. Poienar, J. Alloys Compd. 848 (2020) 156595.

[7] M. Poienar, P. Svera, B.-O. Taranu, C. Ianasi, P. Sfirloaga, G. Buse, P. Veber, P. Vlazan, Crystals 12 (2022) 1803.

[8] B.-O. Taranu, E. Fagadar-Cosma, P. Sfirloaga, M. Poienar, Energies 16 (2023) 1212.

[9] W. Zhang, W. Lai, R. Cao, Chem. Rev. 117 (2017) 3717.

[10] Q. Li, Y. Bao, F. Bai, MRS Bull. 45 (2020) 569.

[11] B. Yao, Y. He, S. Wang, H. Sun, X. Liu, Int. J. Mol. Sci. 23 (2022) 6036.

[12] B. B. Beyene, C.-H. Hung, Coord. Chem. Rev. 410 (2020) 213234.

[13] R. J. Mortimer, N. M. Rowley, in: J. A. McCleverty, T. J. Meyer (Eds.), Comprehensive Coordination Chemistry II, vol. 9, Elsevier Ltd., Amsterdam, The Netherlands, 2003, pp. 581.

[14] E. Fagadar-Cosma, D. Vlascici, G. Fagadar-Cosma, Porfirinele de la sinteză la aplicații, Eurostampa, Timisoara, Romania, 2008, pp. 10.

[15] B.-O. Taranu, E. Fagadar-Cosma, Nanomater. 12 (2022) 3788.

[16] N.I. Ramli, N.A.B Ismail, F. Abd-Wahab, W.W.A.W. Salim, in: K. Pal (Ed.), Transparent Conducting Films, IntechOpen, London, UK, 2018, pp. 75.

[17] H. Pang, C. Wei, Y. Ma, S. Zhao, G. Li, J. Zhang, J. Chen, S. Li, ChemPlusChem 78 (2013) 546.

[18] H. Yang, S. Zhang, L. Han, Z. Zhang, Z. Xue, J. Gao, Y. Li, C. Huang, Y. Yi, H. Liu, Y. Li, ACS Appl. Mater. Interfaces 8 (2016) 5366.

[19] C.A. Garcia-Perez, C. Menchaca-Campos, M.A. Garcia-Sanchez, Y.I. Vega-Cantu, O. Rodriguez-Perez, J. Uruchurtu, Diam. Relat. Mater. 96 (2019) 44.

[20] M. Poienar, A. Maignan, P. Sfirloaga, S. Malo, P. Vlazan, A. Guesdon, F. Laine, J. Rouquette, C. Martin, Solid State Sci. 93 (2014) 92.

[21] E. Fagadar-Cosma, C. Enache, R. Tudose, I. Armeanu, E. Mosoarca, D. Vlascici, O. Costisor, Rev. Chim. 58 (2007) 451.
[22] B.-O. Taranu, S. D. Novaconi, M. Ivanovici, J. N. Goncalves, F. S. Rus, Appl. Sci. 12 (2022) 6821.
[23] B.-O. Taranu, E. Fagadar-Cosma, I. Popa, N. Plesu, I. Taranu, Dig. J. Nanomater. Biostructures. 9 (2014) 667.
[24] A. Kellenberger, D. Ambros, N. Plesu, Int. J. Electrochem. Sci. 9 (2014) 6821.

AGGREGATION BEHAVIOUR STUDY OF A SYMMETRICALLY SUBSTITUTED CATIONIC Zn(II)-PORPHYRIN APPLIED FROM DIFFERENT SOLVENTS

Bogdan-Ovidiu Taranu[1], Eugenia Fagadar-Cosma[2]

[1]National Institute of Research and Development for Electrochemistry and Condensed Matter, Dr. A.P. Podeanu street, No. 144, 300569, Timisoara, Romania
[2]Institute of Chemistry "Coriolan Dragulescu", Mihai Viteazu Ave. 24, 300223 Timisoara, Romania
e-mail: b.taranu84@gmail.com

Abstract

The aggregation behaviour of 5,10,15,20-tetrakis(N-methyl-4-pyridyl)porphyrin-Zn(II) tetrachloride (ZnTMPyP) was investigated *via* transmission electron microscopy (TEM). The samples were prepared by drop-casting the metalloporphyrin from solvents with different polarities. The recorded images revealed a variety of structures resulted from the spontaneous association of the porphyrin molecules. The main factors responsible for the shape of the architectures were ZnTMPyP's peripheral substituents and central metal cation, the nonpolar carbon film of the TEM grid and the polarity of the solvents employed to obtain the TEM specimens. This morphological study supplements the existing literature data with respect to the self-assembly of metallated porphyrins.

Introduction

Porphyrins are a class of organic aromatic nitrogenous pigments that are found in nature (e.g., chlorophylls and the haem) but that can also be obtained artificially as synthetic porphyrin powders or dyes. Regarding their structure, they are macrocyclic tetrapyrrole derivatives that can be peripherally substituted with a broad variety of functional groups and the centre of their ring system can be complexed with almost all metal cations. Structural modifications lead to functional changes and are responsible for the many applications identified for both free-base and metallated porphyrin compounds [1,2].

One of the properties shared by porphyrin molecules is their ability to self-assemble [3]. Basically, they can spontaneously associate *via* non-covalent interactions, giving rise to stable and well-defined architectures [4]. There are some aspects regarding the self-assembling process that are noteworthy [5-7]. One of them is its non-destructive nature with respect to the chemical structure of the participating molecules and of the substrate. Another is that it can occur in solution, as well as at the solution/gas or solution/solid substrate interface. Furthermore, the resulting structures usually exhibit properties that are distinct from the ones possessed by the molecules.

The simplest porphyrin assemblies are the side-by-side (or J-type) and the face-to-face (or H-type) stacking arrangements, while the aggregates displaying a higher degree of complexity are based on the subsequent ordering of these less complicated structures [8].

The scientific literature includes numerous studies that outline the morphology of porphyrin-based architectures [9-11], and the current paper brings its own contribution to this constantly expanding body of research by providing a morphological characterization of the aggregates formed by a symmetrically substituted cationic metalloporphyrin applied on TEM grids from solvents having different polarities.

Experimental

5,10,15,20-Tetrakis(N-methyl-4-pyridyl)porphyrin-Zn(II) tetrachloride (ZnTMPyP) was synthesized based on a previously published procedure [12,13], and its chemical structure is presented in Scheme 1. The solvents used to obtain the porphyrin solutions were: laboratory produced double distilled water, as well as dimethylsulfoxide (DMSO), N,N-dimethylformamide (DMF), acetonitrile (AcN) and ethanol (EtOH), purchased from Sigma Aldrich, Merck and Honeywell. These solvents exhibit different polarities that decrease in the following order: H_2O > DMSO > DMF > AcN > EtOH [14,15].

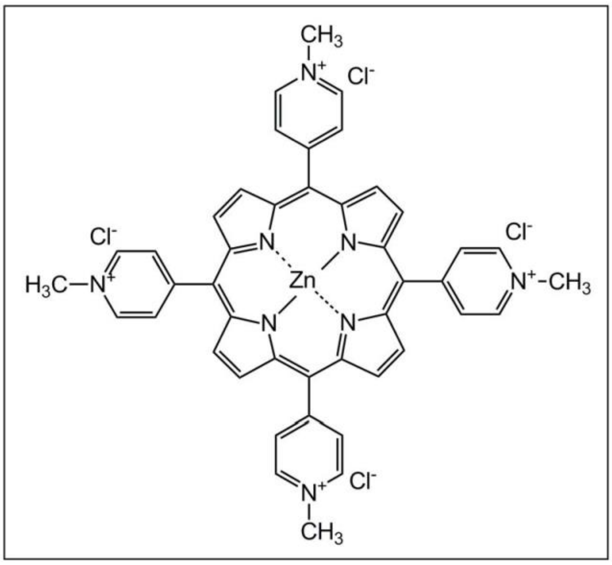

Scheme 1. The chemical structure of ZnTMPyP

A Titan G2 80-200 microscope from FEI Company (Eindhoven, The Netherlands) was operated at 200 KV acceleration voltage in transmission and scanning transmission electron microscopy modes (TEM and STEM) in order to record images of the Zn(II)-porphyrin assemblies formed on the surface of TEM grids. To prepare the samples, the porphyrin was dissolved in H_2O, DMSO, DMF, AcN and EtOH. The samples were obtained by drop-casting a volume of 3 μL from 0.15 mM porphyrin solutions on the carbon film covered TEM copper grids.

Results and discussion

Figure 1a presents the image recorded on the specimen resulted by applying the metalloporphyrin dissolved in double distilled water on the carbon support. Porphyrin aggregates (some of which overlap) having different dimensions and shapes can be observed and include a large quasi-squared plate (side length of ~ 2.7 μm), smaller and irregularly shaped flat formations, as well as bundles. The smaller structures may belong to intermediary stages in the assembling of large plates [16]. It should be pointed out that the aggregation behaviour of ZnTMPyP from aqueous solution was also investigated by Dudas *et al.* [13], but the solvent was acidified and this affected the shape of the obtained architectures that resembled triangular plates.

When DMSO was employed as solvent for the Zn(II)-porphyrin solution, the STEM analysis of the specimen revealed intricate networks of irregular rows of rings such as the one shown in Figure 1b. The sizes of the self-assemblies were of a few hundreds of nanometres, while the higher order aggregate networks resulted from their assembling extended over several micrometres.

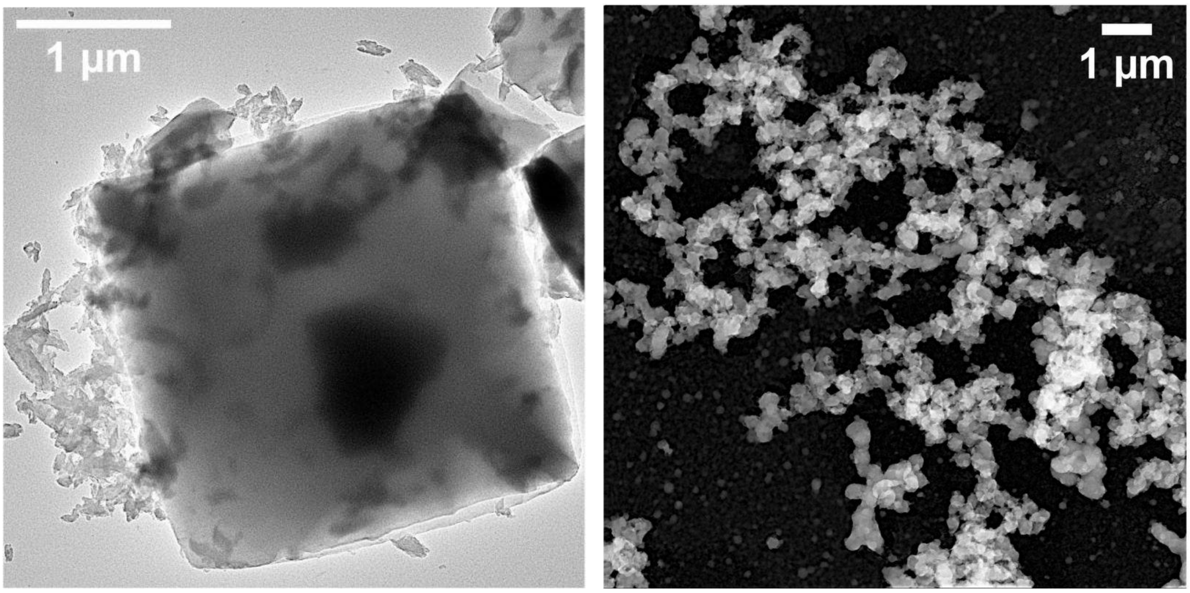

(a) (b)

Figure 1. (a) TEM image recorded on the sample obtained by depositing ZnTMPyP from H_2O; (b) STEM image recorded on the ZnTMPyP specimen resulted by employing DMSO as solvent

Under the effect of DMF (Figure 2a), the molecules of the metalated porphyrin arranged either as spots with submicrometric dimensions or as ramified islands resembling incomplete fern-type aggregates [5].

The replacing of DMF with AcN led to the formation of different architectures, as can be seen in Figure 2b. The ZnTMPyP molecules organized as crumpled sheets with some of the folds having the appearance of acicular structures.

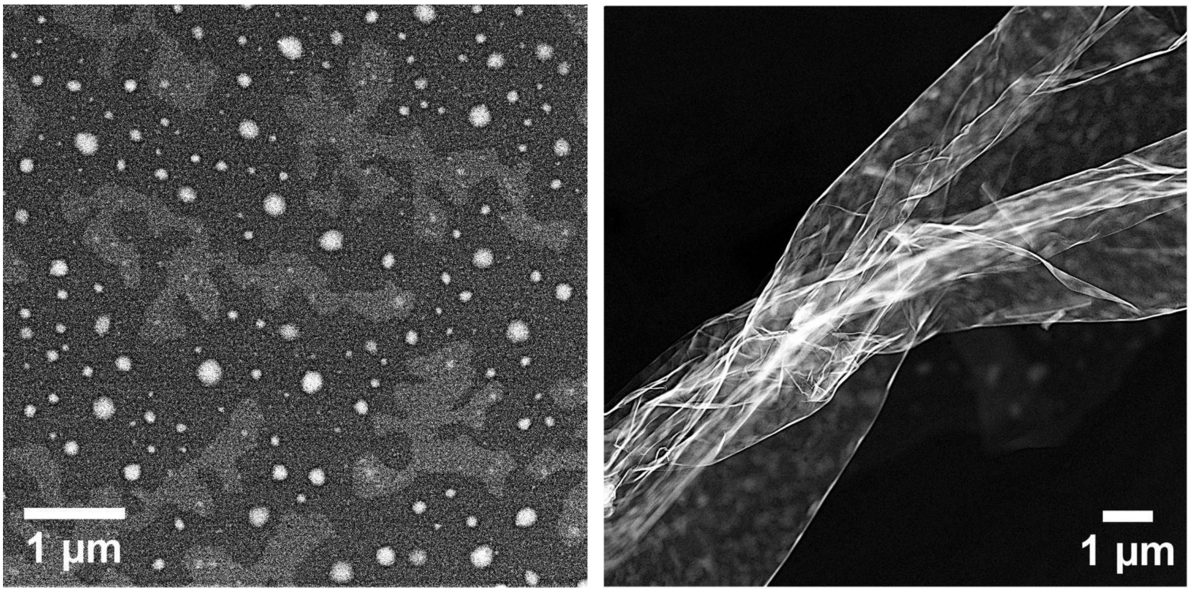

(a) (b)

Figure 2. (a) STEM image scanned on the specimen resulted from the drop-casting of the Zn(II)-porphyrin from DMF; (b) STEM image recorded on the metalloporphyrin sample obtained using AcN as solvent

Lastly, when the porphyrin derivative was applied from ethanol, quasi-annular arrangements were evidenced (Figure 3) that appeared to exhibit a high degree of homogeneity when observed from a distance. However, from up-close it was difficult to find two formations that were identical.

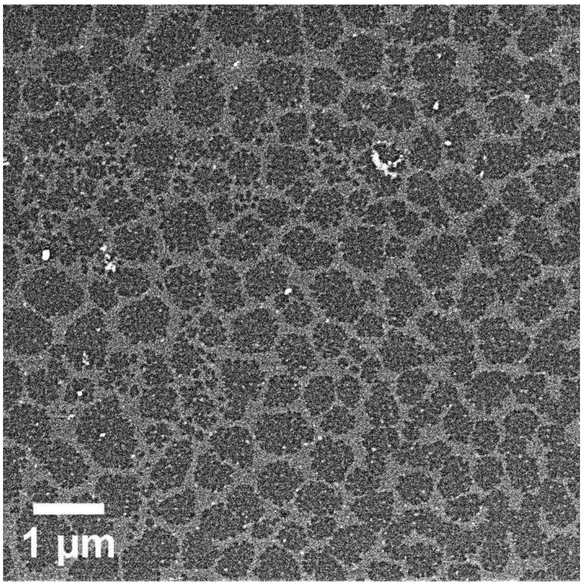

Figure 3. STEM image recorded on the specimen obtained by drop-casting ZnTMPyP from EtOH

Conclusion

The TEM/STEM analysis of the zinc-metalated porphyrin samples revealed several types of aggregates produced *via* the self-assembling of the complex's molecules from solvents having different polarities. The shapes of the formations varied from one solvent to another, regardless of their organic or inorganic nature. The observed architectural heterogeneity is attributable to the interplay between the structure of the symmetrically substituted cationic metalloporphyrin, its hydrophilic/hydrophobic balance, the properties of the solvents employed to dissolve it (including their polarities), as well as the properties of the continuous and amorphous nonpolar carbon film covering the TEM grids.

The results supplement the scientific literature relevant to the self-assembly of metalloporphyrins.

References

[1] M. Tahoun, C.T. Gee, V.E. McCoy, P.M. Sander, C.E. Muller, RSC Adv. 11 (2021) 7552.
[2] E. Fagadar-Cosma, D. Vlascici, G. Fagadar-Cosma, Porfirinele de la sinteză la aplicații, Eurostampa, Timisoara, Romania, 2008, pp. 10.
[3] Y.-B. Jiang, Z. Sun, MRS Bull. 44 (2019) 167–171.
[4] G.M. Whitesides, J.P. Mathias, C.T. Seto, Science 254 (1991) 1312–1319.
[5] B.-O. Taranu, E. Fagadar-Cosma, Processes 10 (2022) 611.
[6] I. Fratilescu, A. Lascu, B.O. Taranu, C. Epuran, M. Birdeanu, A.-M. Macsim, E. Tanasa, E. Vasile, E. Fagadar-Cosma, Nanomater. 12 (2022) 1930.
[7] B.-O. Taranu, E. Fagadar-Cosma, Nanomater. 12 (2022) 3788.
[8] M. Birdeanu, E. Fagadar-Cosma, in: M.V. Putz (Ed.), Quantum Nanosystems: Structure, Properties, and Interactions, Apple Academic Press, Toronto, Canada, 2015, pp. 173.
[9] G. Magna, D. Monti, C.D. Natale, R. Paolesse, M. Stefanelli, Molecules 24 (2019) 4307.
[10] L. Zhang, T. Wang, J. Jiang, M. Liu, Aggregate (2022) e198.

[11] F.A. Helmich, Multi-component porphyrin self-assembly, Ph.D. Thesis, Technische Universiteit Eindhoven, Eindhoven, The Netherlands, 2012, pp. 1.
[12] E. Fagadar-Cosma, I. Creanga, B. Maranescu, A. Palade, A. Lorinczi, G. Fagadar-Cosma, M. Popescu, Dig. J. Nanomater. Biostructures 6 (2011) 75.
[13] Z. Dudas, E. Fagadar-Cosma, A. Len, L. Romanszki, L. Almasy, B. Vlad-Oros, D. Dascalu, A. Krajnc, M. Kriechbaum, A. Kuncser, Materials 11 (2018) 565.
[14] L.R. Snyder, J.J. Kirkland, J.L. Glajch, Practical HPLC Method Development, Vol. 3, 2nd Ed., John Wiley & Sons, Inc., Hoboken, NJ, USA, 1997, pp. 721.
[15] Z. Szabadai, L. Sbarcea, L. Udrescu, Analiza fizica si chimica a medicamentului, Vol. 1, Victor Babes Publishing House, Timisoara, Romania, 2016, pp. 243.
[16] B.-O. Taranu, Contribuții la caracterizarea fizico-chimică a porfirinelor. Aplicații în senzoristică și coroziune, Ph.D. Thesis, Institute of Chemistry Timisoara of Romanian Academy, Timisoara, Romania, 2016, pp. 105.

THE ELECTROCATALYTIC ACTIVITY OF $YMnO_3$-BASED ELECTRODES FOR THE O_2 AND H_2 EVOLUTION REACTIONS IN A STRONG ALKALINE MEDIUM

Bogdan-Ovidiu Taranu[1], Paula Sfirloaga[1,2]

[1]National Institute for Research and Development in Electrochemistry and Condensed Matter, Dr. A.P. Podeanu street, No. 144, 300569, Timisoara, Romania
[2]Spin-off Nattive-Senz SRL, Dr. A.P. Podeanu street, No. 144, 300569, Timisoara, Timis, Romania
e-mail: b.taranu84@gmail.com

Abstract

$YMnO_3$ perovskites synthesized using the sol-gel method were studied regarding their electrocatalytic properties for the O_2 and H_2 evolution reactions (OER and HER) in a strong alkaline medium. The highest activity was observed during HER experiments, especially for the electrodes manufactured using suspensions containing Nafion, Carbon Black and either Co^{2+} doped $YMnO_3$ or Sn^{2+} doped $YMnO_3$. For these samples, the HER overpotential value at $i = -10$ mA/cm^2 was 0.83 V. The main conclusions are the following: (a) the inclusion of Carbon Black into the electrode manufacturing process improved the HER catalytic activity of all perovskite-modified electrodes and (b) the HER activity of the samples modified with the catalysts, Nafion and Carbon Black was similar despite the different temperatures applied during perovskite synthesis.

Introduction

Two side effects of the comparatively recent and rapid global economic development consist of climate change and the global energy crisis currently facing humanity [1]. These two issues are at the heart of the present efforts to replace the fossil fuel-based infrastructure with an alternative energy-based one [2]. The ongoing research revealed hydrogen, a carbon-free energy carrier and energy source, as promising for a sustainable alternative energy-oriented infrastructure [3]. There are several known methods for generating hydrogen [4], but the one that is both eco-friendly and economically effective is water-splitting, either by photo- or electrocatalysis [5,6].

Electrocatalytic water-splitting consists of the decomposition of water – an abundant source of H_2 – using electrical current. The two half-cell reactions occurring during this process, namely the hydrogen evolution reaction (HER) taking place at the cathode and the oxygen evolution reaction (OER) unfolding at the anode, make its large-scale application difficult because of high overpotentials (which are a measure of the kinetic energy barriers) [1,7]. To resolve this issue, researchers are actively looking to identify materials that can serve as effective and stable electrocatalysts for the specified reactions. Such catalysts would minimize the overpotentials, ensuring more efficient hydrogen production [8].

The present paper describes a study in which the electrocatalytic activity for the two half-reactions involved in water-splitting of $YMnO_3$ perovskite materials synthesized at different temperatures using the sol-gel method is evaluated in a strong alkaline medium.

Experimental

The materials were synthesized by the sol-gel method, followed by thermal treatments at different temperatures. The subsequent perovskites were obtained: YMO-800 ($YMnO_3$ synthesized at 800 °C), YMO-1000 ($YMnO_3$ synthesized at 1000 °C), YMO-15 (0.005 mmol Co^{2+} doped $YMnO_3$) and YMO-16 (0.005 mmol Sn^{2+} doped $YMnO_3$). Glassy carbon

(GC) pellets were acquired from Andreescu Labor & Soft SRL, Nafion® 117 solution from Sigma-Aldrich, Carbon Black - Vulcan XC 72 from Fuel Cell Store, potassium hydroxide from Merck, and acetone and ethanol from Chimreactiv.

The role of Carbon Black was to enhance the charge transfer at the interface between the sample and the electrolyte solution [9]. Nafion was utilized as binder, ensuring adherence between the deposited composition and the substrate surface [10].

The perovskite catalysts were employed to manufacture modified electrodes by adapting a previously published protocol [11]. The samples were obtained by pursuing the steps described in what follows. The GC pellets served as conductive support. They were washed with water and detergent, water, bidistilled water, acetone and ethanol. After drying, one of their surfaces was covered with suspensions containing the catalytic materials. The suspensions were prepared following two procedures: (1) 5 mg catalyst and 50 μL Nafion solution were added to 450 μL ethanol and (2) 5 mg catalyst, 50 μL Nafion solution and 5 mg Carbon Black were added to 900 μL ethanol. The suspensions were ultrasonicated for 30 min., and a volume of 10 μL was taken from each of them and drop-casted on one of the surfaces of the GC pellets to obtain each modified electrode. The samples were used in the experiments after drying at RT. For each experiment one of the electrodes was inserted into a polyamide support which restricted its geometrical surface to 0.28 cm^2.

The names of the samples are presented in Table 1 along with the compositions of the suspensions used to obtain them.

Table 1. Names of investigated electrodes and compositions of suspensions

Electrode name	**Catalyst (5 mg)**	**Carbon Black (mg)**	**5% Nafion solution (μL)**	**Ethanol (μL)**
GC_0	-	-	-	-
$GC_{YMO-800}$	YMO-800	-	50	450
$GC_{YMO-1000}$	YMO-1000	-	50	450
GC_{YMO-15}	YMO-15	-	50	450
GC_{YMO-16}	YMO-16	-	50	450
$GC_{CB-YMO-800}$	YMO-800	5	50	900
$GC_{CB-YMO-1000}$	YMO-1000	5	50	900
$GC_{CB-YMO-15}$	YMO-15	5	50	900
$GC_{CB-YMO-16}$	YMO-16	5	50	900

The electrochemical setup consisted of a potentiostat – Voltalab model PGZ 402 from Radiometer Analytical – connected to three electrodes inserted into a glass cell containing the electrolyte solution. Each modified sample, as well as an unmodified GC pellet, served as the working electrode. The auxiliary electrode was a Pt plate having a geometrical surface of 0.8 cm^2, while an Ag/AgCl (sat. KCl) electrode was utilized as reference.

The electrolyte solution employed in all experiments was 1 M KOH. Aqueous solutions were obtained with bidistilled water. Linear sweep voltammograms (LSVs) were iR-corrected and recorded at the scan rate (v) of 5 mV/s. For the HER investigations, the electrolyte solution was degassed by bubbling N_2. The electrochemical potential (E) values were represented in terms of the Reversible Hydrogen Electrode (RHE) with equation (1) [12]. The OER and HER overpotential values were obtained with equations (2) and (3), respectively [13,14].

$$E_{RHE} = E_{Ag/AgCl(sat.\ KCl)} + 0.059 \times pH + 0.197 \quad (1)$$

$$\eta_{O2} = E_{RHE} - 1.23 \quad (2)$$

$$\eta_{H2} = |E_{RHE}| \qquad (3)$$

Where: E_{RHE} is the reversible hydrogen electrode potential (V); $E_{Ag/AgCl(sat.\ KCl)}$ is the potential *vs.* the Ag/AgCl (sat. KCl) reference electrode (V); η_{O2} is the oxygen evolution overpotential (V) and η_{H2} is the hydrogen evolution overpotential (V);

Results and discussion

OER investigations. Figure 1 shows the LSVs obtained on the unmodified electrode and on electrodes modified with suspensions containing the perovskite materials and Nafion. The lowest OER overpotential value at i = 10 mA/cm^2 – the current density value often considered as a measure of OER catalytic performance [15] – is 1.15 V and was determined for the $GC_{YMO-800}$ sample. The addition of Carbon Black to the suspensions utilized to manufacture the modified electrodes led to the LSVs presented in Figure 2. The presence of an oxidation peak at E values > 2.2 V hampered the determination of the η_{O2} value at i = 10 mA/cm^2. Thus, the presence of Carbon Black is not advantageous for the study of the OER activity of the perovskite-based modified electrodes.

HER investigations. Figure 3 outlines the polarization curves recorded on GC_0 and the electrodes modified with the perovskite materials and Nafion. It can be seen that the η_{H2} values at i = −10 mA/cm^2 are close to each other for all samples, including the unmodified GC pellet (η_{H2} for GC_0 = 0.9 V). The lowest η_{H2} value was determined for GC_{YMO-16} as 0.88 V. In the presence of Carbon Black in the suspensions used to manufacture the modified electrodes, an improvement in their HER catalytic activity was evidenced (Figure 4). The η_{H2} values of the modified samples remained similar, but the lowest one was determined for both $GC_{CB-YMO-15}$ and $GC_{CB-YMO-16}$ as 0.83 V. According to this result, the differences in the thermal treatment applied during the synthesis of the YMO-15 and YMO-16 perovskites did not affect their HER electrocatalytic activity.

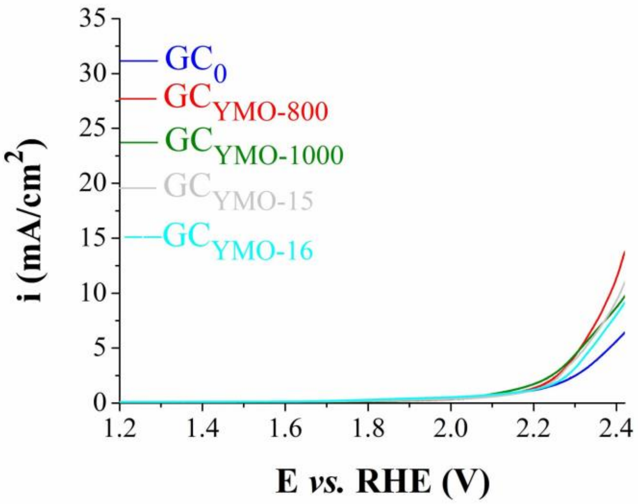

Figure 1. OER polarization curves recorded on the GC_0, $GC_{YMO-800}$, $GC_{YMO-1000}$, GC_{YMO-15}, GC_{YMO-16} electrodes, in 1 M KOH solution, at v = 5 mV/s

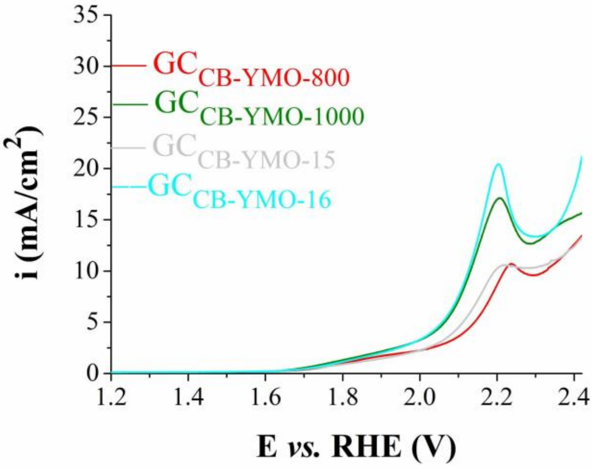

Figure 2. OER polarization curves recorded on the GC$_0$, GC$_{CB-YMO-800}$, GC$_{CB-YMO-1000}$, GC$_{CB-YMO-15}$, GC$_{CB-YMO-16}$ electrodes, in 1 M KOH solution, at v = 5 mV/s

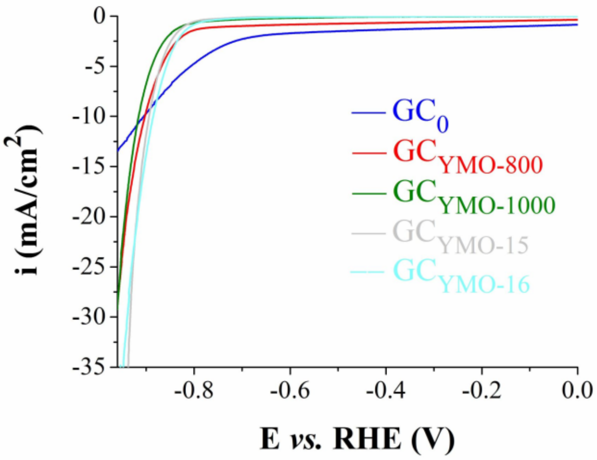

Figure 3. HER polarization curves recorded on the GC$_0$, GC$_{YMO-800}$, GC$_{YMO-1000}$, GC$_{YMO-15}$, GC$_{YMO-16}$ electrodes, in 1 M KOH solution, at v = 5 mV/s

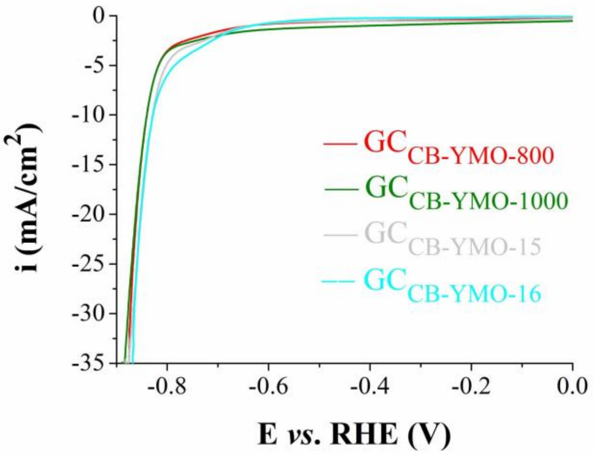

Figure 4. HER polarization curves recorded on the GC$_{CB-YMO-800}$, GC$_{CB-YMO-1000}$, GC$_{CB-YMO-15}$, GC$_{CB-YMO-16}$ electrodes, in 1 M KOH solution, at v = 5 mV/s

Conclusion

The OER and HER experiments performed in a strong alkaline medium (1 M KOH) on modified electrodes manufactured using $YMnO_3$ perovskite materials synthesized at different temperatures revealed that these electrodes are more suitable for the HER. The highest electrocatalytic activity was evidenced for the GC_{YMO-15} and GC_{YMO-16} samples. However, despite different temperatures being applied during the synthesis of the perovskites no significant differences in the HER electrocatalytic activity of the materials were observed. Compared to the samples obtained without using Carbon Black the ones containing this type of conductive carbon displayed lower HER overpotentials.

Acknowledgements

This work was supported by the Experimental Demonstrative Project 683PED⁄2022.

References

[1] X. Xiao, L. Yang, W. Sun, Y. Chen, H. Yu, K. Li, B. Jia, L. Zhang, T. Ma, Small 18 (2022) 2105830.
[2] J.A. Luque-Urrutia, T. Ortiz-García, M. Solà, A. Poater, Inorganics 11 (2023) 88.
[3] A. Pareek, R. Dom, J. Gupta, J. Chandran, V. Adepu, P.H. Borse, Mater. Sci. Energy Technol. 3 (2020) 319.
[4] R. Chaubey, S. Sahu, O.O. James, S. Maity, Renew. Sust. Energ. Rev. 23 (2013) 443.
[5] A. Gupta, B. Likozar, R. Jana, W.C. Chanu, M.K. Singh, Int. J. Hydrog. Energy 47 (2022) 33282.
[6] A. Raveendran, M. Chandran, R. Dhanusuraman, RSC Advances 13 (2023) 3843.
[7] S. Wang, A. Lu, C.-J. Zhong, Nano Converg. 8 (2021) 4.
[8] Y. Kim, S.E. Jun, G. Lee, S. Nam, H.W. Jang, S.H. Park, K.C. Kwon, Materials 16 (2023) 3044.
[9] M. Poienar, B.-O. Taranu, P. Svera, P. Sfirloaga, P. Vlazan, J. Therm. Anal. Calorim. 147 (2022) 11839.
[10] B.-O. Taranu, P. Vlazan, P. Svera (m. Ianasi), M. Poienar, P. Sfirloaga, J. Alloys Compd. 892 (2021) 162239.
[11] J. Chang, Q. Lv, G. Li, J. Ge, C. Liu, W. Xing, Appl. Catal. B 204 (2017) 486.
[12] B.-O. Taranu, E. Fagadar-Cosma, P. Sfirloaga, M. Poienar, Energies 16 (2023) 1212.
[13] I. Fratilescu, A. Lascu, B.O. Taranu, C. Epuran, M. Birdeanu, A.-M. Macsim, E. Tanasa, E. Vasile, E. Fagadar-Cosma, Nanomaterials 12 (2022) 1930.
[14] P. Sfirloaga, B.-O. Taranu, M. Poienar, P. Vlazan, Surf. Interfaces 39 (2023) 102881.
[15] B.-O. Taranu, E. Fagadar-Cosma, Processes 10 (2022) 611.

MASS SPECTROMETRIC PROFILING OF EPIGENETIC DNA MODIFICATIONS IN AN *EPICOCCUM NIGRUM* STRAIN

Kitti Tari*[1]*, Adiyadolgor Turbat*[2]*, Enkh-Amgalan Jigjiddorj*[2]*, Mónika Varga*[1]*,
***Csaba Vágvölgyi*[1]*, András Szekeres*[1]**

[1]*Department of Microbiology, Faculty of Sciences, University of Szeged, 6726, Közép fasor 52, Szeged, Hungary*
[2]*Laboratory of Microbiology, Institute of General and Experimental Biology, Mongolian Academy of Science, Ulaanbaatar, Mongolia 13330*
e-mail: kittitari2000@gmail.com

Bioactive compounds produced by endophytic fungi have great potential and can be utilized by the pharmaceutical and food industries, as well as in agriculture. However, it was observed that the genes responsible for the production of bioactive metabolites from fungal endophytes are usually not expressed in axenic cultures [1,3]. The media used for the culture of fungal endophytes in the laboratories do not contain the nutrients available/found in their native hosts. As a result of the lack of the host stimulus in the medium, many genes encoding biosynthetic pathways become silent, limiting their production of secondary metabolites [1]. Silent biosynthetic pathways of new bioactive secondary metabolites can be induced using epigenetic modifiers due to the change of the genomic chromatin structure. DNA methyltransferase (DNMT) and/or histone deacetylase (HDAC) inhibitors can be a possible treatment in the laboratory to activate these secondary metabolites to modify the chromatin structure of the coding genes [2,3]. The use of these epigenetic modifiers can increase the amount of medicinally useful compounds and improve the efficiency of the microbial production of these compounds [2].

In our research, we selected an endophytic fungus that had already been characterized as a hypericin producer. However, during sub-cultivations, this secondary metabolite production ability of the fungus was lost. To recover the disappeared character and to reveal the possible altered secondary metabolite set, valproic acid (VPA) and sodium-butyrate (SB) were applied as epigenetic modifiers. Both VPA and SB are also members of HDAC inhibitors. The effect of both compounds was examined by the mass spectrometric metabolic profiling of the treated strains. Initially, the concentrations of the epigenetic treatments were defined by the inhibition zone determination of both VPA and SB in agar plate assays. Based on our results, it was observed that there was not any inhibition of the compounds within the applied concentration range. Thus, a relatively high concentration (1000 μM) was applied to form enough high epigenetic pressure on the fungal strain. After the cultivation with the epigenetic modifiers, both the ferment broth and mycelium of grown fungal cultures were subsequently extracted using ethyl acetate and mixture of chloroform-methanol (4:1). The resulted extracts were evaporated and high-resolution mass spectrometric analysis was performed to investigate the possible alterations of the produced metabolites.

This work was supported by the bilateral project 2019-2.1.11-TÉT-2020-00148.

References

[1] L.C. Pillay, L. Nekati, P.J. Makhwitine, S.I. Ndlovu, Front. Microbiol. 13, (2022) 815008.
[2] S. Gupta, M.G. Kulkarni, J.F. White, J.V. Staden, S. Afr. J. Bot. 134, (2020) 394.
[3] T. Asai, S. Morita, N. Shirata, T. Taniguchi, K. Monde, Y. Oshima, Org. Lett. 14(21), (2016) 5456.

HYBRID PEROVSKITE/POLYMER MATERIAL. PREPARATION AND PHYSICOCHEMICAL PROPERTIES

Nick Samuel Ţolea[1], Adina Căta[1], Antonina Lazăr[1], Ioana M.C. Ienaşcu[1,2], Paula Svera[1], Daniel Ursu[1], Corina Orha[1], Anamaria Dabici[1], Paula Sfîrloagă[1,3]

[1]National Institute of Research and Development for Electrochemistry and Condensed Matter, Dr. A. P. Podeanu 144, 300569, Timişoara, Romania
[2]"Vasile Goldiş" Western University of Arad, Faculty of Pharmacy, Liviu Rebreanu 86, 310045, Arad, Romania
[3]Spin-off Nattive-Senz SRL, Dr. A.P. Podeanu 144, 300569, Timisoara, Timis, Romania
e-mail: samy_nick2008@yahoo.com

Abstract

Organic–inorganic hybrid perovskites are a promising class of processable semiconducting materials that combine the favorable properties of the inorganic semiconductor with the flexibility and low-temperature processability of the organic material [1].

Here, we report on the synthesis and investigation of the properties of a novel polymer-perovskite nanoparticles system based on $LaMnO_3$:Ag nanocrystals protected by sodium polyacrylate polymer. The mixture of $LaMnO_3$:Ag and sodium polyacrylate (1:20, m/m) were wet-triturated for 30 minutes, using water, until hydrogels were obtained. The resulting hydrogels were dried at 60 °C for 12 h and then mortared until obtaining a powder with particle dimensions up to 1 mm. Finally, the powder was subjected to another drying stage at 60 °C for 4 h.

The hybrid material was investigated by various characterization techniques, i.e. SEM/EDAX, X-ray diffraction, UV-VIS, FT-IR, and RAMAN spectroscopy. The obtained results confirm the formation of a novel polymer-perovskite nanoparticles system whose electrical and optical properties will be studied later.

References

[1] G.C. Papavassiliou, G.A. Mousdis, I. Koutselas, in: T.-C. Sum, N. Mathews (Eds)., Halide Perovskites: Photovoltaics, Light Emitting Devices, and Beyond, Wiley-VCH GmbH & Co.: Hoboken, NJ, USA, 2019.

Acknowledgements

This work was supported by the Experimental Demonstrative Project 683PED/2022.

ANTIMICROBIAL AND ANTI-ADHESION ACTIVITY OF ESSENTIAL OILS AGAINST BACTERIA *Salmonella* Typhimurium AND *Staphylococcus aureus*, AND YEAST *Candida albicans* AND *Saccharomyces cerevisiae*

Zorica Tomičić[1], **Ružica Tomičić**[2] , **Sunčica Kocić-Tanackov**[2], **Peter Raspor**[3]

[1]Institute of Food Technology in Novi Sad, University of Novi Sad, 21000 Novi Sad,
Bulevar cara Lazara 1, Serbia
[2]Faculty of Technology, University of Novi Sad, 21000 Novi Sad,
Bulevar cara Lazara 1, Serbia
[3]Biotechnical Faculty, University of Ljubljana, 1000 Ljubljana,
Jamnikarjeva 101, Slovenia
e-mail: zorica.tomicic@fins.uns.ac.rs

Introduction

In recent years, the growing resistance of microorganisms to the currently used antimicrobial agents has opened promotional research in the identification of new, more effective drugs with a wide spectrum of action. The use of natural substances with antimicrobial activity, such as essential oils and their bioactive compounds, has become a promising area of research. Therefore, the aim of this study was to evaluate the antimicrobial and anti-adhesion activity of fifteen essential oils and their compounds against gram-negative *Salmonella* Typhimurium ATCC 25923 and gram-positive *Staphylococcus aureus* ATCC 14208 bacteria, and two yeast species *Candida albicans* ATCC 10231 and *Saccharomyces cerevisiae* ATCC 9763 highly important for food spoilage and infectious diseases.

Experimental

Antimicrobial activity was determined by testing the minimum inhibitory concentration (MIC), the minimum bactericidal concentration (MBC) and the minimum fungicidal concentration (MFC) of essential oils and compounds. The method used to assess adhesion was crystal violet staining.

Results and discussion

Susceptibility tests indicated that the essential oils of *Cinnamomum zeylanicum* and *Eugenia caryophyllus* showed the highest antimicrobial activity with MICs ranging from 0.078 to 1.25 mg/mL, and 0.039 to 1.25 mg/mL, respectively. On the other hand, essential oils of *Eucalypti aetheroleum* and *Salvia officinalis* had significantly weaker antimicrobial properties than the others. Furthermore, the MIC values were used to assess the inhibition of adhesion of the tested bacteria and yeast in a microtiter plate. A high inhibitory effect on the initial phase of biofilm formation was observed for most of the tested essential oils, with the strongest effect of *E. caryophyllus* essential oil with a percentage of inhibition of 53.5, 73, 63.5 and 51.5 % on *S.* Typhimurium ATCC 14208, *S. aureus* ATCC 25923, *C. albicans* ATCC 10231 and *S. cerevisiae* ATCC 9763, respectively. The essential oils of *C. zeylanicum*, *Origanum vulgare* and *Thymus vulgaris* also showed a strong anti-adhesion effect. The activity was more pronounced against gram-positive bacteria than gram-negative bacteria, and the most resistant strain was yeast *S. cerevisiae*. In addition, the most active anti-adhesion compounds were carvacrol and thymol which showed the remarkable anti-adhesion effect against bacterial and yeast strains with a percentage of inhibition up to 66 %.

Conclusion

Understanding more about the antimicrobial activity of the tested essential oils and their mechanism of action will be helpful for their application in the treatment of many infectious diseases and food preservation in the future.

Acknowledgements

Ružica Tomičić thank Provincial secretariat for higher education and scientific research, Autonomous Province of Vojvodina, Republic of Serbia (project no. 142-451-2623/2021-01).

PLANT EXTRACTS AS ANTIFUNGAL AND ANTI-ADHESION AGENTS AGAINST YEAST CONTAMINANTS

Ružica Tomičić[1], Zorica Tomičić[2], Sunčica Kocić-Tanackov[1], Peter Raspor[3]

[1]Faculty of Technology, University of Novi Sad, 21000 Novi Sad,
Bulevar cara Lazara 1, Serbia
[2]Institute of Food Technology in Novi Sad, University of Novi Sad, 21000 Novi Sad,
Bulevar cara Lazara 1, Serbia
[3]Biotechnical Faculty, University of Ljubljana, 1000 Ljubljana,
Jamnikarjeva 101, Slovenia
e-mail: ruzica.tomicic@yahoo.com
ruzica.tomicic@uns.ac.rs

Introduction

Yeasts are used in food and drink fermentation, but they can also cause spoilage in a wide range of fermented and non-fermented foods. Food spoilage is a serious sensorial and economical problem for the food industry as microbial contamination can occur during processing, storage and consumption of the end products. *Candida* and *Pichia* are the genera mainly involved in spoilage of products in the food and beverage industry. These contaminating microorganisms can form biofilms on food contact surfaces, being difficult to eradicate, increasing the probability of microbial survival and further dissemination during food processing. It is well known that biofilms are more resistant to antimicrobial agents compared to planktonic cells and this makes them difficult to eliminate. Among the strategies used to overcome resistance to antifungal drugs and preservatives, the use of natural substances such as plant extracts has shown particular promise in controlling biofilms. Taking this into account, our study was designed with the objectives of evaluating the effects of *Humulus lupulus*, *Alpinia katsumadai* and *Evodia rutaecarpa* extracts on the initial phase of biofilm formation and preformed biofilms of *Candida albicans* ATCC 10261, *Candida glabrata* ZIM 2369 and *Pichia membranifaciens* ZIM 2417 to the surface of stainless steel.

Experimental

The minimal inhibitory concentrations (MICs) of plant extracts were determined using the broth microdilution method CLSI M27-A3, while the method used to assess antibiofilm activity was crystal violet staining.

Results and discussion

Based on the MIC values, all plant extracts exerted significant antifungal effects with MIC values ranged from 100 to 400 µg/mL. Our data showed a significant reduction of biofilm formation and preformed biofilm of *C. albicans* ATCC 10261 to stainless steel surface after exposure to the *H. lupulus*, *A. katsumadai* and *E. rutaecarpa* extracts at concentrations of 1/2 × MIC and 1 × MIC. All three tested extracts were equally effective against *C. albicans*. In the case of *C. glabrata* ZIM 2369, it was evident that both concentrations (1/2 × MIC and 1 × MIC) of *A. katsumadai* extract significantly reduced the initial phase of biofilm formation during 24 h of incubation. However, exposure of preformed 24 h biofilms with *A. katsumadai* extract for 3 h had no effect on the formed biofilm. These findings highlighted that the extracts were more efficient in the case of *C. albicans* than in *C. glabrata*. Regarding *P. membranifaciens* ZIM 2417, it was found that *A. katsumadai* and *E. rutaecarpa* extracts significantly increased biofilm formation at a concentration of 1/2 × MIC. The enhanced biofilm development observed upon exposure to some extracts in this study may be due to the presence of certain compounds within the extracts that favour the development of these biofilms.

Conclusion

The obtained data may contribute to a better understanding of the antifungal properties of plant extracts such as *H. lupulus*, *A. katsumadai* and *E. rutaecarpa* which can be promoted as an alternative antifungal agents.

Acknowledgements

Ružica Tomičić thank Provincial secretariat for higher education and scientific research, Autonomous Province of Vojvodina, Republic of Serbia (project no. 142-451-2623/2021-01).

EFFICIENCY OF XANTHAN BIOSYNTHESIS BY LOCAL *Xanthomonas* ISOLATE USING INDUSTRIAL EFFLUENTS GENERATED IN AP VOJVODINA

Zorana Trivunović, Ida Zahović, Jelena Dodić

Department of Biotechnology, Faculty of Technology Novi Sad, University of Novi Sad,
Bulevar cara Lazara 1, Novi Sad 21101, Serbia
e-mail: ida.zahovic@uns.ac.rs

Abstract

Rapid industrialization and intensification of agricultural production are responsible for the exploitation of natural resources and the simultaneous generation of different effluents. The emission of untreated effluents into the environment is ecologically unacceptable due to its high negative environmental impact. Since developed treatment methods mainly result in waste conversion from one form into another, there is an urgent need for suitable utilization of agro-industrial effluents in their crude form. Industrial effluents, which include various biodegradable waste streams and by-products, are characterized by high presence of organic and inorganic compounds, and hence, they have a great potential for valorisation in biotechnological production of value-added products. One of valuable bioproducts that can be obtained by cultivation of microorganisms on different effluents is xanthan, biopolymer of microbial origin. Due to its outstanding rheological properties, biodegradability, non-toxic nature and biocompatibility, xanthan is widely exploited and has high commercial value. Although this biopolymer is generally produced by the reference strain *Xanthomonas campestris* ATCC 13951 on glucose or sucrose containing medium, the other members of the genus *Xanthomonas* are also examined as xanthan-producing microorganisms especially when alternative raw materials are used. Therefore, the aim of this study was to compare the success of xanthan biosynthesis by local *Xanthomonas* isolate on media based on industrial effluents in relation to the biosynthesis performed with reference strain *Xanthomonas campestris* ATCC 13951 on commonly applied semi-synthetic medium with glucose.

Within the experimental part, the cultivation of reference strain on standard semi-synthetic medium was performed simultaneously with cultivation of local isolate on media based on effluents generated by the biodiesel, wine, dairy and confectionery industry in the AP Vojvodina. Applied alternative production media contained glycerol, fructose and glucose, lactose, and starch as a carbon sources, respectively. Xanthan biosynthesis was carried out at laboratory level (300 mL Erlenmeyer flasks) in aerobic conditions on media with the same initial concentrations of carbon source (20 g/L) at temperature of 30°C and agitation of 150 rpm for 120 h. Bioprocess success was estimated based on the quantity of produced xanthan. In order to conduct mutual comparison and to easier interpret the obtained results, experimental data for xanthan concentration in media at the end of biosynthesis were relativized. Cultivation of reference strain on semi-synthetic medium is considered as 100% successful, and in relation to this, the values of xanthan concentration in alternative media were relativized.

Based on the obtained results, xanthan biosynthesis by applied isolate on medium prepared with winery effluents was 97.38% successful, while xanthan production on medium containing effluents from biodiesel and confectionery industry conducted with the same producing strain resulted in 50.86% and 48.69 of success, respectively. The lowest success of 26.56%, in applied experimental conditions, was achieved when xanthan biosynthesis was performed on medium based on effluents originated from diary industry. These differences in the xanthan quantity probably are the consequence of different carbon sources in alternative media, as well as the

presence of other compounds originating from the raw material that can inhibit the metabolic activity of producing strain.

The obtained results confirm the possibility of xanthan biosynthesis by local *Xanthomonas* isolate on media based on effluents from selected branches of industry that is generated in the AP Vojvodina. Considering the discussed values, it can be concluded that effluents generated during the wine production have a high potential for valorisation in xanthan production by examined isolate, which represents the basis for further research aimed to improve this production process.

Acknowledgments

This research was funded by the Ministry of Science, Technological Development and Innovation of the Republic of Serbia (Grant No. 451-03-47/2023-01/200134) and the Provincial Secretariat for Science and Technological Development of Vojvodina, Republic of Serbia (Project No. 142-451-3166/2023-01/01).

POTENTIAL OF *Xanthomonas* STRAINS ISOLATED IN SERBIA FOR XANTHAN PRODUCTION FROM CRUDE GLYCEROL

Ida Zahović, Jelena Dodić, Zorana Trivunović

Department of Biotechnology, Faculty of Technology Novi Sad, University of Novi Sad,
Bulevar cara Lazara 1, Novi Sad 21101, Serbia
e-mail: ida.zahovic@uns.ac.rs

Abstract

Xanthan is a natural polysaccharide that is biosynthesized by metabolic activity of Gram-negative bacteria from the genus *Xanthomonas.* Commercial production of xanthan is mainly performed as aerobic submerged batch cultivation of the reference strain *X. campestris* ATCC 13951 on a medium of appropriate composition and under optimal conditions. The success of xanthan production is largely influenced by the selection of producing strains, formulation of cultivation medium composition, and control and regulation of bioprocess parameters. The aim of this study was to examine xanthan production on medium containing crude glycerol from domestic biodiesel industry using reference strain *Xanthomonas campestris* ATCC 13951 and *Xanthomonas* strains locally isolated from different vegetable cultures. Xanthan was produced by submerged cultivation of examined producing strains at a laboratory level under aerobic conditions at 30°C and 150 rpm for 168 h. Bioprocess efficacy was estimated based on the xanthan concentration in media at the end of biosynthesis. According to the obtained results, xanthan production on crude-glycerol based medium was possible by all applied *Xanthomonas* strains. The highest potential for successful xanthan production has PL4 strain, while strain Xp 3-1 has the lowest ability to biosynthesize xanthan in applied experimental conditions.

Keywords: Biodiesel industry, crude glycerol, biotechnological production, xanthan, *Xanthomonas* isolates

Introduction

Biopolymers are attracting enhanced attention due to environmental concerns and their outstanding properties. Among them, microbial biopolymers are a promising alternative for existing polymers. Xanthan represents most commercially successful example of a microbial exopolysaccharide, which is produced by metabolic activity of Gram-negative bacteria from the genus *Xanthomonas* [1]. Because of its unique chemical structure, outstanding rheological properties, biodegradability, non-toxic nature and biocompatibility, this biopolymer is widely used as a thickener, rheological modifier, stabilizer, and emulsifier in the food, biomedical, pharmaceutical, petrochemical, chemical, and textile industry [2-4]. Xanthan occurs as a white or cream-colored free-flowing powder of neutral smell and taste [5] and has been classified as a food additive number E 415 by the European List of Permitted Food Additives, while the United States Food and Drug Administration has given the GRAS status (Generally Recognized as Safe) to an ethanol precipitate of xanthan [6]. Xanthan production is mainly performed as aerobic submerged batch cultivation of reference strain *X. campestris* ATCC 13951 on the medium of appropriate composition and under optimal conditions. Sucrose and glucose are mostly used as carbon sources in medium for xanthan production [7]. Taking into account that the cost of substrate is an important factor for commercial xanthan production and that an actual rise in prices of aforementioned sugars is present, it is clear that there is a need for exploitation of carbon sources of lower price in order to reduce the overall production costs [8]. Use of waste streams and by-products from different industries which contain aforementioned carbon sources can reduce the total costs of xanthan production, as well as reduce the environmental pollution caused by their disposal into environment [9]. Since the previous research have confirmed that *Xanthomonas* strains have the ability to metabolize glycerol it can be concluded that crude glycerol from the biodiesel industry have a great potential to be one of the promising alternative substrates of lower market value which may be used as a carbon source in the cultivation medium for xanthan production [8, 10].

The aim of this study was to examine xanthan production on media containing crude glycerol from domestic biodiesel industry by reference strain *Xanthomonas campestris* ATCC 13951 and *Xanthomonas* strains locally isolated from different vegetable cultures. The bioprocess efficacy was estimated based on xanthan concentration in media at the end of biosynthesis.

Experimental

Producing microorganisms

The reference strain *X. campestris* ATCC 13951, eight *Xanthomonas* strains isolated from crucifers (Am, CF, CB, KA, Xp 3-1, Xp 7-2, Mn 7-2, 12-2) and five *Xanthomonas* strains isolated from pepper leaves (PL1, PL2, PL3, PL4, PL5) were used as the producing microorganisms in these experiments. All strains were stored at 4ºC on agar slant (Yeast Maltose Agar, HiMedia, India) and subcultured every four weeks. *Xanthomonas* strains isolated from infected crucifers were stored in the Microbial Culture Collection of the Faculty of Technology Novi Sad, Serbia and *Xanthomonas* strains isolated from infected pepper leaves were stored in the Microbial Culture Collection of the Faculty of Agriculture in Novi Sad, Serbia.

Cultivation media

Agar slant was used for refreshing of producing microorganisms, and commercial liquid medium (Yeast Maltose Broth, HiMedia, India) was used for incubation of producing microorganisms in inoculum preparation procedure. Xanthan biosynthesis was performed on medium containing crude glycerol from the biodiesel production in the Republic of Serbia. Glycerol content in the medium was 20.00 g/L. The cultivation medium also contained yeast extract (3.0 g/L), $(NH_4)_2SO_4$ (1.5 g/L), K_2HPO_4 (3.0 g/L) and $MgSO_4 \cdot 7H_2O$ (0.3 g/L). The pH value of all used media was adjusted to 7.0±0.2 and then sterilized by autoclaving (121°C, 2.1 bar, 20 min).

Inoculum preparation

Xanthomonas strains were subcultured on agar slant and incubated at 25°C for 48 h. Further, inoculum preparation procedure was included suspending of producing microorganism cells in commercial liquid medium. The prepared suspension was then incubated in aerobic conditions at 25°C and 150 rpm (laboratory shaker KS 4000i control, Ika® Werke, Germany) for 48h.

Xanthan production

The xanthan production was carried out in 300 mL Erlenmeyer flasks with 100 mL of the cultivation medium. Inoculation was performed by adding 10% (v/v) of inoculum prepared as previously described. The biosynthesis was performed under aerobic conditions at 30°C and 150 rpm (laboratory shaker KS 4000i control, Ika® Werke, Germany) for 168 h.

Xanthan separation

At the end of biosynthesis, the xanthan was separated from the supernatant of cultivation medium by precipitation with cold 96% (v/v) ethanol, as described in previous research [11].

Results and discussion

In accordance with the defined aim of this research, xanthan was produced by reference strain *X. campestris* ATCC 13951 and local *Xanthomonas* isolates on medium prepared with crude glycerol generated in domestic biodiesel facility. In order to conduct mutual comparison of the obtained results and to easier interpret them, experimental data for xanthan concentration in media at the end of biosynthesis were relativized by assigning the largest obtained value to be maximally successful (100%) while the other values were expressed in a proportion of the maximum. The relativized values of xanthan concentration in media at the end of biosynthesis are shown in Figure 1.

Figure 1. Relativized values of xanthan concentration in medium at the end of biosynthesis by different *Xanthomonas* strains

From the graphically presented results (Figure 1) it can be noticed that cultivation of strain PL4 exhibited the maximal xanthan production, hence it is considered as 100% successful, and in relation to this, the other values of xanthan concentration in media were relativized. Xanthan production by *Xanthomonas* strain Am was also very successful since the relativized value of xanthan concentration in medium amounted 97.25%. More than 80% of success was achieved by strains PL2, PL5 and Xp 7-2, based on the relativized values of xanthan concentration in medium of 89.40%, 84.09% and 81.66%, respectively. PL1 strain, reference strain *X. campestris* ATCC 13951, as well as strains CB, KA and Mn 7-2 showed somewhat lower ability to produce xanthan on crude glycerol containing medium considering that the success of xanthan production by these strains was 78.60%, 72.74%, 72.50%, 72.34% and 71.80%, respectively. The obtained results show that success of xanthan production by strains PL3, 12-2 and CF was 69.35%, 63.73% and 60.77%, respectively, indicating that these strains have low ability to produce xanthan on crude glycerol containing medium. However, Xp 3-1 strain exhibited the lowest ability to produce xanthan on medium with crude glycerol in applied experimental conditions since the success of this bioprocess was 57.57%.

The results obtained in this study indicate that all the used *Xanthomonas* strains isolated in Serbia have ability to biosynthesize xanthan on medium containing crude glycerol from domestic biodiesel industry. The highest potential for successful xanthan production on crude glycerol-based medium have PL4 strain, while strain Xp 3-1 has the lowest ability to produce xanthan in applied experimental conditions. The difference in productivity among previously discussed *Xanthomonas* strains is probably due the fact that different *Xanthomonas* species possess different metabolic pathways and cycles [12].

Conclusions

The results of this study have confirmed that reference strain *X. campestris* ATCC 13951, as well as *Xanthomonas* strains isolated from crucifers and pepper leaves have the ability to produce xanthan on medium containing crude glycerol from the biodiesel industry of the Republic of Serbia. This is very important from economic aspect considering that crude glycerol can substitute commonly used carbon sources in cultivation media for xanthan and reduce the costs of cultivation media preparation which leads to the reduction in the total production costs. Results of this study have also a great importance from an ecological aspect, since the biotechnological production of xanthan on crude glycerol-based media represents a promising solution for valorisation of this effluent. Results obtained in this study represent valuable information that can be used in further investigation related to development of biotechnological production of xanthan on crude glycerol-based media.

Acknowledgments

This study is part of the projects (451-03-47/2023-01/200134 and 337-00-110/2023-05/25) which are supported by the Ministry of Science, Technological Development and Innovation of the Republic of Serbia.

References

[1] I. Rottava, G. Batesini, M. Fernandes Silva, L. Lerin, D. de Oliveira, F. Ferreira Padilha, G. Toniazzo, A. Mossi, R.L. Cansian, M. Di Luccio, H.Treichel, Carbohydr. Polym. 77 (2009) 65–71.
[2] A.S. Demirci, I. Palabiyik, D. Apaydın, M. Mirik, T. Gumus, LWT - Food Sci. Technol. 101 (2019) 40–47.
[3] S. Kalia, A.R. Choudhary, Int. J. Biol. Macromol. 137(2019) 475–482.
[4] T. Riaz, M.W. Iqbal, B. Jiang, J. Chen, Int. J. Biol. Macromol. 186 (2021) 472–489.
[5] T. Khan, J. Park, J. Kwon, Korean J. Chem. Eng. 24 (2007) 816-826.
[6] A. Dzionek, D. Wojcieszyńska, U. Guzik, Bioresour. Technol. 351 (2022) 126918.
[7] L.V. Brandão, D.J. Assis, J.A. López, M.C.A. Espiridião, E.M. Echevarria, J.I. Druzian, Braz. J. Chem. Eng. 20 (2013) 737-746.
[8] Z. Wang, J. Wu, L. Zhu, X. Zhan, Bioresour Technol. 211 (2016) 390-397.
[9] J.A. da Silva, L.G. Cardoso, D. de Jesus Assis, G.V. Gomes, M.B. Oliveira, C.O. de Souza, J.I. Druzian, Appl. Biochem. Biotechnol. 186 (2018) 750-763.
[10] D. de Jesus Assis, L.V. Brandão, C.L.A. de Sousa, T.V.B. Figueiredo, L.S. Sousa, F.F. Padilha, J.I. Druzian, Biotechnol. Appl. Biochem. 172 (2014) 2769-2785.
[11] Z. Rončević, B. Bajić, J. Grahovac, S. Dodić, J. Dodić, Acta Period. Technol. 45 (2014) 234-246.
[12] I. Zahović, J. Dodić, S. Markov, J. Grahovac, M. Grahovac, Z. Trivunović, Rom. Biotechnol. Lett. 26 (2021) 2800-2807.

QSAR ANALYSIS OF TOXICITY FOR A SERIES OF AROMATIC COMPOUNDS

Marina Alexandra Tudoran, Zoltan Szabadai

National Institute of R&D for Electrochemistry and Condensed Matter - INCEMC,
144 Aurel Păunescu-Podeanu, RO-300569, Timişoara, Romania
e-mail: r_alliy@yahoo.com

Abstract

Aromatic compounds are particularly interesting to scientists due to environmental and human health concerns. QSAR models are increasingly used to investigate the relationship between the toxicity of a pollutant and its structural properties, on the assumption that pollutants similar in structure and physicochemical properties are likely to be similar in toxicity. Based on the above mentioned, this paper investigates the relationship between electron affinity, ionization potential, and the toxicity of some aromatic compounds. Correlation and linear regression are used as QSAR analysis methods.

Introduction

Polycyclic aromatic hydrocarbons (PAHs) are aromatic compounds consisting of carbon and hydrogen atoms, highly stable, hydrophobic and lipophilic, characterised by their property of bioaccumulating, and considered harmful pollutants for the environment. Depending on the number of aromatic rings, PAHs are classified into two groups: low molecular weight compounds with less than four aromatic rings, and high molecular weight compounds with four or more aromatic rings. Studies have shown that polycyclic aromatic hydrocarbons have different environmental impacts depending on their molecular weight. Thus, while low molecular weight molecules are volatilised or easily decomposed in the environment, high molecular weight molecules with a large number of benzene rings are more chemically stable, exhibit high toxicity and persistence in the environment, thus remaining in soil, sediment, and water for a longer period of time [1-3].

The number and orientation of the benzene rings also affect the physical and chemical properties of PAH molecules, which in turn affect their mobility and distribution between different environmental compartments. Acute toxicity, which increases with increasing molecular size (up to 4-5 benzene rings), has also been shown to be influenced by molecular structure [2, 4, 5]. Predicting the toxicity of chemical compounds, however, remains a major challenge for the scientific community. Defined as the extent to which a chemical compound (or mixture) can harm, injure or kill a living organism, toxicity can be estimated using a range of sophisticated in vitro or in vivo experimental techniques. Because these techniques are expensive, time-consuming and raise ethical concerns (by using of animals or animal tissues), researchers have developed in silico (computer-based) methods to address these issues. One of the most widely used in silico methods is the quantitative structure-activity/property relationship (QSAR/QSPR) method, which is based on the assumption that chemical molecules that are similar in structure will have similar activities and properties. Thus, based on the relationship between chemical structures and activities/properties of known compounds, models can be constructed to predict the activities/properties of unknown (but structurally similar) chemicals using multivariate statistical techniques [6].

Starting from these considerations, this current work is intended to presents the relationship between LC_{50} (data from literature), electron affinity and ionization potential respectively (computationally calculated) for a series of aromatic compounds using QSAR analysis. The obtained results show that the toxicity of benzene and linear PAHs is different from the toxicity of angular and clustered PAHs.

Experimental

The molecules from the working set were generated by HyperChem 8.0.10 software [7] and pre-optimized using the MM+ force field. Then, using Gaussian View 6.0.16 and Gaussian 3.0 (DFT 3-21G, B3LYP method), we generate the optimized structures and calculate the energy. The electron affinity (*EA*), considered as the energy difference resulted by an electron addition to a neutral molecule, was calculated with the formula: $EA = \left(E_{Neutral} - E_{Anion}\right)$, with $E_{Neutral}$ – the energy of neutral form, and E_{Anion} – the energy of anion. The ionization potential (*IP*), considered as the energy necessary for an electron removal from a neutral molecule, was calculated with the formula: $IP = \left(E_{Cation} - E_{Neutral}\right)$, with E_{Cation} – the energy of cation [8]. The distribution type of the data was determined using Kolmogorov-Smirnov Test. The association between LC_{50} (*Daphnia magna*) – as dependent variable, and the ionization potential and electron affinity – as independent variables, was assessed using Pearson correlation (*2-tailed*). Linear regression was computed in order to determine the line of the best fit for the data. All statistical calculations were performed using Origin 9 program.

Results and discussion

The optimized structures of the aromatic compounds are presented in Figure 1. The physical-chemical parameters computed using Gaussian program and the LC_{50} computed with ADMETlab 2.0 [9] are given in Table 1. For all of the parameters in study the Kolmogorov-Smirnov test returned $p > 0.05$ (0.39477 for electron affinity, 0.71116 for ionization potential, and 0.13844 for LC_{50}), meaning that the data is normally distributed.

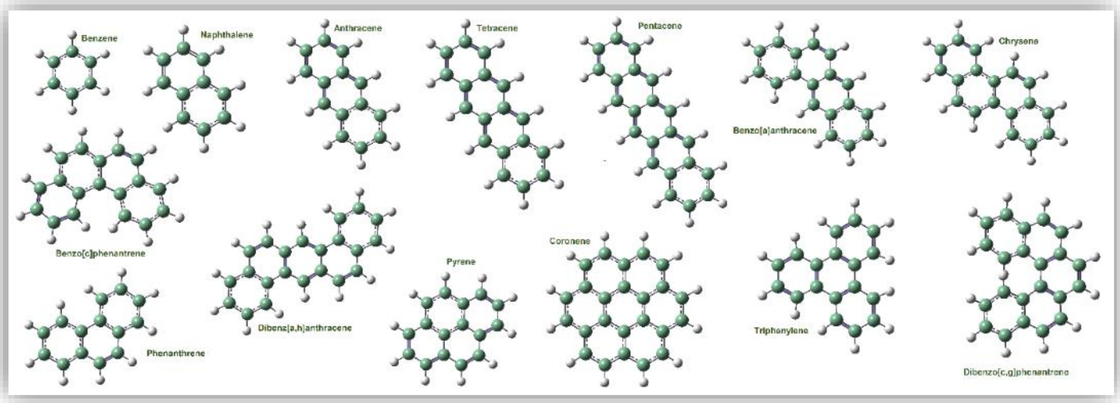

Figure 1. Optimized structures of neutral form of the molecules in study (ball-and-stick model)

According to the Pearson correlation results, there was a significant correlation in positive direction between LC_{50} and electron affinity ($r = 0.782$, $p < 0.01$), and a significant correlation in negative direction between LC_{50} and ionization potential ($r = -0.779$, $p < 0.01$).

Table 1. Values of electron affinity, ionization potential, and LC_{50} for the molecules in study

NAME	**EA (A.U.)**	**IP (A.U.)**	**LC_{50} (*Daphia magna*)**

Benzene	-0.078	0.335	3.378
Naphthalene	-0.029	0.285	4.597
Anthracene	0.003	0.253	5.256
Tetracene	0.026	0.232	5.688
Pentacene	0.042	0.217	6.085
Phenanthrene	-0.017	0.272	5.742
Benzo[c]phenanthrene	-0.001	0.264	6.060
Dibenzo[c,g]phenantrene	-0.001	0.259	6.465
Benzo[a]anthracene	0.008	0.250	5.945
Coronene	0.009	0.253	6.092
Pyrene	-0.003	0.258	5.924
Chrysene	-0.001	0.258	6.060
Triphenylene	-0.024	0.279	5.890
Dibenz[a,h]anthracene	0.009	0.248	6.151

The relationship between electron affinity and LC_{50} of aromatic molecules is described by equation (1), and plotted in Figure 2a.

$$\boldsymbol{MODEL\ 1}: LC_{50} = 5.75719 + 22.23965 \times \mathrm{EA} \quad (1)$$

In Figure 2a, two areas of distribution of molecules in the working set can be seen. Benzene and PAHs molecules with linear structure follow a linear distribution, while PAHs molecules with angular and clustered structure follow a growth/sigmoidal (MichaelisMenten) type distribution.

Table 2. Summary of simple linear regression with LC_{50} (*Daphnia magna*) as dependent variable and electron affinity (***MODEL 1***) and ionization potential (***MODEL 2***) respectively as independent variables (N = 14).

	Intercept		**Slope**		**Statistics**
	Value	*SE*	*Value*	*SE*	*Adj.* R^2
MODEL 1	5.75719	0.14002	22.23965	5.11828	0.57902
MODEL 2	11.61867	1.39023	-22.74868	5.28673	0.57399

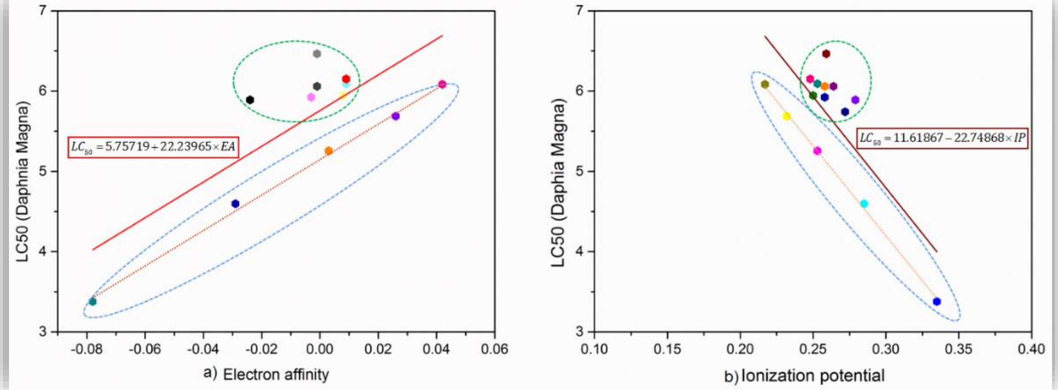

Figure 2. LC_{50} values of the studied polycyclic aromatic hydrocarbons as a function of a) electron affinity (***MODEL 1***) and b) ionization potential (***MODEL 2***).

The relationship between electron affinity and LC_{50} of aromatic molecules is described by equation (2), and plotted in Figure 2b.

$$\boldsymbol{MODEL\ 2}: LC_{50} = 11.61867 - 22.74868 \times \mathrm{IP} \quad (2)$$

In Figure 2b, the two areas of distribution are maintained as in privous case. Thus, benzene and PAHs molecules with linear structure follow a linear distribution, while PAHs molecules with angular and clustered structure follow a distribution described by the ratio of two polynomial functions (Rational0).

Conclusion

Linear regression was employed to produce the best-fit line through which the electron affinity and ionization potential of a series of PAHs molecules could be related to their LC_{50} values. For the associated regression lines, close values of the Adj.-R^2 coefficient were obtained (0.57902 for electronic affinity and 0.57399 for ionization potential, respectively), implying that the toxicity of an unknown aromatic compound with similar structure as the working set can be predicted with about 60% accuracy if either electronic affinity or ionization potential values are known. In addition, it was found that, in the case of the studied set, the association between toxicity and electron affinity and the ionization potential is strongly influenced by the way the benzene nuclei are arranged in molecules. Thus, in terms of the manifestation of toxicity in relation to the studied parameters, in case of molecules with angular and clustered structure, other variables play a role which in case of linear molecules either play no role or have a constant value.

References

[1] H. Ha, K. Park, G. Kang, S. Lee, Ecotoxicology 28 (2019) 333.
[2] H.I. Eldos, N. Zouari, S. Saeed, M.A. Al-Ghouti,Arab. J. Chem. 15(7) (2022) 103918.
[3] M. Honda, N. Suzuki, IJERPH 17(4) (2020) 1363.
[4] A. Alalaiwe, Y.K. Lin, C.H. Lin, P.W. Wang, J.Y. Lin, J.Y. Fang, Chemosphere 255 (2020) 126955.
[5] M.J. Munoz, J.V. Tarazona, Bull. Environ. Contam. Toxicol. 50 (1993) 363.
[6] A. Karim, V. Riahi, A. Mishra, M.H. Newton, A. Dehzangi, T. Balle, A. Sattar, Acs Omega, 6(18), (2021) 12306.
[7] HyperChem™ Professional, Hypercube, Inc., 1115 NW 4th Street, Gainesville, Florida 32601, USA.
[8] J.B. Foresman, Æ. Frisch, Exploring Chemistry With Electronic Structure Methods: A Guide to Using Gaussian 2nd Edition, Gaussian, Pittsburg, 1996, pp. 142-143.
[9] https://admetmesh.scbdd.com/service/evaluation/cal

HYDROTHERMAL SYNTHESIS OF AgNW@TiO$_2$ CORE SHELL FOR *PLASMON-INDUCED* CHARGE SEPARATION

Daniel Ursu[1*], Radu Banica[1], Cristina Mosoarca[1]

National Institute of Research and Development for Electrochemistry and Condensed Matter,
Dr. A.P. Podeanu street, No. 144, 300569, Timisoara, Romania
**e-mail:danielhoratiu@yahoo.com*

Abstract

AgNW@TiO$_2$ core shell architecture was synthesized by a facial hydrothermal method. The features of the sample were characterized by XRD, SEM, and UV-VIS-NIR. The hydrothermal synthesis was performed between 100 - 200°C using different concentration of Titanium butoxide (TBT)/ethanol as precursor.

From the X-ray diffraction spectra, one can see the corresponding diffraction maxima for Ag (01-087-0718) at the position $2\theta = 38.201$, 44.401 and 64.601; AgCl (00-006-0480) at position $2\theta = 27.831$, 32.244, 46.234, 54.830, 57.480 as well as for TiO$_2$ anatase (01-071-1169) at position $2\theta = 25.156$ and 47.782.

Figure 1a shows the SEM images of the AgNW@TiO$_2$ compound obtained by the hydrothermal method at different synthesis temperatures using an autoclave time of 12h. The average thickness of the nanowires is approximately 80 nm. It can be seen that the deposition of TiO$_2$ on the AgNWs surface is uniform. It can also be observed that in addition to the silver nanowires there is also a surplus of TiO$_2$ nanoparticles. Thus for the AgNW_3 experiment which is obtained at a temperature of 200°C, the silver nanowires are completely embedded in TiO$_2$ nanoparticles. Thus it can be said that the synthesis temperature affects the surface of the structures by detaching the semiconductor from their surface.

With the increase of the autoclaving temperature, it can be observed that the silver nanowires are embedded in TiO$_2$ and the fine structure of absorption maxima characteristic of AgNWs are observed very little. The plasmonic absorption characteristic of Ag reach the value of 350 nm and 380 nm. The absorption for TiO$_2$ is at the value of 265 nm (figure 1b).

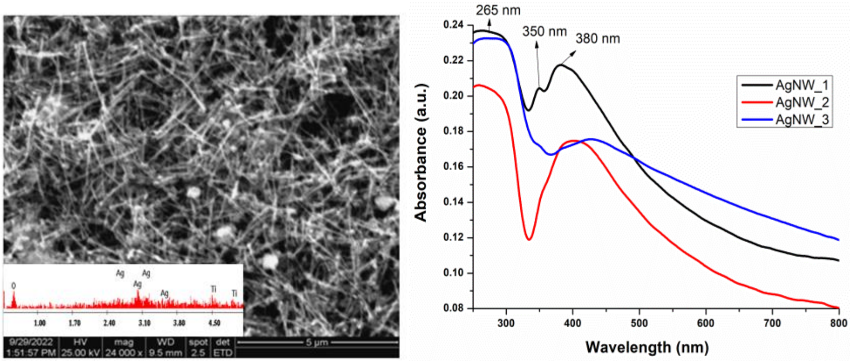

Fig.1 a) SEM images and b) absorbance spectra of AgNW@TiO$_2$ compound

Acknowledgements

This work was supported by a grant of the Ministry of Research, Innovation and Digitization, CCCDI-UEFISCDI, project number PN-III-P2-2.1-PED-2021-2541, within PNCDI II.

PHOTOCATALYTIC ACTIVITY INDUCED BY ZINC PHTHALOCYANINE SYNTHESIZED BY MICROWAVE IRRADIATION

Bojana Vasiljević, Jovana Prekodravac, Dragana Marinković

University of Belgrade, Vinča Institute of Nuclear Sciences, National Institute of the Republic of Serbia, University of Belgrade, P. O. Box 522, 11001 Belgrade, Serbia
e-mail: bojana.vasiljevic@vin.bg.ac.rs

Abstract

Zinc phthalocyanine, synthesized under microwave irradiation proved to be an interesting photocatalyst. The degradation of Rose Bengal, as model organic dye, under visible light irradiation was used to study the adsorption/photocatalytic activity. The huge potential of the synthesized molecule for the removal of organic pollutants was demonstrated by its absorption capacity, which was far larger than that of dye degradation.

Introduction

Many manufacturing industries across the world directly discharge their wastes into freshwater bodies utilized for drinking and agricultural purposes. The most common contaminants that could be found are synthetic colors, and dye chemicals used to color various substances and materials. These are persistent and stable environmental pollutants waiting for unconventional wastewater treatment methods. To immediately address these challenges, the development of more efficient and low-cost protocols and photocatalysts is required.

Photocatalysis is an effective technique for the degradation and mineralization of hazardous pollutants from the environment. In that context, a variety of photocatalysts have been studied. Zinc phthalocyanine (ZnPc), a symmetrical 18π-electron aromatic macrocycle has won considerable research interest and enjoys applications in fields of non-linear optics, chemical sensors, semiconductors, and catalysts[1]. However, there hasn't been as much focus on developing advanced synthetic techniques and photocatalytic testing for this kind of molecule. In this work, we present a detailed study of the photocatalytic activity of ZnPc synthesized under microwave irradiation. The macrocyclic compound was obtained in high yield and purity after only a few minutes of heating.

Experimental

All chemicals: zinc (II) acetate dehydrate (>99%, Sigma-Aldrich), 1,2-dicyanobenzene (≥98%, Sigma-Aldrich), *N*, *N*-dimethylformamide (>99%, Alfa Aesar), dimethyl sulfoxide (>99%, Fisher Chemicals), and methanol (≥ 99%, Sigma Aldrich) were of the highest purity commercially available and were used without further purification. Mili-Q deionized water (electrical resistivity = 18.2 MΩ cm^{-1}) was used.

ZnPc was synthesized in a microwave reactor (noted as $ZnPc_{MW}$) as described in our previous work[2]. The starting compounds 1,2-dicyanobenzene (2.5 mmol, 0.320 g), zinc (II) acetate dihydrate (0.63 mmol, 0.138 g), and 1 mL of DMF were heated at 250 °C for 5 minutes in microwave reactor. After cooling to room temperature precipitate was filtered off and washed with 3% HCl, water, methanol, and dried. The resulting deep purple crystals remain after the processing of the reaction mixture. The yield of $ZnPc_{MW}$ is 68 %.

Photocatalytic testing was performed in the presence of a $ZnPc_{MW}$ photocatalyst in concentration of 0.5 mg/ml and RB organic dye (0.03 mM). The reaction was performed in the cylindrically shaped closed homemade photoreactor with six LEDs operating at 370 nm. For the experiments of photolysis and photocatalysis, samples were kept in dark conditions for 60 minutes in order to establish the adsorption/desorption equilibrium followed by irradiation for 240 minutes.

Microwave-assisted synthesis was performed in a mono-mode microwave reactor Anton Paar Monowave 300. Attenuated total reflectance Fourier transform infrared (ATR-FTIR) spectroscopic measurements were performed in 400–4000 cm^{-1} range with a spectral resolution of 4 cm^{-1} at room temperature by Thermo Scientific Nicolet iS50 FT-IR spectrometer equipped with built-in all reflective ATR diamond. The ultraviolet-visible (UV/Vis) absorption spectra were recorded on Shimadzu 1800 UV–Vis spectrophotometer equipped with a temperature controller in the range of 200–800 nm.

Results and discussion

The development of robust and cheap photocatalysts for visible-light-induced organic substrate transformations is a significant uprising research topic at the crossroads of green chemistry and modern synthetic methodology. A microwave-enhanced synthetic route has been evaluated as a fast and efficient method for obtaining $ZnPc_{MW}$ after only five minutes of heating, at 250 °C, compare to six hours for traditional methods[2] (Figure 1a).

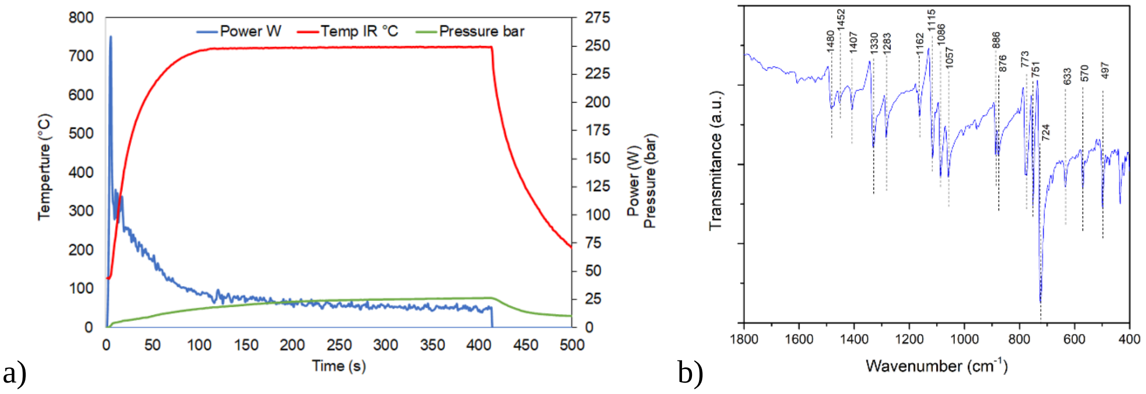

a)

b)

Figure 1. Microwave heating profile for $ZnPc_{MW}$ synthesis, and FTIR spectra of synthesized crystals.

The FT-IR spectral measurement is carried out to ascertain the functional group structures for $ZnPc_{MW}$. The absorption peaks at 480 cm^{-1}, 1452 cm^{-1}, 1330 cm^{-1}, 1162 cm^{-1}, 1115 cm^{-1}, and 886 cm^{-1} were assigned to Pc skeletal vibration (Figure 1b). The peaks located at 1407 and 1283 cm^{-1} are assigned to the stretching vibration of the aromatic phenyl ring and C–N= covalent bond, respectively. Absorption peaks observed around 1086 cm^{-1} and 1057 cm^{-1} were assigned to C–H in-plane bending vibrations. The peaks observed at 773 cm^{-1} and 724 cm^{-1} were assigned to C–H out-of-plane bending vibrations. The bands at 751 cm^{-1}, 633 cm^{-1}, 570 cm^{-1}, and 497 cm^{-1} also belong to in-plane skeletal deformation vibrations of the isoindole fragments. The absence of metal-free Pcs characteristic absorption peak around 1000 cm^{-1} confirmed the reaction selectivity and purity of the synthesized compound.

The photocatalytic reaction of Rose Bengal (0.03 mM) removal in water media under UV (370 nm) light was performed in the presence of $ZnPc_{MW}$ as photocatalyst. Reaction was carried out at pH5 (Figure 2). After 60 min of adsorption/desorption the $ZnPc_{MW}$ showed strong adsorption capacity towards RB dye with 96% of the dye adsorbed after 60 min in dark.

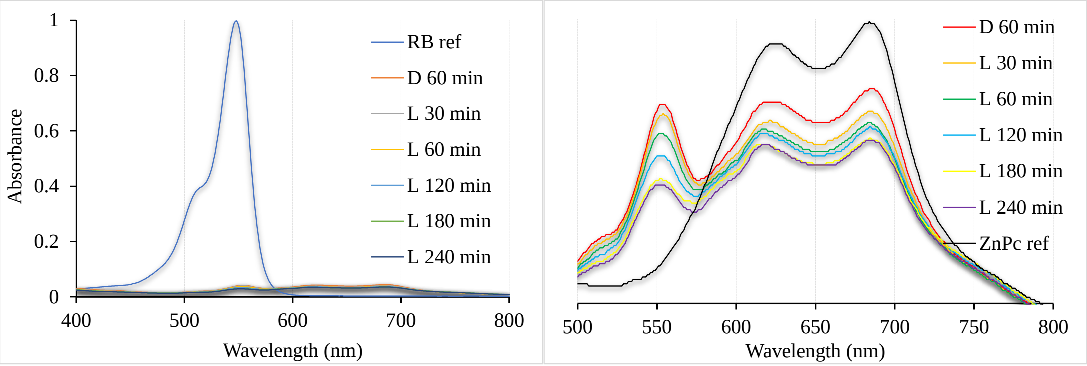

Figure 2. a) The absorbance spectra of RB degradation in the presence of ZnPc photocatalyst, and b) RB absorbance and ZnPc peak in time under UV light irradiation.

In terms of the photocatalyst removal efficiency towards RB organic dye, under 240 min of exposure to the UV light, 97% of the RB dye was successfully removed from water media (Figure 3). Obtained results suggested strong capacity of ZnPc as adsorbents for toxic organic dyes.

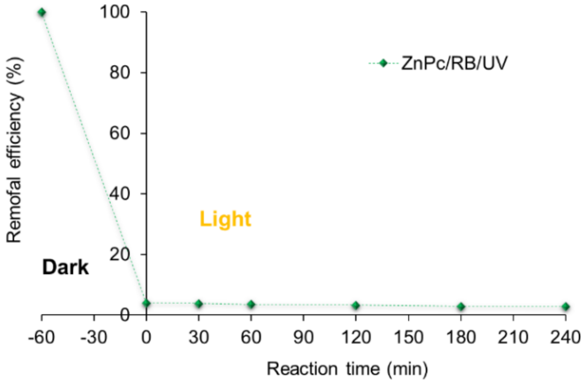

Figure 3. RB removal efficiency in the presence of $ZnPc_{MW}$.

Conclusion

Significant rate enhancements, purity and stability of macrocyclic compound of $ZnPc_{MW}$ lead to valuable and efficient photocatalyst. Photocatalytic testing revealed a strong potential for the ZnPc photocatalyst application as an adsorbent for RB in a water medium. Dye removal is followed by its high percent of final degradation.

Acknowledgements

The research was funded by the Ministry of Science, Technological Development and Innovation of the Republic of Serbia (grant number 451-03-47/2023-01/200017).

References

[1] R.R. Cranston, B.H. Lessard, RSC Adv. 35 (2021) 21716.
[2] B. Vasiljević, D. Milivojević, T. Barudžija, M. Budimir, D. Mijin, M. Marinović-Cincović, D. Marinković, Mater. Lett. 350 (2023) 134911.

CORROSION INHIBITION OF STAINLESS AND CARBON STEELS BY QUERCETIN IN ALCOHOLIC SOLUTIONS

Cristian-George Vaszilcsin[1], **Mihai V. Putz**[1], **Mircea L. Dan**[2], **George D. Dima**[1,2]

[1]National Institute of Research and Development for Electrochemistry and Condensed Matter, Dr. A. P. Podeanu 144, 300569, Timişoara, Romania
[2]University Politehnica Timişoara, 300006, Piaţa Victoriei 2, Timisoara, Romania
e-mail: cristi_vasz@yahoo.com

Abstract

Quercetin (QUE) is a flavone derivative, its rational name being 3,5,7-trihydroxy-2-(3,4-dihydroxy-phenyl)-4-chromenone. In pure state, it is a yellow solid, slightly soluble in water, but soluble in alcohol and alkaline solutions [1,2]. It is found in many plants such as citrus fruits, apples, onions, parsley, sage, tea and red grapes [1]. QUE has inhibitory potential due to the presence of oxygen heteroatoms in the molecule, as well as a number of 8 pairs of π electrons. The molecular parameters relevant to the inhibitory properties of QUE were determined by Zhixiong Xu et al. [3].

In this paper, the results obtained by the potentiodynamic polarization (PDP) method in the study of the inhibitory efficiency of QUE for stainless steel AISI 304L and carbon steel OLC 45 in 12% aqueous alcoholic solution are presented (table 1). The authors have took into account the fact that the mentioned metals are used in the food industry where they come into contact with such solutions.

Table 1. Electrochemical parameters and inhibitory efficiency η_{inh} obtained by PDP.

QUE conc. [mol L^{-1}]	304L			OLC 45		
	E_{corr} [mV]	i_{cor} [μA cm^{-2}]	η_{inh} [%]	E_{corr} [mV]	i_{cor} [μA cm^{-2}]	η_{inh} [%]
SB	-151	0.271	-	-676	15.9	-
10^{-6}	-144	0.226	16.6	-670	13.0	18,2
10^{-5}	-134	0.186	31,4	-665	11.1	30.2
10^{-4}	-106	0.153	43.5	-660	7.86	50.6
10^{-3}	-75.7	0.106	60.9	-656	5,25	67.0

The results obtained by PDP have been validated by electrochemical impedance spectroscopy. The nature of the metal - QUE interactions was evaluated based on the values of the Gibbs energy of adsorption ΔG^{o}_{ads}, determined using the adsorption constants K_{ads} assessed from the adsorption isotherms. The obtained results near -40 kJ mol^{-1} demonstrate the strength of the metal - inhibitor interactions, which are chemical in nature.

References

[1] Priyanka Singh, Yamshi Arif, Andrzej Bajguz, Shamsul Hayat, *Plant Physiology and Biochemistry*, 166 (2021) 10–19.
[2] M. H. Abraham, W. E. Acree Jr., *Journal of Molecular Liquids*, 197 (2014) 157–159.
[3] Zhixiong Xu, Bochuan Tan, Jida Chen, Jie Liu, Xingwen Zheng, Lei Guo, Fan Zhang, Nabil Al-Zaqri, Ruilai Zhang, Wenpo Li, *Journal of the Taiwan Institute of Chemical Engineers*, 150 (2023) 105044.

MEDICINAL PLANTS – IMPORTANT SOURCE OF ESSENTIAL MICROELEMENTS

Ariana-Bianca Velciov[1], Antoanela Cozma[2], Andreea Adriana Petcov[3], Georgeta-Sofia Popescu[1], Daniela Stoin[1], Iasmina-Madalina Anghel[4], Adrian Riviș[1], Nicoleta Gabriela Hădărugă[1], Maria Rada[5*]

[1] University of Life Sciences "King Michael I" Timisoara, Faculty of Food Engineering, Food Science Department, Calea Aradului, 300645, Timisoara, Romania
[2] University of Life Sciences "King Michael I" Timisoara, Faculty of Agriculture, Department of Soil Sciences, Calea Aradului, 300645, Timisoara, Romania
[3] University of Life Sciences "King Michael I" Timisoara, Faculty of Engineering and Applied Technologies, Department of Soil Sciences, Calea Aradului, 300645, Timisoara, Romania
[4] Politehnica University of Timişoara, Materials and Manufacturing Engineering Department, 300222, Timişoara, Romania
5University of Medicine and Pharmacy "Victor Babes", 2 EftimieMurgu Sq., 300041, Timisoara, Romania
e-mail: radamariam@gmail.com

Abstract

The purpose of this paper was to evaluate the concentration of some essential microelements (Fe, Mn, Zn and Cu) from the leaves of two plants: stinging nettle (*Urtica dioica*) and sage (*Salvia officinalis*), species of plants with multiple uses in the food and medical field due to their high content of compounds with beneficial action for organisms. Samples were obtained by washing, drying and calcination of fresh leaves. The results obtained by atomic absorption spectrometry regarding Mn, Fe, Zn and Cu concentration in sage and nettle leaves shows that the samples contains important amounts of essential microelements, Cu (1.72-1.87 μg/g), Fe (25.43-65.67 μg/g), Mn (7.86 – 9.30 μg/g), Zn (54.61 – 73.12 μg/g). The appreciable contents of essential microelements recommend the use of these plants as a supplementary source of essential elements.

Keywords: *essential microelements, sage, nettle, medicinal plants*

Introduction

Medicinal plants are known through the prism of their double status – foods and medicine [1]. The beneficial effects of medicinal plants are due to the large number and diversity of active biological compounds present in their composition: alkaloids, tannins, oils, vitamins, mineral elements, that makes possible the use for different therapeutic purposes – prevention and healing of numerous health conditions as herbal teas [2,3].

The levels of essential microelements in medicinal plants can be influenced by soil and climate conditions and by the plants' ability of assimilating these elements [4].

Stinging nettle (*Urtica dioica*), is a perennial plant whose leaves are a relatively good source of caloric energy, protein, fiber, and an array of health-promoting bioactive compounds which include vitamins A, C, and K, fatty acids (α-linoleic and linoleic acid), minerals (Fe, Mn, K, and Ca) and carotenoids [5]. Nettle leaves are rich in proteins, fats, carbohydrates, vitamins, minerals and trace elements [6].

Sage (*Salvia officinalis*) is a plant well known due to its important healing and flavoring properties. From sage leaves numerous active principles were identified: constituents of the essential oil, diterpenes, phenolic acids, flavonoids and tannins [7].

The purpose of this experiment was to analyze nettle (Urtica dioica) and sage (Salvia officinalis) leaves grown spontaneously in gardens and to evaluate the concentration of some essential microelements from their leaves, based on the fact that they can be used as a supplementary (alternative) source of essential elements.

Materials and methods

Plant material.

For samples we used nettle (Urtica dioica) and sage (Salvia officinalis) leaves, grown spontaneously in gardens, cultivated alongside fruits and vegetables. They were cleaned and washed under running tap water to remove mechanical impurities, after which they were left to dry at room temperature, until the crispy texture was observed. Until the analysis, samples were placed in brown glass vials and kept cold.

Determination of mineral elements.

The essential mineral element in sage and nettle leaves were carried out according to the method recommended and used by Velciov et al. (2015) when a similar product was analyzing [8]. The determination consists in the calcination of the leaves sample at 550°C, followed by the solubilization of the ash in HNO_3 0.5 N and the measurement of mineral element concentrations using the FS Varian 280 Spectrometer.

Results and discussions

The results obtained from the analysis, regarding Mn, Fe, Zn and Cu concentration in sage and nettle leaves shows that the samples contains important amounts of essential microelements (figure 1).

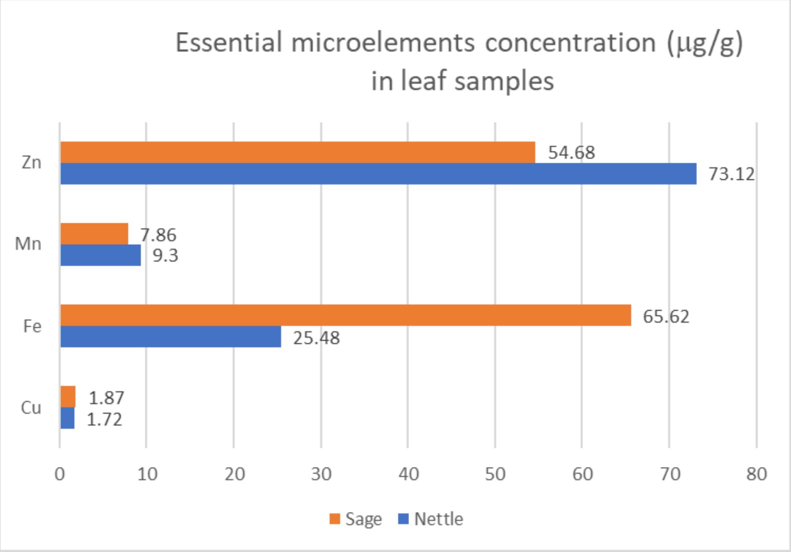

Figure 1. Distribution of Fe, Mn, Zn and Cu in sage and nettle leaf samples

The distribution of bioelements analyzed in sage and nettle leaves is uneven, depending on the plant from which they come (nettle or sage) and the analyzed bioelement: 1.72 µg/g Cu, 25.48 µg/g Fe, 9.3 µg/g Mn, 73.12 µg/g Zn - in nettle leaves and 1.87 µg/g Cu, 65.62 µg/g Fe, 7.86 µg/g Mn, 54.68 µg/g Zn - in sage leaves.

From all the analyzed elements, zinc and iron are the best represented. Compared to these, manganese and copper were determined in lower concentrations. Comparing the mineral concentrations of the two medicinal plants leaf, it can be seen that the both have an important content of essential microelements.

Conclusion

The nutritional and therapeutic qualities of nettle (*Urtica dioica*) and sage leaves (*Salvia officinalis*), two of the well-known medicinal plants, are influenced by their content of essential microelements.

The concentrations of microelements in the two analyzed medicinal plants follow the same decreasing trend Zn> Fe> Mn> Cu. Zinc is the most abundant trace element, followed by iron, smaller amounts of Mn and much smaller Cu amounts.

Comparing the concentrations of microelements in the analyzed medicinal plants, it is observed that, compared to the sage leaves, nettle leaves are richer in Zn and Mn, and sage leaves are richer in Fe. Copper show similar values in both plants.

The appreciable contents of essential microelements recommend the use of these plants for the preparation of teas or other products with therapeutic effects, but also as an additional supply of microelements.

Acknowledgements

The present paper was funded by the Research Project “Research on the use of biologically active substances in order to obtain high-nutrition foods", No 1545/28.02.2019.

References

[1] Akinyemi O., Oyewole S.O., Jimoh K.A., Medicinal plants and sustainable human health: a review, Horticult Int J., **2018**, 2(4), 194-195.

[2] Gogoasa I., Jurca .V, Alda L.M., Velciov A., Rada M., Alda S., Sirbulescu C., Bordean D.M. and Gergen I., *Journal of Horticulture, Forestry and Biotechnology*, **2013**, 17(4), 65- 67;

[3] Paciana I., Butnariu M., Highlighting the compounds with pharmacological activity from some medicinal plants from the area of Romania**,** *Med Aromat Plants (Los Angeles)*, **2021**, 10(1), 370;

[4] Mehri A. and R.F. Marjan, Trace elements in human nutrition: A Review, *Int. j. Med. invest.*, **2013**, 2(3), 115-128.

[5] Bauman, H, Perez, J. Food as medicine: Stinging nettle *(Urtica dioica, Urticaceae*), Herbal Egram, 2018, 15(7).

[6] Bhusal, K.K., Magar, S.K., Thapa, R., Lamsal, A., Bhandari, S., Maharjan, R., Shrestha, S., Shrestha, J. (**2022**), *Nutritional and pharmacological importance of stinging nettle (Urtica dioica L.): A review*, Heliyon 8. e09717. https://doi.org/10.1016/j.heliyon.2022.e09717]

[7] Aradski, A.Z.A., Oalde, M.M., Duletić-Laušević, S.N. Salvia officinalis: Traditional medicinal plant with novel therapeutical perspectives, *Salvia officinalis: Production, Cultivation and Uses*, (2021) pp. 1-72, https://novapublishers.com/shop/salvia-officinalis-production-cultivation-and-uses/ ISBN: 978-153619647-4; 978-153619531-6

[8] Velciov, A., Popescu, S., Riviş, A., David, I., Gogoaşă, I.. The evaluation of some bioelements in different types of herbal teas and their infusions, pp. 863-870, 15th International Multidisciplinary Scientific Geoconference, Ecology and Environmental Protection Section, vol I, Albena, Bulgaria, 2015, ISBN 978-619-7105-39-1, ISSN 1314-2704, DOI: 10.5593/sgem2015B51.

THE EFFECT OF PEROXYMONO- AND PEROXYDISULFATE IONS ON THE PHOTOCATALYTIC EFFICIENCY OF ZNO

Bence Veres, Benjámin Vas, Tünde Alapi

Department of Molecular and Analytical Chemistry, University of Szeged, H-6720 Szeged,
Dóm tér 7, Hungary
e-mail: veres0629@gmail.com

One of the urgent problems in water treatment is the effective removal of non-biodegradable and biologically active trace pollutants. The application of advanced oxidation processes (AOP) as an additive method is suitable for the effective removal of most organic pollutants from biologically treated wastewater. One of the promising AOPs is heterogeneous photocatalysis, based on the excitation of a semiconductor photocatalyst. The photogenerated charges (hole (h^+_{vb}) and electron (e^-_{cb})) can initiate oxidation and reduction of various materials on the surface. The oxidation of organic pollutants requires an effective e^-_{cb} capture to hinder the fast recombination of photogenerated charges. During complex, multi-step processes, radicals are formed, which contribute to the transformation and mineralization of organic materials. The combination of heterogeneous photocatalysis with an oxidizing agent, such as H_2O_2, and persulfate ions (peroxymonosulfate (HSO_5^-, PMS) and peroxydisulfate ($S_2O_4^{2-}$, PDS)) can result in enhanced efficiency due to the formation $^{\bullet}OH$ and $SO_4^{\bullet-}$.

In this work, we studied the ZnO/PMS, and ZnO/PDS systems and compared them to the ZnO/H_2O_2 process. Suspensions were irradiated with LEDs having an emission maximum of 365 nm. Trimethoprim (TRIM) antibiotic, hydroquinone (HQ), and nitrobenzene (NB) were used as target substances to test the efficiency and investigate the contribution of various radicals to the transformation. Both PMS and PDS greatly increased the photocatalytic efficiency of ZnO. In the presence of PMS and PDS, dissolved oxygen was not required for the degradation of the organic substances, proving the excellent electron acceptance properties of persulfate ions. The effect of radical scavengers proved that besides $SO_4^{\bullet-}$, the $^{\bullet}OH$ formation was also enhanced, and its contribution to the transformation was significant. The photocatalytic activity of ZnO did not change during 3 consecutive cycles, even in the presence of persulfate ions.

The effect of biologically treated communal wastewater (BTWW) as a matrix, containing large amounts of Cl^- (3.4×10^{-3} M) and HCO_3^- (8.6×10^{-3} M) was also studied. Inorganic ions can heavily influence the surface properties of the photocatalyst, and processes that occur on the surface. Moreover, they react with $^{\bullet}OH$ and $SO_4^{\bullet-}$ and change the radical set. Their effects on the transformation rate of TRIM and PDS were studied. The co-presence of the organic substances, inorganic ions, and dissolved oxygen results in a competition that occurs between various substances for adsorption sites and photogenerated charge carriers. Besides radical scavenging processes, this is also responsible for the change in the radical set and, in this way, the photocatalytic efficiency.

Acknowledgments

This work was sponsored by the National Research, Development, and Innovation Office-NKFI Fund OTKA, project number FK132742. Bence Veres was supported by the ÚNKP-23-3-SZTE-534 New National Excellence Program of the Ministry for Culture and Innovation from the source of the National Research, Development, and Innovation Fund.

EFFECT OF SYNTHESIS CONDITIONS ON THE PROPERTIES OF MAGNETIC NANOFLOWERS

Viktória Hornok[1], **Erzsébet Illés**[2]

[1]*Department of Physical Chemistry and Materials Science, University of Szeged, H-6720 Szeged, Aradi vt. tere 1, Hungary*
[2]*Department of Food Engineering, University of Szeged, H-6724 Szeged, Mars tér. 7, Hungary*
e-mail: vhornok@chem.u-szeged.hu

Abstract

Magnetic nanoflowers (MNF) can be applied in complementary cancer therapy treatment, however, some of the preparation conditions and stability experiments have not been examined in great detail. In this study, magnetite nanoparticles (NPs) with flower-like architecture were synthesized, characterized and tested by magnetic hyperthermia. The preparation and characterization of flower-shaped magnetic objects were optimized in two types of reaction vessels. The two different synthesis methods resulted in magnetic nanoparticles (MNP) of slightly different morphology, resulting in different behavior for hyperthermia. The stability of the NPs was achieved by the application polymer functionalization both by in situ and post-coating methods.

Introduction

The colloid aqueous dispersion of superparamagnetic iron oxide nanoparticles (SPIONs) is very popular partly due to their potential theranostic application, indicating the combined possibility of therapy and diagnosis. Moreover, SPIONs can be used as a complementary therapy in cancer treatment. Their favorable magnetic properties can be further improved by preparing flower-like structures [1]. There have been some studies in recent years, aiming to prepare magnetite nanoflowers (MNF), however, the preparation conditions are quite different and lack detailed stability experiments.

Experimental

In this study, the MNFs were prepared from Fe(II) and Fe(III) chloride salts and NaOH dissolved in diethylene glycol (DEG) and N-methyl-diethanolamine (NMDA) mixture. The reaction was carried out both in an autoclave and in a round-bottom flask (either with or without continuous mixing) at 220 °C [2]. The magnetite structure was verified by X-ray diffraction measurements. As a stabilizing agent, based on earlier results [3], polyacrylic acid (PAA) and a copolymer, poly(acrylic acid-co-maleic acid) (PAM) was applied both during and after synthesis. The optimal pH and amount of stabilizing polymer were confirmed by both zeta-potential and dynamic light scattering (DLS) measurements. To provide information about their potential medical application, magnetic hyperthermia measurements were carried out [4].

Results and discussion

The results verified the crucial importance of some preparation conditions, such as the composition of the reaction solvent mixture, reaction time and rate of heating and cooling. Transmission electron microscopic images (TEM) of the nanoparticles revealed that as an effect of mixing, more fluffy structures with were obtained (Figure 1B).

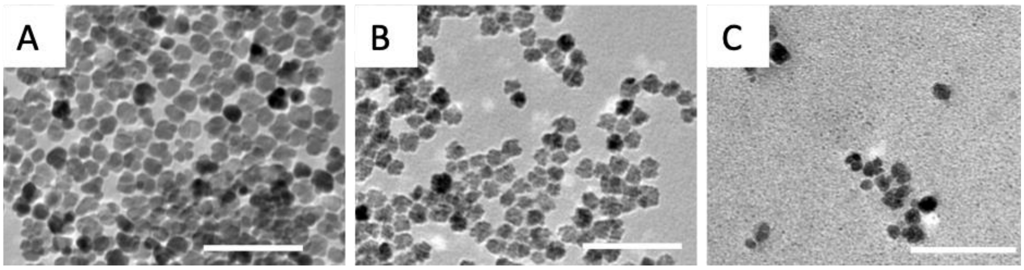

Figure 1. TEM images of MNF prepared without (A), with continuous mixing (B) and in-situ stabilized by PAA (C). The scale-bar above represent 100 nm.

To ensure NP stability for potential medical applications, the addition of polymers was carried out and zeta-potential measurements indicated the pH-dependent characteristics. If PAM polymer was added to the system during synthesis, the NP average diameter, determined by TEM, was significantly smaller, 14.0 ± 2.8 nm compared to the value of 19.5 ± 4.8 nm obtained for the NPs prepared in autoclave. During the post-coating method, a minimum of 0.7 mmol/g of polymer proved to be necessary for the stabilization of MNF.

Conclusion

Magnetic flower-like structures were prepared by the polyol method by two methods with difference in mixing or not. As a result, MNFs were obtained with similar average diameter but different primary particle size, resulting in different fine structures. With the variation of synthesis parameters, it has been revealed that the cooling rate plays a crucial part in the resulting NPs with an average particle diameter ranging from about 72 nm to ~20 nm. To obtain stable NPs, both in situ and post-coated method was applied with the help of two polymers. As for the hyperthermia result, our MNFs unquestionably possess a high effect, underlying the morphology suggestion for increased effect of the cooperation of small magnetic individuals. As a result, our NPs define the requirement of stabile flower structures with increased hyperthermia effect.

Acknowledgements

This research was supported by the Hungarian National Research Development and Innovation Office (NRDIH) through the FK131739 project and by the ÚNKP-23-5-SZTE-700 New National Excellence Program of the Ministry for Culture and Innovation from the source of the National Research, Development and Innovation Fund.

References

[1] V. Socoliuc *et al.*, Magnetic nanoparticle systems for nanomedicine-a materials science perspective”, Magnetochemistry 6 (2020) 1.

[2] D. Caruntu *et al.*, Synthesis of Variable-Sized Nanocrystals of Fe_3O_4 with High Surface Reactivity, Chem. Mater. 16 (2004) 5527.

[3] I. Y. Tóth, E. Illés, R.A. Bauer, D. Nesztor, M. Szekeres, I. Zupkó, E. Tombácz, Langmuir, 2012, 28: 16638 – 16646.

[4] L. Lartigue *et. al.*, Cooperative Organization in Iron Oxide Multi-Core Nanoparticles Potentiates Their Efficiency as Heating Mediators and MRI Contrast Agents, ACS Nano 6, 12 (2012) 10935-10949.

CLIMATIC, HYDROLOGICAL AND SOIL CHARACTERISTICS AS A DRIVING FORCE OF BIOLOGICAL INVASION: A CASE STUDY OF HUNGARY

Georgina Veronika Visztra [1], **Kata Frei** [2], **Alida Anna Hábenczyus** [2], **Anna Soóky** [2],
Zoltán Bátori [2], **Annamária Laborczi** [3], **László Pásztor** [3] **and Péter Szilassi**[1]

[1]Department of Geoinformatics, Physical and Environmental Geography, University of Szeged, Egyetem utca 2-6, H-6722 Szeged, Hungary
[2]Department of Ecology, University of Szeged, Egyetem utca 2-6, H-6726 Szeged, Hungary
[3]Department of Soil Mapping and Environmental Informatics, Institute for Soil Sciences, Centre for Agricultural Research, Herman Ottó út 15, H-1022 Budapest, Hungary
e-mail: myosotis.sylvatica12@mail.com

Abstract

Invasive plants are a serious threat to biodiversity, biological invasion is a significant problem in protected areas. In order to control their spread, we need to identify the soil, hydrological and climatic conditions which provide favorable conditions for their occurrence. Soil conditions, such as pH level, organic matter and calcium carbonate content and the rooting depth can influence the occurrence of invasive plant species. Many plant species can be associated with surface water, and thus distance from surface water can also be a determining factor for biological invasion. Mean annual temperature and precipitation are climatic factors that can also influence the spread of invasive plants.

We mapped the occurrence one of the most aggressively spreading non-native plants of Eurasia (*Ailanthus altissima*, *Asclepias syriaca*, *Elaeagnus angustifolia*, *Robinia pseudoacacia*, *Solidago* spp.) in Hungary, using field photos from the EUROSTAT Land Use and Coverage Area Frame Survey (LUCAS) and CORINE Land Cover databases, and investigated with geostatistical methods (ANOVA test in R statistics) how spatial characteristics of infection are related to soil and climatic characteristics and habitat types of Hungary.

We found that all the considered soil, hydrological and climatic factor had significant effect for the spread of the investigated invasive plant species. Our results confirm that environmental preference differs between the examined species, climate change may also have a different role on the occurrence.

Introduction

Invasive species are a serious threat to natural habitats, undemanding to their environment and therefore more successful at displacing native species from their natural habitat and invading anthropogenic areas. Biological invasion is the main problem in protected habitats [1–4].

The most effective control against invasive plants is to prevent their spread [5–7]. To find the most effective way to prevent the spreading of invasive species, we need to explore the environmental factors that influence their spread. The environmental (geographical) factors influencing invasion may be the quality and water management of the soil, or even temperature and amount of precipitation [7–12]. In this study, we investigated the influence of soil parameters such as organic matter content, pH, calcium carbonate content, rooting depth; climatic parameters such as mean annual temperature and mean annual precipitation, and distance from surface water on the occurrence of the most aggressively spreading invasive plant species: Tree of heaven (*Ailanthus altissima*), Common milkweed (*Asclepias syriaca*), Russian olive (*Elaeagnus angustifolia*), Black locust (*Robinia pseudoacacia*) and two invasive goldenrod species (*Solidago canadensis, Solidago gigantea*)). The two goldenrod species are mentioned as *Solidago* spp.

Experimental

The study was carried out in the territory of Hungary. The distribution of invasive species was obtained using the National GIS Database of Invasive Plant Species, which is a point-based database. A point is invaded if at least one individual of the plant is present at that point. If the plant is not detected at the point, it is considered as a non-invaded point [8] (Figure 1.). For the analysis of the environmental parameters, we used the Digital, Optimized, Soil Related Maps and Information in Hungary (DOSoReMI.hu) database [13].

Using ArcGIS software, we overlaid the environmental parameters (soil, hydrological, and climatic data) with the invaded and non-invaded points. This method was used to determine the environmental parameters at the given points. For statistical analysis, one-way ANOVA model was used and performed using Rstudio software.

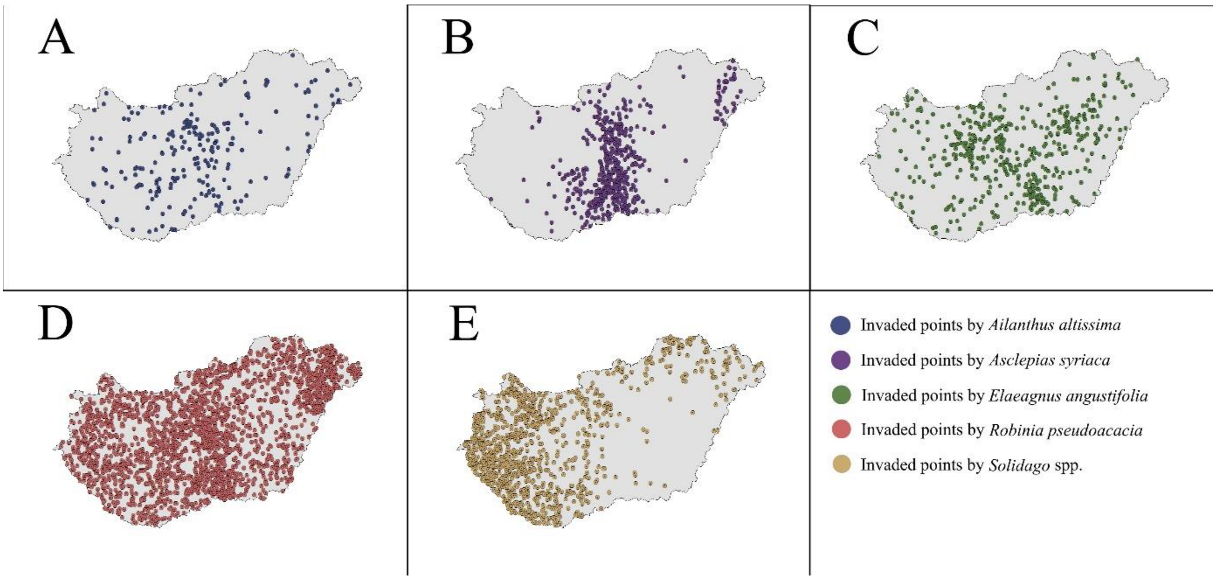

Figure 1. Distribution of the investigated invasive plant species in the territory Hungary, where A, *Ailanthus altissima;* B, *Asclepias syriaca;* C, *Elaeagnus angustifolia;* D, *Robinia pseudoacacia* and E, *Solidago* spp.

Results and discussion

The results show that all the considered environmental parameters have an influence on the occurrence of invasive plants studied. All soil and climatic factors (except mean annual precipitation) have significant impacts on the spread of *Ailanthus altissima*. The organic matter content was significantly lower, soil pH, calcium carbonate content, rooting depth, distance from surface water and mean annual temperature was significantly higher at the invaded points. In the case of *Asclepias syriaca*, all soil characteristics and climatic factors had a very high significant effect. Organic matter content and mean annual precipitation were significantly lower, soil pH, calcium carbonate content, rooting depth, distance from surface water and mean annual temperature were significantly higher at the invaded points by *Asclepias syriaca*. To *Elaeagnus angustifolia* we found that the soil pH, calcium carbonate content and mean annual temperature were significantly higher and mean annual precipitation was significantly lower at the invaded points. All soil characteristics (except calcium carbonate content) showed significant differences between invaded and non-invaded points by *Robinia pseudoacacia*. Organic matter content of the soil and soil pH were significantly lower, rooting depth and distance from surface water were significantly higher at the invaded points. Mean annual temperature was significantly lower at the invaded points, but we found no difference in the case of mean annual precipitation. Examining *Solidago* spp. we found significant differences in all of the investigated soil and climatic characteristics (except rooting depth) between invaded and non-inveded points (Table 1.).

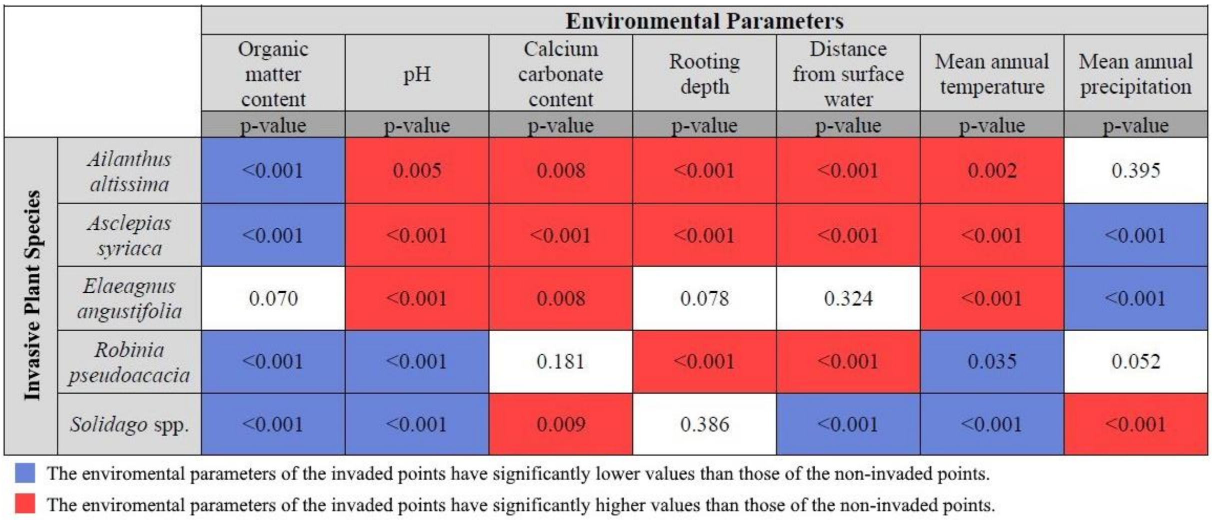

		Environmental Parameters						
		Organic matter content	pH	Calcium carbonate content	Rooting depth	Distance from surface water	Mean annual temperature	Mean annual precipitation
		p-value	p-value	p-value	p-value	p-value	p-value	p-value
Invasive Plant Species	*Ailanthus altissima*	🟦 <0.001	🟥 0.005	🟥 0.008	🟥 <0.001	🟥 <0.001	🟥 0.002	0.395
	Asclepias syriaca	🟦 <0.001	🟥 <0.001	🟥 <0.001	🟥 <0.001	🟥 <0.001	🟥 <0.001	🟦 <0.001
	Elaeagnus angustifolia	0.070	🟥 <0.001	🟥 0.008	0.078	0.324	🟥 <0.001	🟦 <0.001
	Robinia pseudoacacia	🟦 <0.001	🟦 <0.001	0.181	🟥 <0.001	🟥 <0.001	🟦 0.035	0.052
	Solidago spp.	🟦 <0.001	🟦 <0.001	🟥 0.009	0.386	🟦 <0.001	🟦 <0.001	🟥 <0.001

🟦 The enviromental parameters of the invaded points have significantly lower values than those of the non-invaded points.

🟥 The enviromental parameters of the invaded points have significantly higher values than those of the non-invaded points.

Table 1. Differences between invaded and non-invaded points as a function of the soil, hydrological, and climatic parameters for the invasive species investigated.

The results confirm that this method is well applied to investigate which environmental parameters influence the spread of invasive plants. The results show that these species are well tolerant of soils with low organic matter content and that high calcium carbonate content has a positive effect on their occurrence (Figure 2.). This does not necessarily mean that these plants prefer soils with low organic matter content and high calcium carbonate content. The results explain that invasive plants can grow well in poorer quality habitats where native species do not [4,13].

The results show that high precipitation has a positive effect on the occurrence of *Solidago* spp., but high temperatures inhibit its spread. In contrast, the opposite is true for *Asclepias syriaca* and *Elaeagnus angustifolia*. These plants prefer drier and warmer habitats [12] (Figure 2.).

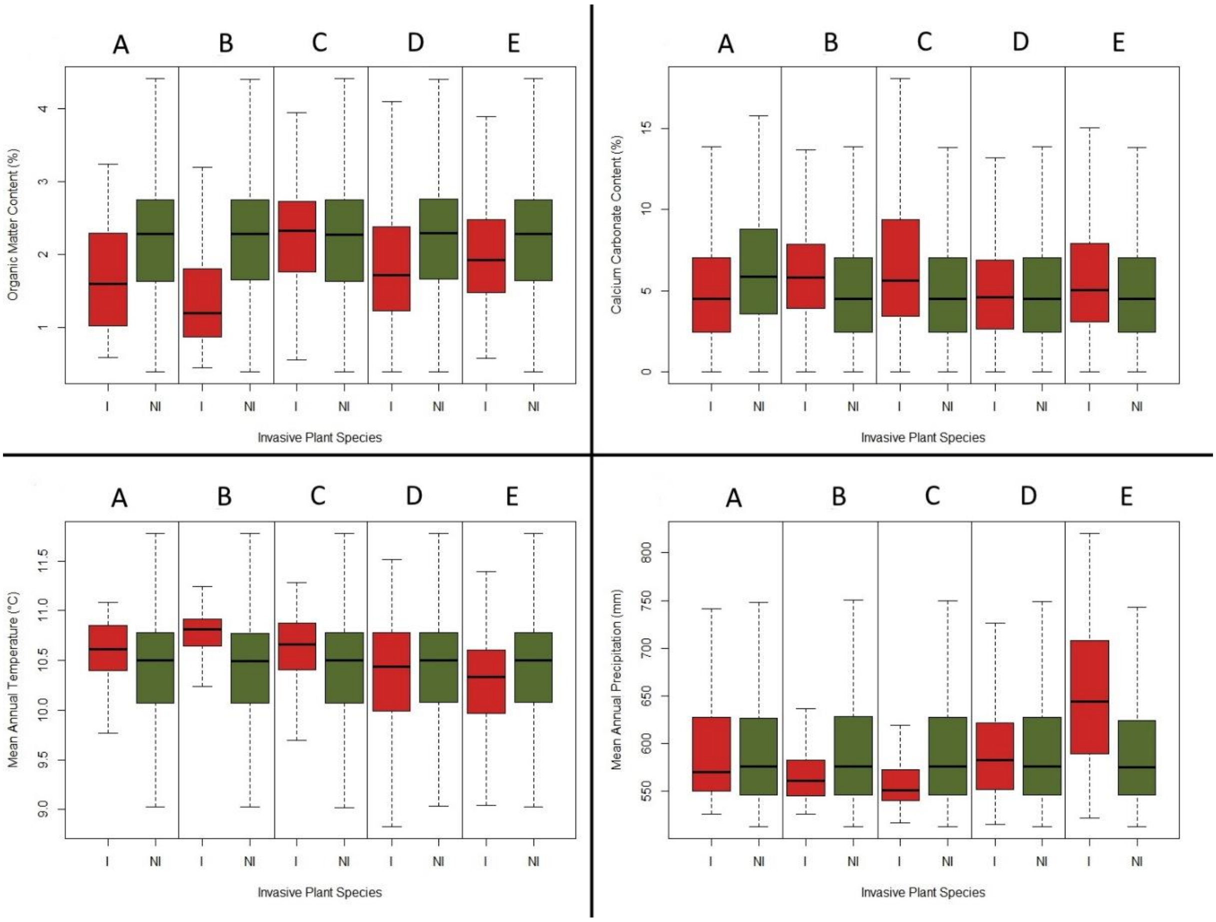

Figure 2. Differences between invaded and non-invaded points regarding organic matter content, calcium carbonate content, mean annual temperature and mean annual precipitation; (A, *Ailanthus altissima;* B, *Asclepias syriaca;* C, *Elaeagnus angustifolia;* D, *Robinia pseudoacacia* and E, *Solidago* spp.)

Conclusion

Like any other plant, the spread of invasive plants is highly dependent on environmental parameters. Some environmental factors promote, and others inhibit the occurrence of these plants [7-12]. Our results confirm that invasive plant species tolerate low soil organic matter and calcareous soils well.

The results show that *Asclepias syriaca* and *Elaeagnus angustifolia* prefer warmer and drier climatic conditions, while *Solidago* spp. prefers cooler and wetter conditions. This suggests that climate change promotes the occurrence of *Asclepias syriaca* and Elaeagnus *angustifolia*, but inhibits that of *Solidago* spp.

Acknowledgements

I would like to take this opportunity to thank all my co-authors for their dedicated work. I would especially like to thank my supervisor, Dr. Szilassi Péter for his help, without him this study would not have been possible.

References

1. Follak, S.; Bakacsy, L.; Essl, F.; Hochfellner, L.; Lapin, K.; Schwarz, M.; Tokarska-Guzik, B.; Wołkowycki, D. Monograph of Invasive Plants in Europe N°6: Asclepias Syriaca L. *Bot Lett* **2021**, *168*, 422–451, doi:10.1080/23818107.2021.1886984.
2. Gurevitch, J.; Padilla, D.K. Are Invasive Species a Major Cause of Extinctions? *Trends Ecol Evol* **2004**, *19*, 470–474, doi:10.1016/j.tree.2004.07.005.
3. Csiszár, Á.; Kézdy, P.; Korda, M.; Bartha, D. Occurrence and Management of Invasive Alien Species in Hungarian Protected Areas Compared to Europe. *Folia Oecologica* **2020**, *47*, 178–191, doi:10.2478/foecol-2020-0021.
4. Paź-Dyderska, S.; Ladach-Zajdler, A.; Jagodziński, A.M.; Dyderski, M.K. Landscape and Parental Tree Availability Drive Spread of Ailanthus Altissima in the Urban Ecosystem of Poznań, Poland. *Urban For Urban Green* **2020**, *56*, doi:10.1016/j.ufug.2020.126868.
5. Mehta, S. V.; Haight, R.G.; Homans, F.R.; Polasky, S.; Venette, R.C. Optimal Detection and Control Strategies for Invasive Species Management. *Ecological Economics* **2007**, *61*, 237–245, doi:10.1016/j.ecolecon.2006.10.024.
6. Maxwell, B.D.; Lehnhoff, E.; Rew, L.J. The Rationale for Monitoring Invasive Plant Populations as a Crucial Step for Management. *Invasive Plant Sci Manag* **2009**, *2*, 1–9, doi:10.1614/ipsm-07-054.1.
7. Royimani, L.; Mutanga, O.; Odindi, J.; Dube, T.; Matongera, T.N. Advancements in Satellite Remote Sensing for Mapping and Monitoring of Alien Invasive Plant Species (AIPs). *Physics and Chemistry of the Earth* 2019, *112*, 237–245.
8. Szilassi, P.; Szatmári, G.; Pásztor, L.; Árvai, M.; Szatmári, J.; Szitár, K.; Papp, L. Understanding the Environmental Background of an Invasive Plant Species (Asclepias Syriaca) for the Future: An Application of Lucas Field Photographs and Machine Learning Algorithm Methods. *Plants* **2019**, *8*, doi:10.3390/plants8120593.
9. Szilassi, P.; Soóky, A.; Bátori, Z.; Hábenczyus, A.A.; Frei, K.; Tölgyesi, C.; van Leeuwen, B.; Tobak, Z.; Csikós, N. Natura 2000 Areas, Road, Railway, Water, and Ecological Networks May Provide Pathways for Biological Invasion: A Country Scale Analysis. *Plants* **2021**, *10*, doi:10.3390/plants10122670.
10. Vaz, A.S.; Alcaraz-Segura, D.; Campos, J.C.; Vicente, J.R.; Honrado, J.P. Managing Plant Invasions through the Lens of Remote Sensing: A Review of Progress and the Way Forward. *Science of the Total Environment* 2018, *642*, 1328–1339.
11. Wang, R.; Gamon, J.A. Remote Sensing of Terrestrial Plant Biodiversity. *Remote Sens Environ* **2019**, *231*, doi:10.1016/j.rse.2019.111218.
12. Visztra, G.V.; Frei, K.; Hábenczyus, A.A.; Soóky, A.; Bátori, Z.; Laborczi, A.; Csikós, N.; Szatmári, G.; Szilassi, P. Applicability of Point-and Polygon-Based Vegetation Monitoring Data to Identify Soil, Hydrological and Climatic Driving Forces of Biological Invasions-A Case Study of Ailanthus Altissima, Elaeagnus Angustifolia and Robinia Pseudoacacia. **2023**, doi:10.3390/plants.
13. Pásztor, L.; Laborczi, A.; Takács, K.; Illés, G.; Szabó, J.; Szatmári, G. Progress in the Elaboration of GSM Conform DSM Products and Their Functional Utilization in Hungary. *Geoderma Regional* 2020, *21*.

SUBACUTE EXPOSURE TO DIBUTYL PHTHALATE RESULTS IN AN INCREASED NUMBER OF OVARIAN CORPUS LUTEUM IN FEMALE WISTAR RATS

Jelena Vukčević, Ivana Ivelja, Nebojša Andrić, Jelena Marković Filipović

Department of Biology and Ecology, Faculty of Sciences, University of Novi Sad, Trg Dositeja Obradovića 2, Serbia
e-mail: jelena.karan@dbe.uns.ac.rs

Abstract.

Dibutyl phthalate (DBP) is a phthalic acid ester, widely used as a plasticizer to add flexibility to plastics. Due to its weak chemical bonding with polymer products, DBP can easily be released into the environment. It has been shown that DBP act as an endocrine disruptor with estrogenic activity, primarily targeting the ovary.

The objective of this study was to determine whether a subacute exposure to DBP affects the number of ovarian corpus luteum.

Twenty-four female Wistar rats, 40 days old at the beginning of the experiment, were divided into four groups (6 rats per group). They underwent subacute exposure for 28 days with DBP incorporated into their diet at doses of 0, 100, 500 and 5000 mg DBP/kg diet, that correspond to 8.58, 41.34 and 447.33 mg/kg BW/day. Bouin's-fixed ovaries were embedded in paraffin and then serially sectioned into 5 µm slices. The slides were stained with hematoxylin and eosin. The numbers of ovarian corpus luteum were determined under Olympus light microscope. Statistical analysis was performed using STATISTICA® version 13.0 (StatSoft, Inc). Data from control and treated rats were compared using One-way analysis of variance (ANOVA) for multiple comparisons, followed by Tukey post-hoc tests.

Statistical analysis revealed no differences in the number of corpus luteum in the group exposed to 100 mg DBP/kg diet when compared with control group. However, in the group exposed to 500 and 5000 mg DBP/kg diet, a significant increase in the number of corpora lutea was observed.

The results indicated that short-term exposure to higher doses of DBP result in an elevated number of ovarian corpus luteum. Based on these data, we can infer that under these experimental conditions, DBP has the capacity to induce accelerated ovarian aging.

CHARACTERZATION OF POLY(N-IZOPROPYLACRYLAMIDE) HYDROGEL NANOCOMPOSITES INFLUENCED BY ANIZOTROPIC SILVER NANOPARTICLES

Ivana Vukoje, Jelena Spasojević, Nikolina Nikolić , Milica Milošević, Vesna Vodnik, Aleksandra Radosavljević

Vinča Institute of Nuclear Sciences, National Institute of the Republic of Serbia, University of Belgrade, Mike Petrovića Alasa 12-14, 11351 Vinča, Belgrade, Serbia
e-mail: ivanav@vin.bg.ac.rs

Abstract

Hydrogels possess distinctive characteristics that can be tailored to meet specific needs, especially in the field of biosciences, which is continuously expanding and advancing. Adjustability of gel porosity, followed by tunability of swelling properties, environmental responsiveness, and stability, are properties that are easily adjusted, offering researchers and engineers the flexibility to fine-tune these properties to suit the specific requirements of diverse applications. As a result of environmental responsivity, one class of these materials emerged, referred to as stimuli-responsive or smart hydrogels. Such hydrogels can change their properties in response to specific external stimuli or environmental conditions in a controlled and reversible manner. Depending on the specific type of smart hydrogel, this feature can enable targeted drug delivery, tissue engineering, and controlled release systems while maintaining their biocompatibility. Poly(N-isopropylacrylamide) (PNiPAAm) is a thermosensitive polymer with a well-defined volume phase transition temperature (VPTT) around 32°C. Conversely, silver nanoparticles (AgNPs) continue to preserve academic interest due to their size-dependent optical, catalytic, and electronic properties, as well as their significant antimicrobial potential. One of the primary obstacles encountered by scientists is establishing the broader range of practical applications of AgNPs as well as improving the existing ones. Optimizing their properties often involves controlling size and shape, stability, and surface properties. In order to determine how anizotropic Ag NPs alter and influence the physicochemical properties of PNiPAAm we present a simple, straightforward two-step synthesis of AgNPs/PNiPAAm hydrogel nanocomposites. This method involves the chemical synthesis of both spherical and triangular AgNPs, followed by the crosslinking of PNiPAAm through gamma irradiation in the presence of nanoparticles. The validation of employing gamma irradiation is based on the fact that this technology integrates the processes of sterilization and synthesis, resulting in a consolidated technical step that enhances efficiency and enables the exploration of numerous innovative biomedical applications. The porous sponge-like structure was observed by SEM analysis, while the formation of stable and uniformly distributed AgNPs in the polymer was confirmed by UV-VIS spectroscopy. Swelling and deswelling processes were performed in water at 25°C and 48°C, respectively. In addition, AgNPs were shown to influence VPTT values. The primary objective of this study is to examine the correlation between various morphologies of AgNPs and the physicochemical characteristics of nanocomposite samples. This investigation considers the possible uses and the current demand for the extensive utilization of biocompatible materials.

Acknowledgements

This work was supported by the Ministry of Science, Technological Development and Innovations of the Republic of Serbia (Contract No. 451-03-47/2023-01/200017).

BIODEGRADATION AND DEGRADATION PATHWAY OF DIISOPROPYL ETHER BY *MYCOLICIBACTERIUM* SP. STRAIN CH28

Ingrid Zsilinszky[1], Balázs Fehér[1], József Varga[2], István Kiss[1], Attila Komóczi[1], Zsolt Szabó[1]

[1]Department of Applied Microbiology, Division for Biotechnology, Bay Zoltán Nonprofit Ltd. for Applied Research, H-6726 Szeged, Derkovits fasor 2., Hungary
[2]IMSYS Engineering Services Ltd. H-1033 Budapest, Mozaik utca 14/a, Hungary
e-mail: ingrid.zsilinszky@bayzoltan.hu

Abstract

A diisopropyl ether (DIPE) degrader bacterium, *Mycolicibacterium* sp. strain CH28 was isolated from a pharmaceutical groundwater. Based on our results strain CH28 is capable of the complete mineralization of DIPE with a maximum degradation rate of 1.63 ± 0.03 nmol min^{-1} mg biomass^{-1}. We proposed the metabolic pathway of microbial DIPE degradation in our isolate based on the detection of 2-propanol, acetone, and acetate as degradation intermediates. Our results revealed that strain CH28 holds great potential in the bioremediation of sites contaminated with fuel oxygenate ethers (e.g.: DIPE).

Introduction

Fuel oxygenate ethers, like methyl *tert*-butyl ether (MTBE), ethyl *tert*-butyl ether (ETBE), *tert*-amyl methyl ether (TAME), and diisopropyl ether (DIPE) have been increasingly used since the 1970s as octane enhancers to replace lead and induce complete fuel combustion [1]. There are various treatment methods for degrading ether oxygenates from the contaminated medium including air stripping, absorption [2], adsorption [3], chemical oxidation [4], additionally several combined physical/chemical and biological processes are also spreading [5]. Despite these compounds are usually poorly biodegradable because of their highly stable ether bonds and branched carbon structure [1], biological treatment is the most common method of remediating ether-polluted wastewaters [6].

DIPE is widely used as an industrial solvent for oils, waxes, dyes, and resins [7], and for the extraction and purification of many compounds [8]. To date, only three bacterial isolates have the ability to degrade DIPE have been described: *Rhodococcus ruber* IFP 2001 [9], *Pseudonocardia* sp. strain ENV478 [10], and *Aquincola tertiaricarbonis* L108 [11].

In this abstract, we describe the kinetics and some intermediates of DIPE biodegradation observed regarding *Mycolicibacterium* sp. strain CH28, furthermore, we propose a part of the degradation pathway of aerobic DIPE mineralization as well.

Results and discussion

Resting cell experiments with Mycolicibacterium sp. strain CH28

To measure the DIPE-degrading capacity of strain CH28 resting cell, experiments were carried out with 200 mg l^{-1} DIPE. The total amount of DIPE was efficiently mineralized in less than 11 hours, the maximum degradation rate was 1.63 ± 0.03 nmol min^{-1} mg biomass^{-1}. The rate of DIPE degradation was seemed to be of the same magnitude as for the previously described strains [9-11]. During the experiment, acetone and acetate were detected as intermediates (Figure 1). This was the first time that acetate had been identified as a degradation intermediate of DIPE biodegradation.

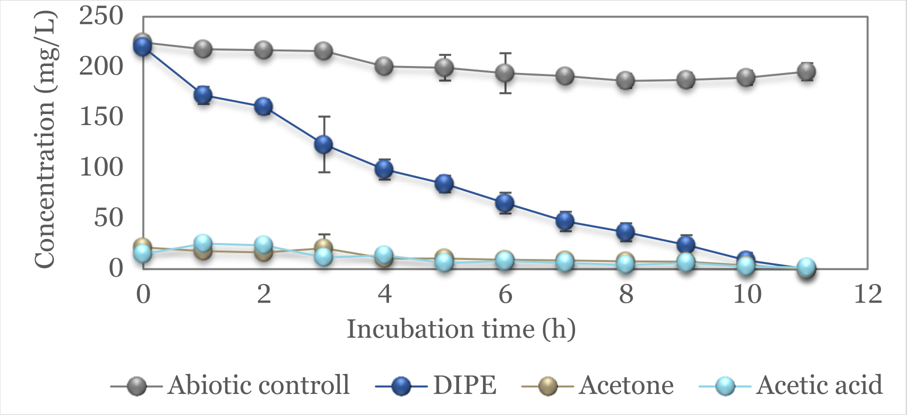

Figure 1. Degradation of DIPE by *Mycolicibacterium* sp. strain CH28 resting cells. Cells were pre-grown in SMM supplemented with 200 mg l^{-1} DIPE. The concentrations of DIPE (abiotic controls (□); bioaugmented systems (▲)), acetone (●), and acetate (◊) were monitored. Error bars indicate the standard deviations of three parallel measurements.

Biodegradation pathway of DIPE in Mycolicibacterium sp. strain CH28

Biodegradation of ether oxygenates such as MTBE, ETBE, dimethyl ether, diethyl ether, and aralkyl ethers was described to proceed through an *O*-dealkylation reaction [12]. Generally, this process is catalyzed by monooxygenases, during the degradation an oxygen atom incorporates to the alpha carbon atom of the ether bond. This results the formation of an unstable hemiacetal structure which spontaneously decomposes to an alcohol and a carbonyl compound [1]. *O*-dealkylation of DIPE generates to the simultaneous formation of 2-propanol and acetone. Most likely, 2-propanol is converted to acetone by a secondary alcohol dehydrogenase. These results are in good agreement with our experiments since we have managed to detect 2-propanol (in microcosm studies, data not shown) and acetone as degradation intermediates (Figure 2). Considering our and the above showed results we propose the upper pathway of DIPE degradation by strain CH28 (Figure 3) resulting in the formation of 2-propanol and acetone as the major intermediates.

The lower pathway of DIPE biodegradation includes the degradation of acetone producing CO_2 and bacterial biomass. Microbial metabolism of acetone has been well-studied in general, five major pathways were revealed [13]. Two of these involve the formation of formaldehyde but we could not detect this intermediate in any of our samples. Strain CH28 is not capable of the biodegradation of formaldehyde, so if it had been formed, it would have accumulated. During the biodegradation of DIPE, acetate was generated by strain CH28. Accordingly, it could be formed virtually in all the reported acetone degradation pathways. However, further research is required to clarify the actual biodegradation pathway of acetone in strain CH28 (Figure 3).

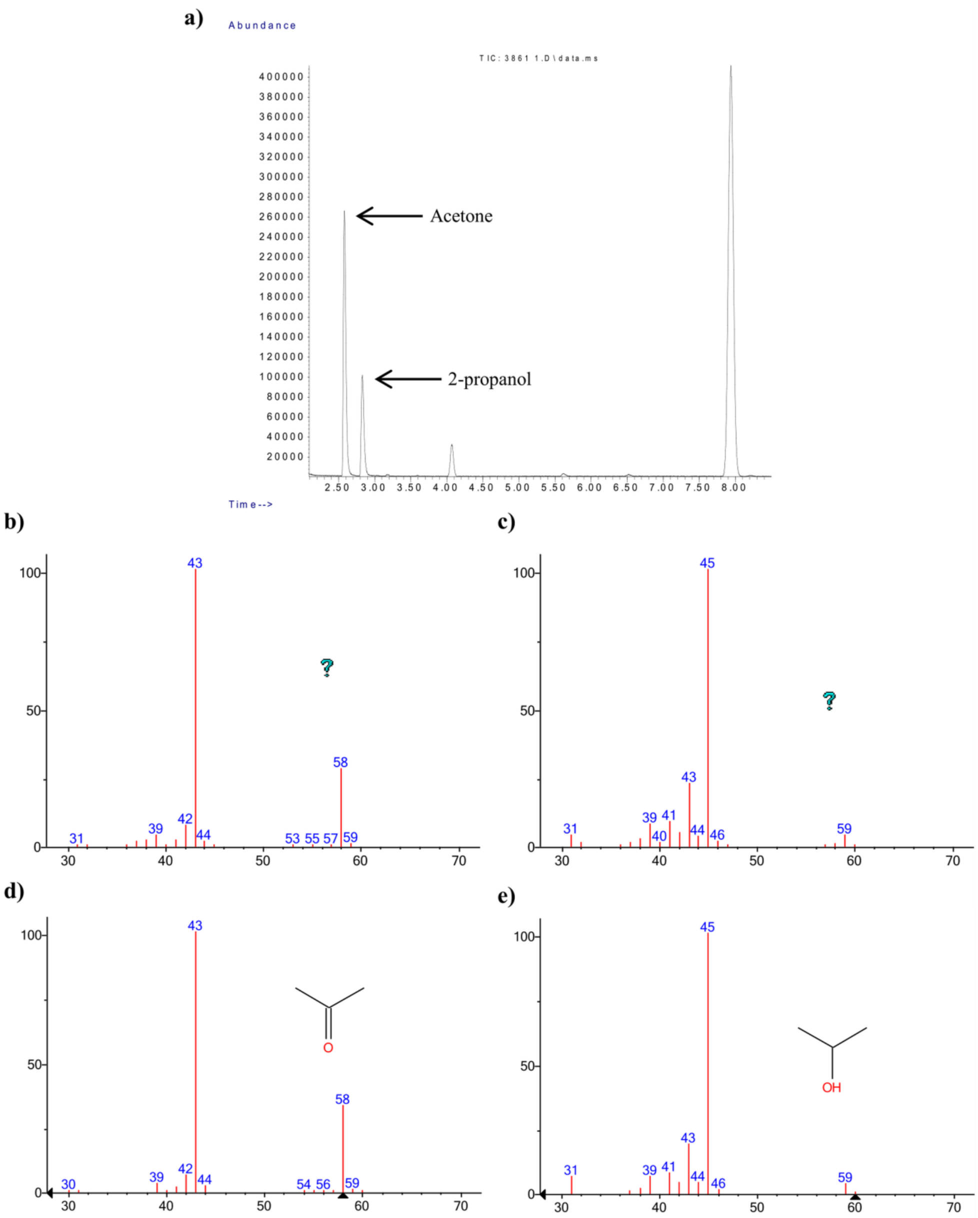

Figure 2. Acetone (at t_R=2.578 min) and 2-propanol (at t_R=2.829 min) as identified intermediates of DIPE degradation by *Mycolicibacterium* sp. strain CH28 in our experiments (**a**), with mass spectra of acetone and 2-propanol from the microcosm samples (**b** and **c**, respectively) and from the NIST/EPA/NIH Mass Spectral Library (Version 2.0f, NIST, Gaithersburg, MD, USA) (**d** and **e**, respectively).

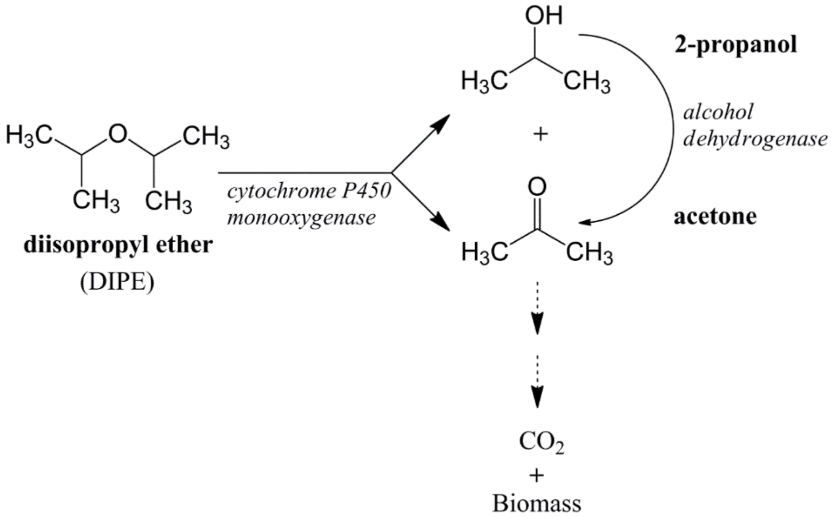

Figure 3. Upper pathway of DIPE biodegradation by *Mycolicibacterium* sp. strain CH28.

Conclusions

Mycolicibacterium sp. CH28, isolated from a pharmaceutical groundwater, is a powerful DIPE-degrader. Regarding strain CH28, major part of upper DIPE-degradation pathway was revealed, however, further studies are needed to clarify the exact lower degradation pathway as well.

Acknowledgements

This work was supported by National Research Development and Innovation Office, Hungary. Project: KFI_16-1-2017-0377 "Intensified Microbiological Degradation and Development of Analytical Methods"

National Research, Development and Innovation Office
Hungary
PROJECT
FINANCED FROM
THE NRDI FUND
MOMENTUM OF INNOVATION

References

[1] White, G. F., N. J. Russell, and E. C. Tidswell. 1996. Bacterial scission of ether bonds. Microbiological Reviews 60 (1):216–32.

[2] Cortez, J. S. A., B. I. Kharisov, T. E. S. Quezada, and T. C. H. García. 2017. Micro- and nanoporous materials capable of absorbing solvents and oils reversibly: The state of the art. Petroleum Science 14 (1):84–104.

[3] Vakili, M., M. Rafatullah, B. Salamatinia, M. H. Ibrahim, N. Ismail, and A. Z. Abdullah. 2017. Adsorption studies of methyl tert-butyl ether from environment. Separation & Purification Reviews 46 (4):273–90.

[4] Kashir, M., and R. McGregor. 2018. Stabilized hydrogen peroxide for the remediation of hydrocarbons and MTBE in high temperature and saline groundwater. Remediation Journal 29 (1):27–36.

[5] Liang, J., S. Tang, J. Gong, G. Zeng, W. Tang, B. Song, P. Zhang, Z. Yang, and Y. Luo. 2020. Responses of enzymatic activity and microbial communities to biochar/compost amendment in sulfamethoxazole polluted wetland soil. Journal of Hazardous Materials 385: 121533.

[6] Borisov, I., I. Podtynnikov, E. Grushevenko, O. Scharova, T. Anokhina, S. Makaev, A. Volkov, and V. Volkov. 2020. High Selective Composite Polyalkylmethylsiloxane Membranes for Pervaporative Removal of MTBE from Water. Polymers 12: 1213.

[7] Patnaik, P. 2007. A comprehensive guide to the hazardous properties of chemical substances. 3rd ed. Hoboken, NJ: Wiley-Interscience

[8] Harrington, P.J. 2011. Pharmaceutical Process Chemistry for Synthesis: Rethinking the Routes to Scale-Up. 1st ed. Hoboken, N.J: Wiley.

[9] Hernandez-Perez, G., F. Fayolle, and J.-P. Vandecasteele. 2001. Biodegradation of ethyl *t*-butyl ether (ETBE), methyl *t*-butyl ether (MTBE) and *t*-amyl methyl ether (TAME) by Gordonia terrae. Applied Microbiology and Biotechnology 55: 117–121.

[10] Vainberg, S., K. McClay, H. Masuda, D. Root, C. Condee, G.J. Zylstra, and R.J. Steffan. 2006. Biodegradation of ether pollutants by *Pseudonocardia* sp. strain ENV478. Applied and Environmental Microbiology 72: 5218–5224.

[11] Lechner, U., D. Brodkorb, R. Geyer, G. Hause, C. Härtig, G. Auling, F. Fayolle-Guichard, P. Piveteau, R.H. Müller, and T. Rohwerder. 2007. *Aquincola tertiaricarbonis* gen. nov., sp. nov., a *tertiary* butyl moiety-degrading bacterium. International Journal of Systematic and Evolutionary Microbiology 57: 1295–1303

[12] Kim, Y.-H., and K.-H. Engesser. 2005. Inhibition of diethyl ether degradation in *Rhodococcus* sp. strain DEE5151 by glutaraldehyde and ethyl vinyl ether. FEMS Microbiology Letters 243: 317–322.

[13] Hausinger, R.P. 2007. New insights into acetone metabolism. Journal of Bacteriology 189: 671–673.